Advancements of Stepped Planing Hulls

Evan J. Lee

Dissertation submitted to the Faculty of the
Virginia Polytechnic Institute and State University
in partial fulfillment of the requirements for the degree of

Doctor of Philosophy
in
Aerospace Engineering

Leigh S McCue-Weil, Chair
Alan J. Brown
Timothy Coats
Wayne L Neu

October 30, 2014
Blacksburg, Virginia

Keywords: Stepped Planing Hull, High Speed Craft, Hydrodynamics

Advancements in the Analysis of Stepped Planing Hulls

Evan J. Lee

(ABSTRACT)

The straight line calm water performance of stepped planing hulls has been studied experimentally, by prediction method, and numerically. A model test was conducted to provide a systematic understanding of the effects that displacement and step location have on the performance of a stepped planing hull. Ten different step configurations were tested at three different displacements and over a range of four different speeds in calm water. Seven of these configurations were tested at two different Longitudinal Center of Gravity (LCG) locations. Of all the configurations tested, the stepped hull configurations showed reduced resistance compared to the unstepped hull. The configurations with the largest step height aft showed the least amount of resistance over the speed range tested. Increasing displacement and shifting LCG had similar effects on craft performance for both stepped and unstepped hulls. The current stepped hull prediction method was expanded to include a three dimension wave profile and the ability for the stagnation line to cross the step. Using previous model test data and existing two dimension wave profile equations, a single equation was developed to predict the three dimension wave profile aft of a step. Formulations were added to Savitsky's planing prediction method to include very high speed craft and chines dry conditions. Lastly, two simulations were performed using two computational fluid dynamics numerical tools, OpenFOAM, and NFA. The results of these simulations were compared to the experimental test results to assess each code's relative strengths and weaknesses for use in detail design of stepped planing craft.

This work received support from Naval Surface Warfare Center Carderock Division IAR and Section 219 Programs

Acknowledgments

First I would like to thank God for blessing me with the opportunity to study and earn my PhD. I would also like thank the following people, my wife, Jessica, for her love as I completed this dissertation. My parents for their support growing up. Dr. Leigh McCue-Weil for her support, encouragement and guidance as I earn my PhD. Dr. Tim Coats, Dr. Alan Brown, and Dr. Wayne Neu for being on my committee. Gordon Hatchell for encouraging me to get my PhD. Steve Brandis for assisting in the construction of the model, Dr. Michael Morabito for the conversations about stepped planing hulls, and United States Naval Academy Hydromechanics Lab for their assistance in conducting the model test. Dr. John Barkyoumb, Dr. Jack Price, Dr. Jack Templeton, and Dan Goodwin for their support of the model test. Dr. Tom Fu and Dr. Tom O'Shea for their assistance with Numerical Flow Analysis. Dr. Joseph Gorski for assisting with computational resources.

Contents

List of Figures

List of Tables

Variables

α=Volume Fraction
B=Beam
β=Deadrise angle, degrees
β_i=Deadrise angle of ith step
$C_v = \frac{V}{\sqrt{gB}}$=Speed coefficient
$C_{L,s}$=Lift coefficient based on bottom area
d=Draft at transom
D_{f_i}=Friction resistance force on the ith planing surface
Δ=Hull displacement
ϵ=Propulsion force angle
h=Height of Step
L=Lift
L_c=Wetted chine length
L_k=Wetted keel length
λ=Mean wetted length to beam ratio
l_p=Center of pressure
L_{S_i}=Horizontal length from transom to ith planing surface
N_i=Normal force on the ith planing surface
n=Number of planing surfaces
ρ=Density
T=Propulsion force
τ=Trim angle, degrees
θ_i=Difference in angle between planing surface ith planing surface and horizontal, degrees
U_s=Tangential velocity at transom
u=x-component of flow velocity due to velocity potential component $Ar^n \cos n\theta$
V=Hull Velocity
w=z-component of flow velocity due to velocity potential component $Ar^n \cos n\theta$
X=Distance aft of transom, Beams
Y=Distance off centerline, Beams
Z=Height of wave profile above keel, Beams

Chapter 1

Introduction

Stepped planing hulls are a type of planing hull form where there are transverse discontinuities, also known as steps, in the planing surface. Figure 1.1 shows an example of a stepped planing hull with two steps. At high speeds, the flow separates off of the step and allows for a stepped hull to have less resistance than an unstepped hull. Steps can be applied to both planing monohulls and planing catamarans. This thesis will focus on the application of steps on planing monohulls.

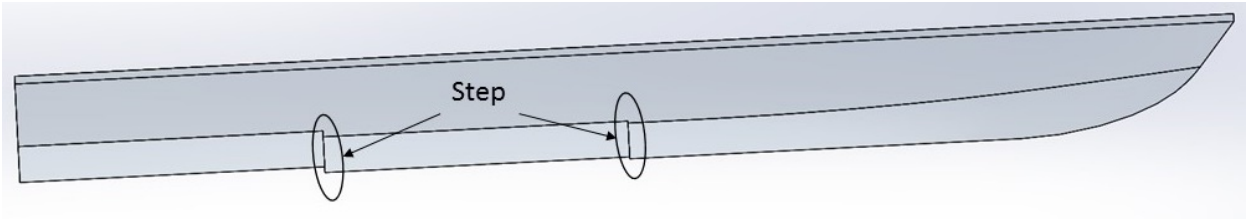

Figure 1.1: Example of a Stepped Planing Hull

It is commonly thought that stepped planing hulls do not perform well at off design conditions. The idea is that a stepped planing hull is designed so that it performs optimally at a specific speed, displacement, and LCG location. When the stepped hull is not operating at its design condition, the performance is thought to be very poor.

Industry is currently using stepped planing hulls in many high speed applications, such as offshore racing boats and sport fishing boats. Industry has developed the stepped planing hull through the process of trial and error. The cost to modify the hull is small compared to the cost to perform trade studies. Companies are not willing to publish what information that they have learned so that they can protect their competitive advantage.

A brief history of the research that is available on stepped planing hulls are presented in the following sections. Most of the early research of steps were conducted for seaplanes. A number of different researchers have conducted model tests of stepped planing hulls in recent years. Researchers have also expanded Savitsky's planing prediction method to include the ability to predict stepped planing hulls.

1.1 Early History of Stepped Hulls

The first stepped hull was proposed by Reverend C.M. Ramus in 1872. This hull was intended to be used for a 2,500 ton, 370 ft long, ship rather than a smaller planing craft [1]. The hull did not have any deadrise and the keel had an angle of 8 ° to the baseline [1]. William Froude tested a model of this hull form at the Torquay Towing Tank [1]. The stepped hull model was compared against two other models, a traditional hull shape of the time with the same dimensions as the stepped hull and a model of the HMS Greyhound which has been tested extensively at the time [1]. Up to 50 knots full scale speed, the stepped hull had more resistance than the other two hull forms [1]. Froude noted that at the highest speed, a dynamic instability occurred where, in calm water, the hull would either ride solely on the aft planing surface or on both planing surfaces. [1]

Further research on the hydrodynamics of stepped planing hulls started with seaplane research performed by the National Advisory Committee for Aeronautics [2] [3] . Stepped planing hulls were used as floats and integrated into the plane as flying boats. Table 1.1 shows a summary of the difference between typical seaplanes and stepped planing hulls. There are many differences between the stepped planing hull and seaplanes. First, stepped planing hulls use much smaller step height than the float or the flying boat. Secondly, the afterbody angle is much higher on a float or a flying boat compared to a stepped planing hull. For the flying boat, this was important because the afterbody was the aft part of the plane and aerodynamic considerations also needed to be taken into account. Lastly, the length to beam ratio of a stepped hull is smaller than for a float or a flying boat. Another consideration is that the seaplanes were designed for take off speeds that are higher than the speeds that most planing hulls operate.

Table 1.1: Seaplane vs. Stepped Planing Hull Comparison

	Stepped Planing Hull	Float [3]	Flying Boat [2]
Step Height (% of Beam)	1-2	7	16
Afterbody Angle (°)	±2	7	7
Length to Beam Ratio	4-5	7	15

Eugene Clement [4] started researching a stepped planing hull design in the 1960s at Naval Surface Warfare Center Carderock Division (NSWCCD) called the Dynaplane. The Dynaplane is different from modern stepped planing hulls in a few respects. First, the Dynaplane was designed so that the afterbody is completely out of the water and additional lift is generated at the transom with a hydrofoil. The hull has keel camber near the step to generate additional lift. NSWCCD has tested this model at the David Taylor Model Basin. This form of the stepped planing hull has not been utilized by industry.

1.2 History of Stepped Planing Hull Model Testing

R. Rodstrom, Hans Edstrand, and H. Bratt in 1953 [5] was one of the first to conduct model tests on a stepped planing hull. They conducted a systematic series of experiments on a single step planing hull. They investigated the effect of beam on resistance and transverse stability. The model with the lowest deadrise angle showed the least amount of resistance of all the models tested [5]. The results show that resistance decreased with increased beam, but the model with the greatest beam showed porpoising above a speed coefficient of 3.54 [5]. Increasing the afterbody angle eliminated this porpoising but increased the resistance. In that configuration, the afterbody has a higher initial trim angle than the forebody. Decreasing the afterbody length increased the resistance. The large step height variations showed small variations resistance. The 0° afterbody angle shows the least resistance up until porpoising [5].

Over the years, a number of stepped planing hull tests have been conducted at Webb Institute. The first stepped planing hull model test was performed by James Filling in 1993 [6]. His hull model test consisted of three phases. The first phase was the test of a stepped planing hull model that was free to trim and heave. The second phase was a fixed trim and heave test to determine the lift and moment of each planing surface. The forebody and afterbody were mounted separately on the carriage, and the forces were measured on each planing surface [6]. The presence of the forebody increased the lift on the afterbody [6]. Phase three was a model test similar to phase one, but the afterbody was angled in relation to the forebody. The change in angle did not have an appreciable impact on the static trim, but had an effect on the running trim. William Gassman and Scott Kartinen continued Fillings work in 1994 [7]. They used his existing model and tested more variables. They concluded that the 50% step location and the furthest aft LCG location had the least resistance [7]. Testing of LCG locations further aft are needed because the furthest aft location that they tested exhibited the least resistance and the optimum LCG for the step configuration is unknown. Therefore, one cannot decisively conclude that they found the optimal LCG location for their step configuration. Chris Becker, Anthony Loreto, and Justin Shell revisited stepped planing model testing in 2008 [8]. These tests focused on the

pre-planing regime. The deep vee monohull had lower resistance than the stepped hull at the speeds tested. They concluded that the stepped hull was not beneficial until higher speeds. They found that the step type did not have a large effect on the speed at which separation occurs.

The United States Naval Academy (USNA) has performed two different stepped planing hull tests. The first was performed by William Garland as a senior project [9]. It was found that when the step height was 3.67% of the beam, the stepped hull had the lowest resistance [9]. Holes were drilled behind the step to ensure that the step was always ventilated. Runs were repeated with the holes plugged and the results showed that there was no difference between the holes plugged or open. The step was always properly ventilated. At high speeds, the flow no longer separated from the forebody at the chine and started separating at the step. Greg White at the USNA performed a series of model tests of a stepped hull in a single and double step configuration [10]. This test focused on a single design speed and trim. The results from this test show that the stepped planing hull had lower resistance than a traditional hull at the design condition [10].

D.J. Taunton, D.A. Hudson, and R.A. Shenoi performed a systematic model test of planing hulls in calm water [11]. As part of the series, two stepped hull models were tested. Model C was a deep vee monohull and the two stepped hull (Model C1 and Model C2) were derived from this parent hull. The resistance for both stepped models were less than the parent Model C [11]. C1 at a speed coefficient of 4.7 was the only condition to show signs of porpoising [11]. They concluded that the steps did not have any effect on dynamic heave or dynamic trim.

Table 1.2 is a summary of previous stepped planing hull model tests.

Table 1.2: Previous Model Tests

Tester	Rodstrom et al	Filling	Gassman et al	Becker et al	Garland	White	Taunton et al
Year	1953	1993	1994	2007	2010	2010	2010
Length (inches)	112.6	50.875	50.875	52	60	63.54	78.75
Beam (inches)	20.5	5.25	5.25	11.25	17.4	14.4	18.11
Step Height (% of Beam)	5.8, 10.1, 14.4	20.95	10	0.56, 1.11, 1.67	2, 4, 5.98	0.87, 1.74, 3.47, 5.21, 6.94	
Step Location (% of Length forward of transom)	50	50	38.33, 50.12, 61.92		33.54	33.64 (fwd), 18.89 (aft)	
Step Type	Transverse	Transverse	Transverse	Transverse, Apex Forward, Apex Aft	Transverse	Transverse	Transverse
Displacement (lbf)	150	19.95	19.95	27	57.45	43.81	54.7
Deadrise Angle (°)	7.5 and 10	15	15	20	15	24	22.5
LCG (% of Length forward of transom)		35.4, 38.33, 44.23	34.62	39.4		33	
Speed Coefficient	2.39-4.87	1.066-3.81	1.07-4.4	1.64-2.73	0.73-4.54	4.4	1.88-5.65

1.3 Prediction Methods

1.3.1 Savitsky's Planing Prediction Method

Daniel Savitsky in 1964 published a paper that outlined an empirical method to predict the trim and resistance of an unstepped planing hull [12]. Before his work leading up to the paper, a number of different researchers studied prismatic planing hulls to describe the hydrodynamic characteristics at fixed trim, mean wetted length, and speed [12]. His goal was to develop empirical equations that would relate the different physical characteristics of a planing hull to the hydrodynamic lift, drag, pitch moment and wetted surface area of the hull [12]. To add to the data missing from previous research, a series of model tank tests conducted at Davidson Laboratories where prismatic planing hulls were tested in a fixed trim and heave condition. The lift, resistance, trim moment, and mean wetted length to beam ratio was measured. All of the collected data was analyzed and empirical relationships between the different hydrodynamic characteristics were found to develop Savitsky's planing prediction method. This method has been useful to the naval architect for years because it is a quick method to estimate straight line performance of an unstepped planing hull in calm water. Savitsky's method is an iterative procedure which one iterates upon trim angle to balance trim moment. The process for solving the Savitsky planing prediction method starts with selecting an initial value for the trim angle. Once the initial value of the trim angle is selected, the flat plate lift coefficient is iterated or found from the design graphs provided by Savitsky [12]. Using the flat plate lift coefficient, the mean wetted length to beam ratio is iterated or found from the design charts. With the mean wetted length to beam ratio, the center of pressure for the lift is calculated from an empirically based equation. The center of pressure is the point where the lift force acts on the planing surface. The friction resistance is calculated by using the wetted surface area and the Schoenherr friction coefficient. The Schoenherr friction coefficient is iterated or found from design graphs. Using the weight of the craft, the planing lift, the propulsive thrust, and the friction resistance, the moment about the LCG is calculated. The trim angle is iterated until the moment is zero.

1.3.2 Stepped Planing Hull Prediction Method

Previous work has been done to extend Savitsky's planing prediction method to stepped planing hulls. Morabito presented a method for predicting performance of stepped planing hulls [13]. His work focused on developing a way to predict the three dimension wave profile. His method requires a number of equations to calculate the wave profile. Svahn presented a more detailed method for predicting the performance of stepped planing hulls [14]. Svahn's method predicts the performance of a single step planing hull [14]. Svahn assumes a percentage of the total lift is generated on the forward planing surface and the rest of the lift is generated on the aft planing surface. His method only uses the wave profile

to calculate the parameters for calculating the friction resistance. The lift on the aft planing surface is assumed to be the lift that is not supported by the forward planing surface. He also assumes that the flow aft of the step is two dimensional and is linear in the transverse direction. Therefore, the flow will reattach the aft planing surface in a similar manner as the flow attaches the forward planing surface. As a result, the aft planing surface will have a straight stagnation line from keel to chine. Danielsson and Stromquist developed a method for predicting performance of stepped planing hulls as part of conceptual design for a yacht tender[15]. Their method was extended to a double step planing hull. For their work, they simplified the flow aft of the step and assumed that it is horizontal.

1.4 Numerical Methods

For unstepped hulls, numerical tools have been introduced to supplement model tests. There are many factors to consider in the simulation of planing hulls. First, the domain needs to be large to capture the far field wave profile. The form resistance of a hull as it moves through the water is manifested by the waves that it generates. Therefore, the far field wave profile needs to be accurately simulated to determine the correct form resistance. For planing hulls, the friction resistance is a large contributor to the overall resistance, so the cells near the hull need to be small to capture the boundary layer and friction resistance. Lastly, when using simulation to predict the performance of planing craft, the running trim angle and draft are not known. So an initial trim angle and draft must be given and the simulation then must solve for the running trim angle and draft. Therefore the numerical tool must have some implementation for a moving mesh.

1.5 Objectives

To test the current thought that stepped planing hulls do not perform well at off design conditions, the effect of Displacement and LCG on stepped hull performance is needed to be determined. Based on the previous model tests, displacement has not been systematically varied and only one other model test has systematically varied LCG. Chapter 2 furthers the existing stepped planing hull model test data and provides a detailed look into the influence of displacement and LCG on stepped hull performance. Observations from the model test revealed areas of improvements for stepped planing hull predictions to increase its accuracy and applicability. First, the stagnation line crossed the step. It is thought to be ideal to design the step so that at the design condition, the stagnation line crosses the chines of the forward planing surface. At off design conditions, this may not happen and the stagnation line might cross the step. Second, it was always thought that the reattachment line

aft of the step was always straight, but underwater photographs show it was curved rather than straight. These are two areas that are not implemented in current prediction methods. Chapter 3 extends the current prediction method to include a three dimension wave profile and the ability for the stagnation line to cross the step. Numerical methods have been used to simulate unstepped hulls. The added feature of the step increases the complexity of the already difficult simulation by adding a tiny flow feature that has a large influence of the simulation results. Chapter 4 assess modeling gaps and computational constraints in current state of the art numerical simulation tools when analyzing stepped planing hulls.

Chapter 2

Model Test

2.1 Model Test Introduction

As discussed in the introductory chapter section 1.2, advances in stepped planing hull model testing have focused on the step height, step location, and step type. However, one variable that has not been systematically varied is displacement. Because many applications require robust performance across loading conditions, it is critical to broaden the understanding of how displacement and LCG location can influence stepped planing hull performance. This chapter describes model tests at the USNA using the Naval Surface Warfare Center 15 ° Extended (NSWC15E) hull. The model was tested with 10 different step configurations; one unstepped and nine stepped. Each configuration was tested at three displacements and two LCG locations.

2.2 Hull Form

The hullform used for this model test, NSWC15E, is derived from the Naval Surface Warfare Center 15 ° deadrise hull form (NSWC15) developed at Naval Surface Warfare Center, Detachment Norfolk (NSWCCD DN) [9]. The NSWC15 was selected because of its parallel sections aft which allow for a constant deadrise planing surface. The parallel sections aft reduce difficulty in hydrodynamic analysis and simplified the step design and construction. There are no strakes or chine flats to reduce potential variables in the model test that would need to be captured in further assessment of simulation. The NSWC15 has a length of 60 inches and a beam of 18 inches. Because the length to beam ratio of 3.33 does not reflect the current length to beam ratio of stepped planing hulls, an additional 20 inches of parallel midbody was added to the length of the NSWC15 to create the NSWC15E. The added

length increases the length to beam ratio to 4.44. The new hull has parallel midbody from Station 4 to the transom. There are two steps located on the hull; one at midships (40 inches forward of the transom) and one 25% of the length overall forward of the transom (20 inches forward of the transom). Each of these steps are transverse from chine to chine. Table 2.1. is a table of the principal characteristics and Figure 2.1 shows the body plan of the hull.

Table 2.1: Principal Characteristics

Length Overall	80 inches
Beam Overall	18 inches
Maximum Chine Beam	17.5 inches
Design Displacement	85 lbf
Deadrise Angle	15 °

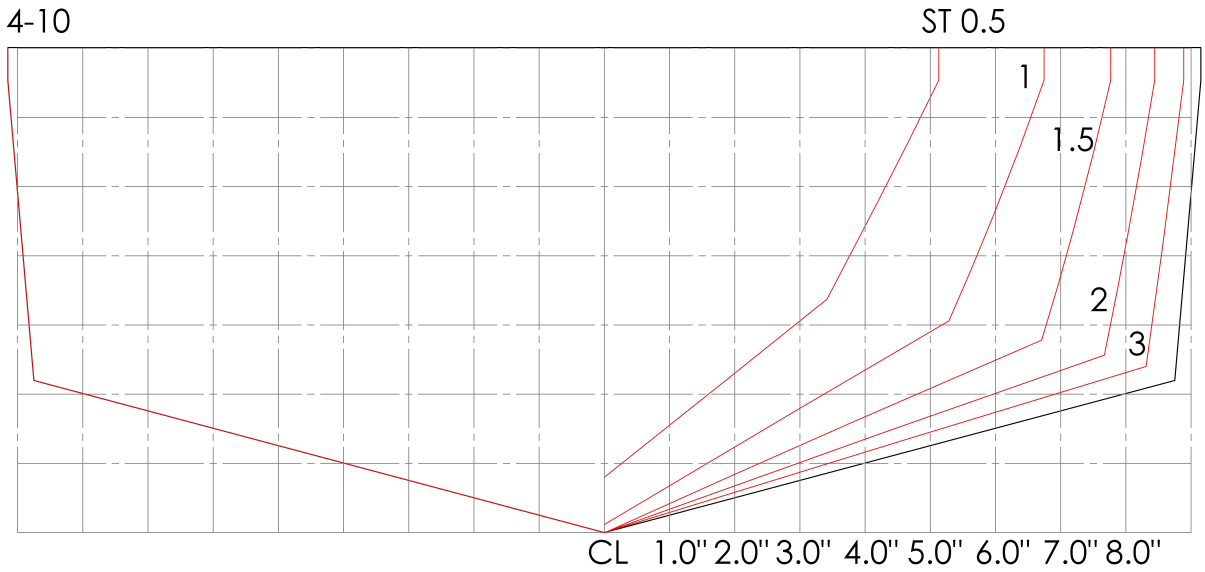

Figure 2.1: Body Plan of NSWC15E

2.3 Model

For stepped planing hull models, a method to systematically vary the steps is needed. To increase the flexibility in selecting the step height of the model, a method was developed to allow for the step to be adjusted over a range of heights at each of the step locations. The model is built in three parts and the parts are connected together by through bolts at the bulkheads. Each bulkhead has three bolts; one near the keel and one on either side near the

shear line. This arrangement ensured a tight fit between each of the parts and did not allow for the parts to rotate while adjusting the step height. In the midbody, 1 inch long slots were drilled to allow the step height to be adjusted. Holes were drilled on the afterbody and the forebody and threaded plates were epoxied to the back to provide threads for the bolts. Each of the bulkheads were cut flat to the same height. An angle aluminum extrusion was epoxied onto the bulkhead of the midbody and forebody so that the angle aluminum extrusion is flush with the top of the bulkhead. This arrangement allows for the step heights to be changed while the model is still mounted to the carriage. To change the step height, each of the bolts are loosened and the step is raised. A piece of flat aluminum bar corresponding to the desired step height is inserted between the angle aluminum extrusion and the top of the bulkhead. The step is lowered until the angle aluminum extrusion is flush with the flat aluminum bar.

2.3.1 Model Construction

The NSWC15E model was built at NSWCCD Combatant Craft Division by Steve Brandis and the author. The model was built in three parts from the NSWC15 mold provided by USNA. The forebody consisted of the forward 40 inches of the craft. The midbody was the 20 inches between the steps and the afterbody was the last 20 inches of the model. The mold is a fiberglass mold that is open on the top and at the transom. A Lexan plate was used to enclose the transom area. To construct the model, a temporary dam was first built from the few inches of the model near the transom (Figure 2.2).

Figure 2.2: Temporary Dam Completed in Mold

This temporary dam was then moved 20 inches forward and secured in place to provide the forward bulkhead of the afterbody (Figure 2.3).

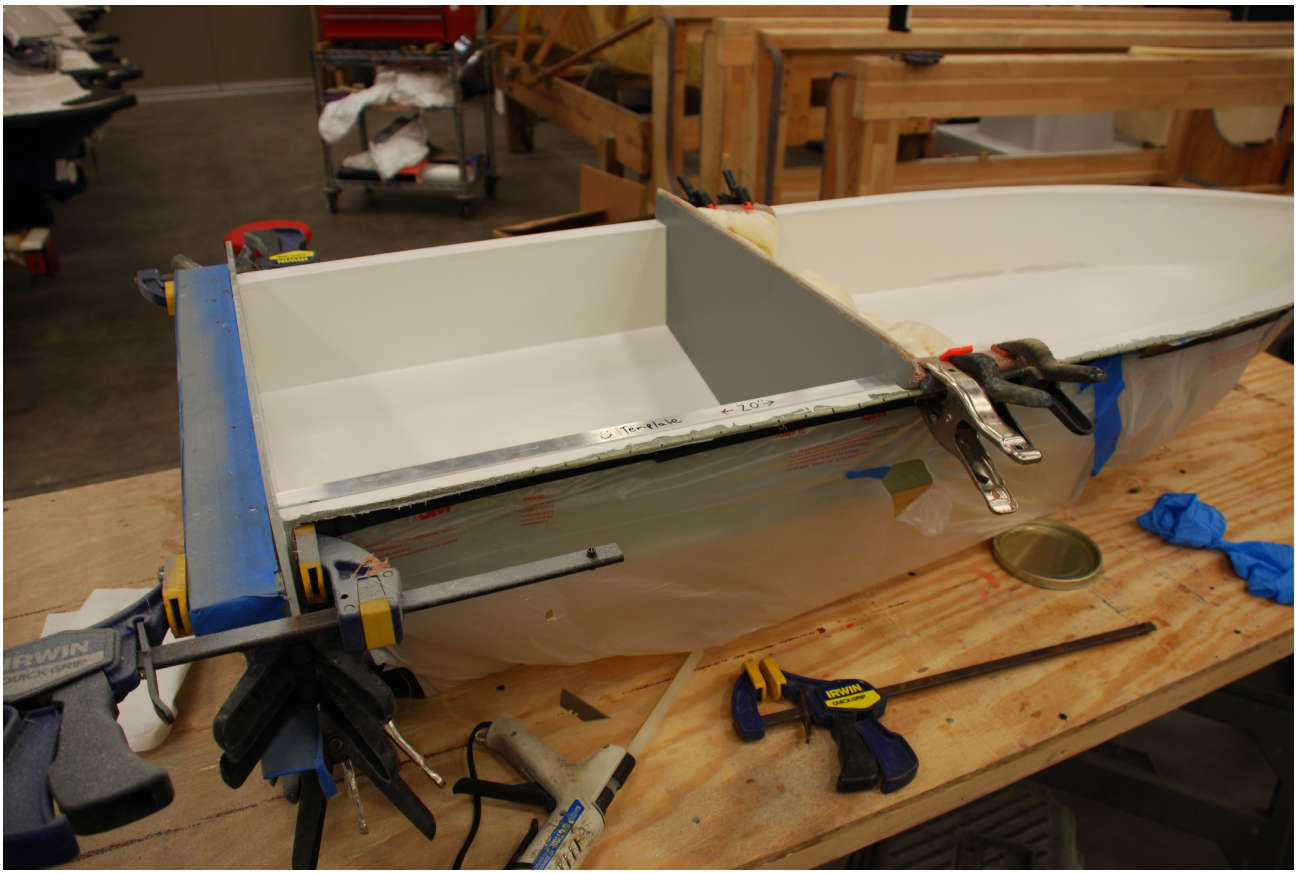

Figure 2.3: Temporary Dam Moved Forward 20 inches

The afterbody was then built, secured in place and the temporary dam removed (Figure 2.4).

Figure 2.4: Afterbody Built in Mold

The forebody was then built using the afterbody to provide the aft bulkhead of the forebody (Figure 2.5).

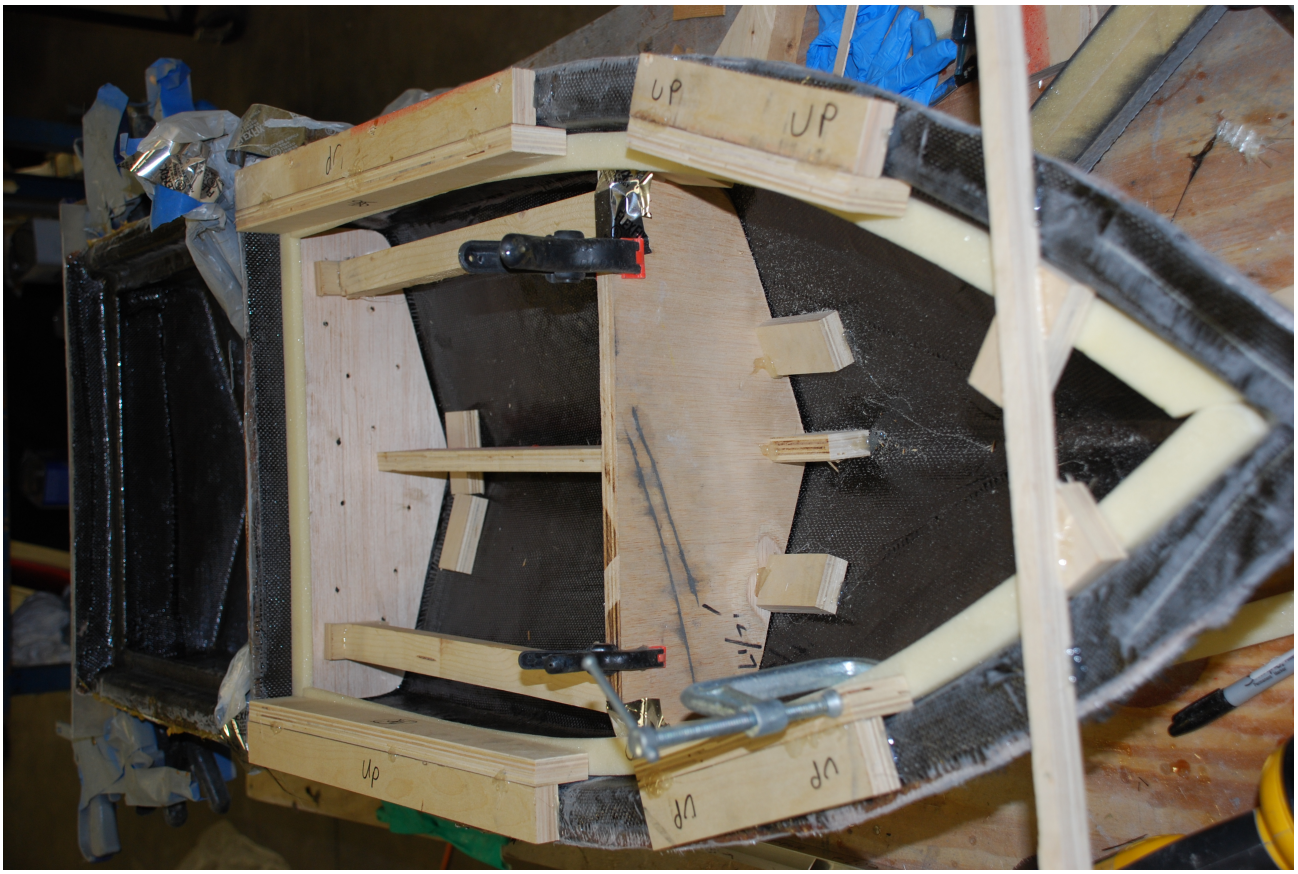

Figure 2.5: Forebody Construction: Installation of the Stiffeners

Once the forebody was built, the afterbody was removed and the forebody was used to create the forward bulkhead of the midbody (Figure 2.6).

Figure 2.6: Midbody Construction: Before layup of Stiffeners

The model is a composite model using carbon fiber, fiberglass, and epoxy. A gel coat was first sprayed into the mold. Once the gel coat dried, ProSet 175/275 [16] was used to fill in the corners to keep the keel and chines sharp as well as protect them from damage. Next a layer of OCV M723A [17] 0.75 oz chop fiberglass was used to provide a foundation for the following directional layers. The rest of the laminate is as follows; two layers of 94101 [18] 0/90 deg 6 oz carbon fiber, one layer of E-BXM 1708 [19] ±45deg 26 oz fiberglass, and another two layers of 94101 0/90 deg 6 oz carbon fiber. The bulkhead of each section were stiffened with a 1/8 inch balsa core and another layer of 0/90 deg 6 oz carbon fiber. To stiffen the top of the model, A500 [20] foam ring stiffeners were mounted 3/4 inch from the shear line. The stiffeners were covered by C-BX 0300 [21] 3oz ±45deg carbon fiber.

It should be noted that the original paint scheme for the model was a black and white checkerboard pattern similar to the pattern used at NSWCCD David Taylor Model Basin. The contrast of the black and white made it difficult to discern the areas where the water was aerated or attached. The USNA retested the model with the paint scheme that they use for most of their tests. The photographs from the second set of tests provided marginally

better results for the wetted surface area. There was still some difficulty in determining the wetted surface area when the area after the step was highly aerated with large bubbles.

2.4 Configurations

Ten different step configurations were tested (Table 2.2). The step heights at each of the steps were 0.125, 0.25, and 0.375 inch corresponding to 0.7%, 1.4%, and 2.1% of the beam. These values cover the range of step heights of current pleasure craft designs [8]. Configuration 1 had no steps thus serving as the unstepped hull for baseline comparison.

Table 2.2: Step Configurations

Configuration	Forward Step Height (% of Beam)	Aft Step Height from Forward Step (% of Beam)
1	0	0
2	0.7	0.7
3	0.7	1.4
4	0.7	2.1
5	1.4	0.7
6	1.4	1.4
7	2.1	0.7
8	1.4	2.1
9	2.1	1.4
10	2.1	2.1

2.5 Variables

The displacement, LCG, speed, and step configuration are the independent variables that are being tested. A model scale full load displacement of 85 lbf was selected to match the full scale displacement of a typical military craft as described in White and Beaver [10]. Two overload displacements (95 lbf and 105 lbf) were selected to determine the effect of future weight growth on craft performance. Two LCG locations (40% and 35% of the LOA forward of the transom) were selected to determine how shifts in weight effect craft performance. The first seven configurations were tested at both the forward and aft LCG locations. The last three configurations were only tested at the aft LCG location.Four speeds were selected that were in the planing regime; 25, 27, 29, and 31 ft/s corresponding to 41.9, 45.2, 48.6, and 52 knots full scale (speed coefficients of 3.6, 3.88, 4.17, and 4.46). The speed coefficient

is a non-dimensional value similar to the Froude number and defined as $C_v = \frac{V}{\sqrt{gB}}$. Since the wetted length of a planing hull varies, the characteristic length used is the hull beam rather than the hull length as would be typical for Froude number. The dependent variables are resistance, heave, pitch and wetted surface area. The resistance, heave, and pitch were measured directly while the wetted surface area was measured after the test using underwater photos.

2.6 Test Setup

The model test was conducted in the 380 ft Towing Tank at the USNA Hydromechanical Lab (USNA HL). The data was collected during two different model tests. In the first model test, the first seven step configurations were tested at the forward LCG location. During the second model test, all ten step configurations were tested at the aft LCG location. The tank is 26 ft wide and has a depth of 16 ft. The high speed carriage was used for the experiments allowing a maximum velocity of 31 ft/s. The model was attached to the carriage with a pivoting single post heave staff allowing the model to be free in pitch and heave. The pivot, located at the LCG and 5.25 inches above the baseline, contained a pitch potentiometer to measure the trim of the model. The heave was measured by a pair of linear potentiometers on the tow post. The resistance was measured using a variable reluctance displacement transducer force block. The static heave and trim was measured for each condition while the hull was at rest. The trim reported is the absolute trim, the angle between the baseline and the horizontal. The heave reported is the distance the boat moved vertically from the static position. Based on previous experiments, no methods were used to supplement the step ventilation. The step ventilated at all the conditions tested. To change displacement, additional weights were added to the model at posts located 20 inches forward and aft of the LCG to maintain a constant LCG location. The radius of gyration changed slightly, but since the tests were for only calm water, this change in radius of gyration was deemed to have a minimal influence on test results; 12.35 inches for 85 lbf displacement and 14.14 inches for 105 lbf displacement. The wetted surface area was calculated from underwater photos of the planing surface. The underwater photography system at the USNA HL consists of a digital SLR housed in a water proof case and two strobe lights. The camera was triggered via a trip mounted on the side of the tank.

2.7 Test Method

The resistance, trim, and heave for a run was recorded by taking the average of the data when the carriage was running at constant velocity. To calculate the wetted surface area, the underwater photos were first corrected for lens distortion (fish eye effect). The lens distortion was corrected using a toolbox developed by Jean-Yves Bouget for MATLAB [22]. For this

method, a series of grided calibration photos are needed. A grid in MATLAB is overlaid onto the calibration photos. The overlaid grid is adjusted until it matches the grid of the calibration photo. The correction factors are then calculated from the overlaid grids. Lastly, the correction factors are applied to the underwater photos. The view was then transformed from a perspective view to an orthogonal view using the perspective tool in GIMP [23], an open source photo editing tool. Once the photos were corrected, Solidworks [24], a 3D CAD program, was used to calculate the wetted surface area.

2.8 Error Analysis

The possible sources of error lie within the data acquisition equipment for the velocity, resistance, trim, and heave along with post-processing, human-introduced errors, in estimating wetted surface areas. To assess the experimental error acquired in data collection, configuration 1 was run twice for each of the 4 velocities tested for the 85 and 95 lbf displacements. The standard deviation of the difference between runs was calculated for each of the runs and presented in Table 2.3. The standard deviation is the variation from the mean value for each individual run. The first two columns are the displacements and the target speed tested while the last four columns are the standard deviation for the velocity as well as the resistnace, trim and heave.

Table 2.3: Repeat Test Standard Deviation

Displacement	Speed	Velocity	Resistance	Trim	Heave
lbf	ft/s	ft/s	lbf	°	in
85	25	0.0047	0.0272	0.0184	0.0050
85	27	0.0049	0.0530	0.0197	0.0180
85	29	0.0055	0.0476	0.0208	0.0182
85	31	0.0030	0.1753	0.0412	0.0281
95	25	0.0051	0.0195	0.0043	0.0220
95	27	0.0056	0.2377	0.0202	0.0080
95	29	0.0059	0.1772	0.0425	0.0307
95	31	0.0051	0.1450	0.0448	0.0264

The 27 ft/s run at the 95 lbf displacement shows the most error with the resistance. As a result, this condition was run an additional 10 times during the first test period and an additional 8 times during the second test period. Including a re-run during the initial set of tests, this run was repeated 22 times. The standard deviation of the difference between the runs is shown in Table 2.4. In this table only the standard deviations are shown.

Table 2.4: Standard Deviation Speed=29 ft/s Displacement=95 lbf

Velocity (ft/s)	Resistance (lbf)	Trim (deg)	Heave (in)
0.0028	0.2625	0.107	0.0313

For each of the variables, a χ-squared test was performed in MATLAB to test if the data is normally distributed [25]. All of the data passed the test, but the sample size is small. Therefore, it was cautiously assumed that the error is normally distributed. The standard deviation for the specific variable was then multiplied by 2 to get a 95% confidence interval with two standard deviations on each side of the mean. For the trim, the error in measuring the static trim was added to the error in the dynamic trim to determine the overall confidence interval. For the wetted surface area, the difference between the wetted chine lengths of the port and starboard side was used to determine the error in length for the wetted surface area calculations. This value was multiplied by the wetted beam to determine the total error in the wetted surface area. This confidence interval based on configuration 1 at 27 ft/s and 95 lbf displacement was then applied to all the configurations, speeds and displacements and the confidence interval can be seen as error bars in the data analysis plots (Table 2.5). For some plots where the horizontal errors are small, the horizontal bars are eliminated for clarity.

Table 2.5: Confidence Interval

Velocity (ft/s)	Resistance (lbf)	Trim (deg)	Heave (in)	Wetted Surface Area (in^2)	Displacement (lbf)
0.0056	0.525	0.214	0.063	33.3	0.5

2.9 Results

2.9.1 Resistance

The plots for the 85 lbf displacement are presented here (Figures 2.7-2.9) while the plots for the other displacements can be found in Appendix B. The results from all ten step configurations are divided into three plots for clarity. The configuration 1, unstepped hull, results were repeated on each plot for reference. The filled symbols were the results from the forward LCG location and the unfilled symbols were from the aft LCG location. Configurations 1-7, which were tested at both LCG locations have the same shape for the data points for easier comparison. Figure 2.7 shows configurations 4, 8 and 10, which all have the large step height aft. Figure 2.8 shows configurations 3, 6 and 9, which all have the medium step height aft. Figure 2.9 shows configurations 2, 5 and 7, which all have the small step height aft. When comparing Figures 2.7-2.9, Figure 2.7 shows that the large step height aft had lowest resistance of all the step configurations tested. As the aft step height decreases from

large to small, from configuration 10 to configuration 4, the reduction in resistance when compared to the unstepped hull decreases. Figure 2.7 shows that with the large aft step height, the forward step height had little effect on the resistance. On the other hand, Figure 2.9 shows that with the small aft step height, the forward step height had a large effect on the resistance. As the forward step height increases, from configuration 2 to configuration 7, the resistance decreases. This shows that large aft step heights contributes significantly to the overall reduction in resistance. As the aft step height got smaller, the forward step height had more of an effect on the reduction in resistance. For all the configurations tested, the hull had more resistance at the forward LCG location than the aft LCG location. As the aft step increased, the difference in resistance between the forward LCG location and the aft LCG location decreased. All the step configurations show a greater reduction in resistance/weight as the speed coefficient increases. This shows that stepped planing hulls perform better than unstepped hulls as speed increases. Similar trends were seen at the two other displacements.

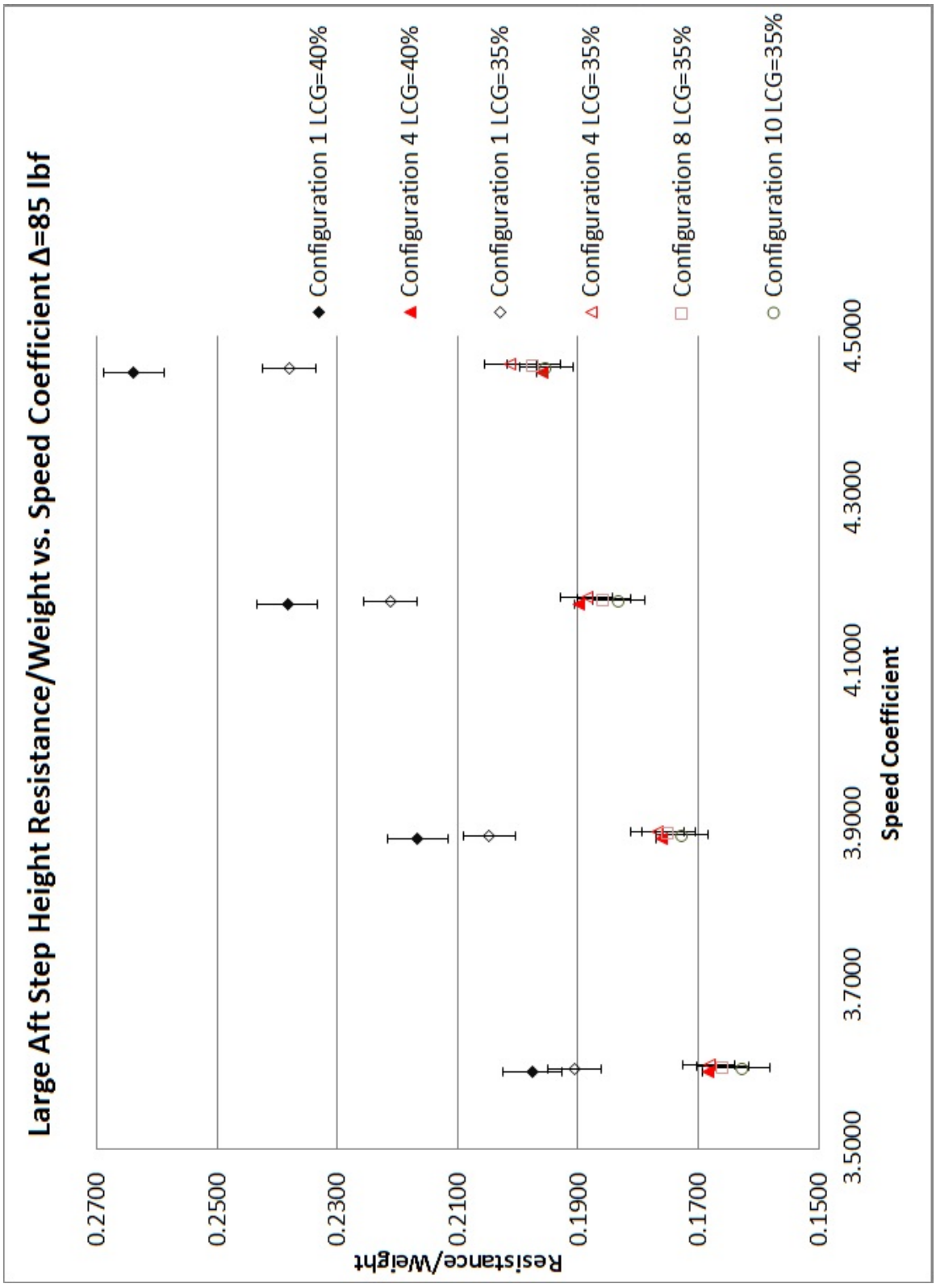

Figure 2.7: Large Aft Step Height Resistance/Weight vs. Speed Coefficient at Δ=85 lbf: Large step height aft had lowest Resistance/Weight of all the step configurations tested. The forward step height did not significantly effect the reduction in resistance

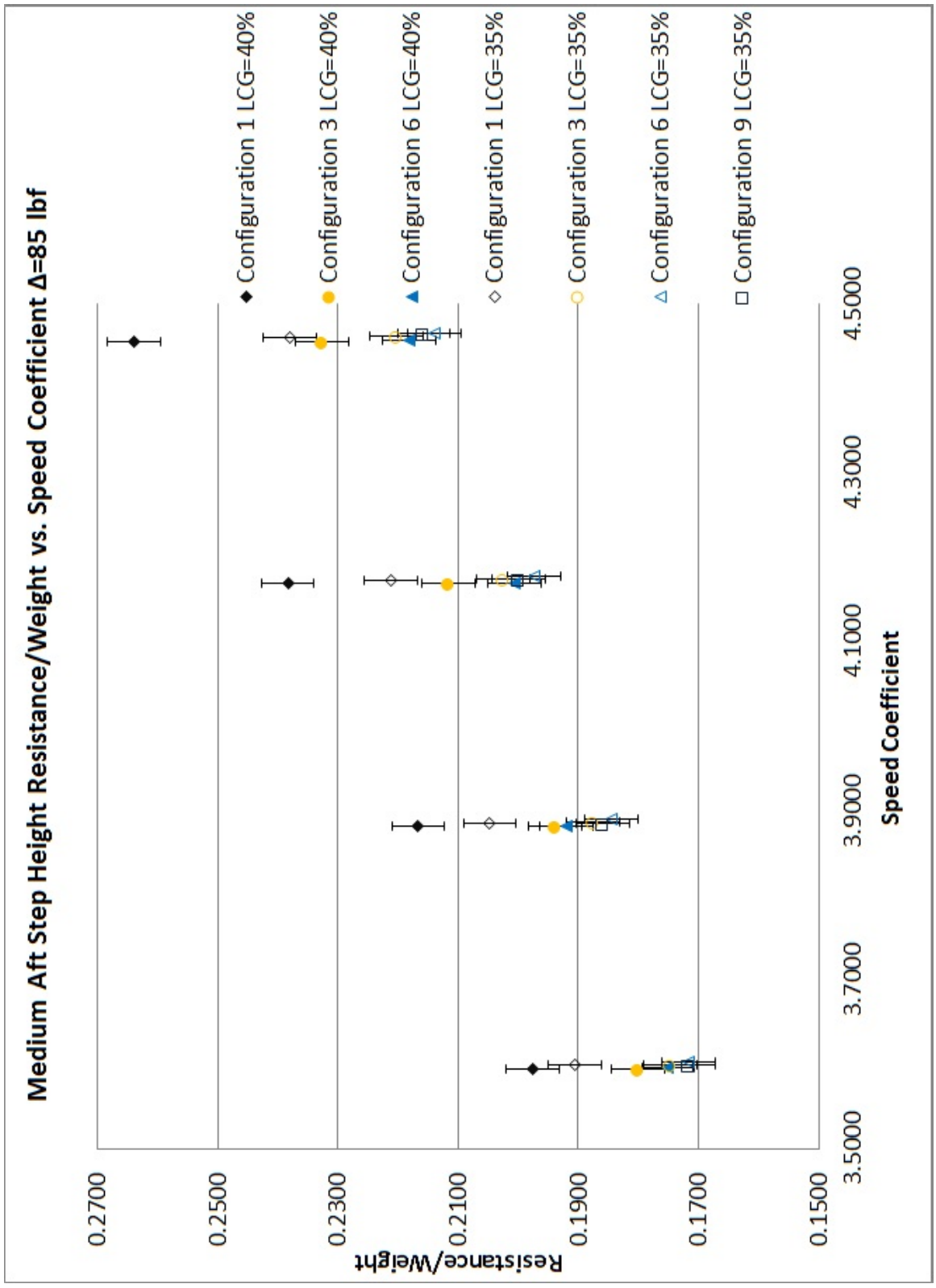

Figure 2.8: Medium Aft Step Height Resistance/Weight vs. Speed Coefficient at Δ=85 lbf: For the middle aft step height, configuration 3 with the small forward step height had most resistance at both LCG locations

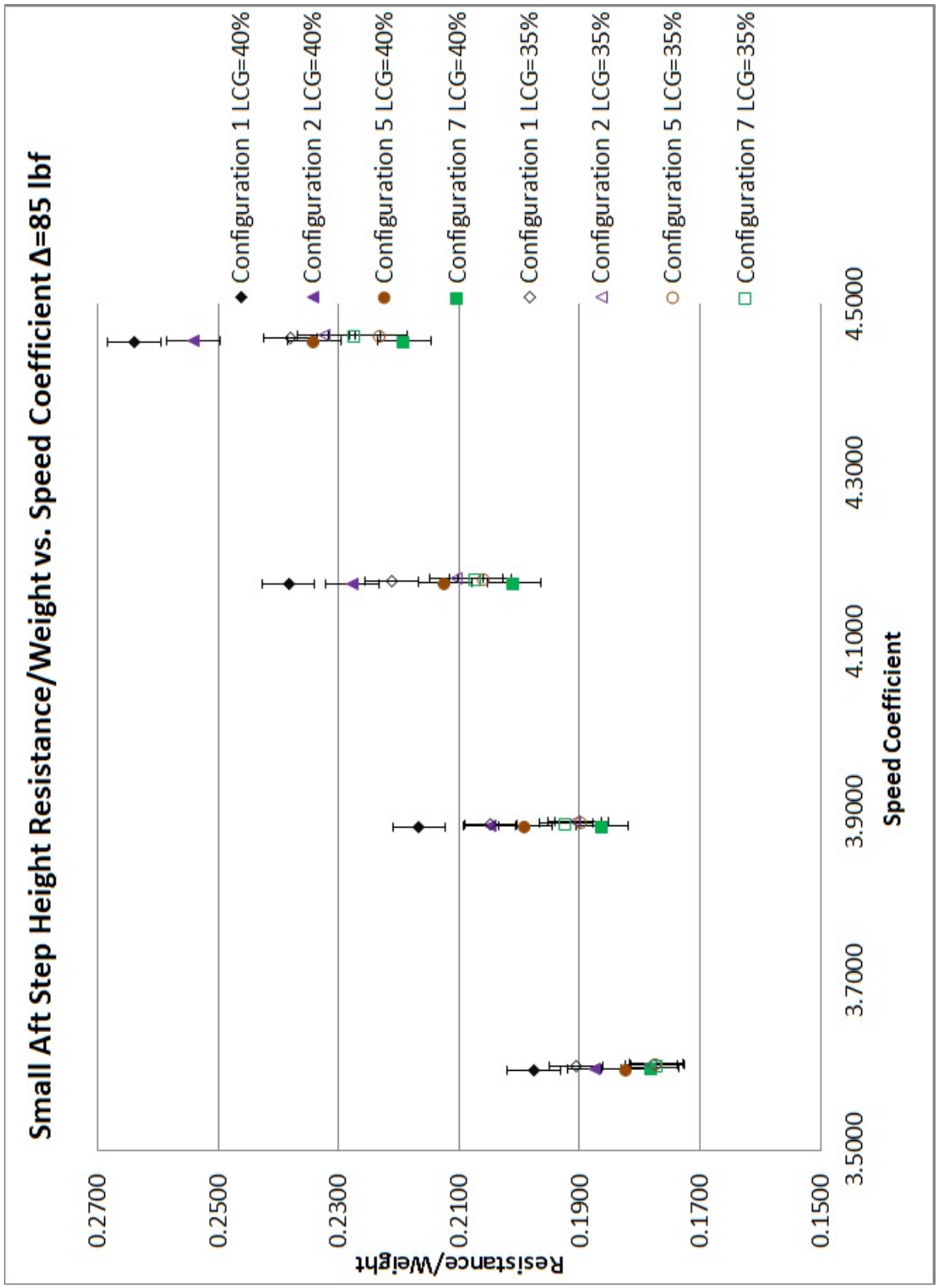

Figure 2.9: Small Aft Step Height Resistance/Weight vs. Speed Coefficient at Δ=85 lbf: For the small aft step height, configuration 2 with the small forward step height forward had most resistance at both LCG locations

2.9.2 Wetted Surface Area

The plots for the 85 lbf displacement are presented here (Figures 2.10-2.12) while the plots for the other displacements can be found in Appendix B. The plots are grouped similarly to the plots for resistance for clarity. Configuration 10 with the large step height aft and forward as well as configuration 8 with the large step height aft and medium step height forward had the least wetted surface area of all the configurations. Having the largest step height for both the forward and aft steps, it would make sense that Configuration 10 would have the least wetted surface area because the large step heights would create large separated zones. These two configurations also had the least resistance of all the configurations tested. The aft step height had a stronger effect on the wetted surface area than the forward step height. When comparing the wetted surface area results to the resistance results, there is a strong correlation between the reduction in wetted surface area and the reduction in resistance. The friction resistance is a large component of the overall resistance of planing hulls at high speeds. Theory states that the friction resistance is proportional to the wetted surface area. Therefore, the reduction in wetted surface area would cause a reduction in resistance. For all the step configurations, the aft LCG location had lower wetted surface area than the forward LCG location. For the aft LCG location, the forward step height had less influence on the wetted surface area than the forward LCG location. Similar trends were seen at the two other displacements.

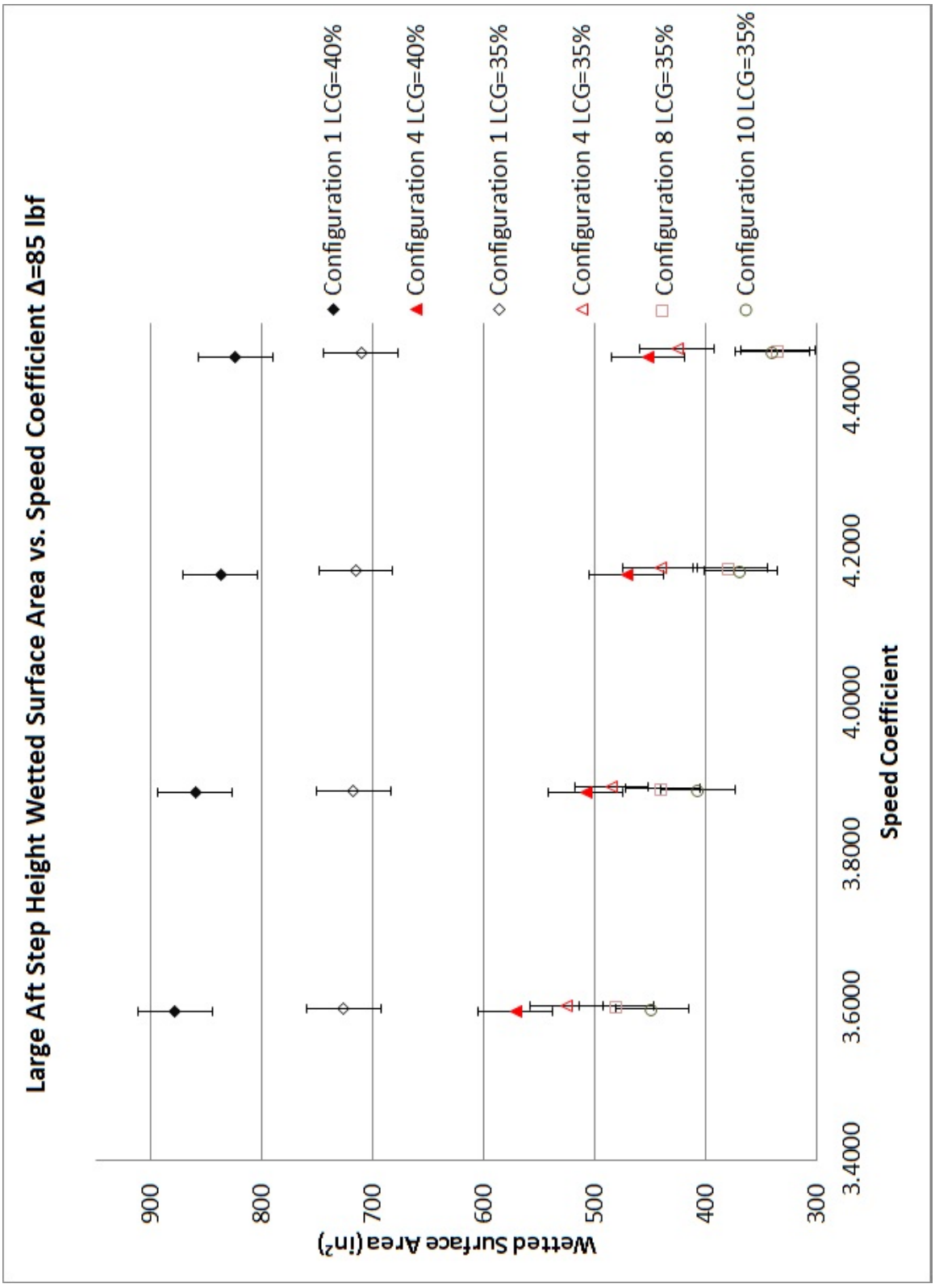

Figure 2.10: Large Aft Step Height Wetted Surface Area vs. Speed Coefficient at Δ=85 lbf: Aft LCG location had lower wetted surface are than forward LCG location. Configuration 10 with large step height aft and forward as well as configuration 8 with large step height aft and medium step height forward had the least wetted surface area of all configurations.

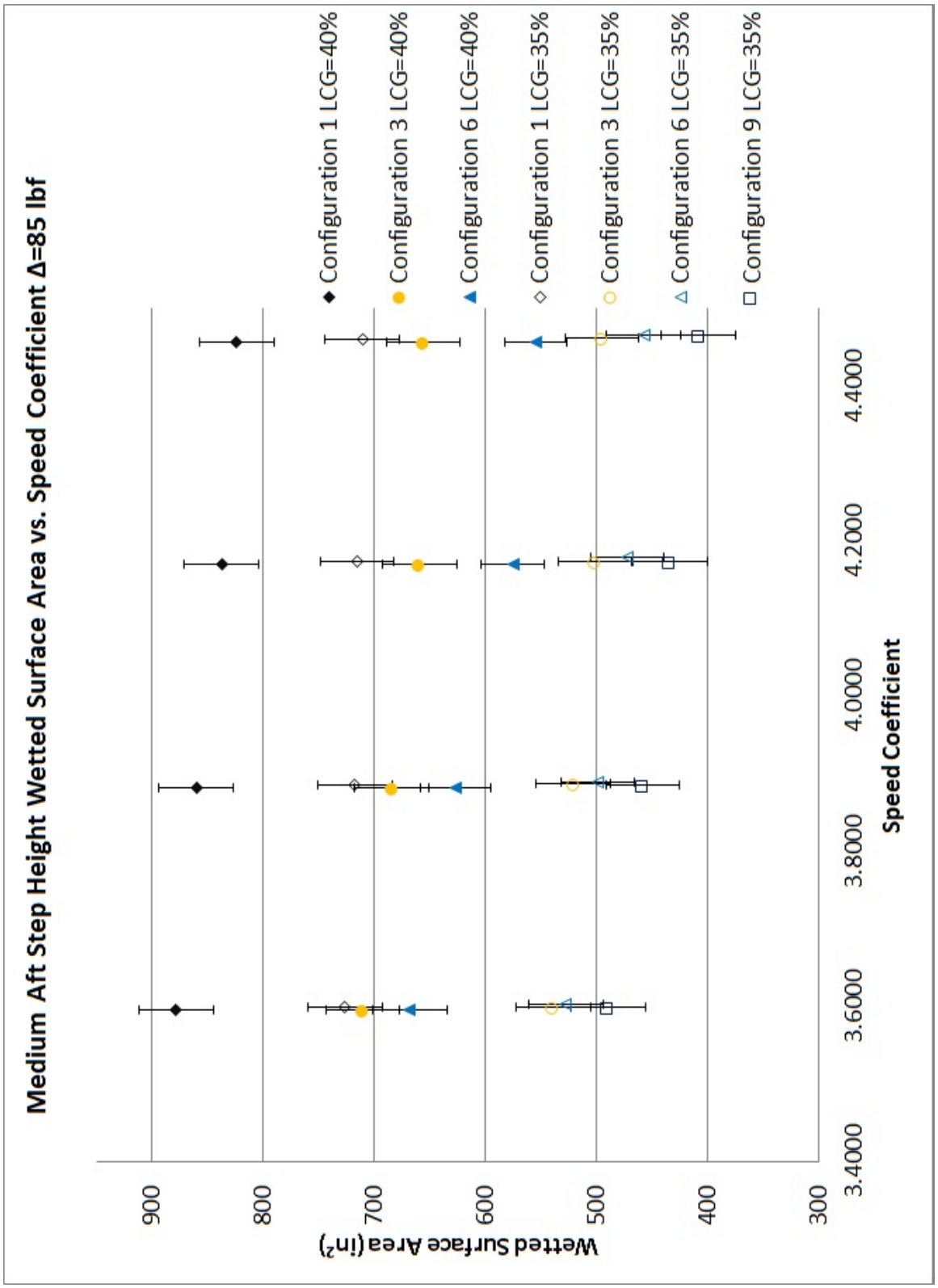

Figure 2.11: Medium Aft Step Height Wetted Surface Area vs. Speed Coefficient at Δ=85 lbf: Aft LCG location had lower wetted surface are than forward LCG location. Configuration 9 with large step height forward and medium step height aft had about same wetted surface area as configuration 4 with large step height aft and small step height forward.

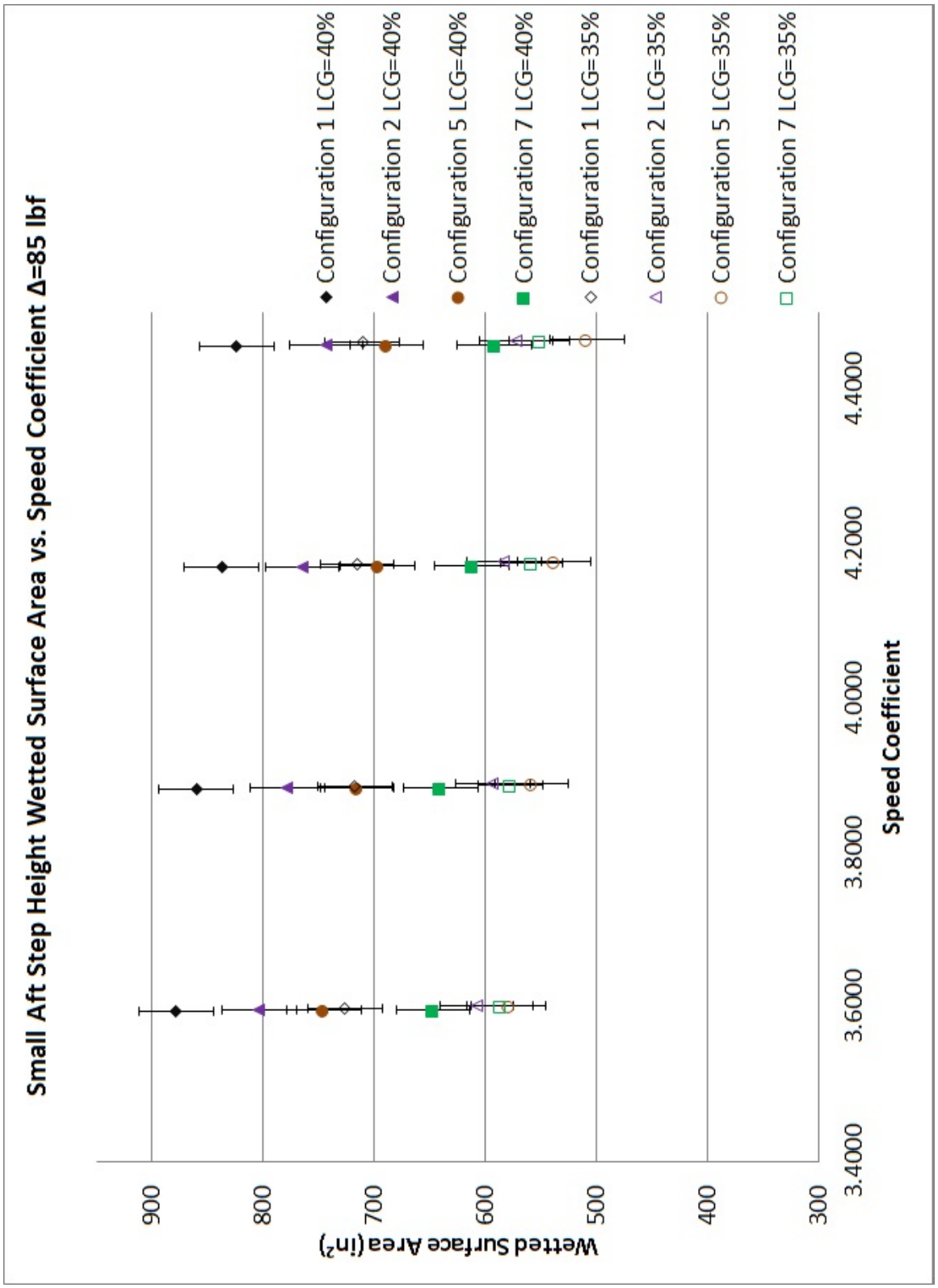

Figure 2.12: Small Aft Step Height Wetted Surface Area vs. Speed Coefficient at Δ=85 lbf: Aft LCG location had lower wetted surface are than forward LCG location.

2.9.3 Trim

The plots for the 85 lbf displacement are presented here (Figures 2.13-2.15) while the plots for the other displacements can be found in Appendix B. The plots are grouped similarly to the plots for resistance for clarity. The aft LCG location decreased more rapidly with increasing speed than the forward LCG location. The aft LCG location had about the same or higher trim at the low speed and had less or about the same trim than the forward LCG location at the higher speeds. Configurations 4, 8 and 10, with the largest step height aft, had the largest trim angles of the configurations tested. The medium and small aft step height configurations had trim angles similar to the unstepped hull. Theory states that the form resistance for unstepped hulls is proportional to the tangent of the trim angle. Assuming that this theory is the same for stepped planing hulls, the similar trim angles between the medium and small aft step height configurations and the unstepped hull would show that the form resistance between these configurations are similar. Referring to Figures 2.10-2.12, the wetted surface area of the stepped configurations are significantly less than the unstepped hull and as a result, the friction resistance of the stepped configurations are less than the unstepped hull. Therefore, the results show that the primary cause for stepped configurations to have less resistance than the unstepped hull is the reduction in wetted surface area and friction resistance. Similar trends were seen at the two other displacements.

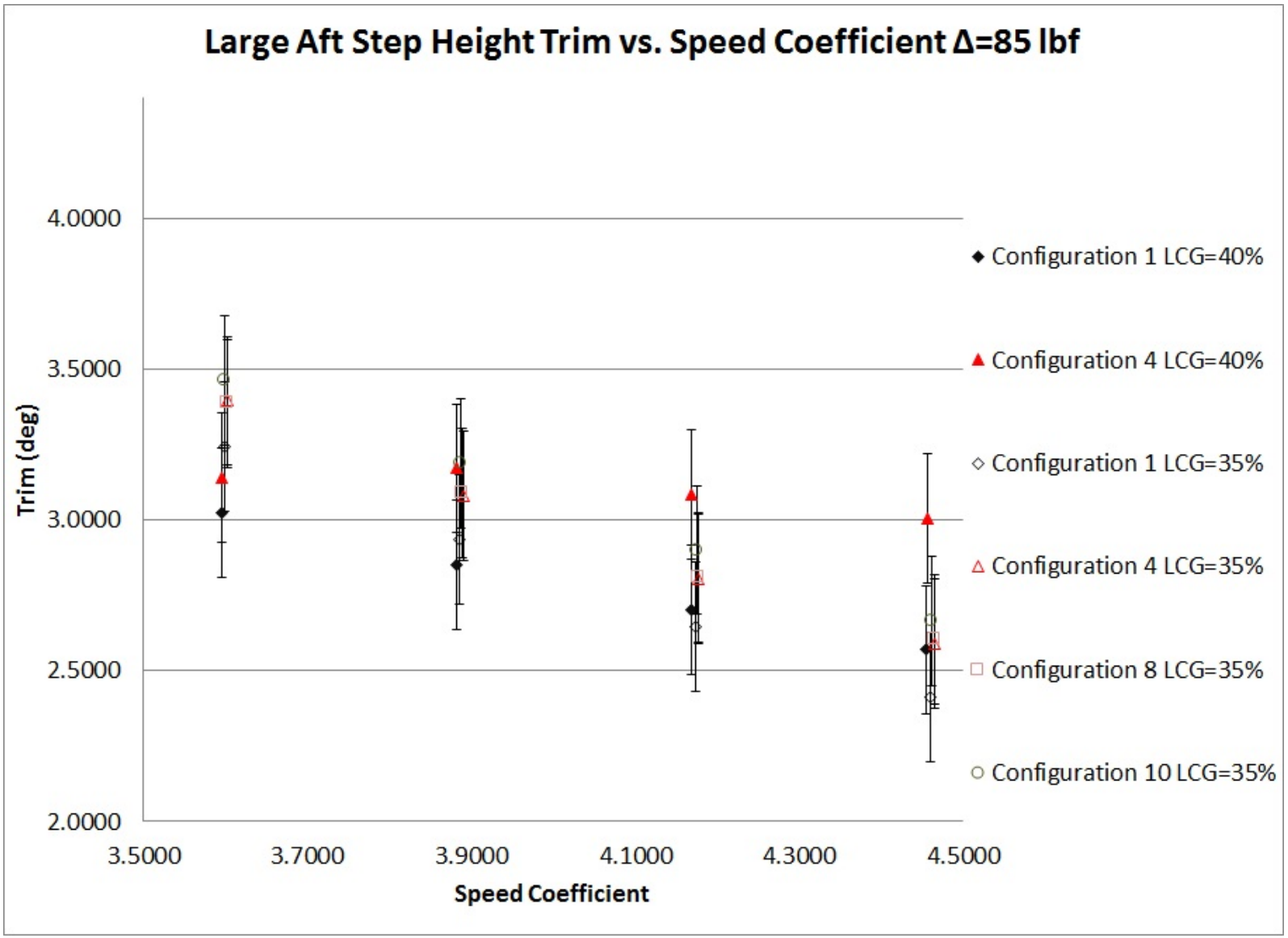

Figure 2.13: Large Aft Step Height Trim vs. Speed Coefficient at Δ=85 lbf: Aft LCG location has slightly higher trim than the forward LCG location at low speeds and about the same trim at the higher speeds

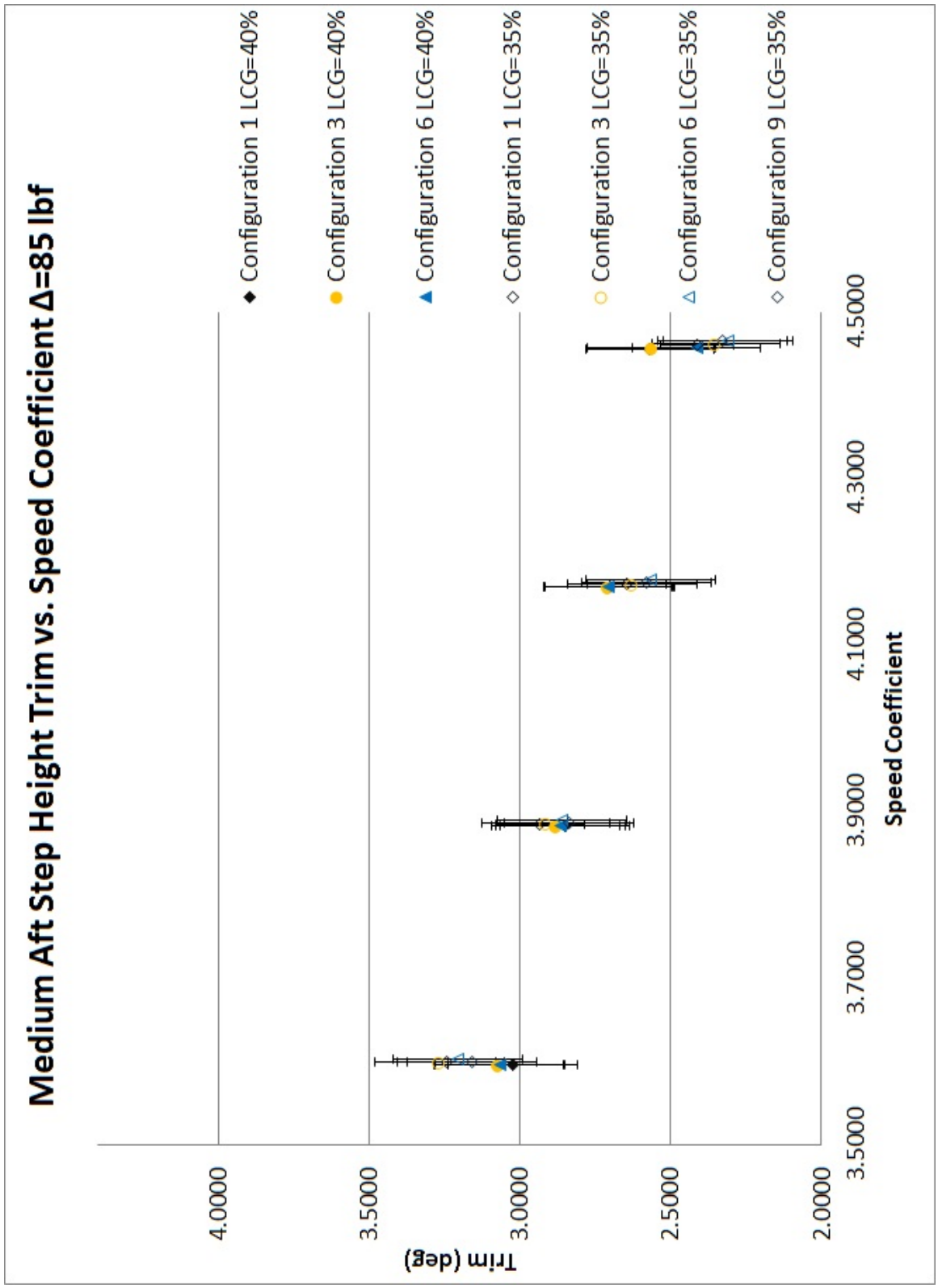

Figure 2.14: Medium Aft Step Height Trim vs. Speed Coefficient at Δ=85 lbf: Aft LCG location has slightly higher trim than the forward LCG location at low speeds and about the same trim at the higher speeds

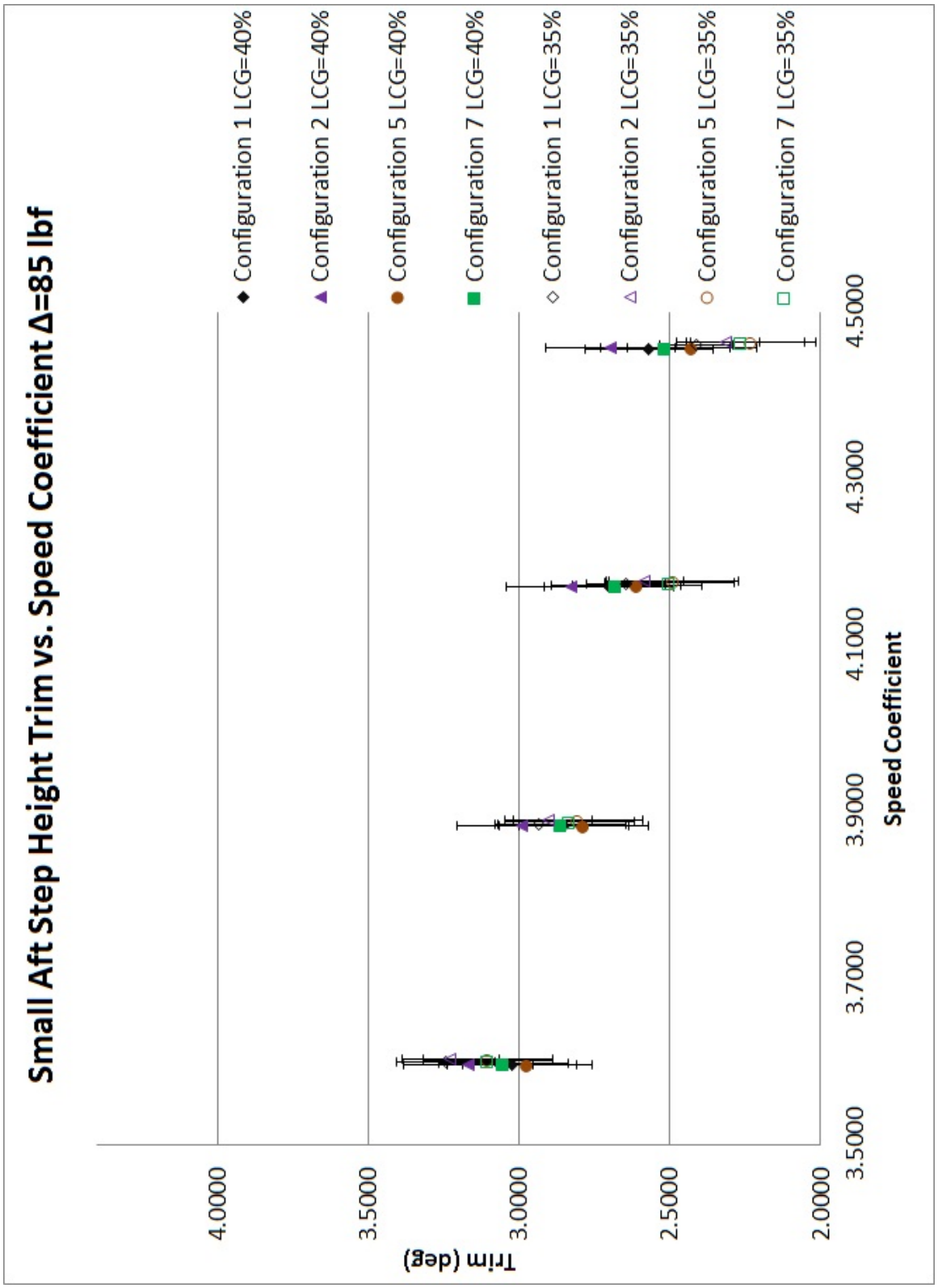

Figure 2.15: Small Aft Step Height Trim vs. Speed Coefficient at Δ=85 lbf: Aft LCG location has about the same trim as the forward LCG location

2.9.4 Heave

The plots for the 85 lbf displacement are presented here (Figures 2.16-2.18) while the plots for the other displacements can be found in Appendix B. The plots are grouped similarly to the plots for resistance for clarity. The heave presented here is the change in the vertical position of the center of gravity between the static and running condition. For all the step configurations, the aft LCG location had higher heave from the static condition than the forward LCG location. The difference in the heave between the stepped and unstepped hull was insignificant. The higher heave, and lower trim angles show that the hull was riding flatter and higher out of the water at the aft LCG location. This in turn correlates to the reduction in wetted surface area and resistance that was seen in the experiment. Similar trends were seen at the two other displacements.

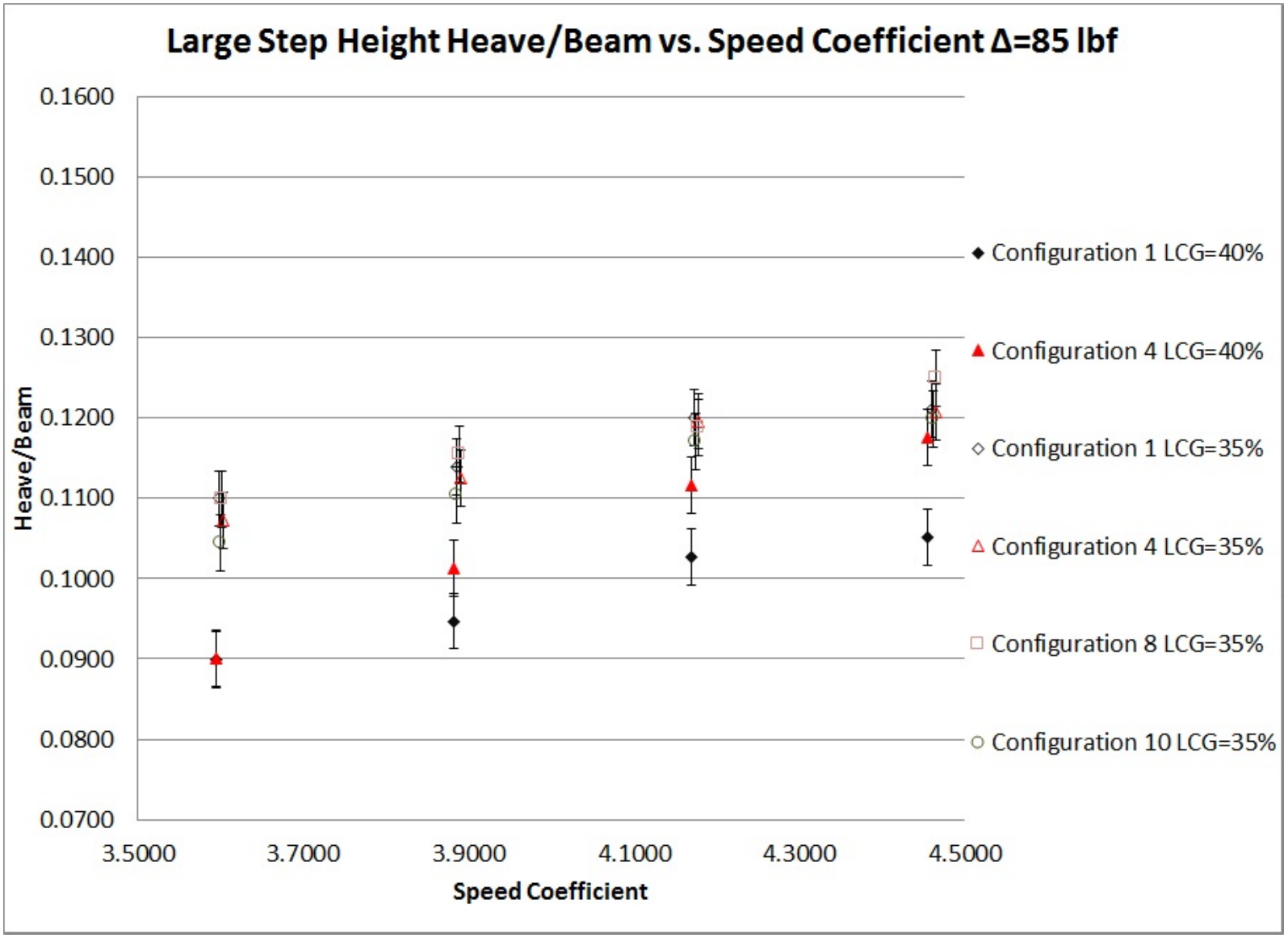

Figure 2.16: Large Aft Step Height Heave/Beam vs. Speed Coefficient at Δ=85 lbf: Aft LCG location had higher heave from the static condition than the forward LCG location

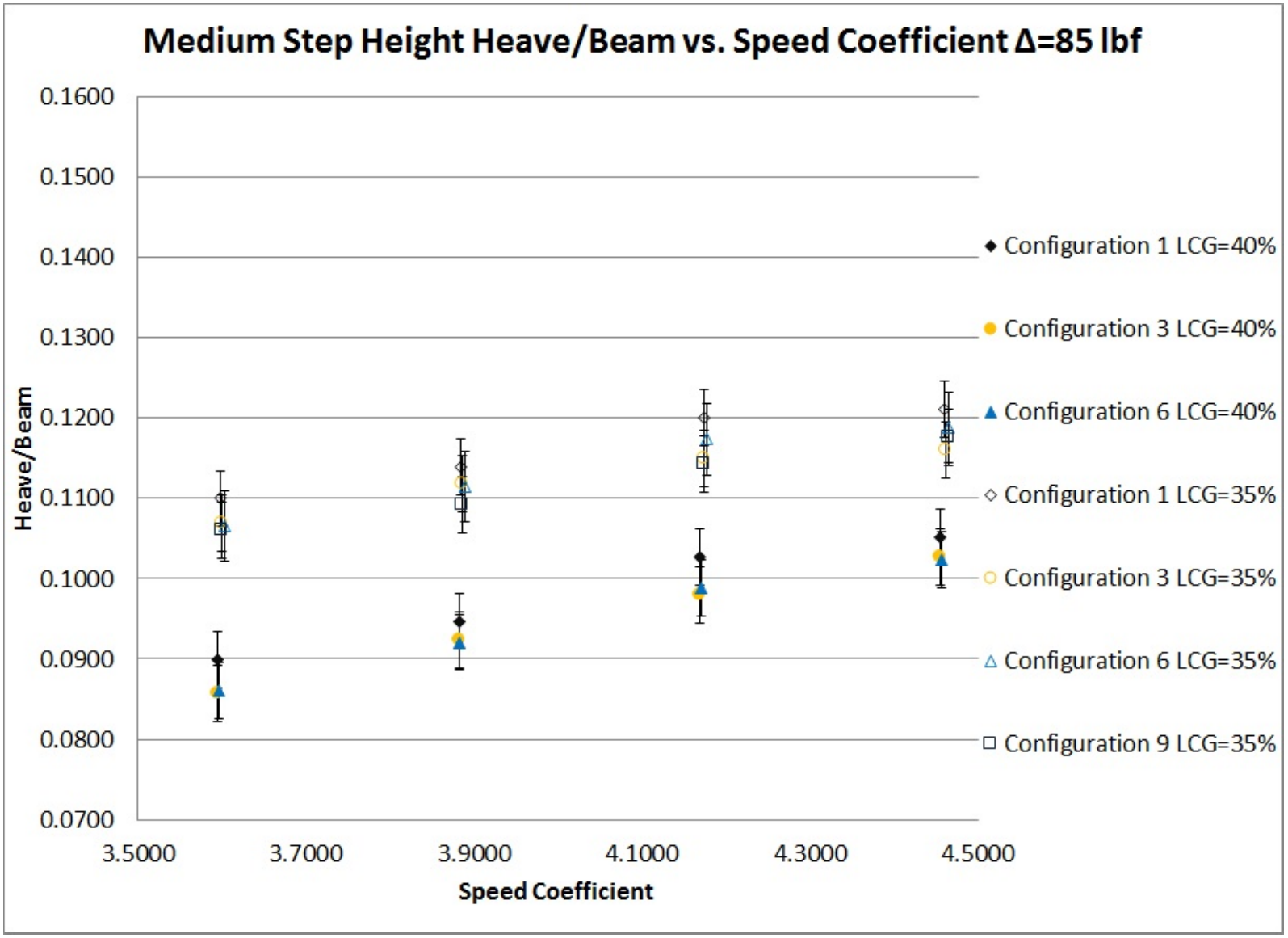

Figure 2.17: Medium Aft Step Height Heave/Beam vs. Speed Coefficient at Δ=85 lbf: Aft LCG location had higher heave from the static condition than the forward LCG location

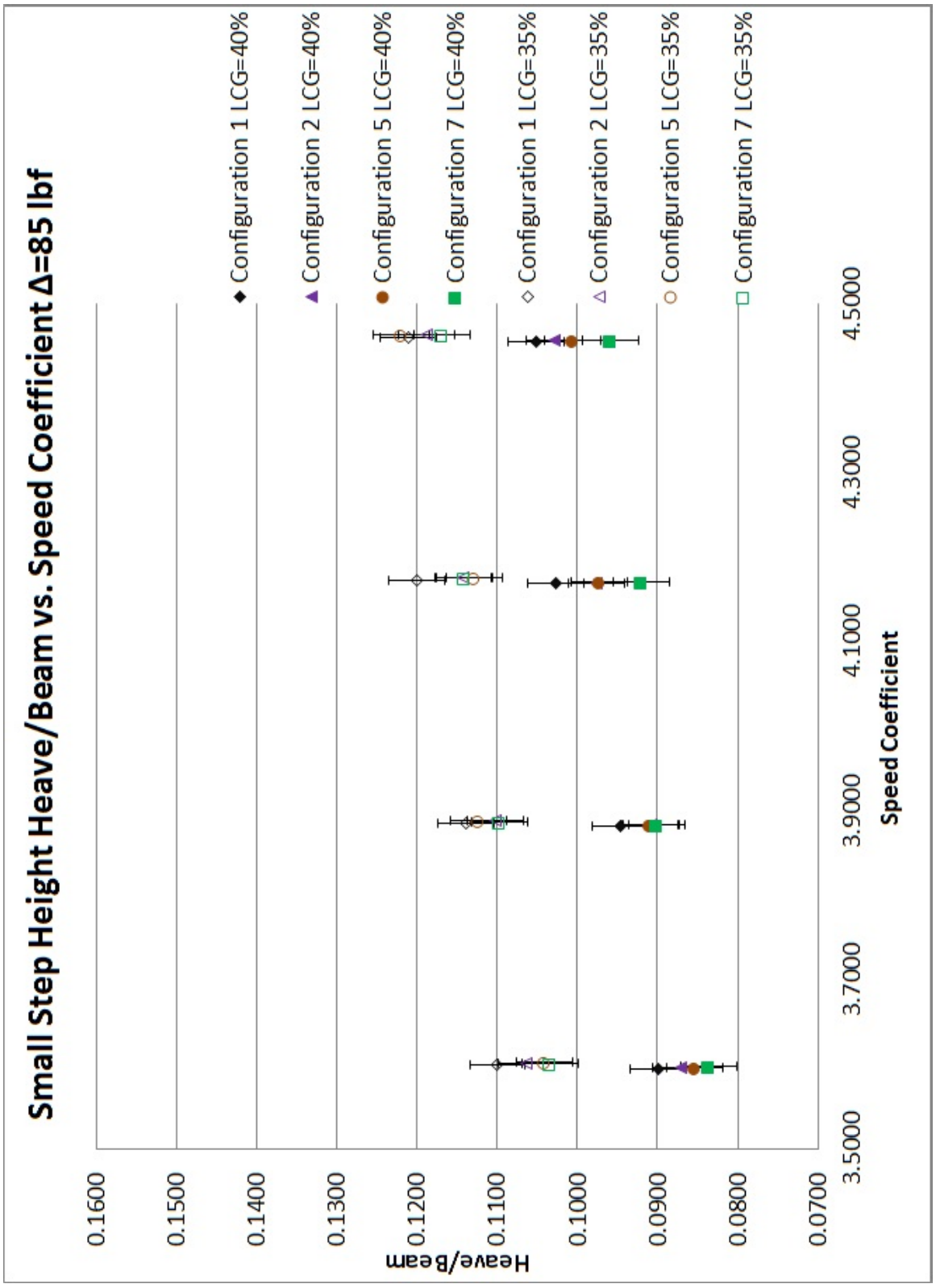

Figure 2.18: Small Aft Step Height Heave/Beam vs. Speed Coefficient Δ=85 lbf: Aft LCG location had higher heave from the static condition than the forward LCG location

2.9.5 Effect of Displacement

One of the main focuses of this research is to determine the effects of changes in displacement on the calm water performance of a stepped planing hull. The plots for the resistance/weight vs. displacement at C_v=4.46 are presented here (Figures 2.19-2.21) while the plots for the other speeds and other parameters can be found in Appendix B. The plots are grouped similarly to the plots for resistance for clarity. Whereas in the previous plots, the focus was the comparison between the unstepped hull and the stepped hull, the main focus of these sets of plots is the slope of the data. Some naval architects think that the stepped planing hull is designed for a specific design condition and when the stepped planing hull becomes heavier, the performance is poor. Configuration 1, the unstepped hull, shows a decrease in the resistance/weight as the displacement increases. All the step configurations show this decrease as well. The slope of this decrease is similar between the stepped hull and unstepped hull. This shows that changes in displacement effect the performance of a stepped hull the same as an unstepped hull. The result is contrary to the current understanding of many naval architects. The speeds tested were all in the planing regime and at all displacements the step was always ventilated. Increasing the displacement did not increase the bottom loading enough to eliminate the separated flow at the step. Similar trends were seen at the other speeds and for the other parameters.

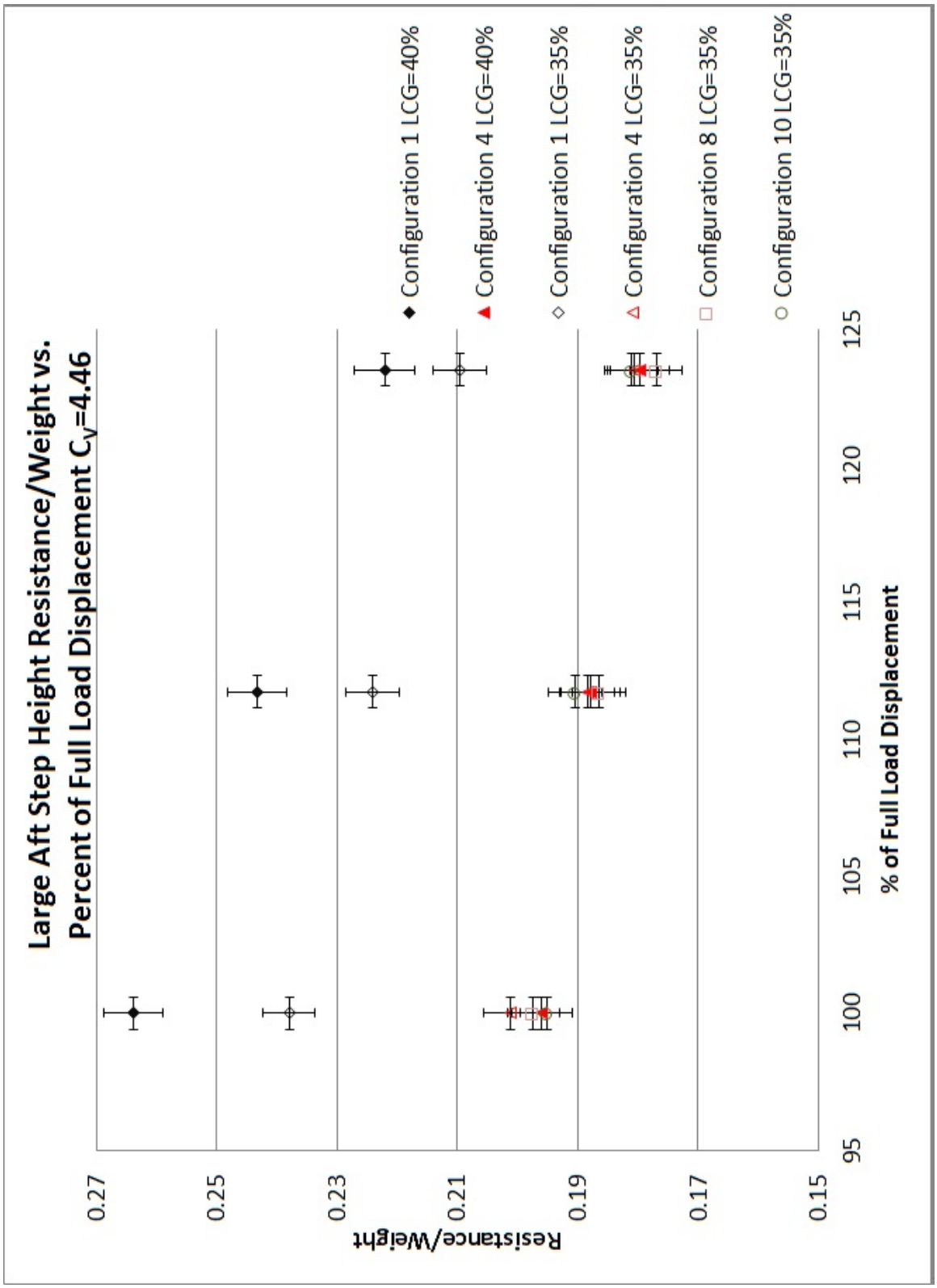

Figure 2.19: Large Aft Step Height Resistance/Weight vs.Percent of Full Load Displacement at C_v=4.46: The change in Resistance/Weight as displacement increases is similar for the unstepped and stepped configurations

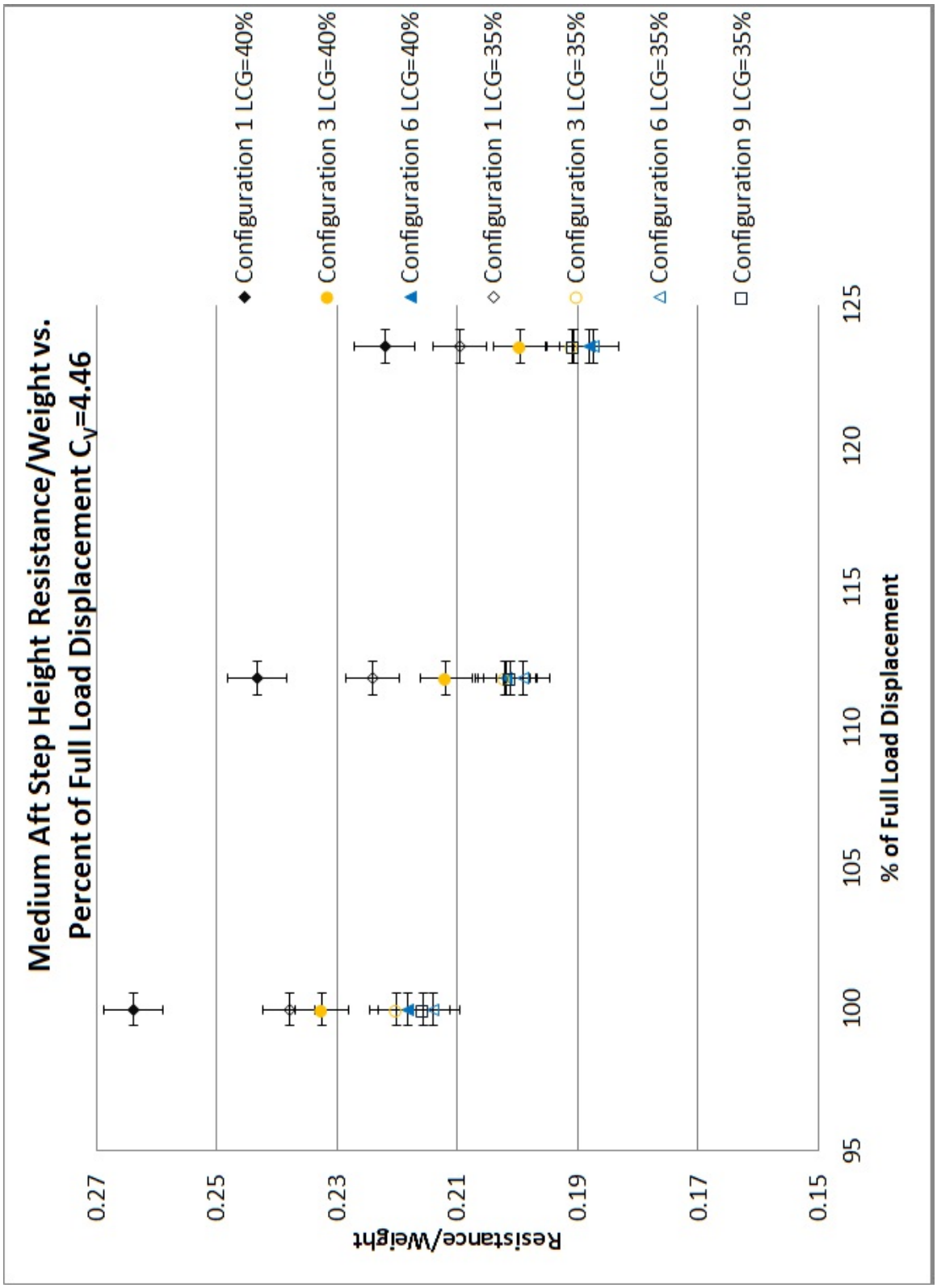

Figure 2.20: Medium Aft Step Height Resistance/Weight vs.Percent of Full Load Displacement at C_v=4.46 : The change in Resistance/Weight as displacement increases is similar for the unstepped and stepped configurations

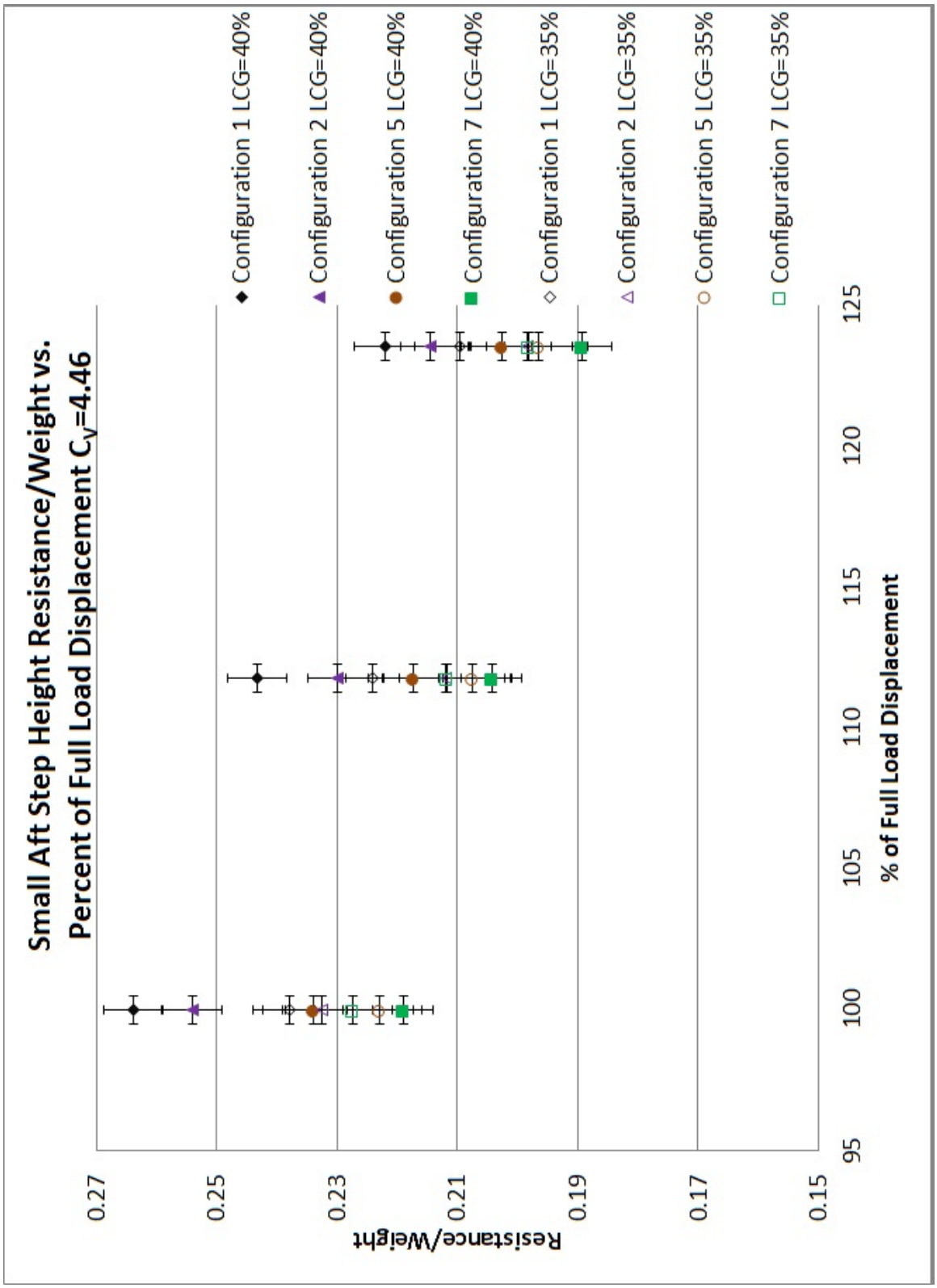

Figure 2.21: Small Aft Step Height Resistance/Weight vs.Percent of Full Load Displacement at C_v=4.46 : The change in Resistance/Weight as displacement increases is similar for all the unstepped and stepped configurations

2.9.6 Effect of LCG

Another of the main focuses of this research is to determine the effects of changes in LCG on the calm water performance of a stepped planing hull. Some naval architects think that the stepped planing hull is designed for a specific design condition and when the stepped planing hull has a shift in LCG, the performance is poor. The plots of the resistance/weight vs the LCG for the first seven step configurations at a displacement of 85 lbf are presented here (Figures 2.22-2.25) while the plots for the other displacements and other parameters can be found in Appendix B. The resistance for the unstepped planing hull, which is at the top with the highest resistance, decreases as the LCG moves further aft. All the step configurations except configuration 4 and 7 follow this trend. For configuration 4, with the large step height aft and the small step height forward, these changes are small and fall within the experimental error. Configuration 7, with the large step height forward and the small step height aft, shows a trend that is opposite of the unstepped hull. The forward LCG location had larger resistance than the forward LCG location. This change in effect of LCG on resistance may be due to the large step height since configurations 4 and 7 were the only two configurations tested at both LCG locations with a large step height.

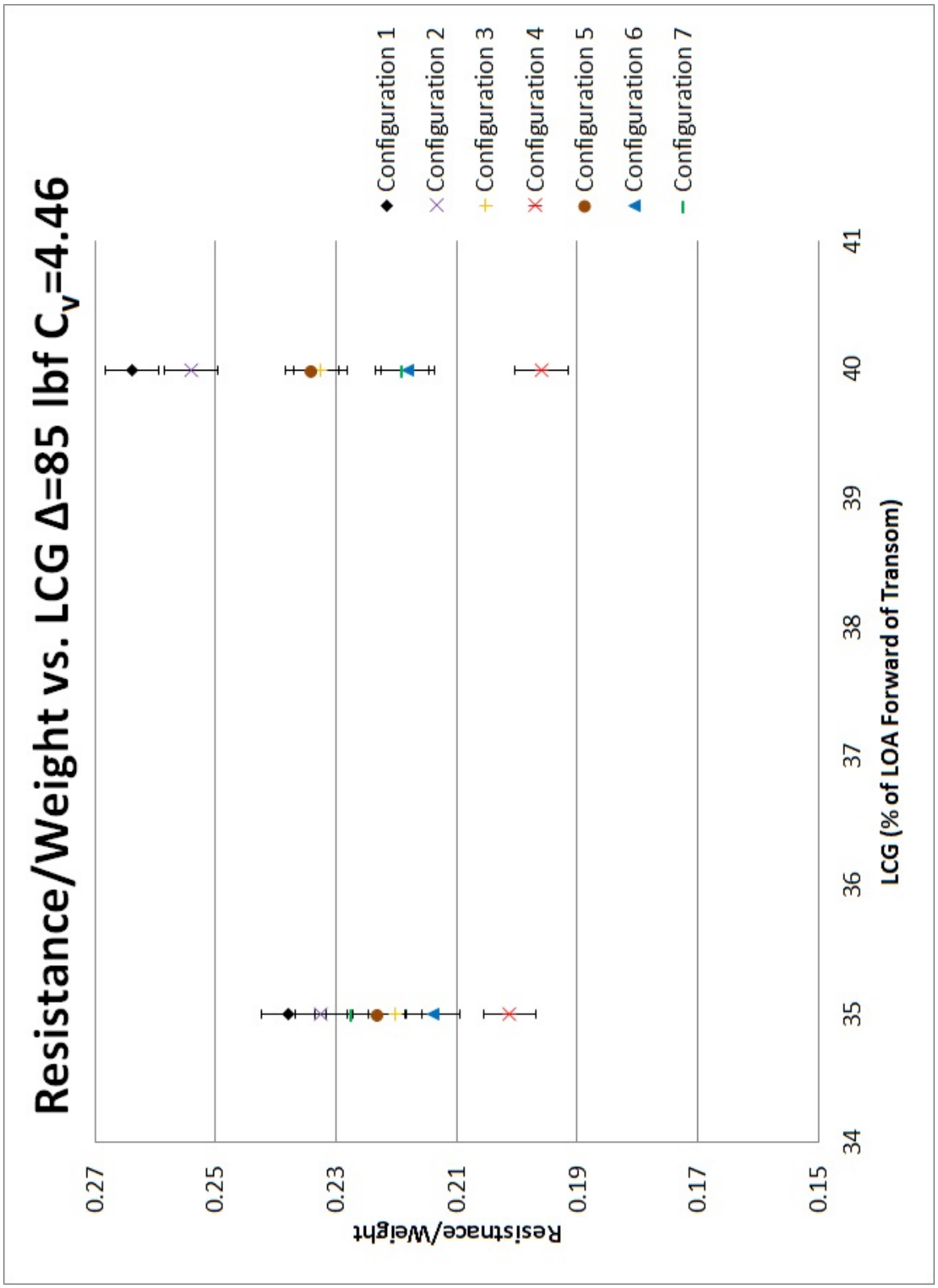

Figure 2.22: Resistance/Weight vs. Longitudinal Center of Gravity at Δ=85 lbf C_v=4.46: Configuration 4 and 7 only configurations that do not have the same change in Resistance/Weight as LCG changes

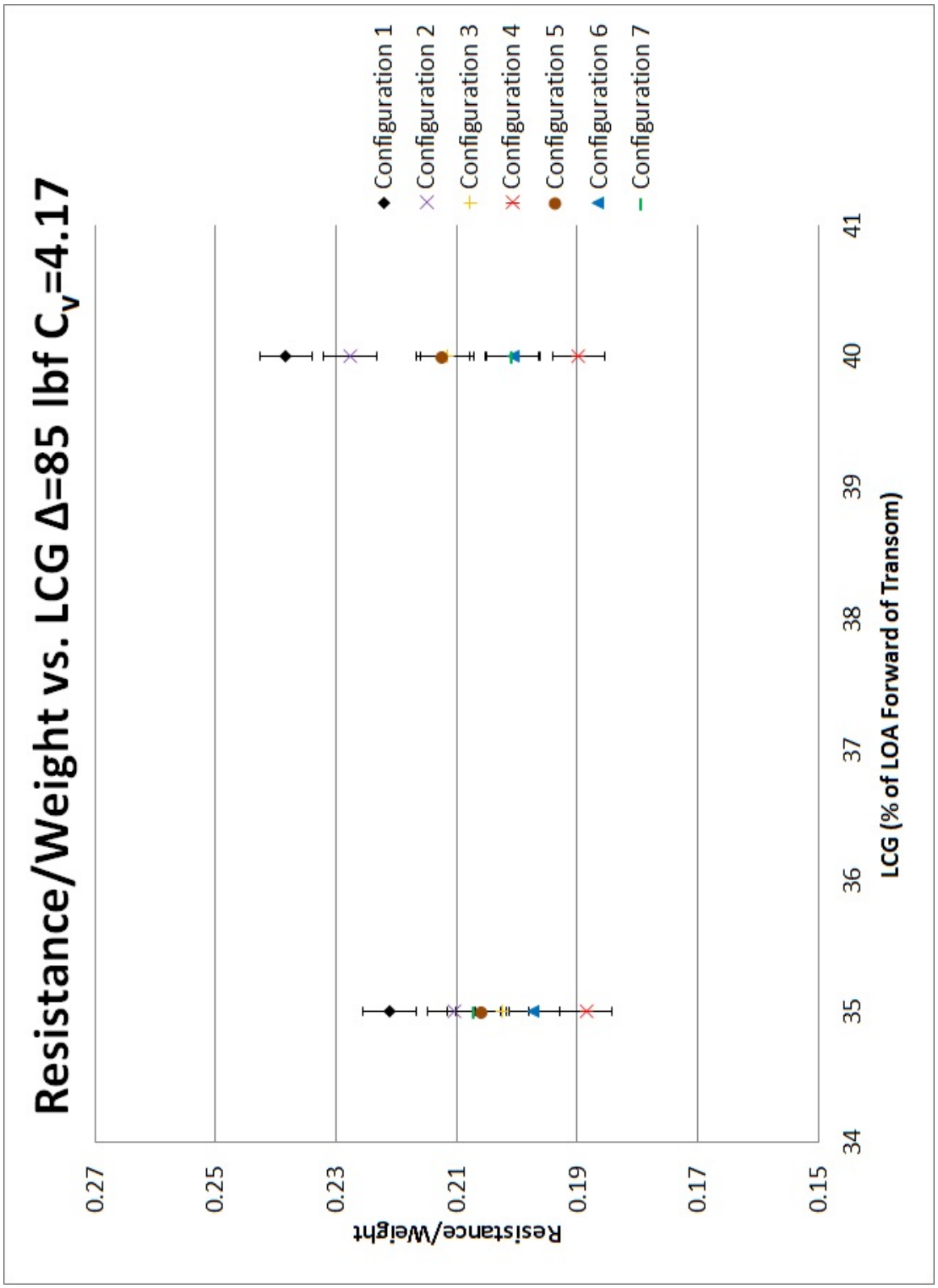

Figure 2.23: Resistance/Weight vs. Longitudinal Center of Gravity at Δ=85 lbf C_v=4.17: Configuration 7 only configuration that does not have the same change in Resistance/Weight as LCG changes

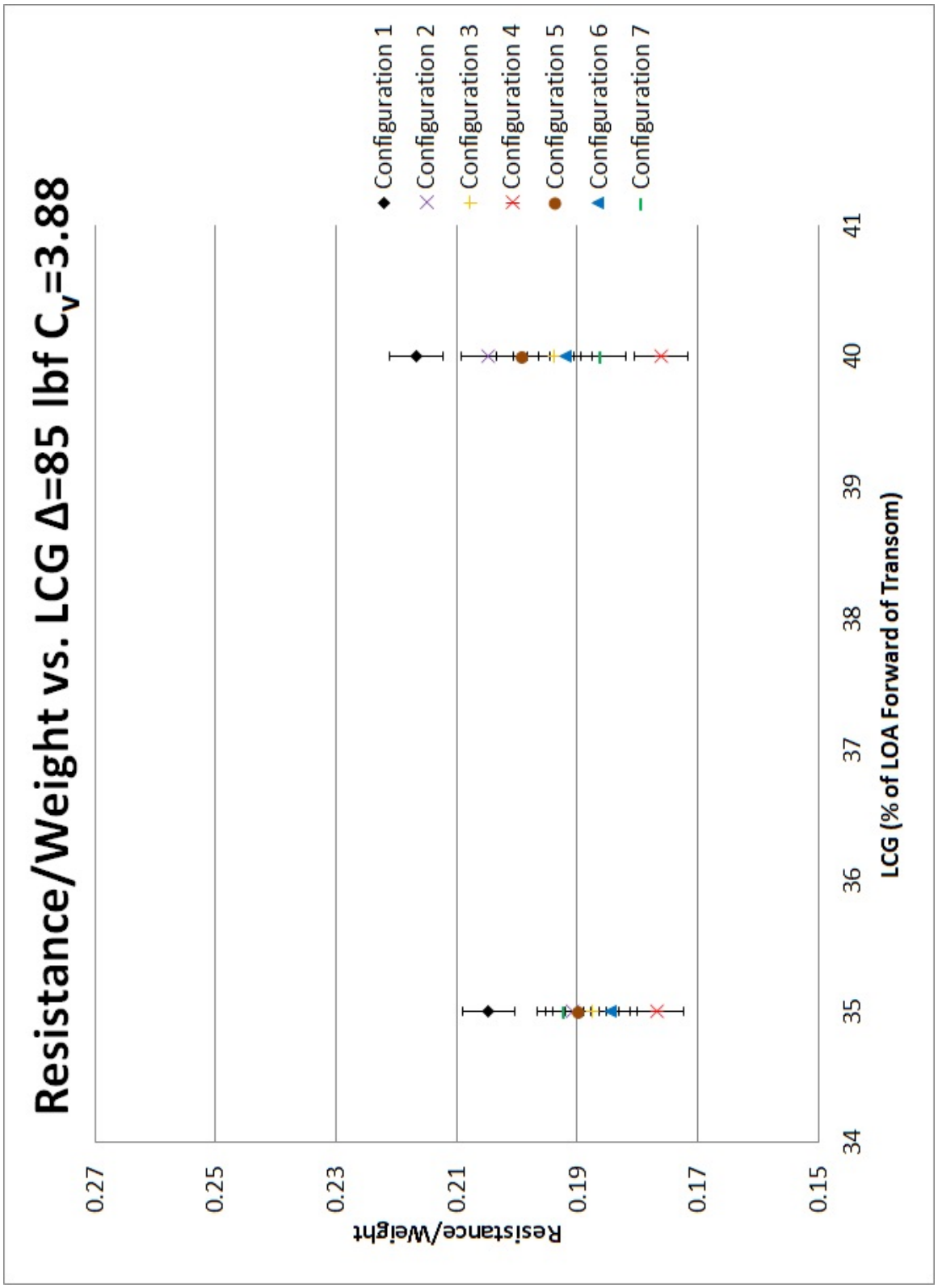

Figure 2.24: Resistance/Weight vs. Longitudinal Center of Gravity at Δ=85 lbf C_v=3.88: Configuration 4 and 7 only configurations that do not have the same change in Resistance/Weight as LCG changes

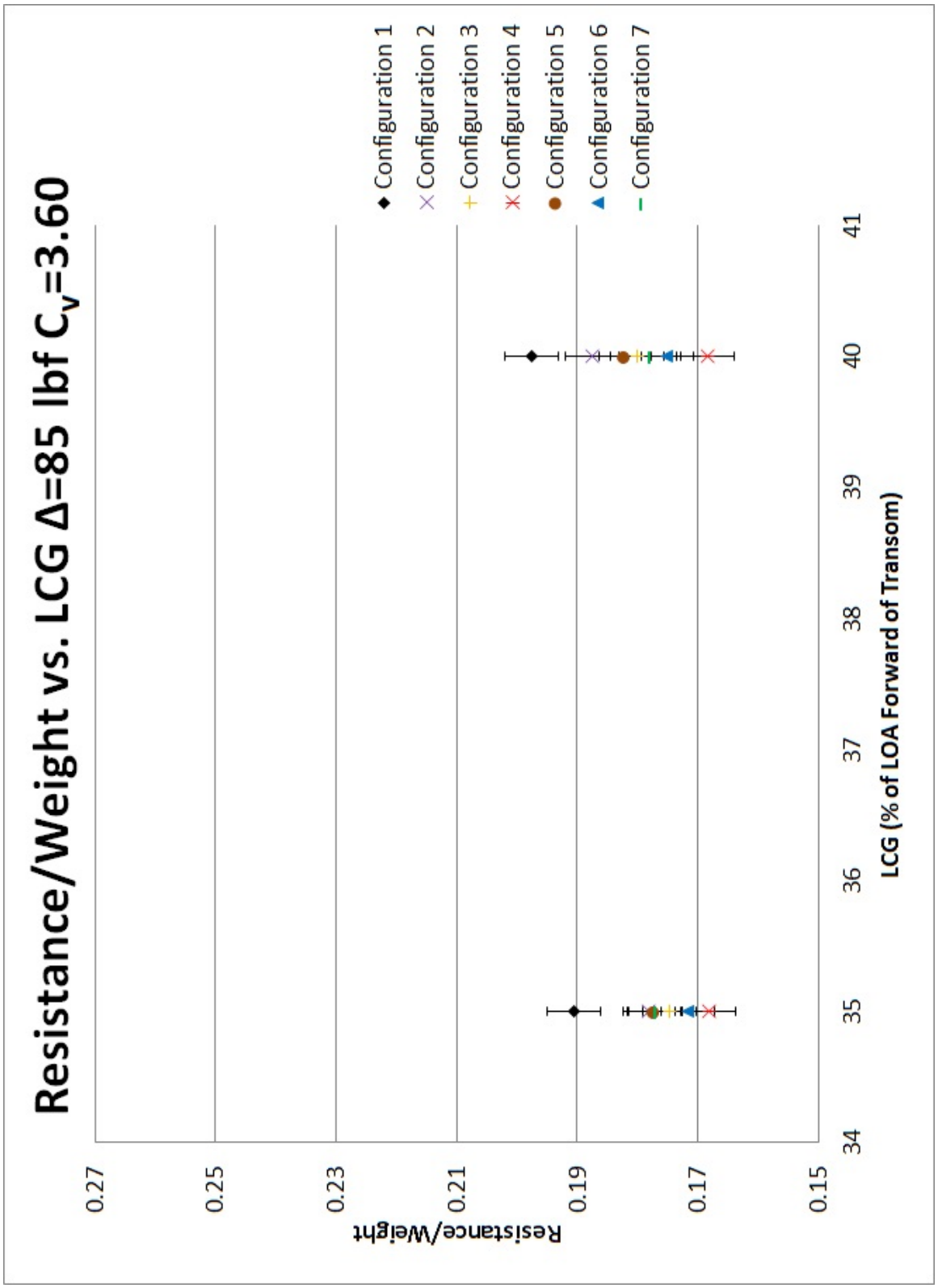

Figure 2.25: Resistance/Weight vs. Longitudinal Center of Gravity at Δ=85 lbf C_v=3.60: Configuration 4 and 7 only configurations that do not have the same change in Resistance/Weight as LCG changes

Figure 2.26 is a plot of the trim angle vs. the LCG for the first seven step configurations at a displacement of 85 lbf and C_V=4.46. The data is presented in the same fashion as for the resistance/weight. For the unstepped configuration and all of the stepped configurations, the trim angle decreased as the LCG moved further aft. This opposite of theory and trends of other ustepped hulls, such as Series 62. All of the sensors were reaclibrated and check to ensure that this change in trim angle was not caused by experimental error. The Test personnel at the USNA noted that the NSWC15, parent hull to the NSWC15E, had a dynamic trim instability where it was stable in either a bow up or a bow down condition. The hull could be in a bow up condition and if a downward force was applied on the bow, it would transition to the bow down condition. Underwater photography showed that in the forward LCG position, the bow section was clearly in the water. In the aft LCG position, the bow was further out of the water. The NSWC15E only extended the prismatic section of the NSWC15, so the bow on the NSWC15E was very bluff and is not typical of a modern stepped planing hull. The NSWC15 was selected as a parent model for its prismatic sections assuming that the bow would be out of the water, but at the trim angles and LCG locations tested, the bow did have an influence on the results.

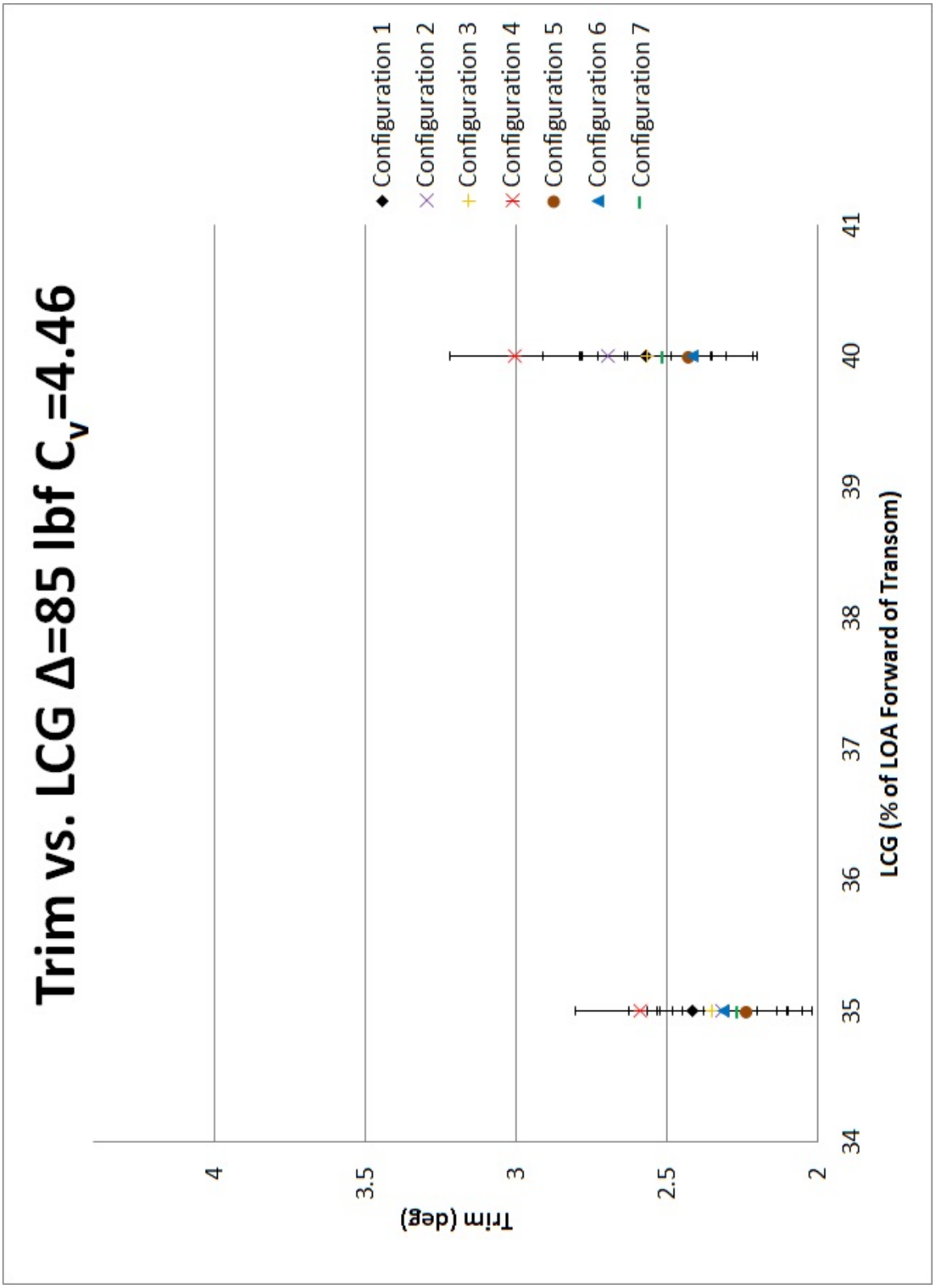

Figure 2.26: Trim vs. Longitudinal Center of Gravity at Δ=85 C_v=4.46: All of the configurations have the same change in trim angle as LCG changes

2.10 Discussion

All of the step configurations tested had less resistance than the unstepped hull. Since all of the step configurations showed lower resistance than the unstepped hull, the results of the model tests supports the conclusion that the stepped planing hull can reduce the resistance for a boat even if operated in a somewhat sub-optimal configuration. The results show that the stepped hull configurations had less wetted surface area than the unstepped hull. The reduction of the wetted surface area corresponds to a reduction in the friction resistance and thus the overall drag for the boat.

The stepped planing hull configurations tested have higher static trim angles than the unstepped hull, but the model test shows that they may have lower running trim angles than the unstepped hull. All of the stepped hull configurations have higher static trim angles compared to the unstepped hull because of the volume that is being removed by the steps in the stern area. On the other hand, the running trim angles for the step configurations were not necessarily higher than the unstepped hull like the static trim angle. Configurations 4, 8, and 10, with the large aft step height, had the highest running trim angles. Eugene Clement has predicted an optimum trim angle that causes the planing surface to have the least amount of resistance for a given deadrise angle and planing surface aspect ratio [26]. The optimum trim angle minimizes the two major components of planing craft resistance; friction and form. Friction resistance increases at lower trim angles due to the increased wetted surface area needed to support the hull. For a given displacement, the form resistance increases because the pressure force normal to the planing surface has a larger rearward component as the trim angle increases. As a general assumption the optimum trim angle is about 4° [26]. For all the conditions tested, the unstepped hull was running at below the optimum trim angle. Therefore the higher trim angles of the step configurations with the large step height aft have a more optimum trim angle.

Configurations 4, 8, and 10, with the large aft step height, exhibited the least amount of resistance for the configurations tested. Referring back to Figures 2.7-2.9, configurations 4, 8, and 10, with the large aft step height, had the least amount of wetted surface area of all of the configurations. Figure 3.1. shows an underwater photograph of the planing surface for configuration 4 at a displacement of 85 lbf and a speed coefficient of 4.46. As seen in the photograph, the bubbles behind the aft step shows that configuration 4, with the large step aft, has most of the aft planing surface out of the water. The middle planing surface also benefited from the small step height at the forward step further reducing wetted surface area.

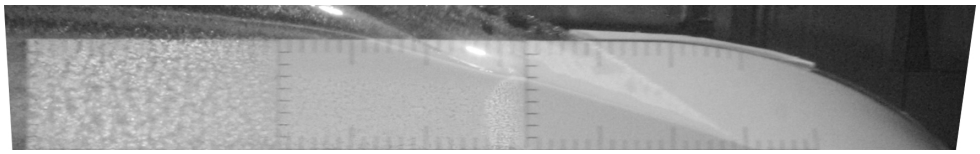

Figure 2.27: Underwater Photograph showing stagnation line for Configuration 4 Displacement=85 lbf Cv=4.46

Figures 2.13-2.15. show that the configurations with the large aft step height had a higher trim angle than all of the other configurations. It is hypothesized that the configurations with a large aft step height runs at a higher trim angle because the aft planing surface is out of the water and the hull can be effectively modeled as a shorter planing surface. Instead of a planing surface that is 80 inches long, it is functioning as though it is 60 inches long. The LCG relative to the planing surface has changed as well. Instead of an LCG 40% of the original length overall (32 inches) from the transom, the LCG is now 20% of the shorter length overall (12 inches) from the transom. Thus the configurations with the large aft step heights are running at a higher, more optimum, trim angle as predicted by Clement [26].

At the high speeds where the stepped planing hulls have less resistance than the unstepped hull, friction resistance is a large portion of the overall resistance. Therefore it has been shown that the reduction of wetted surface area is the main cause of the reduction in resistance in stepped planing hulls. Configuration 2, with the small step height both forward and aft has about the same trim angle as the unstepped hull so the form resistance for both step configurations are about the same. Even the small step heights created some separation and reduced the wetted surface area, reducing the friction resistance and the overall resistance.

The stepped hull was not significantly more or less sensitive to increased displacement or LCG. The results show that there is no significant difference in the sensitivity to displacement or LCG between a stepped hull and an unstepped hull. Therefore there are stepped hull configurations that can support changes in displacements in the same way as unstepped monohulls.

There was still a reduction in resistance of the stepped hull when the stagnation line crossed the step. As seen previously in Figure 3.1, the stagnation line from the forward planing surface crosses the step instead of the chine. Therefore, the forward planing surface is operating in a chines dry regime. The midbody now has the stagnation line crossing the chine. As a result, the first part of the middle planing surface is chines dry. This is also the region of separated flow aft of the step. It would be assumed that there is increased resistance because of the flow, but the increased resistance is not great enough so that the stepped planing hull has more resistance than the unstepped hull. The figure also shows that the flow reattaches near the chine closer to the step near the chine than in the middle of planing surface. This

can be seen on the aft planing surface near the chine. This would seem counter intuitive, but this reattachment may be caused by the spray generated from the stagnation line separating at the middle planing surface. With stepped planing hulls that have their step far forward, it can be assumed that the stagnation line will cross the step. These model tests have shown that the stagnation crossing has no significant detrimental effects to the performance of the stepped planing hull in calm water. For this planing condition, the fundamental physics is more complex as there is a stagnation line and flow separation occurring next to each other.

2.10.1 LCG

When changing the LCG location from the forward to aft position, it is generally expected that the trim angle should increase. At the high speeds, as seen in Figure 2.26, the trim angle was lower at the aft LCG location and higher at the forward LCG location. A prediction was made of the NSWC15E using Savitsky's planing prediction method and the model test results were compared to a similar Series 62 model. In both cases, it was predicted for the trim angle to be higher at the aft LCG location than the forward LCG location. The configuration 4 tests from the first year were re-run in year two and the results were within experimental error. The resistance, pitch and heave sensors are bench calibrated before being installed on the carriage and to determine if there was an error in the measurements, the calibrations were verified while the model was connected to the carriage as if ready for a run. The weight of the model was also verified on the carriage. The static measurements for trim and heave were verified again. Since the experimental setup has been verified, the cause for the NSWC15E not to follow theory is most likely due to hull form and hydrodynamics. Test personnel noted that the NSWC15 had a dynamic trim instability where it was stable in either a bow up or a bow down condition. The hull could be in a bow up condition and if a downward force was applied on the bow, it would transition to the bow down condition. Based on the underwater photography, in the forward LCG position, the bow section was clearly in the water. In the aft LCG position, the bow was further out of the water. Since the NSWC15 had a bluff bow and the NSWC15E only extended the prismatic section, the bow on the NSWC15E was very bluff and is not typical of a modern stepped planing hull. The NSWC15 was selected as a parent model for its prismatic sections assuming that the bow would be out of the water, but at the trim angles and LCG locations tested, the bow did have an influence on the results.

2.11 Recommendations for Future Work

Based on the model test, the following is a list recommendations for future work that will further improve the understanding of stepped planing hulls. 1. Use the NSWC15E and

conduct the same model test as the aft LCG location at an even further aft LCG location (30% of the LOA forward of the transom). This will give a better understanding of the effect of LCG on stepped planing hull performance.
2. Restrain the model in both trim and heave so that some fixed cases can be run for numerical validation as it is easier to simulate fixed cases than free cases because mesh motion is not needed.
3. Build a prismatic bow section for the NSWC15E model to determine if the bow section is causing the model test results to differ from theory.

Chapter 3

Prediction Method

3.1 Background

Two observations can be drawn from the model tests in Chapter 2. These observations have not been implemented in stepped planing hull prediction methods. Figure 3.1 is an underwater photograph from the model tests discussed in Chapter 2 of configuration 4 at 85 lbf displacement showing the wetted surface area of the hull.

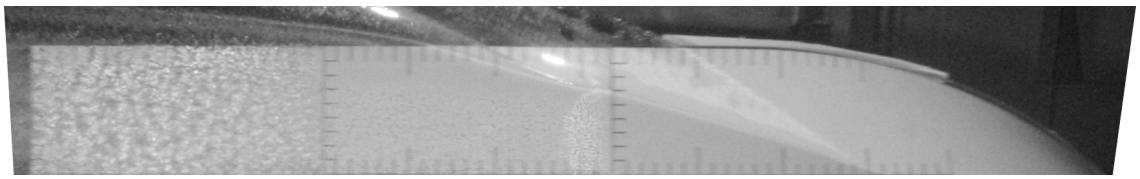

Figure 3.1: Underwater Photograph showing separated flow for Configuration 4 Displacement=85 lbf Cv=4.46

In the figure, the two vertically marked lines are the steps. The dark portion of the hull show areas where the flow is fully attached. Aft of the aft step, the distorted area shows a large area of separated flow. The separated zone aft of the forward step shows the first observation. The reattachment of the flow aft of the forward step shows a smooth, but nonlinear curve in the transverse direction. If the flow was linear in the transverse direction, the reattachment of the flow would look like a triangle pointing forward much like the stagnation line of the hull intersecting the calm water. This shows that a three dimension wave profile instead of a two dimension wave profile is needed to improve the stepped planing hull prediction method. Morabito [13] has presented a method using multiple equations for calculating the three dimension wave profile.

This figure also shows the second obervation, that the stagnation line crosses the step. Current methods are designed to predict the performance of a stepped hull when the stagnation line crosses the chines similar to Savitsky's planing prediction method with unstepped hulls. Further research can increase the capability of the Savitsky's planing prediction method. Savitsky's planing prediction method assumes that the chines are always wet; meaning that the stagnation line always crosses the chine. At very high speeds, the stagnation line would cross the transom of an unstepped planing hull and the stagnation line would cross the step on a stepped planing hull at any speed. Savitsky's planing prediction method can predict a non-physical negative wetted chine lengths when the stagnation line is actually crossing the transom. The prediction method is only valid up to a speed coefficient of 13 [12]. There are some extreme cases, such as offshore racing boats when an unstepped hull can have a speed coefficient greater than 13.

In addition to the two observations mentioned above, the lift equation that Savitsky developed for his planing prediction method and used in previous stepped planing hull prediction methods is limited to a speed coefficient of 13. For stepped planing hulls, the speed coefficient can also be very high when the wetted beam on the aft planing surfaces is small. The also may be stepped planing hulls that would exceed the speed coefficient limit.

This current thesis updates current stepped planing hull prediction methods to develop a more accurate prediction tool. First, a new lift equation for speed coefficients greater than 13 will be implemented. Second, a new physics based method for determining the three dimension wave profile aft of the step using a single equation will be developed. Lastly, a method for allowing the stagnation line to cross the step will be used.

3.1.1 Lift

The first area for updating Savitsky's planing prediction method are the lift equations. These updates are applicable to both the stepped and unstepped hull.

High Speed Lift

Savitsky has developed a lift equation for most planing speeds in which the stagnation line crosses the chine in a straight line. The Shuford-Brown lift equation can be used if the speed coefficient is greater than 13 as an alternative to Savitsky's lift equation at high speeds, Equation (3.1) [27].

$$
\begin{gathered}
C_L = C_{L,L} + C_{L,X} + C_{L,S} \\
C_{L,L} = \frac{0.5\pi \sin\tau \cos^2\tau}{1 + \frac{1}{\lambda}} \\
C_{L,X} = \frac{4}{3}\lambda \sin^2\tau \cos^3\tau \cos\beta \\
C_{L,S} = \tau 0.0109 \frac{\lambda^2}{{C_v}^2} \\
C_{L,L} = \text{Linear Term Determined from Lifting-Line Theory [27]} \\
C_{L,L} = \text{Crossflow Term} \\
C_{L,S} = \text{Hydrodstatic Lift}
\end{gathered}
\tag{3.1}
$$

The Shuford-Brown lift equation can be used for a speed coefficient up to 44, which covers the speed of any currently available stepped planing hull [27]. The center of pressure is calculated using the same method as used by Savitsky in the Savitsky planing prediction method [12]

Chines Dry Lift

To account for when the hull is chines dry, a formulation to calculate the chines dry lift is needed. Daniel Savitsky's formulation based on Milwitzky's test data was used for the chines dry lift coefficient, Equation (3.2)[28].

$$
C_L = \pi(\frac{\pi}{2\beta} - 1)^2 sin^3\tau(1 - \frac{tan\tau}{2tan\beta})
\tag{3.2}
$$

Once the lift coefficient is calculated, the lift can be found, Equation (3.3) [28].

$$Lift = \frac{1}{2} C_L \rho V^2 L_k^2 \tag{3.3}$$

The reduced beam can be found by using Equation (3.4) and setting L_c to zero and solving for the beam, Equation (3.5) [12].

$$L_k - L_c = \frac{B}{\pi} \frac{\tan\beta}{\tan\tau} \tag{3.4}$$

$$B = L_k \pi \frac{\tan\tau}{\tan\beta} \tag{3.5}$$

The mean wetted length to beam ratio is given by Equation (3.6).

$$\lambda = \frac{L_k + L_c}{2B} \tag{3.6}$$

With the wetted chine length equaling zero, Equation (3.6) becomes (3.7). Using the wetted keel length and the reduced beam, the mean wetted length to beam ratio can be calculated.

$$\lambda = \frac{L_k}{2B} \tag{3.7}$$

For the chines dry condition, the center of pressure is assumed to be 0.4 times the wetted keel length.

3.1.2 Wave Profiles

Model Test Background

Korvin-Kroukovsky et al. published the first papers with wave profile measurements for planing surfaces [29] [30] [31]. Finger probes were used to measure the wave heights at various locations. The deadrise angle, trim angle, loading coefficient, and speed were varied over

the ranges summarized in Table 3.1.

Table 3.1: Wave Profile Range of Applicability

	Korvin-Kroukovsky et al.	Savitsky and Morabito
Transverse Measurement Locations (Beams)	Keel, 0.2, 0.4	Keel, 0.25
Longitudinal Measurement Locations (Beams)	0-6 in 1 Beam Intervals	0-3 in 0.33 Beam Intervals
Deadrise Angle (degrees)	10, 20, 30	10, 20, 30
Trim Angle (degrees)	4, 8, 12	2, 3, 4, 5
Loading Coefficient	Various	0.4, 0.6, 0.8
Speed Coefficient	Various	4, 6, 8
Experimental Error (Beams)	0.01	0.03

The Korvin-Kroukovsky data focused on sea plane applications so the range of trim angles tested are higher than the typical planing hull range of 3 °-5 ° and the wave profile does not have great fidelity in the longitudinal direction near the transom. From the test data, an equation to predict the wave profile at the keel was developed. Morabito expanded on this test data by developing equations for the wave profile at 0.4 beams from the keel and the wave crest [13]. Faltinsen derived an analytical form of the wave profile at the keel and using the previous test data presents a simpler form of the wave profile for the keel [32]. Savitsky and Morabito conducted new wave profile tests in 2009 focusing on the application of stepped planing hulls [28]. The range of the variables tested are presented in Table 3.1. The trim angles tested was more suitable for planing hulls and the wave profile had more fidelity in the longitudinal direction near the transom. The drawback with the Savitsky and Morabito set of data is that the wave profile was only measured in two transverse locations and the three dimensional wave profile is unknown.

Cavity Pressure Assumption

To date, no known experiments have been conducted to measure the shape of the separated flow aft of a step. If one assumes that the air pressure in the cavity is atmospheric, then models for the wave profile aft of an unstepped planing hull can be used to model the separated flow aft of a step. Garland has shown in his model test that the assumption that

the air pressure in the cavity is atmospheric is valid [9]. To test this assumption, holes were drilled behind the step to ensure that the step was always ventilated. Three sets of runs were conducted to determine the effect the holes had on the craft performance. The three test conditions were; before the holes were installed, the holes were plugged, and the holes were open. The ventilation length, the resistance, and the trim angle were all in agreement within experimental error when the ventilation holes were open, plugged, and not used. Therefore, the step was always ventilated and no holes are needed to assist in ventilation.

Faltinsen's Analytical Method

Faltinsen derived an analytical solution to determine the form of the wave profile equation [32]. The derivation is shown from Equation (3.8) to Equation (3.13). For the solution near the separation point, the flow is assumed to be two-dimensional in the vertical plane (Figure 3.2) [32]. The body boundary condition is that there is no flow through the body boundary and the dynamic free surface boundary condition is that the pressure is atmospheric on the free surface.

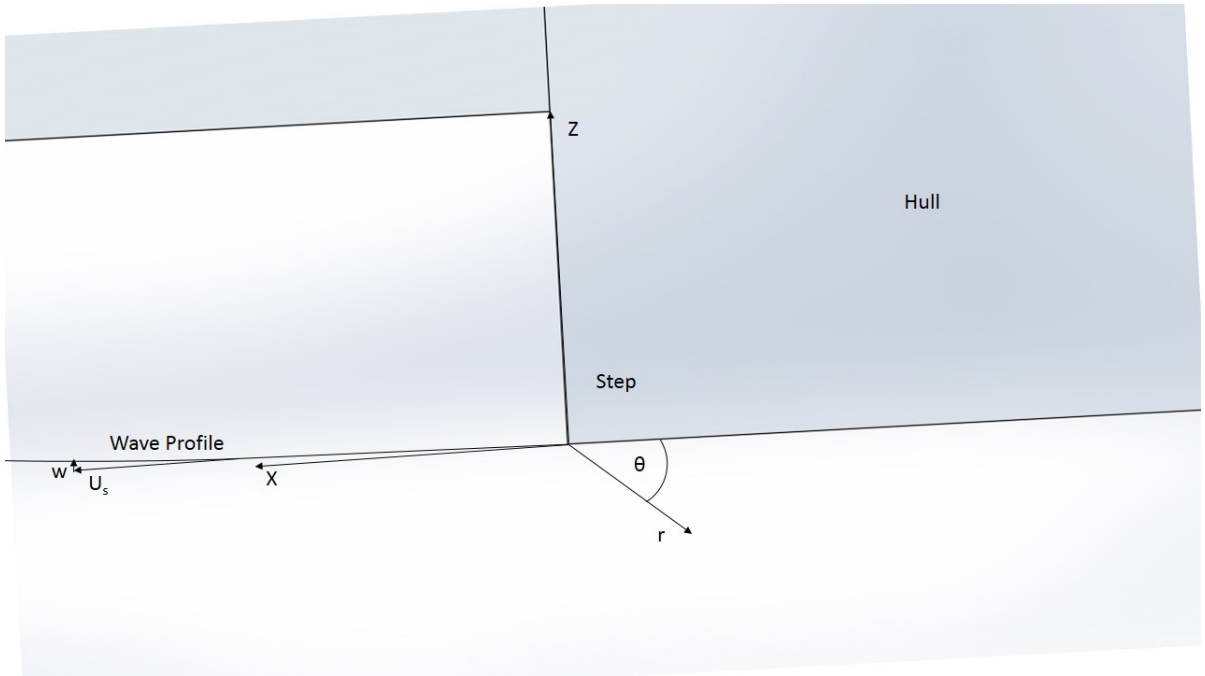

Figure 3.2: Local Coordinate System at the Step

Using polar coordinates and assuming that r is small, the velocity potential is Equation (3.8) [32].

$$\Phi = U_s X + Ar^n \cos n\theta \tag{3.8}$$

Bernoulli's equation with the velocity potential then becomes Equation (3.9) [32].

$$\frac{\rho}{2}((U_s + u)^2 + w^2) - \rho g(d - Z) = \frac{\rho}{2}U \tag{3.9}$$

The second order term of Equation (3.9) on $\theta = \pi$ or $z = 0$ becomes $\rho U_s u = 0$ and on $z = 0$ u can be written as Equation (3.10) [32].

$$u = \frac{\partial}{\partial r} Ar^n \cos n\theta \tag{3.10}$$

To satisfy Equation (3.9), $\cos n\pi = 0$. The smallest value for n must be chosen since r is assumed to be small. $n = \frac{1}{2}$ is not possible since the velocity will be infinite at $r = 0$. Therefore, $n = \frac{3}{2}$ is chosen and w becomes Equation (3.11) at $z = 0$ [32].

$$w = \frac{1}{r} Ar^{3/2} \frac{d}{d\theta} \cos \frac{3}{2}\theta = \frac{3}{2} Ar^{\frac{3}{2}} \tag{3.11}$$

The free surface can be approximated by the streamline at the free surface. Thus the free surface slope ($\frac{dz}{dx}$) is approximately Equation (3.12) [32].

$$\frac{dz}{dx} = \frac{w}{U_s} \tag{3.12}$$

Substituting w and solving the equation gives the wave profile height in the form of Equation (3.13) [32].

$$z = \frac{A}{U_s} x^{\frac{3}{2}}$$
$$A = \text{Unknown Constant} \tag{3.13}$$

When non-dimensionalizing z and x by the Beam (B), Equation (3.13) becomes Equation (3.14).

$$ZB = \frac{A}{U_s}(XB)^{\frac{3}{2}}$$
$$Z = z/B$$
$$x = x/B \tag{3.14}$$

Simplifying Equation (3.14) to Equation (3.15)

$$Z = \frac{A}{\frac{U_s}{\sqrt{B}}}(X)^{\frac{3}{2}} \tag{3.15}$$

Realizing that $\frac{U_s}{\sqrt{B}}$ is similar to the speed coefficient, Equation (3.15) is multiplied by the gravitational constant to form (3.16).

$$Z = \frac{A}{\frac{U_s\sqrt{g}}{\sqrt{gB}}}(X)^{\frac{3}{2}}$$
$$g = \text{gravitational constant} \tag{3.16}$$

The gravitational constant can be absorbed into the unknown constant A to form Equation (3.17).

$$Z = \frac{A}{C_v} X^{\frac{3}{2}} \tag{3.17}$$

2D Wave Profile

The Savitsky and Morabito wave profile equation takes the form of Equation (3.18) [28].

$$\begin{gathered} H = 0.17(C + 0.03 L_k \tau^{1.5}) \sin \frac{\pi}{C_v} (\frac{X}{3})^{\frac{3}{2}} \\ H = \text{Height of Wave Profile Above Keel, Beams} \\ \text{At the keel, for } \beta = 10\,^{\circ}\text{: } C = 1.5 \\ \text{At the keel, for } \beta = 20\,^{\circ}\text{and } \beta = 30\,^{\circ}\text{: } C = 2.0 \\ \text{At the} \frac{1}{4} \text{Beam : } C = 0.75 \end{gathered} \tag{3.18}$$

C is a coefficient that varies based on transverse transom location and deadrise angle. The equation assumes that the origin is at the keel and transom intersection and the x axis extends aft parallel with the keel.

Morabito and Savitsky's wave profile equation has a form that is similar to the analytical form presented in Equation (3.17). Assuming that at small angles, the sine of an angle can be approximated as the angle, Equation (3.18) can take a form similar to the analytical form of Equation (3.17) resulting in Equation (3.19)).

$$H = 0.17(C + 0.03 L_k \tau^{\frac{3}{2}}) \frac{\pi}{C_v} (\frac{X}{3})^{\frac{3}{2}} \tag{3.19}$$

Further combining the constant coefficients results in equation (3.20).

$$H = 0.103(C + 0.03L_k\tau^{\frac{3}{2}})\frac{1}{C_v}X^{\frac{3}{2}} \tag{3.20}$$

In Savitsky and Morabito's wave profile equation, at the keel, $C = 1.5$ when $\beta = 10\,^\circ$ and $C = 2.0$ when $\beta = 20\,^\circ$ and $30\,^\circ$ [28]. At the quarter Beam, $C = 0.75$ for all deadrise angles.

3D Wave Profile Equation

Based on the change in the factor C between the keel and the quarter beam in Savitsky and Morabito's [28] wave profile, the idea for a three dimension wave profile equation varying the constant C in the transverse direction was developed. For the three dimension wave profile equation, a new form of C as a function of the transverse location was assumed (Equation (3.21)). A number of different equations were tested to determine the best fit. Two power equations, y^2 and $y^{\frac{3}{2}}$ and an exponential equation e^y were tried. The $y^{\frac{3}{2}}$ equation was selected based on the Faltinsen derivation for the longitudinal wave profile [32]. The quadratic equation gave the best fit to the experimental data of the equations tested.

$$C = C_1(\frac{y}{B})^2 + C_2(\frac{y}{B}) + C_3 \tag{3.21}$$

The new form of Equation (3.19) becomes Equation (3.22)

$$0.103(C_1(\frac{y}{B})^2 + C_2(\frac{y}{B}) + C_3 + 0.03L_k\tau^{\frac{3}{2}})\frac{1}{C_v}(\frac{x}{B})^{\frac{3}{2}} \tag{3.22}$$

To determine the unknown coefficients C_1,C_2, and C_3, Equation (3.22) was compared to Korvin-Kroukovsky's wave profile data [29] [30] [31] and the coefficients were found that minimized the error between the equation and the data. The wave profile heights were presented in figure, not numerical values in the papers. To obtain the numerical values, the figures from Korvin-Kroukovsky's papers were imported into Solidworks [24] and the faired wave profile was measured. The data for all of the $\tau = 4^\circ$ runs was measured from the transom to 3 beams aft of the transom in $\frac{1}{3}$ beam increments. A total of seventeen runs were used with deadrise angles of 10°, 20°, 30° at various speeds and displacements. The Savitsky and Morabito wave profile equation was applicable over a range of trim angles from 3° to 5°. Since the Savitsky and Morabito wave profile was the basis for the three dimension wave

profile, Equation (3.22) was compared to the Korvin-Kroukovsky data at $\tau = 4°$.

The figures from the Korvin-Kroukovsky papers presented the data with the origin at the calm water line. The hull trimmed and sunk to the running conditions such that the keel at the step is below the origin. Equation (3.22) references the origin at the intersection of the keel and the step. Therefore, equation (3.22) had to be rotated and shifted to account for the coordinate system of the Korvin-Kroukovsky wave profile data. For the wave profiles that were not located transversely at the keel, an additional shift is needed to account for the height of the hull at the transverse location. Equation (3.23) is the modified version of Equation (3.22) that was used to compare the wave profile equation to the test data.

$$H = 0.103(C_1(\frac{y}{B})^2 + C_2(\frac{y}{B}) + C_3 + 0.03L_k\tau^{\frac{3}{2}})\frac{1}{C_v}(\frac{x}{B})^{\frac{3}{2}} - \frac{L_k}{B}\sin\tau + \frac{y}{B}\tan\beta \tag{3.23}$$

The error was calculated as in Equation (3.24).

$$Error = |z_{estimated} - z_{measured}| \tag{3.24}$$

The solver add-in feature in Excel [33] was used to determine the coefficients C_1, C_2, and C_3 in Equation (3.21) by minimizing the error as in Equation (3.24). The coefficients were also calculated with limitations such as forcing the equation to match Savitsky and Morabito's coefficients at the keel and quarter beam. It was found that letting all three coefficients be independent minimized the error with the experimental data. With the coefficients, Equation (3.22) is (3.25).

$$H = 0.103(4.14(\frac{y}{B})^2 - 3.59(\frac{y}{B}) + 1.33 + 0.03L_k\tau^{\frac{3}{2}})\frac{1}{C_v}(\frac{x}{B})^{\frac{3}{2}} \tag{3.25}$$

3.1.3 Process

Savitsky's method is an iterative procedure which one iterates upon trim angle to balance trim moment. The stepped hull planing prediction method requires a second iterative unknown variable. The wetted keel length is also iterated to balance the vertical forces. Therefore, there are two dependent (vertical force and moment) and two independent variables (trim angle and wetted keel length on the forward planing surface) solved for in this method. The result of interest, resistance, is a third dependent variable that comes out of the method. Figure 3.3 is a flow chart of the stepped hull planing prediction method. The procedure starts on the upper left and ends on the upper right.

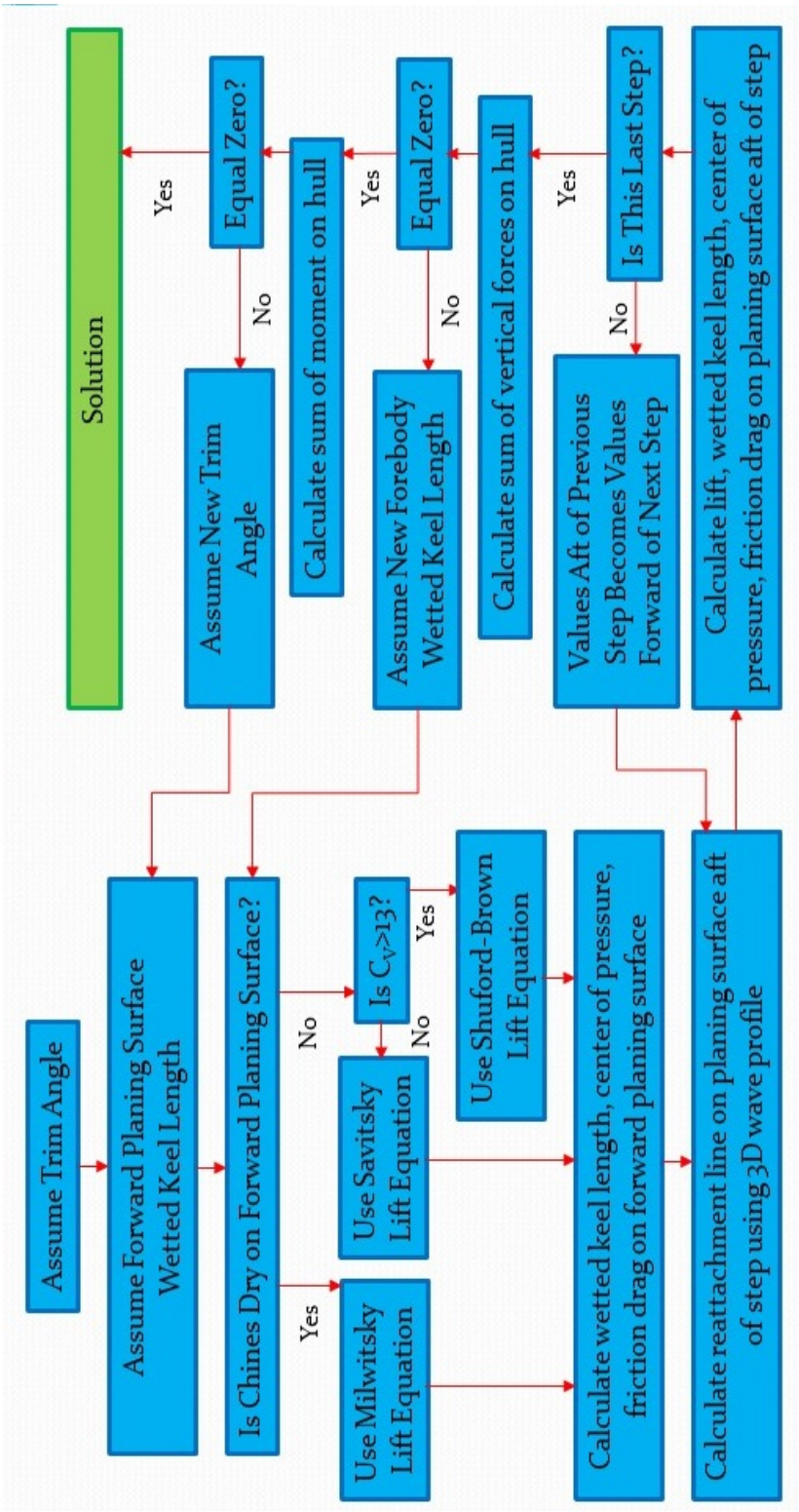

Figure 3.3: Stepped hull planing prediction method. Procedure starts on the uper left and ends on the upper right

The method starts by assuming a trim angle. Once a trim angle is assumed, a wetted keel length on the forward planing surface is assumed. All the other methods for predicting the performance of the stepped planing hull(Morabito [28], Danielsson [15], and Svahn [14]) assumes a lift generated by the forward planing surface instead of a wetted keel length on the forward planing surface. The upper limit of lift generated by the forward planing surface is limited by the length of the wetted keel length of the forward planing surface. The wetted keel length cannot be longer than the length of the forward planing surface. In reality, since the bow section is not prismatic, but highly shaped, this limit may be less. If a lift is assumed on the forward planing surface, the wetted length required to generate the assumed lift could be longer than the length of the forward planing surface. This method assumes that the stagnation line crosses the forward planing surface, so the wetted keel length is limited to the length of the forward planing surface. Once these two variables are selected the calculation begins on the forward planing surface.

Forward Planing Surface

First, the hull is divided into a number of longitudinal sections creating a transverse grid. At each of these grid points, the longitudinal position of the stagnation line is calculated in two different reference frames, longitudinal position from the transom (L_{Stag}) and longitudinal position from the step ($L_{L_{Stag}}$). Both L_{Stag} and $L_{L_{Stag}}$ are matrices where the columns are the transverse position and the rows are the planing surfaces. When the stagnation line is on a planing surface, the longitudinal position is stored in the row corresponding to the planing surface the stagnation line is on. If the stagnation line crosses the step, the new reduced beam is calculated and stored as the local beam. Figure 3.4 shows the stagnation line crossing the step. The black lines represent the two steps. The blue line represents the stagnation line on the forward planing surface. The green line represents the stagnation line on the middle planing surface.

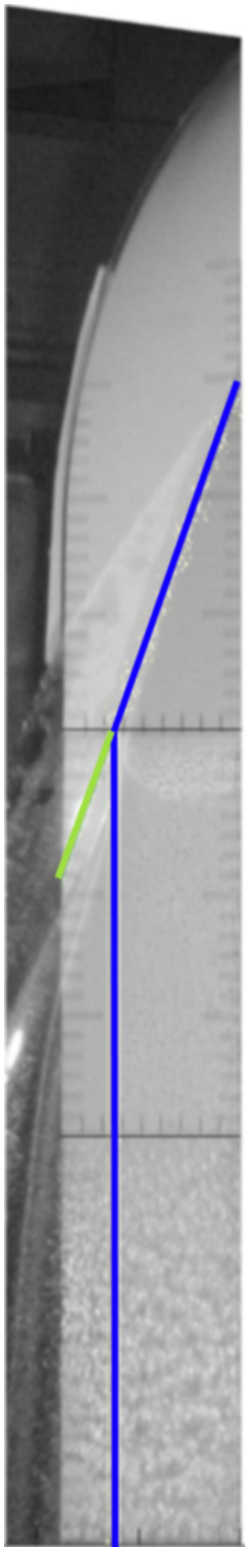

Figure 3.4: Predicted Stagnation Line. Black lines represent the two steps. Blue line represents the stagnation line on the forward planing surface. Green line represents the stagnation line on the middle planing surface

The lift and center of pressure is calculated based on the conditions of the forward planing surface. If the chines are dry, Milwitzky's chines dry lift equation is used. For the chines wet condition, if the speed coefficient is above 13, the Shuford-Brown lift equation is used Otherwise, the Savitsky lift equation is used. The friction resistance on the forward planing surface is found using the wetted surface area of the forward planing surface and the ITTC '57 friction line.

Aft planing surfaces

Utilizing the trim angle, the wetted keel length, beam, and the deadrise angle of the planing surface forward of the step, the longitudinal distance of the reattachment line from the step at each transverse location (x) is calculated from the three dimension wave profile equation. The three dimension wave profile, Equation (3.22), is set so that the height, z, on the left hand side is equal to the height of the planing surface aft of the step. Equations (3.26) to (3.28) show the three components that contribute to the height of the planing surface aft of the step. Equation (3.26) is the height of the step.

$$z = \frac{h}{B} \tag{3.26}$$

Equation (3.27) is the height due to difference in angle between the planing surface forward and aft of step.

$$z = \frac{x}{B} \tan \theta_{i+1} \tag{3.27}$$

Equation (3.28) is the height due to difference in deadrise angle between the planing surface forward and aft of step.

$$z = \frac{y}{B} (\tan \beta_{i+1} - \tan \beta_i) \tag{3.28}$$

The combined equation is shown in Equation (3.29).

$$0.103(C_1(\frac{y}{B})^2 + C_2(\frac{y}{B}) + C_3 + 0.03L_k\tau^{\frac{3}{2}})\frac{1}{C_v}(\frac{x}{B})^{\frac{3}{2}} = \frac{h}{B} + \frac{x}{B}\tan\theta_{i+1} + \frac{y}{B}(\tan\beta_{i+1} - \tan\beta_i) \tag{3.29}$$

The longitudinal position from the reattachment point to the aft end of the planing surface is calculated and stored in a new matrix ($L_{L_{Wake}}$). This position is also transferred to the transom reference frame (L_{Wake}). If the longitudinal distance of the reattachment point is longer than the planing surface then the longitudinal distance from the reattachment point to the aft end of the next planing surface is calculated and stored in matrices (L_{Extra}) and ($L_{L_{Extra}}$). The wetted length at each transverse location is found by calculating the minimum longitudinal position of the stagnation line, the reattachment point from the separated flow off the step, and the reattachment point from the separated flow off any step forward of the step of interest. The mean wetted length to beam ratio is calculated by taking the average of the wetted lengths. If the flow crosses the end of the planing surface, the new local beam is calculated as well.

Svahn suggests using the slope of the wave profile as it reattaches to the step as the local trim angle for calculating the friction resistance as well calculating the forces and moments [14]. While the direction of the flow at the free surface is the slope of the wave profile as it reattaches the step, it must be noted that as the hull moves through the water, the flow encountering the hull aft of the step is seen by the hull at the overall trim angle. Therefore the local trim angle used for this method is the overall trim angle.

The local deadrise angle is no longer the deadrise angle of the hull with respect to the flat calm water, but is now the deadrise angle of the hull with respect to the 3D wave profile. Therefore the local deadrise angle is the difference between the deadrise angle of the hull and the angle of the transverse wave profile at the reattachment point for each transverse location. The angle of the transverse wave profile at the reattachment point can be found by taking the arctangent of the slope of the wave profile at the reattachment point. To determine the slope of the wave profile at the reattachment point, the derivative of Equation (3.29) is taken with respect to y and the result is shown in Equation (3.30)

$$\frac{dF}{dy} = 0.103B(2C_1\frac{y}{B^2} + \frac{C_2}{B})\frac{1}{C_v}(\frac{x}{B})^{\frac{3}{2}} - \frac{1}{B}(\tan\beta_{i+1} - \tan\beta_i) \tag{3.30}$$

Taking the arctangent of Equation (3.30) and subtracting it from the deadrise angle and the local deadrise angle is given in Equation (3.31)

$$\beta_{Li} = \beta_i - \arctan(0.103B(2C_1\frac{y}{B^2} + \frac{C_2}{B})\frac{1}{C_v}(\frac{x}{B})^{\frac{3}{2}} - \frac{1}{B}(\tan\beta_{i+1} - \tan\beta_i)) \tag{3.31}$$

The average deadrise angle is found by averaging the deadrise angle at each transverse position.

The lift, center of pressure, and the friction resistance is found on the planing surface in a similar manner to how they are found on the forward planing surface. This process is repeated for each planing surface aft of the forward planing surface.

3.1.4 Equilibrium Equations

With the lift, center of pressure, and the friction resistance known for each planing surface, the vertical forces are calculated. The forces in the vertical direction are the hull displacement, the vertical components of the lift forces on each planing surface, and the vertical component of the friction resistance, Equation (3.32).

$$\sum_{i=1}^{n} N_i\cos(\tau_i + \theta_i) - \sum_{i=1}^{n} D_{f_i}\sin(\tau_i + \theta_i) - \Delta = 0$$
$$N_i = \frac{Lift_i}{\cos(\tau_i + \theta_i)} \tag{3.32}$$

For a given trim angle, recognizing the sum of vertical forces must be zero, the wetted keel length on the forward planing surface is iterated until a solution is found. The trim moment is then calculated.

The trim moment can be measured in reference to the center of gravity as following Savitsky's method [12]. The a coefficient is the Vertical Center of Gravity (VCG) minus the step heights of the steps forward of the ith planing surface minus the height of the quarter beam. The c coefficient is the LCG minus the distance from the transom to the step aft of the ith planing surface minus the center of pressure on the ith planing surface. The sum of the moments is the sum of the normal force on each planing surface multiplied by the lever arm c and the friction drag on each planing surface multiplied by the lever arm a.

$$\begin{gathered} a_i = VCG - \sum_{j=1}^{i}(h_j) - \frac{B_{Li}}{4} tan\beta \\ c_i = LCG - L_{S_{i-1}} - C_{p_i} \\ \sum_{i=1}^{n}(N_i \cos(\theta_i) c_i) + \sum_{i=1}^{n}(D_{f_i} a_i) = 0 \\ n = \text{Total number of steps} \end{gathered} \tag{3.33}$$

For the stepped planing hull to be in equilibrium, trim moment must be in in equilibrium. Therefore, the trim angle is iterated until the trim moment equals zero.

A constrained optimization routine was required to determine the forward planing surface wetted keel length and trim angle that would make the vertical forces and trim moment in equilibrium. The constraints of the routine had to be individually tailored for each specific run configuration studied.

The forces in the horizontal direction are the horizontal components of the lift forces on each planing surface and the horizontal component of the friction resistance. The sum of these forces is the total drag (resistance) on the stepped hull, Equation (3.34).

$$D = \sum_{i=1}^{n} N_i \sin(\tau_i + \theta_i) + \sum_{i=1}^{n} D_{f_i} \cos(\tau_i + \theta_i) \tag{3.34}$$

Grid Convergence

The number of grid points in the transverse direction that define the stagnation line and the reattachment lines was varied to determine the effects of grid spacing on the results. Figure 3.5 shows the average percent error in resistance/weight as the number of grid points increases. The figure shows that the resistance/weight converges as the number of points in the transverse direction increases. Figure 3.6 shows the average percent error in trim angle as the number of grid points increases. The figure shows that the trim angle converges as the number of points in the transverse direction increases.

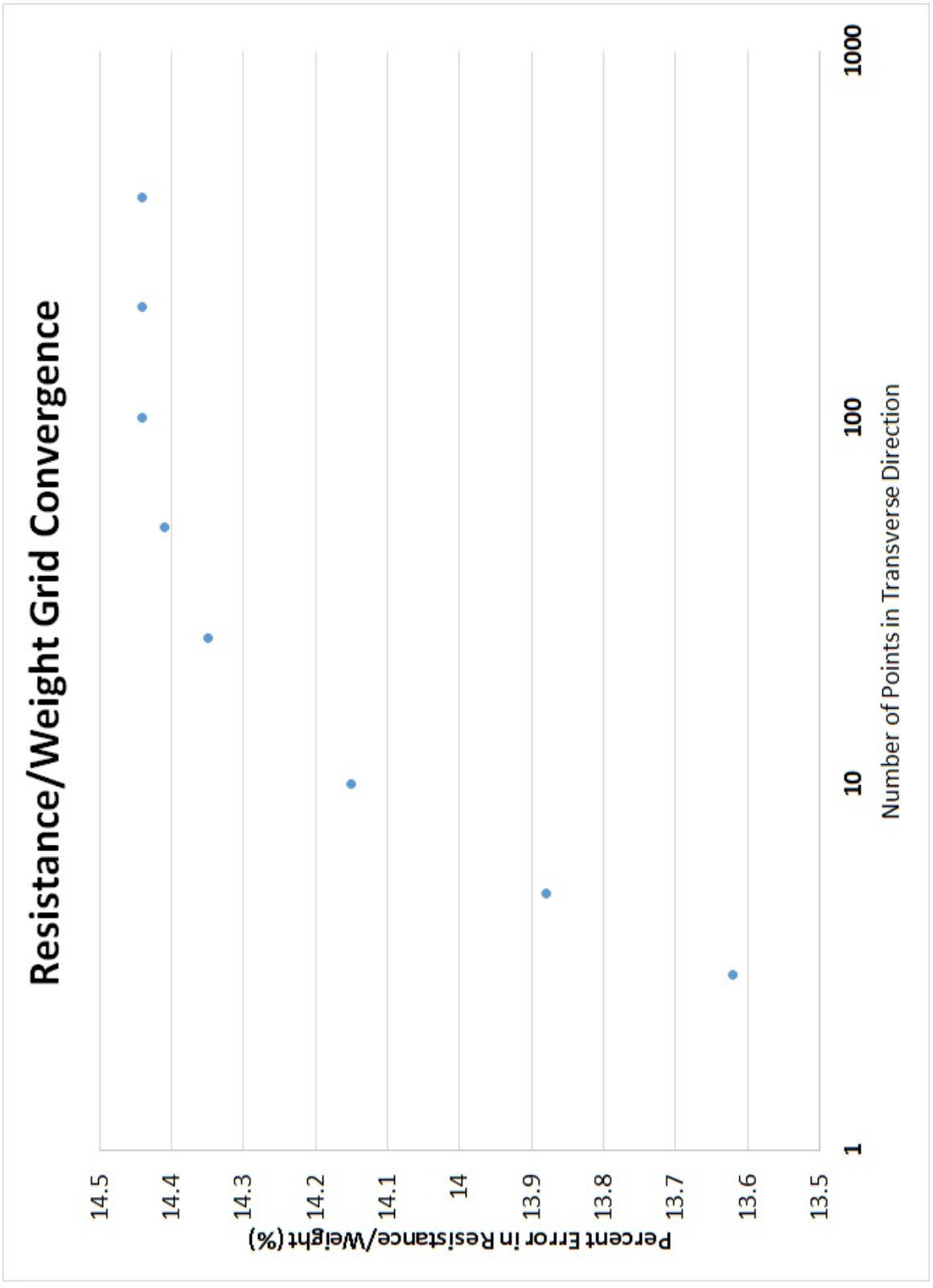

Figure 3.5: Resistance/Weight Grid Convergence: Average percent error in resistance/weight as number of grid points increases

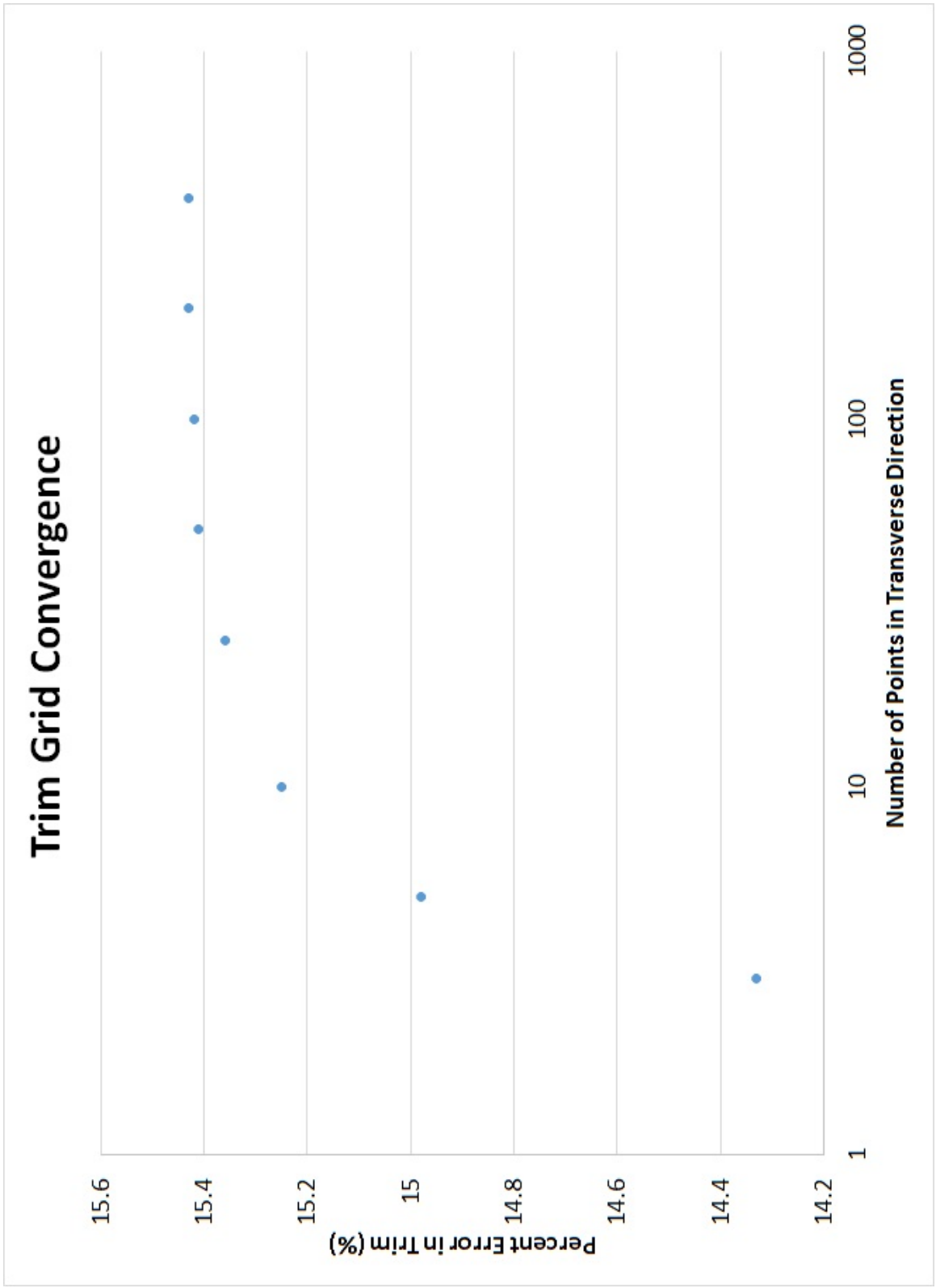

Figure 3.6: Trim Angle Grid Convergence: Average percent error in trim angle as number of grid points increases

Two hundred grid points were selected as the number of grid points for further analysis since both the resistance/weight and the trim angle has converged. Four hundred grid points was not selected due to the increase in computational time compared to two hundred points and the difference in values are small.

Tolerance Analysis

The tolerance used to to determine if the sum of the vertical forces and sum of the moments were in equilibrium was varied to determine the effects the tolerance value on the results. The tolerance value was the same for both the vertical force and the moment. The tolerance ranged from a value of 5 to 0.001. The plots show the tolerance values on a logarithmic base 10 scale. Figure 3.7 shows the average percent error in resistance/weight as the tolerance value increases. The figure shows that the resistance/weight converges as the tolerance value decreases. Figure 3.8 shows the average percent error in trim angle as the tolerance value increases. The figure shows that the trim angle converges as the tolerance value decreases.

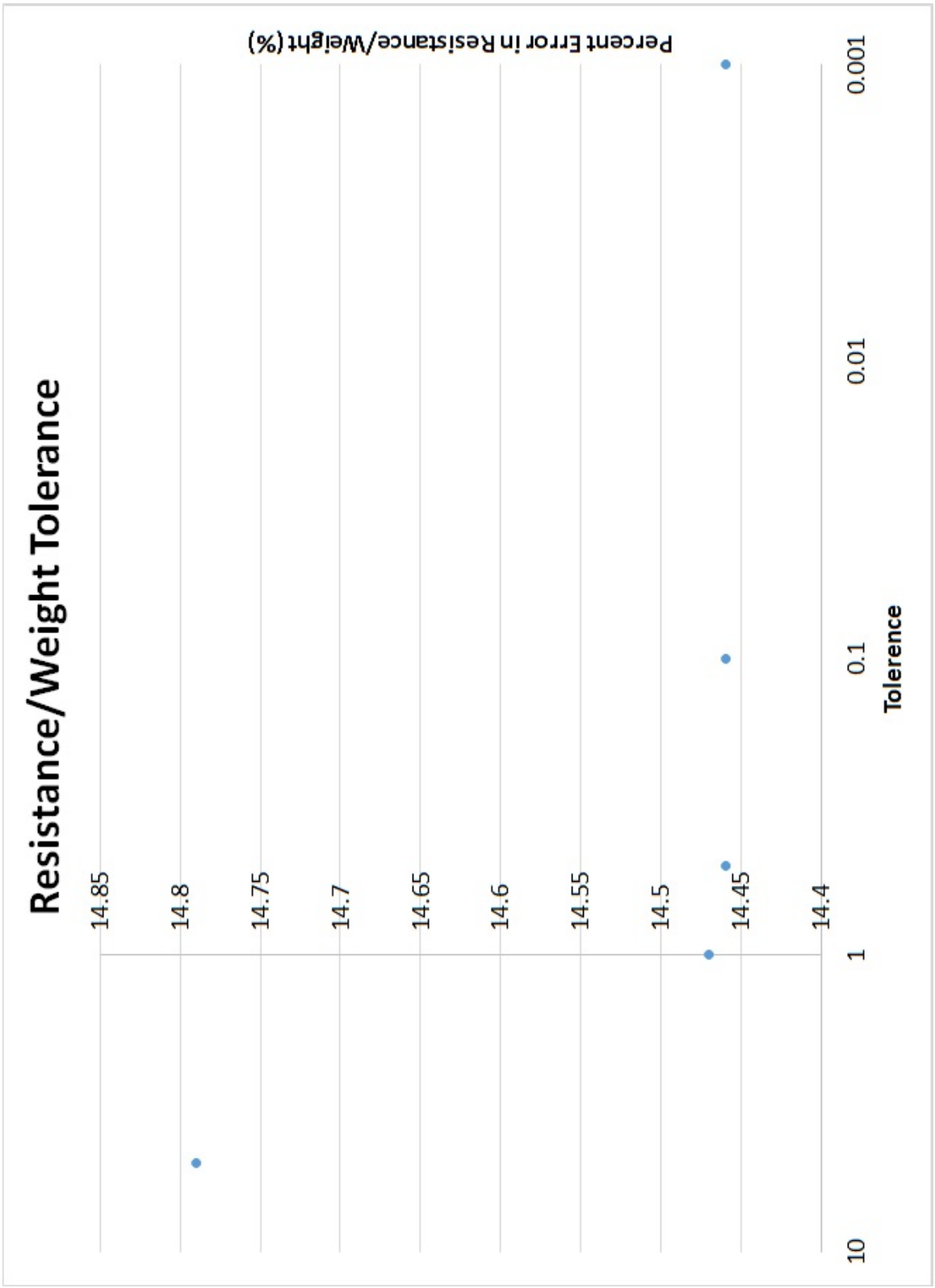

Figure 3.7: Resistance/Weight Tolerance: Average percent error in resistance/weight as tolerance value decreases

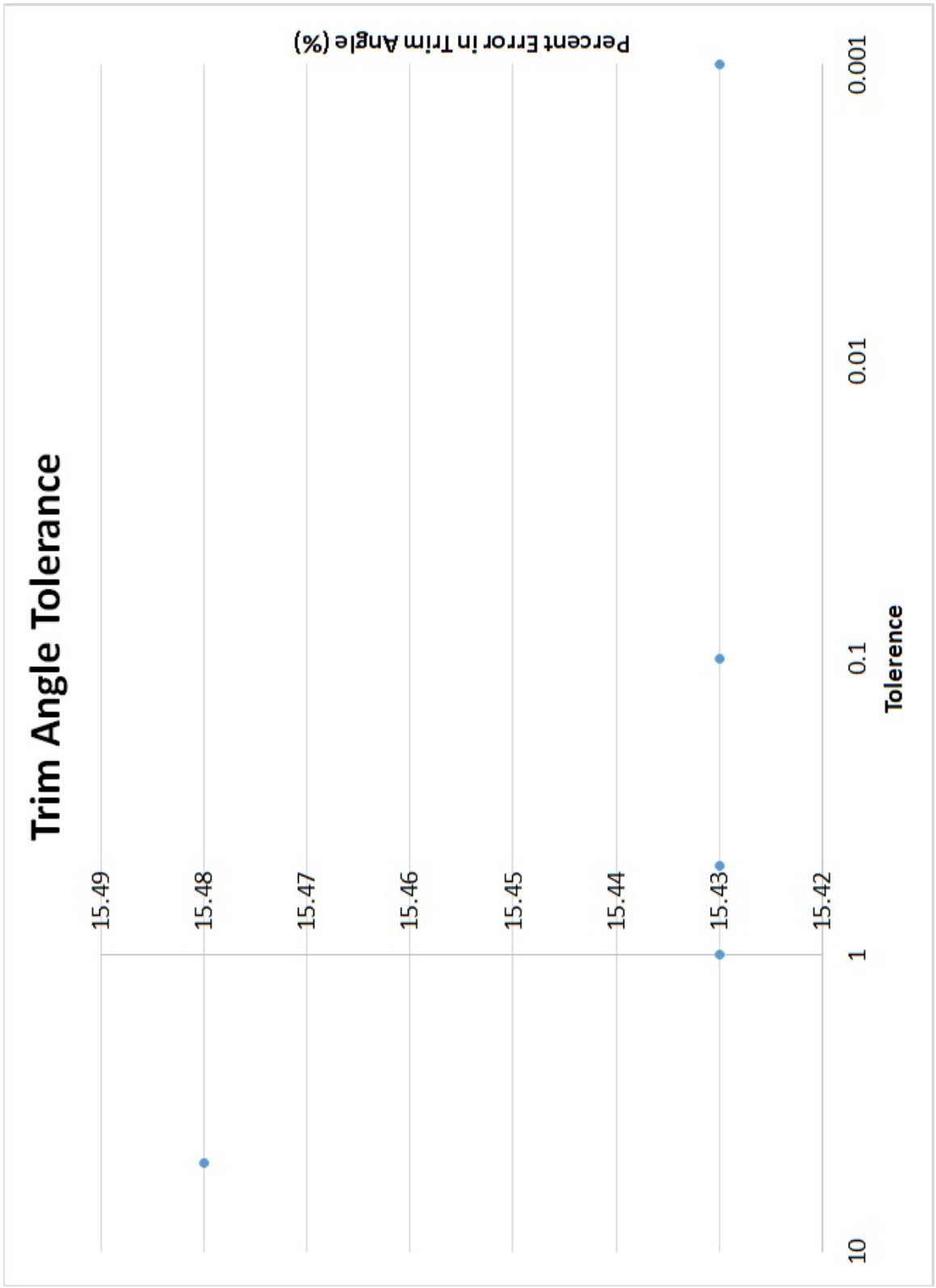

Figure 3.8: Trim Angle Grid Tolerance: Average percent error in trim angle as tolerance value decreases

A tolerance value of 0.001 was selected for further analysis because there was no significant increase in speed in reducing the tolerance value among the converged tolerance values.

3.2 Results

3.2.1 Overview

Table 3.2 shows the average percent error for the resistance/weight and the trim angle for Savitsky's planing prediction method to predict configuration 1, the unstepped hull.

Table 3.2: Savitsky Unstepped Hull

Run	Average Percent Error in Resistance/Weight	Average Percent Error in Trim Angle
configuration 1 LCG=35% LOA forward of Transom	12.63%	9.09%
All unstepped hull runs	12.45%	7.29%

Table 3.3 shows the average percent error for the resistance/weight and the trim angle for the various planing prediction methods to predict stepped hull.

Table 3.3: Stepped Hull

Method	Runs	Average Percent Error in Resistance/Weight	Average Percent Error in Trim Angle
Savitsky	Configuration 2 LCG=35%	7.65%	11.52%
Savitsky	All stepped hull runs	3.96%	8.73%
2D	Configuration 2 LCG=35%	8.60%	5.77%
2D	All stepped hull runs	12.63%	18.67%
3D	Configuration 2 LCG=35%	10.18%	2.13%
3D	All stepped hull runs	14.44%	15.43%
Modified 3D	Configuration 2 LCG=35%	4.14%	1.61%
Modified 3D	All stepped hull runs	3.60%	6.96%

3.2.2 Savistky

Unstepped Hull

The resistance and trim angle results of configuration 1, the unstepped hull, was compared to the Savitsky's planing prediction method. The measured data is presented with the experimental error bars calculated from the model test. For the LCG=35% condition, the resistance was under predicted and the trim angle was over predicted, Figures 3.9 and 3.10). Savitsky's planing prediction method under predicts the resistance more at higher speeds than at lower speeds. Savitsky's planing prediction method over predicts the trim angle more at lower speeds than at higher speeds. The form drag is proportional to the tangent of the trim angle, therefore the over prediction of the trim angle would lead to an over prediction of the form resistance. Since the resistance is under predicted and the form resistance is over predicted, one can surmise that the friction drag is under predicted.

Figure 3.9: Savtisky Prediction of Resistance/Weight of the unstepped hull at LCG=35%. Savitsky prediction method under predicted the resistance for all displacements

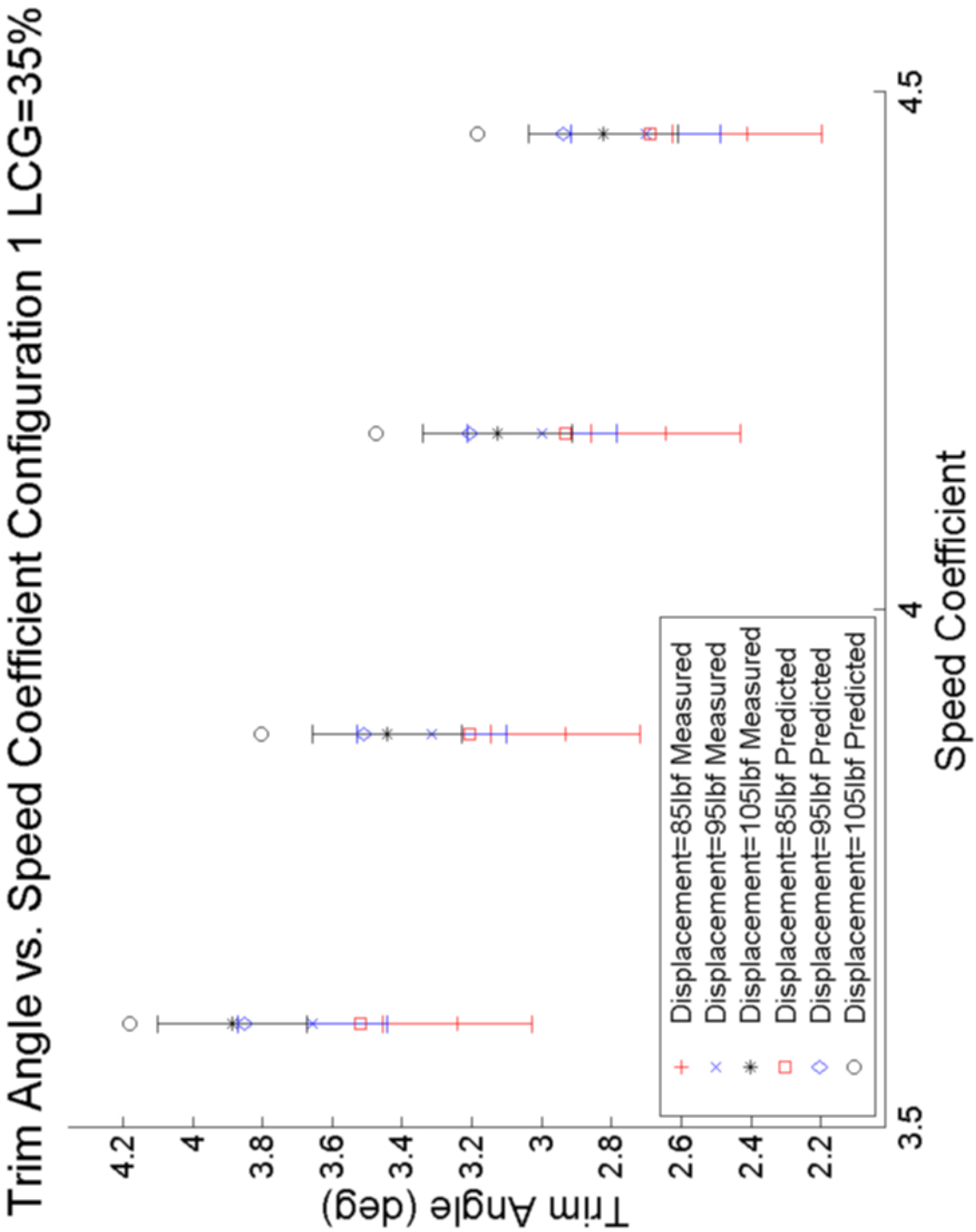

Figure 3.10: Savtisky Prediction of Trim Angle of the unstepped hull at LCG=35%. Savitsky prediction method over predicted the trim angle for most displacements

For configuration 1 at LCG=35%, the average error in the resistance/weight was 12.63% and the error in the trim angle was 9.09%. For all 24 conditions of configuration 1, the average error in the resistance/weight was 12.45% and the error in the trim angle was 7.29%.

Stepped Hull

Configuration 2 at LCG 35% was compared to the Savitsky's planing prediction method unstepped prediction, Figures 3.11 and 3.12. The data is presented in a similar fashion to configuration 1. Configuration 2 was selected for analysis because it has the small (0.125in, 0.007 Beam) step height for the forward and aft step. The wave profile would have the most impact on the reattachment length for the small step height. Similar to configuration 1, the predicted resistance was under predicted and the predicted trim angle was over predicted for step configuration 2. Savitsky's Prediction Method under predicts the resistance more at higher speeds than at lower speeds. Savitsky's planing prediction method over predicts the trim angle more at lower speeds than at higher speeds. If one assumes that the like an unstepped hull, the form resistance is proportional to the tangent of the trim angle, the over prediction of the trim angle would lead to an over prediction of the form resistance. For an unstepped hull, Savitsky assumes the form resistance to be $D_{Form} = \Delta tan(\tau)$. In other words, the higher the trim angle, the more of the hull that has to be pushed through the water and higher form resistance. Since the resistance is under predicted and the form resistance is over predicted, one can surmise, similar to configuration 1, that the friction drag is under predicted. Since the results of the Savitsky's planing prediction method does not account for steps and are the same for configuration 2 and configuration 1, the reduced resistance of configuration 2 causes the Savitsky Prediction Method to more accurately predict the resistance of configuration 2.

Figure 3.11: Savtisky Prediction of Resistance/Weight of Configuration 2 at LCG=35%. Savitsky prediction method under predicted the resistance for all displacements

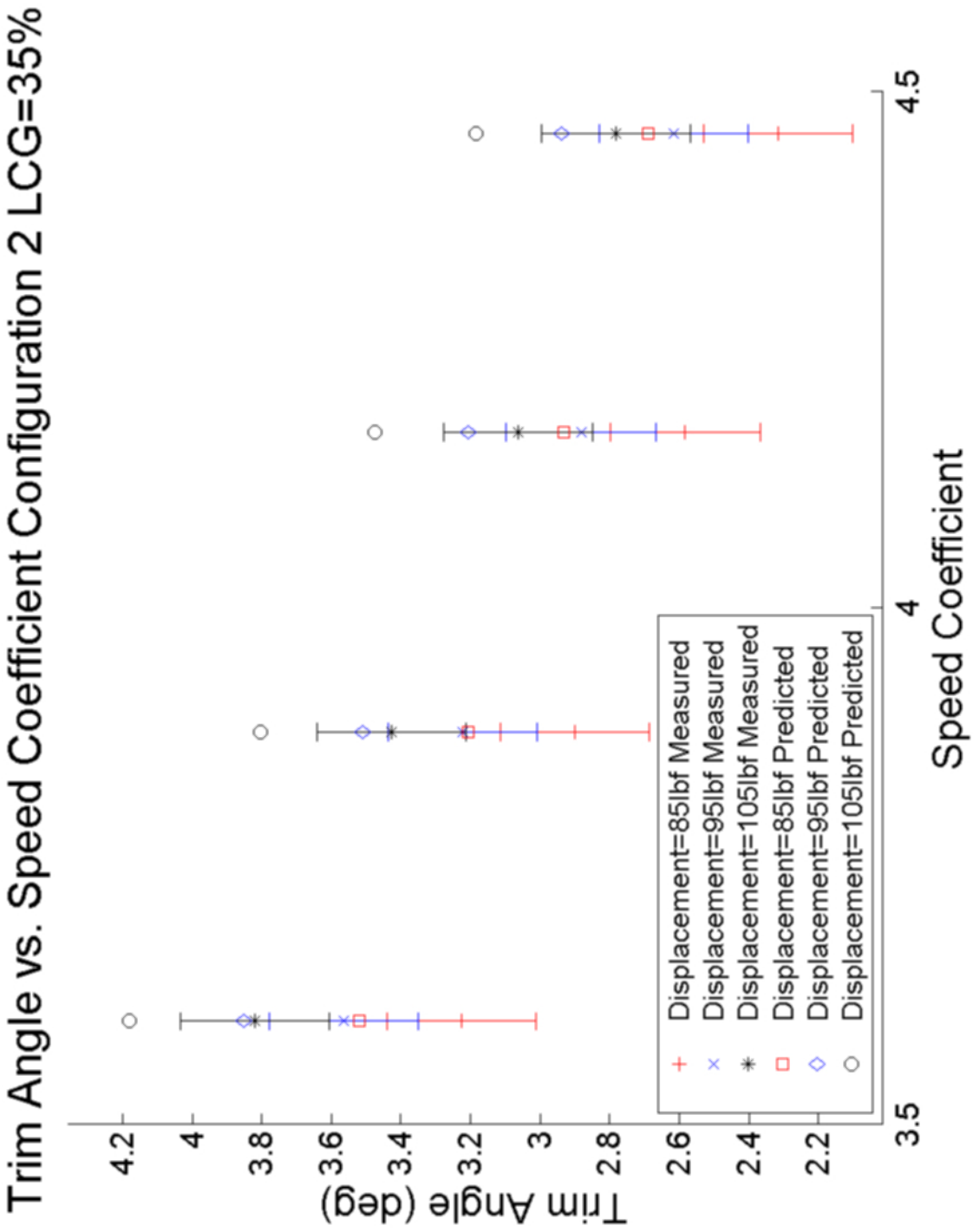

Figure 3.12: Savtisky Prediction of Trim Angle of Configuration 2 at LCG=35%. Savitsky prediction method over predicted the trim angle for all displacements

For configuration 2 at LCG=35%, the average error in the resistance/weight was 7.65% and the error in the trim angle was 11.52%. For all 180 conditions of the stepped hull tested in the model test, the average error in the resistance/weight was 3.96% and the error in the trim angle was 8.73%.

3.2.3 2D Wave Profile

Configuration 2 at LCG 35% was compared to the stepped hull planing prediction method using the two dimension wave profile, Figures 3.13 and 3.14. The data is presented in a similar fashion to configuration 1. For configuration 2, the resistance was slightly under predicted and the predicted trim angle was predicted within experimental error for step configuration 2. The resistance was under predicted slightly more at high speeds. The form resistance is proportional to the tangent of the trim angle, therefore the good prediction of the trim angle would lead to a good prediction of the form resistance. Since the resistance is slightly under predicted and the form resistance is predicted well, one can surmise that the friction drag is slightly under predicted.

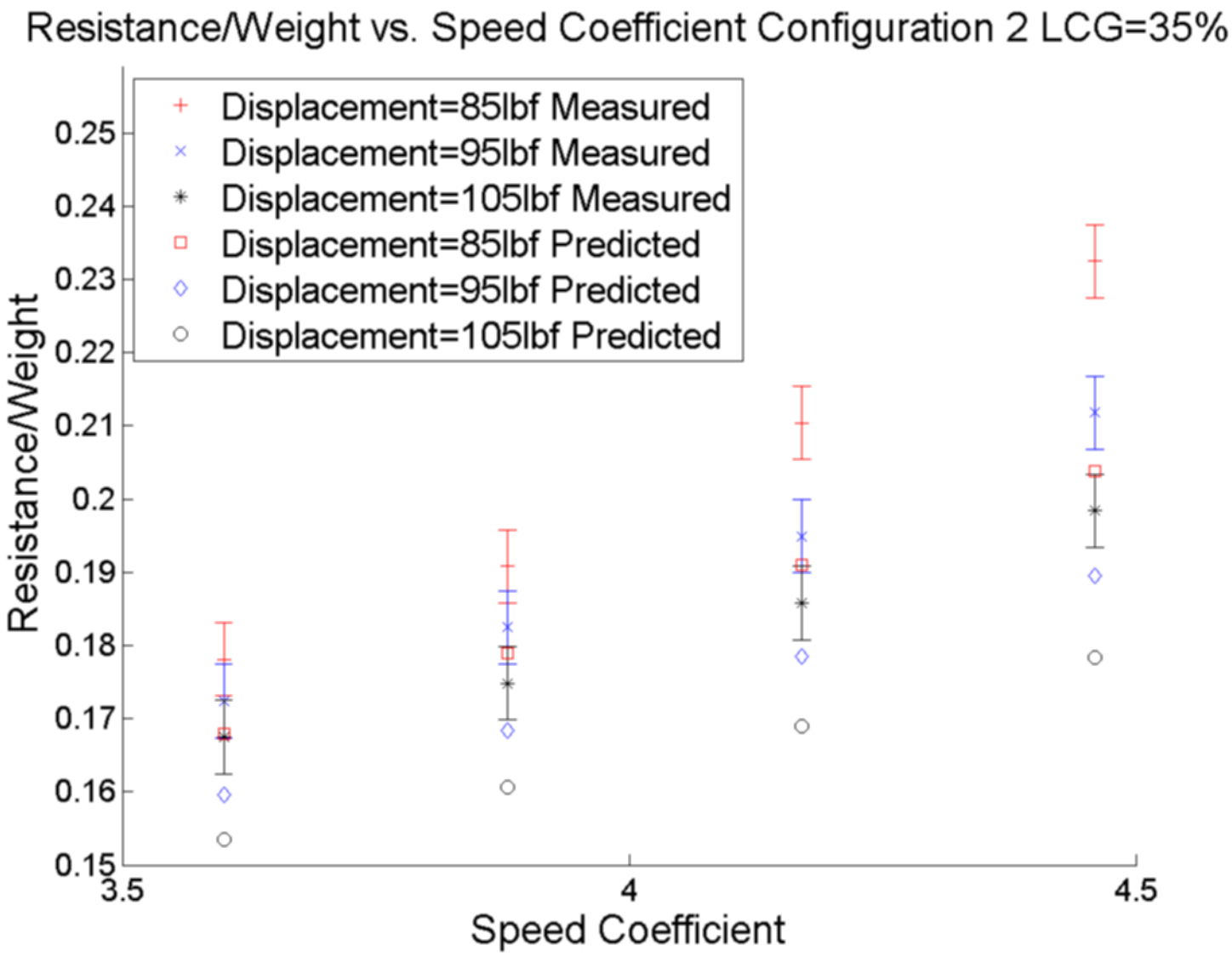

Figure 3.13: Stepped Hull Prediction with 2D Wave Profile of Resistance/Weight of Configuration 2 at LCG=35%. The 2D wave profile slightly under predicted the resistance for all displacements

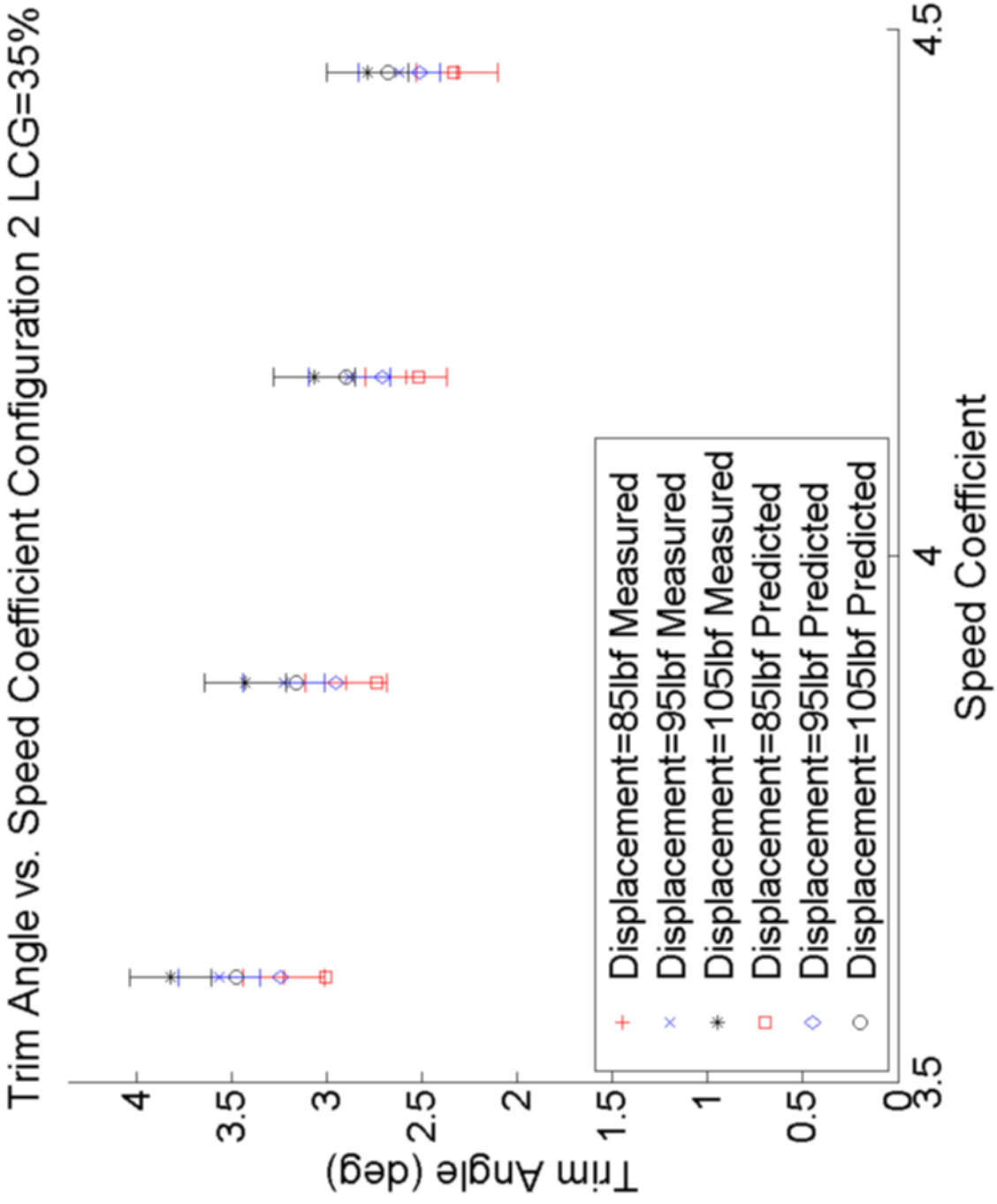

Figure 3.14: Stepped Hull Prediction with 2D Wave Profile of Trim Angle of Configuration 2 at LCG=35%. The 2D wave profile predicted the trim angle for all displacements within experimental error

For configuration 2 at LCG=35%, the average error in the resistance/weight was 8.60% and the error in the trim angle was 5.77%. The two dimension wave profile was more accurate in predicting the trim angle for configuration 2 than Savitsky's planing prediction method. The two dimension wave profile was slightly less accurate than Savitsky's planing prediction method in predicting the resistance. For all 180 conditions of the stepped hull tested in the model test, the average error in the resistance/weight was 12.63% and the error in the trim angle was 18.67%. The two dimension wave profile was about as accurate in predicting the resistance of the stepped hulls than Savitsky's planing prediction method for the unstepped hull.

Figure 3.15 shows the predicted wetted surface using the two dimension wave profile. The black lines represent the two steps. The blue line represents the stagnation line on the forward planing surface. The green line represents the reattachment line on the middle planing surface. The red line represents the reattachment line on the aft planing surface. The areas aft of the blue, green and red lines would be the portions of the hull that are wetted. Figure 3.1 shows a curved reattachment line on the middle planing surface in the model test. Figure 3.15 does not show this curved reattachment line because the two dimension wave profile is assumed to be linear in the transverse direction.

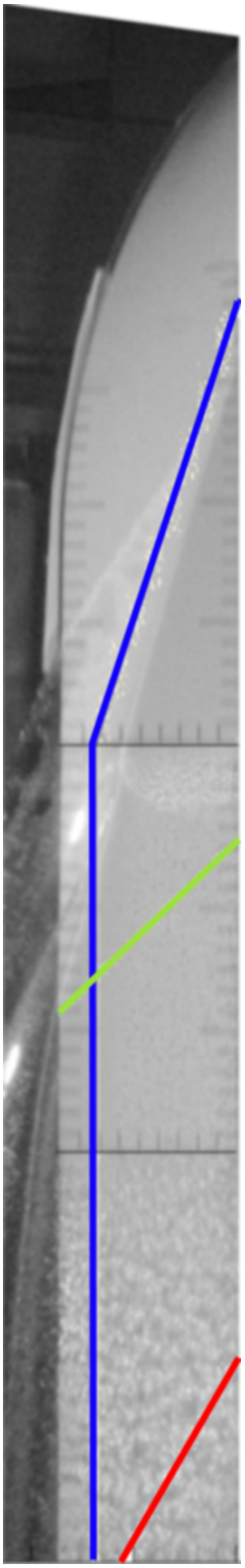

Figure 3.15: 2D Predicted Wetted Surface. Black lines represent the two steps. Blue line represents the stagnation line on the forward planing surface. Green line represents the reattachment line on the middle planing surface. Red line represents the reattachment line on the aft planing surface. The middle planing surface shows a straight reattachment line instead of a curved reattachment line as seen in the model test

3.2.4 3D Wave Profile

Configuration 2 at LCG 35% was compared to the stepped hull planing prediction method using the three dimension wave profile, Figures 3.16 and 3.17. The data is presented in a similar fashion to configuration 1. For configuration 2, the resistance was under predicted and the trim angle was predicted within experimental error. The resistance was more under predicted at high speeds. The form resistance is proportional to the tangent of the trim angle, therefore the good prediction of the trim angle would lead to a good prediction of the form resistance. Since the resistance is slightly under predicted and the form resistance is predicted well, like the two dimension wave profile, one can surmise that the friction drag is slightly under predicted.

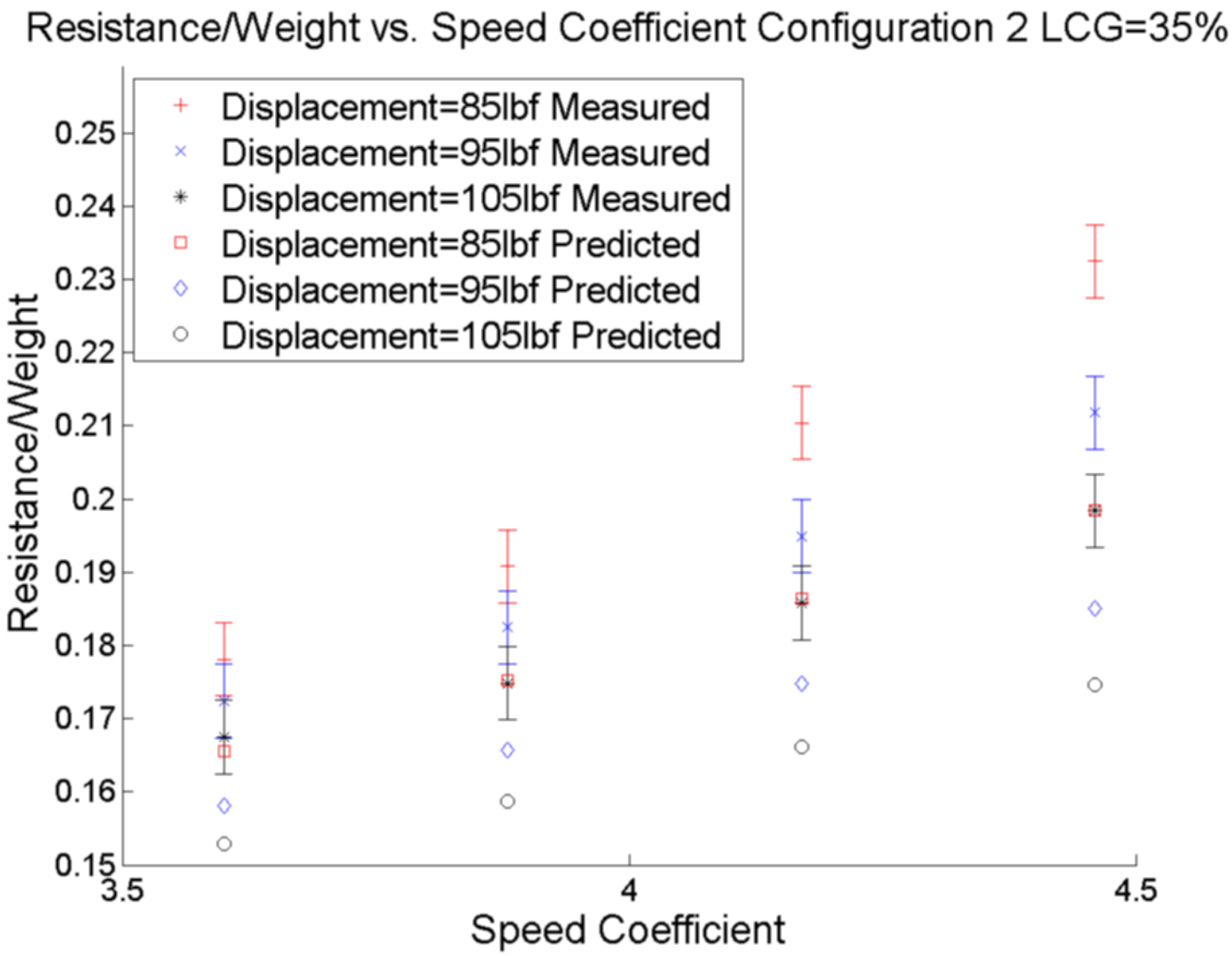

Figure 3.16: Stepped Hull Prediction with 3D Wave Profile of Resistance/Weight of Configuration 2 at LCG=35%. The 3D wave profile under predicted the resistance for all displacements

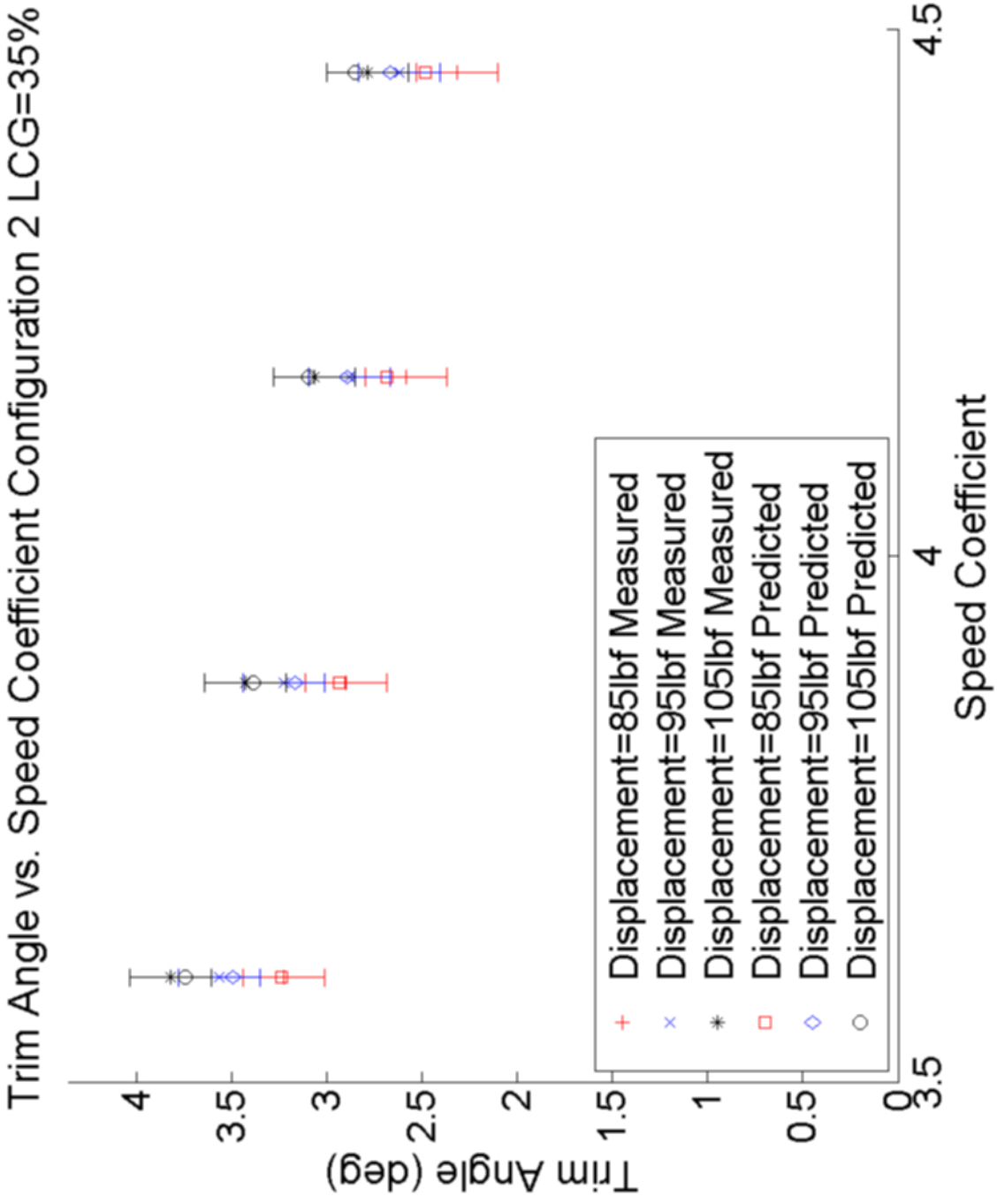

Figure 3.17: Stepped Hull Prediction with 3D Wave Profile of Trim Angle of Configuration 2 at LCG=35%. The 3D wave profile predicted the trim angle for most displacements within experimental error

For configuration 2 at LCG=35%, the average error in the resistance/weight was 10.18% and the error in the trim angle was 2.13%. The three dimension wave profile predicted the resistance and the trim angle better than Savitsky's planing prediction method for the unstepped hull. The three dimension wave profile predicted the trim angle better than the two dimension wave profile, but the three dimension wave profile was less accurate than the two dimension wave profile in predicting the resistance. For all 180 conditions of the stepped hull tested in the model test, the average error in the resistance/weight was 14.44% and the error in the trim angle was 15.43%. The three dimension wave profile was less accurate than the two dimension wave profile in predicting the resistance, but more accurate than the two dimension wave profile in predicting the trim angle.

Figure 3.18 shows the predicted wetted surface using the two dimension wave profile. The black lines represent the two steps. The blue line represents the stagnation line on the forward planing surface. The green line represents the reattachment line on the middle planing surface. The red line represents the reattachment line on the aft planing surface. The areas aft of the blue, green and red lines would be the portions of the hull that are wetted. The curved reattachment line on the middle planing surface is similar the the curved reattachment line seen in Figure 3.1.

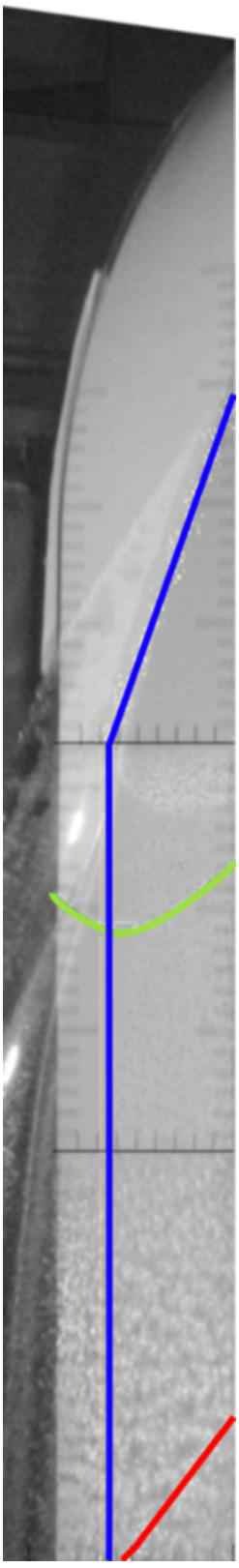

Figure 3.18: 3D Predicted Wetted Surface. Black lines represent the two steps. Blue line represents the stagnation line on the forward planing surface. Green line represents the reattachment line on the middle planing surface. Red line represents the reattachment line on the aft planing surface. The middle planing surface shows the curved reattachment line similar to the model test.

3.2.5 Parameter Sensitivity Study for 3D Wave Profile

When comparing Figure 3.18 to Figure 3.1 the predicted separated region for the middle step was much longer than seen in the model test. To reduce the separated region, the three dimension wave profile would have to be steeper. To understand the sensitivity of the stepped hull planing prediction method to the three dimension wave profile, the coefficients of the three dimension wave profile equation was multiplied by a coefficient factor ranging from 1.25-2.5 making the three dimension wave profile steeper. Values less than one were not selected because it would make the three dimension wave profile shallower.

The Korvin-Kroukovsky test data had an experimental error of 0.01 Beams [13]. Figure 3.19 shows the wave profile using the original three dimension equation at the quarter beam for the forward step of configuration 2. The hull is at the 35% LCG location, 85 lbf displacement and traveling at a speed coefficient of 4.46. The dashed lines show the upper and lower bound of the experimental error. The black line represents the small step height (0.125in, 0.007 Beams). The green line shows the wave profile with a coefficient factor of 1.5 and the red line shows the wave profile with a coefficient factor of 2.5.

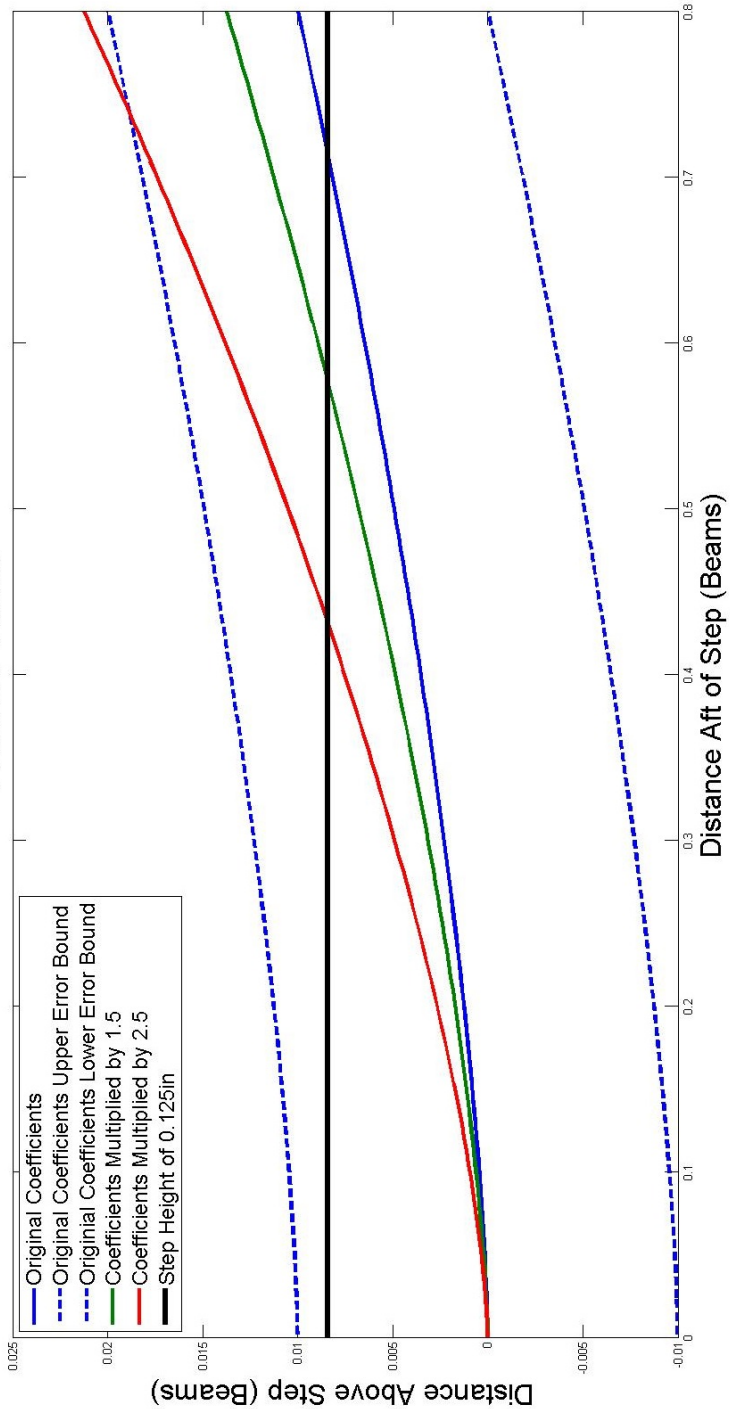

Figure 3.19: Wave Profile: The blue line shows the wave profile using the original equation at the quarter beam. The dashed lines show the upper and lower bound of the experimental error. The black line represents the small step height (0.125in, 0.007 Beams). The green line shows the wave profile with a coefficient factor of 1.5 and the red line shows the wave profile with a coefficient factor of 2.5.

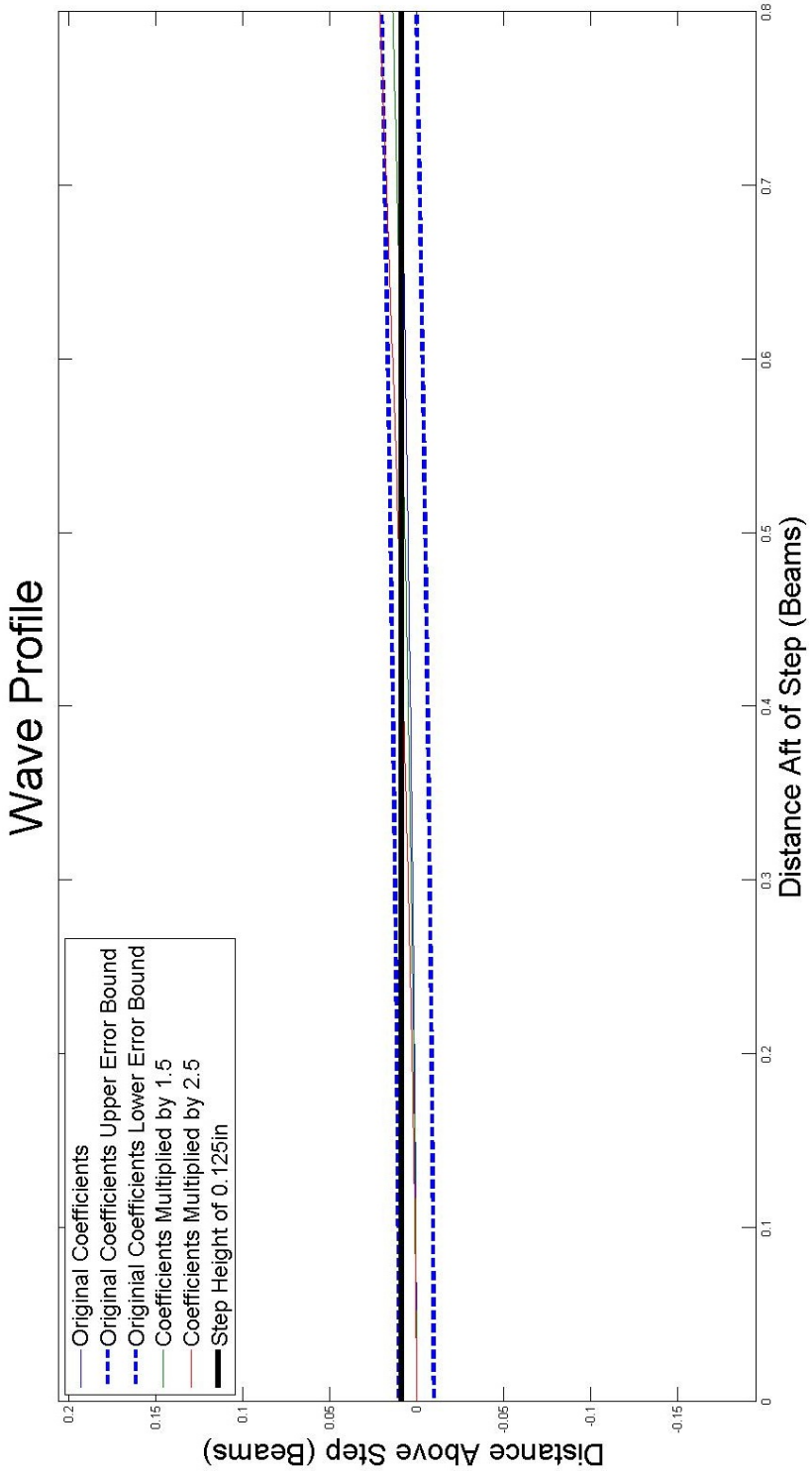

Figure 3.20: Wave Profile: The blue line shows the wave profile using the original equation at the quarter beam. The dashed lines show the upper and lower bound of the experimental error. The black line represents the small step height (0.125in, 0.007 Beams). The green line shows the wave profile with a coefficient factor of 1.5 and the red line shows the wave profile with a coefficient factor of 2.

Increasing the coefficient factor increases the wave profile height and reduces the reattachment length. Over the area of interest, the wave profiles with the coefficient factors fall within the experimental error. Figure 3.20 also shows the difficulty in measuring such small differences in the height of the wave profile.

Figure 3.21 shows the average percent error in resistance/weight for all 180 runs vs. the coefficient factor. As the coefficient factor increases, the error in resistance/weight reduces in a cubic fashion. Coefficient factors greater than about 2.25 have less error in resistance/weight than Savitsky's planing prediction method.

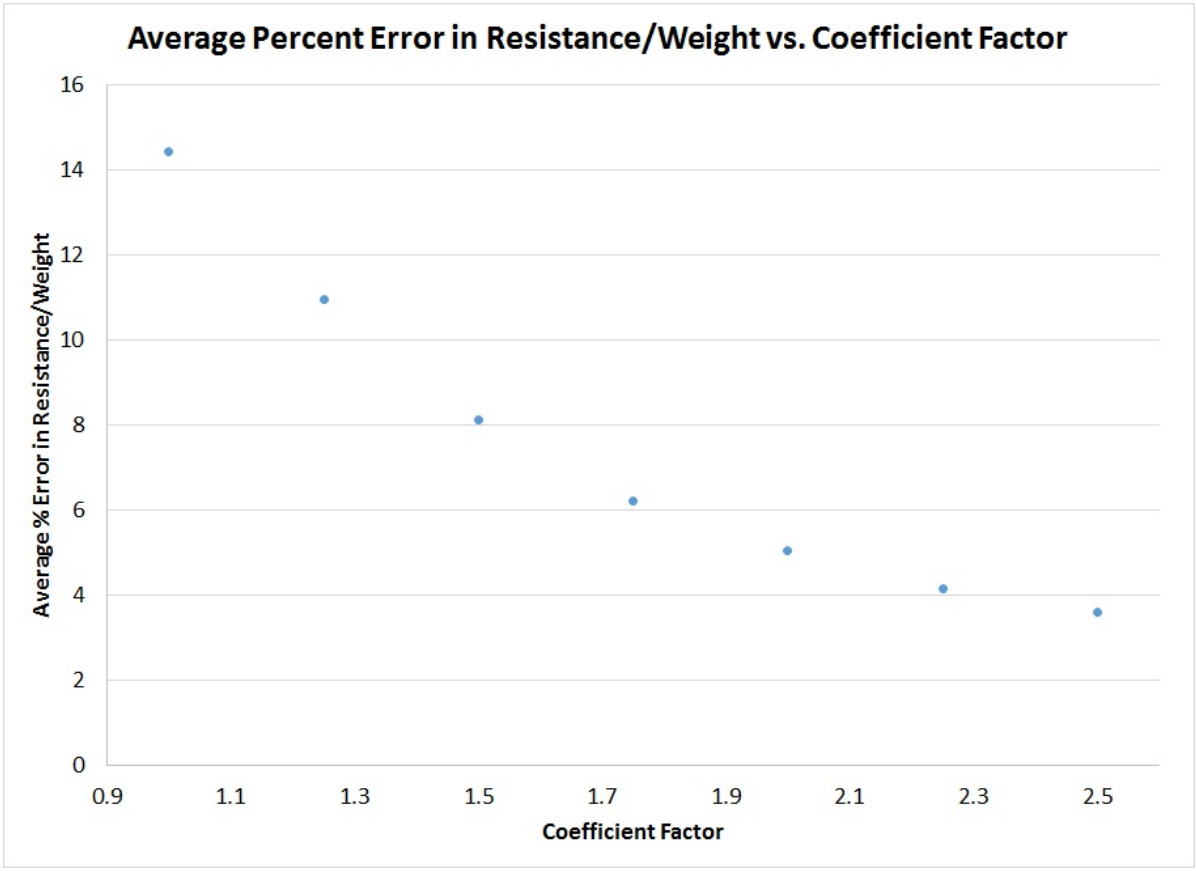

Figure 3.21: Average Percent Error in Resistance/Weight vs. Coefficient Factor: The error in resistance/weight reduces as the coefficient factor is increased. Coefficient factors greater than about 2 have less error in resistance than Savitsky's planing prediction method.

Figure 3.22 shows the average percent error in trim for all 180 runs vs. the coefficient factor. As the coefficient factor increases, the error in trim angle reduces rapidly and asymptotes to about 7% error. Coefficient factors greater than about 1.5 have less error in trim than Savitsky's planing prediction method.

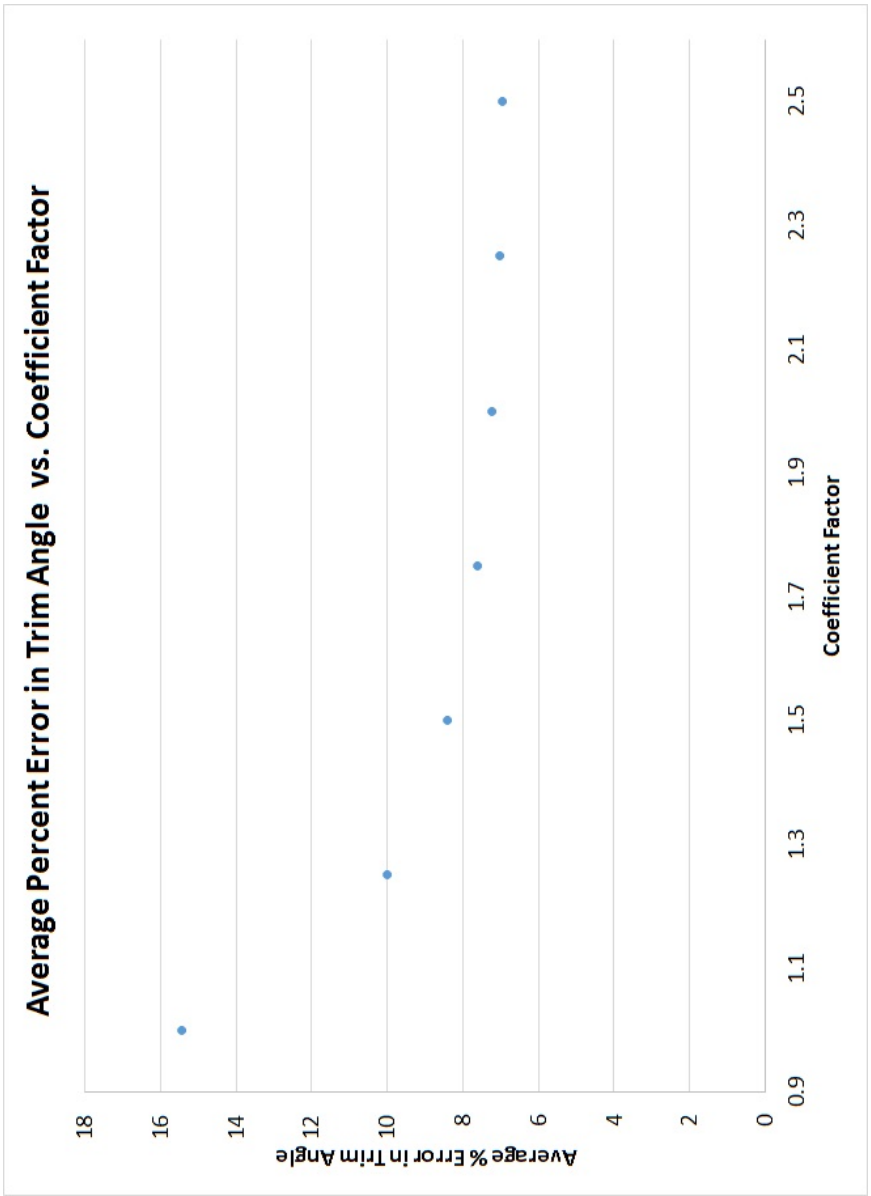

Figure 3.22: Average Percent Error in Trim vs. Coefficient Factor: The error in trim angle reduces as the coefficient factor is increased. Coefficient factors greater than about 1.25 have less error in trim angle than Savitsky's planing prediction method.

The stepped hull planing prediction method using a coefficient factor of 2.5 is shown here for configuration 2 at LCG 35%, Figures 3.23 and 3.24. For configuration 2, the resistance was predicted within experimental error for most displacements and the trim angle was predicted within experimental error for all displacements. The form resistance is proportional to the tangent of the trim angle, therefore the good prediction of the trim angle would lead to a good prediction of the form resistance. Since the resistance and the form resistance is predicted well, one can surmise that the friction drag is also predicted well.

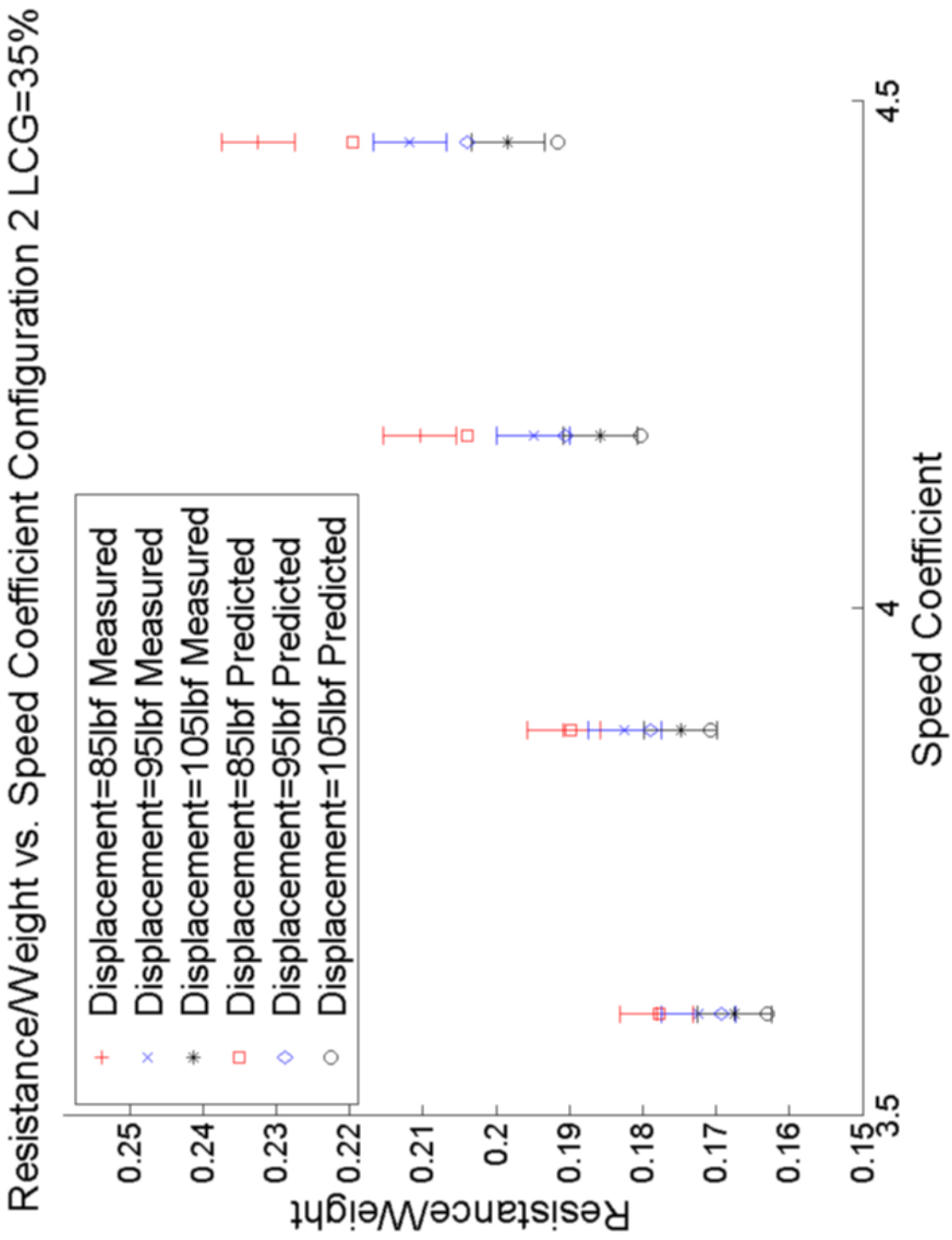

Figure 3.23: Stepped Hull Prediction with Modified 3D Wave Profile of Resistance/Weight of Configuration 2 at LCG=35%. The Modified 3D wave profile predicted the resistance for most displacements within experimental error

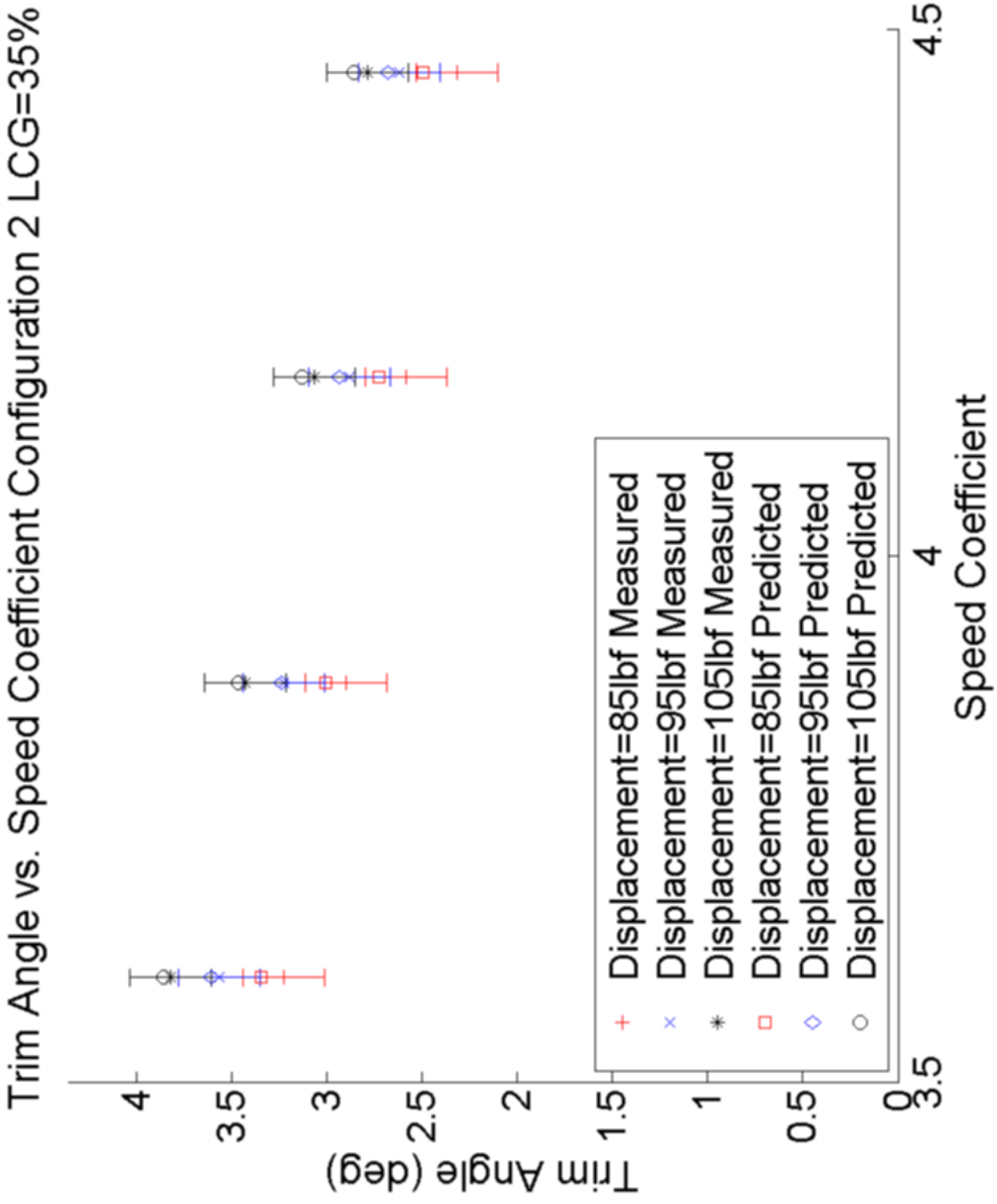

Figure 3.24: Stepped Hull Prediction with Modified 3D Wave Profile of Trim Angle of Configuration 2 at LCG=35%. The 3D wave profile predicted the trim angle for all displacements within experimental error

For configuration 2 at LCG=35%, the average error in the resistance/weight was 4.14% and the error in the trim angle was 1.61%. The modified three dimension wave profile predicted the resistance and trim angle better than all the other prediction methods. For all 180 conditions of the stepped hull tested in the model test, the average error in the resistance/weight was 3.60% and the error in the trim angle was 6.96%. The modified 3D wave profile was more accurate than Savitsky's planing prediction method for predicting the resistance and trim angle.

3.3 Discussion

3.3.1 Savitsky

The Savitsky planing prediction method predicted the results for the stepped hull better than the unstepped hull. The Savitsky planing prediction method consistently under predicted the resistance for the 24 conditions of the unstepped hull. For the 12 runs at the LCG=35% condition, the trim was over predicted and for the 12 runs at the LCG=40% condition, the trim was over predicted.

3.3.2 3D Wave Profile

A single simple closed form physics based empirical equation has been developed to predict the three dimension wave profile aft of a transom or step. The equation has been developed so that the empirical coefficients can be recalculated when new and more accurate test data becomes available. The current equation captures the curvature of the reattachment point seen in the underwater photography from the model test as seen in Figure 3.18. The sensitivity analysis of the coefficients show that a small change in the coefficients can have a large effect on the predicted results. The three dimension wave profile led to a more accurate prediction of the trim angle than the two dimension wave profile. The modified three dimension wave profile showed improvements in the prediction of both the resistance and the trim angle. Figure 3.18 also shows that the predicted reattachment line is further aft than as seen in the experiments. The current coefficients predict the performance of the stepped hull reasonably well, but further research is needed to develop a better three dimension wave profile.

3.3.3 Prediction Method

A number of new features have been added to the existing stepped planing hull prediction methods. First, it utilizes a 3D wave profile for determining the reattachment of the flow aft of each step. Second, this method accounts for the stagnation line crossing the step, thus improving the applicability of this method. This method allows for the stagnation line to cross all of the steps and the transom. Third, this method can be used for an infinite number of steps. Lastly, this method calculates the lift on all the planing surfaces. In previous methods, the lift generated on the planing surface aft of the step was assumed to be the lift that was not being supported by the forward planing surface.

3.3.4 Usage

The stepped planing hull prediction method takes about 1-2 minutes to calculate the prediction for one condition. Since there are fewer calculations, Savitsky's planing prediction method is even faster. Savitsky's planing prediction method can be used for initial preliminary design work. The stepped planing hull prediction method can then be used for further preliminary studies. The stepped planing hull prediction method is another tool for the Naval Architect to predict the performance of stepped planing hulls.

3.4 Recommendations for Future Work

Advancements in sensor technologies has allowed for a number of different methods to more accurately measure the 3D wave profile aft of the step. A new series of tests based on stepped planing hull conditions utilizing the new technologies will provide a better model of he 3D wave profile to use in the stepped planing hull prediction method.

A test understanding the interactions between multiple planing surfaces should be conducted. Instead of having one complete model with multiple steps attached to a single heave post, a test should be conducted with each planing surface attached to its own heave post. This would allow for each of the planing surfaces to be fixed in heave and trim and the lift, resistance and moment on each of the planing surfaces can be measured independently. The model can be run at a number of step configurations, drafts, trim angles and speed. If possible, the pressure distribution on each planing surface can be found and this will help better understand the lift on the aft planing surfaces. This test would also allow for the examination of the assumption that the pressure in the separated zone is indeed atmospheric. It will also show how the turbulent and sometimes bubbly flow can effect the lift on the aft

planing surfaces.

Chapter 4

Numerical Methods

4.1 Introduction

The addition of a step increases the complexity of the simulation of a planing hull. Both the model test and the prediction methods show that the separated flow at the step has a large influence on the overall performance of a stepped planing hull.

Using numerical tools for engineering and design is much different than for research applications. There is a limited amount of time and resources available for numerical simulation in engineering and design. In pure research, one my be able use a large cluster with thousands of cores and run the simulation for a number of weeks. In design, the user may only have access to a few processors due to cost constraints and a week to complete a simulation due to time constraints. While some engineering firms have in-house Computational Fluid Dynamics (CFD) experts, there are other small craft firms that do not have this capability. For these smaller firms, the user of numerical tools for engineering and design may be an engineer who is not a CFD expert. Therefore the meshing, setup and execution of the numerical tool needs to be intuitive so that someone not using the tool all the time can effectively use the tool without having to relearn the the tool every time.

The current research compares two different numerical tools; Numerical Flow Analysis (NFA) and OpenFOAM (Open source Field Operation And Manipulation) for the engineering and detailed hull form design of stepped planing hulls. The comparison assess the modeling gaps and computational constraints in current state of the art numerical simulation tools when analyzing stepped planing hulls. One specific area of interest is each tool's ability to accurately capture the separated flow off of the step.

Configuration 4, with the small step forward and the large step aft, from the model test, discussed in Chapter 2, was selected as the step configuration to be used in the numerical comparison. It was selected because it had the lowest resistance of the conditions tested at the forward LCG location and it was tested at both LCG locations. The small step height forward is a good geometric feature to determine each tool's ability to handle very small features. Multiple test conditions of configuration 4 in the free to pitch and heave condition are tested to determine the resistance and the trim angle of the hull.

The simulations were run with the model free to pitch and heave. The motion of a planing hull from rest to its running condition is highly dynamic. The hull will rise out of the water as the hull is support by hydrodynamic lift and the trim angle will increase during hump speeds and decrease again at planing speeds. Most displacement hulls usually can be run in fixed pitch and heave conditions because the change in the pitch and heave from rest to the running condition is minimal. In the design process, the numerical simulation would often be conducted either before model tests or at different conditions than the model test. Therefore, the running trim angle and draft of the hull is not usually known to run fixed heave and trim simulations.

4.2 Volume of Fluid Method

The volume of fluid (VOF) method is one of two popular methods for describing the free surface to simulate boats and ships within an Eularian grid based representation of the domain[34]. The other method is called the level set method (LSM). Both NFA and OpenFOAM use the VOF method for interface capturing. The VOF method defines a function α, whose value is one at any cell occupied by the fluid; in the case of boats, water [34]. A cell whose value of α is zero would mean that it contains no water and in the case for boats, contains only air. The cells which have a value of α between zero and one contains a mixture of air and water. The air and water interface, free surface for the case of boats, is often defined as an interpolated surface of $\alpha = 0.5$, but can be defined as any fraction between zero and one. The material properties in a cell is defined by averaging the values of the two phases, water and air by the volume fraction α. Equation (4.1) shows how density is calculated in the VOF method. There are also different schemes that work with the VOF advection equations to sharpen the air and water interface, which in the case for boats is the free surface.

$$\rho = \alpha_{water}\rho_{water} + (1 - \alpha_{water})\rho_{air} \tag{4.1}$$

4.3 NFA

4.3.1 Theory

NFA, developed by LEIDOS; formerly SAIC, is a code that was designed as a numerical code to easily model free surface flows. Whereas other numerical tools can solve a wide range of fluids problems, NFA focuses primarily on free surface flows. NFA uses a Large Eddy Simulation (LES) based Cartesian-grid formulation with immersed-boundary (IBM) and VOF methods. A no-slip boundary condition is imposed on the hull, sides and inlet [35]. There is no sub grid turbulence model within the LES simulation [35]. The friction force on the hull is not directly calculated but calculated separately using the wetted surface area determined by the simulation, the overall length of the hull, and the ITTC '57 flat plate approximation. An open boundary condition that is similar to the one specified by Orlanski [36] allows the waves within the domain to pass through the boundary without distortion and reflecting the wave back into the domain. This allows for much shorter domain lengths and reduced computation times. With other numerical tools, the domain has to be long enough so that the waves have dissipated and returned to the calm water level within the domain. To ensure stability, the density as a function of the volume fraction is smoothed by a three-point stencil applied along each axis [37]. Table 4.1 shows the numerical schemes used by NFA.

Table 4.1: NFA Numerical Schemes

Scheme	Type
Momentum Equation	QUICK
Time Integration	Second-Order Runge-Kutta
Volume of Fluid	PLIC

4.3.2 Case Setup

In preparation for meshing, a number of steps need to be completed before the hull can be read into NFA. The hull was exported from Solidworks [24] as an Initial Graphics Exchange Specification (IGES) file which allows for the hull to be imported into other Computer Aided Design (CAD) and Meshing tools. The hull was imported into Rhinoceros 3D (Rhino) [38] to develop the hull surface grid. The hull surface was discretized into 15,000 triangular panels. The panelized hull surface was then exported in the Polygon File Format (PLY) to be used by NFA.

NFA uses an in-house developed Matlab Graphical User Interface (GUI) to facilitate the case setup. The GUI is used to generate the text file that contains all of the inputs for a NFA

simulation. This file is also editable using a standard text editor instead of the GUI. Figure 4.1 shows the main screen that allows for the user to edit a variety of basic parameters. First, the overall number of cells within the domain are determined as seen in the upper right corner of Figure 4.1. The overall number of cells is defined by the number of processors and the number of cells per processor in each direction. The overall number of cells is determined in a number of steps. First, the number of processors in each direction is defined. Second, the number of cells per processors is definied. This process is repeated for the x, y, and z directions. The total number of cells is the product of the number of processors and the number of cells per processors to determine the number of cells in each direction. The three directions are multiplied together to get the total number of cells. The number of time steps and the time step size are defined. The GUI gives the user a suggested time step size based on the requirement that the Courant number be less than 0.5. The hull velocity and hull length overall are also defined as dimensional parameters. In the output tab, the parameters for saving the simulation and outputting data are set. A suggested interval for outputting data is given so that the data can be made into a video. The grid tab allows the user to define the grid. The distribution of cells is controlled by elliptic equations. The user designates zones of constant grid density in each direction and gives a weighting factor to determine the grid density in that zone. Between the zones, the cells are stretched to match the size of the cells in the two adjacent zones. The user can designate any number of these zones as long as it does not violate the elliptic equations. The cells are automatically cut to fit around the hull. The aspect ratio and percent stretching can be reported. The developer stresses the importance of the aspect ratio of the cells being one near the hull to achieve the best results. In the motions tab, the mass, center of gravity, and moment of inertia is defined. NFA also allows for an initial hull offset or velocity. The flow velocity and direction are defined in the current tab. The flow tab allows for the definition of the free surface and the boundary conditions. Linear or pressure forcing waves can be added using the waves tab. The frequency of numerical smoothing is entered in the smoothing tab as the simulation time between each application of the smoothing function. The suggested time interval is 0.1 units of non-dimensional time.

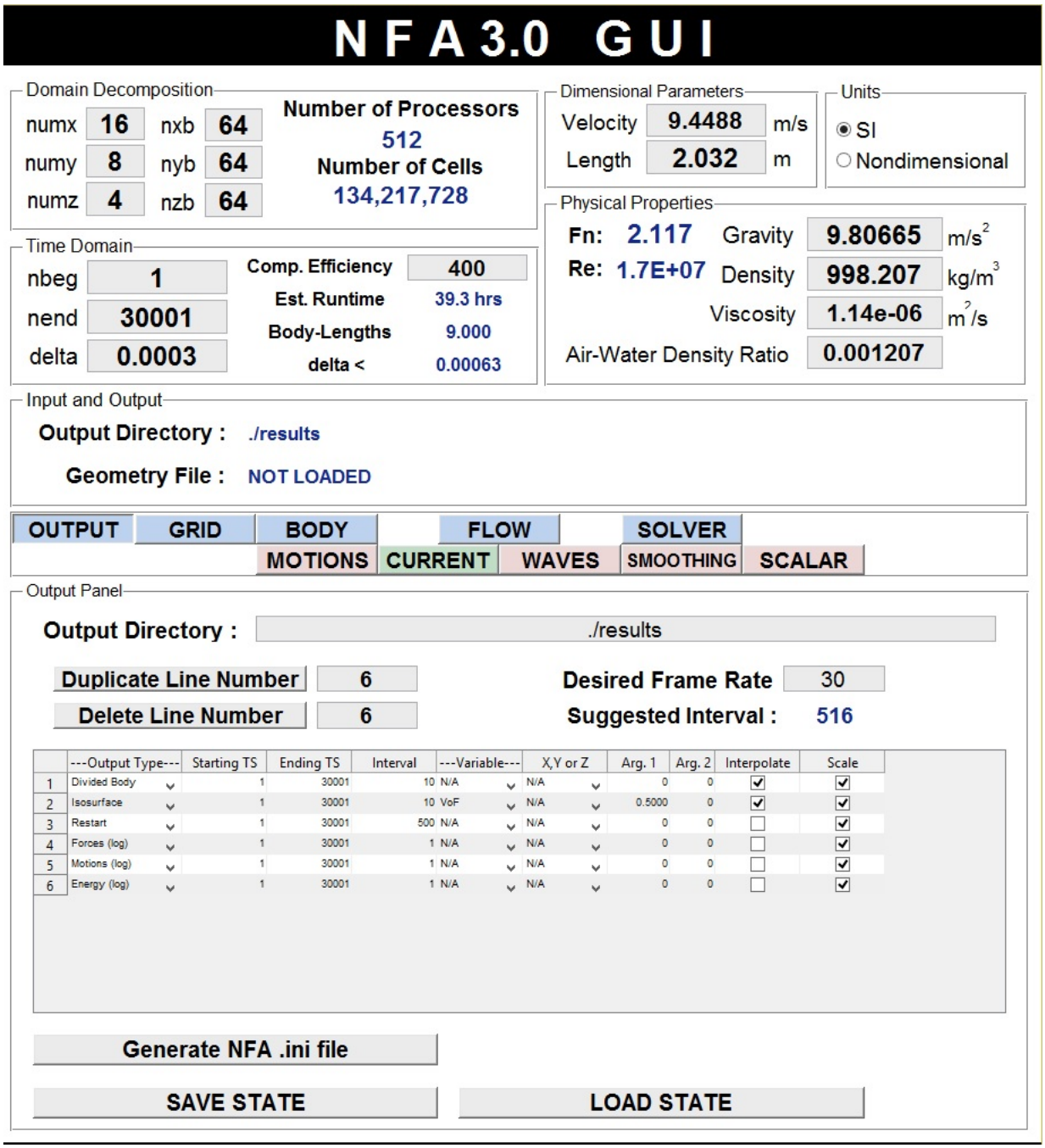

Figure 4.1: NFA GUI: Simple user interface built from Matlab

4.3.3 Mesh

The domain is 3.5 boat lengths long with one boat lengths upstream of the hull and 1.5 boat lengths downstream of the hull. The domain is two boat lengths wide and two boat lengths tall.

Figures 4.2 to 4.4 shows the 134 million cell mesh. Figure 4.2 shows the mesh at the centerline. Figure. 4.3 shows the mesh at the centerline with the number of cells shown cut in one-fifth for so that the hull can be seen within the mesh. Figure 4.4 shows the mesh at the small forward step.

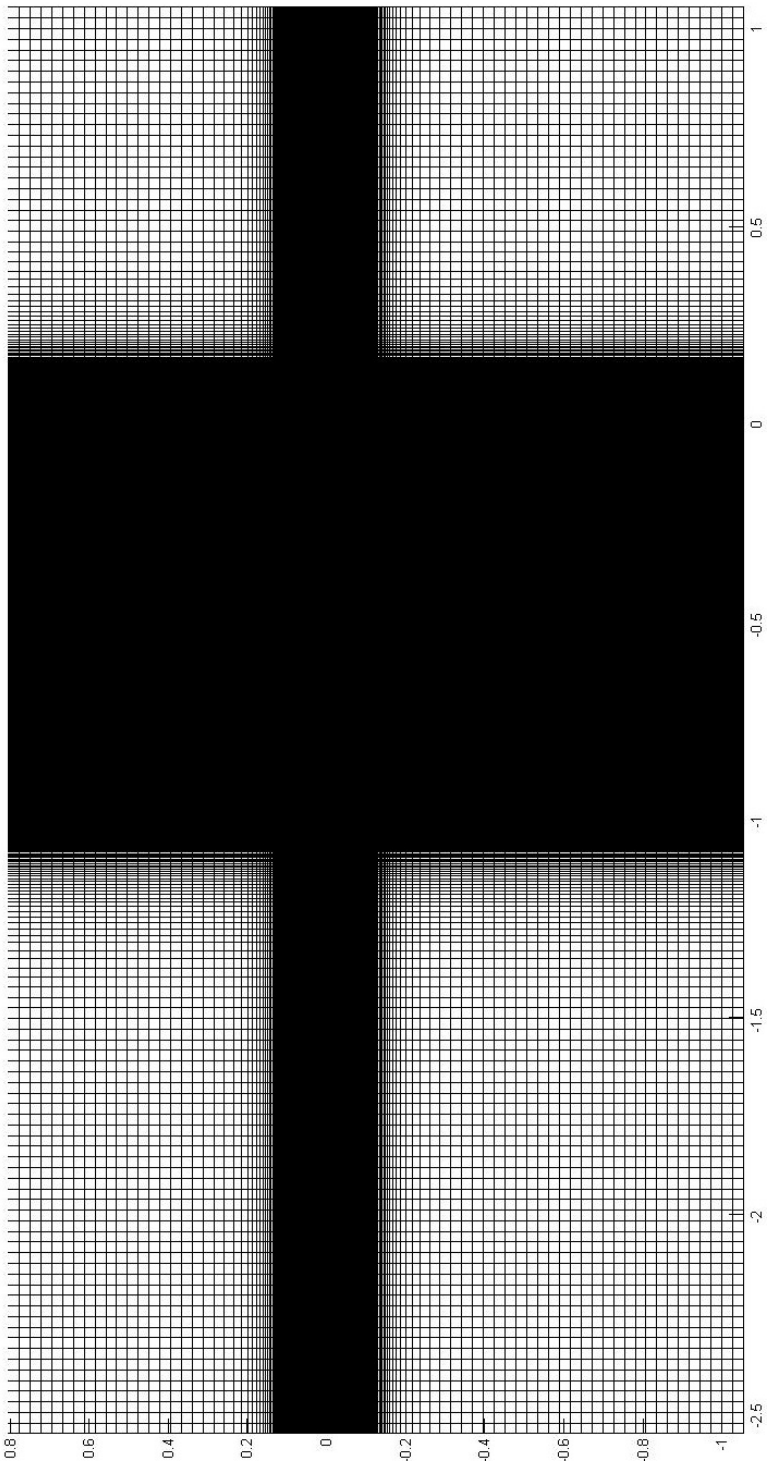

Figure 4.2: Mesh at Centerline.

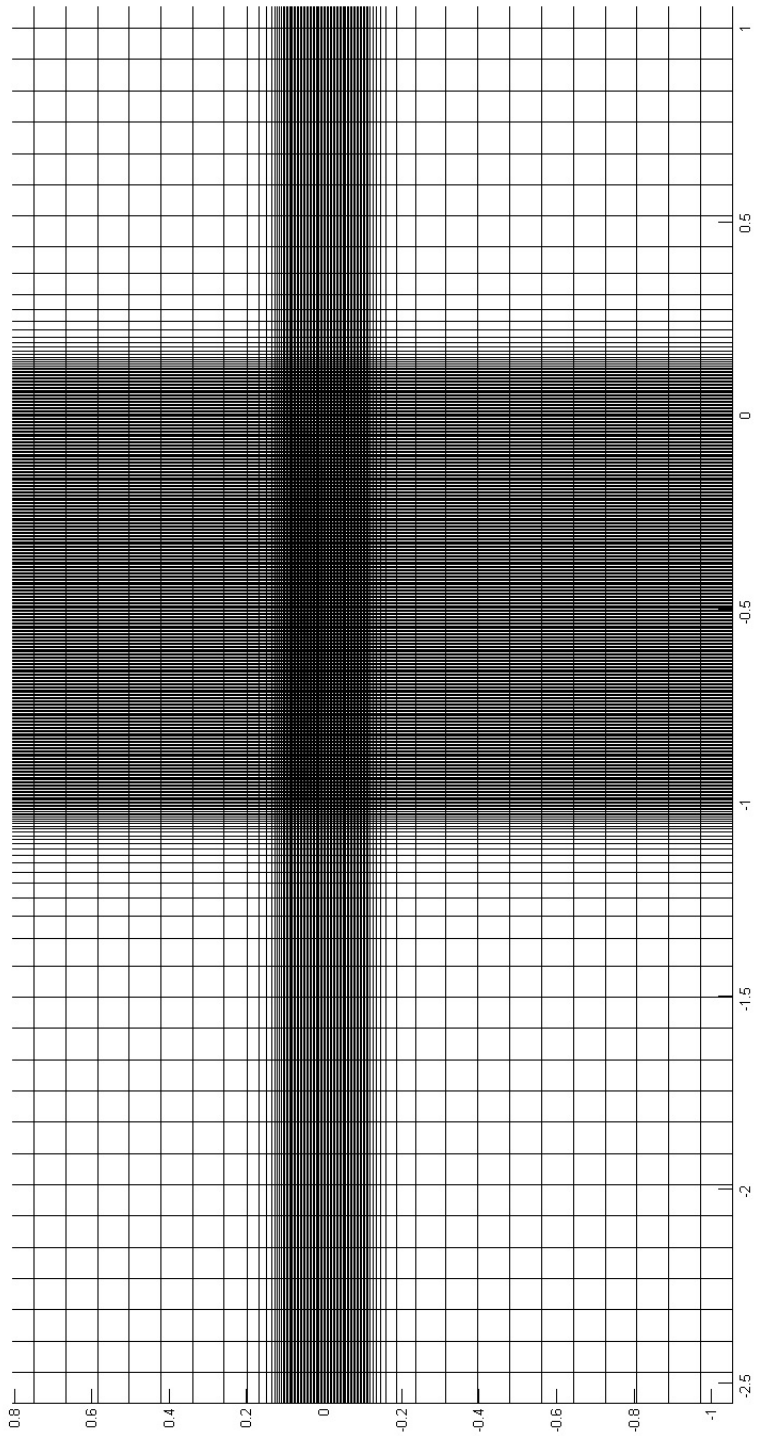

Figure 4.3: Mesh at Centerline showing one-fifth the number of cells for so that the hull can be seen within the mesh.

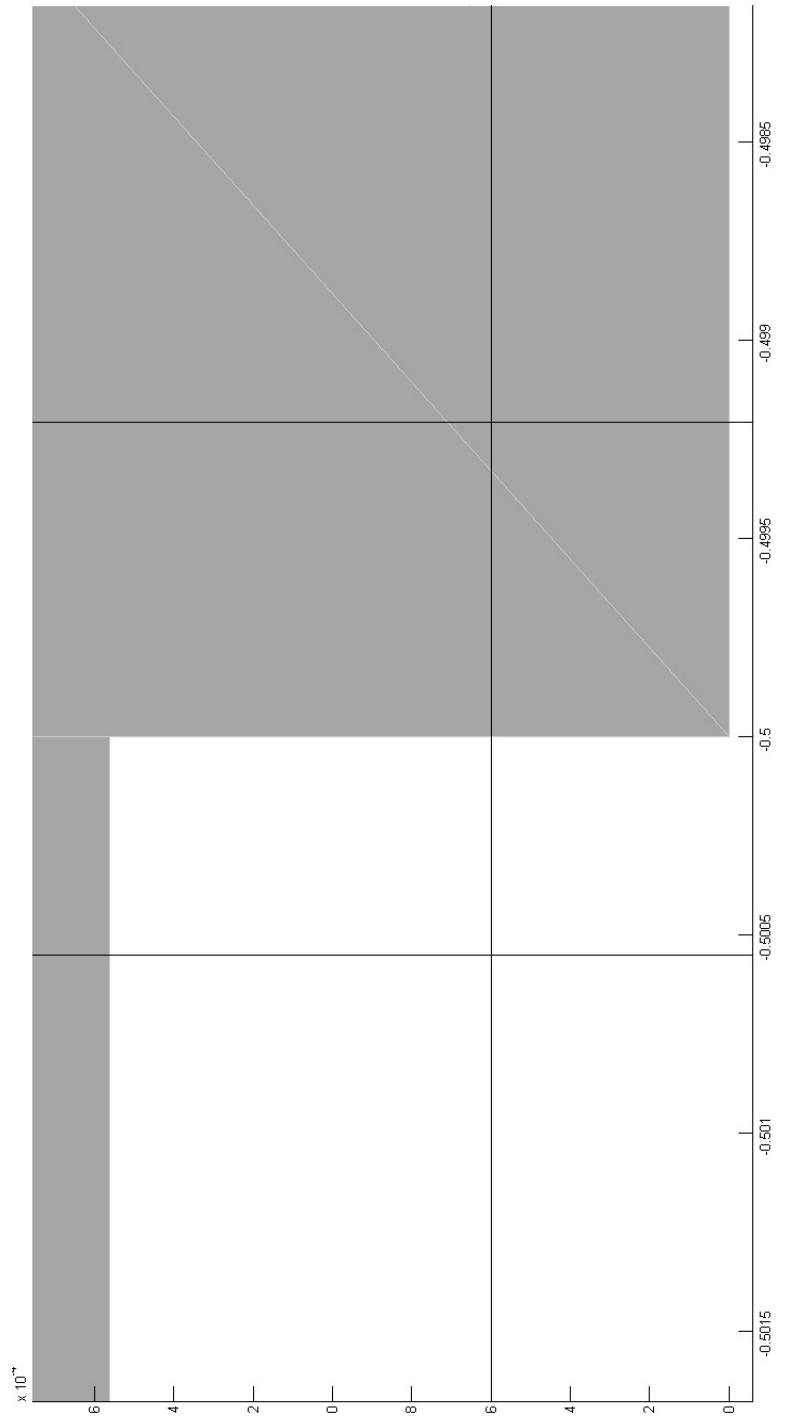

Figure 4.4: Mesh at the small forward step. Few cells across step.

4.3.4 Grid Convergence

The simulation was run with three different grid sizes from about 16 million cells to about 134 million cells. Figure 4.5 shows the resistance as the number cells increases. Figure 4.6 shows the trim angle as the number of cells increases. The grid size was changed by changing the number of cells in each direction. The medium, 57 million cell mesh, is 1.5 times the number of cells in each direction than the small, 16 million cell mesh. The large, 134 million cell mesh, is 2 times the number of cells in each direction than the small, 16 million cell mesh.

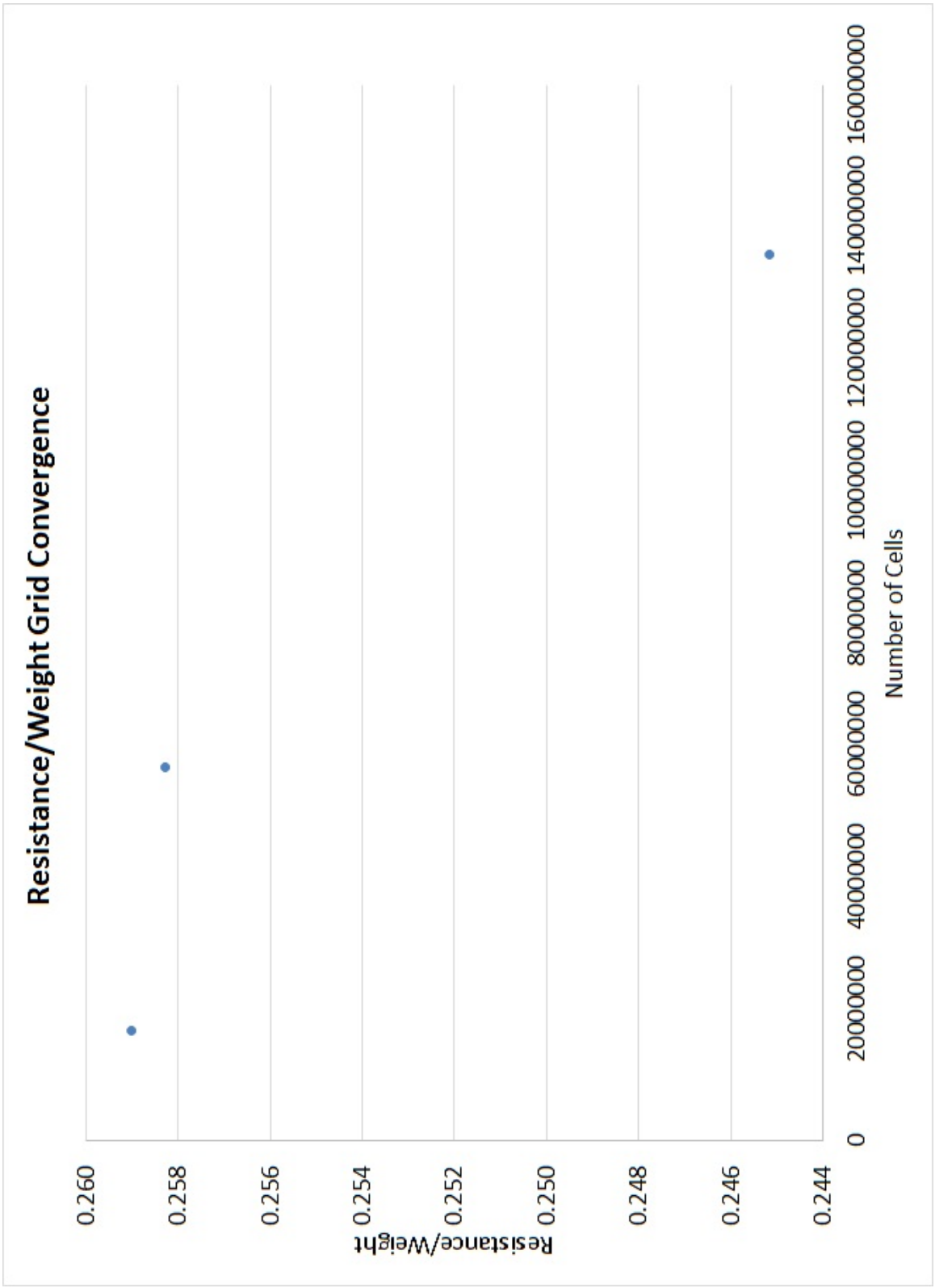

Figure 4.5: Resistance/Weight Grid Convergence: Resistance/Weight as number of cells increases

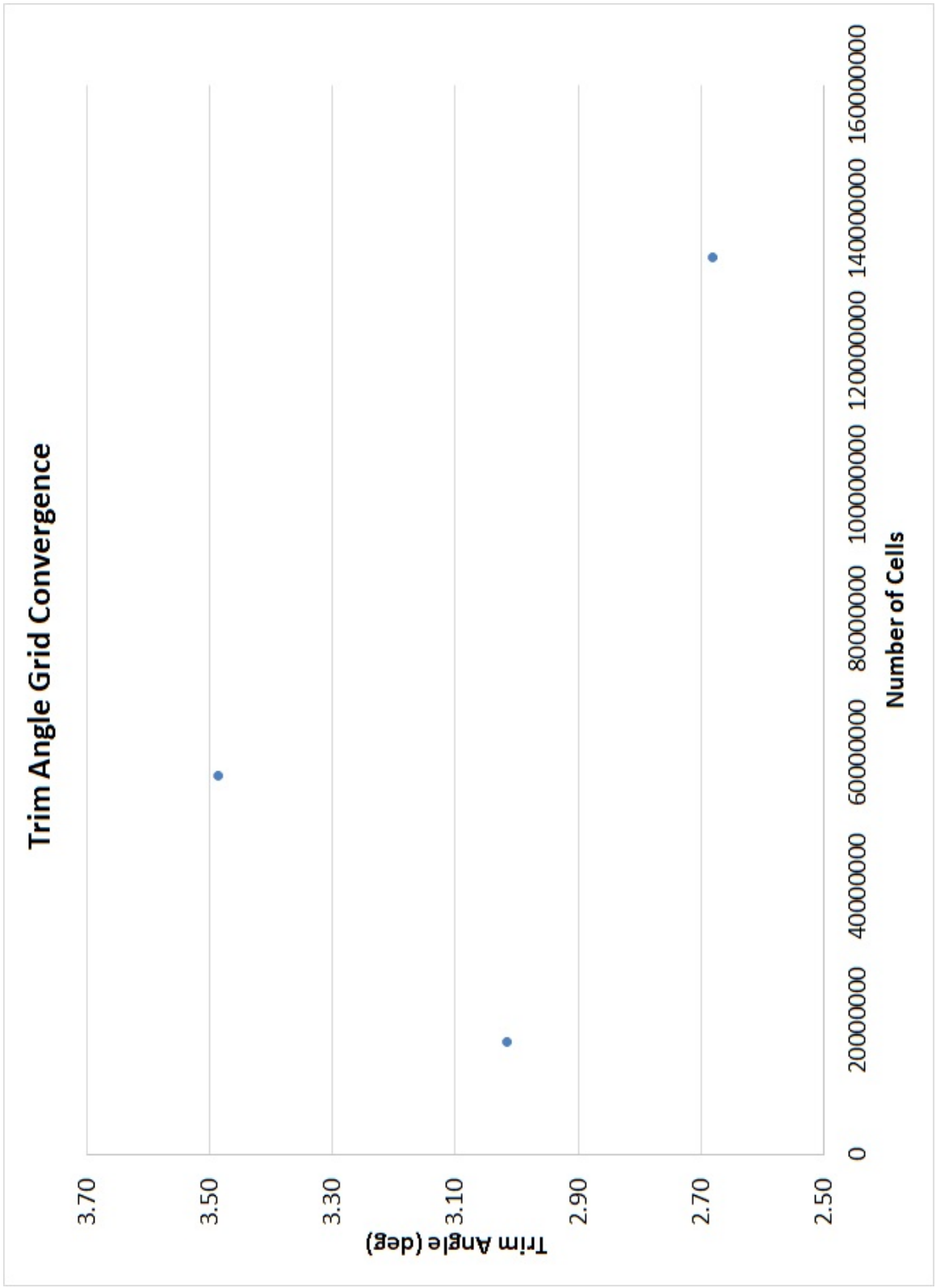

Figure 4.6: Trim Angle Grid Convergence: Trim angle as number of cells increases

Both the resistance and the trim angle did not converge over the grids tested. The lack of convergence calls into question the validity of the results obtained on these grids. The 134 million cell grid was selected for further simulations becuase it was the largest grid that could be simulated within the computational constraints.

4.3.5 Simulation Scalability

The scalability of NFA has been previously tested on the United States High Performance Computing Center. The number of iterations per hour scales with a scaling coefficient of 0.87 to number of processors [39]. As a result, there is nearly a direct trade off between the number of processors and simulation time. Therefore for a given number of cells in a simulation with a constant number of core hours for computation, a larger number of processors can be used with fewer cells per processor to run the simulation quickly or fewer processors can be used to run the simulation for a longer period of time. When using NFA for simulations, there is a balance between simulation speed and processor availability. One is more likely to get a simulation run sooner in a queue with a fewer number of processors, but it would take longer for the simulation to complete.

4.3.6 Simulation Speed

The NFA simulations in this study were run for about 7 seconds of run time at a total of about 25000 core hours on the U.S. Army Engineer Research and Development Center Cray XE6 cluster Garnet [40]. The simulations were either run at 1024 cores for 24 hours or 512 cores for 48 hours depending on processor availability. Based on availability, three or four cases were able to be run simultaneously. The grid size selected provided quick simulation turn around times and allowed for multiple runs to simulated at the same time despite not converging. Therefore, the grid size selected is representative of a grid that would be used for planing hull design.

4.4 OpenFOAM

4.4.1 Theory

OpenFOAM was first developed by Weller et al. in 1998 [41]. The objective of OpenFOAM is to use the tools in the C++ programming language and develop a C++ class library where mathematical and physical models are implemented as high-level mathematical equations [42]. OpenFOAM also utilizes object-oriented programming to allow users to easily

write new solvers within the existing framework. InterDyMFoam, one of the built in solvers, was used for the simulations. InterFoam is OpenFOAM's incompressible two phase solver using VOF method for interface capturing. InterDyMFoam is the dynamic mesh motion version of interFoam. The Reynold's Averaged Navier-Stokes (RANS) solver with the k-ω turbulence model was used for the simulation. The weight of the hull, the center of gravity, and the mass moment of inertia are defined and the motion of hull is solved. OpenFOAM uses multi-dimensional limiter for explicit solutions (MULES) to guarantee the boundedness of the volume fraction[42]. Since MULES is an explicit formulation, the time step is limited due to the Courant number limit [42].

In OpenFOAM 2.3, there are a number of improvements that enhances OpenFOAM's ability to simulate a stepped planning hull. First, a semi-implicit version of MULES was created by applying the MULES limiter to an explicit field rather than the whole domain [42]. The new version of MULES still guarantees boundedness at large Courant numbers [42]. Next, a new solver was developed for rigid body motion that uses a spherical linear interpolation method (Slerp) which enforces smoothness and a cosine profile distance function to maintain the shape of the cells close to the moving surface [42]. The old motion solvers used an elliptic equation that had a tendency to shear the cells [42]. As part of this mesh motion, a new boundary condition was added to calculate rigid body motion. Unlike previous versions, the motion can be constrained in any of the six degrees of freedom. Mesh morphing was chosen over moving reference frame to better capture the free surface. When using moving reference frame, as the whole domain rotates, the incoming free surface is still horizontal and now the domain is not and the free surface is crossing cells at a non-orthongal angle which causes diffusivity of the free surface. Wth the mesh morphing, the cells far from the hull are still orthogonal to the free-surface and only a few number of cells are distorted closer to the hull when it is moving. This ensures a more well defined free surface.

Table 4.2 shows the numerical schemes used for the simulation [43].

Table 4.2: OpenFOAM Numerical Schemes

Scheme	Type
$\frac{\partial}{\partial t}$ Schemes	Euler
$\bigtriangledown$ Schemes	Gauss Linear
$(\bigtriangledown * (\rho UU))$ Schemes	Gauss linearUpwind
$(\bigtriangledown * (U\alpha))$ Schemes	Gauss vanLeer
$(\bigtriangledown * (U_{rb}\alpha_1))$ Schemes	Gauss linear
$(\bigtriangledown * (Uk))$ Schemes	Gauss linearUpwind
$(\bigtriangledown * (U\omega))$ Schemes	Gauss linearUpwind
$(\bigtriangledown * ((\mu_{Eff} * dev(T(\bigtriangledown U)))))$ Schemes	Gauss linear
$\bigtriangledown * (\nu \bigtriangledown U)$ Schemes	Gauss Linear corrected
Interpolation Schemes	Linear
snGradSchemes	corrected
fluxRequired	no

4.4.2 Meshing Tools

Three different meshing tools were examined to generate meshes in OpenFOAM; Pointwise, Boxer, and snappyHexMesh.

Pointwise

Pointwise [44] is a detailed commercial meshing tool that generates both structured hexahedral and unstructured tetrahedral meshes with good user control. The tool is a hybrid of user input building the mesh and automatic meshing. The mesh is built from the hull out to the boundaries. First, the hull is imported as an IGES file. The edges of the hulls are converted to connectors. The number of cells on each connector (edge) are defined by the user. The distribution of the cells are controlled by an elliptic equation and are defined by the cell size on the ends of the connectors. The face meshes in Pointwise are called domains. To create hexahedral face meshes, the domains can consist of more than four connectors, but there must be the same number of cells on opposite edges of the quadrilateral domain. The face mesh is automatically generated by Pointwise and the face mesh might not always be as square as expected. To fix the face mesh, the automatic grid solver can be used to realign the points within the face mesh to generate a more uniform hexahedral mesh. The grid solver has difficulty in solving the grid when the size of the grid is extremely small. If the face mesh is not what is expected and the grid solver does not rectify the problem, there is no further solutions to fix the mesh. Once the face mesh is completed, the face meshes can be extruded to create the volume meshes. A connector is generated in the direction that the face mesh is to be extruded. The cells on the connector are used to define the height of the cells. The face meshes are extruded automatically to create the volume mesh. Since the

extrusion of some of the face meshes does not terminate at a plane, the volume mesh may be stretched by projecting the face mesh to a plane. The generation of the volume mesh is continued until the domain is created. The boundary conditions are set by selecting the outer faces of the domain and assigning the proper boundary condition.

The edge meshing tools allows Pointwise to minimize cell count by accurately growing the cells as defined by the user. The errors in the automatic meshing is problematic and increases meshing time as alternative meshing methods are sought. The overall time required to generate these meshes when compared to Boxer and snappyHexMesh does not promote its use for generating meshes for design iterations. Since each mesh is built from the hull outward to the entire domain, a complete new mesh has to be built for each new hull to be tested.

Boxer

Boxer[45] is a commercial, interactive, and automatic meshing tool that develops hexagonal meshes [45]. Boxer allows for cell refinement and prism layers. To generate the mesh, the hull is imported as an IGES file. The extent of the domain is defined and the initial grid size is set. Regions with finer grids also can be defined. A prism layer on the hull can be defined to capture the boundary layer. Once all the parameters are defined, the mesh is then automatically built. The only drawback of this meshing tool is that the domain grid is made of cubes. There is no allowance for stretching of the cells in the far field. This increases the number of cells used in the domain as extra cells are used in the far field where there is no significant flow physics occuring.

snappyHexMesh

SnappyHexMesh [42] is the free advanced automatic meshing tool that is built into OpenFOAM. A triangular surface mesh is first generated on the hull by a third party meshing tool. The surface mesh was generated by Rhino3D and exported as a Standard Tessellation Language (STL) file to be used by snappyHexMesh. To generate the mesh, three sets of utilities within OpenFOAM are used; blockMesh, topoSet and refineMesh, and snappyHexMesh. The background grid is generated in the basic OpenFOAM meshing utility, blockMesh. BlockMesh generates hexagonal cells and the cells can be stretched in any direction. Using the topoSet and refineMesh tools, certain regions of the mesh can be refined. The user specifies the region that is to be defined and the topoSet tool selects the cells within that region to be refined. The refineMesh tool splits the cells selected for refinement. For the grid used in this simulation, the mesh was refined 6 times. SnappyHexMesh is used for the cutting the hull into the domain and adding prism layers near the hull. SnappyHexMesh uses the cell splitting method of grid refinement. The user can define the number times that the

cells are split, cell refinement level, at certain distances from the hull to improve the mesh near the hull. The minimum and maximum cell refinement level on the hull is also defined. SnappyHexMesh refines the grid and uses the STL file to cut the hull into the existing mesh. A boundary prism layer on the hull can be added after the hull is cut into the mesh. The prism layer cells are defined by the number of layers and the expansion ratio. Unlike other meshing tools, these utilities are not interactive, the parameters for the mesh are defined in a file and the utilities are then run and the mesh is generated.

Comparison

Each of the meshing tools were compared based on quality of mesh, meshing time, ease of use, and compatibility with OpenFOAM. Pointwise gives ultimate control over the mesh, so that the user can generate almost any mesh needed for simulation. SnappyHexMesh has both cell stretching and cell splitting for controlling cell size, so the user has good control over the grid. SnappyHexMesh in OpenFOAM 2.3 also has good prism layer control so that the boundary layer can be accurately modeled. Boxer is very similar to snappyHexMesh without the ability to do cell stretching. As a result, there are a large number of small cells far from the hull. Pointwise is time consuming to generate each new mesh because each hull is built from the ground up. With Boxer and snappyHexMesh, the background grid and the hull are separate entities and the hull is cut into the grid. As a result, the same background grid can be used for different hulls reducing overall meshing time. Boxer and snappyHexMesh both are automatic gridding tools. First the user sets up the parameters from the mesh and then the computer calculates the mesh. The meshing time is less as the user does not have to interact with the mesh while it is actually being created.

SnappyHexMesh was selected to generate the mesh for the OpenFOAM simulations. First, it is the only free meshing tool tested. Secondly, it is seemless for using in OpenFOAM. Both Pointwise and Boxer required the mesh to be exported as a FLUENT mesh and converted into an OpenFOAM mesh.

4.4.3 Mesh

The domain is symmetrical about the centerline to reduce cell count since pitch and heave are the only motions of interest. The domain is seven boat lengths long with two boat lengths upstream of the hull and four boat lengths downstream of the hull. To ensure that the bottom would not interfere with the flow, a depth of sixteen boat lengths would be needed. This would require a large number of cells, so the depth was reduced to 2.5 boat lengths, which is the depth of the USNA towing tank where the model was tested. The domain is

two boat lengths wide.

Figure 4.7 shows the mesh at the centerline after it has reached equilibrium. The red represents the water phase and the blue represents the air phase. Figure 4.8 shows the mesh near the hull with the prism layer near the hull to capture the boundary layer flow. Figure 4.9 shows the mesh at the small forward step. With such few cells near the step, the separation of the flow off of the small step is not well defined.

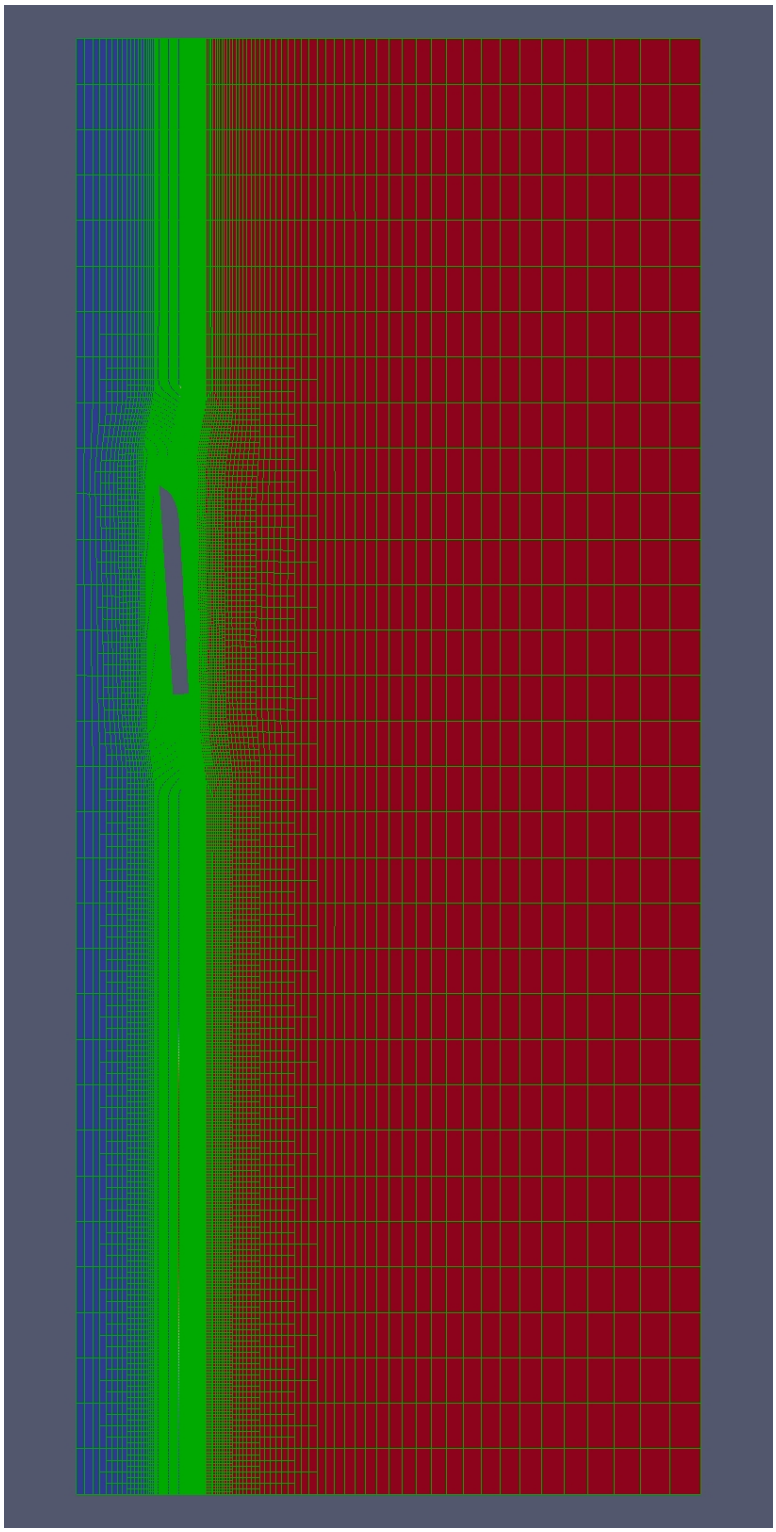

Figure 4.7: Mesh at Centerline (4.8 million cells): Green lines show cells in mesh. Red shows regions of water and blue shows regions of air.

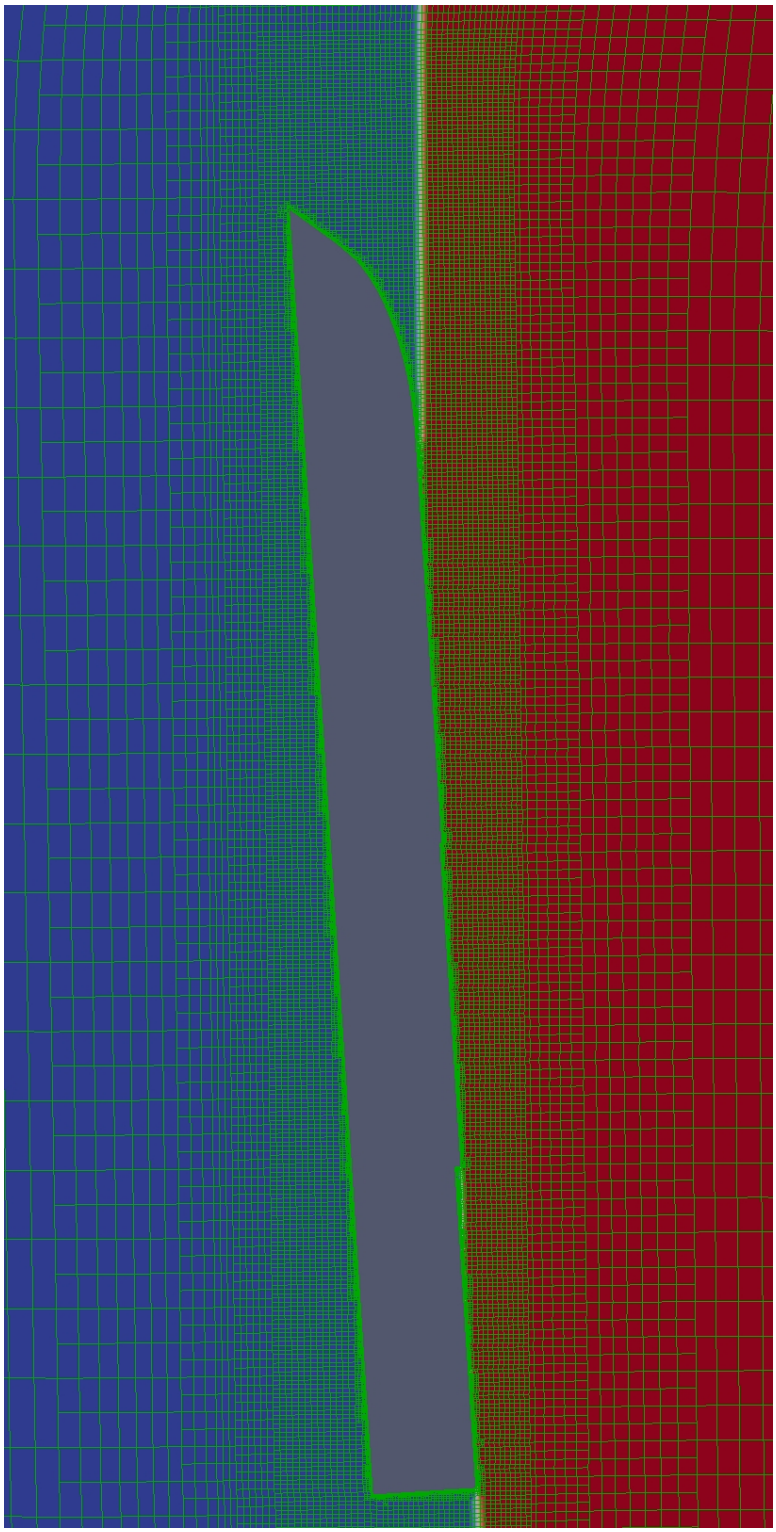

Figure 4.8: Mesh near the hull with the prism layers to capture boundary layer flow (4.8 million cells): Green lines show cells in mesh. Red shows regions of water and blue shows regions of air.

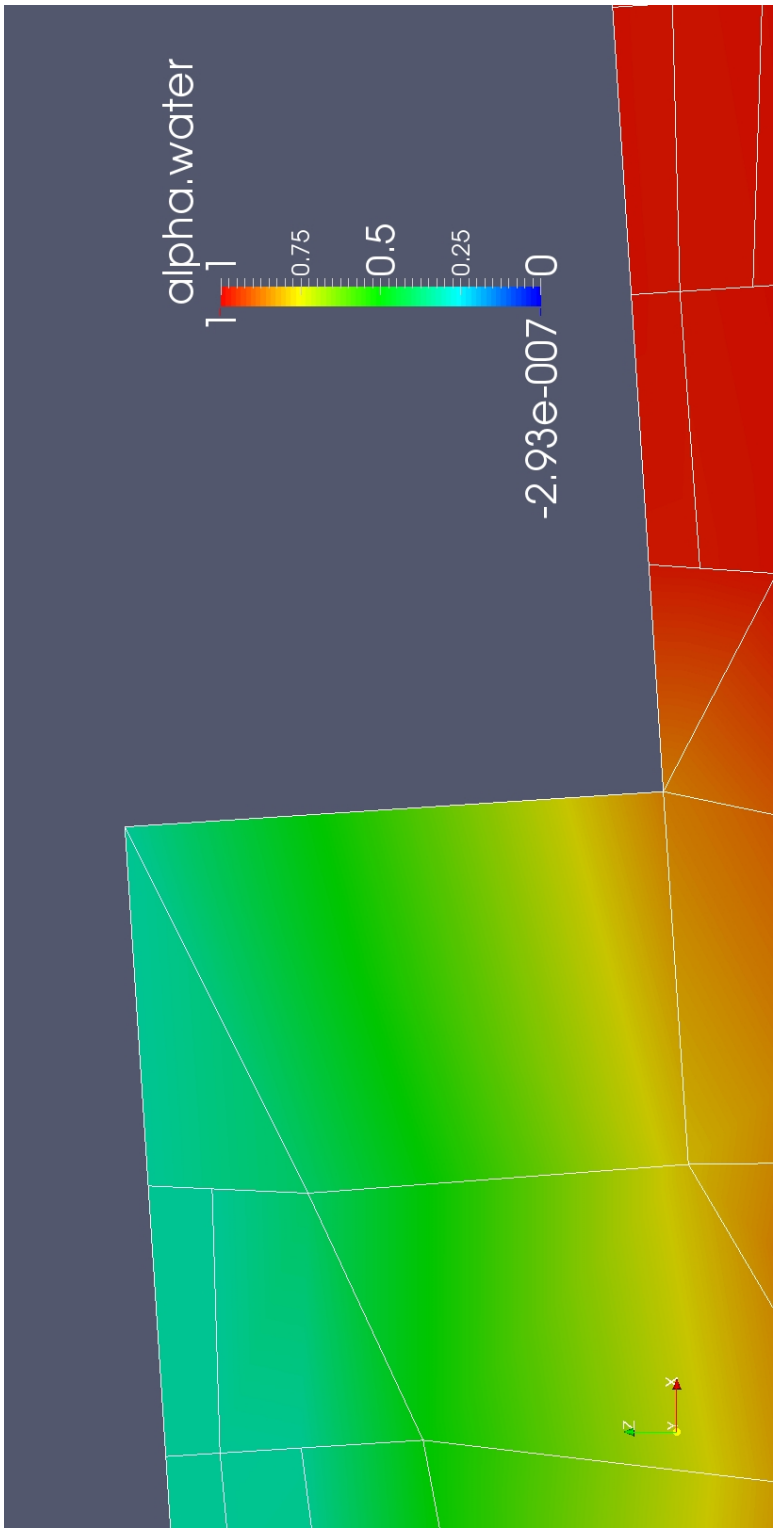

Figure 4.9: 4.8 million cell mesh at the small forward step. Few cells near step. White lines show cells in mesh. Red shows region of water. Blue shows region of air. Green shows region of air/water mixture. Separation off small step not well defined as seen by the gradation of volume fraction across step.

Table 4.3 shows the boundary conditions for the simulation.

Table 4.3: Boundary Conditions

Boundary Conditions			
Patch	Velocity	Pressure	Turbulence
Inlet Sides Bottom	Inflow Velocity	Fixed Flux Pressure	Fixed Value
Outlet	Outlet Phase Mean Velocity	Zero Gradient	Inlet Outlet
Atmosphere	Pressure Inlet Outlet Velocity	Total Pressure	Inlet Outlet
Centerline	Symmetry Plane		

4.4.4 Case Setup

The information needed to run a simulation in OpenFOAM is distributed over a number of different files broken down into three main folders in the file structure. The first type of files are the values of different variable at each time step. The"0" folder contains the definitions of these variables at the initial conditions. When a time step is saved, the values at that time step are stored in a new folder with the time step as the name. The second type are variables that do not change with time. These files are located in the "constant" folder. Files that fall under this type are the mesh, the dynamic mesh motion dictionary, gravity, the fluid properties, and the turbulence model properties. The final type is the system files that are contained in the" system" folder. The dictionary files for all the utilities used in OpenFOAM is stored here as well. The control dictionary controls the actual running of the simulation. It determines the start and end times as well as the time step. It also tells OpenFOAM how often to save data and how to output the data. The fvSchemes file contains all the schemes that are used for solving the equations in OpenFOAM. The fvSolution file contains all the solver information for each of the variables. Figure 4.10 is an example of the file for the velocity at the time step 0, the initial conditions.

```
/*--------------------------------*-
C++ -*----------------------------------*\
| =========                 |
|
| \\      /  F ield         | OpenFOAM: The Open Source CFD
Toolbox           |
|  \\    /   O peration     | Version:  2.3.0
|
|   \\  /    A nd           | Web:      www.OpenFOAM.org
|
|    \\/     M anipulation  |
|
\*---------------------------------------------------------------
------------*/
FoamFile
{
    version     2.0;
    format      binary;
    class       volVectorField;
    location    "0";
    object      U;
}
// * * * * * * * * * * * * * * * * * * * * * * * * * * * * * * * * *
* * * * * * //

dimensions      [0 1 -1 0 0 0 0];

internalField   uniform (-9.449 0 0);

boundaryField
{
    atmosphere
    {
        type            pressureInletOutletVelocity;
        value           uniform (0 0 0);
    }
    inlet
    {
        type            fixedValue;
        value           uniform (-9.449 0 0);
    }
    outlet
    {
        type            outletPhaseMeanVelocity;
        Umean           9.449;
        alpha           alpha.water;
        value           uniform (-9.449 0 0);
    }
    bottom
    {
        type            symmetryPlane;
    }
    side
    {
        type            symmetryPlane;
    }
    midPlane
    {
        type            symmetryPlane;
    }
    hull
    {
        type            movingWallVelocity;
        value           uniform (0 0 0);
    }
}


//
************************************************************************
******** //
```

Figure 4.10: Example of OpenFOAM file for velocity at the initial conditions

4.4.5 Grid Convergence

The simulation was run with four different grid sizes from about 1.95 million cells to about 8.75 million cells. Figure 4.11 shows the resistance/weight as the number cells increases. Figure 4.12 shows trim angle as the number of cells increases. Both the resistance and the trim angle did not show convergence.

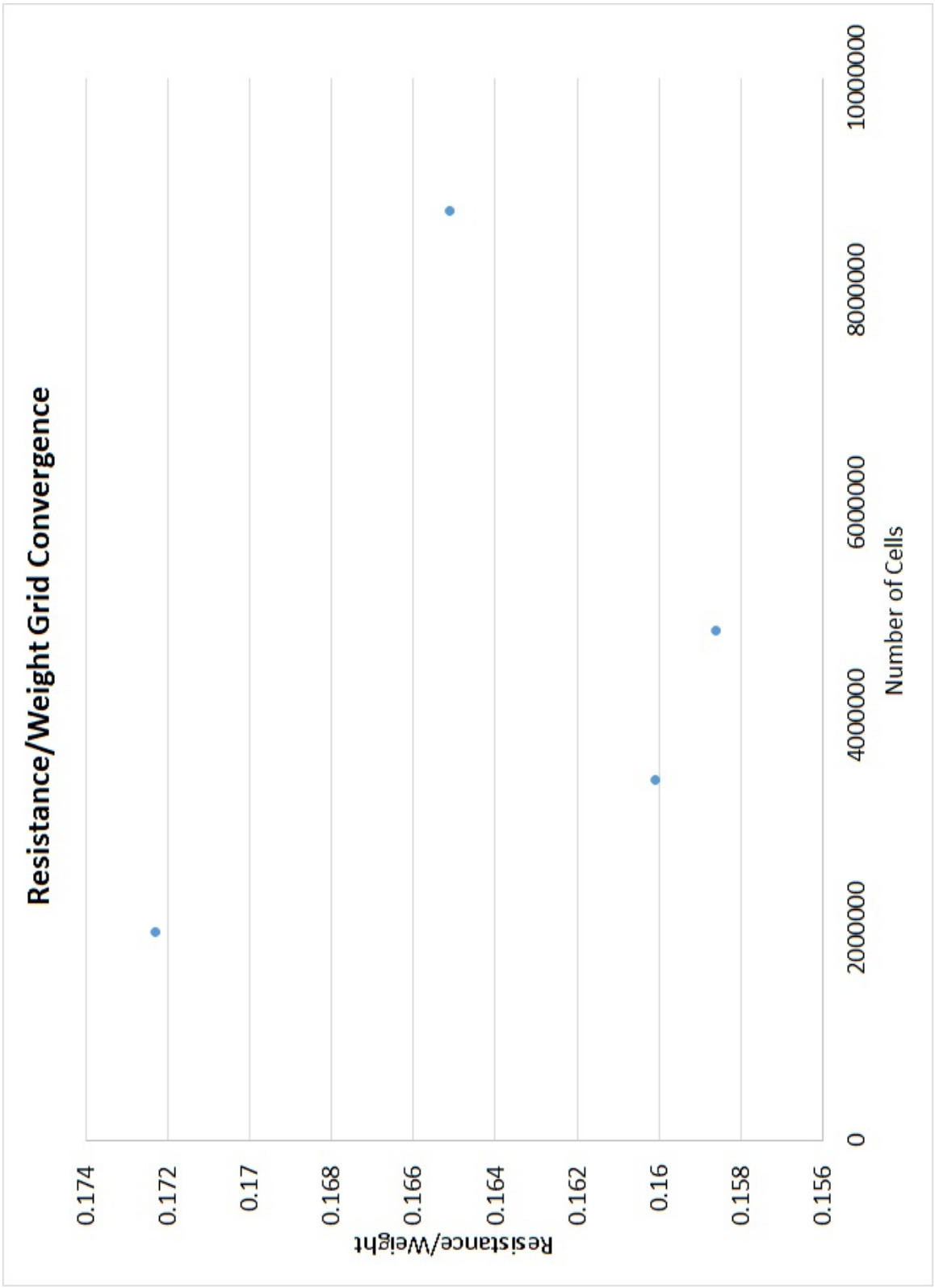

Figure 4.11: Resistance/Weight Grid Convergence: esistance/Δ as number of cells increases

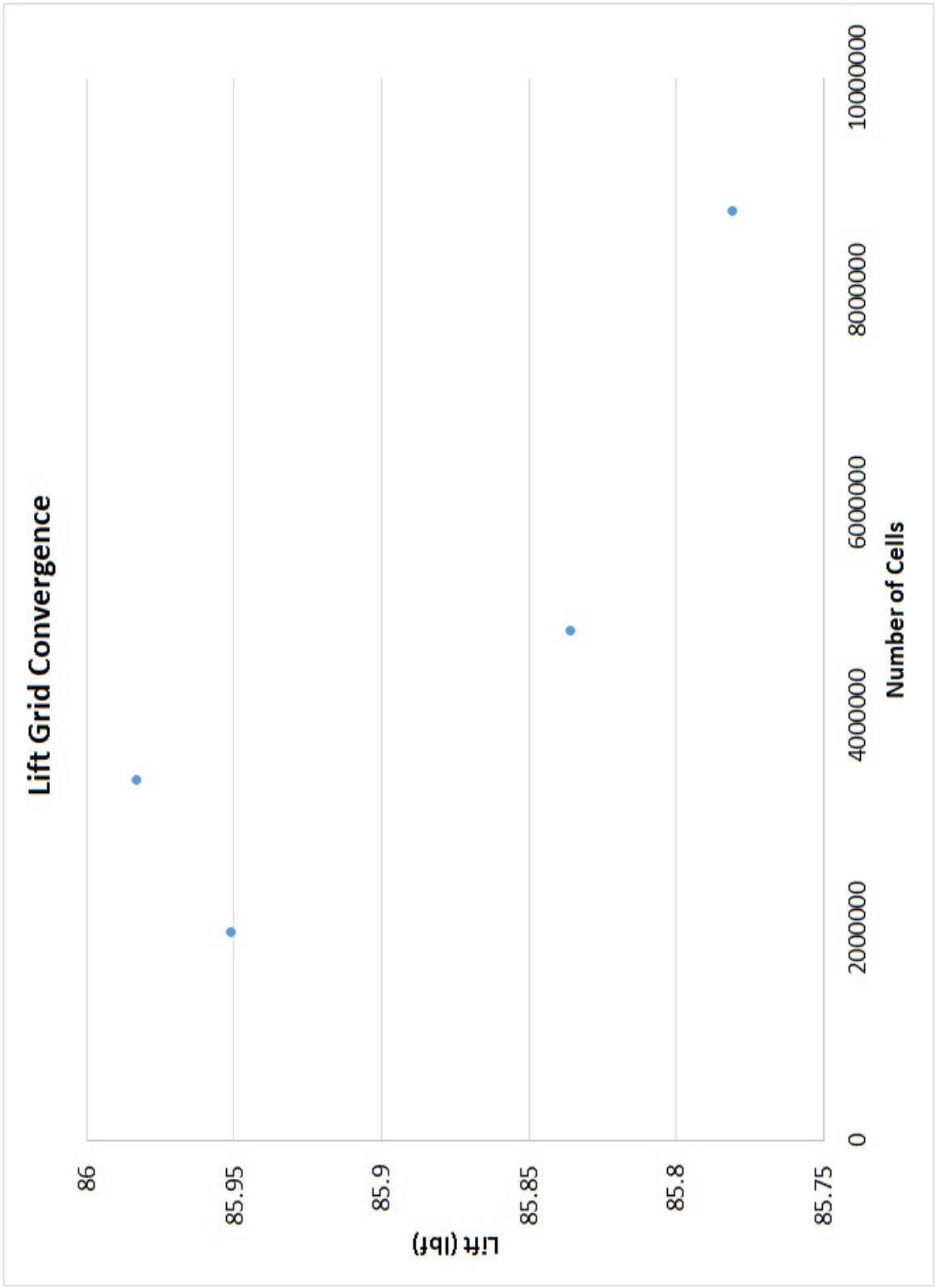

Figure 4.12: Trim Angle Grid Convergence: Trim angle as number of cells increases

Even with the lack of convergence, the mesh with about 4.8 million cells were used for the rest of the simulations based on computational time. The lack of convergence calls into question the validity of the results obtained on these grids.

4.4.6 Simulation Scalability

For OpenFOAM, the user can control the number of cells per processor. It has been recommended that for free surface flows, each processor has about 100,000 cells per processor [42]. Therefore, the number of cells drives the number of processors needed for a simulation and is a large contributor to the overall computation time.

4.4.7 Simulation Speed

The OpenFOAM simulations were run for about 30 seconds of simulated flow time on 48 cores for a total of 6912 core hours on the Virginia Tech Advanced Research Computing Cray CS-300 cluster, Blueridge [46]. Figure 4.13 shows the convergence of resistance/weight over time. Based on availability, four or five cases were able to be run simultaneously. The grid size selected provided quick simulation turn around times and allowed for multiple runs to be simulated at the same time despite lack of convergence. Therefore, the grid size selected is representative of a grid that would be used for design iterations.

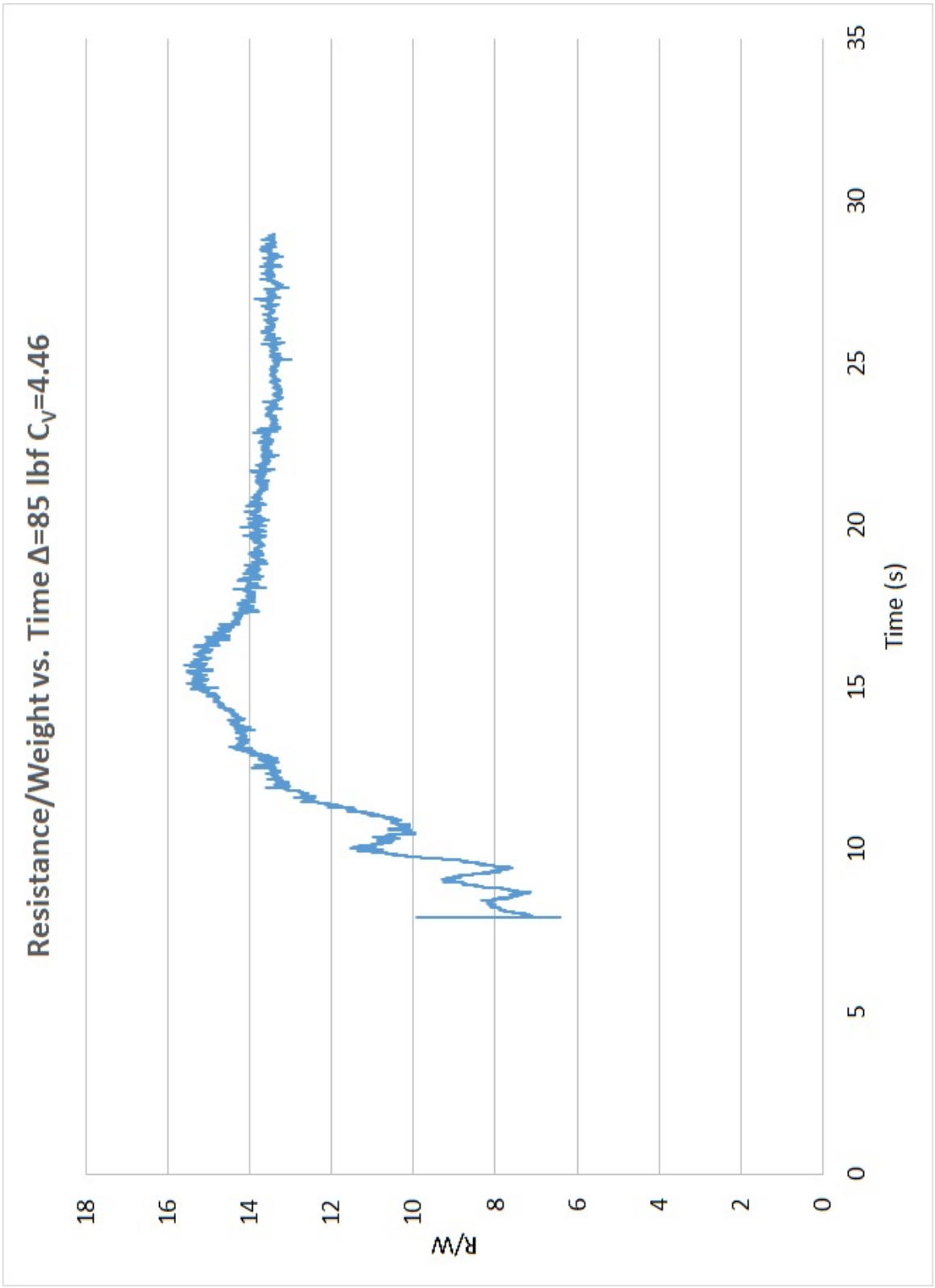

Figure 4.13: Resistance/Weight vs. Time: Resistance/Weight converges to final solution.

4.5 Results

4.5.1 NFA

Tables 4.4 to 4.7 shows the error in resistance/weight and trim angle for the different conditions simulated. The error in resistance/weight is also broken down into the form and friction components. The friction drag from the model test was calculated by using the wetted keel length on each planing surface to determine the Reynold's number and the friction coefficient. The wetted surface area on each planing surface was used to calculate the friction resistance on each planing surface. The total friction resistance was the sum of the friction resistance on each of the planing surfaces. The form resistance is assumed to be the difference between the overall resistance and the friction resistance. A positive percent error shows that the simulation over predicted the result and a negative percent error shows that the simulation under predicted the result. Δ=85 lbf at C_V=4.46 was tested at both LCG locations to determine the simulation's ability to handle the change in LCG location. The simulation over predicted the resistance/weight due to the large over prediction in the friction resistance. The simulation under predicted the trim angle. Even though the trim angle was under predicted, the form resistance was over predicted. This is contrary to theory, which states that the form resistance is proportional to the tangent of the trim angle. So as the trim angle is higher, the form resistance should be higher.

Table 4.4: NFA vs. Model Test Resistance/Weight

Δ (lbf)	C_v	Percent of LOA Forward of the Transom	Predicted Resistance/Weight	Measured Resistance/Weight	Percent Error in Resistance/Weight
85	4.17	40	0.256	0.190	35.03
85	4.46	40	0.273	0.196	39.26
85	4.46	35	0.250	0.201	24.29
95	3.88	40	0.223	0.170	31.59
95	4.46	35	0.236	0.188	25.38
105	3.88	40	0.210	0.167	25.91
105	4.46	40	0.245	0.180	36.42

Table 4.5: NFA vs. Model Test Form Resistance/Weight

Δ (lbf)	C_v	Percent of LOA Forward of the Transom	Predicted Form Resistance/Weight	Measured Form Resistance/Weight	Percent Error in Form Resistance/Weight
85	4.17	40	0.0821	0.0780	5.26
85	4.46	40	0.0846	0.0741	14.21
85	4.46	35	0.0814	0.0713	14.20
95	3.88	40	0.0879	0.0682	28.79
95	4.46	35	0.0861	0.0656	31.17
105	3.88	40	0.0897	0.0740	21.23
105	4.46	40	0.0887	0.0747	18.70

Table 4.6: NFA vs. Model Test Friction Resistance/Weight

Δ (lbf)	C_v	Percent of LOA Forward of the Transom	Predicted Friction Resistance/Weight	Measured Friction Resistance/Weight	Percent Error in Friction Resistance/Weight
85	4.17	40	0.174	0.112	55.81
85	4.46	40	0.188	0.122	54.47
85	4.46	35	0.169	0.130	29.83
95	3.88	40	0.135	0.101	33.48
95	4.46	35	0.150	0.123	22.28
105	3.88	40	0.120	0.093	29.64
105	4.46	40	0.156	0.105	48.78

Table 4.7: NFA vs. Trim Angle

Δ (lbf)	C_v	Percent of LOA Forward of the Transom	Predited Trim Angle	Measured Trim Angle	Percent Error in Trim Angle
85	4.17	40	2.60	3.09	-15.63
85	4.46	40	2.36	3.00	-21.38
85	4.46	35	2.53	2.59	-2.46
95	3.88	40	2.92	3.65	-20.07
95	4.46	35	2.74	2.96	-7.44
105	3.88	40	3.30	3.97	-16.89
105	4.46	40	2.68	3.68	-27.05

Figure 4.14 on the top half shows an underwater photograph of configuration 4 at Δ=85 lbf, $C_v = 4.46$ and LCG=40% forward of the transom. The bottom half shows the simulation of the same condition. The pressure distribution is also plotted on the hull of the simulation. The simulation captures the overall wave profile shape. It does capture the fine spray sheet as seen in the model test and the stagnation line crossing the step. The simulation does not capture the separated flow on the middle planing surface. The separated flow on the aft planing surface in the simulation looks similar to the model test.

Figure 4.14: Comparison of Underwater Photograph to Simulation: Configuration 4, Δ=85 lbf, $C_v = 4.46$ and LCG=40% Forward of the Transom. Simulation captures overall wave profile. Simulation does capture fine spray sheet and stagnation line crossing step. Separation not predicted for forward step and the separated flow on the aft planing surface looks similar.

Resistance

Figure 4.15 is a comparison of the resistance/weight vs. speed coefficient at LCG=40% forward of the transom for the simulation and the model test. The filled symbols show the data measured from the model test with experimental error bars. The unfilled symbols show the corresponding prediction from simulation. The same run conditions for the measured data and the simulation are represented by the same symbol. The plot shows that the simulations over predicted the resistance/weight. The slope of the simulated data for the 95 lbf displacement shows a similar trend to the measured data. On the other hand the slope of the simulated data for the 105 lbf displacement is much steeper than the measured data.

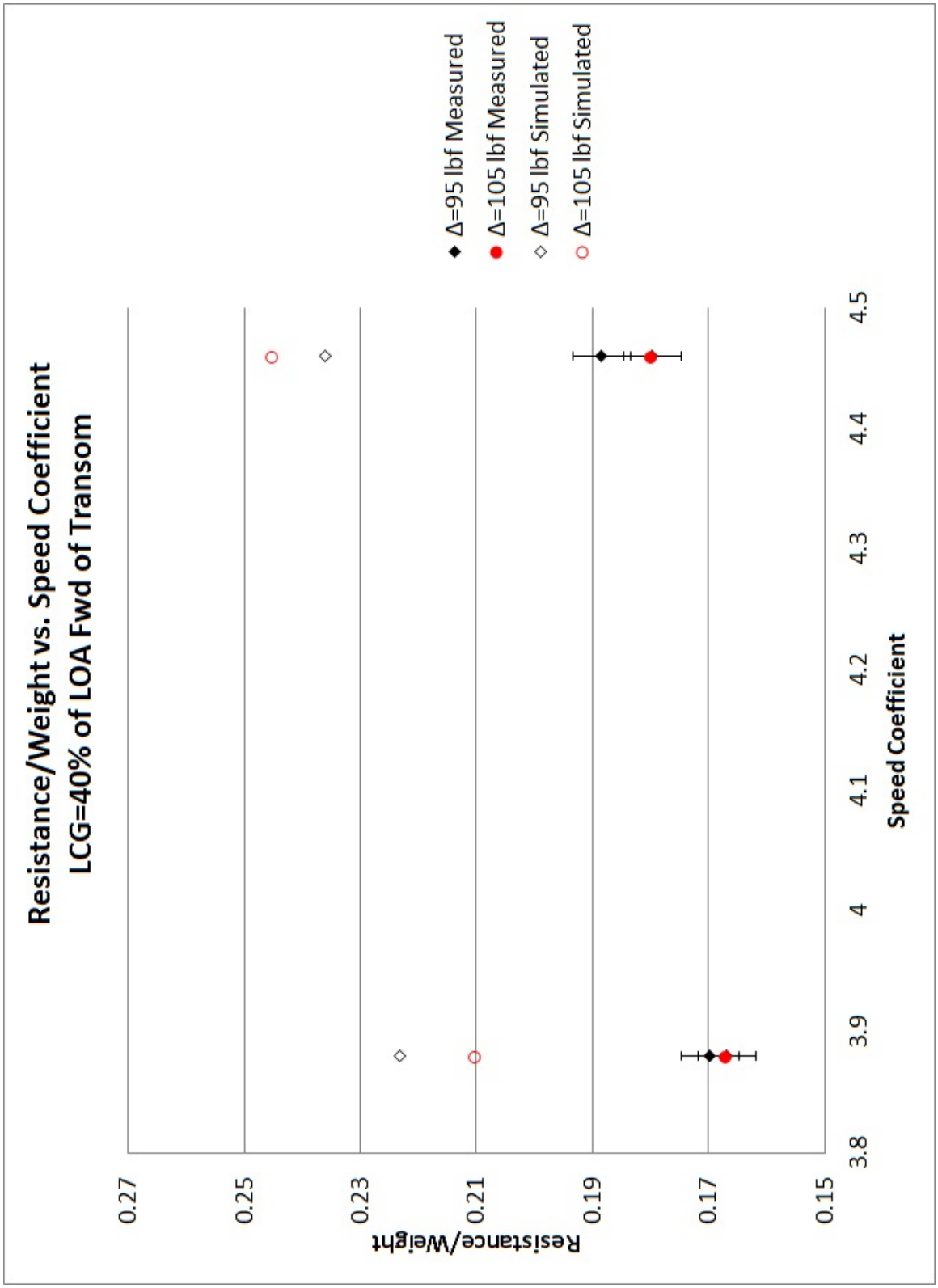

Figure 4.15: Resistance/Weight vs. Speed Coefficient LCG=40% Forward of Transom: Simulations over predicted resistance/weight.

Trim

Figure 4.16 is comparison of the trim angle vs. speed coefficient at LCG=40% forward of the transom for the simulation and the model test. The data is presented in a similar manner to the resistance plots. The plot shows that the simulations under predicted the trim angle. Contrary to the resistance, the simulated data at 105 lbf shows a similar trend to the measured data while the simulated data for the 95 lbf displacement shows a flatter slope. Theory would state that the under prediction of the trim angle would lead to an under prediction of the form resistance. Contrary to what theory states, the form resistance was over predicted, Table 4.6. With the resistance being over predicted, one would assume that the friction drag is also over predicted.

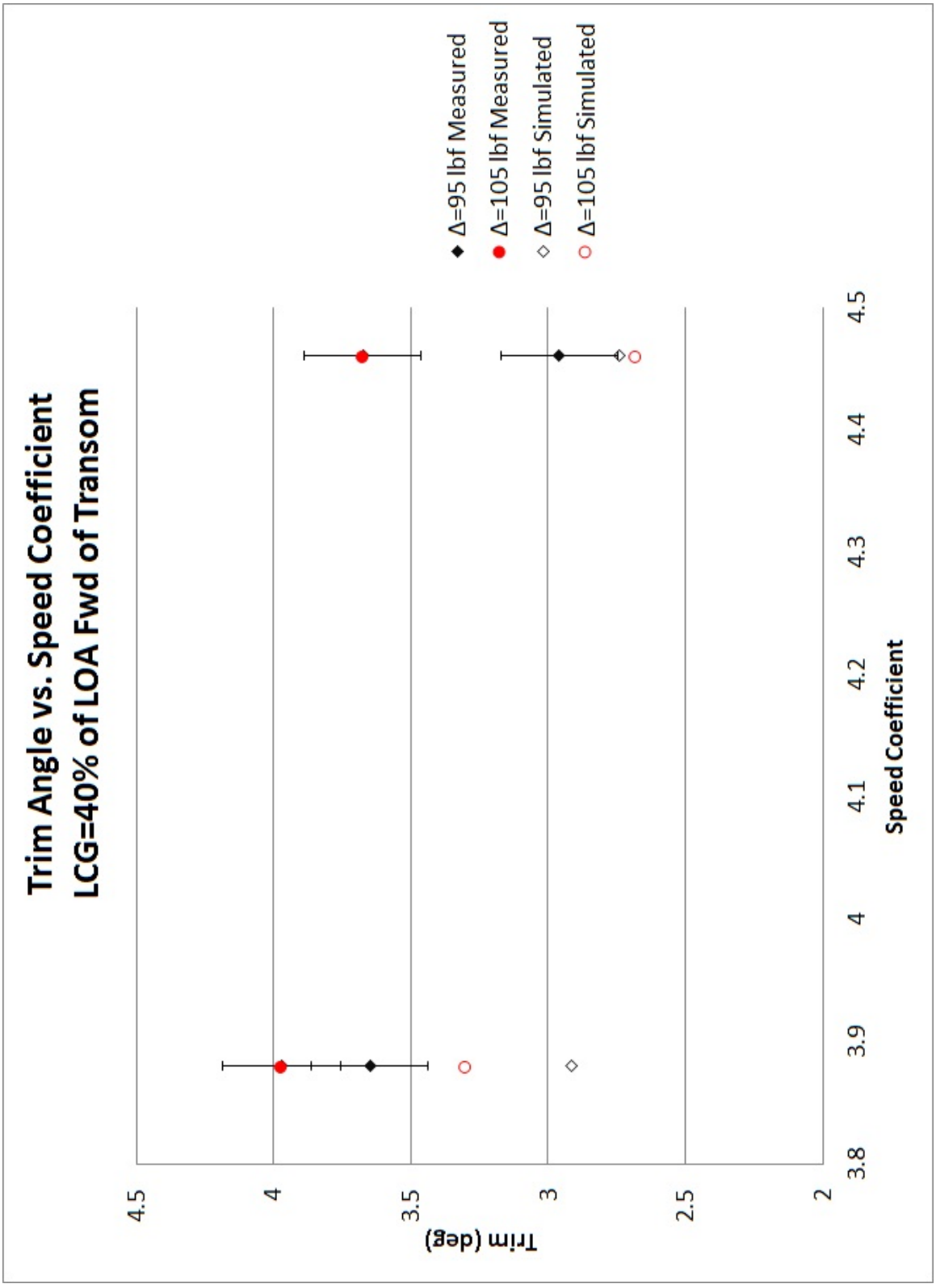

Figure 4.16: Trim Angle vs. Speed Coefficient at LCG=40% Forward of Transom: Simulations under predicted trim angle.

Change in LCG

Figure 4.17 is a comparison of the resistance/weight vs. LCG at C_V=4.46 for the simulation and the model test. The measured data is the filled symbols and the simulated data is the unfilled symbols. The plot shows that the simulations over predicted the resistance/weight. The effect of a LCG shift on resistance/weight from the simulation was opposite of the model test. Figure 4.18 is a comparison of the trim angle vs.LCG at C_V=4.46 for the simulation and the model test. The plot shows that the simulations under predicted the trim angle. The effect of a LCG on trim angle from the simulation was opposite of the model test.

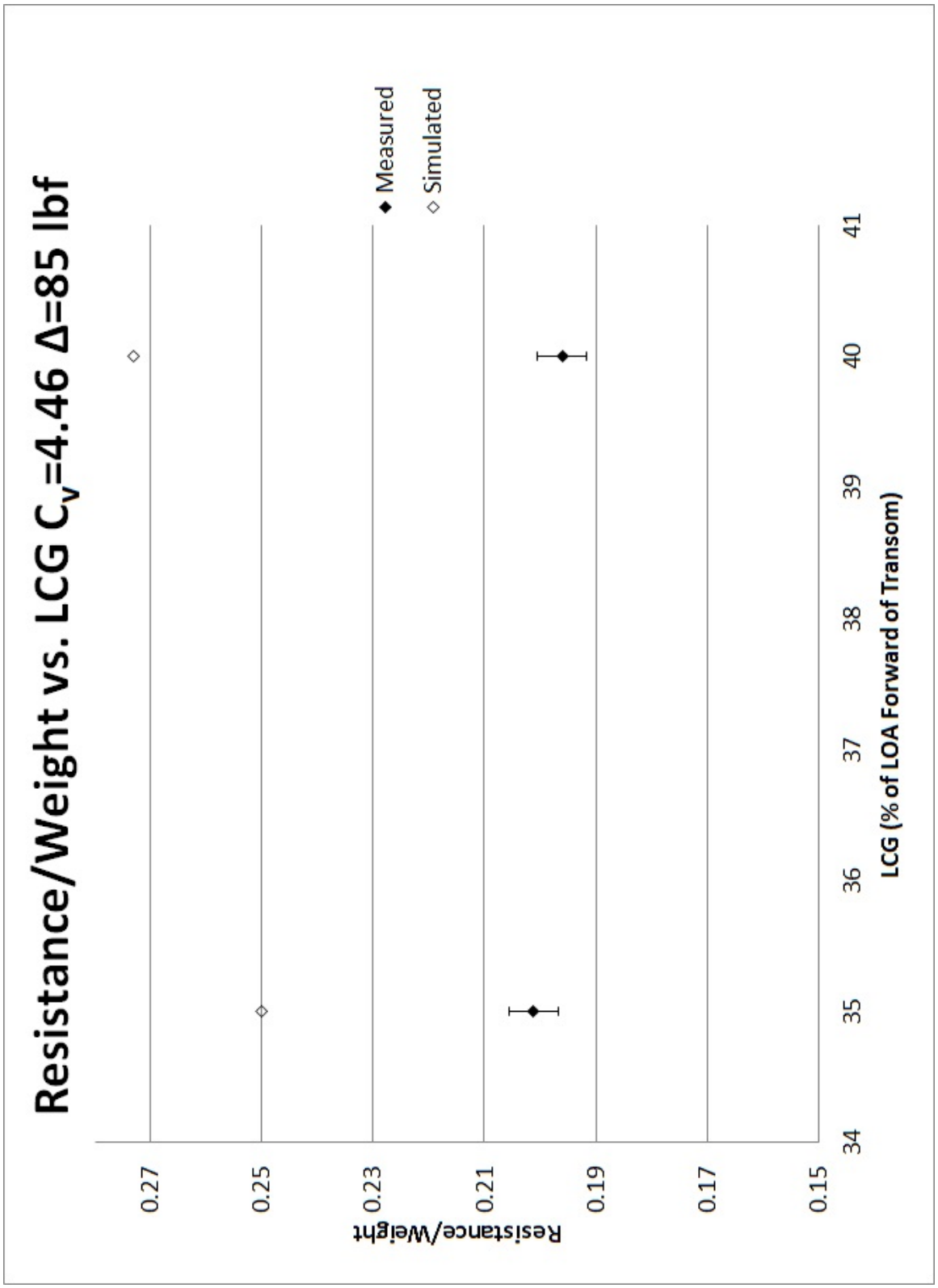

Figure 4.17: Resistance/Weight vs.LCG at C_V=4.46: Simulations over predicted resistance/weight. Effect of LCG shift on resistance/weight from simulation opposite of model test

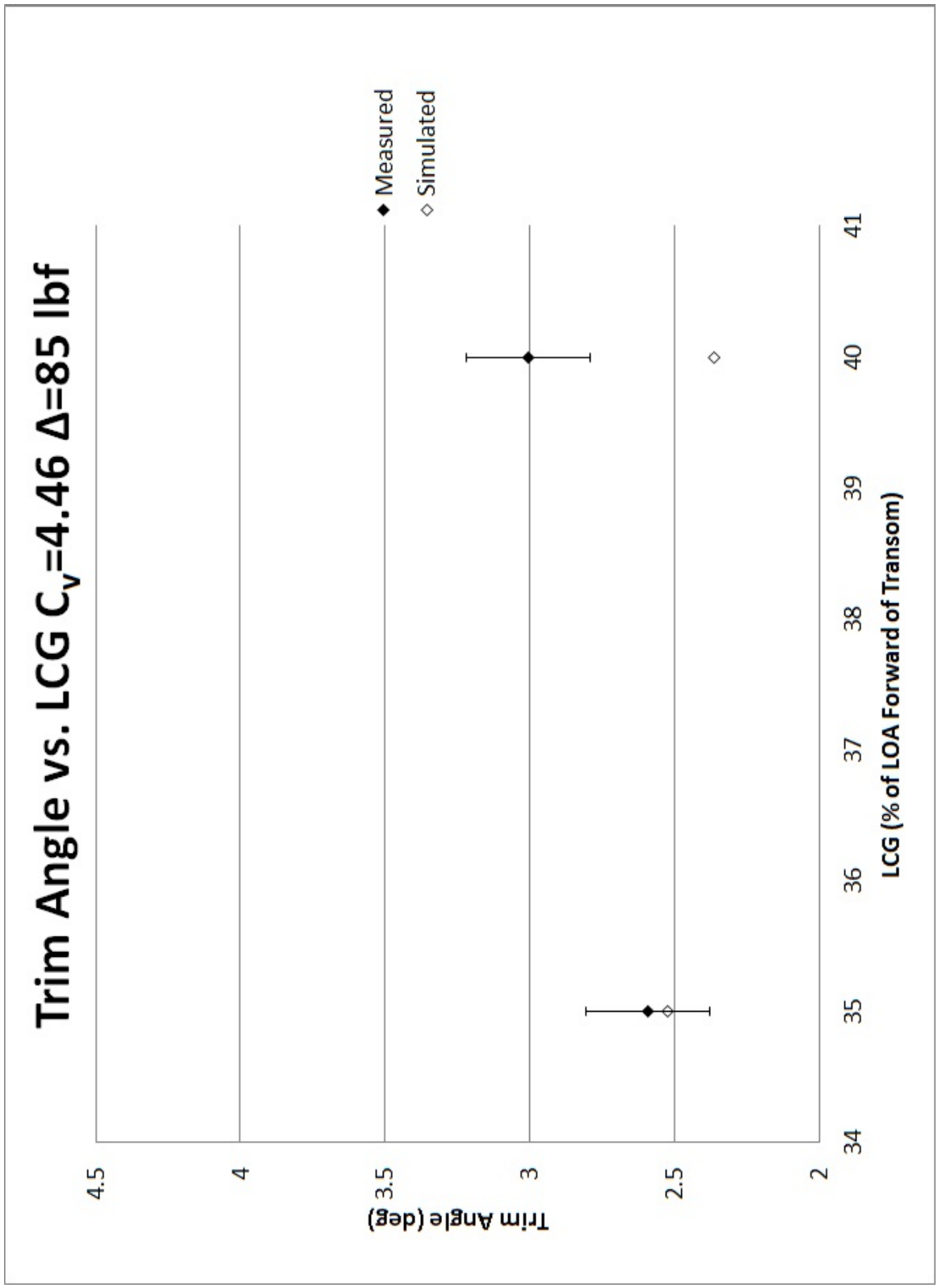

Figure 4.18: Trim Angle vs.LCG at C_V=3.88: Simulations under predicted trim angle. Effect of LCG shift on trim angle from simulation opposite of model test

4.5.2 OpenFOAM

Tables 4.8 to 4.11 shows the error in resistance/weight and trim angle for the different conditions simulated. Three different speeds (C_V=3.88,4.17,4.46) were simulated at Δ=85 lbf to determine the simulation's ability to handle variations in speed. Two speeds (C_V=3.88,4.46) were simulated at all three displacements to determine the simulation's ability to handle the change in displacement. C_V=3.88 was simulated at all three displacements and both LCG locations to determine the simulation's ability to handle the change in LCG location. The simulation was better at predicting the resistance/weight at the lower speeds and the aft LCG location. The simulation was better at predicting the trim angle at the higher speeds and forward LCG location. The large over prediction of the form resistance follows theory as the trim angle is also over predicted. The friction resistance is under predicted and therefore the overall resistance is better predicted than the two main components of the resistance.

Table 4.8: OpenFOAM vs. Model Test Resistance/Weight

Δ (lbf)	C_v	Percent of LOA Forward of the Transom	Predicted Resistance/Weight	Measured Resistance/Weight	Percent Error in Resistance/Weight
85	3.88	40	0.161	0.176	-8.52
85	4.17	40	0.166	0.190	-12.67
85	4.46	40	0.158	0.196	-19.16
85	3.88	35	0.155	0.177	-12.46
95	3.88	40	0.159	0.170	-6.07
95	4.46	40	0.166	0.188	-11.46
95	3.88	35	0.160	0.170	-6.02
105	3.88	40	0.161	0.167	-3.64
105	4.46	40	0.165	0.180	-8.44
105	3.88	35	0.159	0.164	-2.83

Table 4.9: OpenFOAM vs. Model Test Form Resistance/Weight

Δ (lbf)	C_v	Percent of LOA Forward of the Transom	Predicted Form Resistance/Weight	Measured Form Resistance/Weight	Percent Error in Form Resistance/Weight
85	3.88	40	0.094	0.056	67.48
85	4.17	40	0.089	0.054	65.23
85	4.46	40	0.084	0.036	130.77
85	3.88	35	0.101	0.042	142.29
95	3.88	40	0.101	0.058	74.31
95	4.46	40	0.090	0.55	63.09
95	3.88	35	0.109	0.058	89.71
105	3.88	40	0.109	0.066	64.50
105	4.46	40	0.095	0.051	85.92
105	3.88	35	0.117	0.066	78.41

Table 4.10: OpenFOAM vs. Model Test Friction Resistance/Weight

Δ (lbf)	C_v	Percent of LOA Forward of the Transom	Predicted Friction Resistance/Weight	Measured Friction Resistance/Weight	Percent Error in Friction Resistance/Weight
85	3.88	40	0.067	0.105	-36.13
85	4.17	40	0.077	0.112	-31.50
85	4.46	40	0.074	0.122	-39.10
85	3.88	35	0.054	0.113	-52.15
95	3.88	40	0.058	0.101	-42.42
95	4.46	40	0.076	0.111	-31.29
95	3.88	35	0.050	0.102	-50.56
105	3.88	40	0.052	0.094	-45.27
105	4.46	40	0.069	0.113	-38.73
105	3.88	35	0.042	0.093	-55.18

Table 4.11: OpenFOAM vs. Model Test Trim Angle

Δ (lbf)	C_v	Percent of LOA Forward of the Transom	Predicted Trim Angle	Measured Trim Angle	Percent Error in Trim Angle
85	3.88	40	4.43	3.17	39.70
85	4.17	40	4.05	3.09	31.36
85	4.46	40	3.71	3.00	23.51
85	3.88	35	5.03	2.91	72.52
95	3.88	40	4.91	3.65	34.62
95	4.46	40	4.10	3.43	19.54
95	3.88	35	5.58	3.45	61.51
105	3.88	40	5.40	3.97	36.03
105	4.46	40	4.49	3.68	22.15
105	3.88	35	6.10	3.66	66.47

Figure 4.19 on the top half shows an underwater photograph of configuration 4 at Δ=85 lbf, $C_v = 4.46$ and LCG=40% forward of the transom. The bottom half shows the simulation of the same condition. The pressure distribution is also plotted on the hull of the simulation. The simulation captures the overall wave profile shape. It does not capture the fine spray sheet as seen in the model test. The simulation did not capture the stagnation line crossing the step. The simulation does not capture the separated flow on the middle planing surface. The separated flow on the aft planing surface in the simulation looks similar to the model test.

Figure 4.19: Comparison of Underwater Photograph to Simulation: Configuration 4, Δ=85 lbf, $C_v = 4.46$ and LCG=40% Forward of the Transom. Simulation captures overall wave profile. Simulation does not capture fine spray sheet. Simulation did not predict stagnation line crossing step. Separation not predicted for forward step and the separated flow on the aft planing surface looks similar.

Resistance

Figure 4.20 is a comparison of the resistance/weight vs. speed coefficient at Δ=85 lbf and LCG=40% forward of the transom for the simulation and the model test. The filled symbol show the measured data with experimental error bars and the unfilled symbols show the simulated data. The plot shows that the simulations under predicted the resistance/weight. The simulations predicted the results better at the lower speeds. The resistance/weight at the highest speed was lower than the two other speeds. This is not expected as resistance/weight should increase with speed at a given displacement.

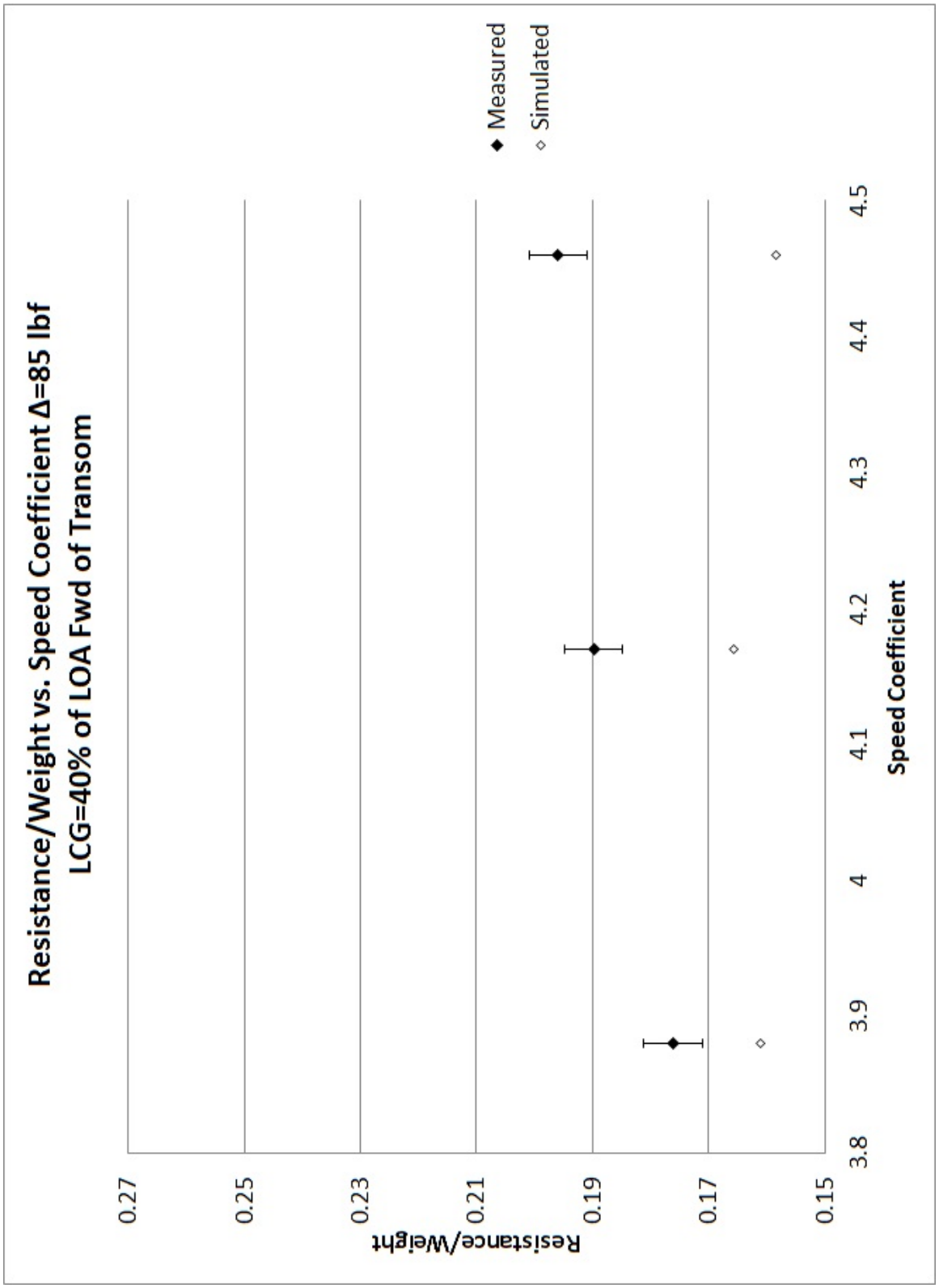

Figure 4.20: Resistance/Weight vs. Speed Coefficient at Δ=85 lbf and LCG=40% Forward of Transom: Simulations under predicted resistance/weight. Simulations predicted results better at lower speeds.

Trim

Figure 4.21 is comparison of the trim angle vs. speed coefficient at Δ=85 lbf and LCG=40% forward of the transom for the simulation and the model test. The data is shown in a similar manner to the resistance. The plot shows that the simulations over predicted the trim angle. The simulations predicted the results better at the higher speeds. Simulations show similar trend in the change of trim as speed increases. Theory would state that the large over prediction of the trim angle would lead to an over prediction of the form resistance. The resistance was under predicted, which would lead to the assumption that the friction resistance was under predicted. The results support this assumption.

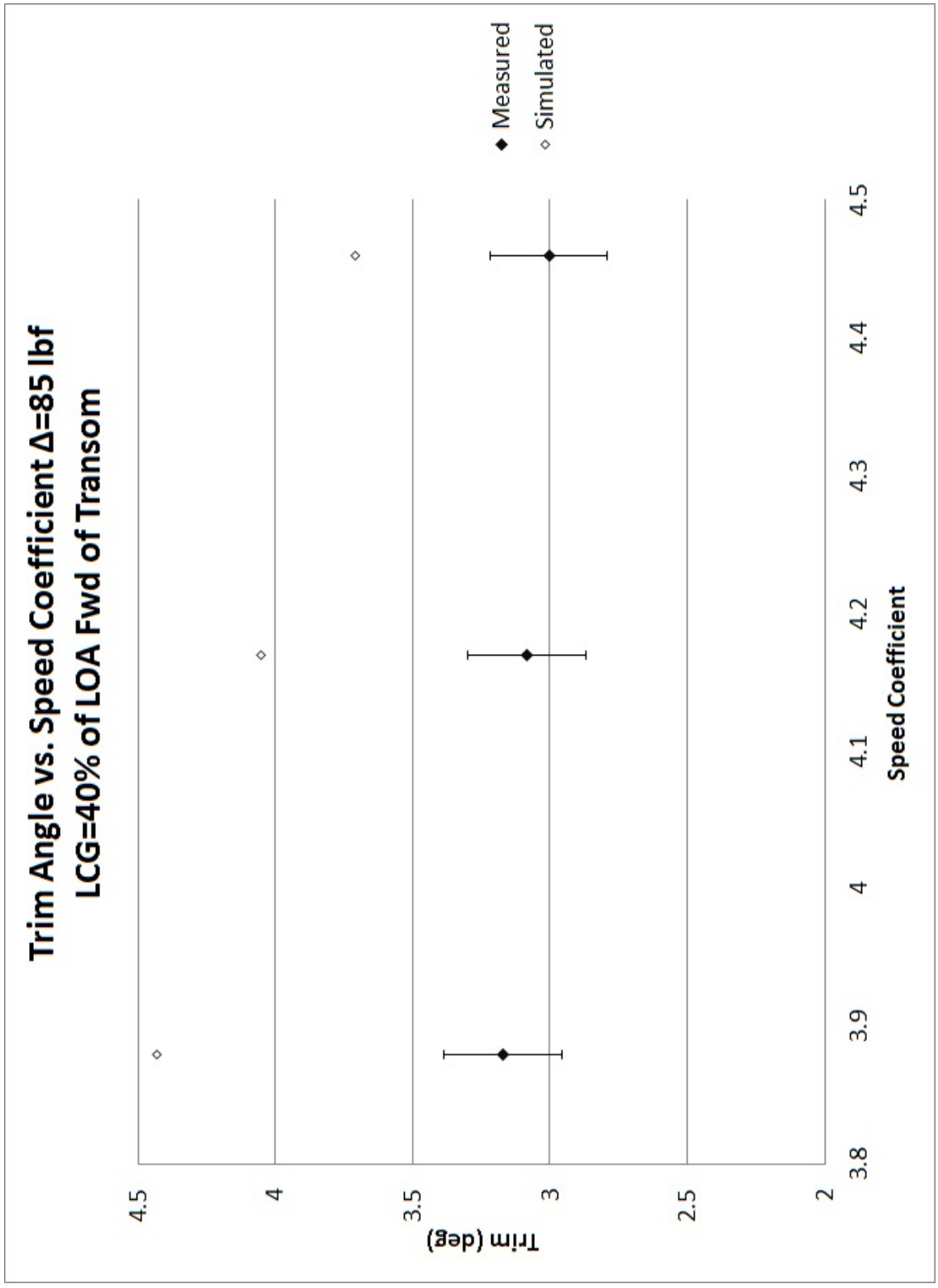

Figure 4.21: Trim Angle vs. Speed Coefficient at 85 lbf displacement and LCG=40% Forward of Transom: Simulations over predicted trim angle. Simulations show similar reduction in trim angle as speed increases.

Change in Displacement

Figure 4.22 is a comparison of the resistance/weight vs. percent of full load displacement for the simulation and the model test. The filled symbols are the measured data from the model test with the experimental error bars. The unfilled symbols are the simulated data. The plot shows that the simulations under predicted the resistance/weight. The simulations predicted the results better at the heavier displacements. The resistance/weight at the lightest displacement is less than the middle displacement. The overall trend of the simulated data does not match the measured data as there is a slight rise in the simulated data between the lightest and middle displacement than a decrease in resistance/weight from the middle to the heaviest displacement. The trend of the measured data is a constant decreasing slope. Figure 4.23 is a comparison of the trim angle vs. percent of full load displacement for the simulation and the model test. The data is presented in a similar manner to the resistance. The plot shows that the simulations over predicted the trim angle. The simulations show similar changes in the trim angle as the displacement changes. The spread of the simulated data is much larger than the measured data.

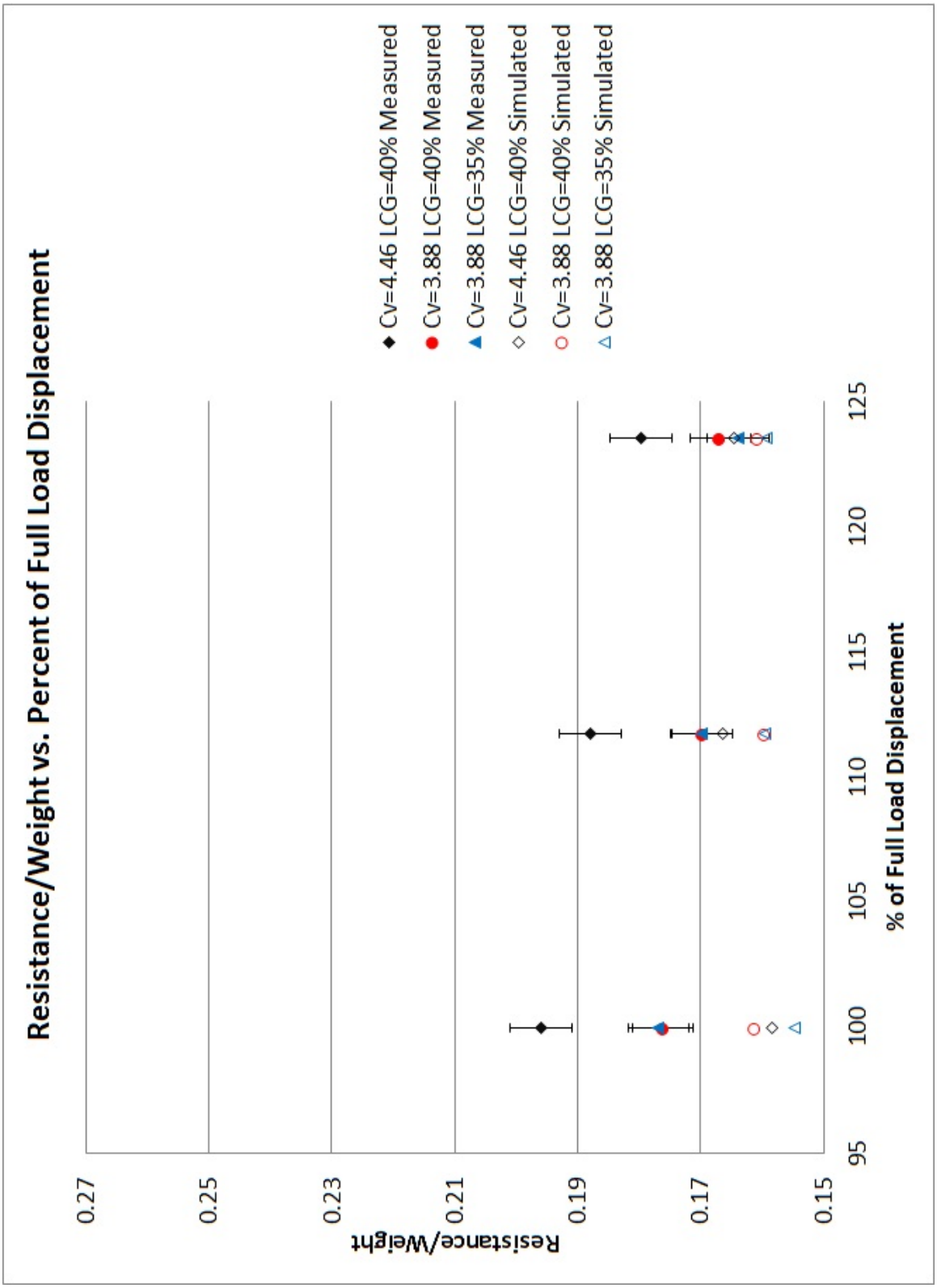

Figure 4.22: Resistance/Weight vs. Percent of Full Load Displacement: Simulations under predicted resistance/weight. Simulations more accurate at heavier displacements

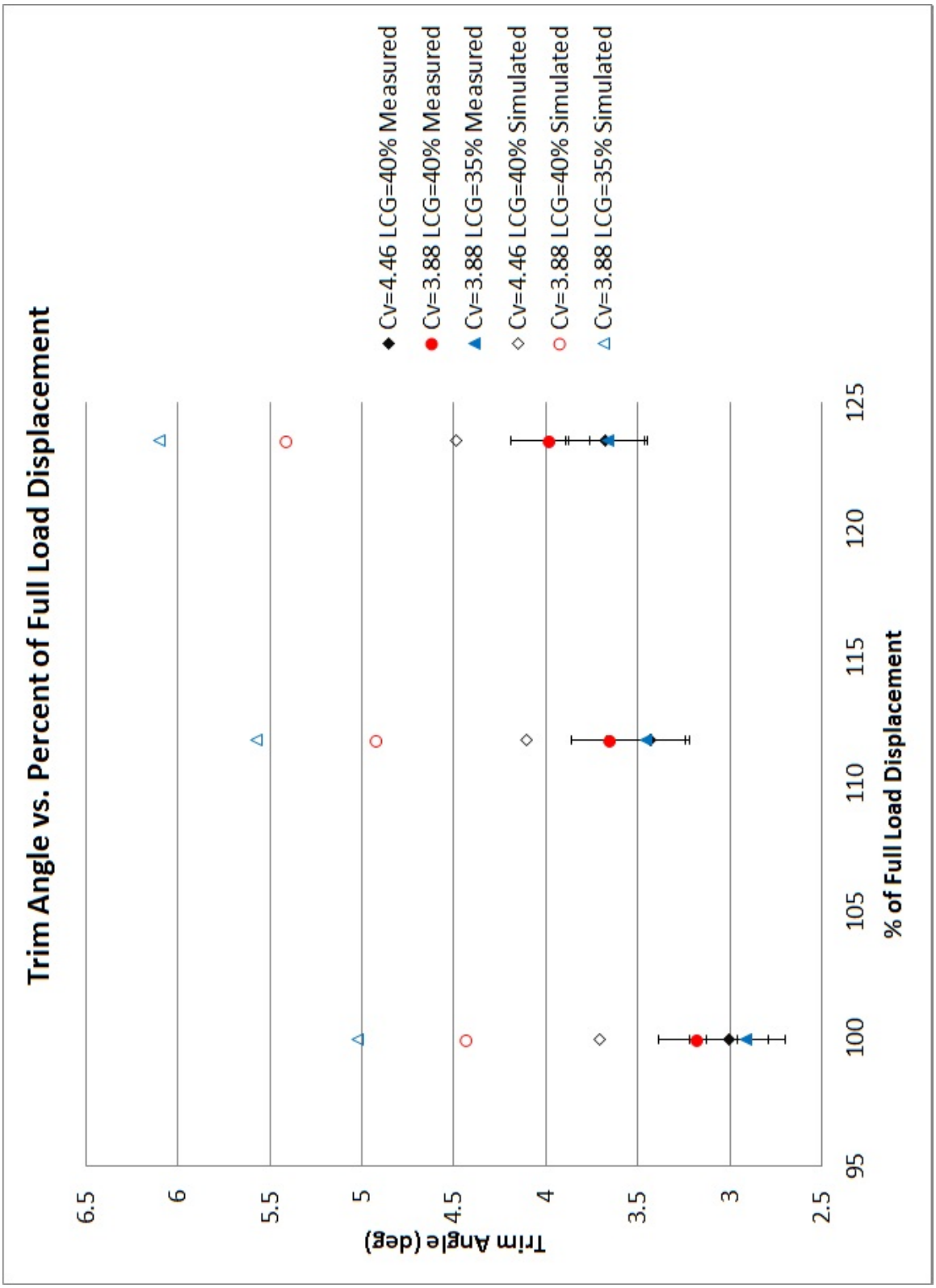

Figure 4.23: Trim Angle vs. Percent of Full Load Displacement: Simulations over predicted trim angle. Simulations show similar changes in trim angle as displacment changes

Change in LCG

Figure 4.24 is a comparison of the resistance/weight vs. LCG at C_V=3.88 for the simulation and the model test. The filled symbols are the measured data from the model test with the experimental error bars. The unfilled symbols are the simulated data. The plot shows that the simulations slightly under predicted the resistance/weight. At the 95 lbf and 105 lbf displacement, the effect of the LCG shift on resistance/weight from the simulation was similar to the model test. For the 85 lbf displacement, the simulated trend is opposite of the model test and the two other simulated displacements. Figure 4.25 is a comparison of the trim angle vs.LCG at C_V=3.88 for the simulation and the model test. The data is presented in a similar manner to the resistance. The plot shows that the simulations over predicted the trim angle. At the 85 lbf and 105 lbf displacement, the effect of the LCG on trim angle from the simulation was opposite of the model test data. At the 95 lbf displacement, the simulated effect of the LCG on trim angle shows the same trend as the model test with a steeper slope. The cause for the model test not to follow theory is most likely due to hull form and hydrodynamics. The NSWC15 had a dynamic trim instability where it was stable in either a bow up or a bow down condition due to the influence of the bow section on the flow. This dynamic instability and its effect on the trim angle is further discussed in Section 2.10.1.

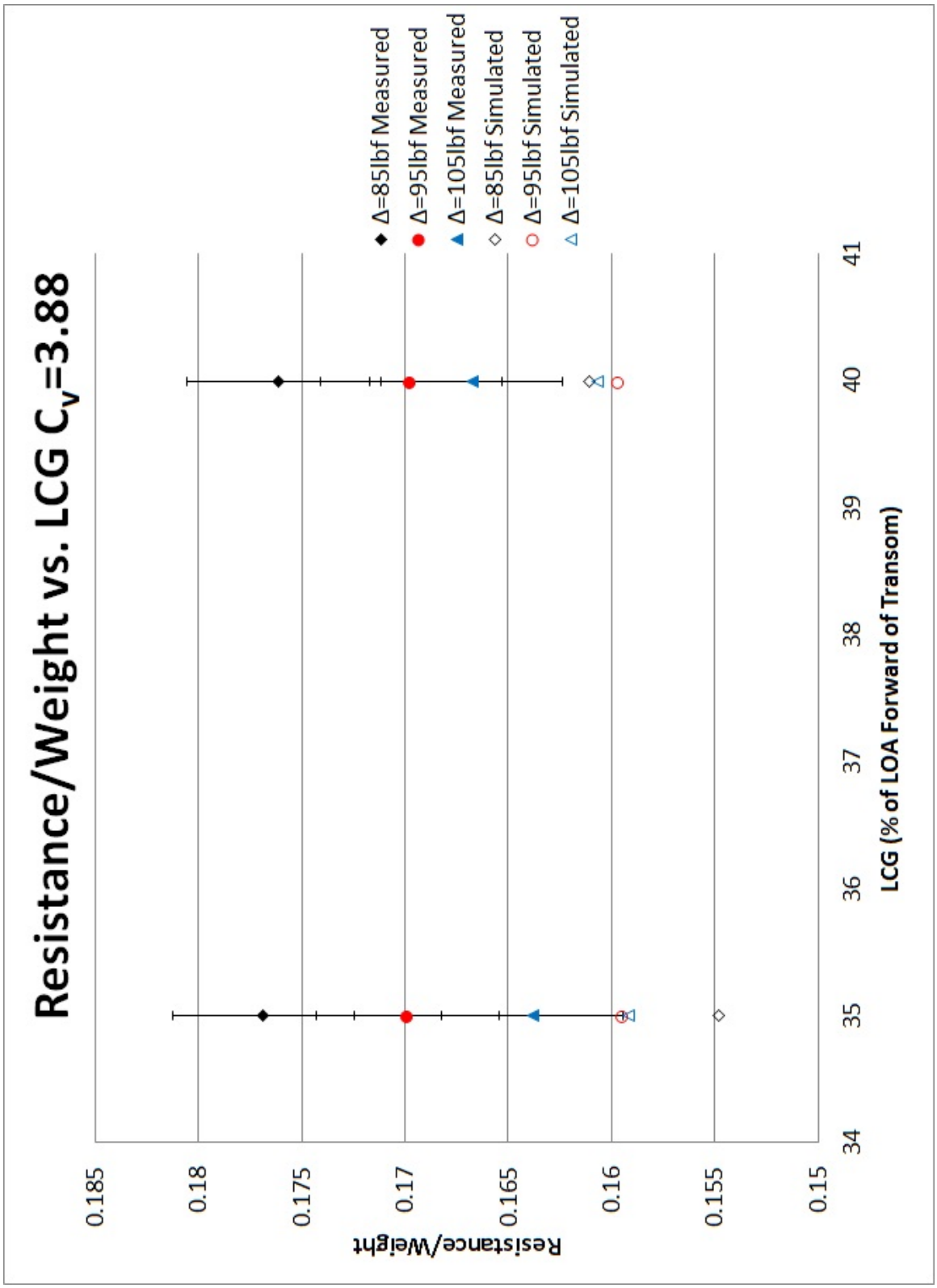

Figure 4.24: Resistance/Weight vs.LCG at C_V=3.88: Simulations under predicted resistance/weight. At Δ=95 lbf and Δ=105 lbf effect of LCG shift on resistance/weight from simulation similar to model tests

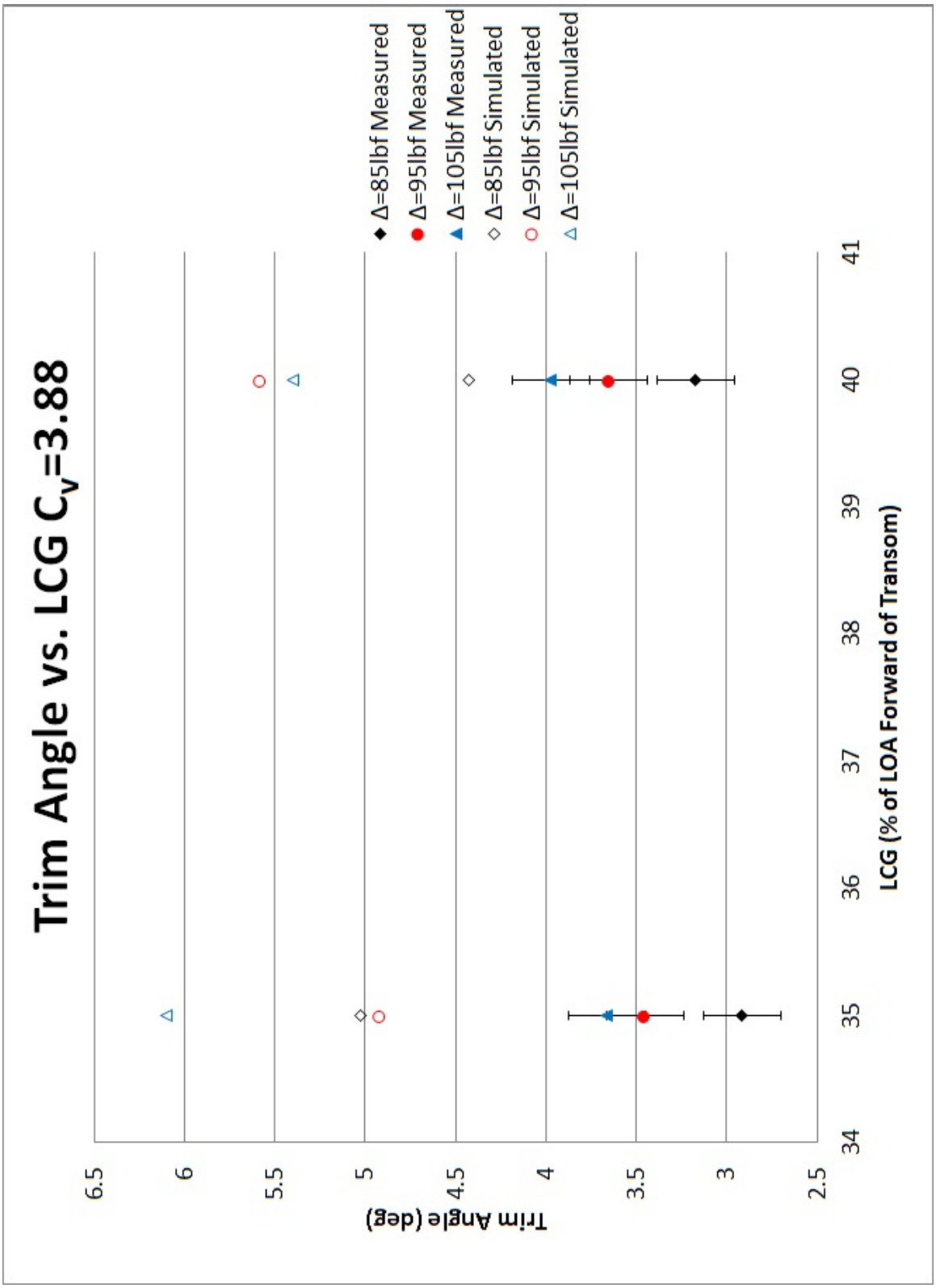

Figure 4.25: Trim Angle vs.LCG at C_V=3.88: Simulations over predicted trim angle. At Δ=85 lbf and Δ=105 lbf effect of LCG shift on trim angle from simulation opposite of model test

4.6 Discussion

Both NFA and OpenFOAM has shown that it is possible to simulate a stepped planing hull going from an initial condition to a steady state planing condition. Both simulation tools implemented mesh motion that allows for multiple degree of freedom motions for planing hulls. The comparison between the separation off of the step seen in the model test and simulation, Figures 4.19 and 4.14, show that to accurately simulate the stepped planing hull, the separated flow off of the step needs to be accurately captured. The inaccuracy in the modeling of the separated flow off of the step can be the cause for the lack of convergence and the error in the results. This shows the importance of high quality meshes and its effect on the solution of the simulation. The computational constraints placed on the simulations requires a concentration of cells near the steps while minimizing the number of cells in the far field to maintain a low cell count. The appropriate meshing, case setup, and application of numerical methods requires a good amount of specialized knowledge and the accurate simulation of a stepped planing hull is beyond the ability of a novice CFD user.

4.6.1 Grid Resolution

One factor that makes simulating a stepped planing hull difficult is the large difference in length scales. The smallest step simulated was 0.0015 boat lengths while the wave profile aft of the hull may be significant a number of boat lengths down stream. The simulations have shown that a large number of cells across the step are needed to resolve the separated flow off the step. This can be difficult to achieve within the constraints of simulation for design applications. NFA does not have any control for prism layers near the hull, so the cell size near the step is driven by the cell distribution. The cell distribution in NFA is controlled by an elliptic equation and the cell stretching needs to be minimized to maintain accuracy of the simulation. This makes the concentration of cells near the step difficult as the ability to create small cells near the step is limited. The smallest cell in the simulation had a height of about 0.0015 boat lengths. SnappyHexMesh, which was used to grid the OpenFOAM mesh, has control over both cell growth and prism layers. The cell splitting in snappyHexMesh allows for a much more rapid change in cell size because a cell split results in eight smaller cells that have edges half the length of the original cell. This prism layers and the cell splitting allows for a concentration of cells near the step with fewer overall number of cells. For the current simulations, about one cell was across the small step in the simulation. The results show that the single cell across the small step was inadequate in resolving the flow off of that step.

4.6.2 NFA

NFA over predicted the resistance when compared to the model test. The Reynold's number for the calculation of the friction resistance is determined by the length overall (LOA) for the hull. For displacement vessels where the load waterline length (LWL) is nearly the LOA, this approximation is suitable, but for planing craft, the wetted keel length can be very different from the LOA. For the stepped planing hull, this is even more important as each of the planing surfaces have a wetted keel length that is much shorter than the LOA. For the speed range covered in the model test, the coefficient of friction using the LOA of the model and the ITTC '57 Friction Line is about 0.0027. Using the wetted length on each of the planing surfaces, the coefficient of friction is about 0.0037. The trim angle was under predicted, which would cause the hull to have an increased wetted surface area and even though the coefficient of friction is lower using the LOA, the friction resistance was still over predicted. The form resistance was over predicted as well. With the lower trim angle, it would be expected that the form resistance would be under predicted rather than over predicted. Theory would state that the under prediction of the trim angle would cause an under prediction of the form resistance. Contray to theory, NFA had over predicted the form resistance.

There are two possible factors that caused errors in NFA's prediction of the results. First, Figure 4.14 shows that the flow separation off of the forward planing surface and the resulting attached flow on the middle planing surface was not accurately modeled by NFA. The two cells across the small forward step of configuration 4 was not sufficient to model the separated flow, Figure 4.9. An increased number of cells would be needed to increase the resolution of the separation zone aft of the step. Secondly, the free slip boundary condition and the absence of modeling the boundary layer could lead to additional error in the results.

4.6.3 OpenFOAM

OpenFOAM under predicted the resistance when compared to the model test. At the heavier displacements the resistance was predicted with results that would probably be acceptable for design work. The trim angle was over predicted and this would lead to the over prediction of the form resistance. Therefore, with a large over prediction of the trim angle, OpenFOAM also over predicted the form resistance. In correlation with the higher trim angle, the hull should have less wetted surface area and a lower friction resistance. OpenFOAM followed this trend and under predicted the friction resistance.

One possible factor for the error in the OpenFOAM results is shown in Figure 4.19. The flow separation off of the forward planing surface and the resulting attached flow on the middle planing surface was not accurately modeled by OpenFOAM. The one cell across the small

forward step of configuration 4 was not sufficient to model the separated flow, Figure 4.9. An increased number of cells would be needed to increase the resolution of the separation zone aft of the step.

4.6.4 Ease of Use

NFA with its simple GUI and single simulation file is much easier to use. The only pre-processing necessary is to develop the hull mesh for NFA. The rest of the simulation setup is done in one location. On the other hand, OpenFOAM required multiple steps to setup the simulation. The mesh was built separately and multiple files had to be changed to update the simulation parameters. Many of these separate steps could be completed in a single script and with some additional programming, a GUI for OpenFOAM could be put together to improve its ease of use.

4.6.5 Simulation Speed

NFA has the benefit of having a processor scaling factor of nearly 1. Therefore, the number of processors can be varied depending on the available time for simulation and available processing power. OpenFOAM on the other hand has a recommended number of cells per processors. Therefore, the cell size would drive the number of processors needed. Other number of cells per processors can be selected to improve speed or reduce processor count. NFA is much more computationally intensive with about 25000 core hours to run a simulation of 7 seconds of simulated time in 48 hours on 512 processors versus about 7000 for OpenFOAM to run a simulation of 30 seconds of simulation time in 144 hours of 48 processors.

4.7 Recommendations for Future Work

4.7.1 NFA

The simulation in NFA can be improved by advancements in the solver so that larger time steps can be used for the simulation. NFA can also be improved with a more accurate interface capturing scheme. The piecewise linear interface capturing method used by NFA can cause diffusivity of the interface. Therefore a large number of small cells are needed to maintain a sharp interface. High resolution capturing schemes such as the Modified High Resolution Interface Capturing (MHRIC) scheme causes less diffusivity of the interface leading to sharper interfaces with fewer number of cells. This will lead to better definition of the

separated flow off of the step.

4.7.2 OpenFOAM

The simulation in OpenFOAM can be improved in a number of ways. First, newer turbulence models for high Reynold's number flows could be added to improve the prediction of the friction resistance such as the Wilcox high Reynold's number k-ω model. Secondly, methods to increase the time step size can be explored. The under relaxation factor can be adjusted to increase time step size. Also, an improved mesh and mesh motion control can ensure that the grid does not move more than one cell size at larger time step sizes. OpenFOAM can also be improved with a more accurate interface capturing scheme. The linear interface capturing method used by OpenFOAM can cause diffusivity of the interface. Therefore a large number of small cells are needed to maintain a sharp interface. Capturing schemes such as the MHRIC scheme causes less diffusivity of the interface leading to sharper interfaces with fewer number of cells, leading to better definition of the separated flow off of the step.

4.7.3 Computational Power

One area of future work is the increased computational capabilities available for simulation. There are three areas to increase computational capabilities; increased availability of high performance computing with current technology, an increase in processing power, and an increase in data transfer between processors. This would allow for larger simulations to be run in the time needed for detailed design. Both NFA and OpenFOAM show that the number of cells in the simulation limited the ability to accurately model the separation off of the small step. Larger simulations will increase grid resolution in this area and increase accuracy.

Chapter 5

Conclusions

This thesis was first started to test the current thought that stepped planing hulls have poor performance when not operating at the design condition. The existing test data did not provide a systematic understanding of the effect of displacement on stepped planing hull performance. As a result a model test, discussed in Chapter 2, was conducted to provide a systematic understanding of the effects that displacement, LCG, and step height have on the performance of a stepped planing hull. Ten different step configurations were tested at three different displacements and over a range of four different speeds in calm water. Seven of these configurations were tested at two difference Longitudinal Center of Gravity (LCG) locations. All of the step configurations tested had less resistance than an unstepped hull. Changes in LCG location and displacement showed that the stepped hull configurations tested has the same sensitivity to changes in LCG location and displacement as an unstepped hull. Therefore, contrary to current understanding, the results have shown that stepped hulls have the same change in performance as unstepped hulls in off design conditions. All of the step configurations tested had less resistance than the unstepped hull The results showed that the primary cause of this reduction in resistance is the reduction in wetted surface area and the reduction of friction drag.

Two observations were made based on the results of the model test. First the flow aft of a step is highly three dimensional because the reattachment line is not straight, but curved. Second, there may be conditions where the stagnation line crosses the step and not the chine of the forward planing surface. The current stepped planing hull prediction methods do not have the capability to handle these two conditions. Chapter 3 probed this further, specifically, a single equation to predict the three dimension wave profile has been developed to account for the three dimensionality of the wave profile and the curved reattachment line. Comparisons with underwater photographs show that the three dimension wave profile captures the reattachment line better than the two dimension wave profile. The method has been expanded to account for the stagnation line crossing the step. A chines dry lift

equation have been added to calculate the lift when the stagnation line crosses the step. A lift equation to predict lift at high speed has been added to expand the applicability of the method to very high speed planing craft. The method has been expanded for use with any number of steps and the lift is calculated on all the planing surfaces thus allowing the method to be used for a stepped planing hull with any number of steps. A sensitivity study has been conducted by increasing the coefficients of the three dimension wave profile. This thesis shows that the modified equation better predicted the reattachment length. Using this modified equation, the stepped planing hull prediction method predicted more accurate results than Savitsky's planing prediciton method.

Simulating an unstepped hull has been difficult due to the many different flow physics that have to be captured. The addition of a step increases the complexity of the simulation. A series of simulations, discussed in Chapter 4, have been run in OpenFOAM and NFA to assess the modeling gaps and computational constraints in current state of the art numerical simulation tools when analyzing stepped planing hulls. The simulation results were compared to the model test results in Chapter 2. Both NFA and OpenFOAM has shown that it is possible to simulate a stepped planing hull going from an initial condition to a steady state planing condition. The comparison between the separation off of the step seen in the model test and simulation show that to accurately simulate the stepped planing hull, the separated flow off of the step needs to be accurately captured. The inaccuracy in the modeling of the separated flow off of the step can be cause lack of convergence and the error in the results. This shows the importance of high quality meshes and its effect on the solution of the simulation. The computational constraints placed on the simulations requires a concentration of cells near the steps while minimizing the number of cells in the far field to maintain a low cell count. The appropriate meshing, case setup, and application of numerical methods requires a good amount of specialized knowledge and the accurate simulation of a stepped planing hull is beyond the ability of a novice CFD user.

In conclusion, this thesis has advanced the current research of stepped planing hulls in the areas of model testing, prediction methods, and numerical methods. A systematic understanding of the effect of displacement, LCG, and step height on stepped planing hull performance has been developed. Additions to the stepped planing hull prediction method have been added that increases its accuracy by incorporating a three dimension wave profile and its applicability by the ability to predict conditions when the stagnation line crosses the step. Numerical methods have shown the importance of capturing the simulated flow off the step to the results.

Bibliography

[1] Froude, William (1872). "Experiments to Determine the Resistances at Various Speeds of a Ship of 2,500 Tons, Designed by Reverend C. Meade Ramus," Enclosure No. 31. Admiralty, United Kingdom.

[2] Kapryan, Walter J. and Clement, Eugene P. (1949). "Effect of Increase in Afterbody Length on the Hydrodynamic Qualities of a Flying-boat Hull of High Length-Beam Ratio," TN-1853. NACA Library, Langley, VA.

[3] Parkinson, John B. et al (1939). "Hydrodynamic and Aerodynamic Tests of a Family of Models of Seaplane Floats with Varying Angles of Deadrise N.A.C.A. Models 57-A, 57-B, and 57-C, TN-716," NACA Library, Langley, VA.

[4] Clement, Eugene (2005). "A Configuration for a Stepped Planing Boat Having Minimum Drag (Dynaplane Boat)" International Hydorfoil Society. November 2005.

[5] Rodstrom, R, Edstrand, Hans, and Bratt, H (1953). "The Transverse Stability and Resistance of Single-Step Boats When Planing, Nr. 25," The Swedish State Shipbuilding Experimental Tank, Goteborg, Sweeden.

[6] Filing, James (1993). "Experimental Procedure and Analysis of Stepped Planing Hulls With Applications to Motor Yachts, Patrol Vessels, and Fast Ferries," Webb Institute, Glen Cove, NY

[7] Gassman, William and Kartinen, Scott (1994). "An Investigation Into the Effects of the Step Location and the Longitudinal Center of Gravity Location on the Performance of Stepped Planing Hulls," Webb Institute, Glen Cove, NY

[8] Becker, Christopher, and Loreto, Anthony, and Shell, Justin (2008). "A Systematic study of stepped planing hulls," Webb Institute, Glen Cove, NY.

[9] Garland, William (2010). "Stepped Planing Hull Investigation," United States Naval Academy, Annapolis, MD.

[10] White, Greg and Beaver, William (2010). "Stepped-Hull High-Speed Boat Model Test," EW-07-10. United States Naval Academy, Annapolis, MD.

[11] Taunton, D.J., Hudson, D.A., and Shenoi, R.A. (2010). "Characteristics of a Series of High Speed Hard Chine Planing Hulls Part 1: Performance in Calm Water," International Journal of Small Craft Technology Vol.2010 B2:96.

[12] Savitsky, Daniel (1964), "Hydrodynamic Design of Planing Hulls. Marine Technology. October 1964.

[13] Morabito, Michael (2005). "Early Racing Power Boats" Bachelor Thesis, Webb Institute, June 2005

[14] Svahn, David (2009) "Performance Prediction Of Hulls With Transverse Steps, Master Thesis, Marina System Centre for Naval Architecture, KTH University, June 2009.

[15] Danielsson, J and Stromquist, J (2012) "Conceptual design of a High-Speed Superyacht Tender", Master Thesis, Marina System Centre for Naval Architecture, KTH University, October 2012

[16] Pro-Set Inc (2006). Pro-Set(r) Adhesive Technical Data. Retrieved from http://www.prosetepoxy.com/adhesive_techdata.html

[17] OCV Reinforcements (2012). M723A Chopped Strand Mat For Conformability. Retrieved from http://ocvreinforcements-a.hansonstatus.com/pdf/products/ChoppedStrandMats_M723A_ww_12_2008_Rev1.pdf

[18] BGF Industries (2012). 94101. Retrieved from http://www.bgf.com/pages/data_sheet_detail/?fabric=1

[19] Vectorply Corporation (2012). E-BXM 1708. Retrieved from http://www.vectorply.com/pdf/e-bxm%201708.pdf

[20] Gurit (2012). Corecell A-Foam. Retrieved from http://www.gurit.com/files/documents/corecell-a-foamv9pdf.pdf

[21] Vectorply Corporation (2012). C-BX 0300. Retrieved from http://www.vectorply.com/pdf/c-bx%200300.pdf

[22] Bouget, Jean-Yves (2010). "Camera Calibration Toolbox for MATLAB," Retrieved from http://www.vision.caltech.edu/bouguetj/calib_doc/index.html#parameters

[23] Kimball, Spencer and Mattis, Peter (1993). GIMP [Computer Software].

[24] Hirschtick, John (1993). Solidworks [Computer Software]. Waltham, Ma: Dassault Systmes SolidWorks Corp.

[25] Moler, Cleve (1984). chi2gof. Natick, Ma: Retrieved from Mathworks.http://www.mathworks.com/help/stats/chi2gof.html

[26] Clement, Eugene P., and Pope, James D. (1961). "Stepless and Stepped Planing Hulls-Graphs for Performance Prediction and Design," 1490. David Taylor Model Basin, Bethesda, MD.

[27] Brown, P.W. (1971) "An Experimental and Theoretical Study of Planing Surfaces with Trim Flaps. Stevens Institute of Technology, Davidson Laboratory Report No. 1463.

[28] Savitsky, Daniel and Morabito, Michael (2009). "Surface Wave Contours Associated With The Forebody Wake of Stepped Planing Hulls",Marine Technology, Volume 47, January 2010.

[29] Korvin-Kroukovsky, B.V., Savitsky, Daniel, and Lehman, William F.: (1948) "Wave Contours in the Wake of a 10-degree Deadrise Planing Surface" Stevens Institute of Technology, Experimenta lTowlng Tank Report No,. 344, November 1948. Sherman M. Fairchild Publication Fund Paper No.: 170, Institute of the Aeronautical Sciences, New

York.

[30] Korvin-Kroukovsky, B.V., Savitsky, Daniel, and Lehman, William F.: (1948) "Wave Contours in the Wake of a 20-degree Deadrise Planing Surface". Stevens Institute of Technology, Experimental Towing Tank Report No. 337, Jun 6 1948. Sherman M. Fairchild Publication Fund Paper No. 168, Institute of the Aeronautical Sciences, New York.

[31] Korvin-Kroukovsky, B.V., Savitsky, Daniel, and Lehman, William F.: (1949) "Wave Profile of a Vee-Planing Surface, Including Test Data on a 30-degree Deadrise Surface." Stevens Institute of Technology, Experimental Towing Tank Report No. 339, Apr 1949. Sherman M. Fairchild Publication Fund Paper No. 229, Institute of the Aeronautical Sciences, New York.

[32] Faltinsen, O (2005). Hydrodynamics of High-Speed Marine Vehicles. Cambridge University Press. New York, NY.

[33] Microsoft Office [Computer Software] Redmond, Wa: Microsoft Corporation. http://office.microsoft.com/en-us/excel/

[34] Hirt, C.W., Nichols, B.D. (1981). "Volume of fluid (VOF) method for the dynamics of free boundaries", Journal of Computational Physics 39 (1): 201225

[35] Sussman, M. and Dommermuth, D. (2001). "The Numerical Simulation of Ship Waves Using Cartesian-Grid Methods" 23rd Symposium on Naval Hydrodynamics, Nantes, France 2001

[36] Orlanski, I (1995). "A Simple Boundary Condition for Unbounded Hyperbolic Flows" Journal of Computational Physics, Volume 21, 1976, pp 251-269

[37] Dommermuth, Douglas G. et al (2006). "The Numerical Simulation of Ship Waves Using Cartesian-Grid and Volume-of-Fluid Methods" 26th Symposium on Naval Hydrodynamics, Rome, Italy 2006

[38] McNeel, Robert (1993). Rhinoceros3D [Computer Software]. Seattle, WA: Robert McNeel & Associates.

[39] O'Shea, Thomas et. al (2013) "Numerical Flow Analysis (NFA) Simulation of Planing Boat in Waves" HPC Insights, Spring 2013, pp 12-17.

[40] U.S. Army Engineer Research and Development Center (ERDC) "High Performance Computing Systems" http://www.erdc.hpc.mil/hardware/

[41] Weller H.G. et al. (1998) "A Tensorial Approach to Comutational Continuum Mechaincs Using Object-Oriented Techniques," Computers in Physics, 12(6), pp. 620-631.

[42] Weller H.G. et al. (1998) . OpenFOAM [Computer Software]. Paris, France: OpenFOAM Foundation

[43] OpenFOAM. 4.4 Numerical Schemes Retrieved from http://www.openfoam.org/docs/user/fvSchemes.php

[44] Chawner, John R. (2007). Pointwise [Computer Software]. Fort Worth, Tx: Pointwise, Inc. http://www.pointwise.com

[45] Dawes, Bill (2007). Boxer Mesh [Computer Software]. Cambridge, UK: Cambridge Flow Solutions Ltd. Retrieved from http://www.cambridgeflowsolutions.com/en/products/boxer-mesh/

[46] Virginia Tech Advanced Research Computing http://www.arc.vt.edu/resources/hpc/blueridge.php

Appendix A

Model Test Data

		Average within truncation limits:									Stern	Middle	Bow	Total
Configuration	Displacement	Vel	Drag	Pitch	Heave	Static Trim (Plate)	Heave/ Beam	Speed Coefficient	R/W	Absolute Trim	Surface Area	Surface Area	Surface Area	Surface Area
Number	lbf	ft/s	lbs	degrees	in	deg				deg	in^2	in^2	in^2	in^2
1	85	24.9838	16.7921	2.8527	1.5638	0.1700	0.0899	3.5949	0.1976	3.0227			878.3835	878.3835
1	85	26.9804	18.4131	2.6820	1.6482	0.1700	0.0947	3.8822	0.2166	2.8520			860.225	860.225
1	85	28.9767	20.2574	2.5324	1.7874	0.1700	0.1027	4.1694	0.2383	2.7024			837.5875	837.5875
1	85	30.9682	22.4297	2.3992	1.8297	0.1700	0.1052	4.4560	0.2639	2.5692			824.005	824.005
1	95	24.9844	17.5634	3.0731	1.7485	0.3400	0.1005	3.5950	0.1849	3.4131			882.8625	882.8625
1	95	26.9786	19.2763	2.8969	1.8823	0.3400	0.1082	3.8819	0.2029	3.2369			864.7525	864.7525
1	95	28.9752	21.1652	2.7178	1.9526	0.3400	0.1122	4.1692	0.2228	3.0578			855.6975	855.6975
1	95	30.9677	23.1142	2.5599	2.0538	0.3400	0.1180	4.4559	0.2433	2.8999			833.06	833.06
1	105	24.9852	18.6803	3.3310	1.9312	0.5700	0.1110	3.5951	0.1779	3.9010			887.39	887.39
1	105	26.9762	19.9079	3.0989	2.0217	0.5700	0.1162	3.8816	0.1896	3.6689			869.28	869.28
1	105	28.9766	21.8595	2.8820	2.1271	0.5700	0.1222	4.1694	0.2082	3.4520			862.4888	862.4888
1	105	30.9684	23.3177	2.6915	2.1777	0.5700	0.1252	4.4560	0.2221	3.2615			842.1615	842.1615
2	85	24.9934	15.9367	2.6168	1.5142	0.5500	0.0870	3.5963	0.1875	3.1668	311	300.3	192.6	803.9
2	85	26.9868	17.4159	2.4420	1.5803	0.5500	0.0908	3.8831	0.2049	2.9920	304.94	294.34	179.28	778.56
2	85	28.9834	19.3585	2.2773	1.6987	0.5500	0.0976	4.1704	0.2277	2.8273	302.14	289.8	173.1	765.04
2	85	30.9738	21.5980	2.1465	1.7910	0.5500	0.1029	4.4568	0.2541	2.6965	301.54	279.8	162.02	743.36
2	95	24.9905	16.9748	2.8753	1.6848	0.7200	0.0968	3.5959	0.1787	3.5953	313.88	306.1	181.74	801.72
2	95	26.9800	18.2784	2.6531	1.7829	0.7200	0.1025	3.8821	0.1924	3.3731	308.1	300.16	167.88	776.14
2	95	28.9792	19.9497	2.4638	1.8811	0.7200	0.1081	4.1698	0.2100	3.1838	306.3	295.5	167.46	769.26
2	95	30.9720	21.8386	2.2961	1.9359	0.7200	0.1113	4.4565	0.2299	3.0161	301.86	290.28	160.48	752.62
2	105	24.9859	18.0703	3.0494	1.8464	0.8500	0.1061	3.5952	0.1721	3.8994	318.42	309.72	167.6	795.74
2	105	26.9815	19.5521	2.8530	2.0071	0.8500	0.1154	3.8823	0.1862	3.7030	308.84	306.88	165.18	780.9
2	105	28.9792	21.0284	2.6477	2.0721	0.8500	0.1191	4.1698	0.2003	3.4977	307.5	301.7	158.24	767.44
2	105	30.9694	22.5185	2.4810	2.1356	0.8500	0.1227	4.4561	0.2145	3.3310	303.26	287.3	150.4	740.96
3	85	24.9848	15.3016	2.6017	1.4917	0.4700	0.0857	3.5950	0.1800	3.0717	209.76	308.32	192.58	710.66
3	85	26.9802	16.4766	2.4109	1.6075	0.4700	0.0924	3.8821	0.1938	2.8809	191.38	303.14	189.8	684.32
3	85	28.9768	17.9781	2.2368	1.7059	0.4700	0.0980	4.1694	0.2115	2.7068	185.88	295.86	177.68	659.42
3	85	30.9695	19.7676	2.0935	1.7859	0.4700	0.1026	4.4562	0.2326	2.5635	179.3	295.28	181.4	655.98
3	95	24.9847	16.4263	2.8180	1.7072	0.8100	0.0981	3.5950	0.1729	3.6280	215.46	316.36	190.52	722.34
3	95	26.9822	17.2887	2.5646	1.8403	0.8900	0.1058	3.8824	0.1820	3.4546	188.64	304.84	187.48	680.96
3	95	28.9763	18.7654	2.4117	1.9161	0.8100	0.1101	4.1694	0.1975	3.2217	186.66	302.24	179.12	668.02
3	95	30.9708	20.1276	2.2498	1.9827	0.8100	0.1140	4.4563	0.2119	3.0598	167.68	300.06	172.1	639.84
3	105	24.9876	17.5242	3.0108	1.8972	0.8900	0.1090	3.5954	0.1669	3.9008	223.36	320.34	185.9	729.6
3	105	26.9808	18.2117	2.7606	2.0139	0.8900	0.1157	3.8822	0.1734	3.6506	206.9	315.78	172.52	695.2
3	105	28.9775	19.3106	2.5496	2.1475	0.8900	0.1234	4.1695	0.1839	3.4396	182.36	313.26	166.78	662.4
3	105	30.9665	20.9618	2.3252	2.2007	0.8900	0.1265	4.4557	0.1996	3.2152	171.62	306.18	163.24	641.04
4	85	24.9850	14.3153	2.5686	1.5673	0.5700	0.0901	3.5951	0.1684	3.1386	88.94	312.46	170.48	571.88
4	85	26.9799	14.9702	2.6010	1.7616	0.5700	0.1012	3.8821	0.1761	3.1710	58.64	304.28	145.48	508.4
4	85	28.9765	16.1290	2.5150	1.9435	0.5700	0.1117	4.1694	0.1898	3.0850	44.22	297.94	129.7	471.86
4	85	30.9684	16.6569	2.4337	2.0461	0.5700	0.1176	4.4560	0.1960	3.0037	40.56	289.38	122.4	452.34
4	95	24.9869	15.6019	2.8811	1.7736	0.9000	0.1019	3.5953	0.1642	3.7811	93.34	314.2	157.7	565.24
4	95	26.9812	16.1230	2.7498	1.9224	0.9000	0.1105	3.8823	0.1697	3.6498	93.12	308.3	147.2	548.62
4	95	28.9785	17.0044	2.6317	2.0500	0.9000	0.1178	4.1697	0.1790	3.5317	77.7	302.44	126.48	506.62
4	95	30.9695	17.8552	2.5331	2.2124	0.9000	0.1272	4.4562	0.1879	3.4331	53.1	295.7	114.88	463.68
4	105	24.9872	16.8133	3.0935	1.9519	1.0500	0.1122	3.5954	0.1601	4.1435	140.04	321.3	173.38	634.72
4	105	26.9865	16.9538	3.0897	1.9690	1.0500	0.1132	3.5953	0.1615	4.1397	140.04	321.3	173.38	634.72
4	105	26.9803	17.5102	2.9216	2.1049	1.0500	0.1210	3.8822	0.1668	3.9716	104.08	315.26	139.88	559.22
4	105	28.9799	18.1188	2.7744	2.2564	1.0500	0.1297	4.1699	0.1726	3.8244	97.08	309.2	136.74	543.02
4	105	30.9723	18.8658	2.6257	2.4079	1.0500	0.1384	4.4566	0.1797	3.6757	95.86	301.42	120.02	517.3
5	85	24.9928	15.4750	2.3738	1.4854	0.6000	0.0854	3.5962	0.1821	2.9738	297.98	216.36	231.12	745.46
5	85	26.9897	16.9170	2.1868	1.5829	0.6000	0.0910	3.8835	0.1990	2.7868	291.06	207.92	216.88	715.86
5	85	28.9868	18.0432	2.0069	1.6914	0.6000	0.0972	4.1709	0.2123	2.6069	286.14	200.36	210.52	697.02
5	85	30.9780	19.8916	1.8258	1.7502	0.6000	0.1006	4.4574	0.2340	2.4258	284.56	197.28	207.38	689.22
5	95	24.9942	16.7176	2.6272	1.6381	0.8800	0.0941	3.5964	0.1760	3.5072	301.26	223.46	237.64	762.36
5	95	26.9898	17.7483	2.4071	1.7655	0.8800	0.1015	3.8835	0.1868	3.2871	292.04	218.7	214.16	724.9
5	95	28.9845	19.0861	2.2090	1.9124	0.8800	0.1099	4.1705	0.2009	3.0890	291.38	205.24	204.54	701.16
5	95	30.9769	20.6463	2.0230	1.8953	0.8800	0.1089	4.4572	0.2173	2.9030	282.64	203.98	201.52	688.14
5	105	24.9911	17.6178	2.8731	1.8057	0.9800	0.1038	3.5959	0.1678	3.8531	302.96	233.26	209.92	746.14
5	105	26.9858	18.8302	2.6203	1.9412	0.9800	0.1116	3.8829	0.1793	3.6003	302.66	287.64	206.9	797.2
5	105	28.9828	19.8845	2.3850	2.0495	0.9800	0.1178	4.1703	0.1894	3.3650	293.64	227.46	195.08	716.18
5	105	30.9763	21.2840	2.1872	2.1359	0.9800	0.1228	4.4571	0.2027	3.1672	292.08	209.22	193.2	694.5
6	85	24.9914	14.8790	2.3755	1.4984	0.6900	0.0861	3.5960	0.1750	3.0655	210.9	226.2	231.58	668.68
6	85	26.9836	16.3228	2.1755	1.6025	0.6900	0.0921	3.8826	0.1920	2.8655	189.36	213.06	224.48	626.9
6	85	28.9820	17.0479	2.0185	1.7194	0.6900	0.0988	4.1702	0.2006	2.7085	167.56	203.58	204.6	575.74
6	85	30.9738	18.5453	1.7242	1.7794	0.6900	0.1023	4.4568	0.2182	2.4142	161.76	192.62	200.64	555.02
6	95	24.9891	15.8601	2.5869	1.6866	0.9800	0.0969	3.5956	0.1669	3.5669	211.14	235.84	215.94	662.92
6	95	26.9839	17.1027	2.3652	1.7695	0.9800	0.1017	3.8827	0.1800	3.3452	202.5	227.28	213.12	642.9
6	95	28.9825	17.9140	2.1747	1.9173	0.9800	0.1102	4.1702	0.1886	3.1547	186.08	221.22	209.96	617.26
6	95	30.9749	19.1857	2.0207	2.0318	0.9800	0.1168	4.4569	0.2020	3.0007	175.16	217.56	213.94	606.66
6	105	24.9866	16.8615	2.8933	1.7979	1.1100	0.1033	3.5953	0.1606	4.0033	212.1	247.46	211.44	671
6	105	26.9859	17.5146	2.6492	1.9018	1.1100	0.1093	3.8830	0.1668	3.7592	203.44	231.42	209.28	644.14
6	105	28.9900	18.6139	2.4289	1.9857	1.1100	0.1141	4.1713	0.1773	3.5389	188.06	227.94	186.46	602.46
6	105	30.9810	19.7482	2.2638	2.0731	1.1100	0.1191	4.4578	0.1881	3.3738	184.98	222.66	180.72	588.36
7	85	24.9975	15.1209	2.2121	1.4539	0.8400	0.0836	3.5969	0.1779	3.0521	313.34	101.6	232.4	647.34
7	85	26.9956	15.8296	2.0182	1.5667	0.8400	0.0900	3.8844	0.1862	2.8582	306.38	92.84	241.18	640.4
7	85	28.9901	17.0706	1.8382	1.6020	0.8400	0.0921	4.1713	0.2008	2.6782	290.84	91.76	229.88	612.48
7	85	30.9782	18.6162	1.6745	1.6686	0.8400	0.0959	4.4574	0.2190	2.5145	285.34	69.56	237.32	592.22
7	95	24.9965	16.0860	2.4345	1.6534	1.1200	0.0950	3.5967	0.1693	3.5545	307.48	141.84	236.34	685.66
7	95	26.9920	16.8584	2.2118	1.7606	1.1200	0.1012	3.8838	0.1775	3.3318	297.04	110.72	230.34	638.1
7	95	28.9884	17.8281	2.0246	1.8342	1.1200	0.1054	4.1711	0.1877	3.1446	289.72	89	237.7	616.42
7	95	30.9816	19.4078	1.8272	1.8922	1.1200	0.1087	4.4579	0.2043	2.9472	282.58	87.88	226.56	597.02
7	105	24.9964	17.2416	2.6814	1.8394	1.2500	0.1057	3.5967	0.1642	3.9314	317.44	164.68	233.72	715.84
7	105	26.9908	18.0786	2.4149	1.9264	1.2500	0.1107	3.8837	0.1722	3.6649	310.48	147.6	236.2	694.28
7	105	28.9862	18.5713	2.1785	1.9729	1.2500	0.1134	4.1708	0.1769	3.4285	305.42	140.84	225.94	672.2
7	105	30.9766	19.8846	1.9632	2.0515	1.2500	0.1179	4.4572	0.1894	3.2132	296.6	141.7	224.32	662.62

Figure A.1: Model Test Data-LCG=40% of LOA forward of the Transom

		Average within truncation limits:									Stern	Middle	Bow	Total
Configuration Number	Displacement lbf	Vel fps	Drag lbs	Pitch degrees	Heave in	Static Trim (Plate) deg	Heave/ Beam	Speed Coefficient	R/W	Absolute Trim deg	Surface Area in^2	Surface Area in^2	Surface Area in^2	Surface Area in^2
1	85	25.00932	16.20191	1.762583	1.91347	1.4800	0.1100	3.5986	0.1906	3.2426				726.7039
1	85	26.99903	17.40004	1.453726	1.98252	1.4800	0.1139	3.8849	0.2047	2.9337				717.6484
1	85	29.00752	18.80031	1.165803	2.08846	1.4800	0.1200	4.1739	0.2212	2.6458				724.44
1	85	31.0009	20.23001	0.933094	2.10554	1.4800	0.1210	4.4607	0.2380	2.4131				710.8568
1	95	25.01964	17.2341	1.937226	2.09692	1.7200	0.1205	3.6000	0.1814	3.6572				715.3845
1	95	27.01877	18.47356	1.594971	2.24184	1.7200	0.1288	3.8877	0.1945	3.3150				715.3845
1	95	29.02143	19.72274	1.279397	2.31943	1.7200	0.1333	4.1759	0.2076	2.9994				706.329
1	95	31.01233	21.29154	0.981191	2.39901	1.7200	0.1379	4.4623	0.2241	2.7012				719.9123
1	105	25.03097	18.43503	2.077736	2.35686	1.8100	0.1355	3.6017	0.1756	3.8877				719.9123
1	105	27.02237	19.43226	1.634436	2.46933	1.8100	0.1419	3.8882	0.1851	3.4444				706.329
1	105	29.02149	20.67296	1.315895	2.53505	1.8100	0.1457	4.1759	0.1969	3.1259				710.8568
1	105	31.01361	22.00329	1.012651	2.5884	1.8100	0.1488	4.4625	0.2096	2.8227				679.1625
2	85	25.03139	15.1369	1.476969	1.84996	1.7500	0.1063	3.6017	0.1781	3.2270	259.52	302.64	91.28	607.8
2	85	27.02723	16.21889	1.150745	1.91777	1.7500	0.1102	3.8889	0.1908	2.9007	249.48	294.98	98.8	593.86
2	85	29.02718	17.88184	0.832771	1.98905	1.7500	0.1143	4.1767	0.2104	2.5828	245.36	287.24	101.94	583.57
2	85	31.02256	19.75987	0.566313	2.06801	1.7500	0.1189	4.4638	0.2325	2.3163	239.58	283.84	98.88	572.86
2	95	25.02224	16.37779	1.625281	2.08329	1.9400	0.1197	3.6004	0.1724	3.5653	259.2	295.42	79.2	594.22
2	95	27.01129	17.33359	1.283173	2.19001	1.9400	0.1259	3.8866	0.1825	3.2232	253.98	288.18	89.54	586.93
2	95	29.01495	18.51731	0.942789	2.21967	1.9400	0.1276	4.1749	0.1949	2.8828	243.26	275.3	86.02	561.57
2	95	31.01151	20.12492	0.676175	2.30328	1.9400	0.1324	4.4622	0.2118	2.6162	267.1	306.52	70.74	608.99
2	105	25.02403	17.58955	1.790943	2.27888	2.0300	0.1310	3.6007	0.1675	3.8209	274.36	310.32	77.16	623.26
2	105	27.02559	18.35513	1.396055	2.40771	2.0300	0.1384	3.8887	0.1748	3.4261	250.92	298.84	71.82	585.67
2	105	29.02432	19.51418	1.032597	2.48422	2.0300	0.1428	4.1763	0.1858	3.0626	248.28	291.96	79.46	579.97
2	105	31.02199	20.82967	0.75288	2.50278	2.0300	0.1438	4.4637	0.1984	2.7829	245.22	281.44	80.64	566.98
3	85	25.0156	14.8434	1.427466	1.85881	1.8400	0.1068	3.5995	0.1746	3.2675	197.84	299.1	84.28	539.08
3	85	27.01133	15.93589	1.073458	1.94644	1.8400	0.1119	3.8866	0.1875	2.9135	187.08	289.92	88.58	521.29
3	85	29.00818	17.21454	0.786536	2.00174	1.8400	0.1150	4.1739	0.2025	2.6265	176.02	278.08	95	501.6
3	85	31.01082	18.713	0.509921	2.0189	1.8400	0.1160	4.4621	0.2202	2.3499	167.52	273.86	108.26	495.51
3	95	25.01713	15.93489	1.547487	2.09255	2.0800	0.1203	3.5997	0.1677	3.6275	198.3	304.8	74.9	540.55
3	95	27.0061	16.81694	1.183238	2.1591	2.0800	0.1241	3.8859	0.1770	3.2632	192.26	298.12	83.34	532.05
3	95	29.01236	17.75317	0.851708	2.19142	2.0800	0.1259	4.1745	0.1869	2.9317	183.32	289.58	86.4	516.1
3	95	31.01243	19.21286	0.565816	2.27532	2.0800	0.1308	4.4623	0.2022	2.6458	170.66	278.32	93.3	495.63
3	105	25.0195	17.14048	1.672152	2.33553	2.1700	0.1342	3.6000	0.1632	3.8422	224.4	312.6	72.94	573.47
3	105	27.01332	17.72499	1.290908	2.36053	2.1700	0.1357	3.8869	0.1688	3.4609	206.74	306.26	74.7	550.35
3	105	29.03796	18.73101	0.986972	2.3648	2.1700	0.1359	4.1782	0.1784	3.1570	190.1	296.34	75.16	524.02
3	105	31.03422	20.03836	0.607451	2.48263	2.1700	0.1427	4.4655	0.1908	2.7775	173.26	286.58	73.68	496.68
4	85	25.03997	14.29934	1.474997	1.86556	1.9200	0.1072	3.6030	0.1682	3.3950	179.96	308.34	75.36	525.98
4	85	27.03674	15.03198	1.159472	1.9585	1.9200	0.1126	3.8903	0.1768	3.0795	157.36	290.1	75.78	485.35
4	85	29.03571	16.02735	0.883702	2.08105	1.9200	0.1196	4.1779	0.1886	2.8037	127.74	277.86	71.28	441.24
4	85	31.03484	17.10135	0.669046	2.10129	1.9200	0.1208	4.4656	0.2012	2.5890	118.82	271.48	71.62	426.11
4	95	25.0285	15.49728	1.613875	2.09067	2.2000	0.1202	3.6013	0.1631	3.8139	187.96	308.48	73.6	533.24
4	95	27.01229	16.13702	1.251855	2.19789	2.2000	0.1263	3.8868	0.1699	3.4519	166.64	297.42	71.94	500.03
4	95	29.01186	16.9612	1.019139	2.30084	2.2000	0.1322	4.1745	0.1785	3.2191	155.3	287.18	66.78	475.87
4	95	31.0084	17.895	0.759636	2.33476	2.2000	0.1342	4.4618	0.1884	2.9596	140.42	280.34	70.2	455.86
4	105	25.01709	16.85687	1.761237	2.33956	2.2900	0.1345	3.5997	0.1605	4.0512	189.42	317.64	71.62	542.87
4	105	27.00604	17.2009	1.372897	2.39026	2.2900	0.1374	3.8859	0.1638	3.6629	178.1	301.62	60.74	510.09
4	105	29.01313	17.93954	1.039491	2.50778	2.2900	0.1441	4.1747	0.1709	3.3295	167.48	293.44	66.02	493.93
4	105	31.00616	18.96908	0.773856	2.5714	2.2900	0.1478	4.4614	0.1807	3.0639	156.14	283.2	64.24	471.46
5	85	25.0334	15.06945	1.284421	1.81148	1.8200	0.1041	3.6020	0.1773	3.1044	264.58	261.64	106.48	579.46
5	85	27.02645	16.12462	0.985122	1.9547	1.8200	0.1123	3.8888	0.1897	2.8051	256.9	245.64	111.96	558.52
5	85	29.0306	17.4913	0.667489	1.9645	1.8200	0.1129	4.1772	0.2058	2.4875	247.42	235.12	112.3	538.69
5	85	31.02611	18.94806	0.41179	2.12334	1.8200	0.1220	4.4643	0.2229	2.2318	235.54	215.6	115.8	509.04
5	95	25.03364	15.9464	1.465618	2.08309	2.1200	0.1197	3.6021	0.1679	3.5856	280.4	274.44	97.44	603.56
5	95	27.0244	17.0999	1.117554	2.16298	2.1200	0.1243	3.8885	0.1800	3.2376	267.02	261.38	97.54	577.17
5	95	29.03128	18.33693	0.761806	2.24831	2.1200	0.1292	4.1773	0.1930	2.8818	261.18	245.88	103.58	558.85
5	95	31.02523	19.71466	0.454515	2.27258	2.1200	0.1306	4.4642	0.2075	2.5745	251.84	232.86	111.58	540.49
5	105	25.03317	17.25417	1.605479	2.29767	2.2400	0.1321	3.6020	0.1643	3.8455	283.08	288.06	88.5	615.39
5	105	27.02252	18.09209	1.208878	2.42792	2.2400	0.1395	3.8882	0.1723	3.4489	277.36	279.2	88.34	600.73
5	105	29.03195	19.07554	0.851221	2.43592	2.2400	0.1400	4.1774	0.1817	3.0912	262.48	260.8	97.74	572.15
5	105	30.99789	20.63431	0.59894	2.45585	2.2400	0.1411	4.4602	0.1965	2.8389	251.5	243.14	104.24	546.76
6	85	25.04107	14.5899	1.245949	1.85373	1.9600	0.1065	3.6031	0.1716	3.2059	207.22	266.78	108.06	528.03
6	85	27.03249	15.68086	0.89882	1.93977	1.9600	0.1115	3.8897	0.1845	2.8588	190.62	254.1	109.18	499.31
6	85	29.03804	16.77679	0.605915	2.04175	1.9600	0.1173	4.1782	0.1974	2.5659	174.38	240.76	114.44	472.36
6	85	31.03217	18.18842	0.349453	2.06795	1.9600	0.1188	4.4652	0.2140	2.3095	165.48	232.38	119.96	457.84
6	95	25.03802	15.69496	1.344587	2.06649	2.2100	0.1188	3.6027	0.1652	3.5546	234.38	279.32	92.1	559.75
6	95	27.0347	16.55741	1.019	2.08453	2.2100	0.1198	3.8900	0.1743	3.2290	225.34	265.8	98.52	540.4
6	95	29.03942	17.71019	0.667847	2.20109	2.2100	0.1265	4.1784	0.1864	2.8778	213.38	241.08	119.9	514.41
6	95	31.03371	18.90984	0.387614	2.24926	2.2100	0.1293	4.4654	0.1991	2.5976	195.54	232.04	103.98	479.57
6	105	25.03821	16.92808	1.507096	2.23328	2.3200	0.1283	3.6027	0.1612	3.8271	236.94	284.54	79.28	561.12
6	105	27.03762	17.65066	1.119203	2.34357	2.3200	0.1347	3.8904	0.1681	3.4392	226.68	275.52	84.7	544.55
6	105	29.03619	18.44987	0.7584	2.42649	2.3200	0.1395	4.1780	0.1757	3.0784	216.52	254.38	99.62	520.71
6	105	31.03148	19.68555	0.43995	2.51807	2.3200	0.1447	4.4651	0.1875	2.7600	202.7	247.22	96.88	498.36
7	85	25.02986	15.04483	1.113927	1.79786	1.9900	0.1033	3.6015	0.1770	3.1039	284	236.36	133.3	587.01
7	85	27.01496	16.33347	0.841678	1.90884	1.9900	0.1097	3.8871	0.1922	2.8317	283.92	223.5	140.28	577.56
7	85	29.02057	17.60802	0.511795	1.98392	1.9900	0.1140	4.1757	0.2072	2.5018	276.1	210.92	143.5	558.77
7	85	31.02144	19.32359	0.274875	2.03458	1.9900	0.1169	4.4636	0.2273	2.2649	270.9	200.54	160.18	551.53
7	95	25.0313	15.99177	1.276105	2.0138	2.2400	0.1157	3.6017	0.1683	3.5161	274.82	261.9	120.1	596.77
7	95	27.02396	17.25187	0.923422	2.13662	2.2400	0.1228	3.8884	0.1816	3.1634	271.96	243.86	129.72	580.68
7	95	29.03372	18.60376	0.6017	2.1851	2.2400	0.1256	4.1776	0.1958	2.8417	270.34	234.92	137.26	573.89
7	95	31.02605	20.10325	0.326494	2.24566	2.2400	0.1291	4.4643	0.2116	2.5665	263.26	213.74	151.08	552.54
7	105	25.0347	17.05828	1.436351	2.25555	2.3600	0.1296	3.6022	0.1625	3.7964	279.04	272.92	114.96	609.44
7	105	27.02968	18.04313	1.019606	2.35191	2.3600	0.1352	3.8893	0.1718	3.3796	274.98	266	117.1	599.53
7	105	29.03188	19.24685	0.652555	2.38196	2.3600	0.1369	4.1774	0.1833	3.0126	270.36	243.34	123.46	575.43
7	105	31.02998	20.80702	0.370113	2.52535	2.3600	0.1451	4.4649	0.1982	2.7301	261.2	231.42	128.84	557.04

Figure A.2: Model Test Data-LCG=35% of LOA forward of the Transom: Configurations 1-7

8	85	25.03504	14.10229	1.285303	1.91264	2.1000	0.1099	3.6023	0.1659	3.3853	159.44	266.04	110.46	480.71
8	85	27.03015	14.8685	0.98855	2.00928	2.1000	0.1155	3.8893	0.1749	3.0885	136.94	252.12	100.22	439.17
8	85	29.03393	15.77808	0.709459	2.06795	2.1000	0.1188	4.1777	0.1856	2.8095	95.04	234.46	98.02	378.51
8	85	31.02917	16.77703	0.50231	2.17474	2.1000	0.1250	4.4647	0.1974	2.6023	57.98	226.86	100.48	335.08
8	95	25.03922	15.21197	1.411756	2.08625	2.3400	0.1199	3.6029	0.1601	3.7518	169.14	275.76	102.08	495.94
8	95	27.02978	15.8619	1.068649	2.21765	2.3400	0.1275	3.8893	0.1670	3.4086	151.38	259.98	92.38	457.55
8	95	29.03546	16.75029	0.752666	2.27177	2.3400	0.1306	4.1779	0.1763	3.0927	120.28	250.66	93.58	417.73
8	95	31.03127	17.71594	0.513551	2.33281	2.3400	0.1341	4.4650	0.1865	2.8536	97.84	236.28	95.06	381.65
8	105	25.03765	16.57273	1.57348	2.279	2.4200	0.1310	3.6026	0.1578	3.9935	201.38	283.32	89.06	529.23
8	105	27.03192	17.12468	1.149795	2.42944	2.4200	0.1396	3.8896	0.1631	3.5698	155.2	272.42	83.96	469.6
8	105	29.03711	17.90571	0.795097	2.52971	2.4200	0.1454	4.1781	0.1705	3.2151	134.02	262.8	83.88	438.76
8	105	31.03086	18.58084	0.550077	2.58175	2.4200	0.1484	4.4650	0.1770	2.9701	122.32	250.62	82.16	414.02
9	85	25.01451	14.58533	1.029573	1.84593	2.1300	0.1061	3.5993	0.1716	3.1596	209.6	213.04	134.64	489.96
9	85	27.00456	15.79761	0.707515	1.90075	2.1300	0.1092	3.8856	0.1859	2.8375	185.7	201.94	141.66	458.47
9	85	29.01026	16.99636	0.451003	1.98893	2.1300	0.1143	4.1742	0.2000	2.5810	173.02	185.46	151.32	434.14
9	85	31.03101	18.33489	0.199773	2.04651	2.1300	0.1176	4.4650	0.2157	2.3298	163.16	162.62	165.8	408.68
9	95	25.04275	15.52085	1.156201	2.05155	2.4100	0.1179	3.6034	0.1634	3.5662	215	233.92	123.52	510.68
9	95	27.03548	16.55263	0.834697	2.11158	2.4100	0.1214	3.8901	0.1742	3.2447	189.54	217.72	127.12	470.82
9	95	29.03912	17.8419	0.495374	2.08641	2.4100	0.1199	4.1784	0.1878	2.9054	178.48	212.38	129.74	455.73
9	95	31.03544	19.10728	0.217501	2.24373	2.4100	0.1289	4.4656	0.2011	2.6275	166.62	190.84	148.8	431.86
9	105	25.04213	16.67701	1.307085	2.25845	2.4900	0.1298	3.6033	0.1588	3.7971	233.98	251.38	109.88	540.3
9	105	27.03499	17.2784	0.895304	2.34085	2.4900	0.1345	3.8900	0.1646	3.3853	219.32	235.54	116.84	513.28
9	105	29.03902	18.59319	0.523718	2.46094	2.4900	0.1414	4.1784	0.1771	3.0137	197.96	221.3	119.36	478.94
9	105	31.03565	20.02918	0.258157	2.44373	2.4900	0.1404	4.4657	0.1908	2.7482	182.3	203.94	128.58	450.53
10	85	25.01465	13.82146	1.203465	1.8178	2.2600	0.1045	3.5993	0.1626	3.4635	163.02	224.74	121.54	448.53
10	85	27.00986	14.6773	0.927665	1.91982	2.2600	0.1103	3.8864	0.1727	3.1877	127.06	218.06	124.02	407.13
10	85	29.01535	15.5719	0.639603	2.03784	2.2600	0.1171	4.1750	0.1832	2.8996	100.92	207.86	119.9	368.73
10	85	31.00769	16.59273	0.405152	2.08559	2.2600	0.1199	4.4617	0.1952	2.6652	81.16	198.46	121	340.12
10	95	25.03333	15.13317	1.22423	2.04811	2.5400	0.1177	3.6020	0.1593	3.7642	176.6	235.8	117.3	471.05
10	95	27.02823	15.90082	0.892604	2.14752	2.5400	0.1234	3.8891	0.1674	3.4326	169.08	226.48	124.42	457.77
10	95	29.03242	16.90555	0.57282	2.22117	2.5400	0.1277	4.1774	0.1780	3.1128	158.88	208.66	121.74	428.41
10	95	31.02852	18.09267	0.293334	2.26863	2.5400	0.1304	4.4647	0.1904	2.8333	149.38	202.04	129.82	416.33
10	105	25.03669	16.36104	1.367953	2.25707	2.6200	0.1297	3.6025	0.1558	3.9880	186.34	248.6	109.02	489.45
10	105	27.00716	17.0739	1.002	2.3902	2.6200	0.1374	3.8860	0.1626	3.6220	178.24	239.3	108.1	471.59
10	105	29.0222	17.96596	0.619321	2.50651	2.6200	0.1441	4.1760	0.1711	3.2393	166.9	228.28	107.8	449.08
10	105	31.01371	19.00651	0.351485	2.51149	2.6200	0.1443	4.4625	0.1810	2.9715	156.48	209.62	115.82	424.01

Figure A.3: Model Test Data-LCG=35% of LOA forward of the Transom: Configurations 8-10

Appendix B

Model Test Plots

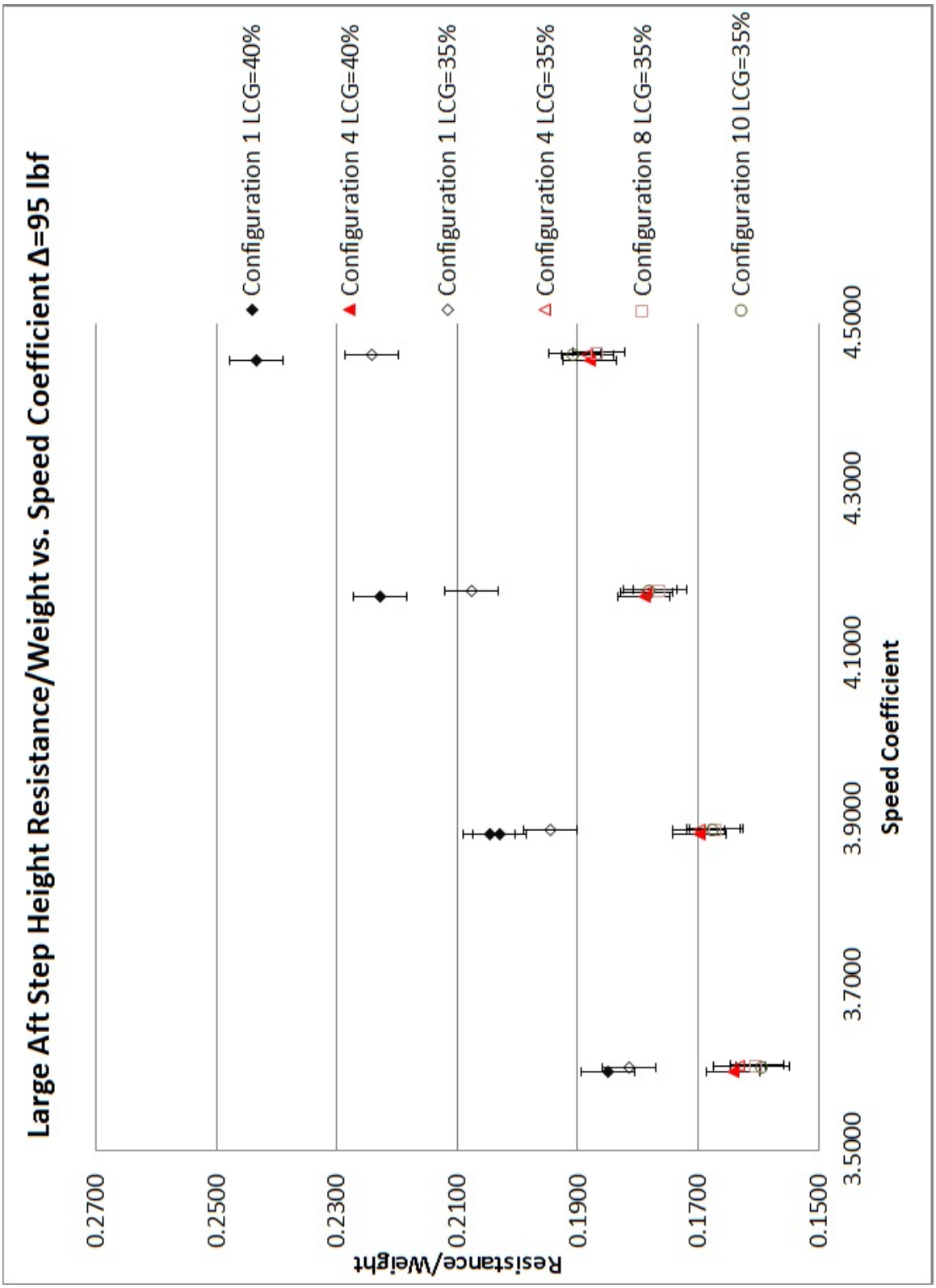

Figure B.1: Large Aft Step Height Resistance/Weight vs. Speed Coefficient at Δ=95 lbf

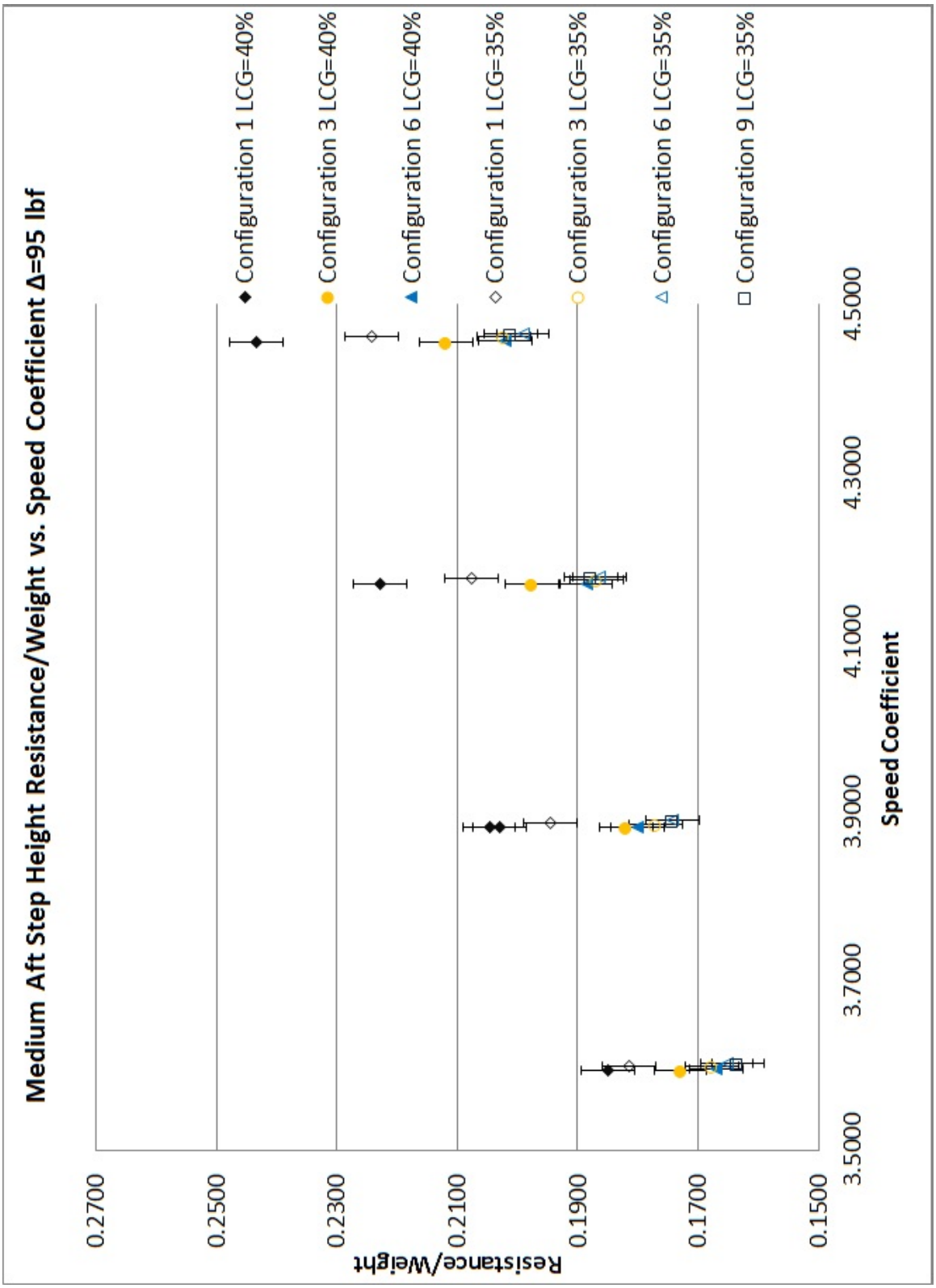

Figure B.2: Medium Aft Step Height Resistance/Weight vs. Speed Coefficient at Δ=95 lbf

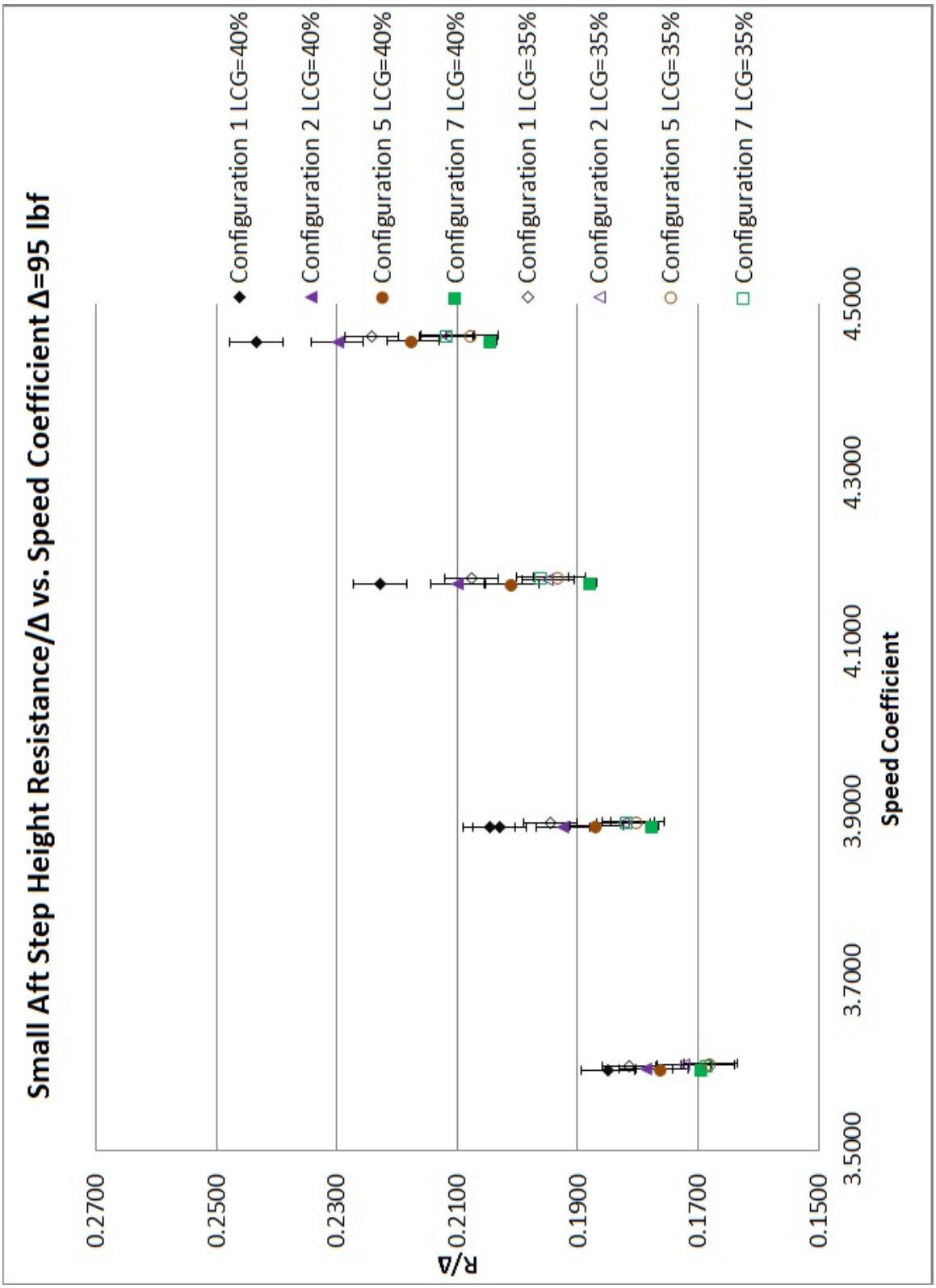

Figure B.3: Small Aft Step Height Resistance/Weight vs. Speed Coefficient at Δ=95 lbf

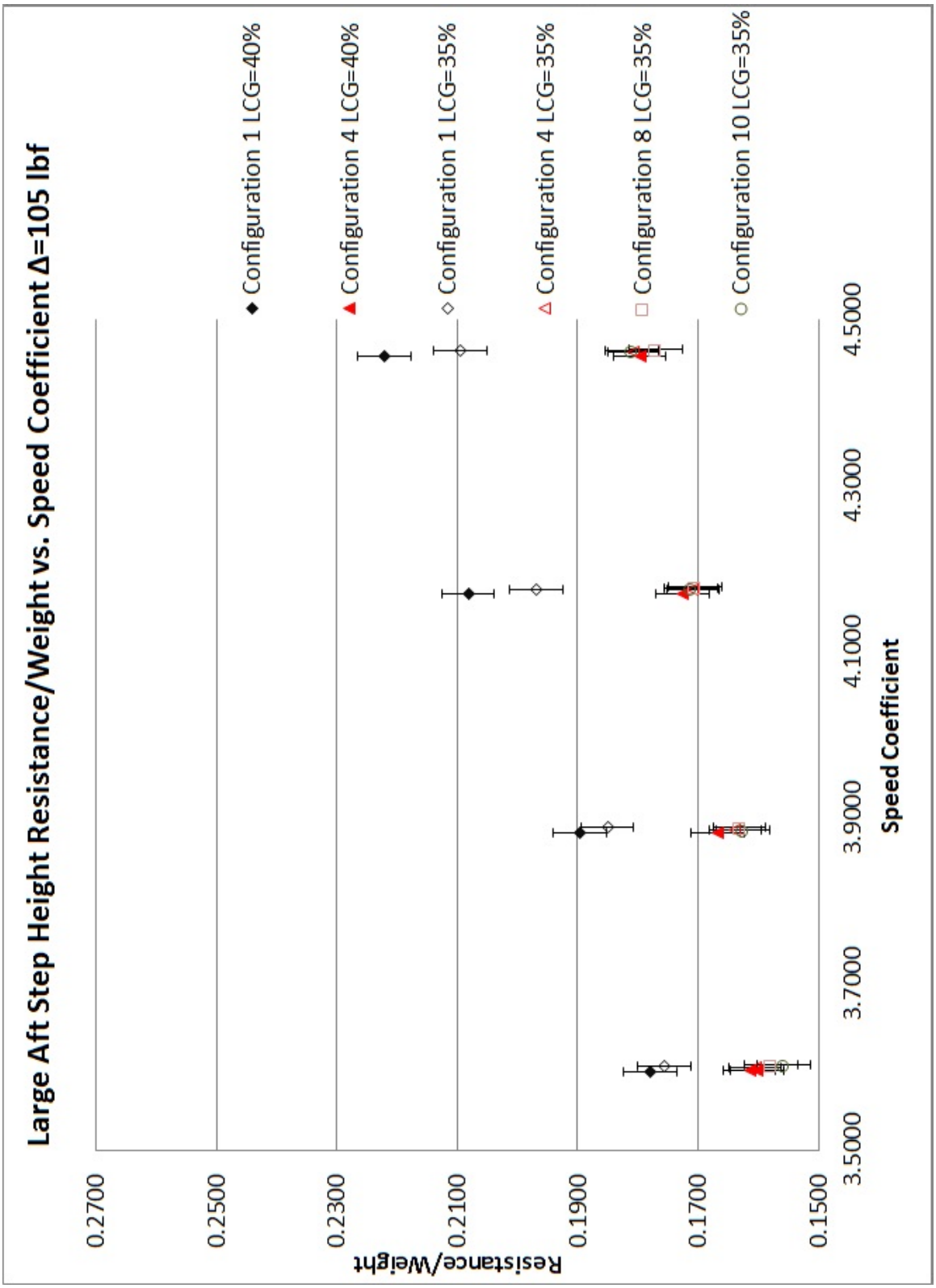

Figure B.4: Large Aft Step Height Resistance/Weight vs. Speed Coefficient at Δ=105 lbf

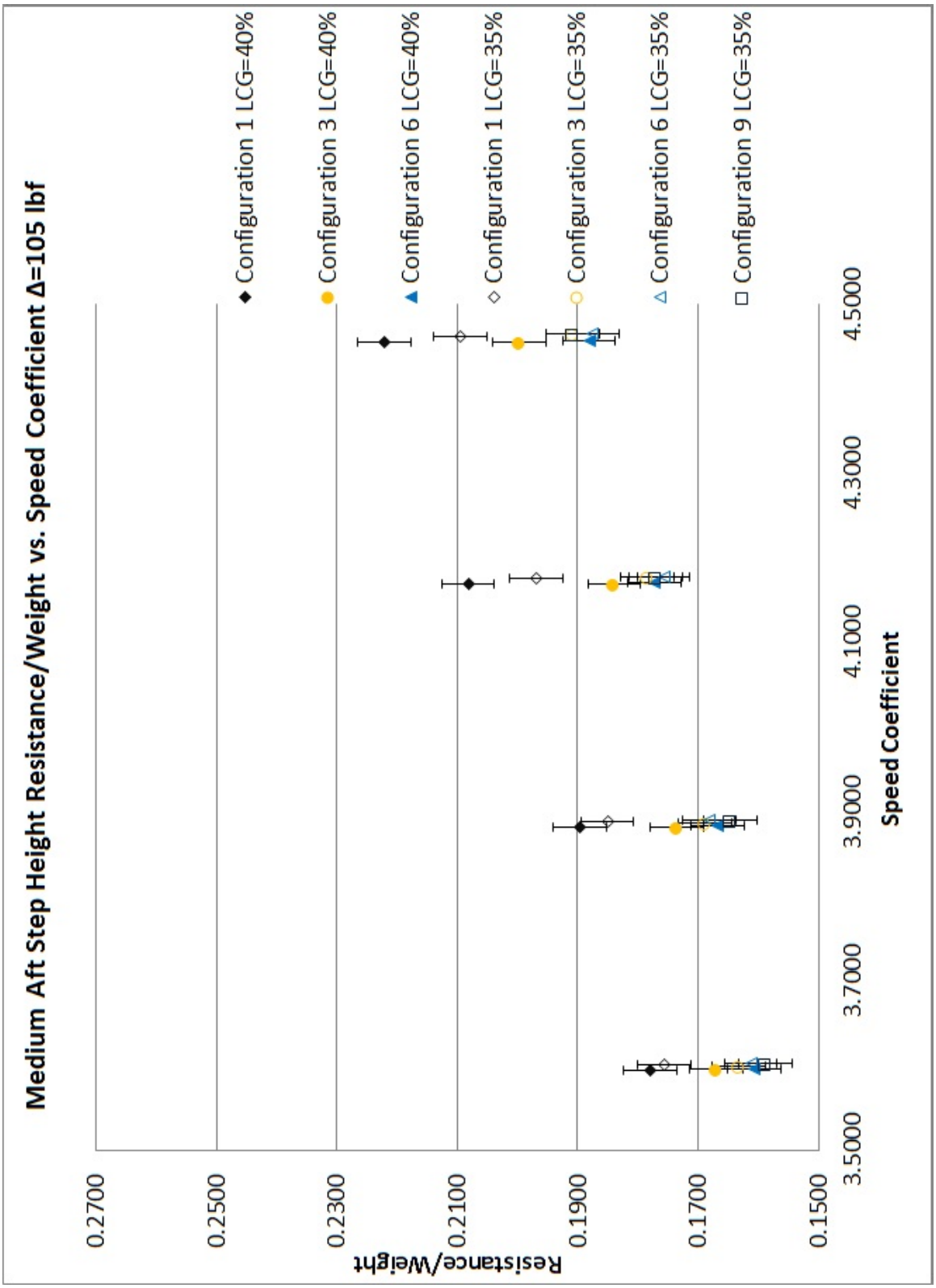

Figure B.5: Medium Aft Step Height Resistance/Weight vs. Speed Coefficient at Δ=105 lbf

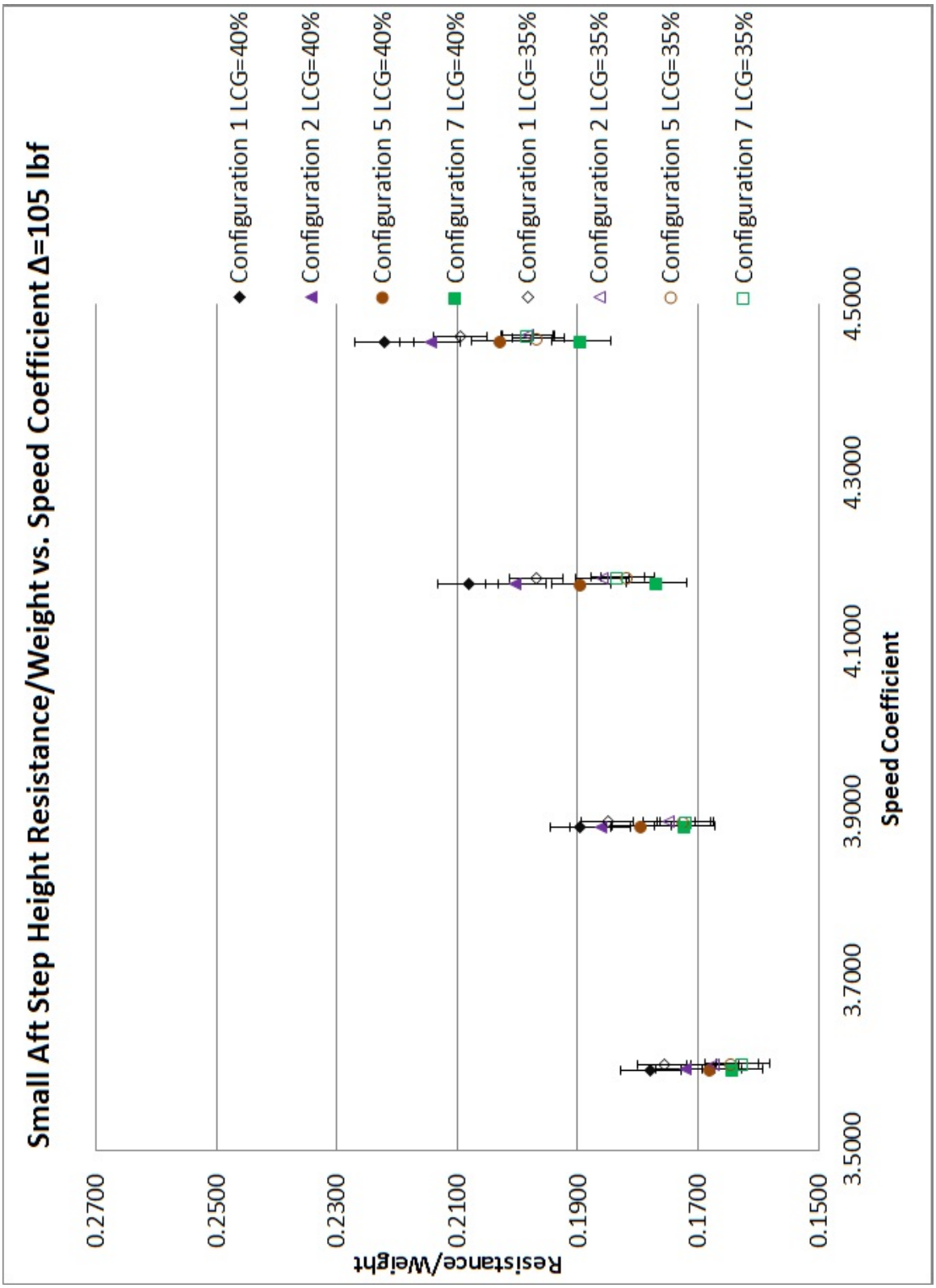

Figure B.6: Small Aft Step Height Resistance/Weight vs. Speed Coefficient at Δ=105 lbf

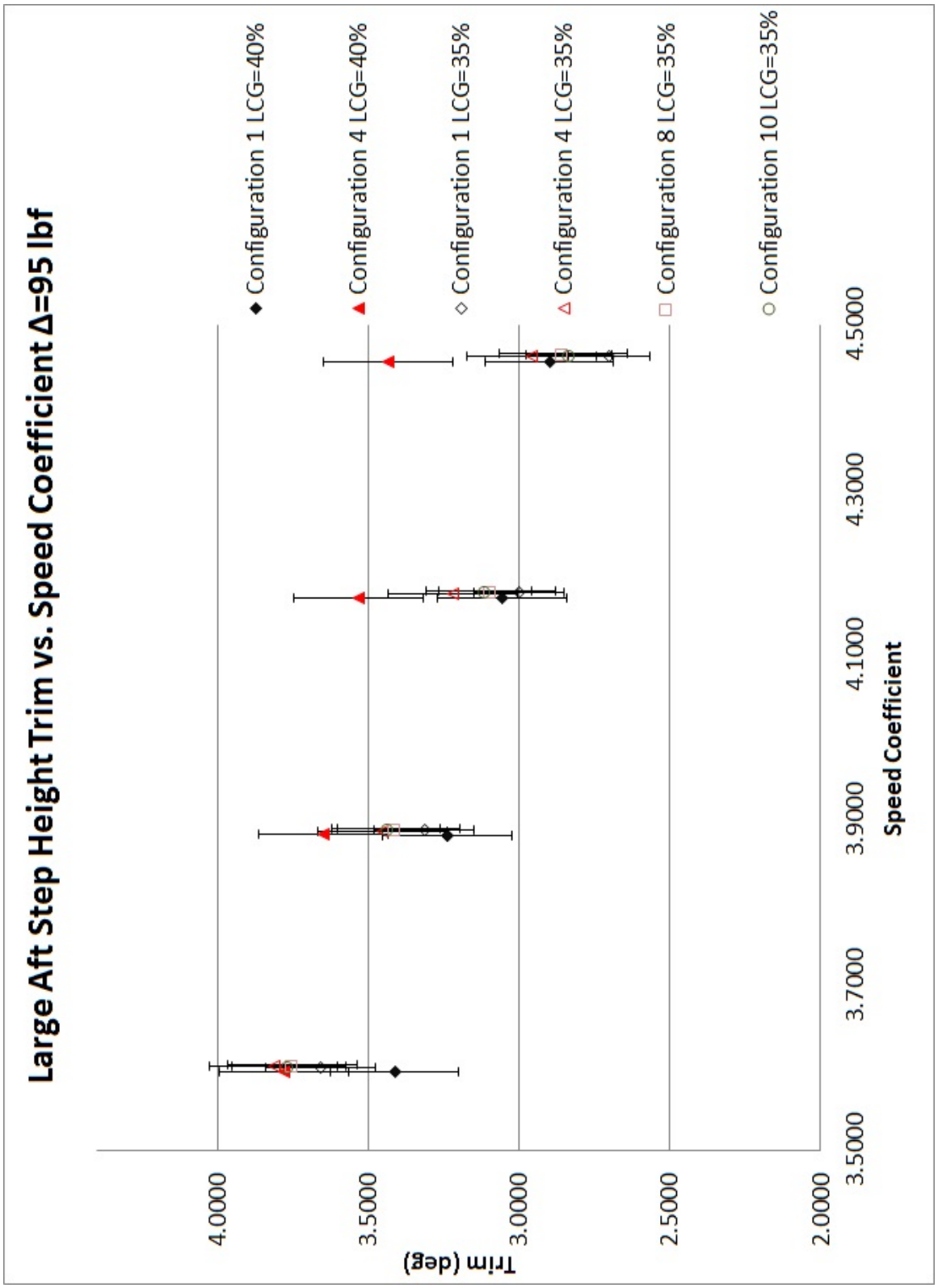

Figure B.7: Large Aft Step Height Trim vs. Speed Coefficient at Δ=95 lbf

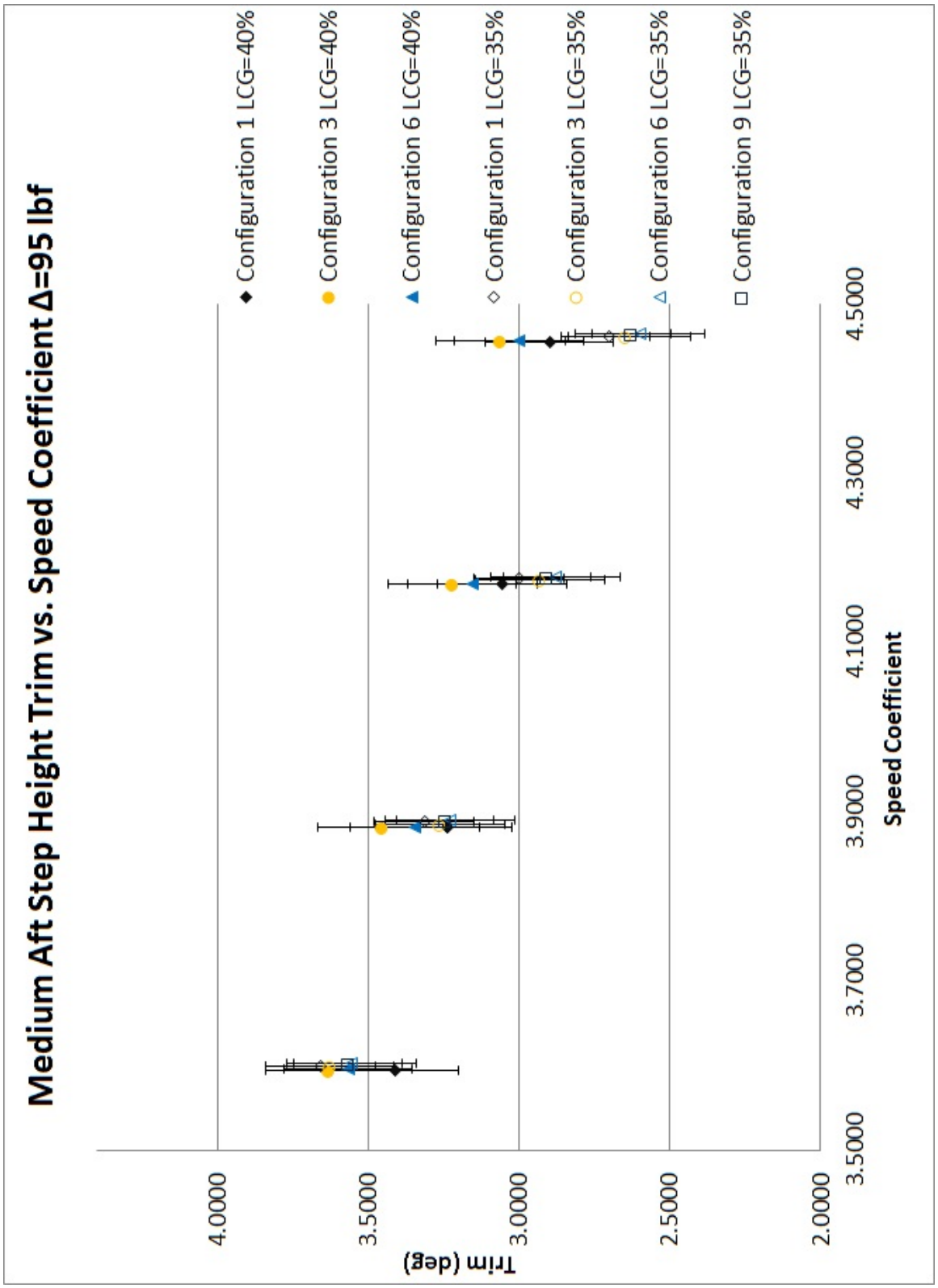

Figure B.8: Medium Aft Step Height Trim vs. Speed Coefficient at Δ=95 lbf

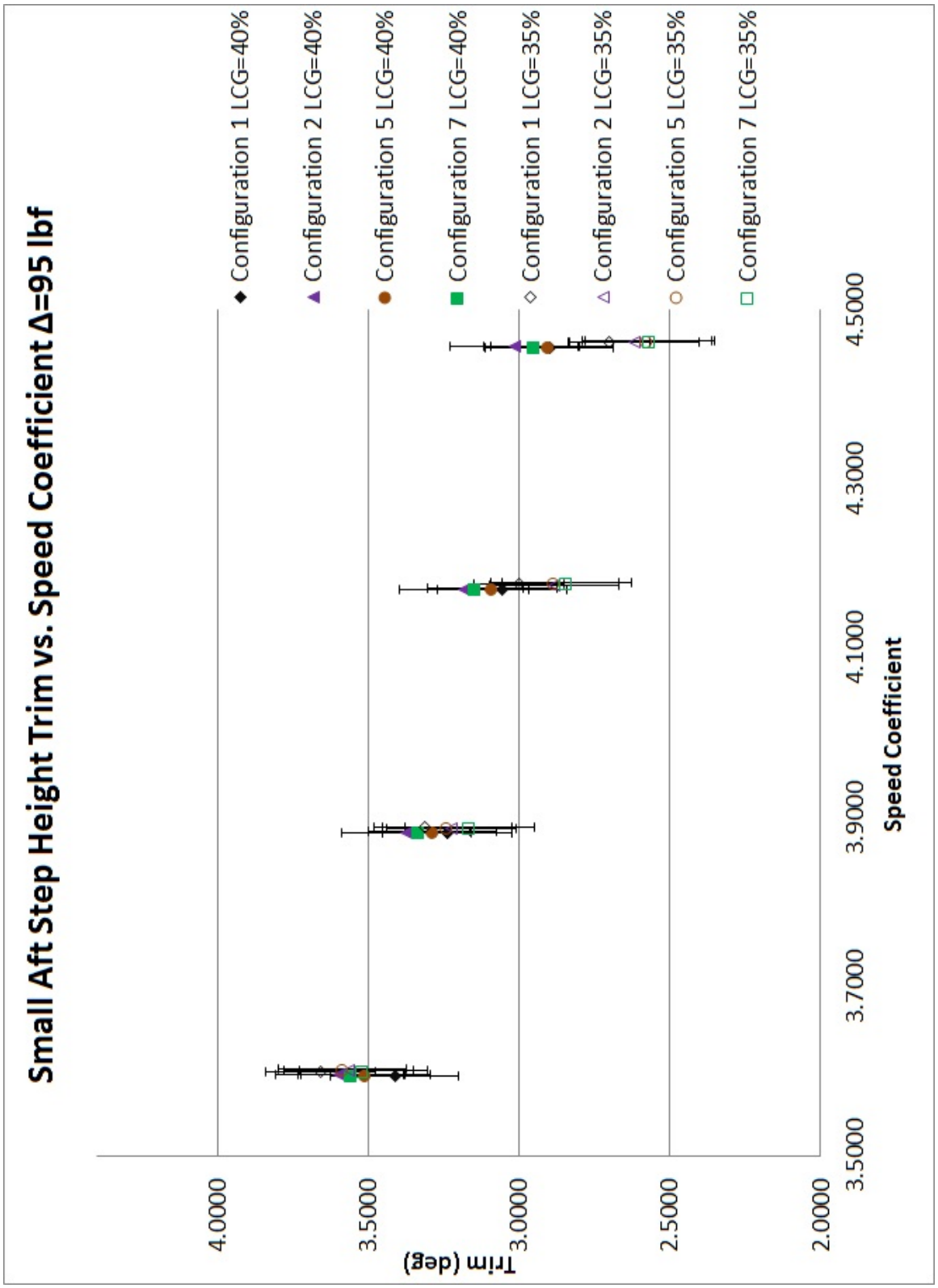

Figure B.9: Small Aft Step Height Trim vs. Speed Coefficient at Δ=95 lbf

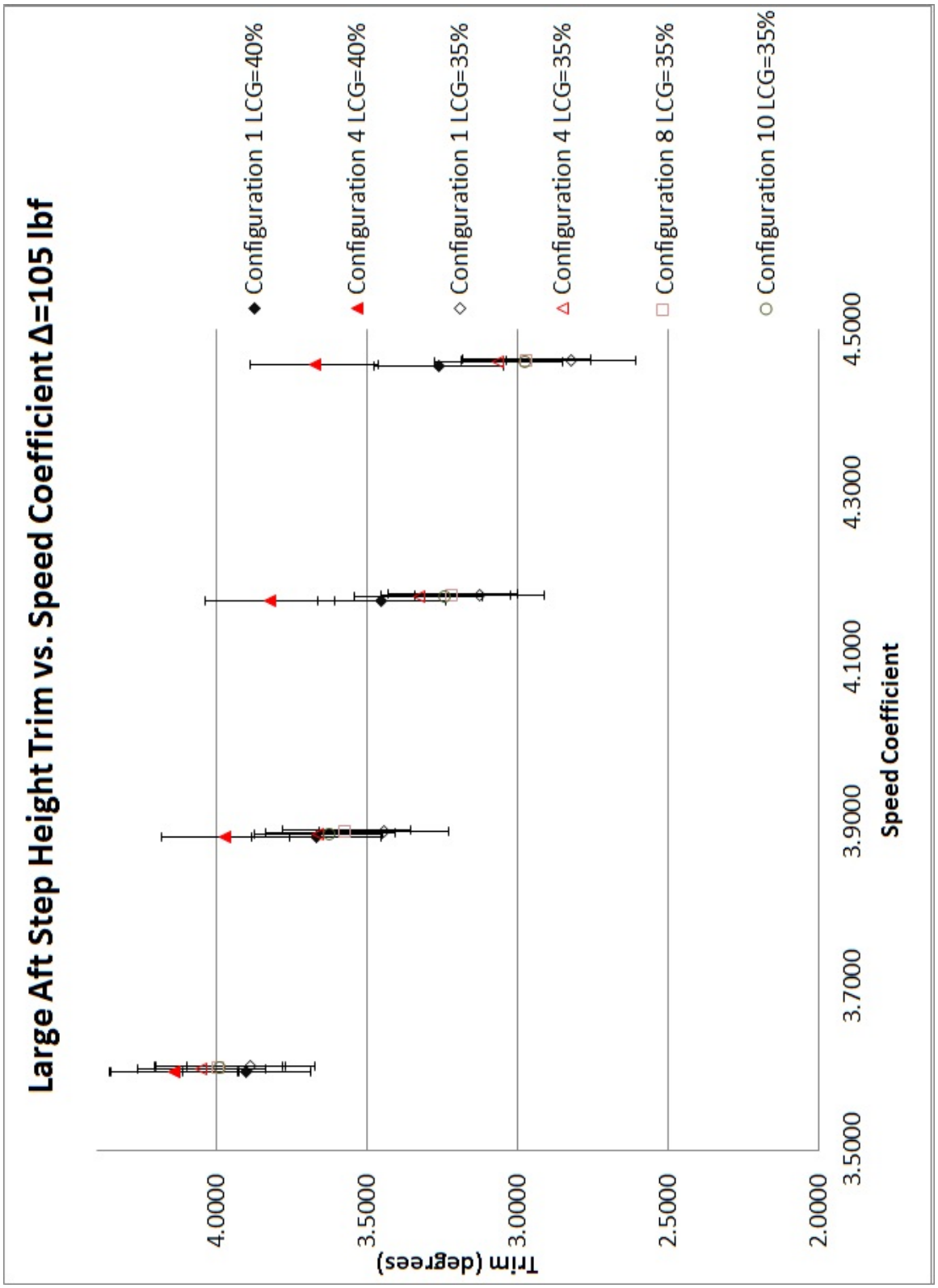

Figure B.10: Large Aft Step Height Trim vs. Speed Coefficient at Δ=105 lbf

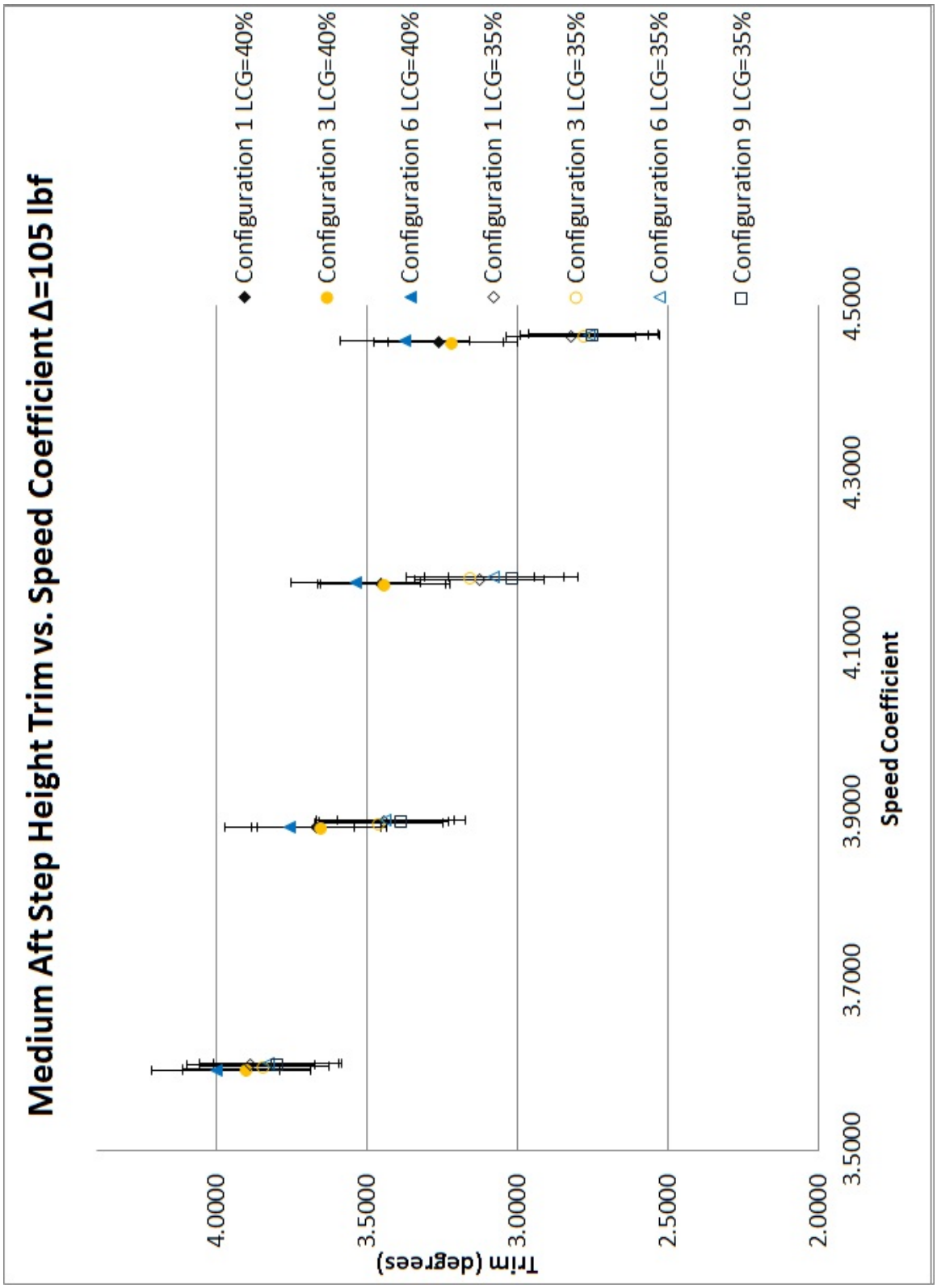

Figure B.11: Medium Aft Step Height Trim vs. Speed Coefficient at Δ=105 lbf

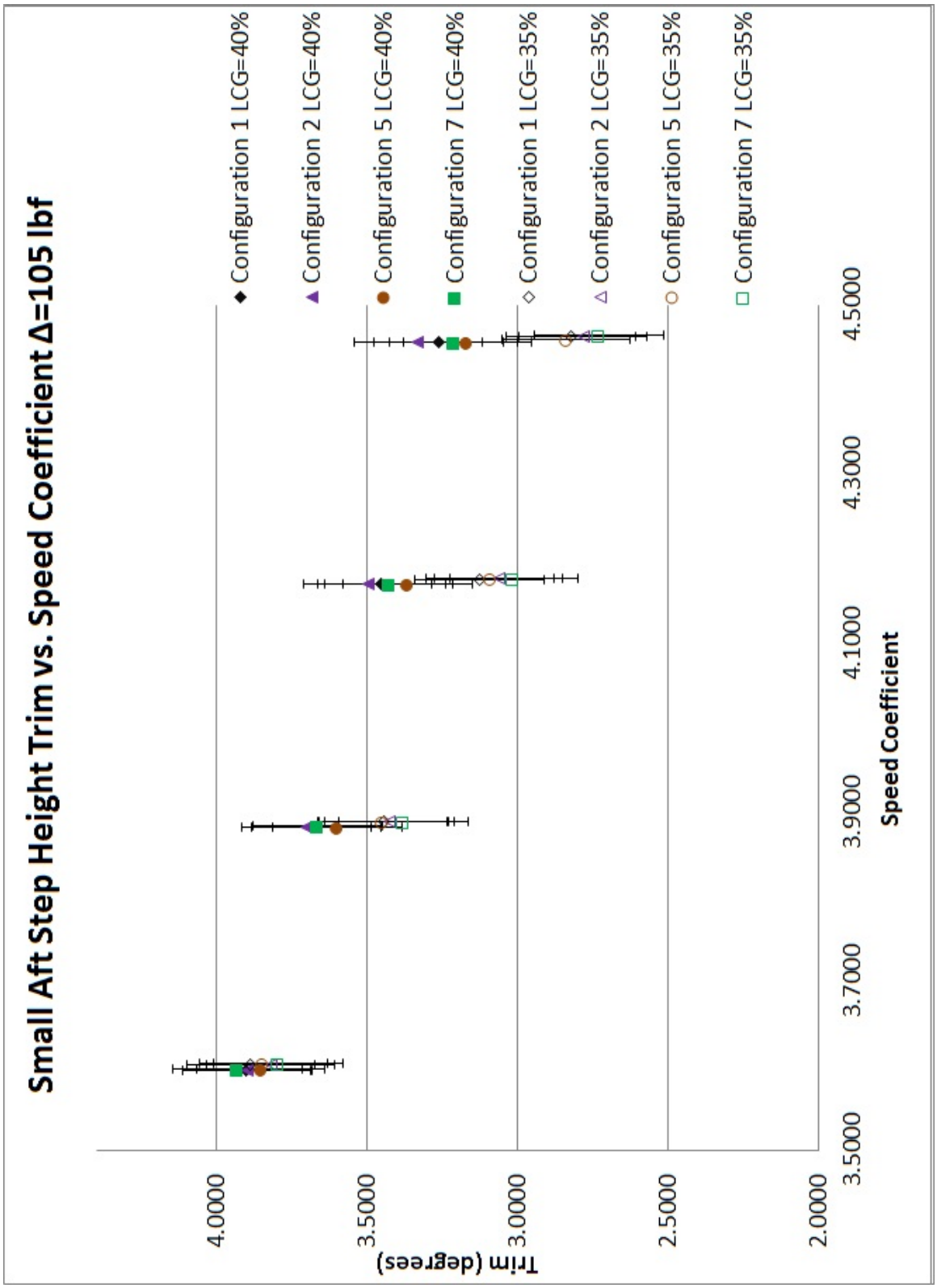

Figure B.12: Small Aft Step Height Trim vs. Speed Coefficient at Δ=105 lbf

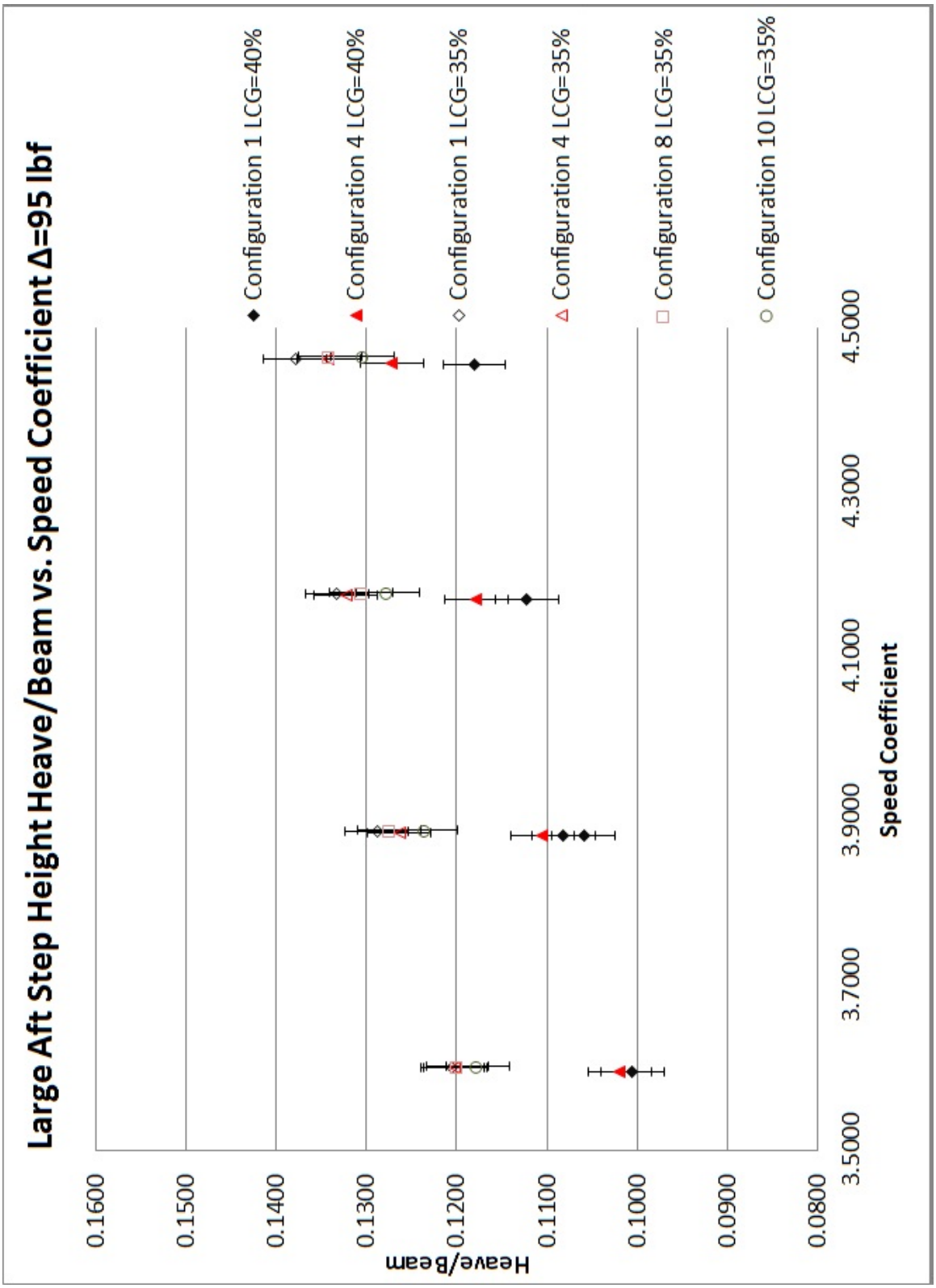

Figure B.13: Large Aft Step Height Heave/Beam vs. Speed Coefficient at Δ=95 lbf

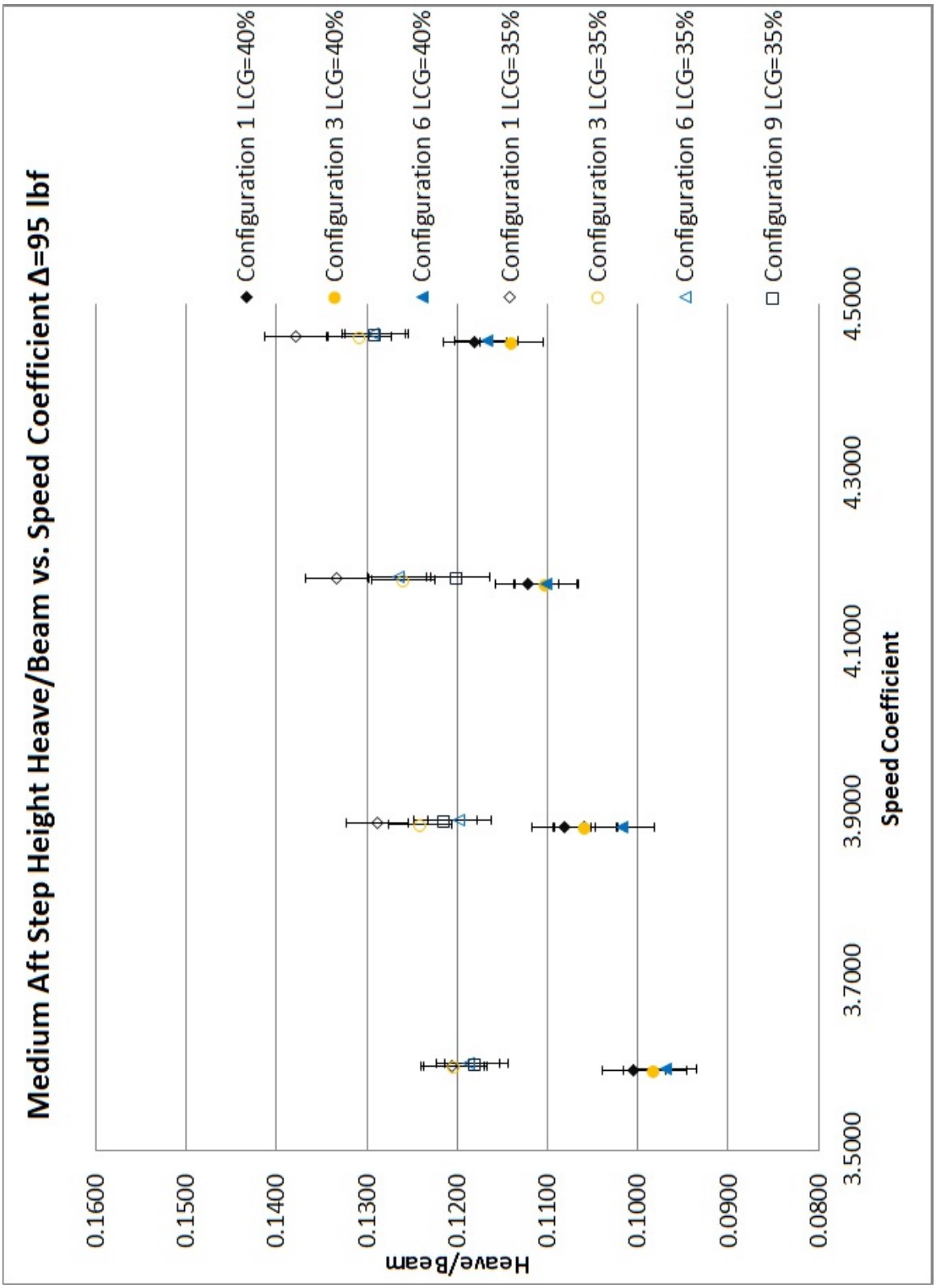

Figure B.14: Medium Aft Step Height Heave/Beam vs. Speed Coefficient at Δ=95 lbf

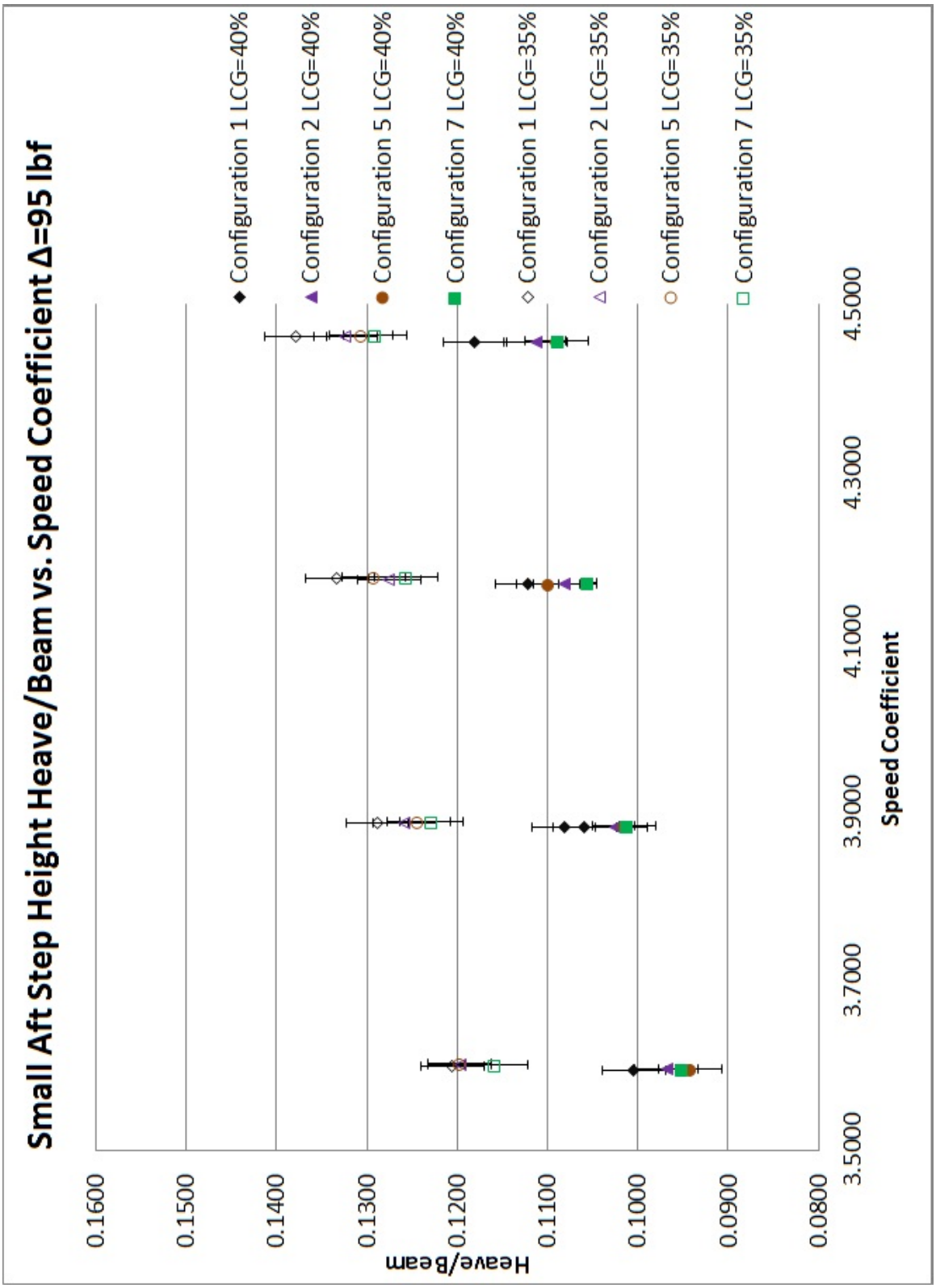

Figure B.15: Small Aft Step Height Heave/Beam vs. Speed Coefficient at Δ=95 lbf

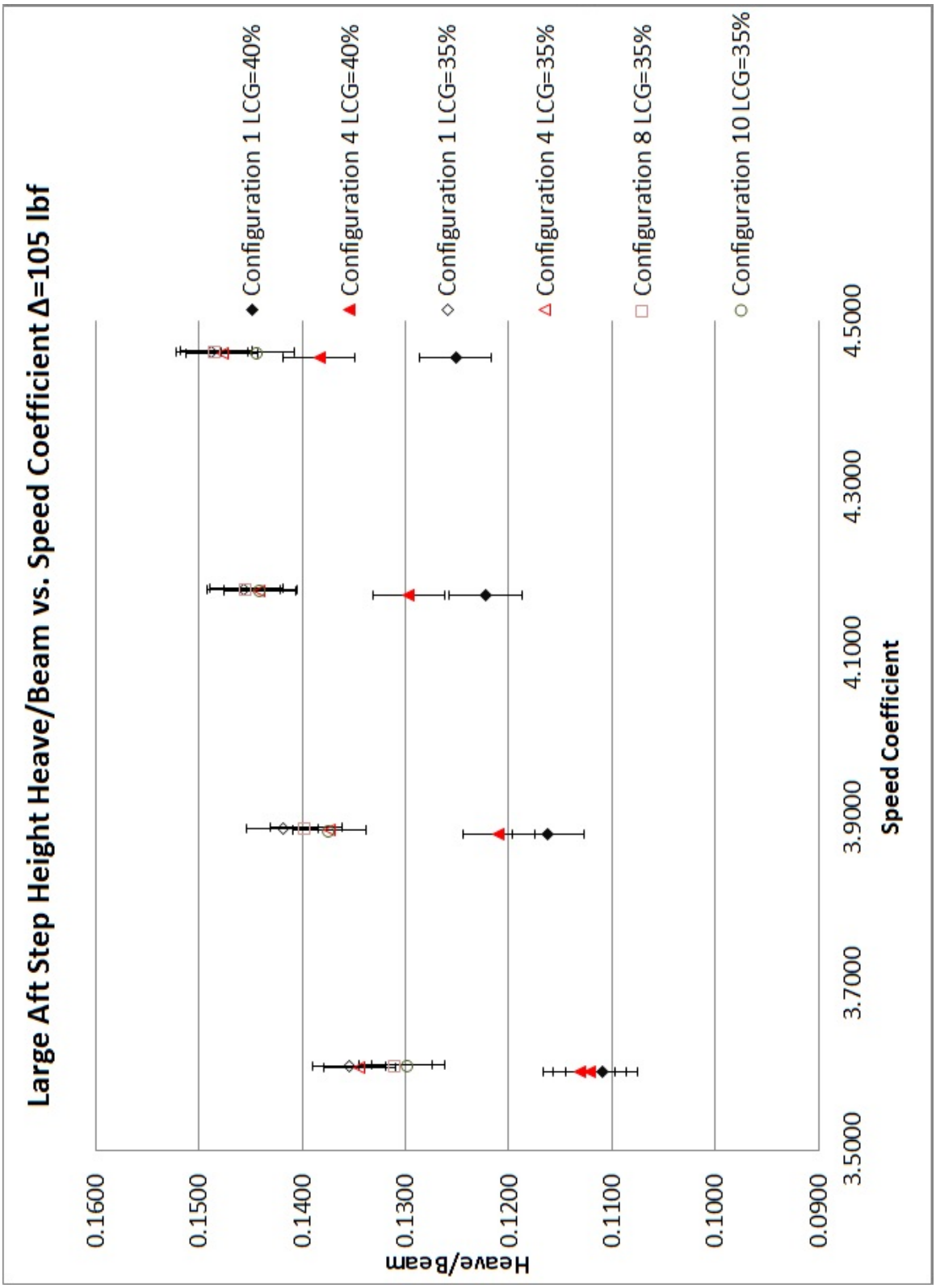

Figure B.16: Large Aft Step Height Heave/Beam vs. Speed Coefficient at Δ=105 lbf

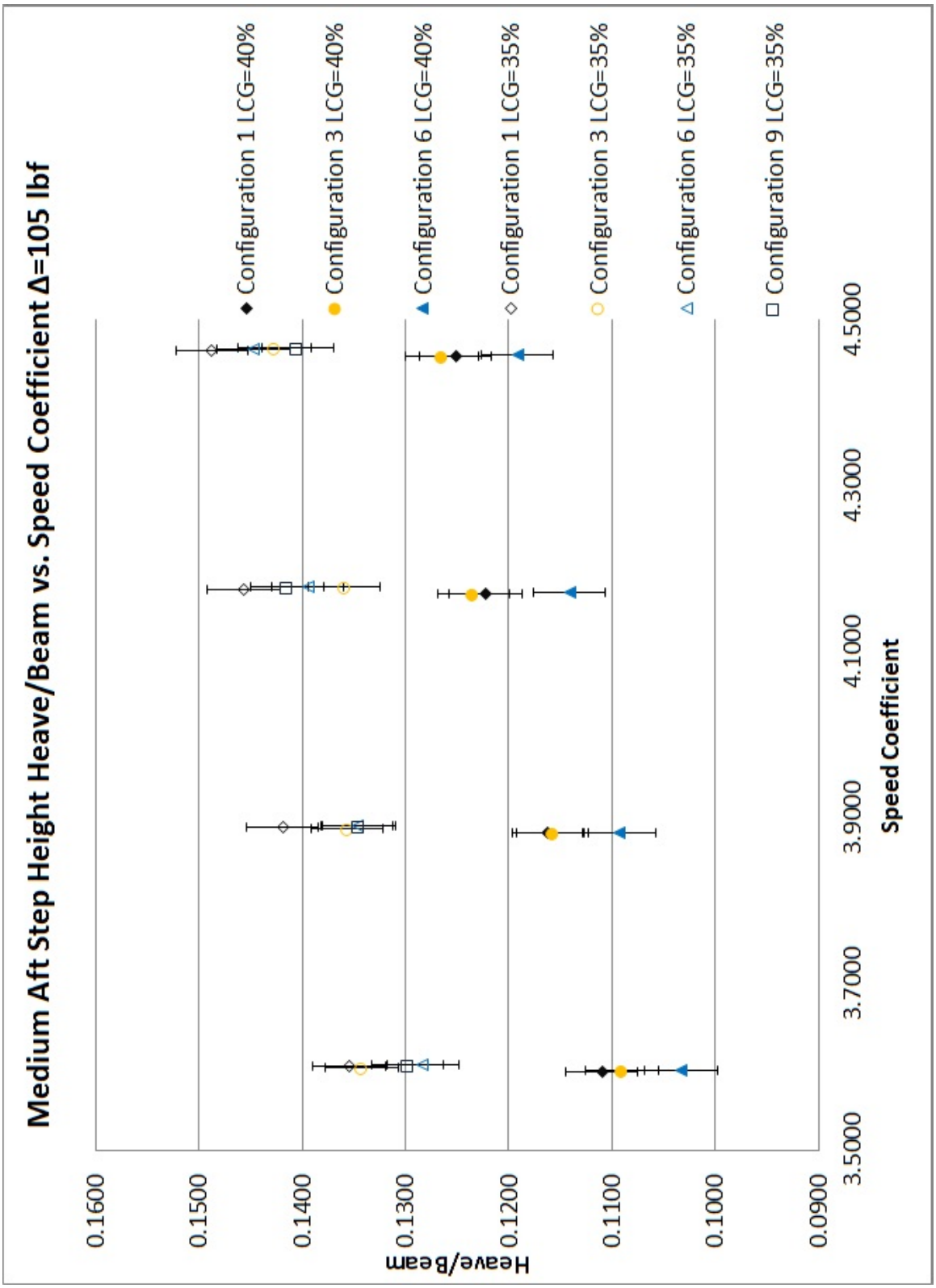

Figure B.17: Medium Aft Step Height Heave/Beam vs. Speed Coefficient at Δ=105 lbf

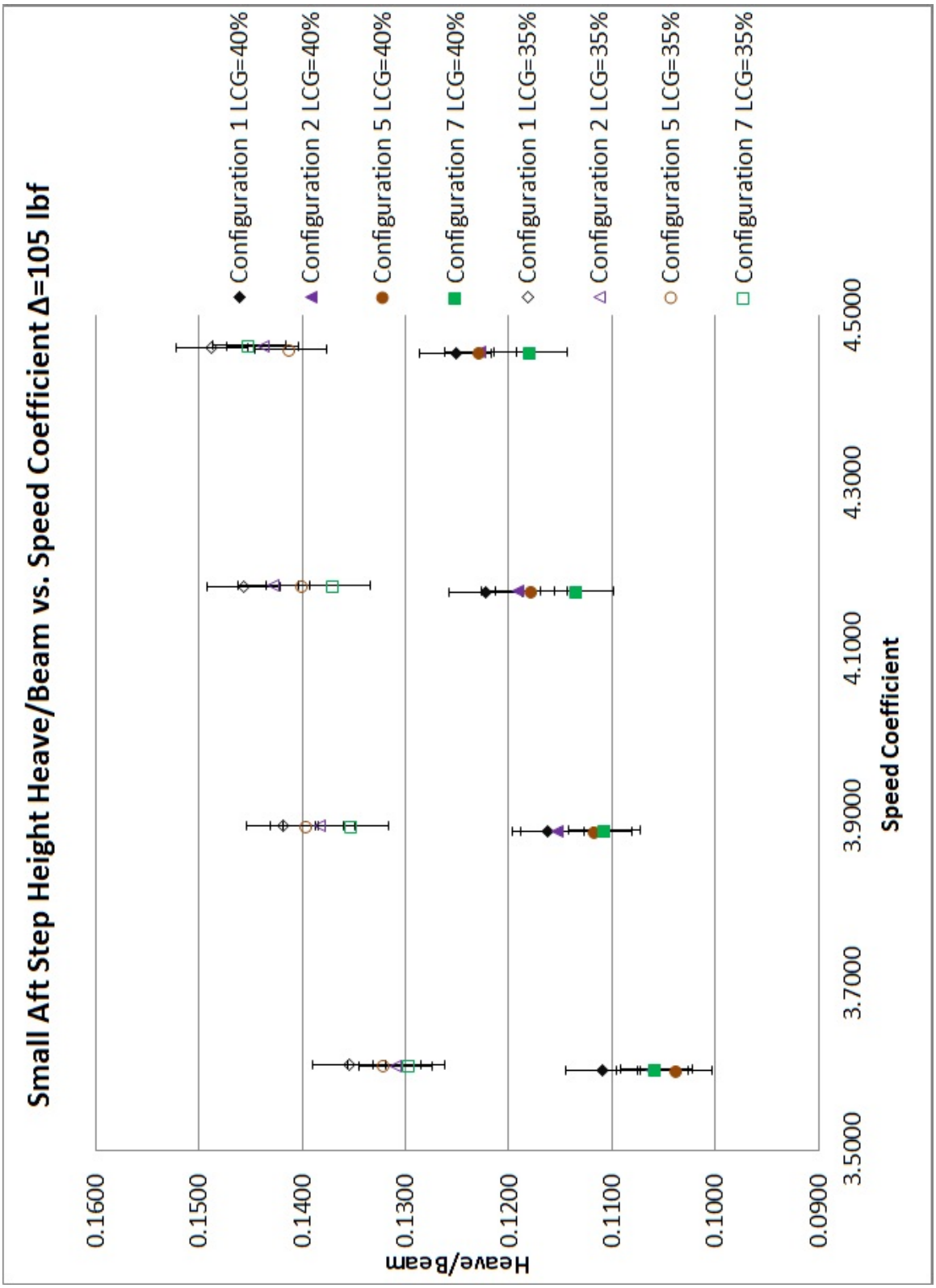

Figure B.18: Small Aft Step Height Heave/Beam vs. Speed Coefficient at Δ=105 lbf

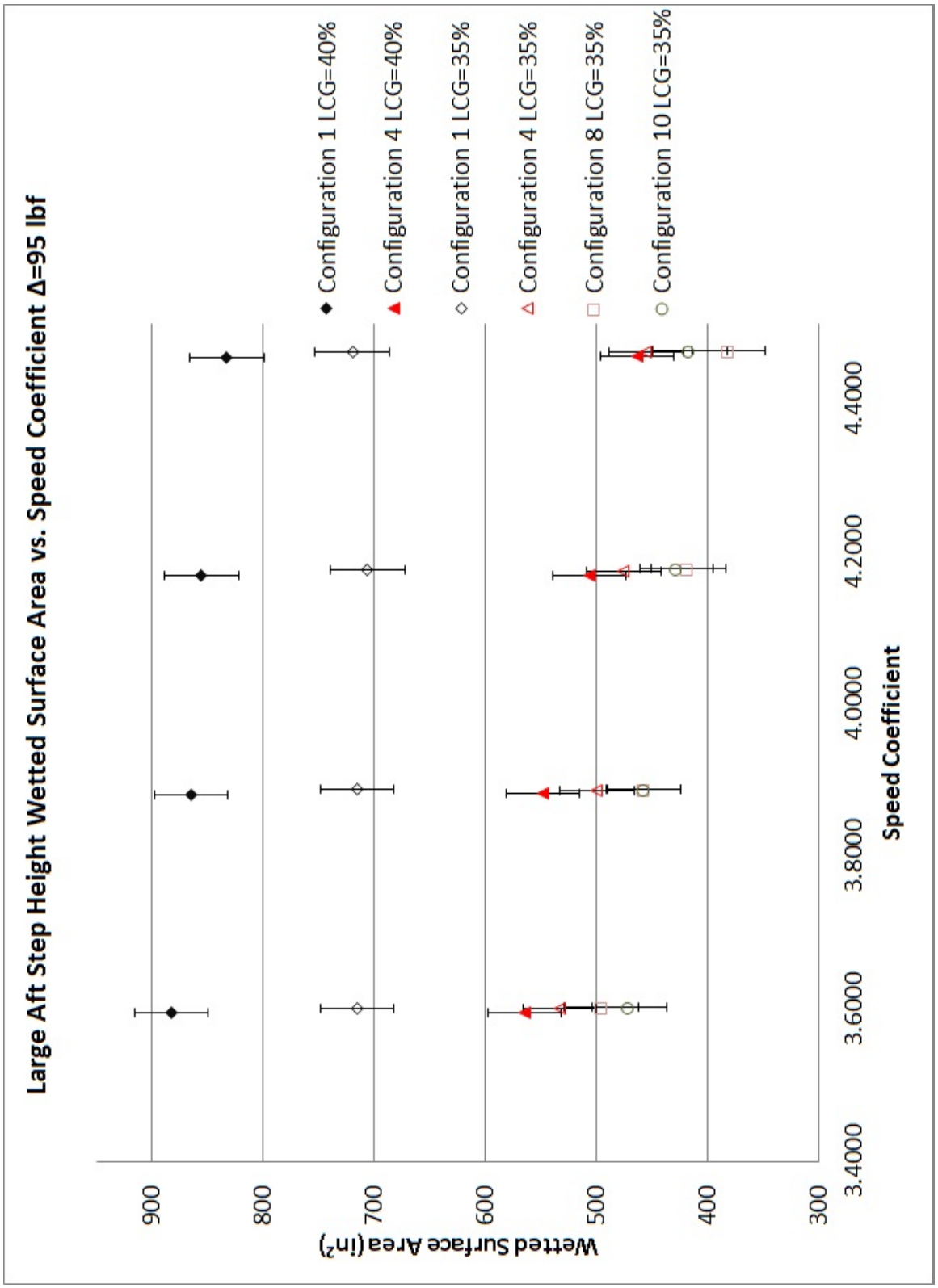

Figure B.19: Large Aft Step Height Wetted Surface Area vs. Speed Coefficient at Δ=95 lbf

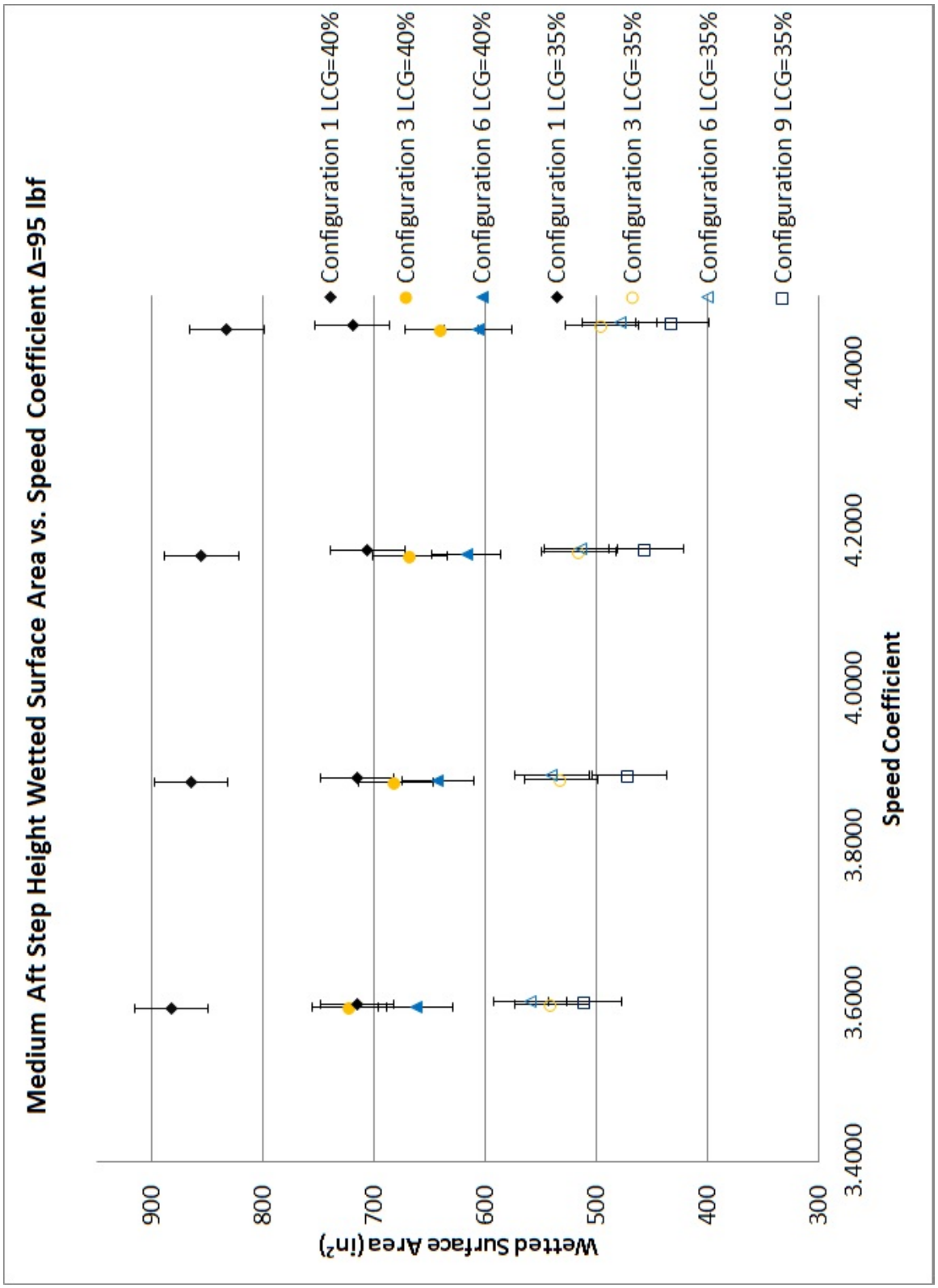

Figure B.20: Medium Aft Step Height Wetted Surface Area vs. Speed Coefficient at Δ=95 lbf

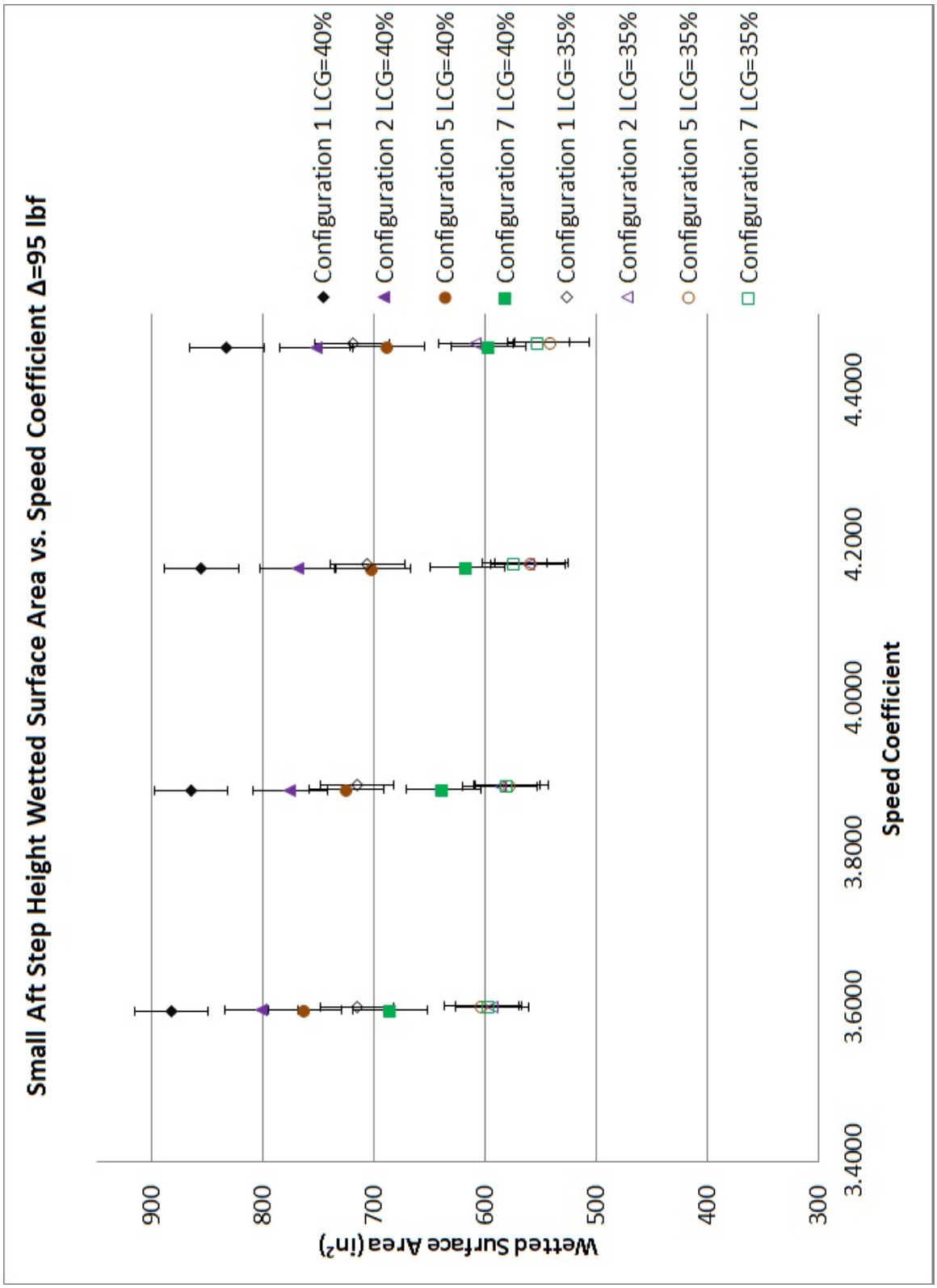

Figure B.21: Small Aft Step Height Wetted Surface Area vs. Speed Coefficient at Δ=95 lbf

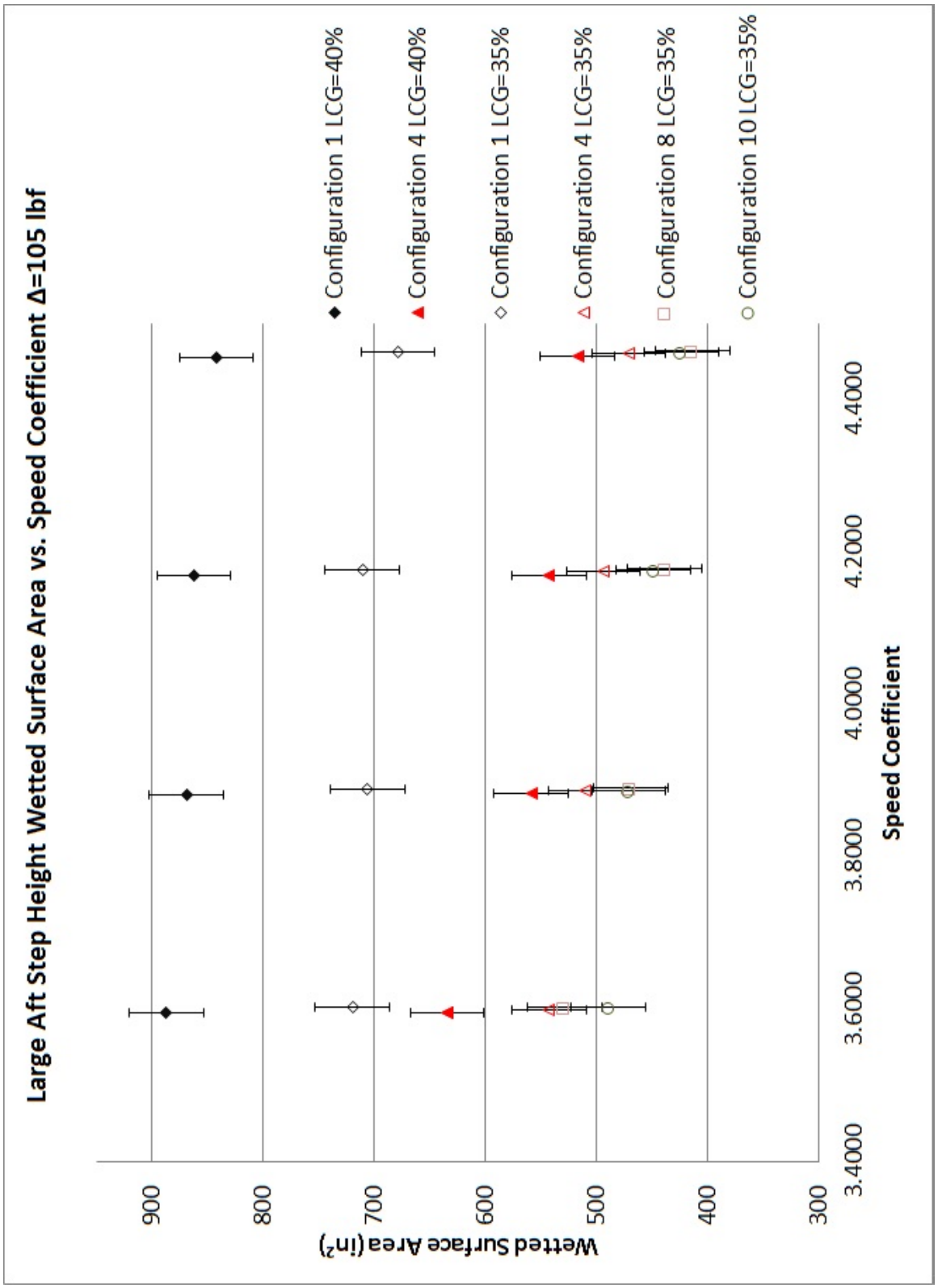

Figure B.22: Large Aft Step Height Wetted Surface Area vs. Speed Coefficient at Δ=105 lbf

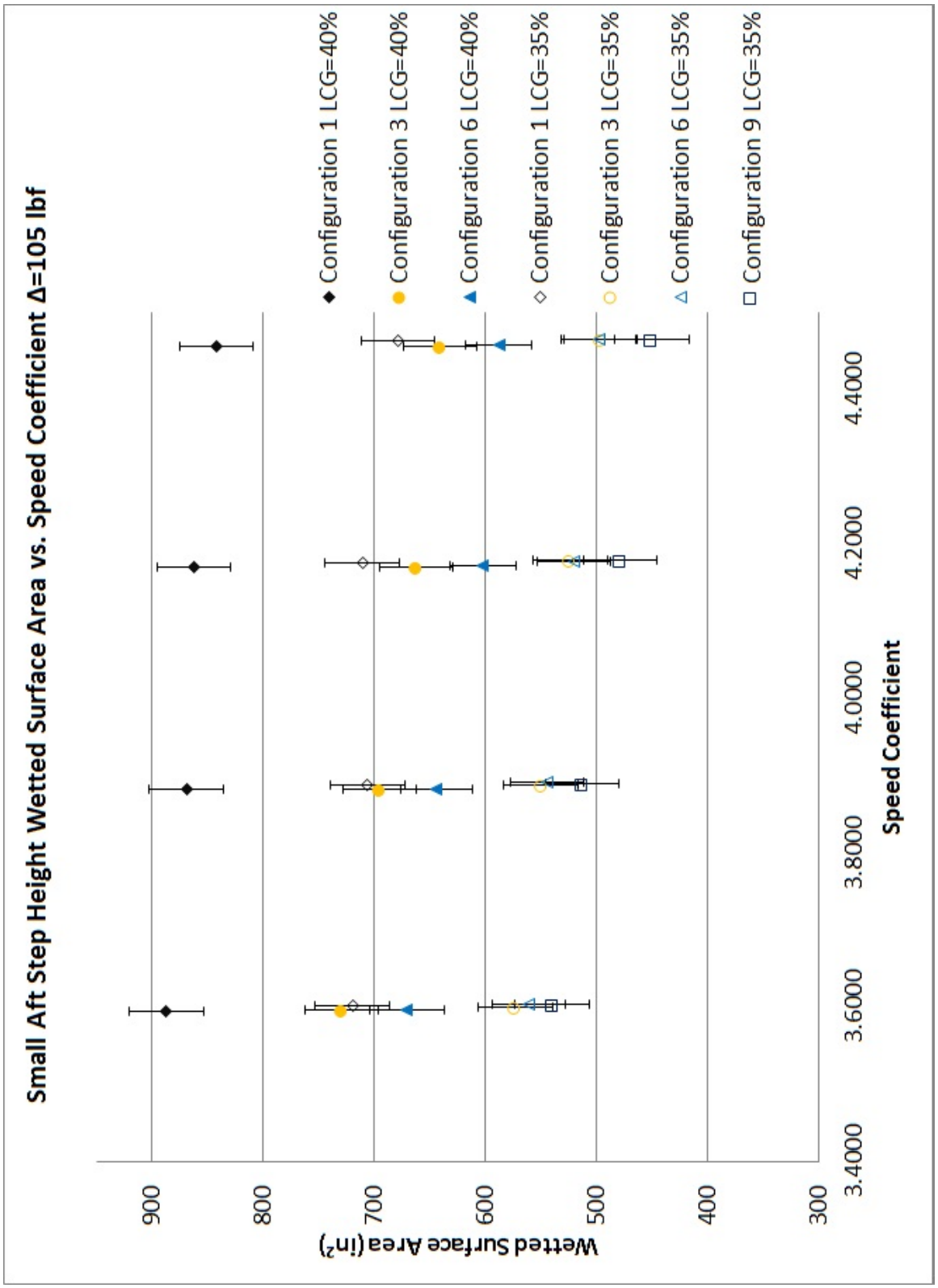

Figure B.23: Medium Aft Step Height Wetted Surface Area vs. Speed Coefficient at Δ=105 lbf

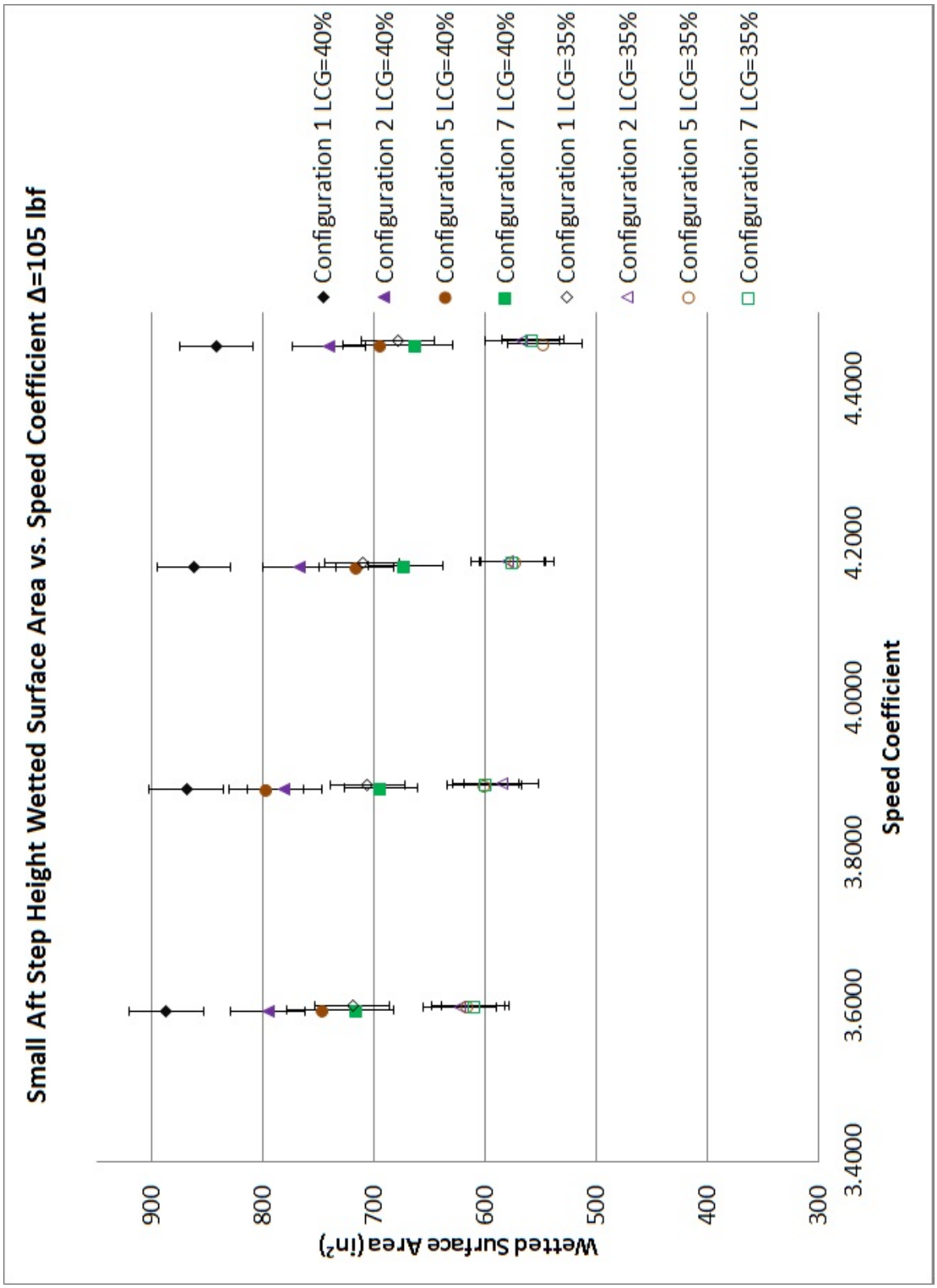

Figure B.24: Small Aft Step Height Wetted Surface Area vs. Speed Coefficient at Δ=105 lbf

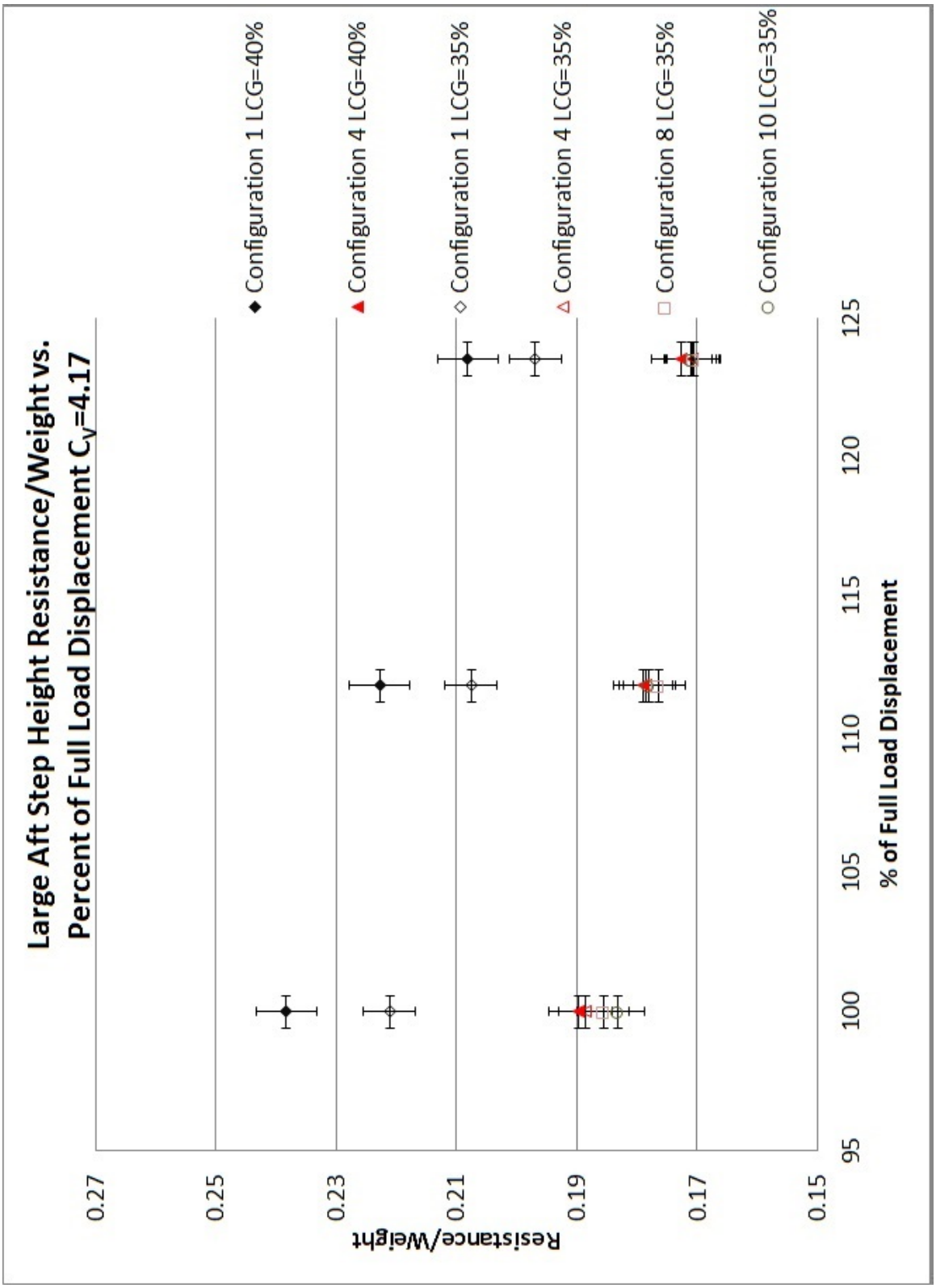

Figure B.25: Large Aft Step Height Resistance/Weight vs. Percent of Full Load Displacement at C_v=4.17

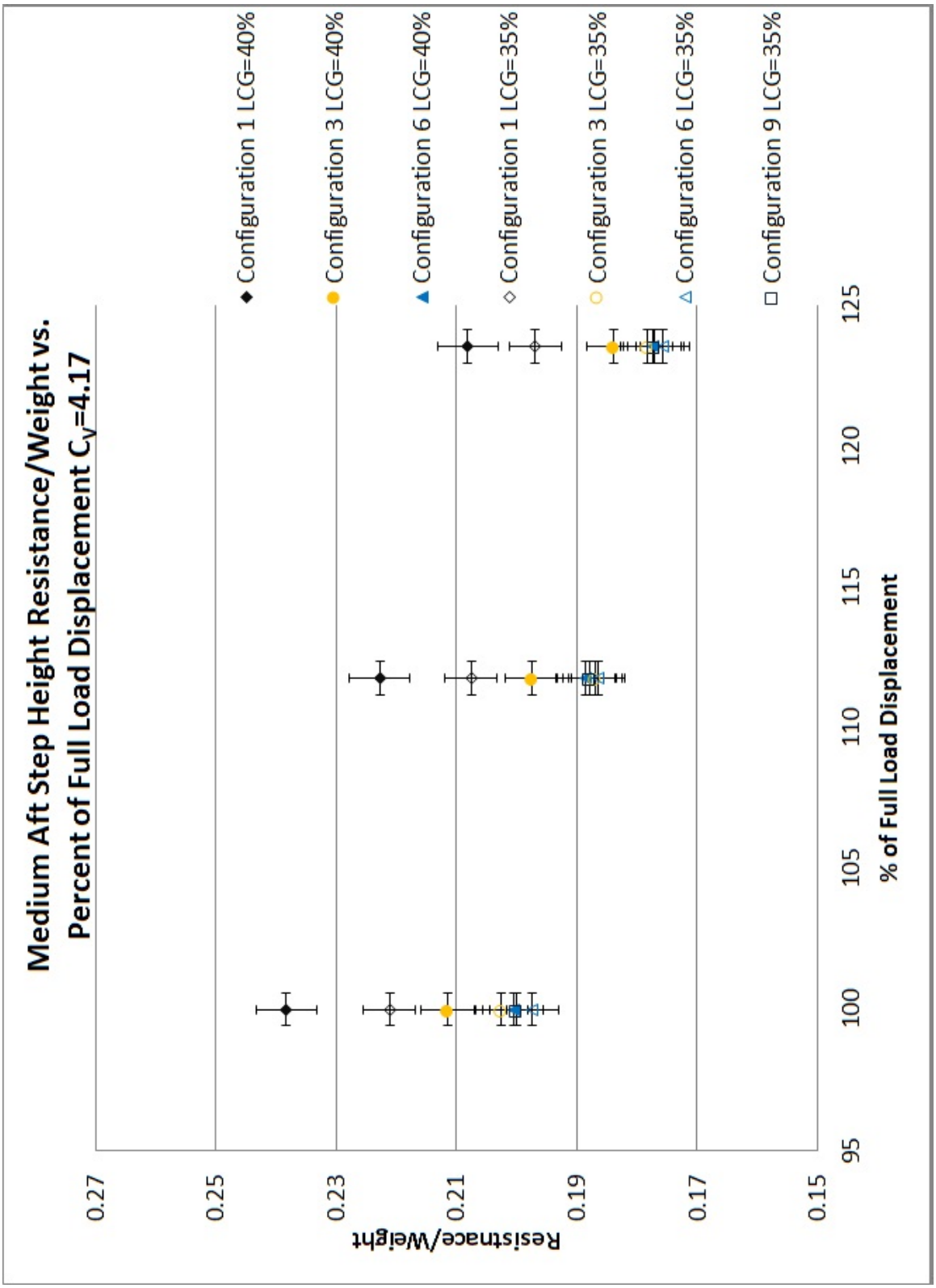

Figure B.26: Medium Aft Step Height Resistance/Weight vs. Percent of Full Load Displacement at C_v=4.17

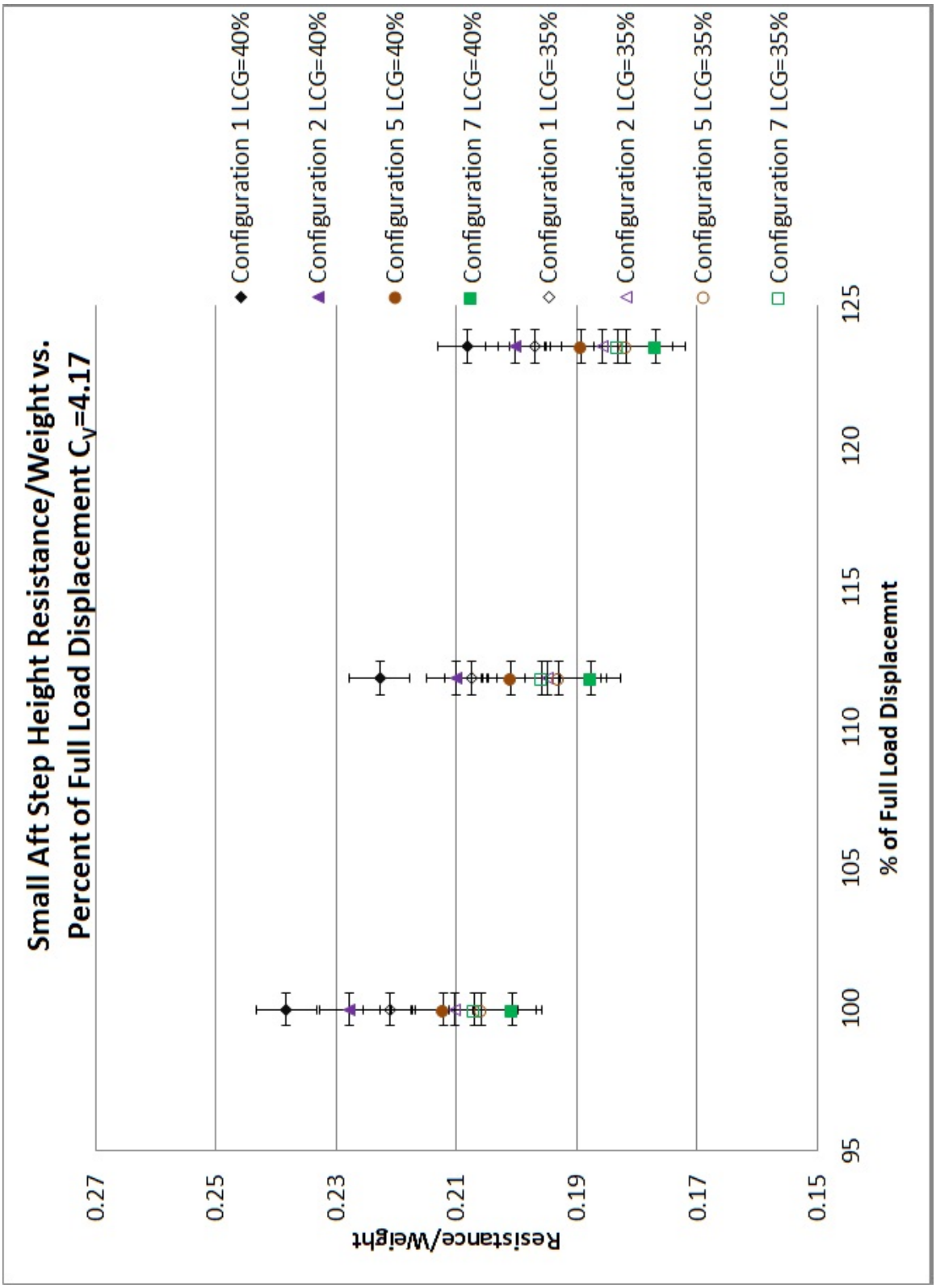

Figure B.27: Small Aft Step Height Resistance/Weight vs. Percent of Full Load Displacement at C_v=4.17

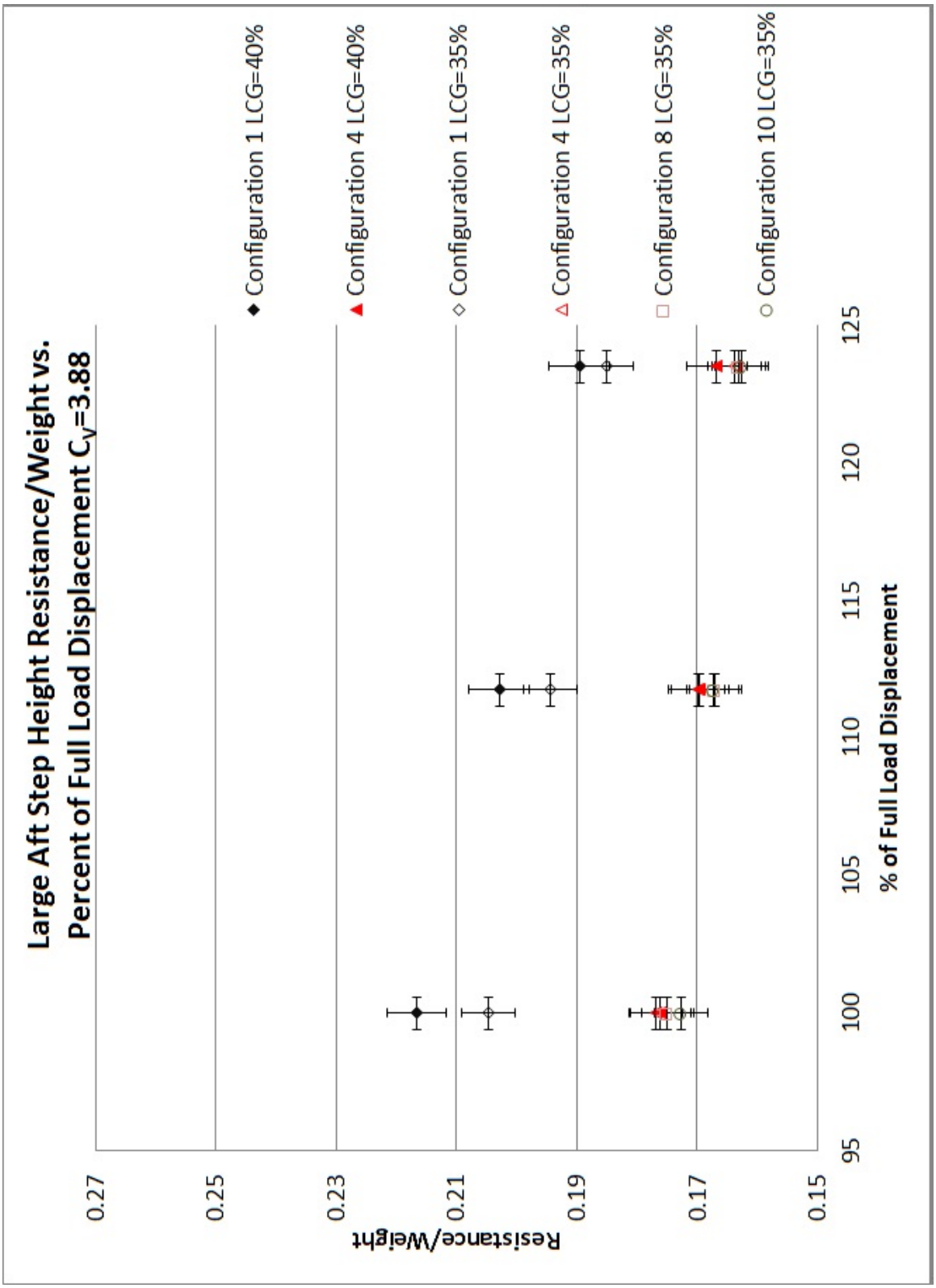

Figure B.28: Large Aft Step Height Resistance/Weight vs. Percent of Full Load Displacement at C_v=3.88

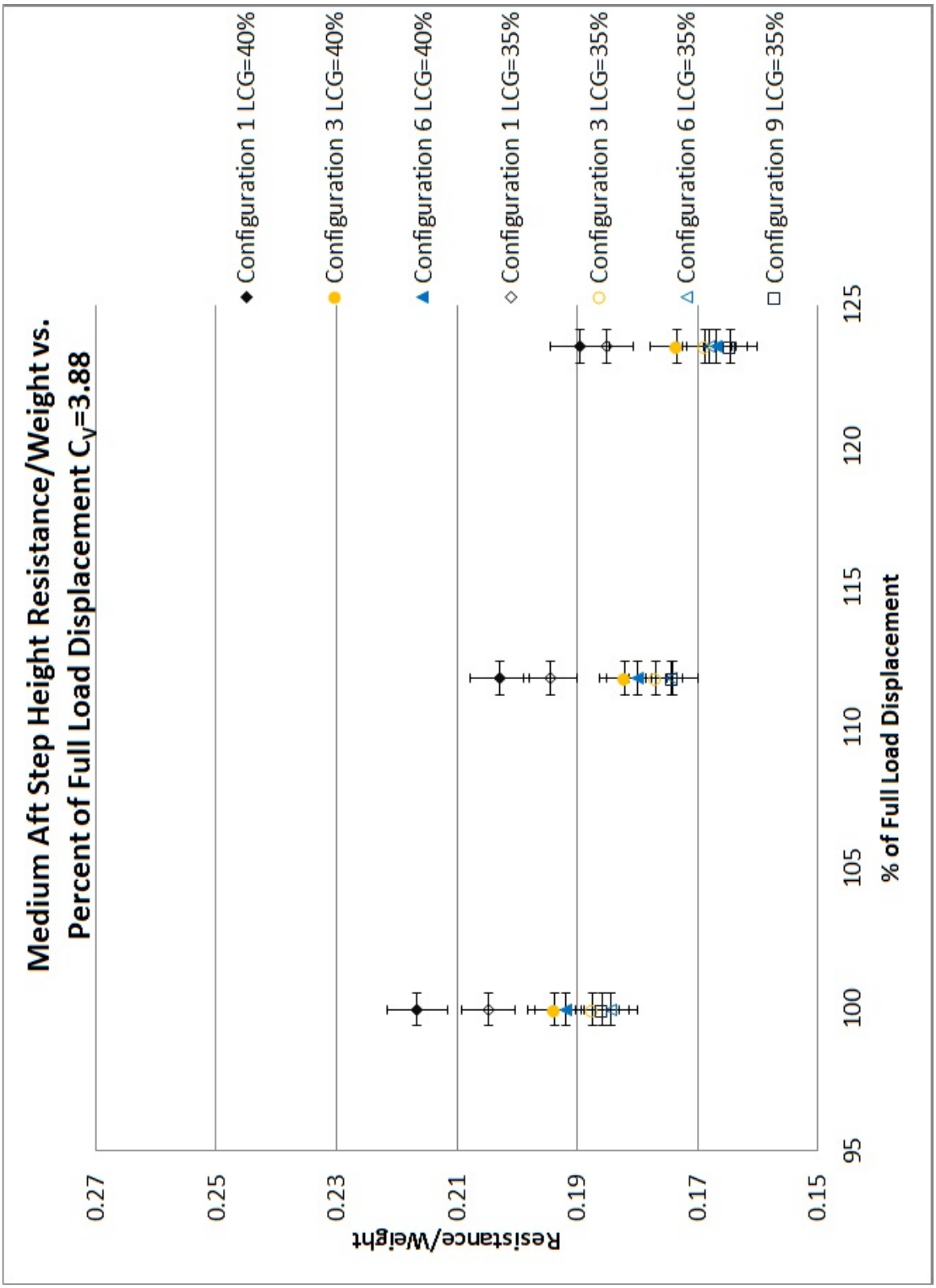

Figure B.29: Medium Aft Step Height Resistance/Weight vs. Percent of Full Load Displacement at C_v=3.88

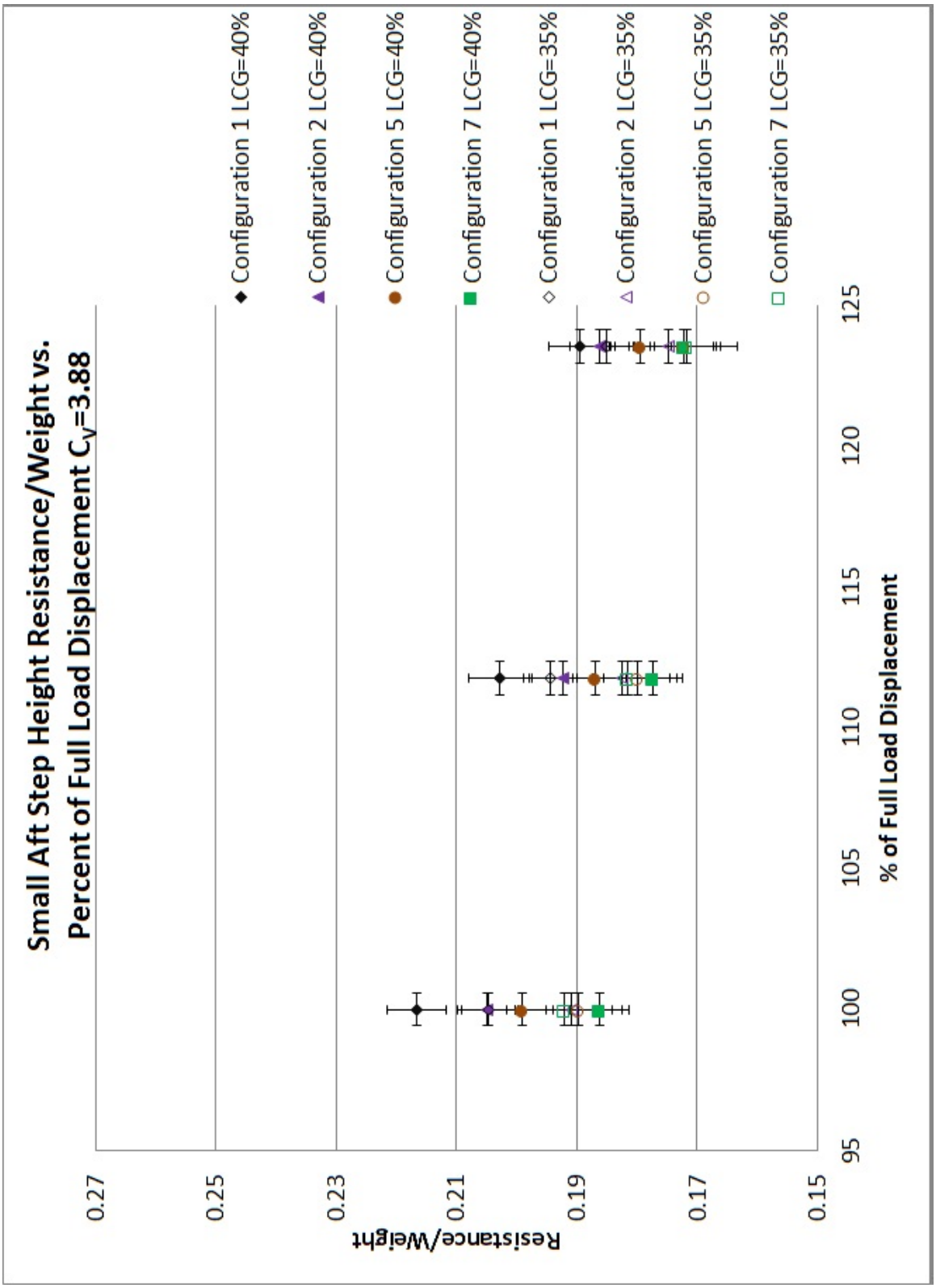

Figure B.30: Small Aft Step Height Resistance/Weight vs. Percent of Full Load Displacement at C_v=3.88

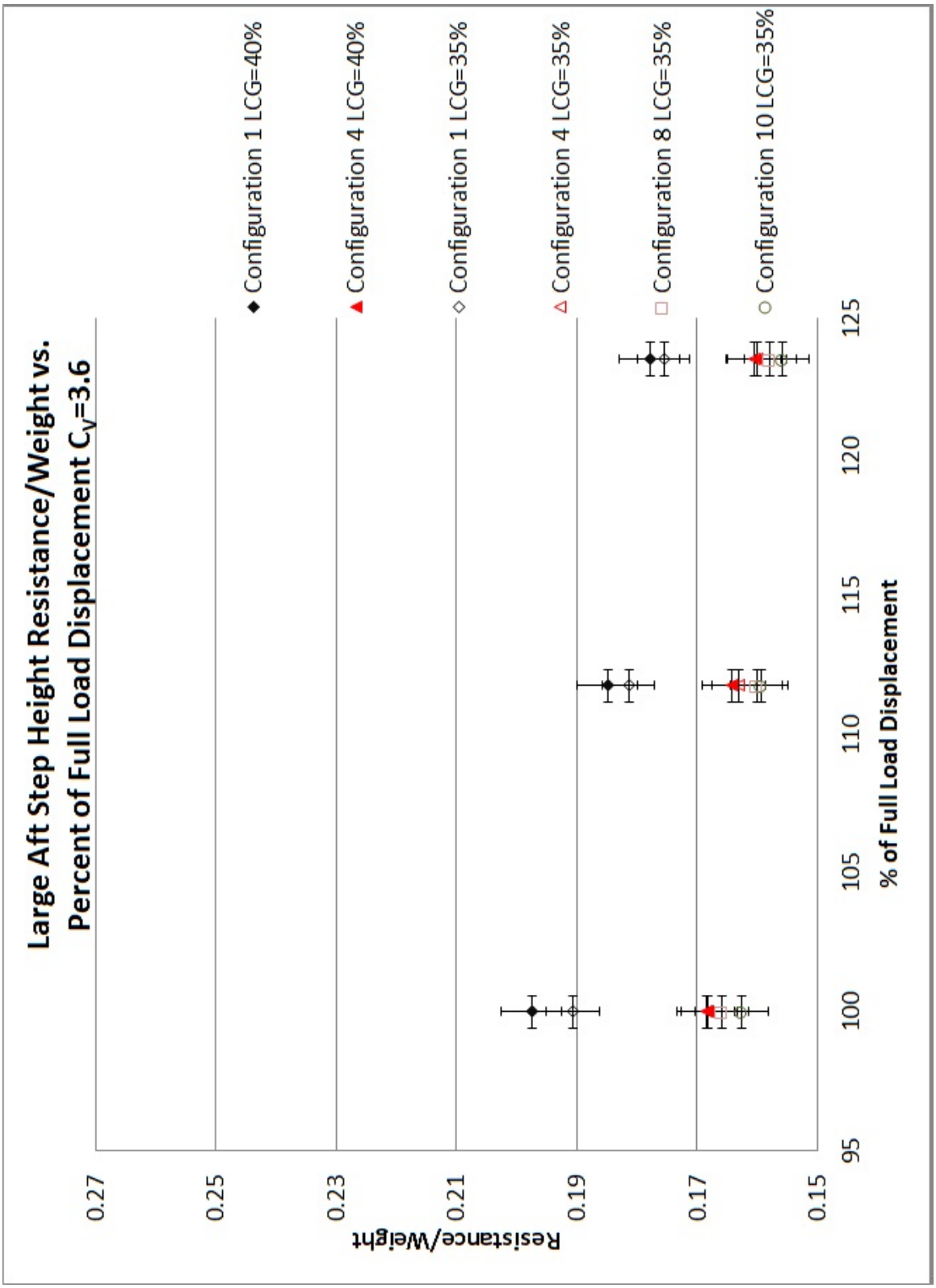

Figure B.31: Large Aft Step Height Resistance/Weight vs. Percent of Full Load Displacement at C_v=3.60

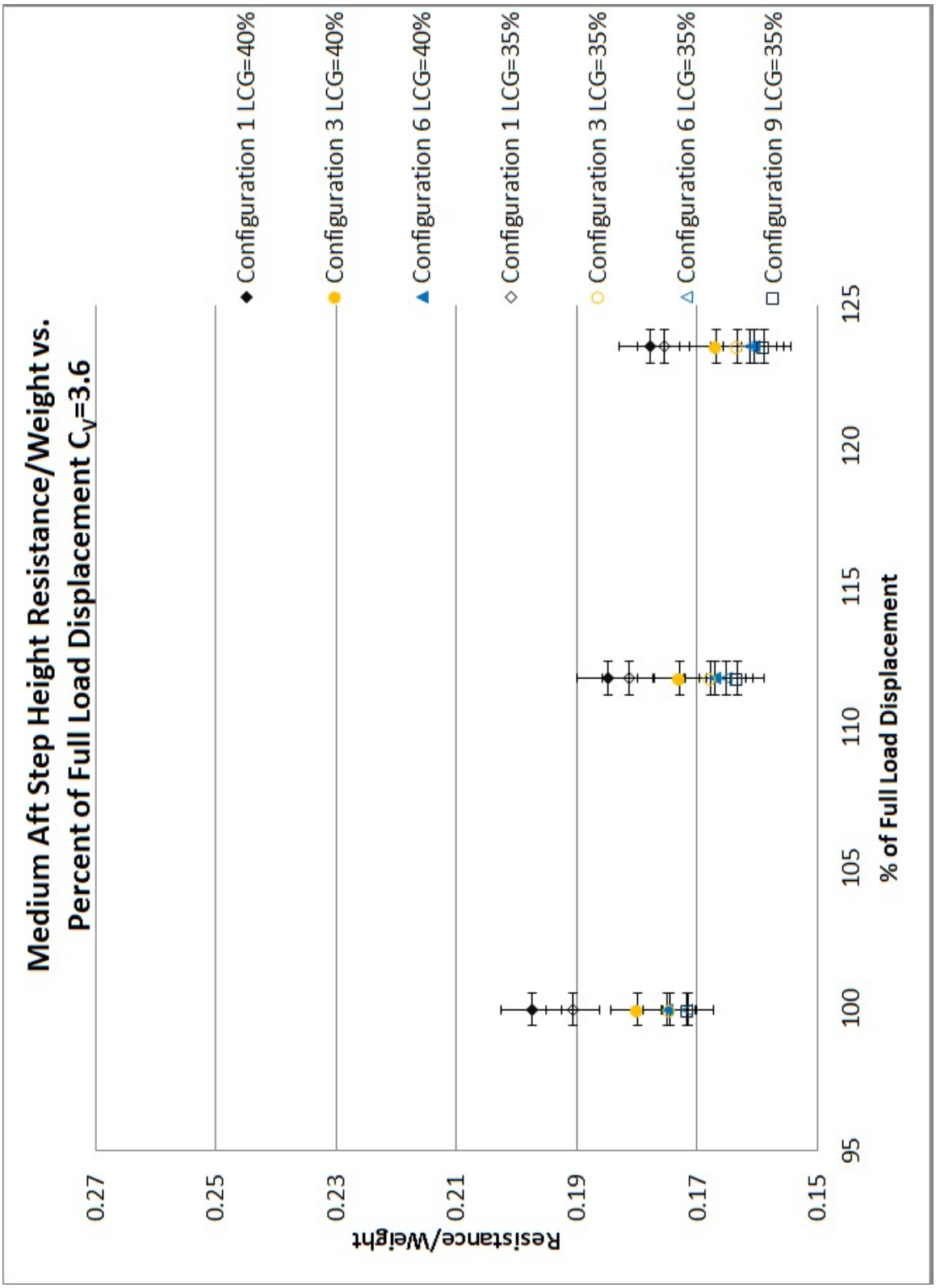

Figure B.32: Medium Aft Step Height Resistance/Weight vs. Percent of Full Load Displacement at C_v=3.60

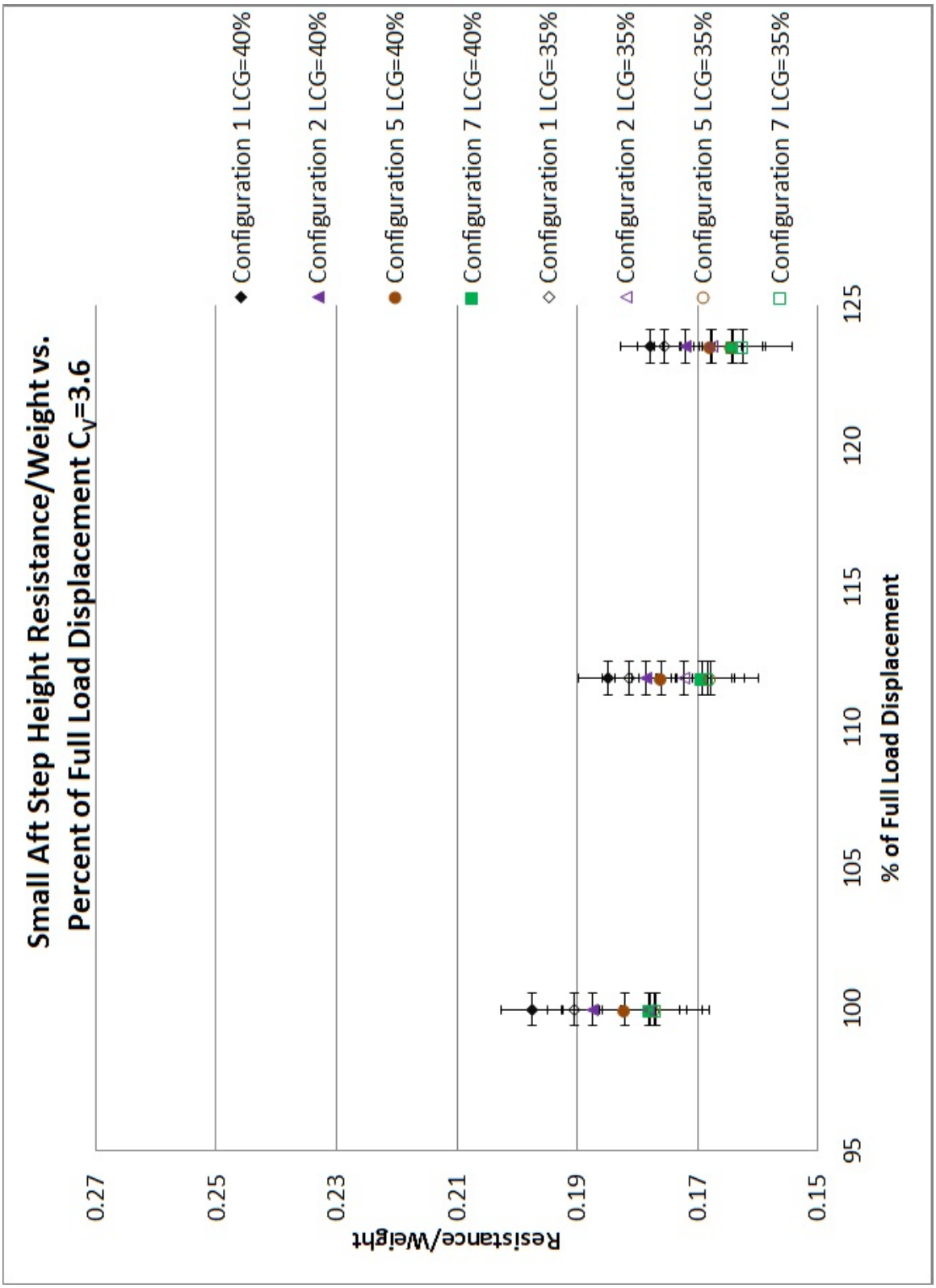

Figure B.33: Small Aft Step Height Resistance/Weight vs. Percent of Full Load Displacement at C_v=3.60

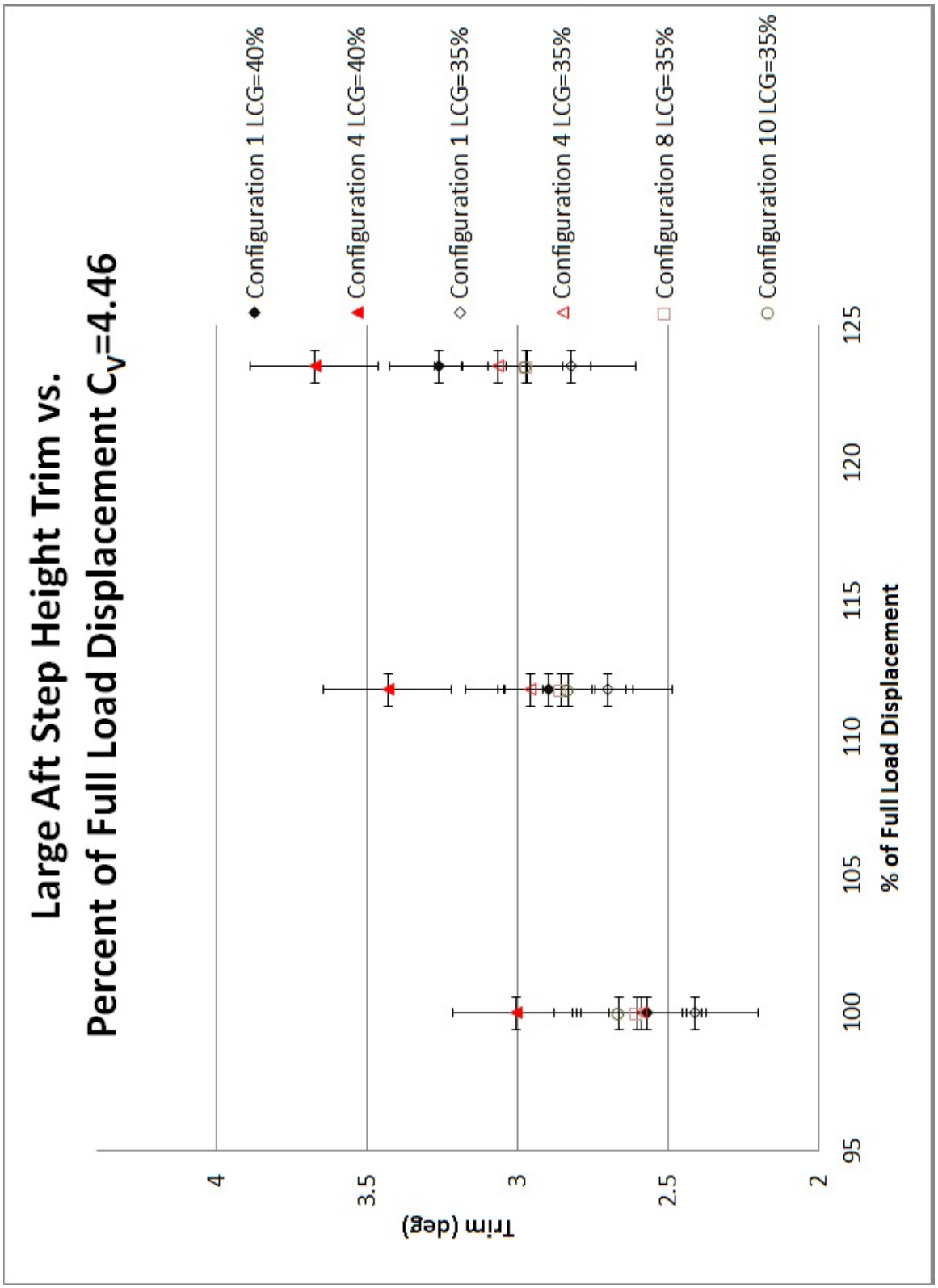

Figure B.34: Large Aft Step Height Trim vs. Percent of Full Load Displacement at C_v=4.46

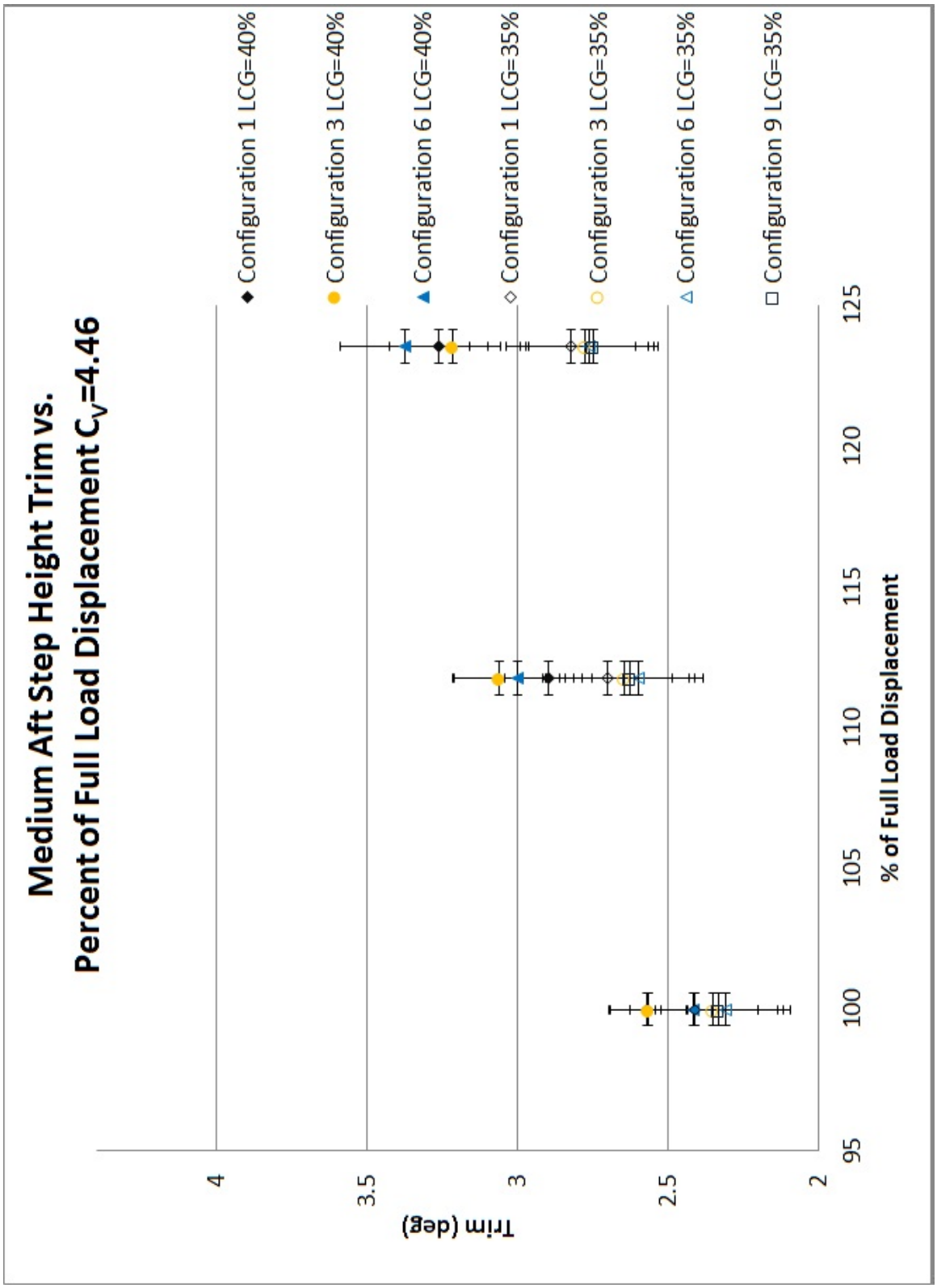

Figure B.35: Medium Aft Step Height Trim vs. Percent of Full Load Displacement at C_v=4.46

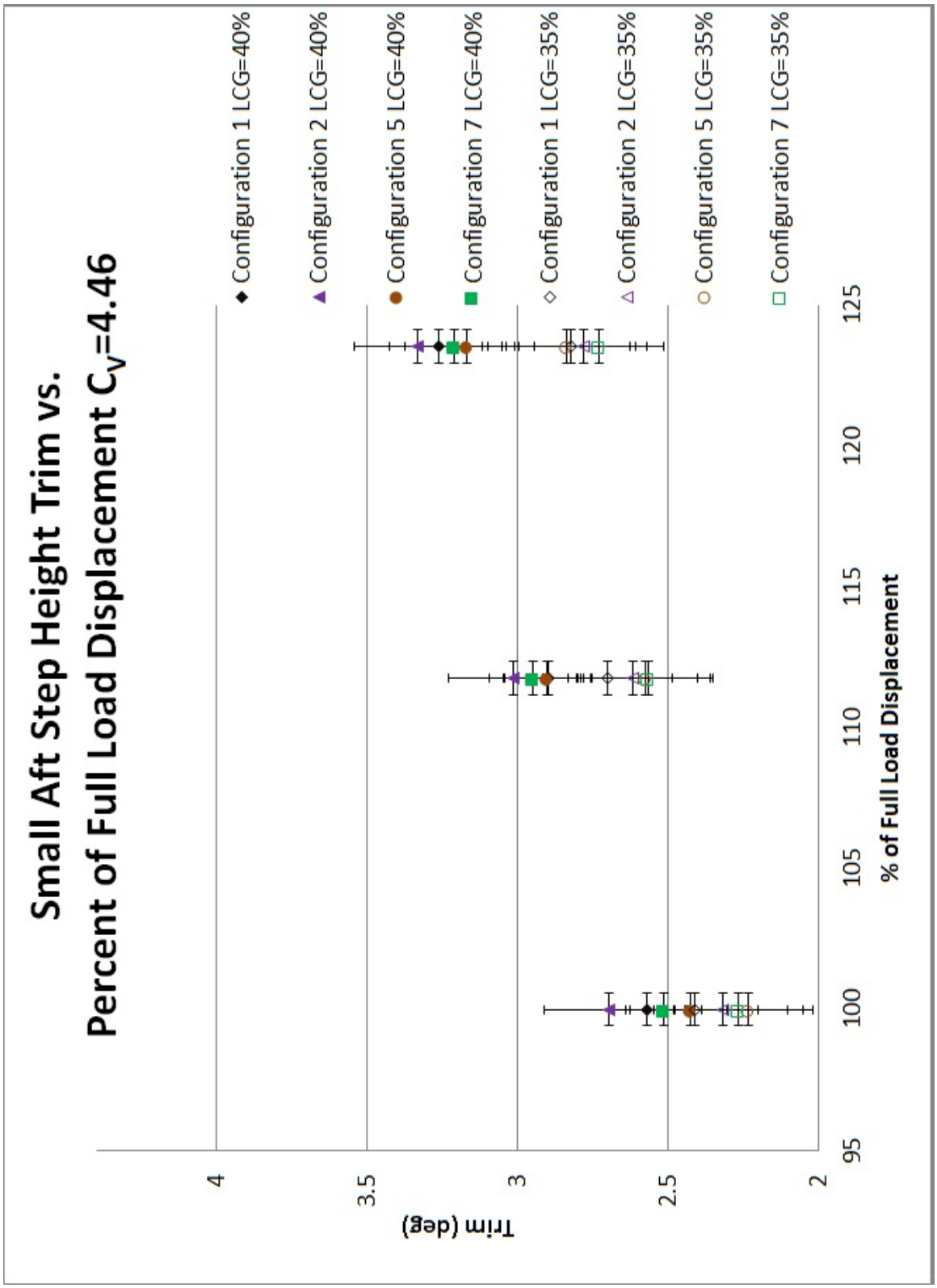

Figure B.36: Small Aft Step Height Trim vs. Percent of Full Load Displacement at C_v=4.46

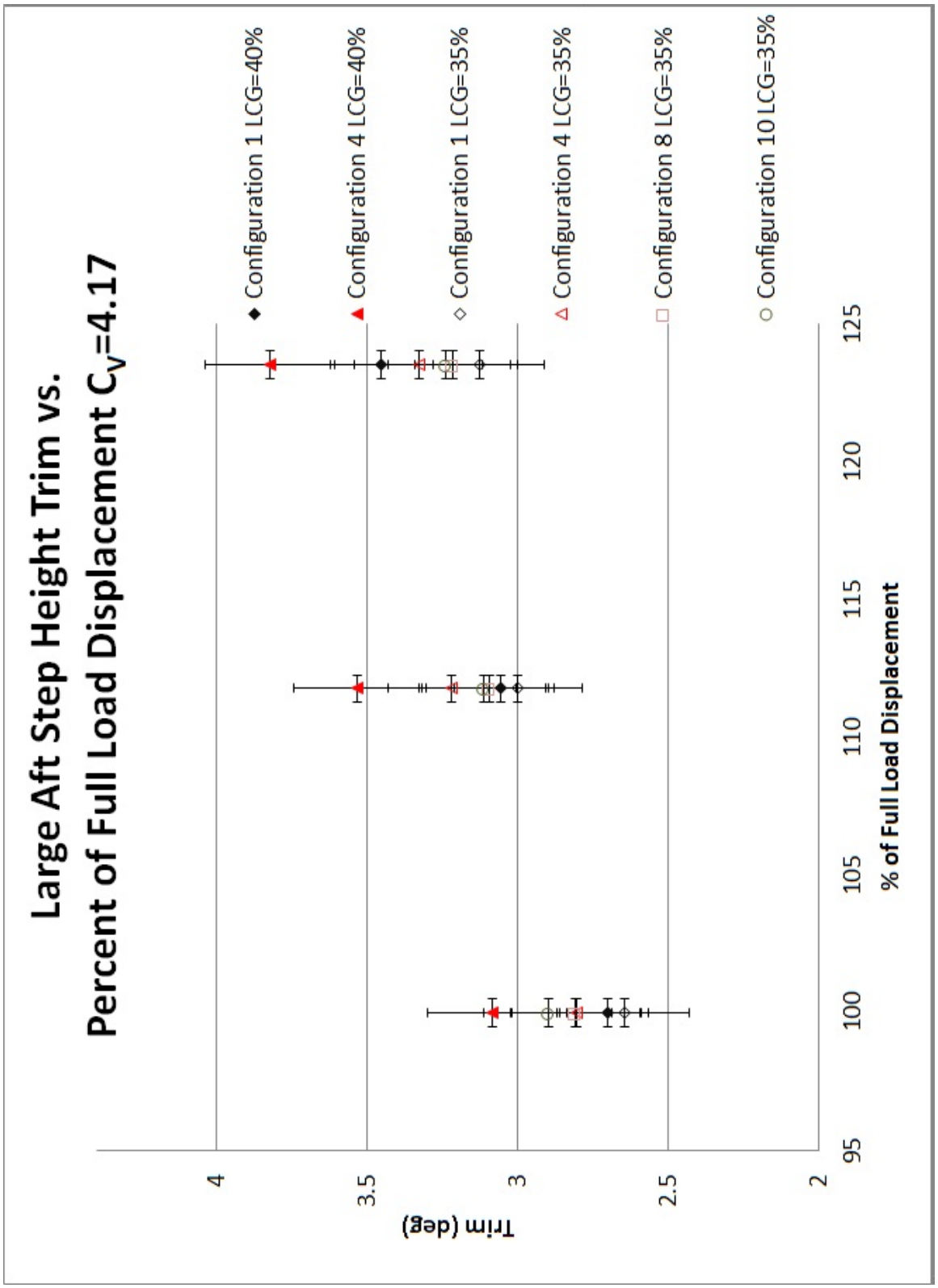

Figure B.37: Large Aft Step Height Trim vs. Percent of Full Load Displacement at C_v=4.17

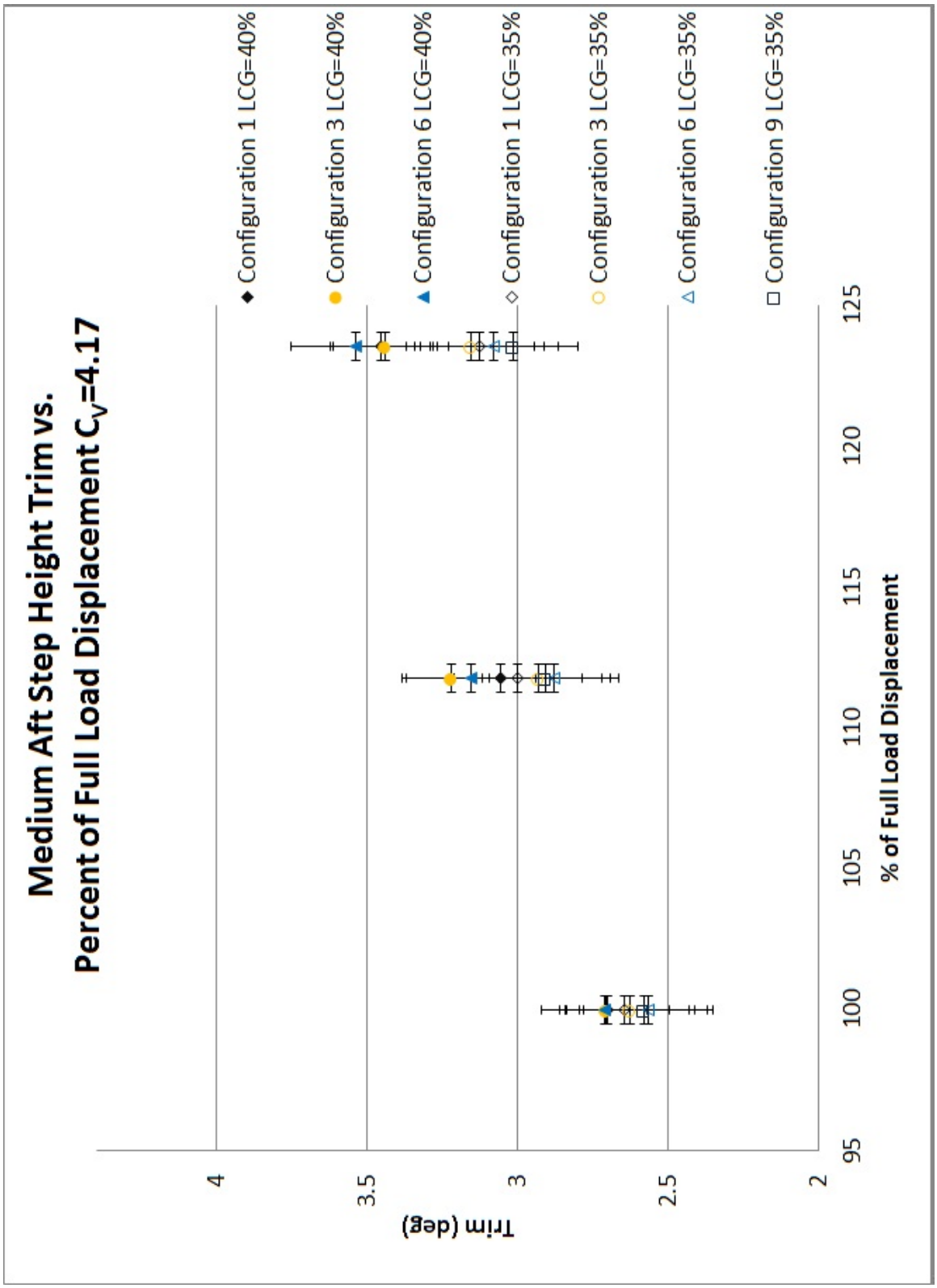

Figure B.38: Medium Aft Step Height Trim vs. Percent of Full Load Displacement at C_v=4.17

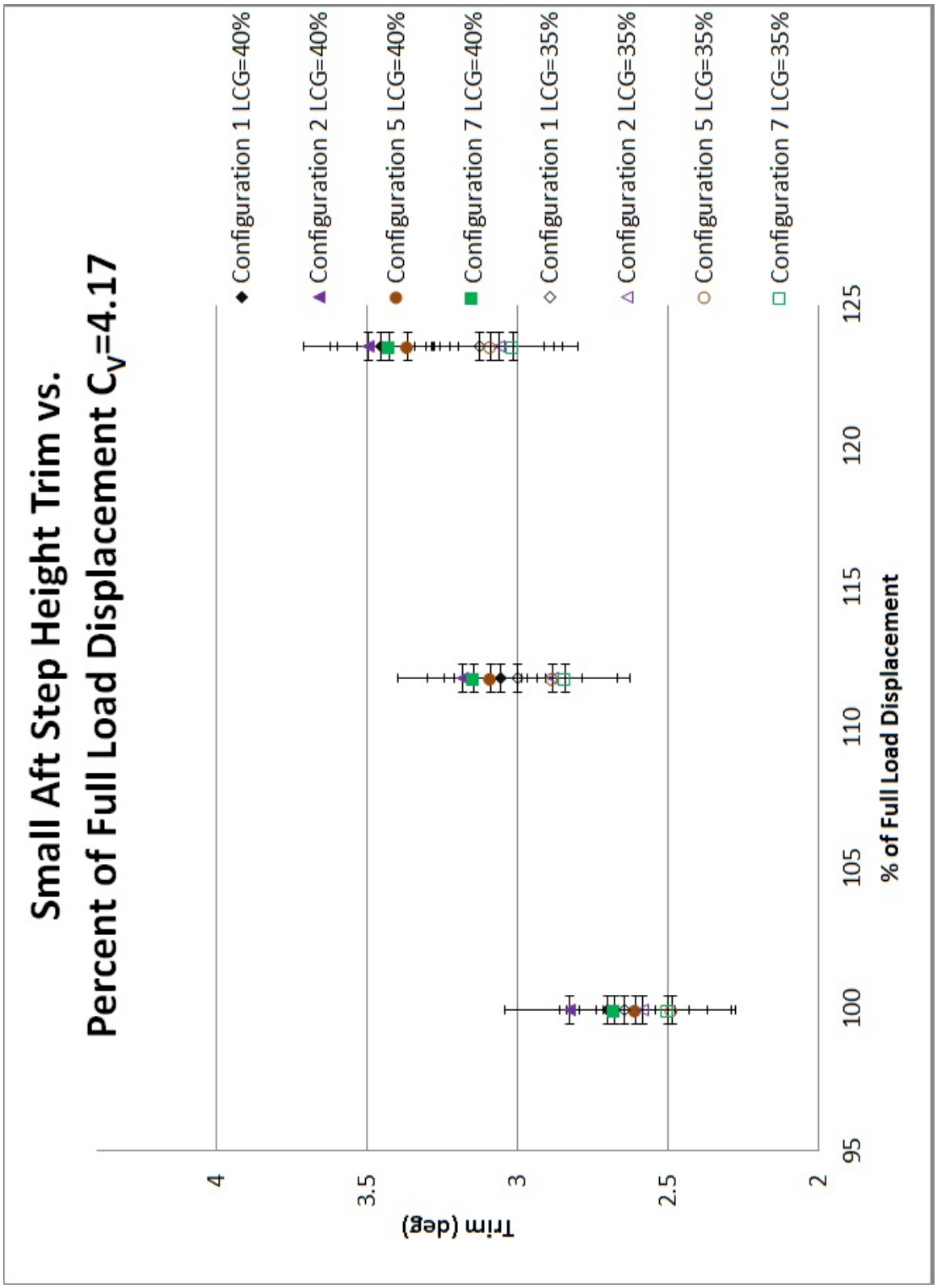

Figure B.39: Small Aft Step Height Trim vs. Percent of Full Load Displacement at C_v=4.17

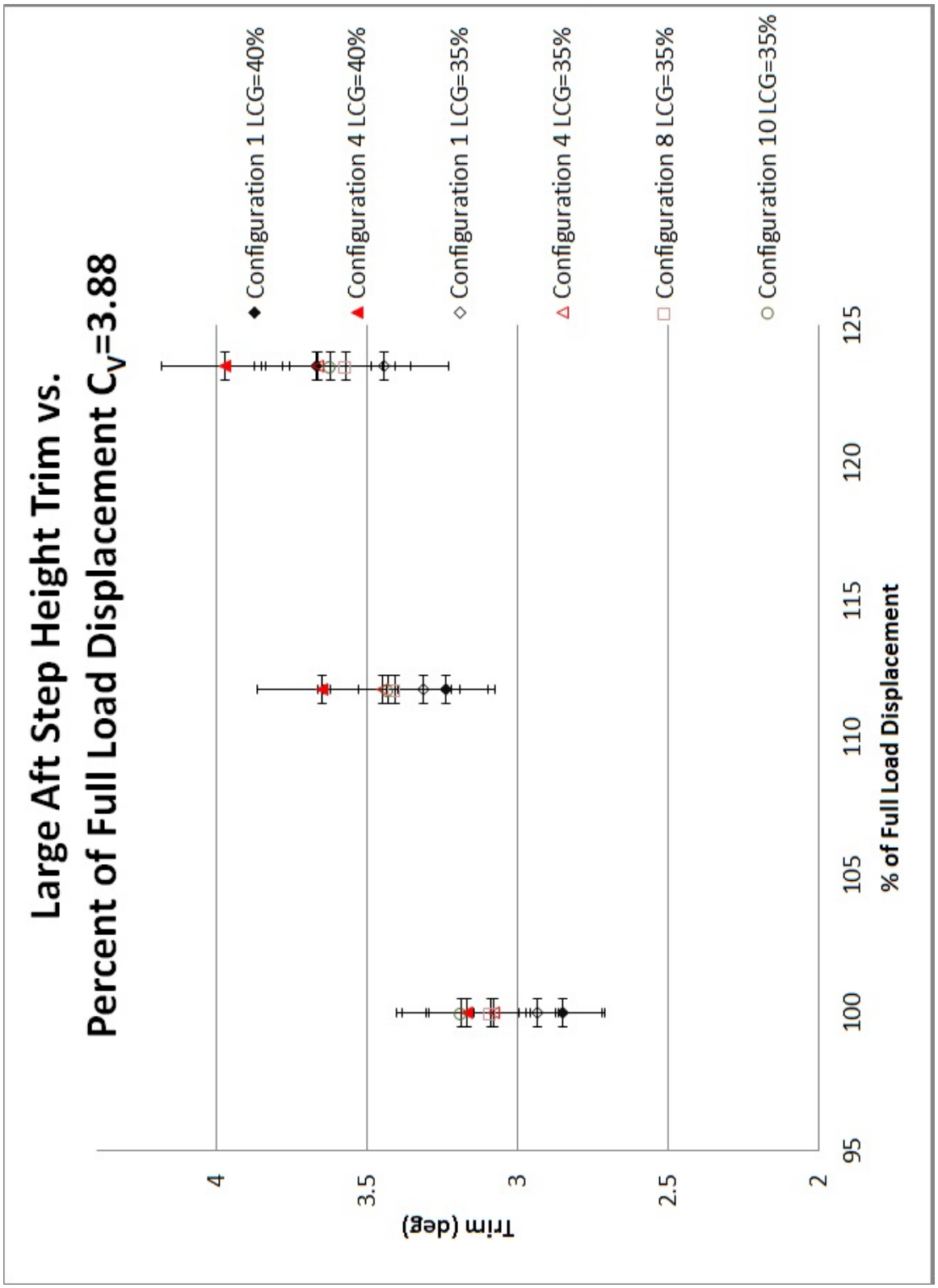

Figure B.40: Large Aft Step Height Trim vs. Percent of Full Load Displacement at C_v=3.88

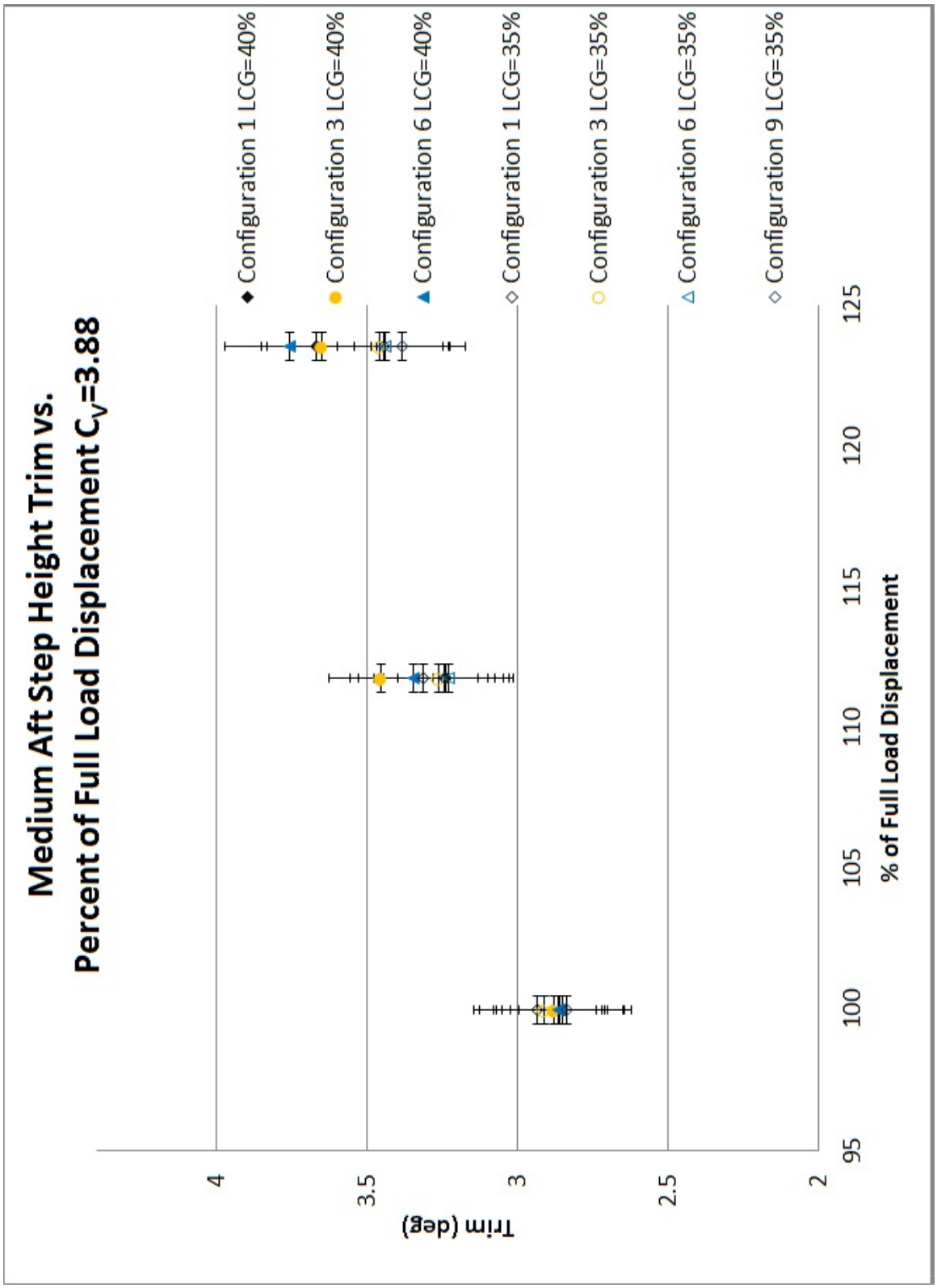

Figure B.41: Medium Aft Step Height Trim vs. Percent of Full Load Displacement at C_v=3.88

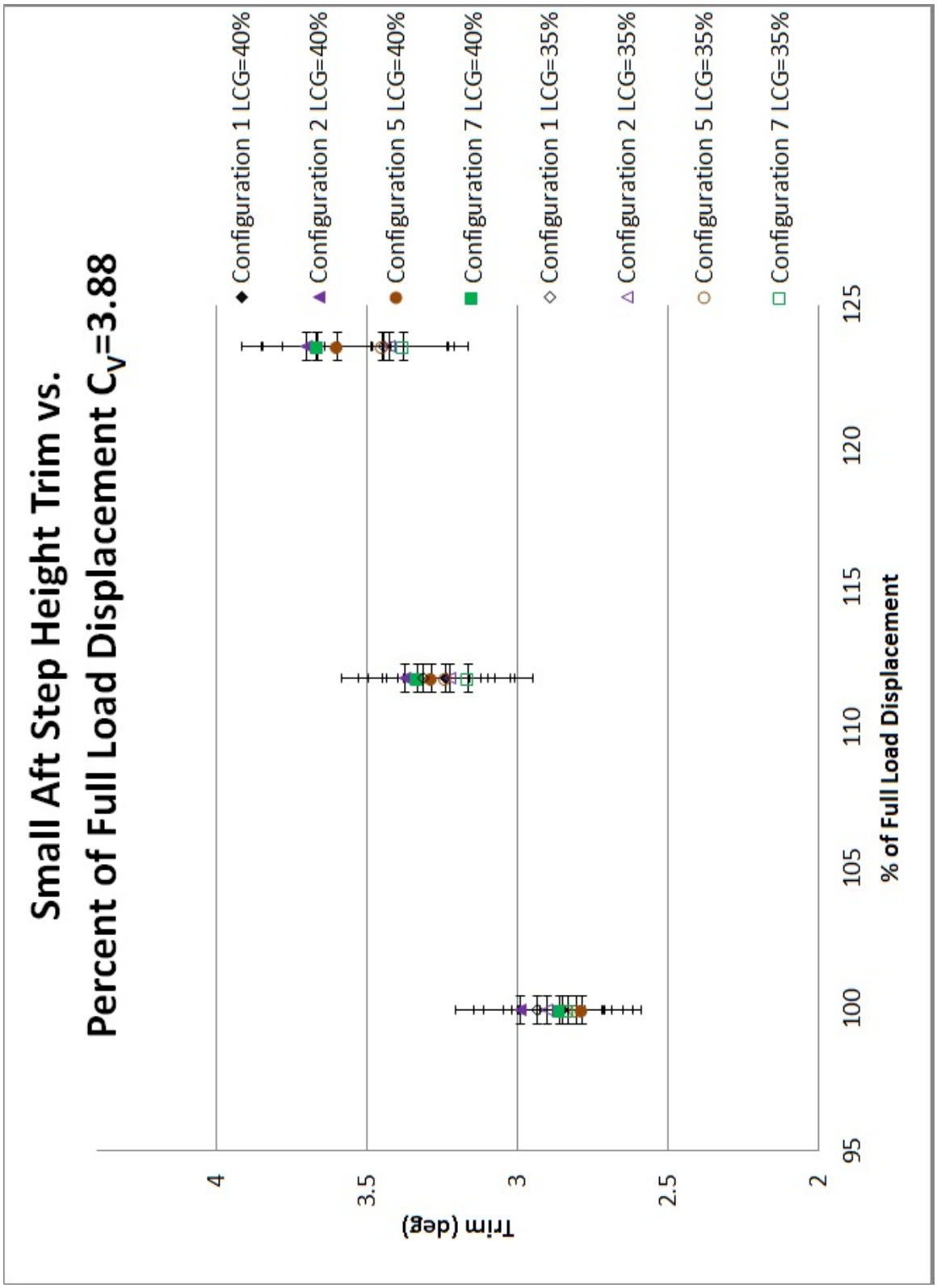

Figure B.42: Small Aft Step Height Trim vs. Percent of Full Load Displacement at C_v=3.88

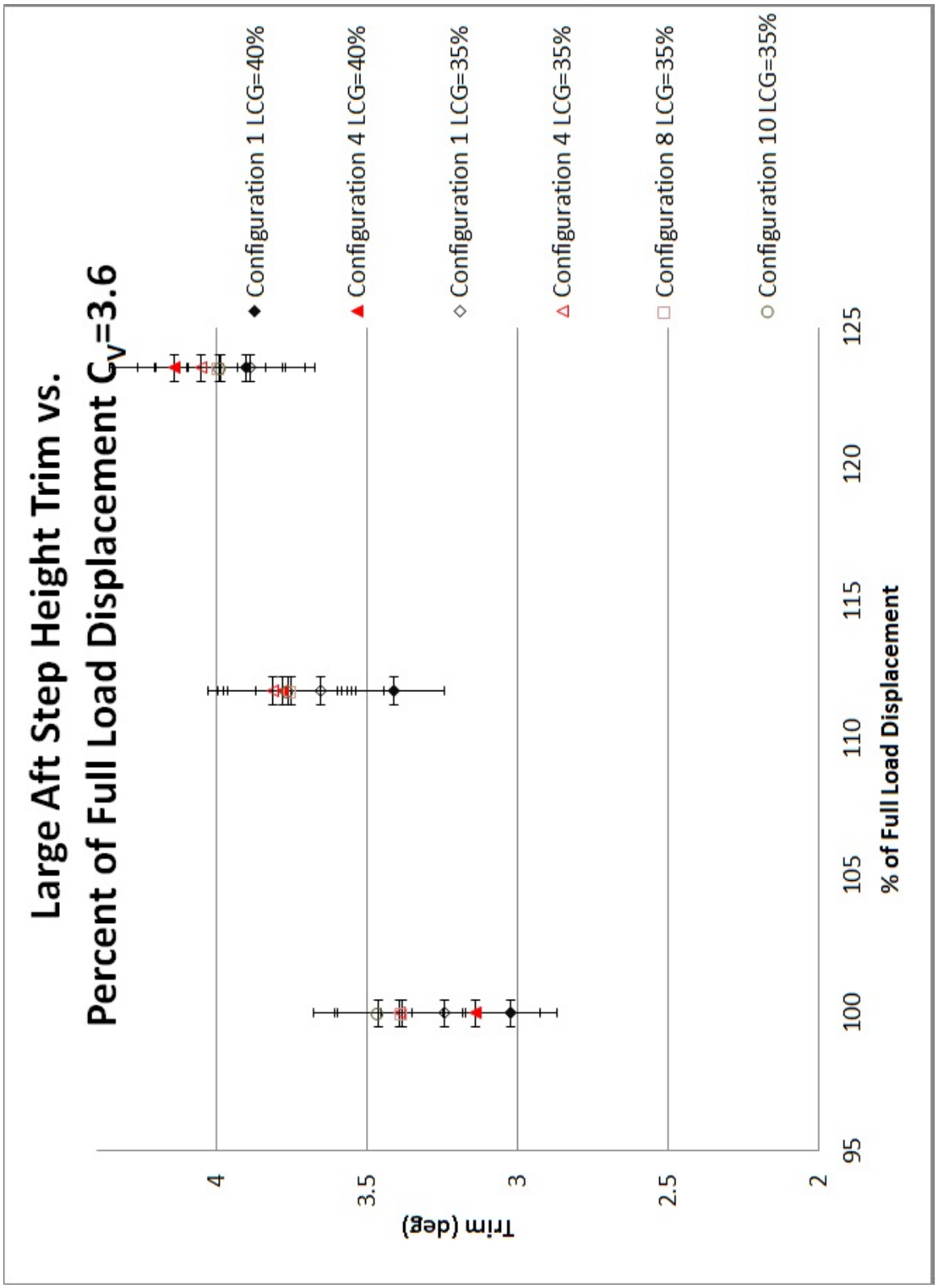

Figure B.43: Large Aft Step Height Trim vs. Percent of Full Load Displacement at C_v=3.60

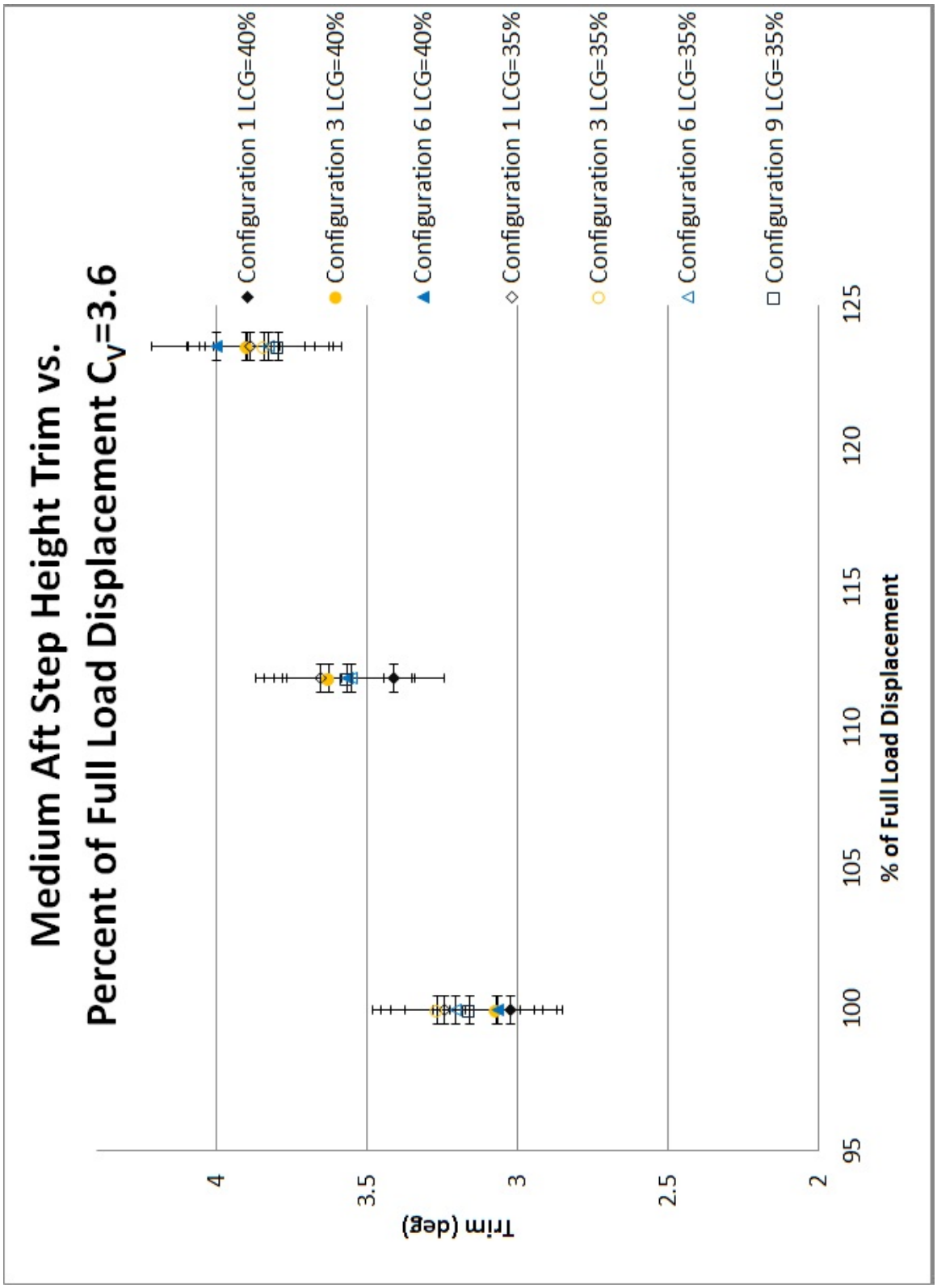

Figure B.44: Medium Aft Step Height Trim vs. Percent of Full Load Displacement at C_v=3.60

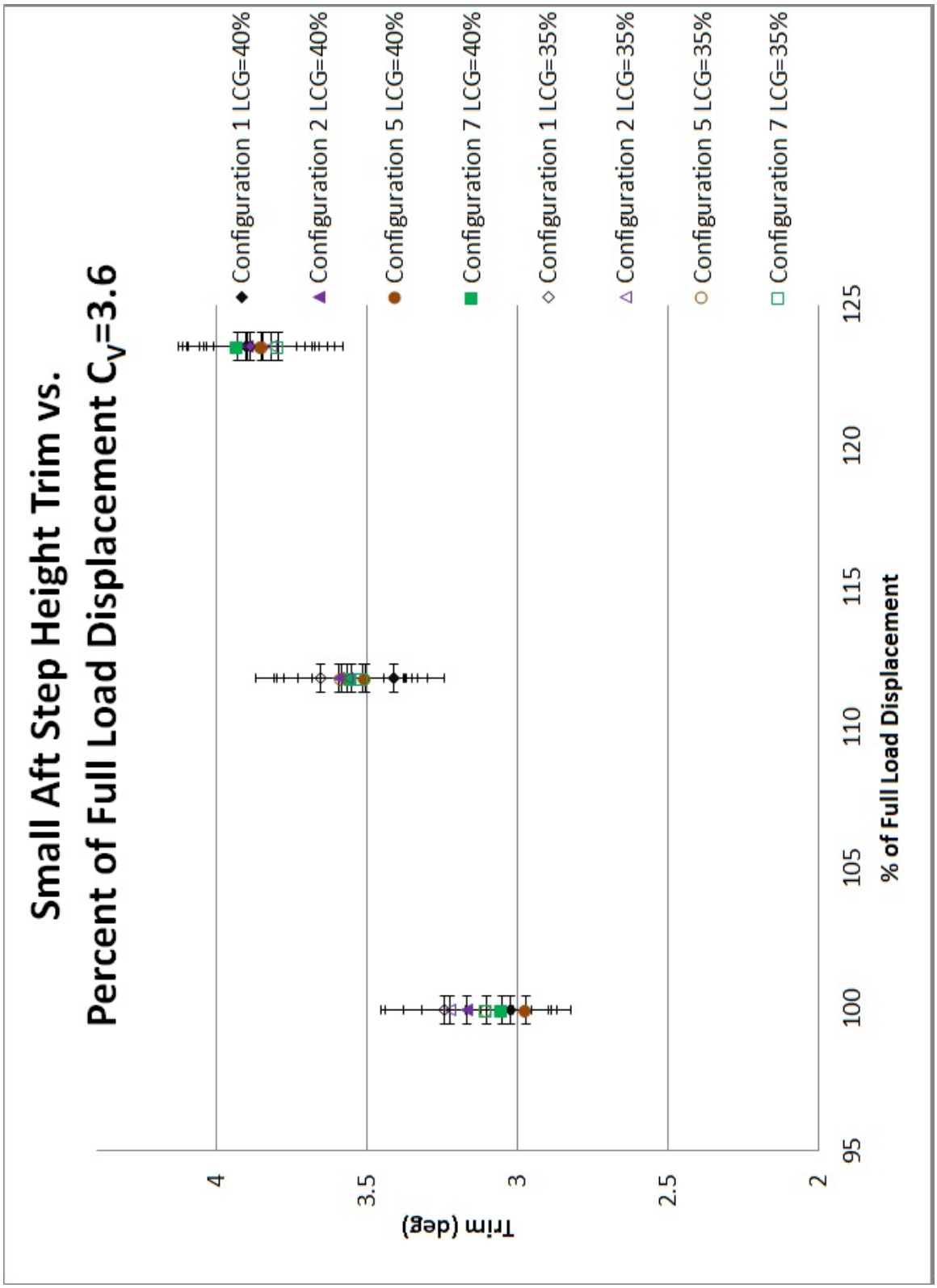

Figure B.45: Small Aft Step Height Trim vs. Percent of Full Load Displacement at C_v=3.60

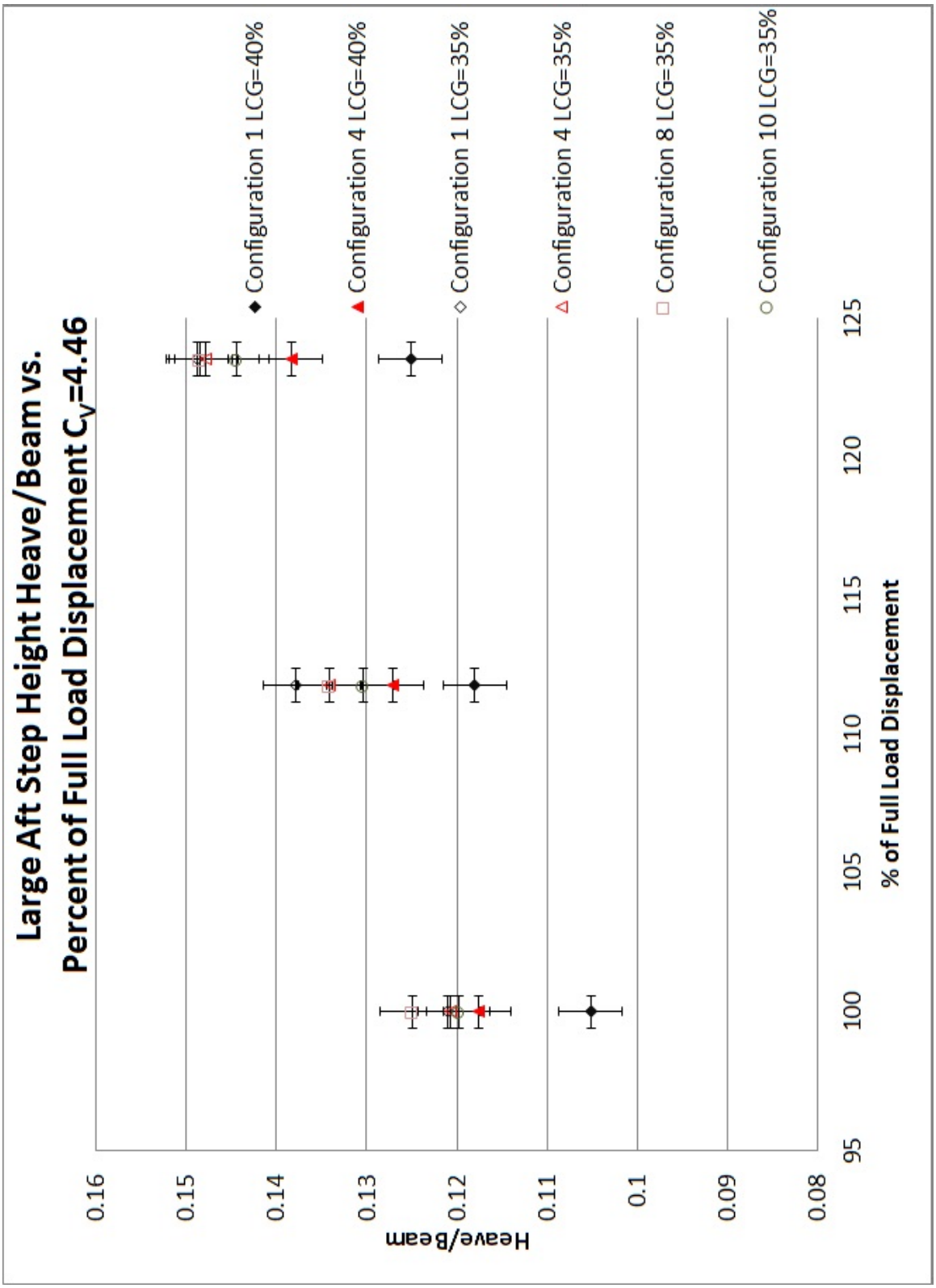

Figure B.46: Large Aft Step Height Heave/Beam vs. Percent of Full Load Displacement at C_v=4.46

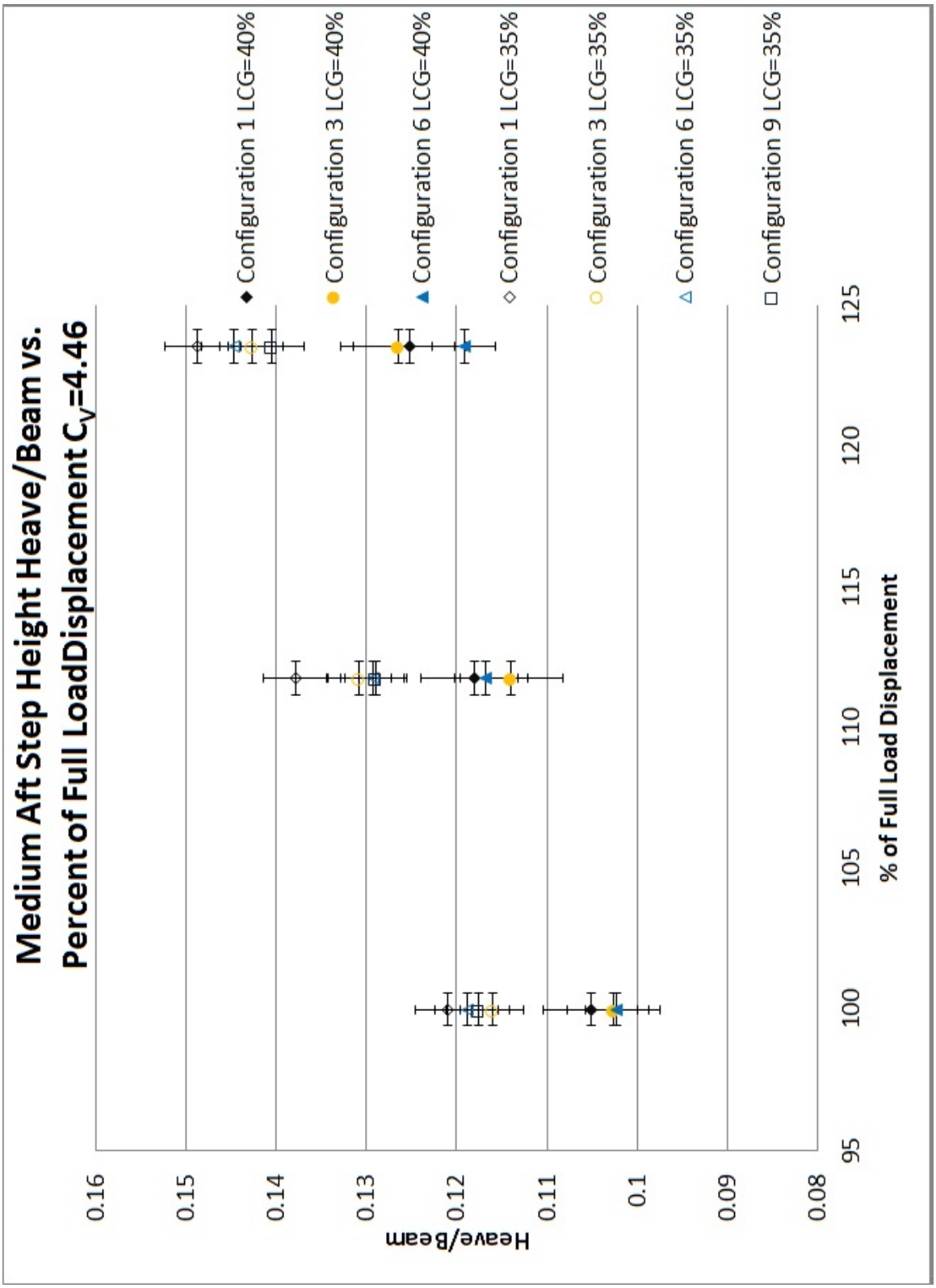

Figure B.47: Medium Aft Step Height Heave/Beam vs. Percent of Full Load Displacement at C_v=4.46

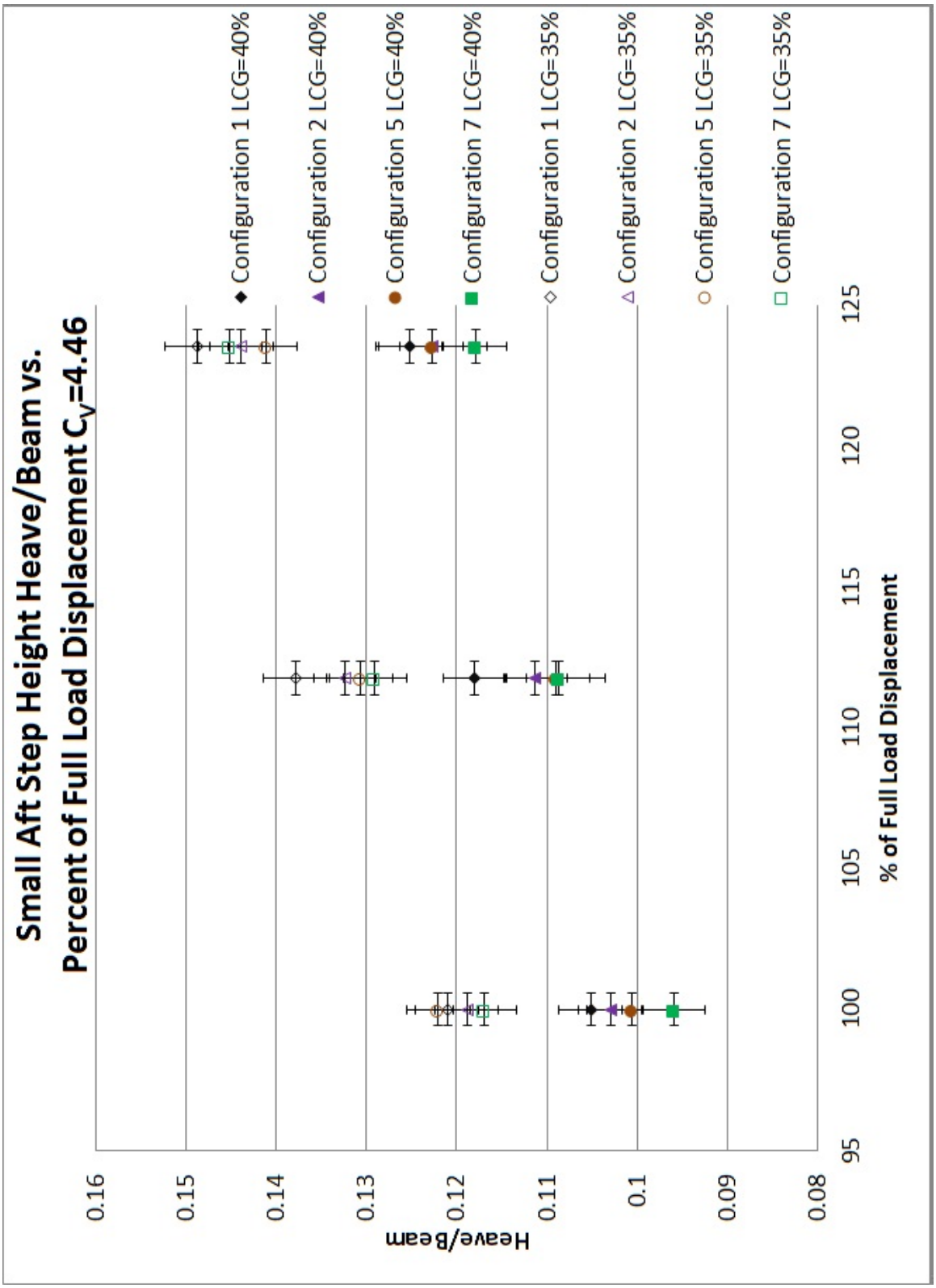

Figure B.48: Small Aft Step Height Heave/Beam vs. Percent of Full Load Displacement at C_v=4.46

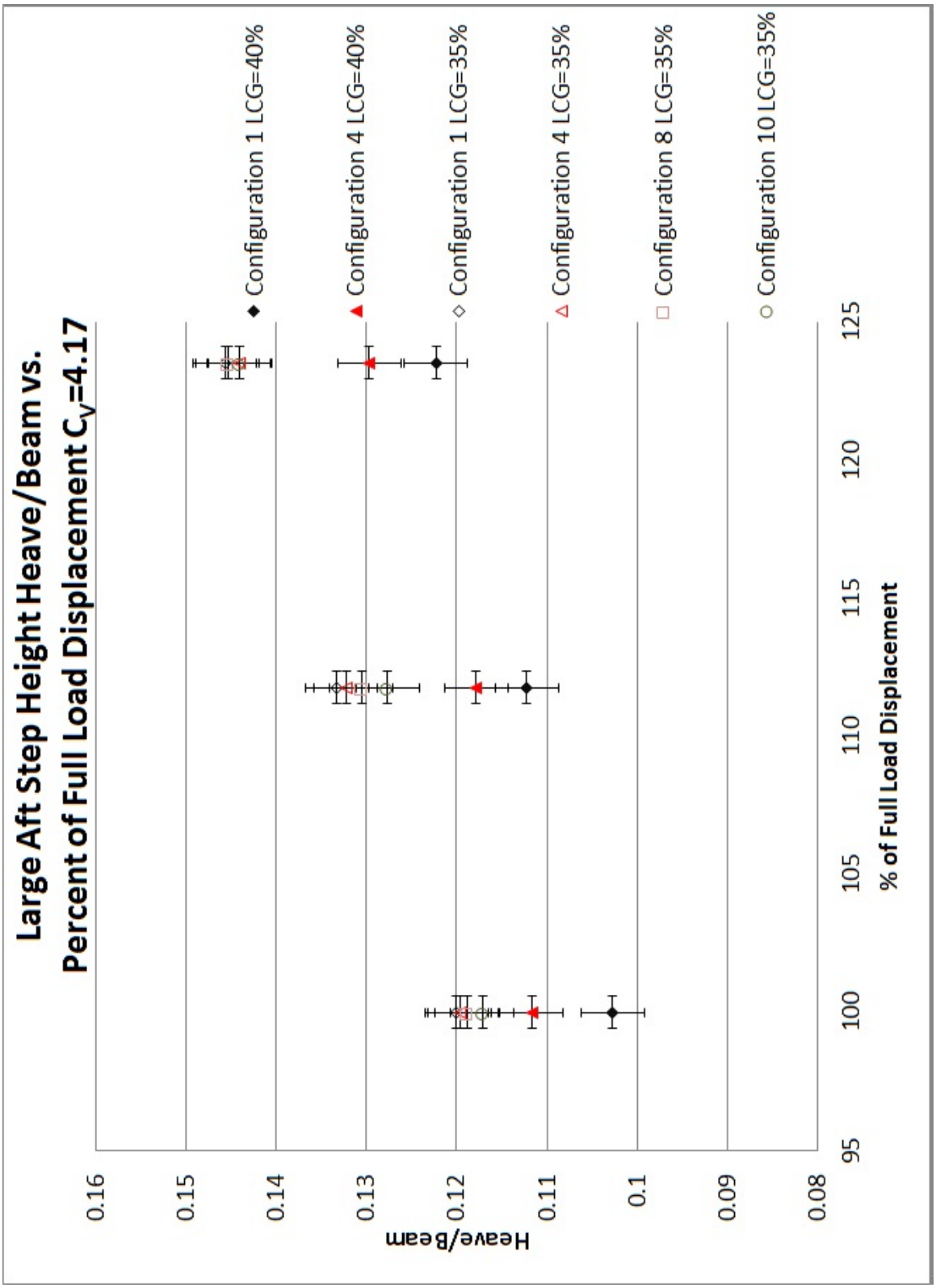

Figure B.49: Large Aft Step Height Heave/Beam vs. Percent of Full Load Displacement at C_v=4.17

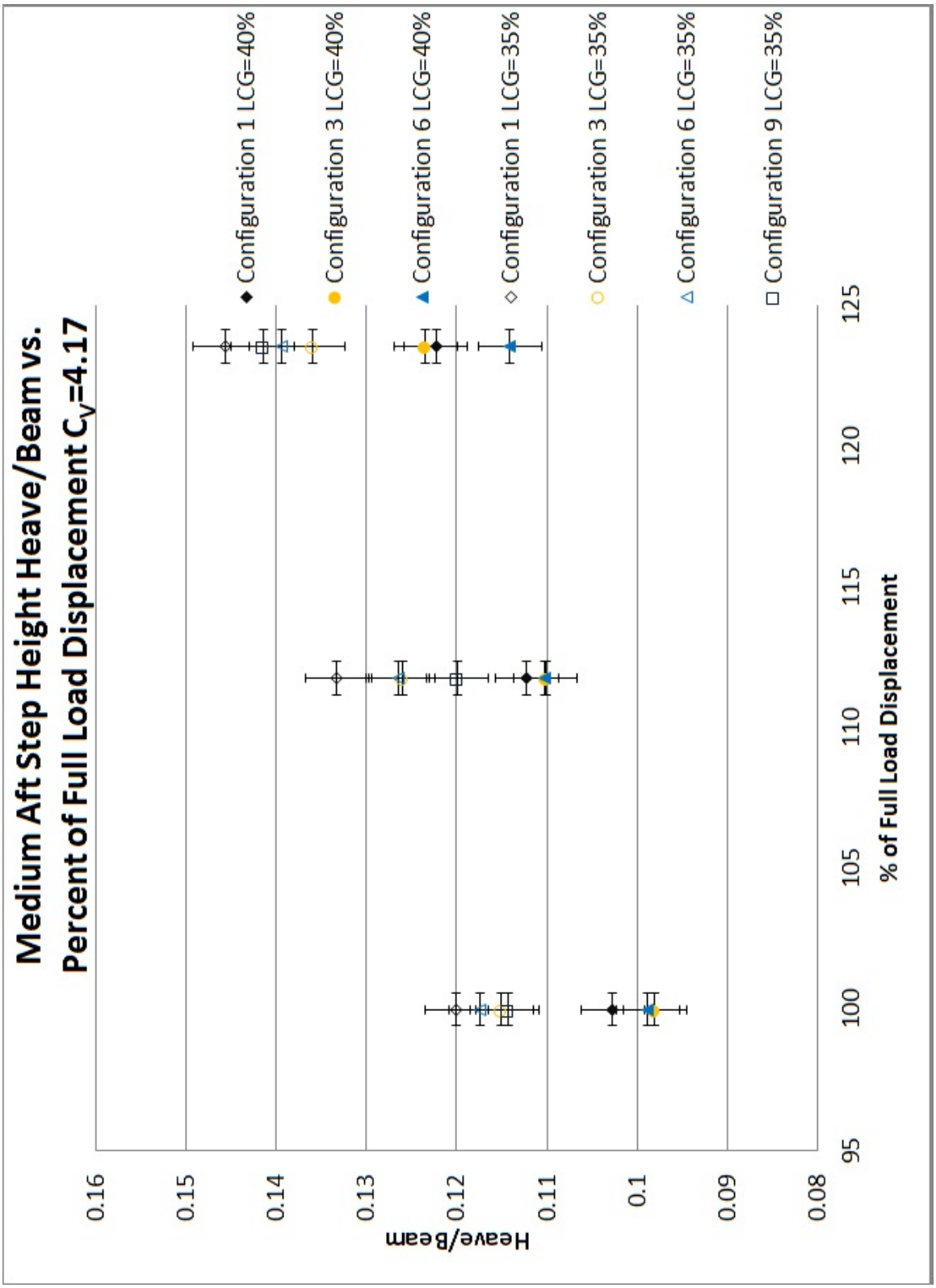

Figure B.50: Medium Aft Step Height Heave/Beam vs. Percent of Full Load Displacement at C_v=4.17

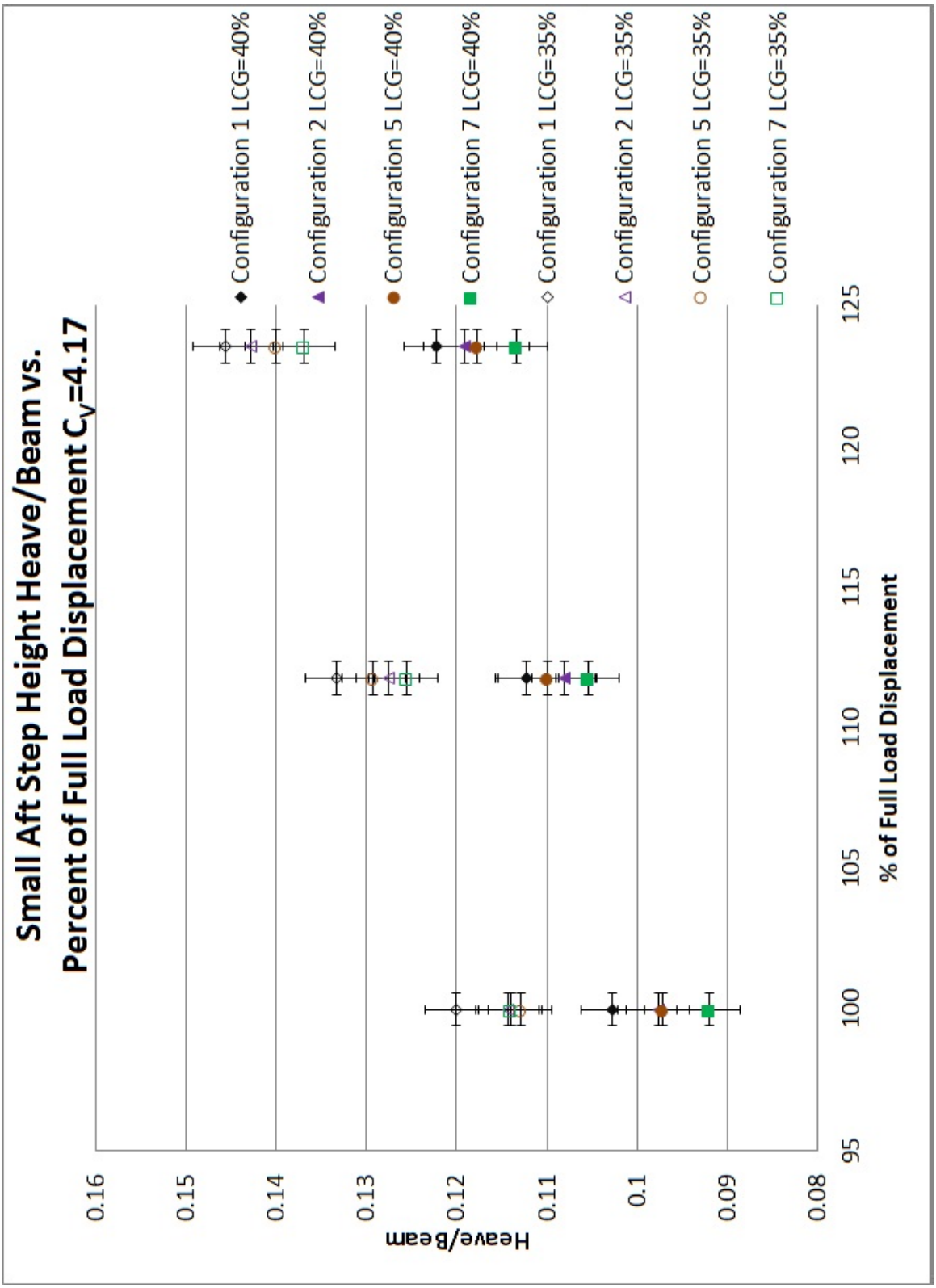

Figure B.51: Small Aft Step Height Heave/Beam vs. Percent of Full Load Displacement at C_v=4.17

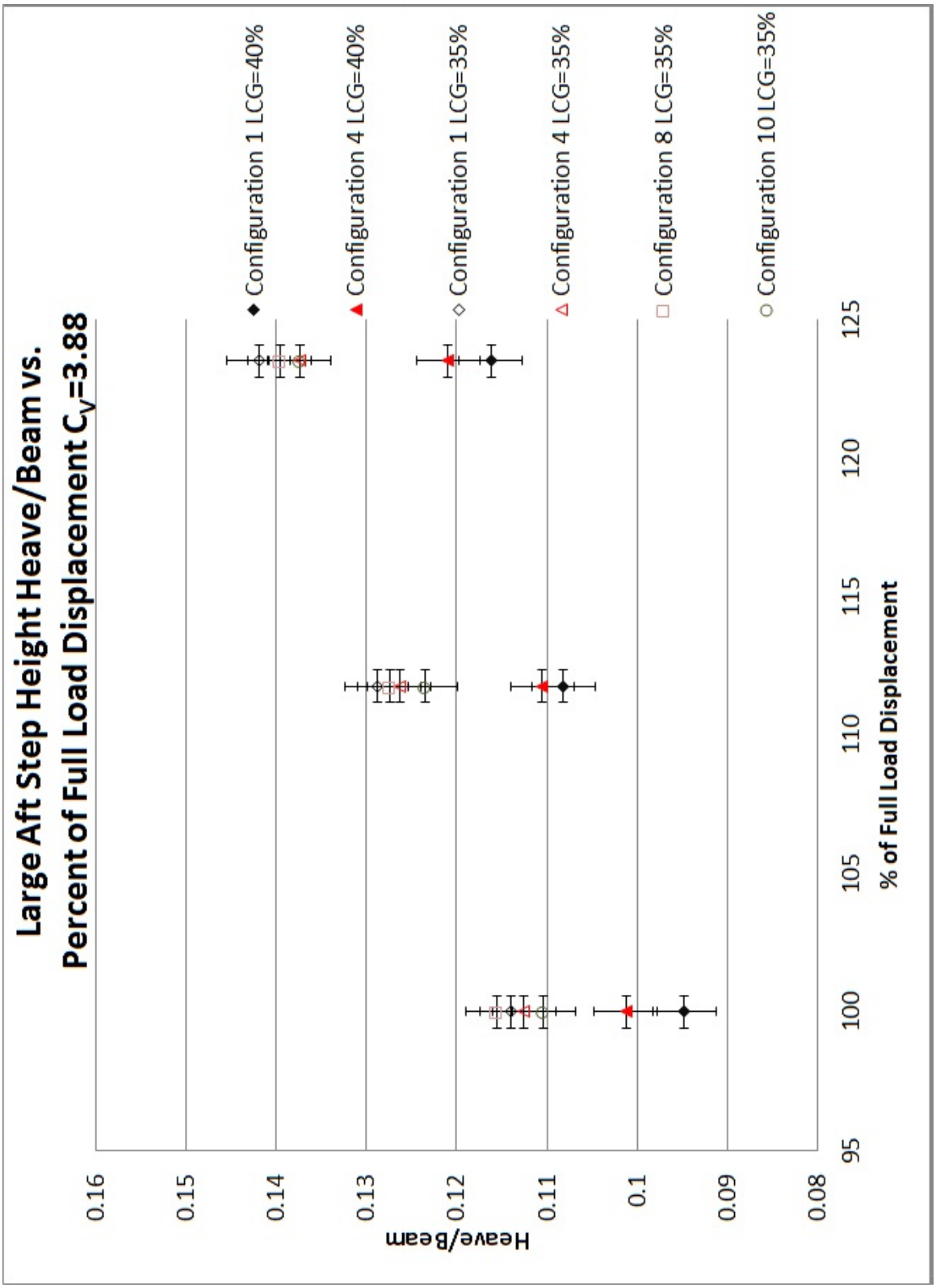

Figure B.52: Large Aft Step Height Heave/Beam vs. Percent of Full Load Displacement at C_v=3.88

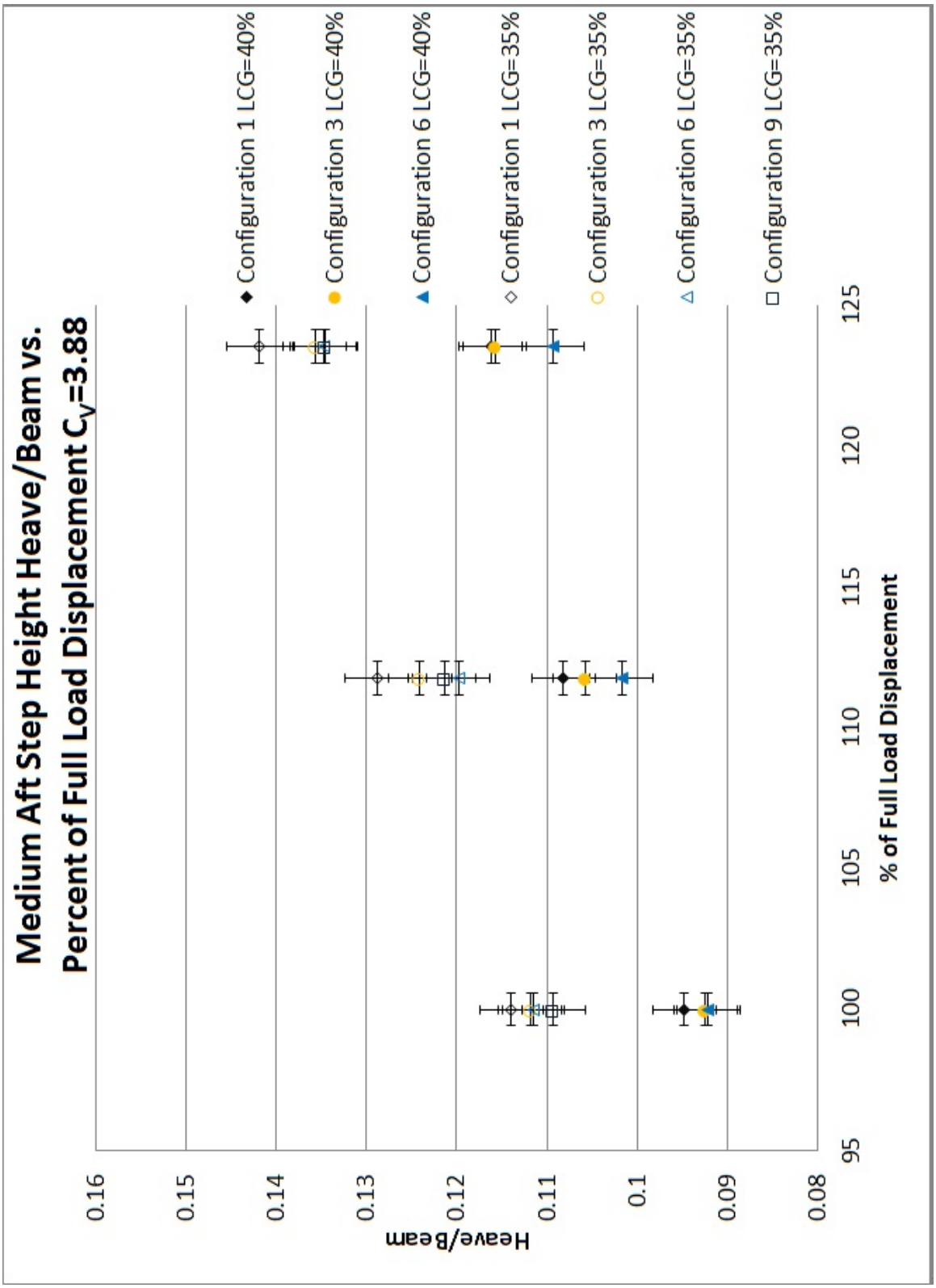

Figure B.53: Medium Aft Step Height Heave/Beam vs. Percent of Full Load Displacement at C_v=3.88

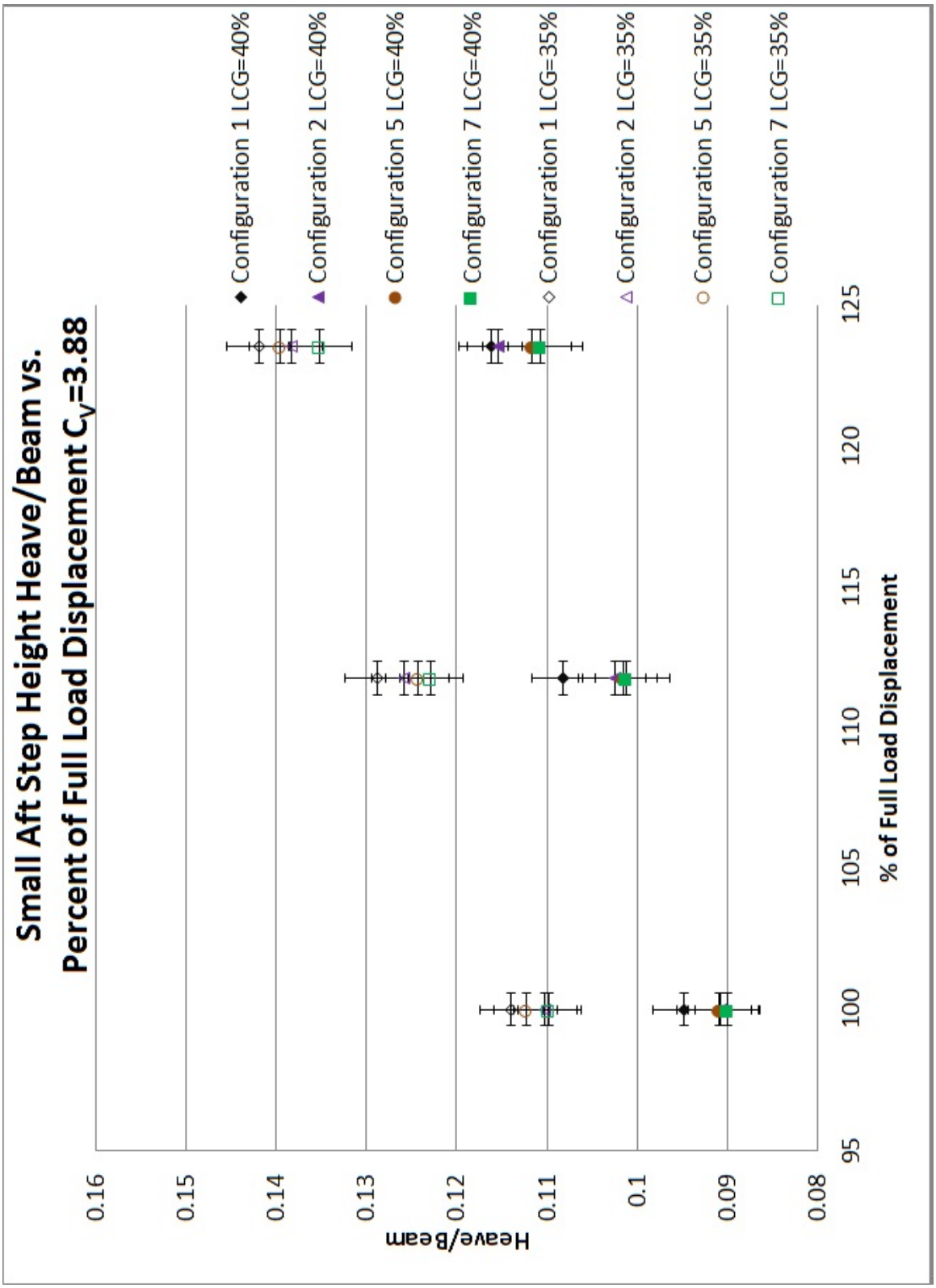

Figure B.54: Small Aft Step Height Heave/Beam vs. Percent of Full Load Displacement at C_v=3.88

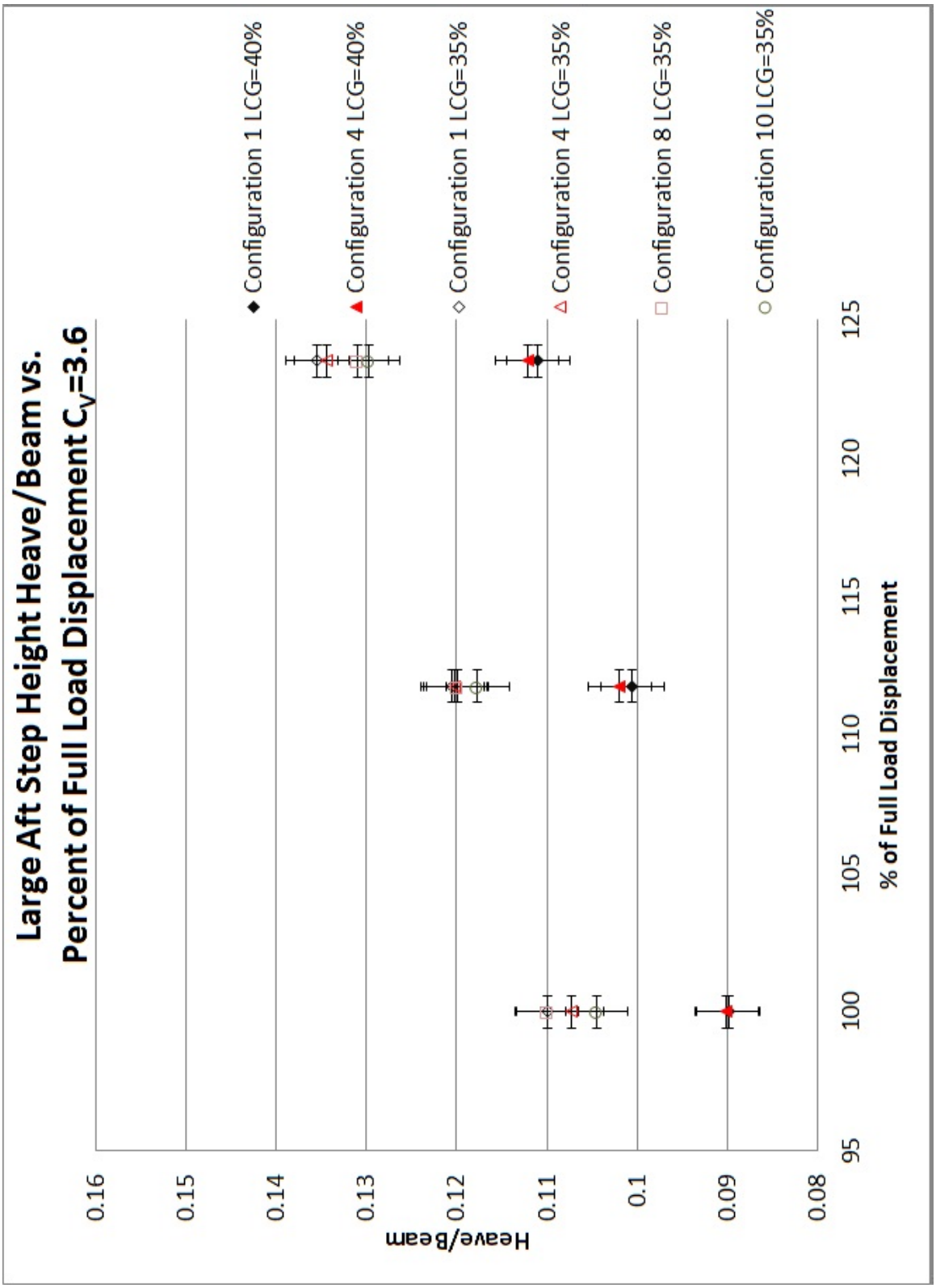

Figure B.55: Large Aft Step Height Heave/Beam vs. Percent of Full Load Displacement at C_v=3.60

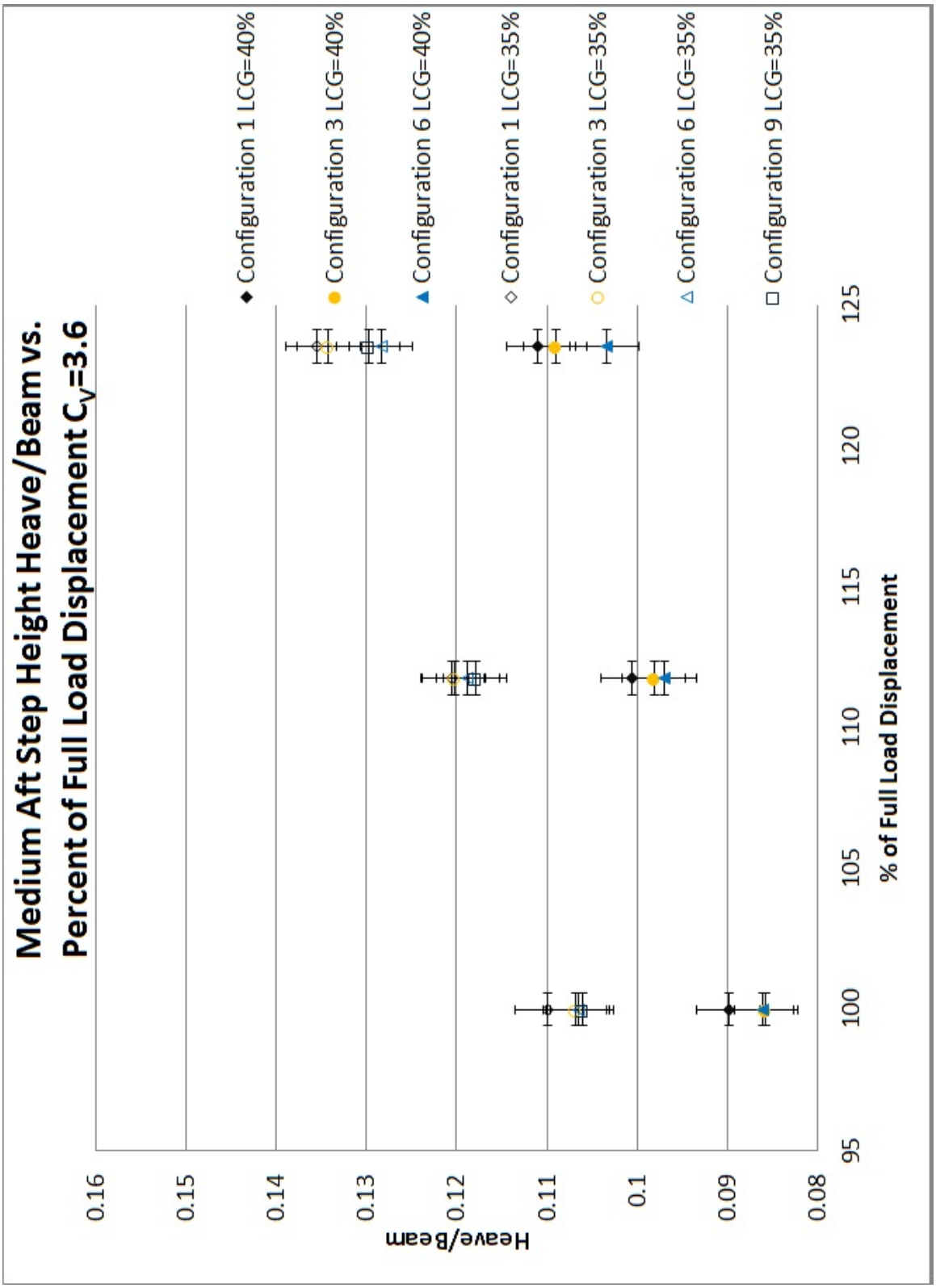

Figure B.56: Medium Aft Step Height Heave/Beam vs. Percent of Full Load Displacement at C_v=3.60

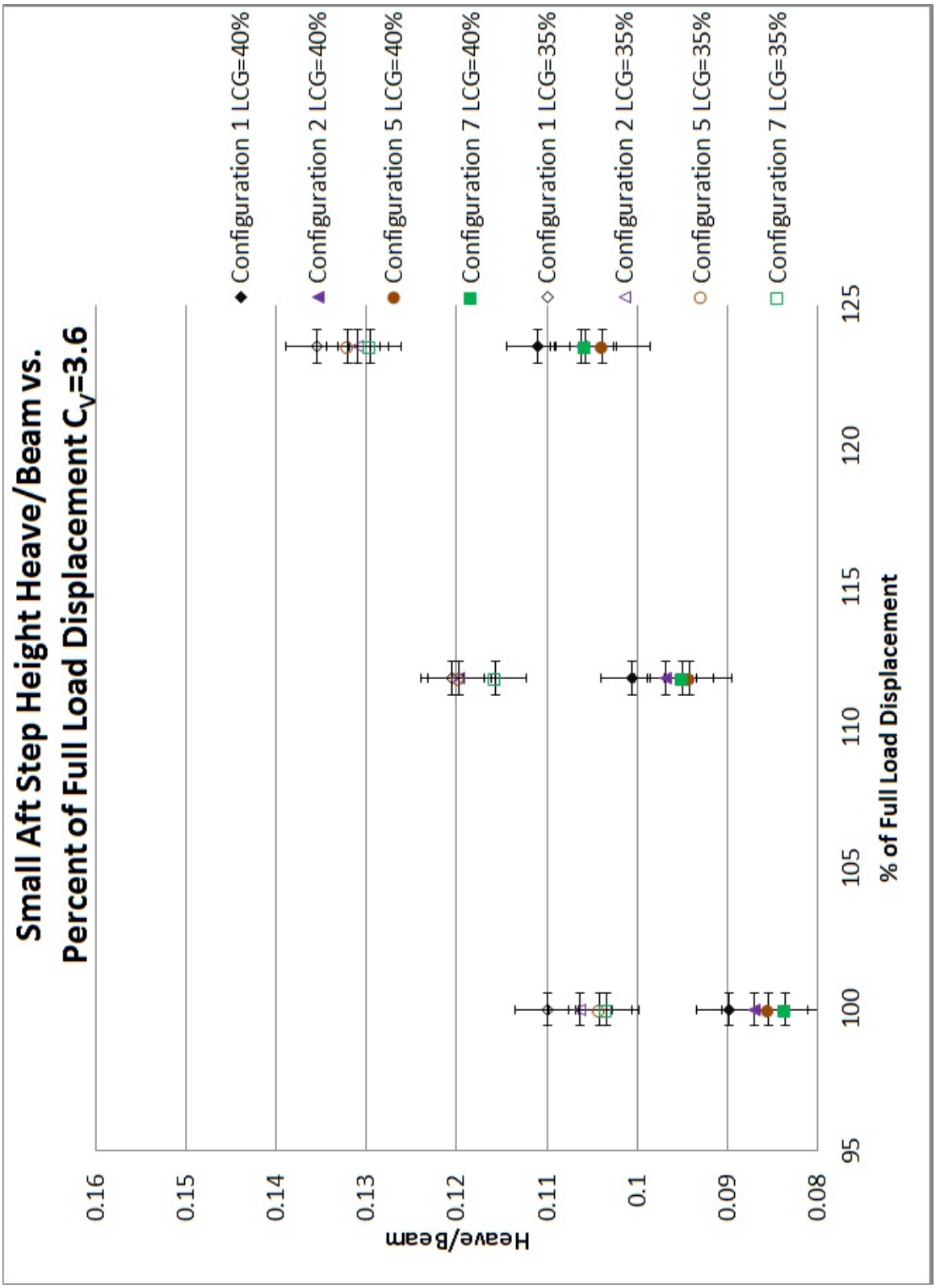

Figure B.57: Small Aft Step Height Heave/Beam vs. Percent of Full Load Displacement at C_v=3.60

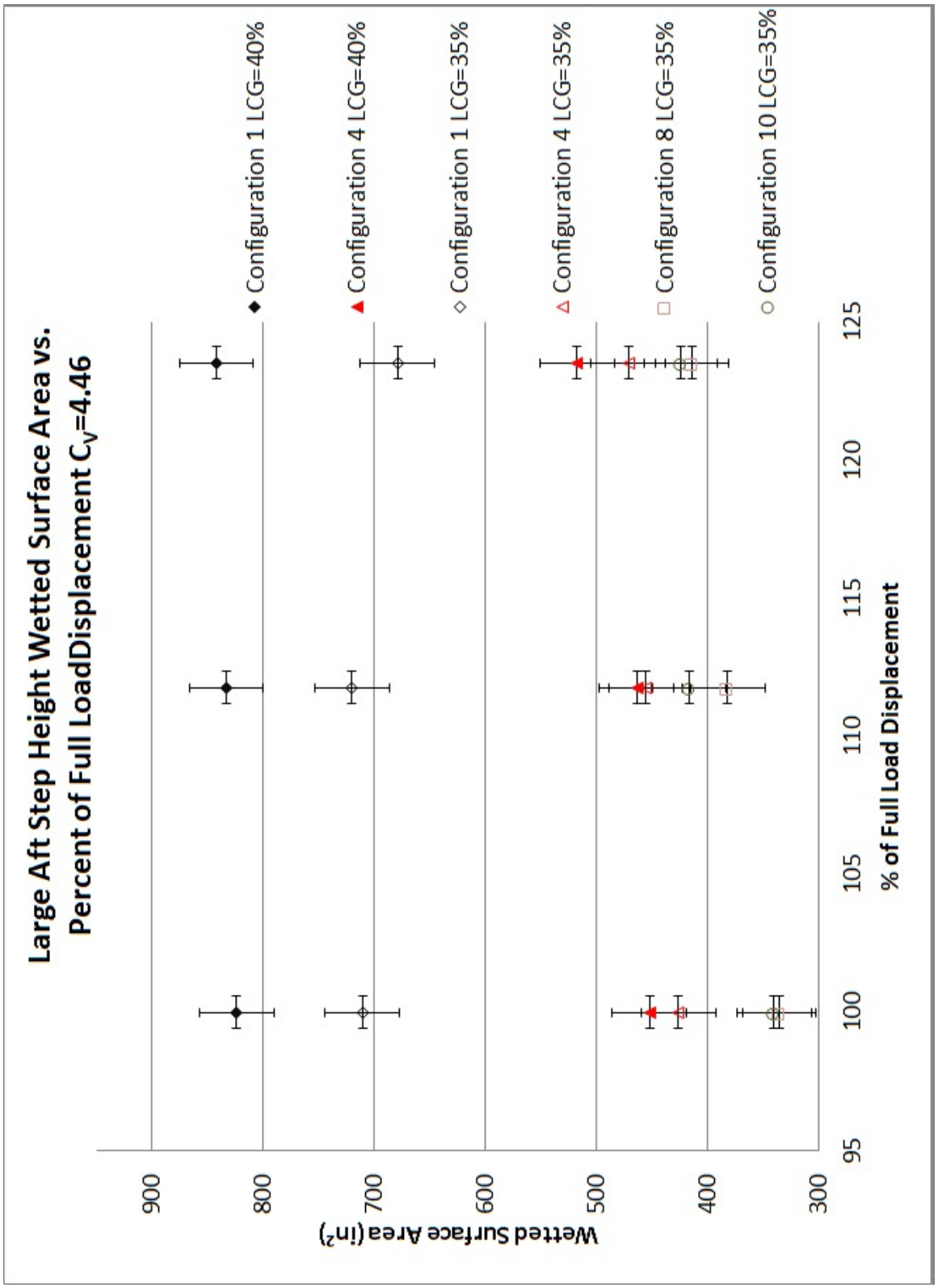

Figure B.58: Large Aft Step Height Wetted Surface Area vs. Percent of Full Load Displacement at C_v=4.46

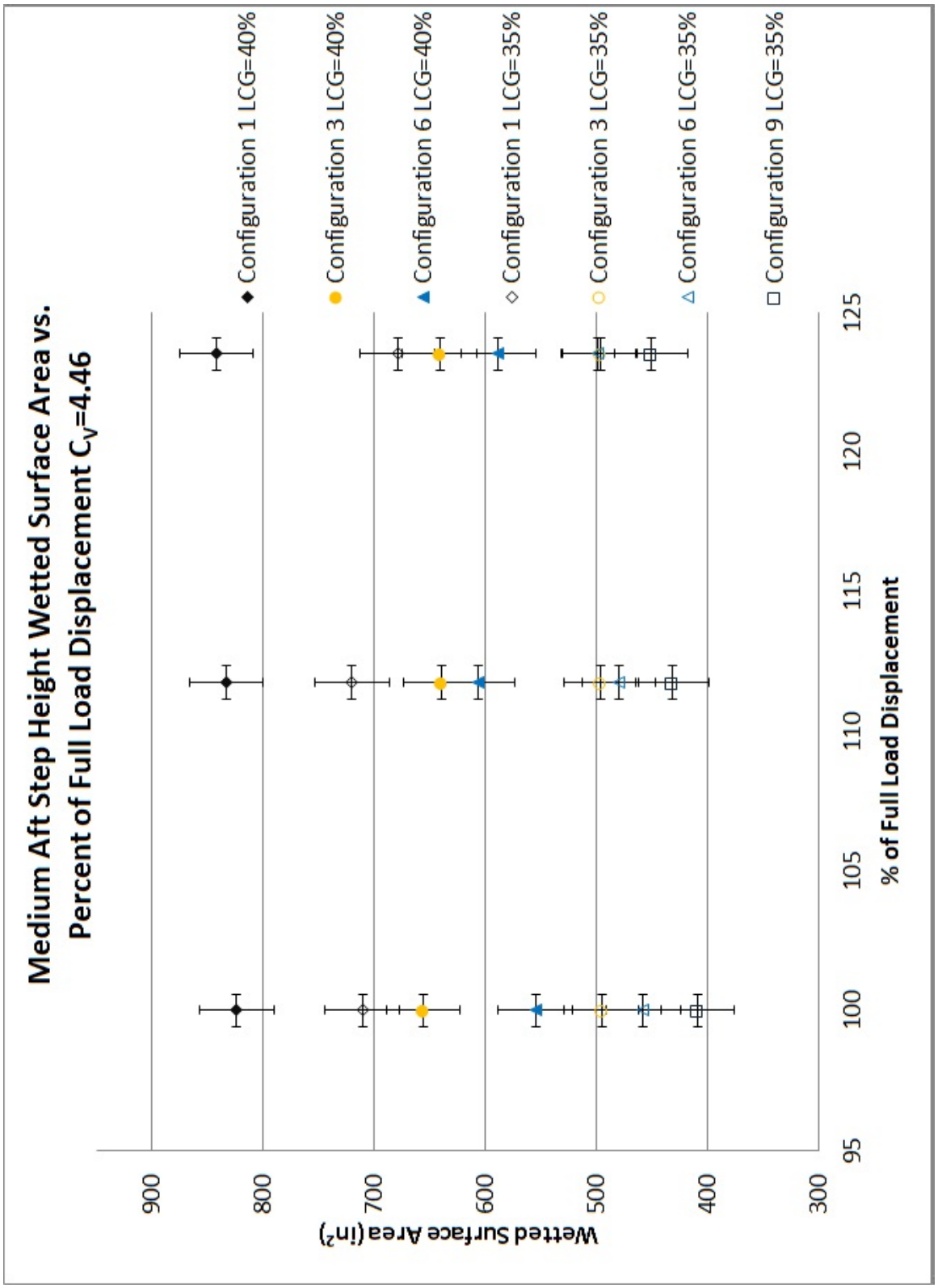

Figure B.59: Medium Aft Step Height Wetted Surface Area vs. Percent of Full Load Displacement at C_v=4.46

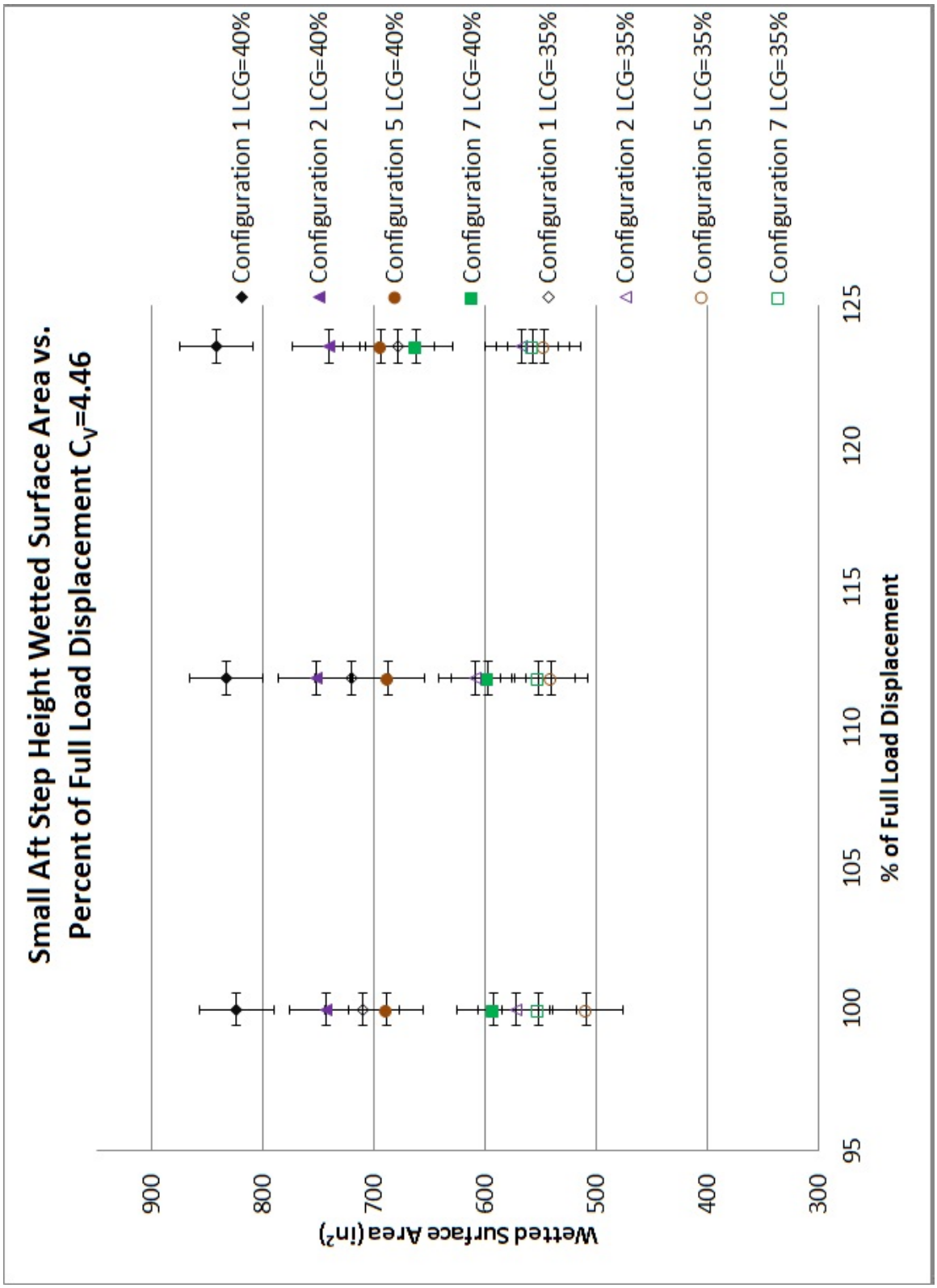

Figure B.60: Small Aft Step Height Wetted Surface Area vs. Percent of Full Load Displacement at C_v=4.46

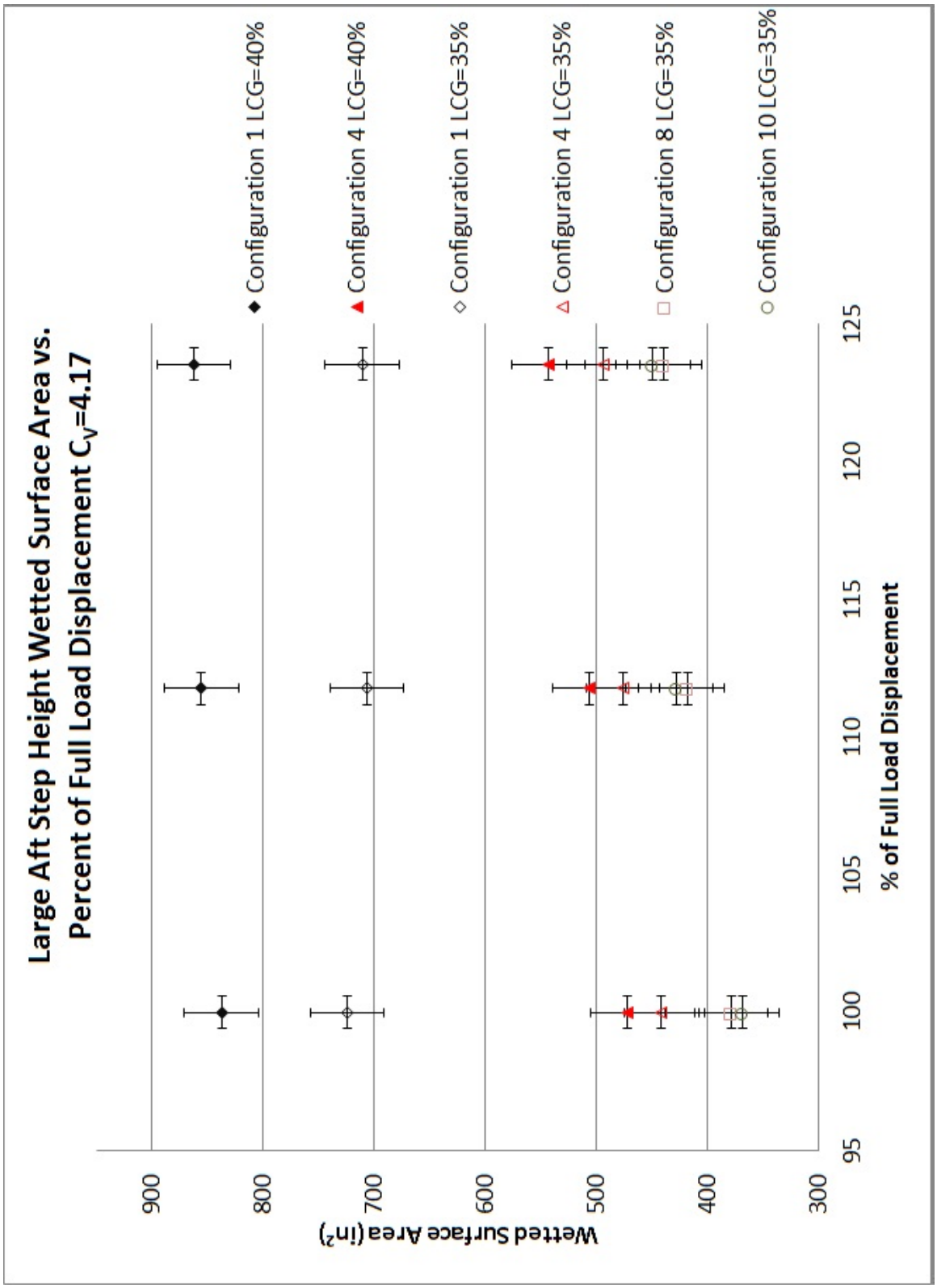

Figure B.61: Large Aft Step Height Wetted Surface Area vs. Percent of Full Load Displacement at C_v=4.17

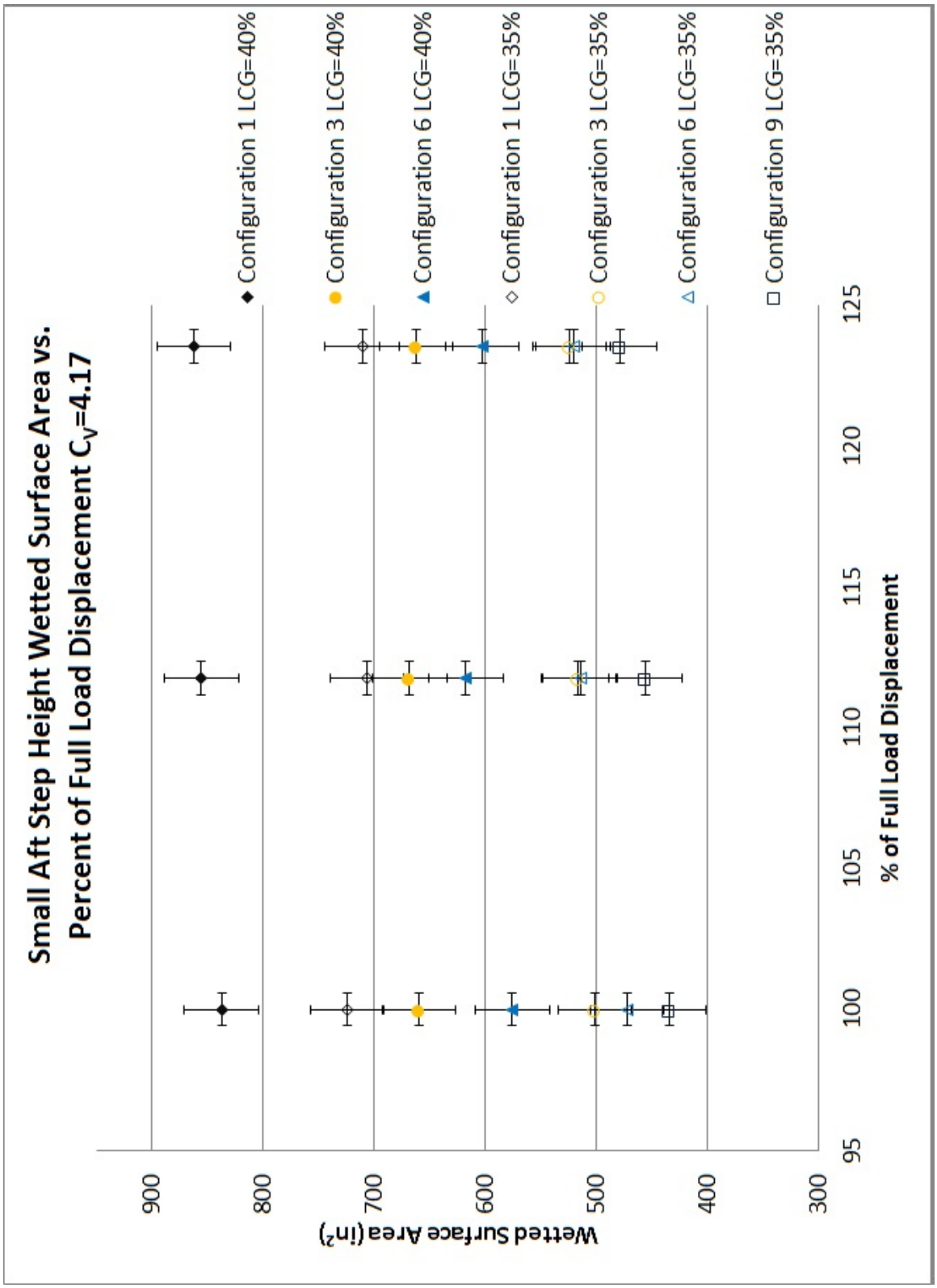

Figure B.62: Medium Aft Step Height Wetted Surface Area vs. Percent of Full Load Displacement at C_v=4.17

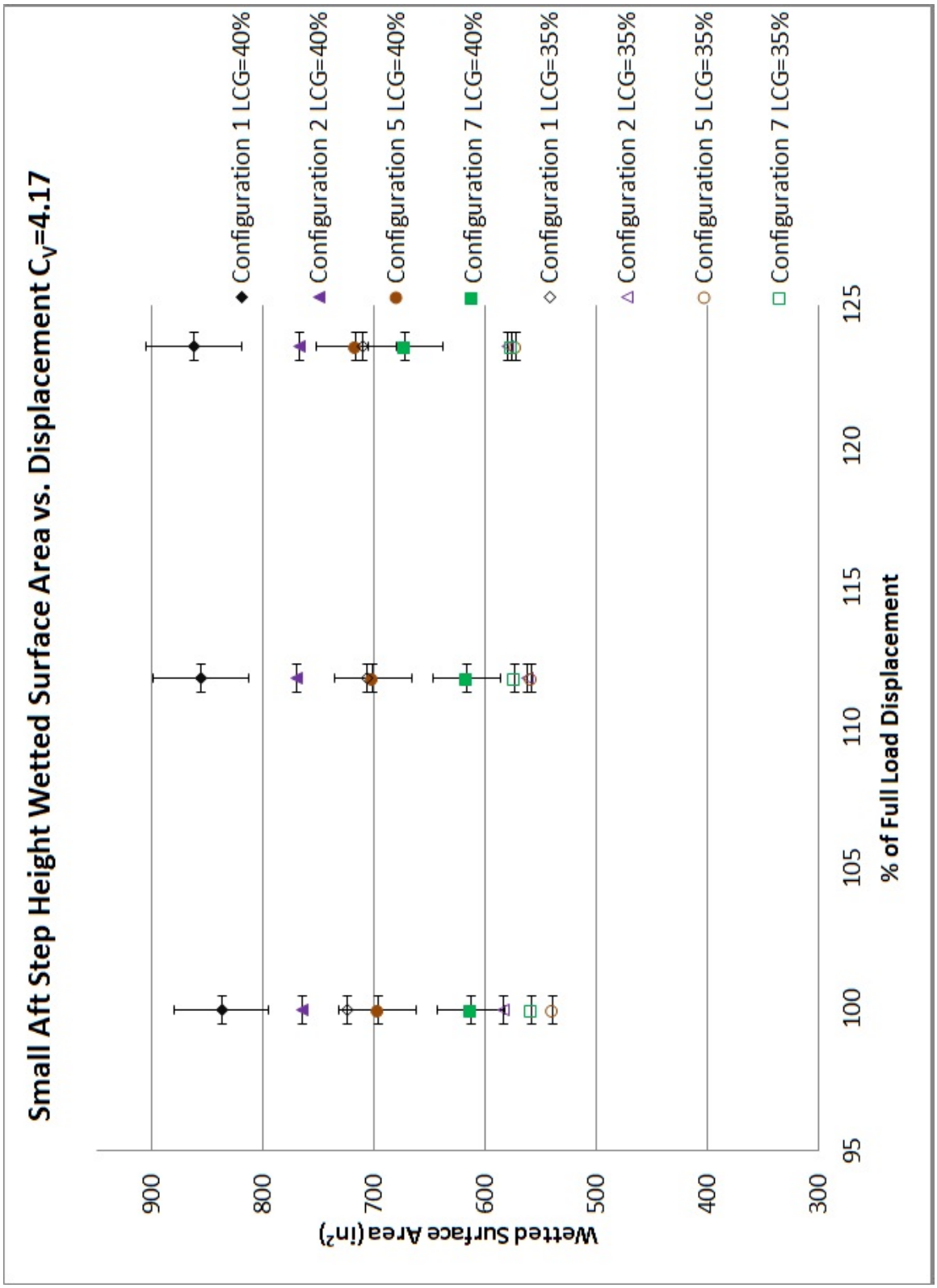

Figure B.63: Small Aft Step Height Wetted Surface Area vs. Percent of Full Load Displacement at C_v=4.17

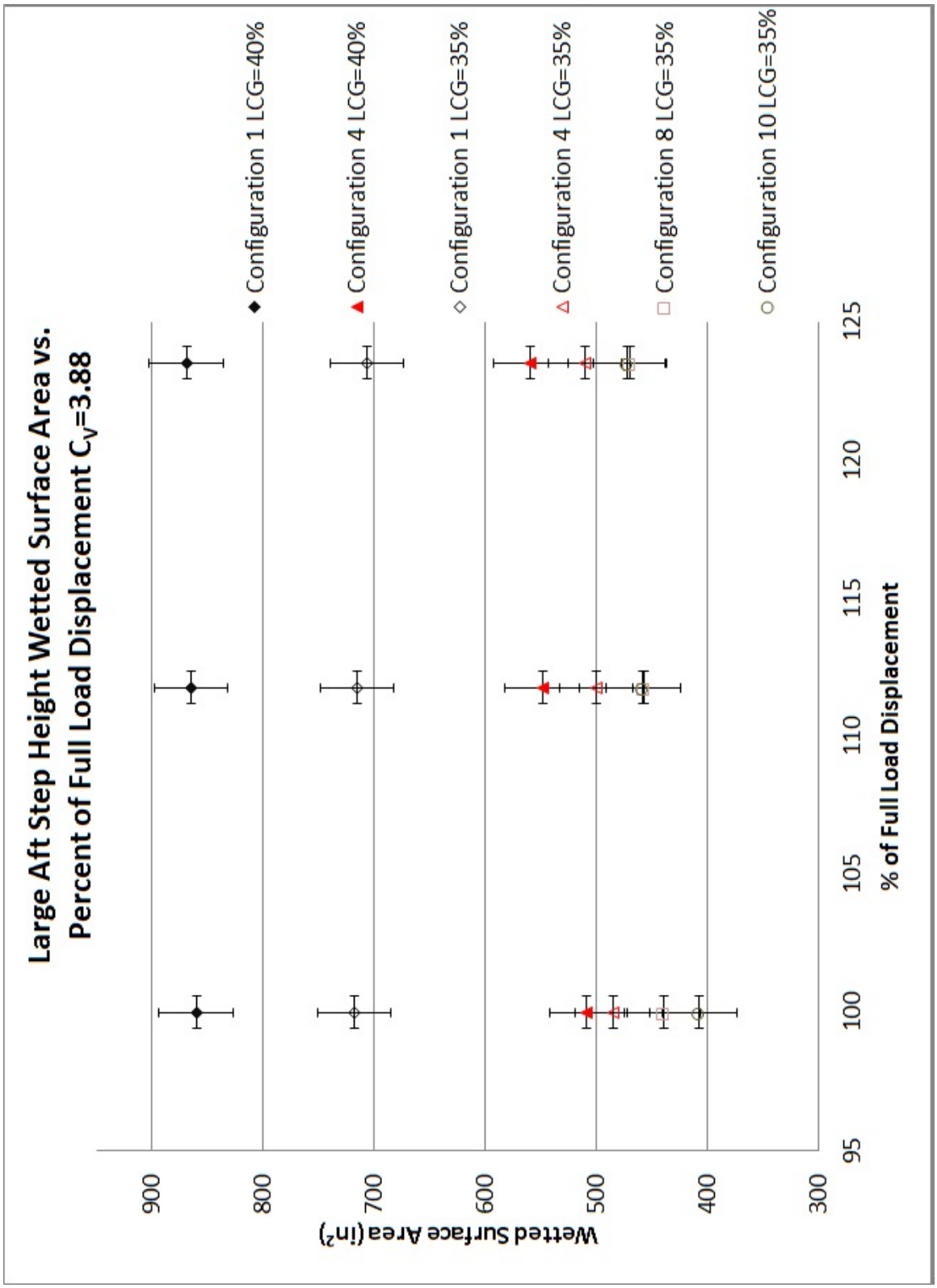

Figure B.64: Large Aft Step Height Wetted Surface Area vs. Percent of Full Load Displacement at C_v=3.88

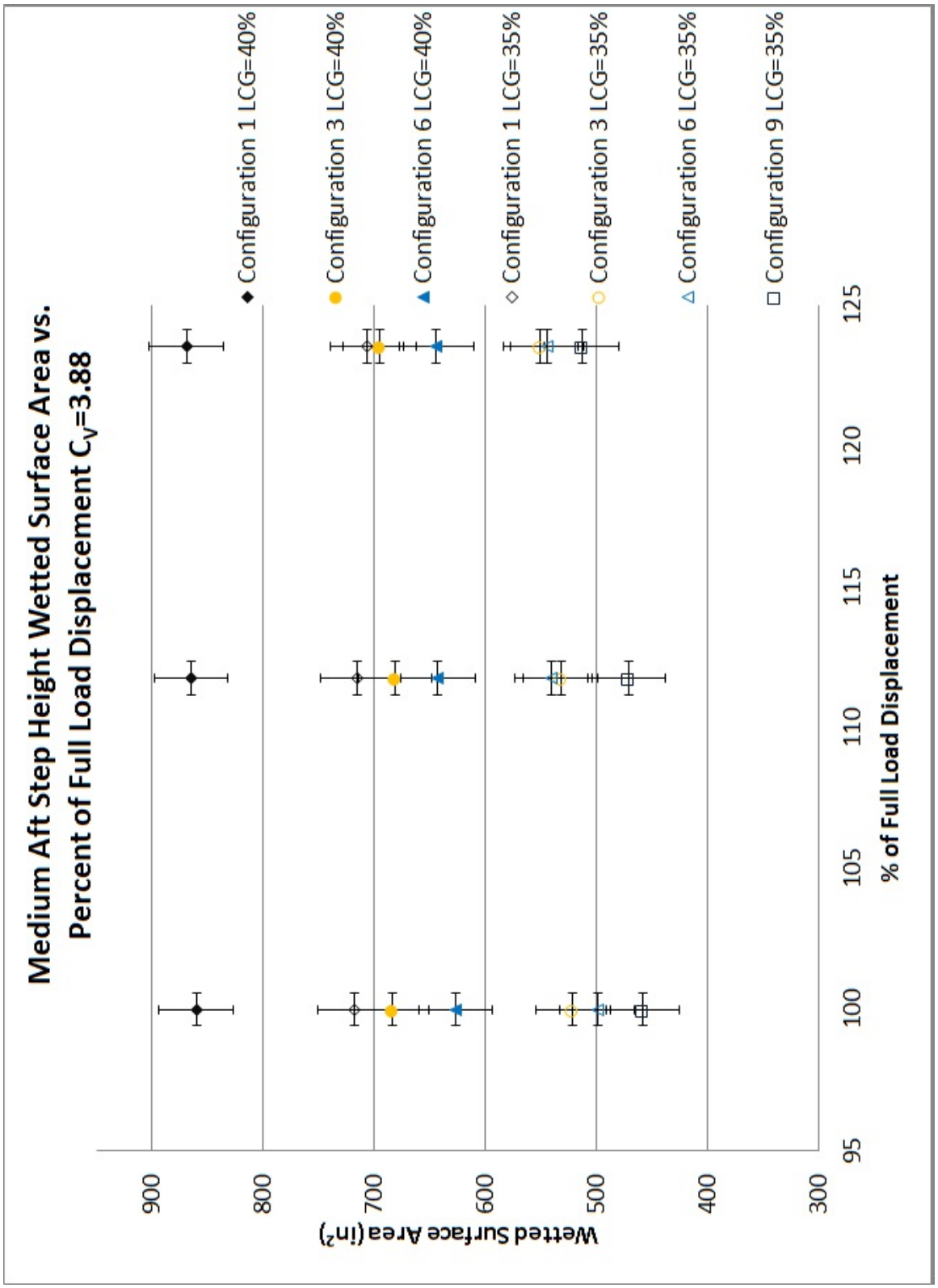

Figure B.65: Medium Aft Step Height Wetted Surface Area vs. Percent of Full Load Displacement at C_v=3.88

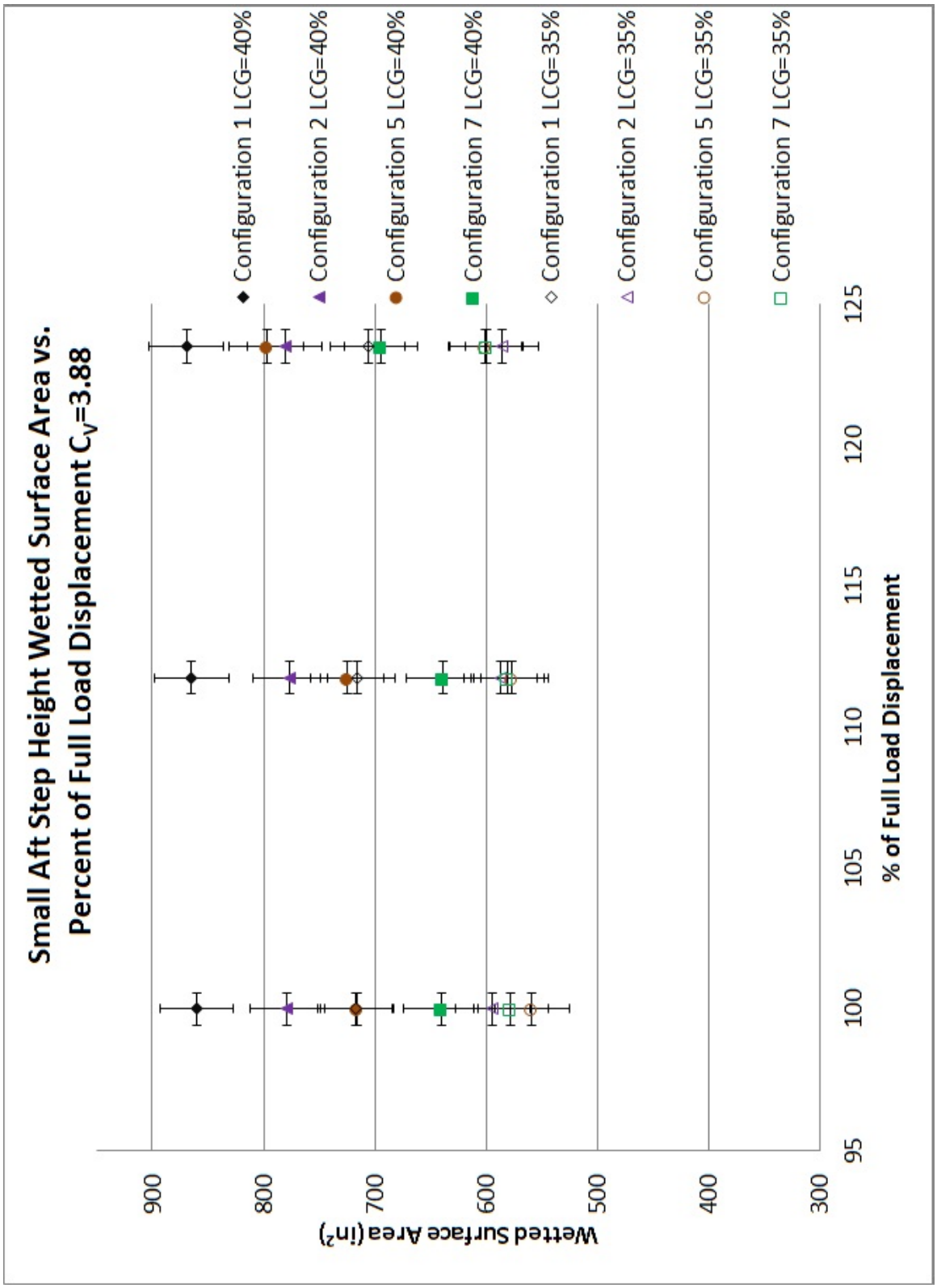

Figure B.66: Small Aft Step Height Wetted Surface Area vs. Percent of Full Load Displacement at C_v=3.88

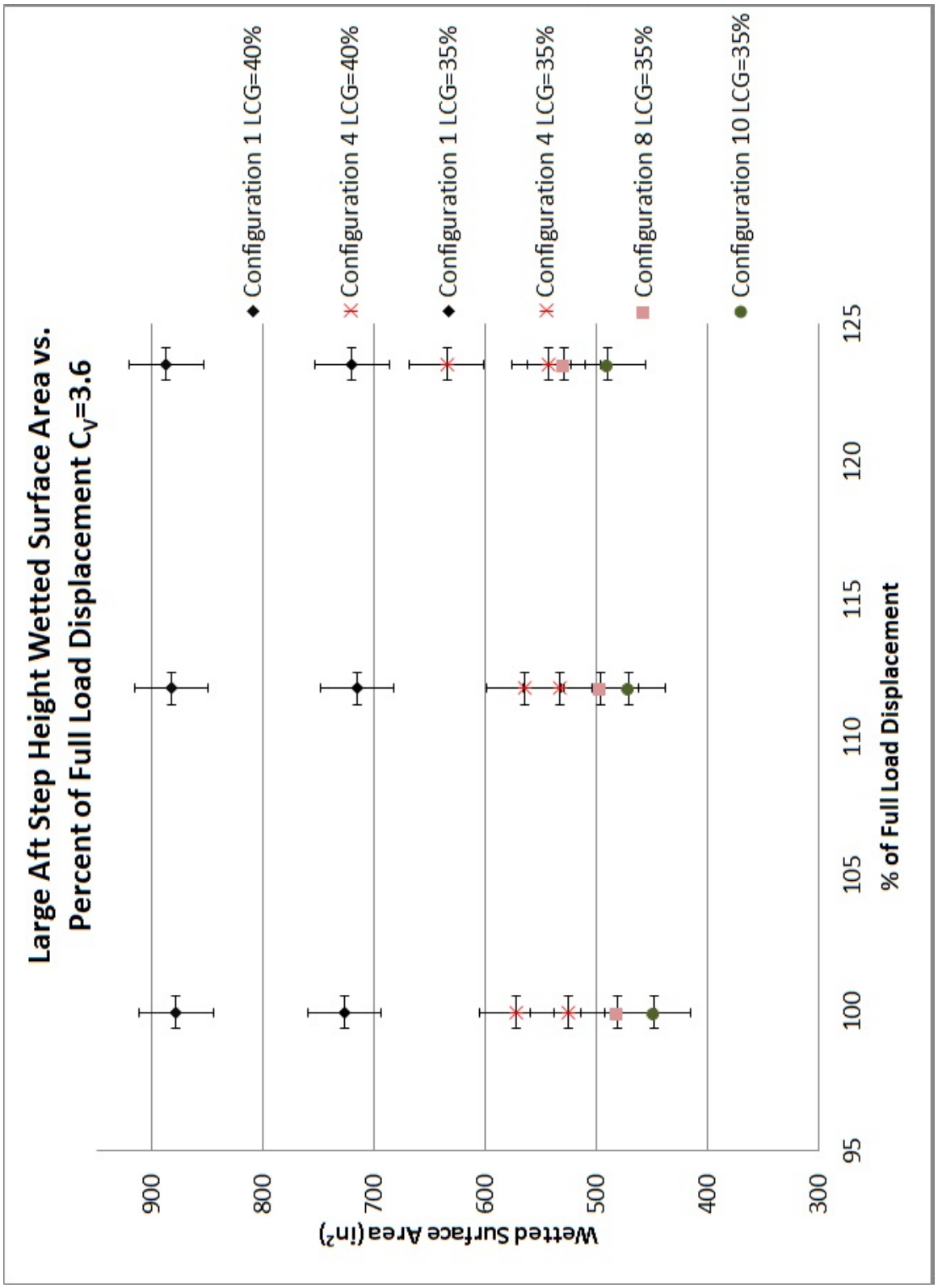

Figure B.67: Large Aft Step Height Wetted Surface Area vs. Percent of Full Load Displacement at C_v=3.60

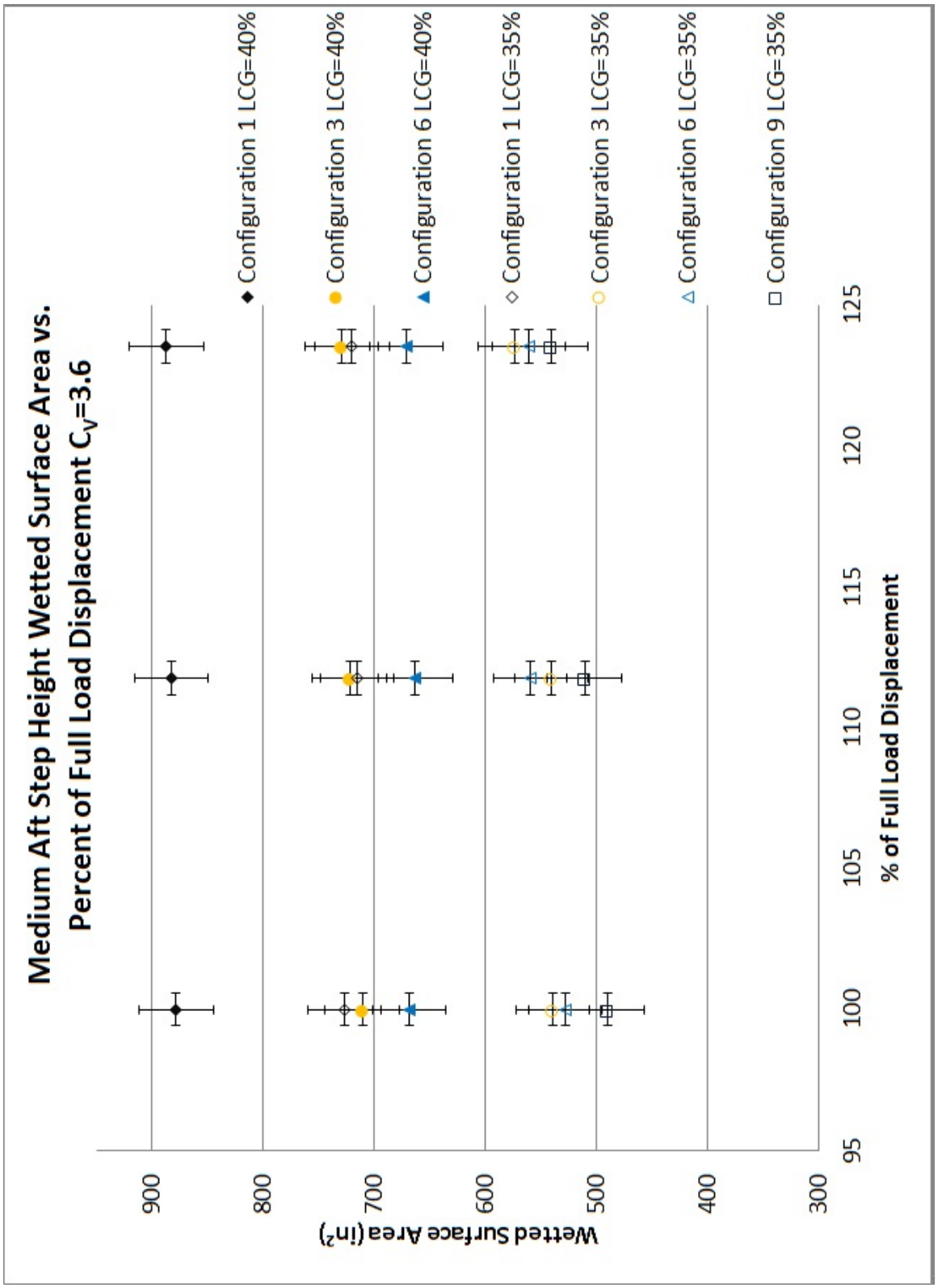

Figure B.68: Medium Aft Step Height Wetted Surface Area vs. Percent of Full Load Displacement at C_v=3.60

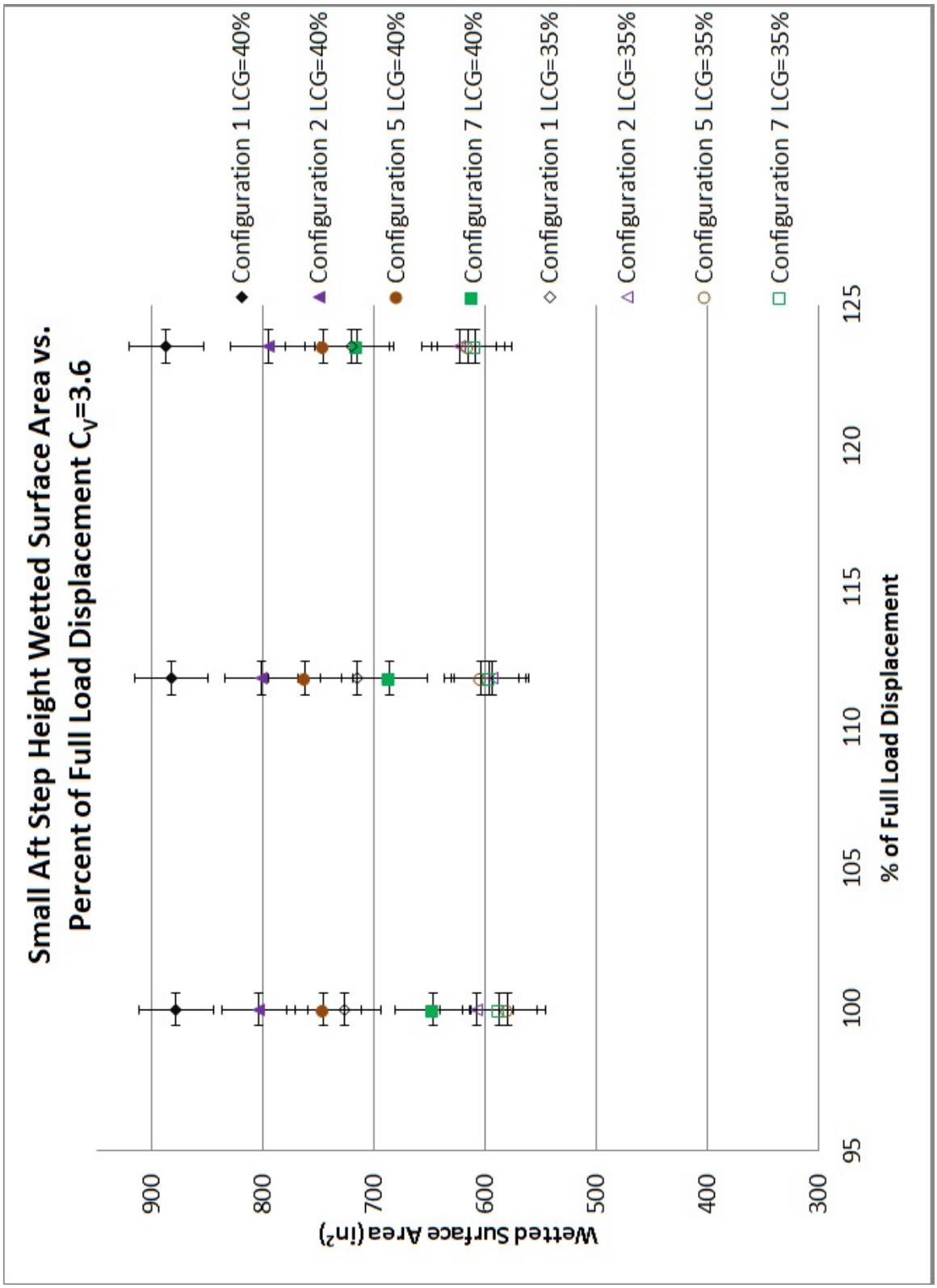

Figure B.69: Small Aft Step Height Wetted Surface Area vs. Percent of Full Load Displacement at C_v=3.60

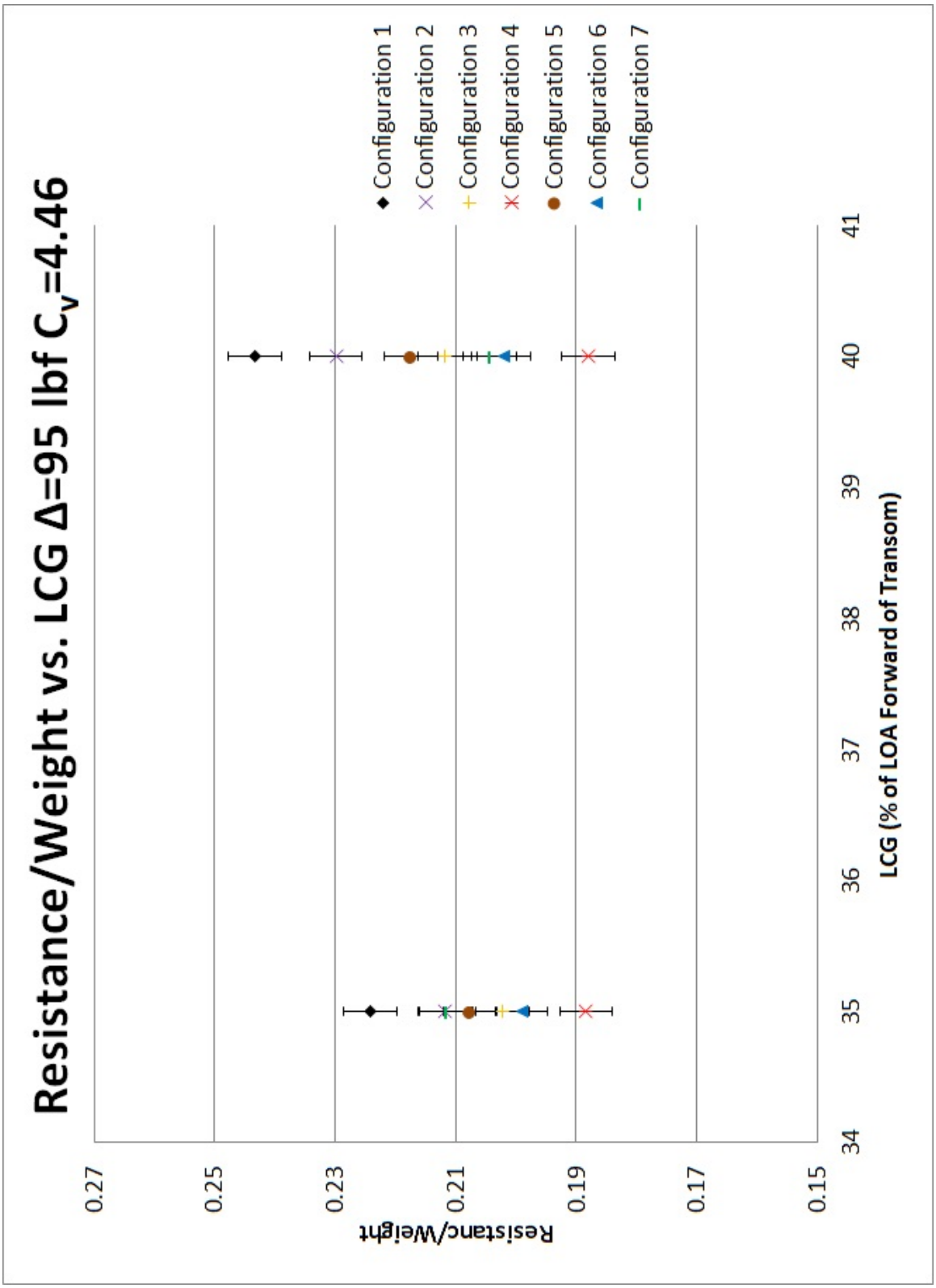

Figure B.70: Resistance/Weight vs. Longitudinal Center of Gravity at Δ=95 C_v=4.46

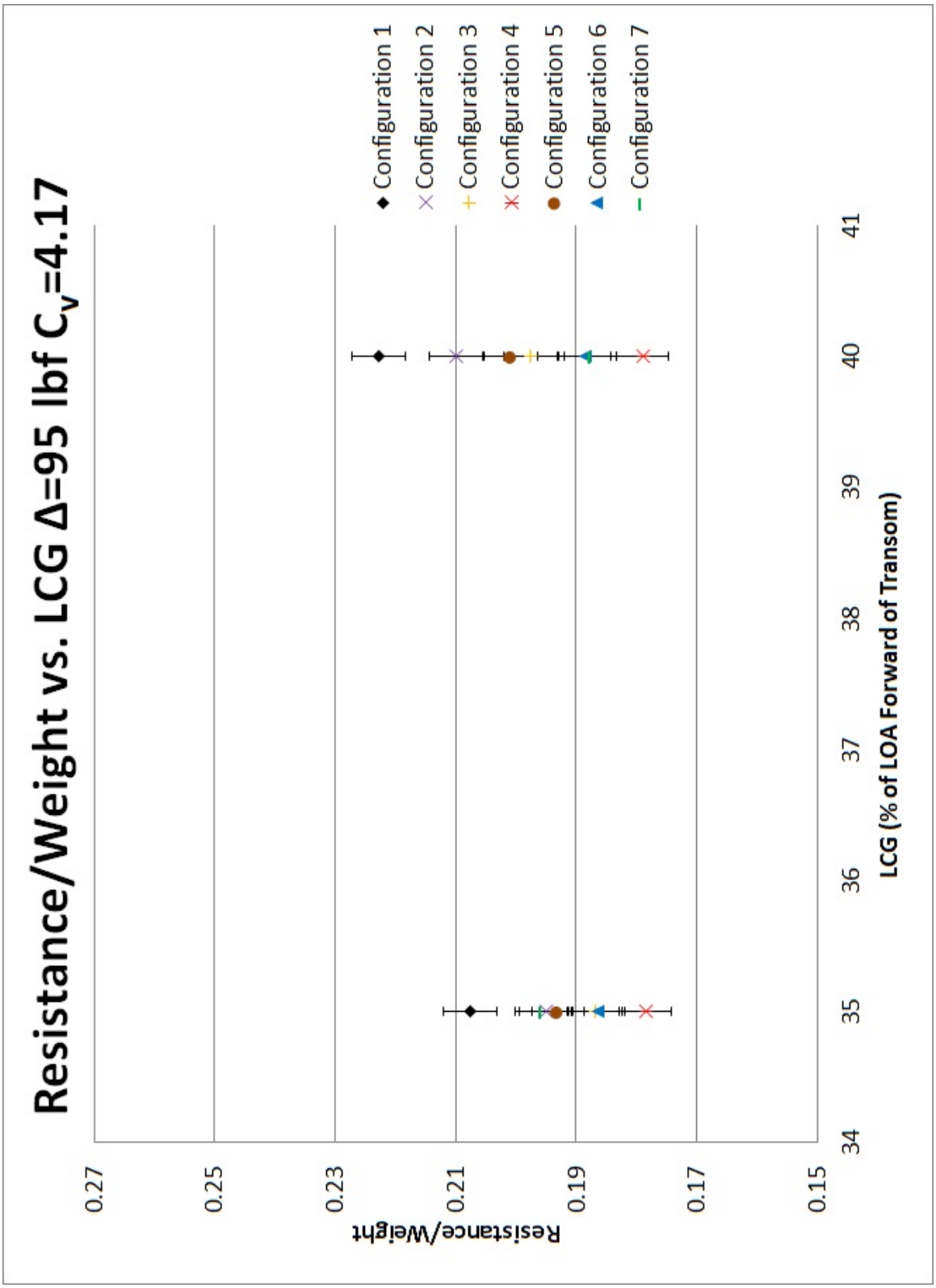

Figure B.71: Resistance/Weight vs. Longitudinal Center of Gravity at Δ=95 C_v=4.17

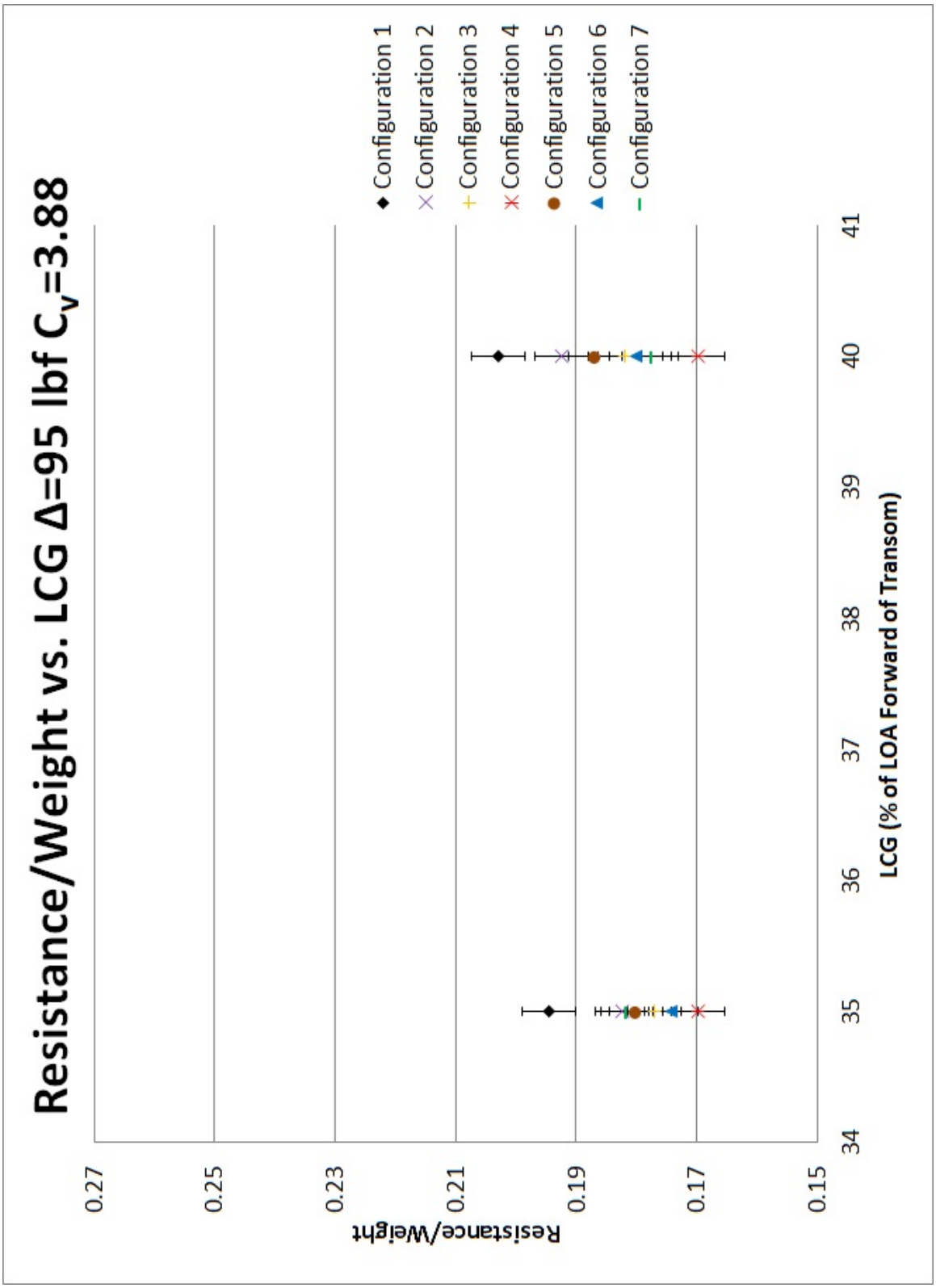

Figure B.72: Resistance/Weight vs. Longitudinal Center of Gravity at Δ=95 C_v=3.88

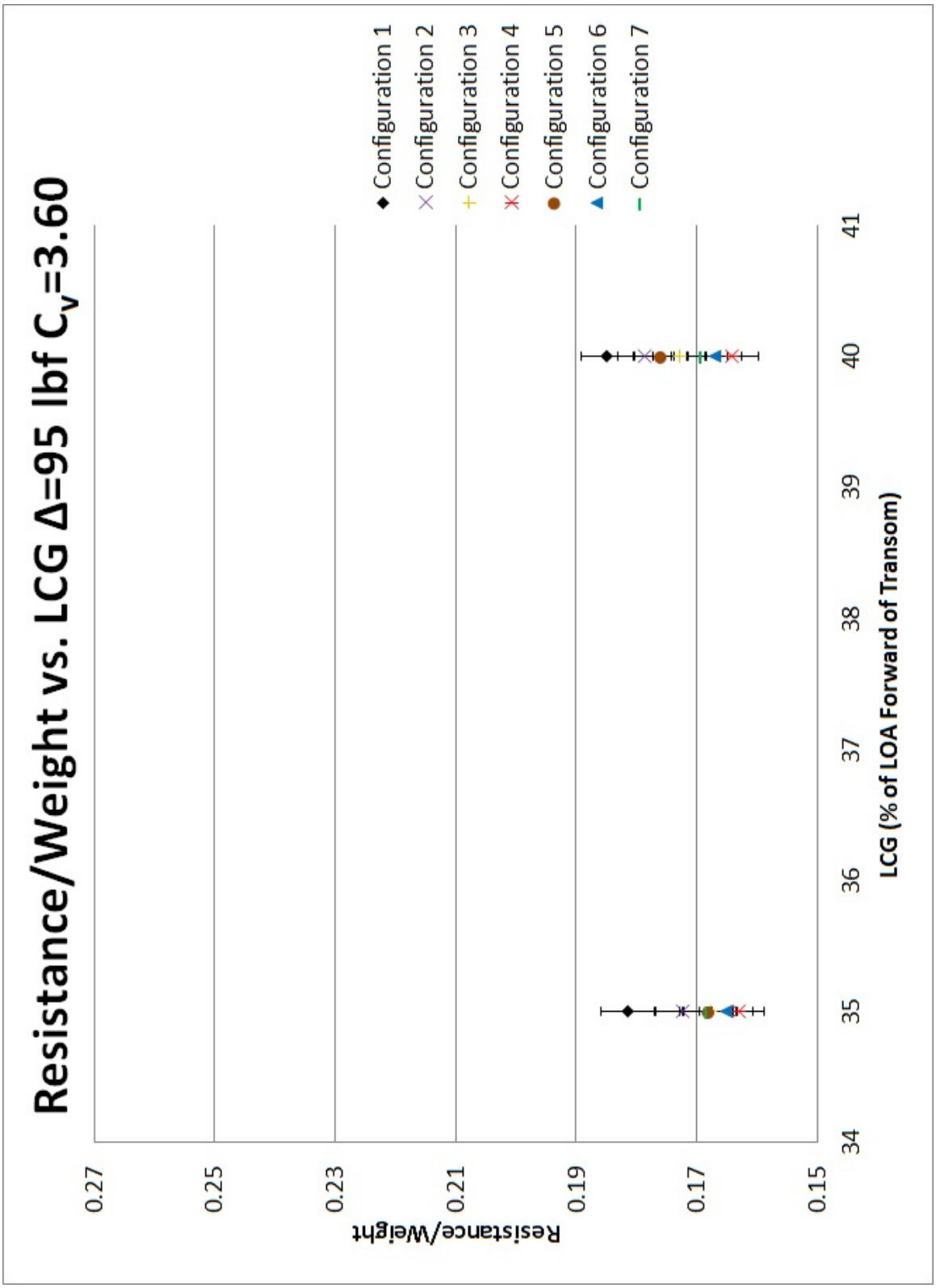

Figure B.73: Resistance/Weight vs. Longitudinal Center of Gravity at Δ=95 C_v=3.60

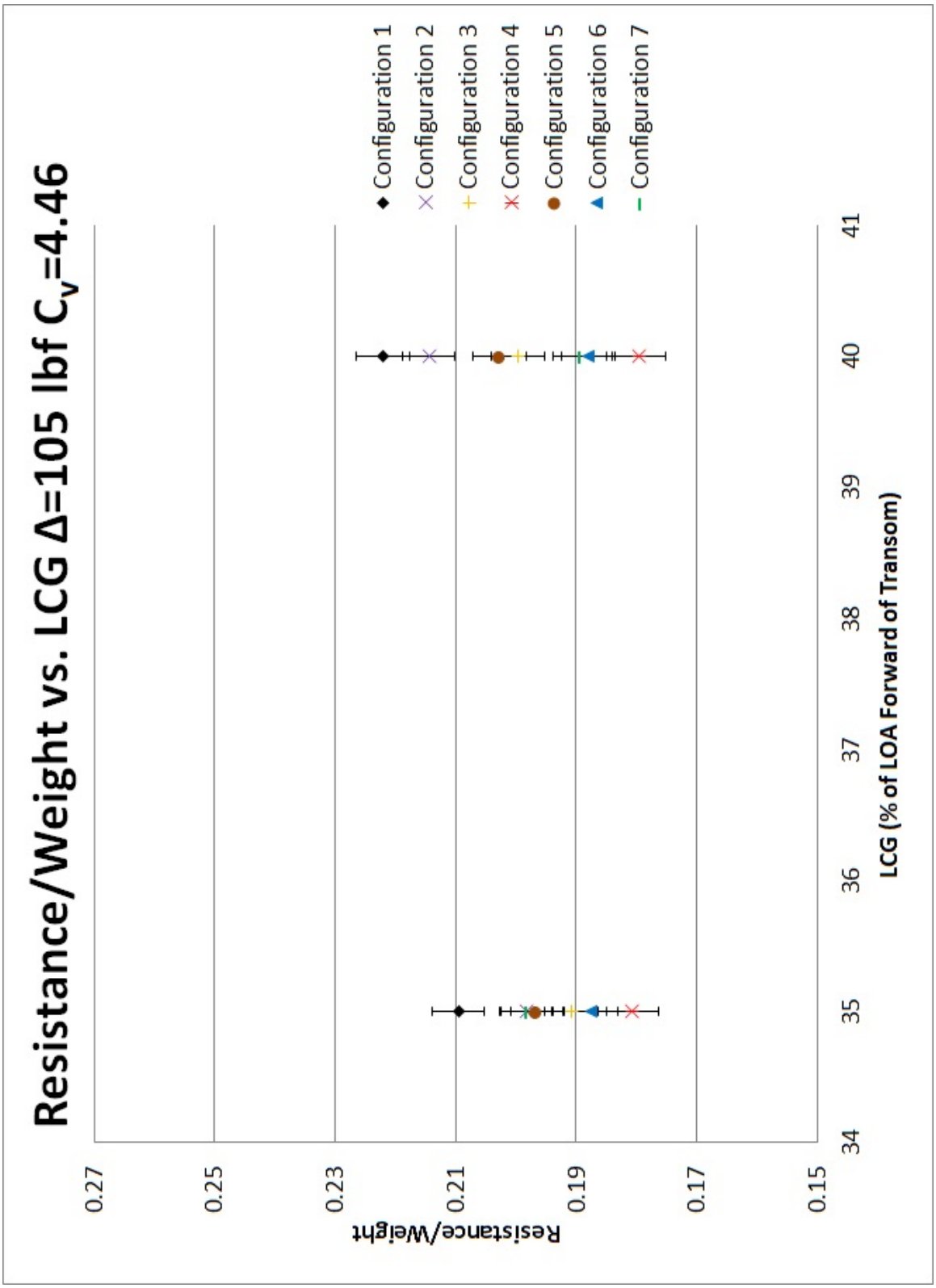

Figure B.74: Resistance/Weight vs. Longitudinal Center of Gravity at Δ=105 C_v=4.46

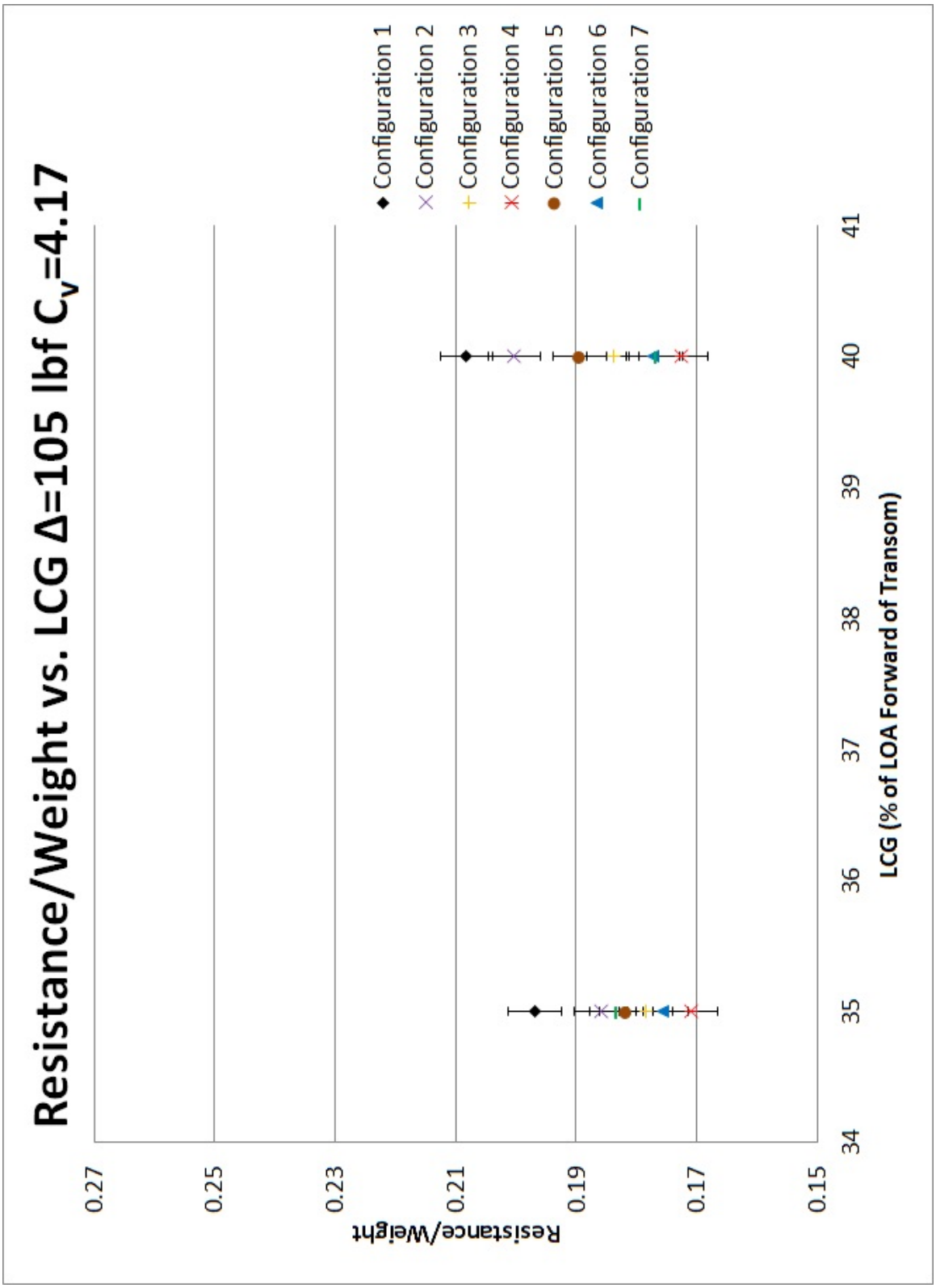

Figure B.75: Resistance/Weight vs. Longitudinal Center of Gravity at Δ=105 C_v=4.17

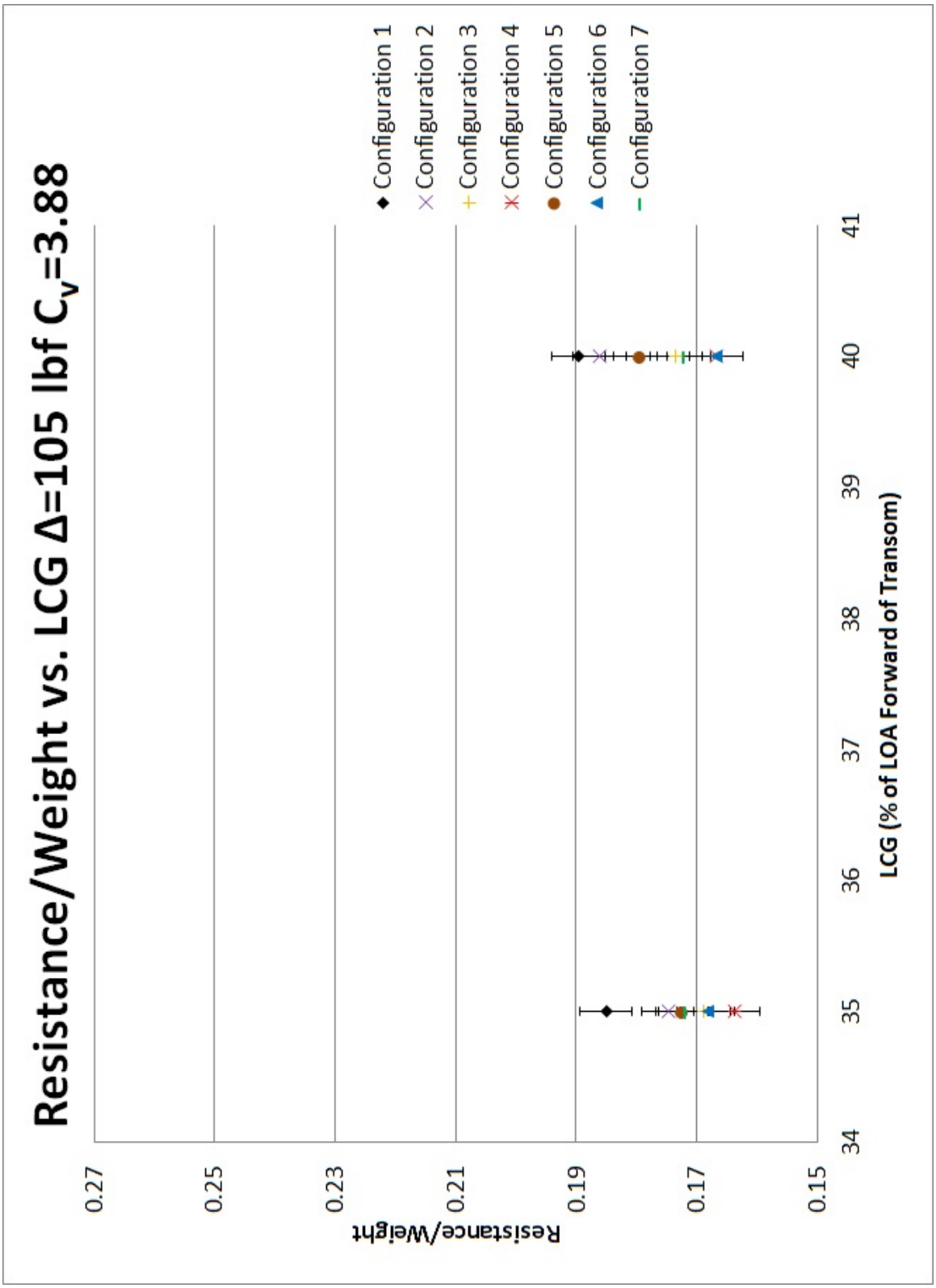

Figure B.76: Resistance/Weight vs. Longitudinal Center of Gravity at Δ=105 C_v=3.88

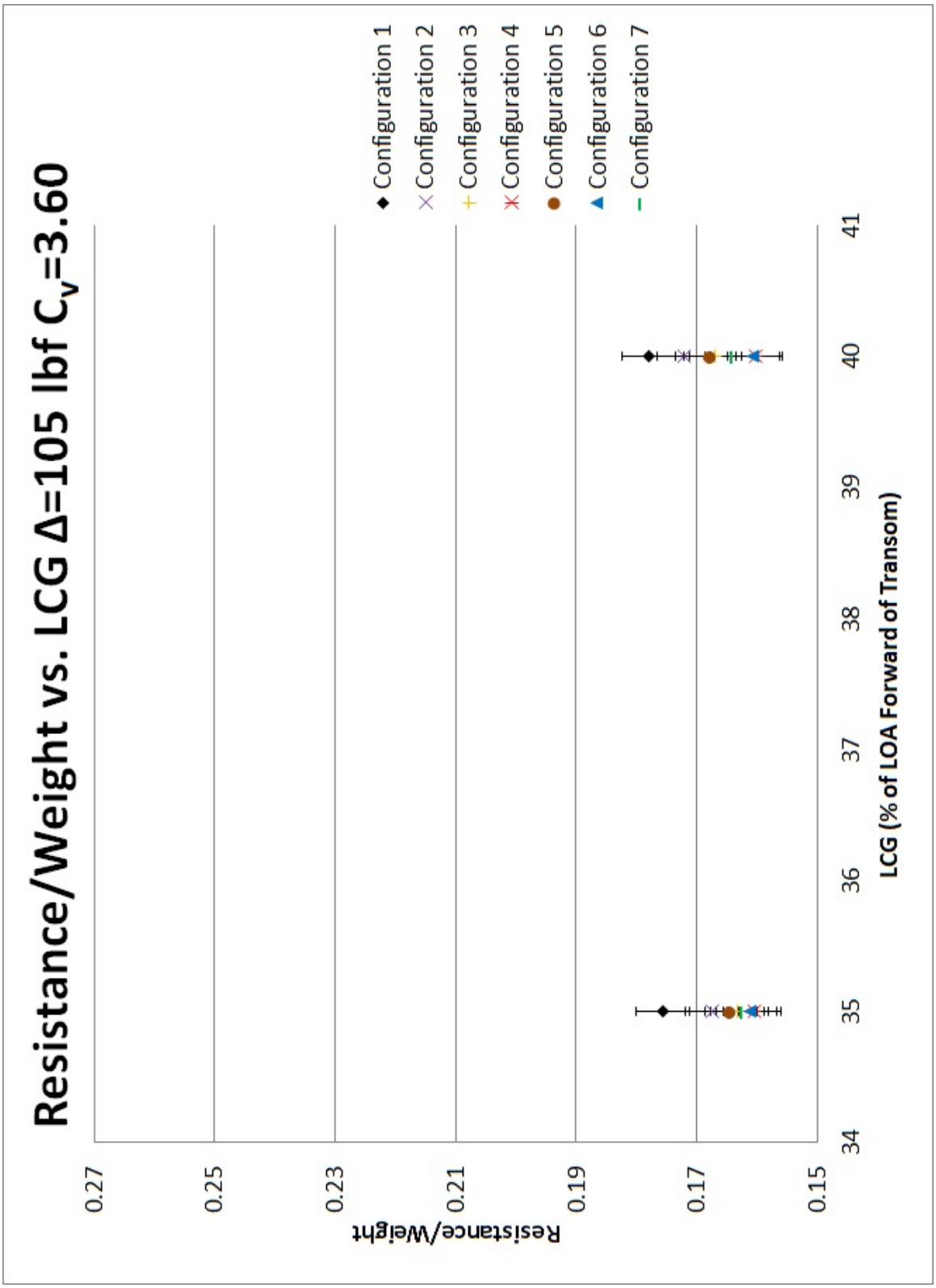

Figure B.77: Resistance/Weight vs. Longitudinal Center of Gravity at Δ=105 C_v=3.60

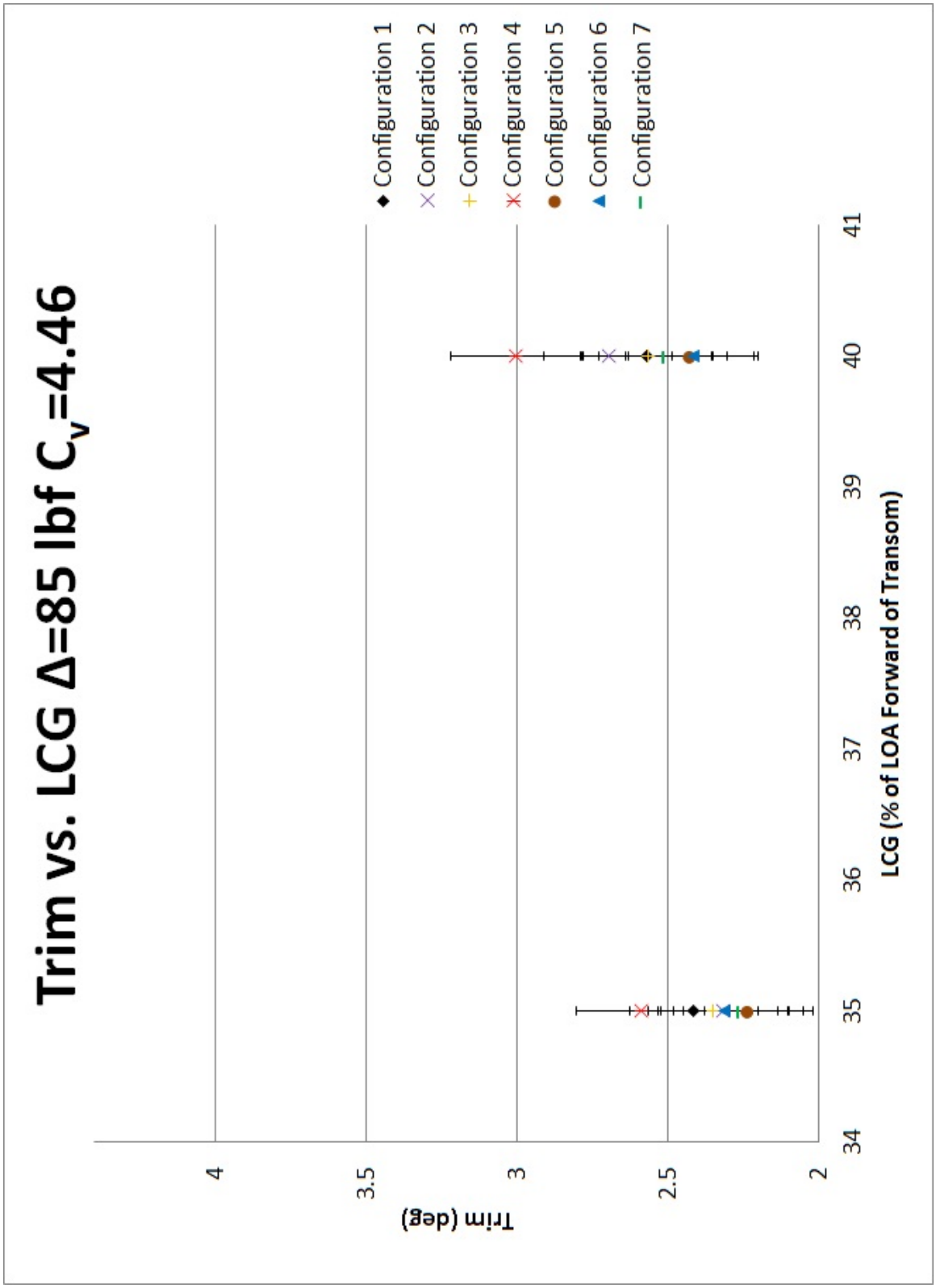

Figure B.78: Trim vs. Longitudinal Center of Gravity at Δ=85 C_v=4.46

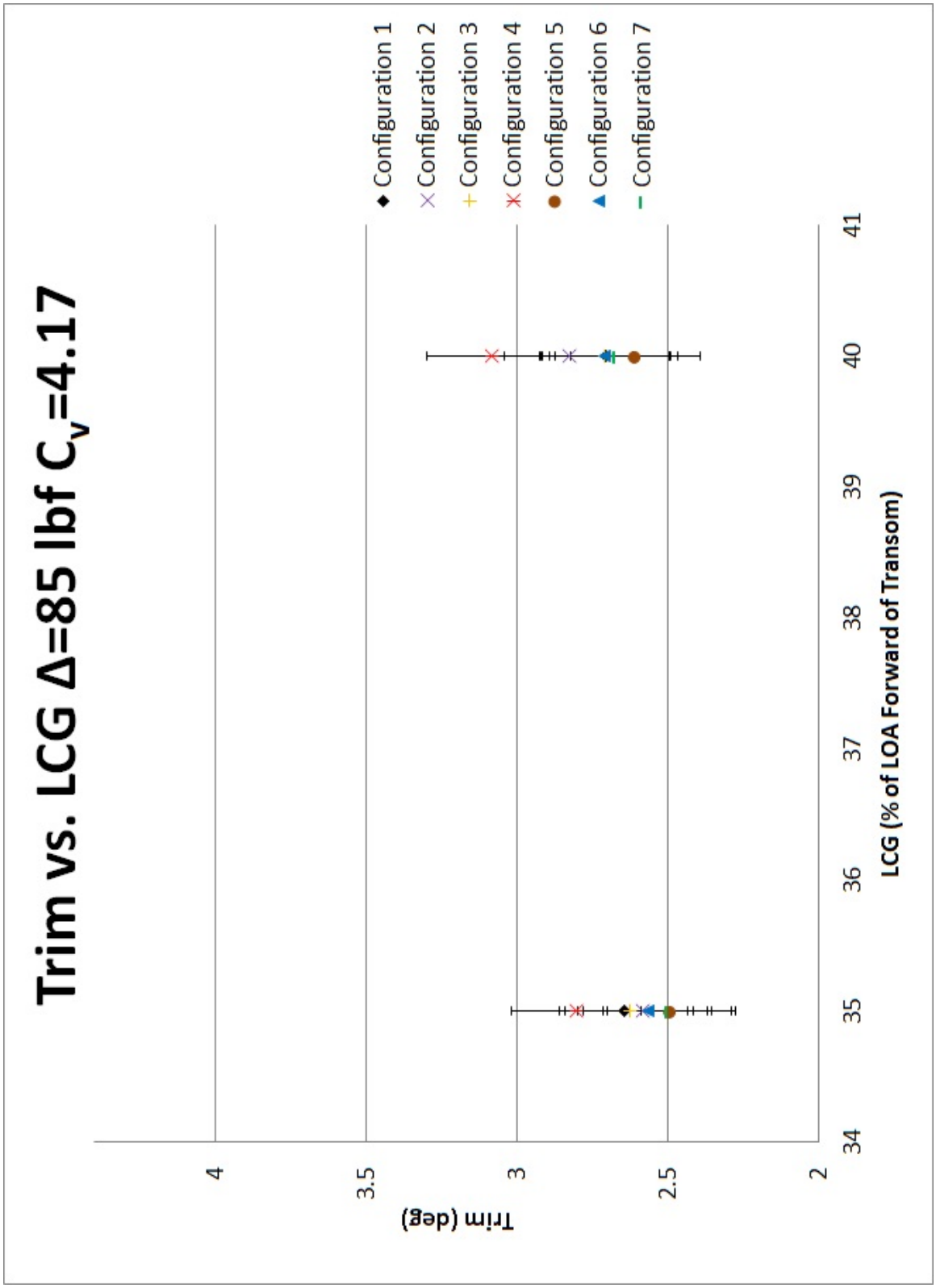

Figure B.79: Trim vs. Longitudinal Center of Gravity at Δ=85 C_v=4.17

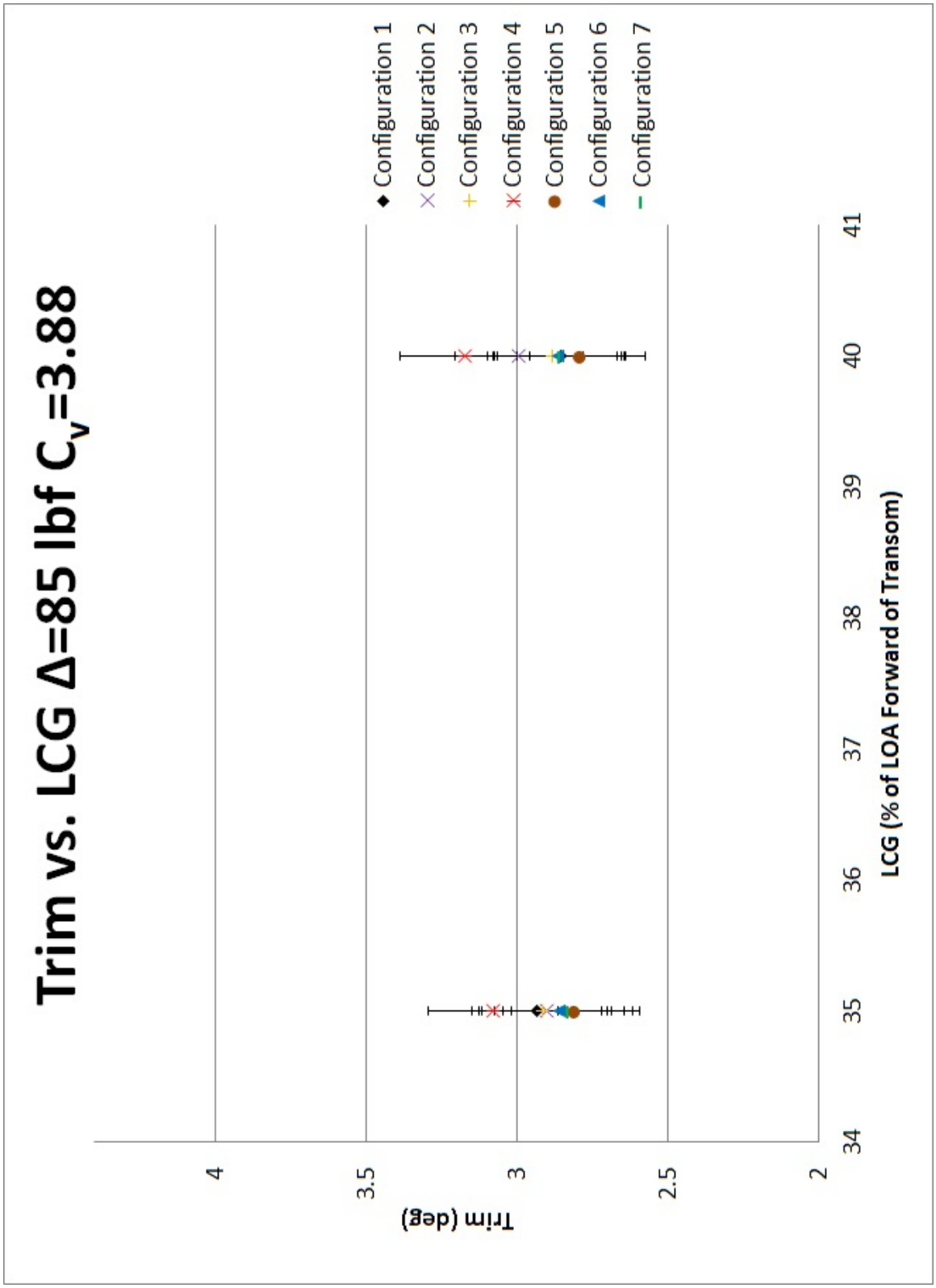

Figure B.80: Trim vs. Longitudinal Center of Gravity at Δ=85 C_v=3.88

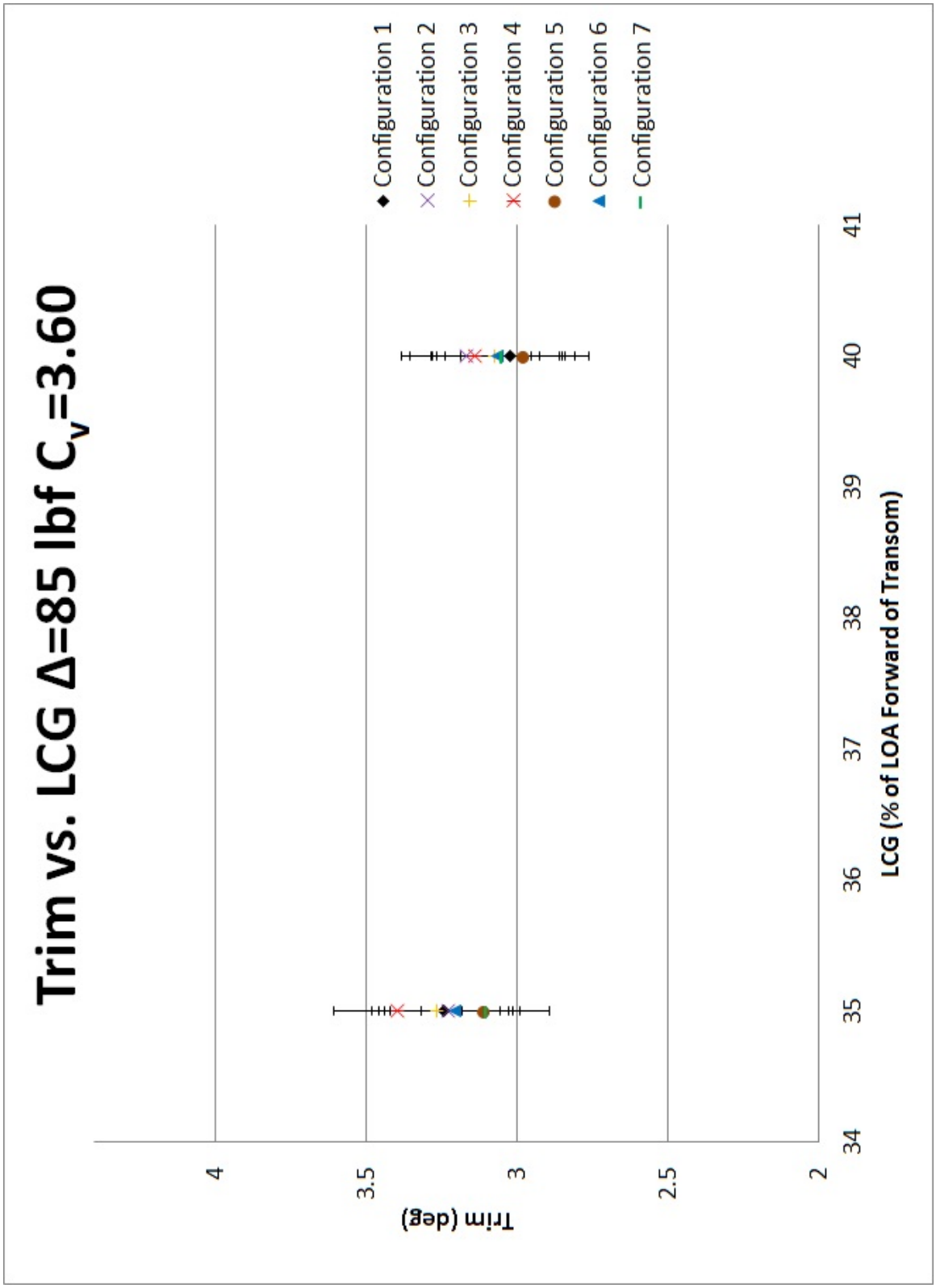

Figure B.81: Trim vs. Longitudinal Center of Gravity at Δ=85 C_v=3.60

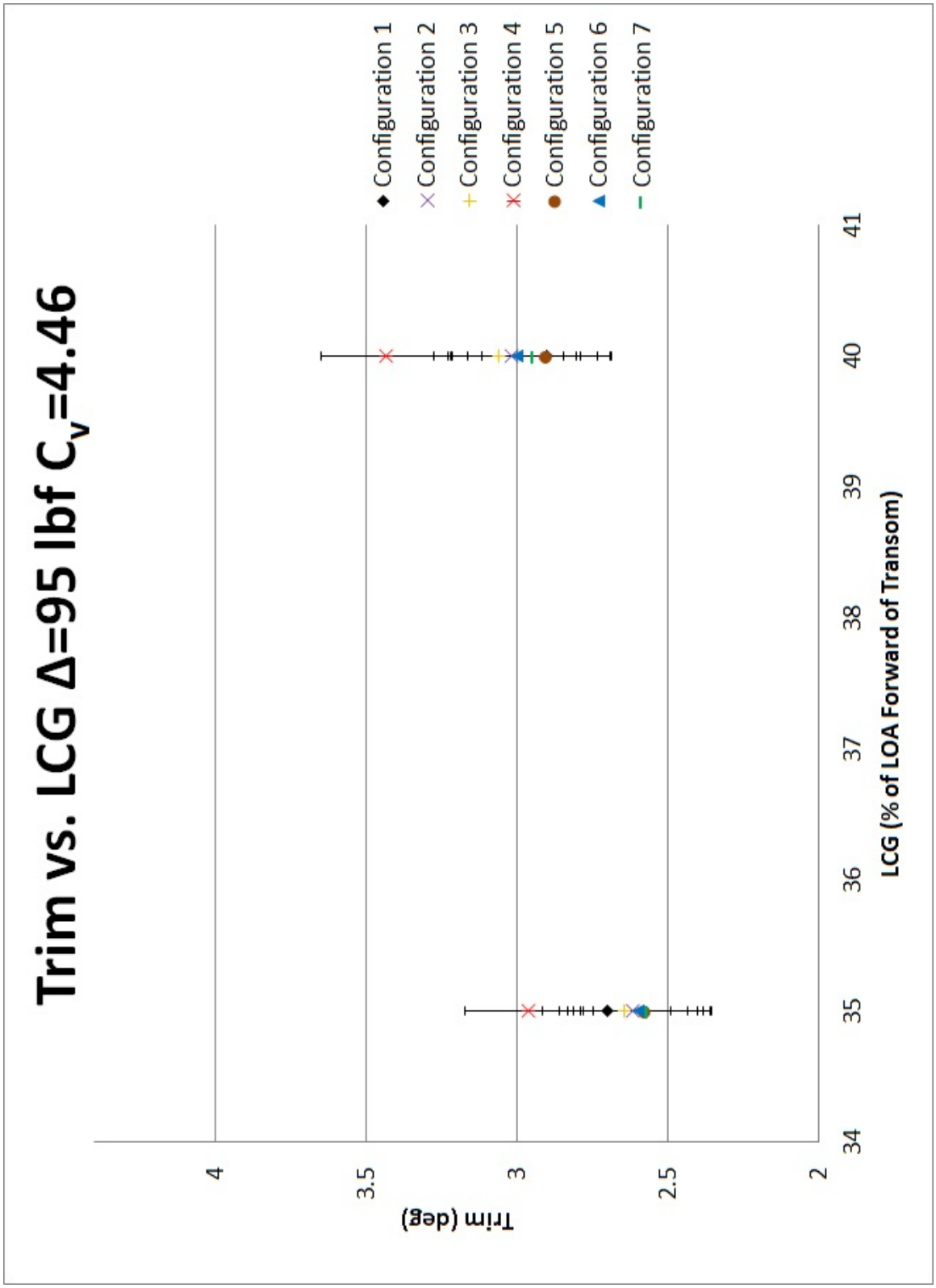

Figure B.82: Trim vs. Longitudinal Center of Gravity at Δ=95 C_v=4.46

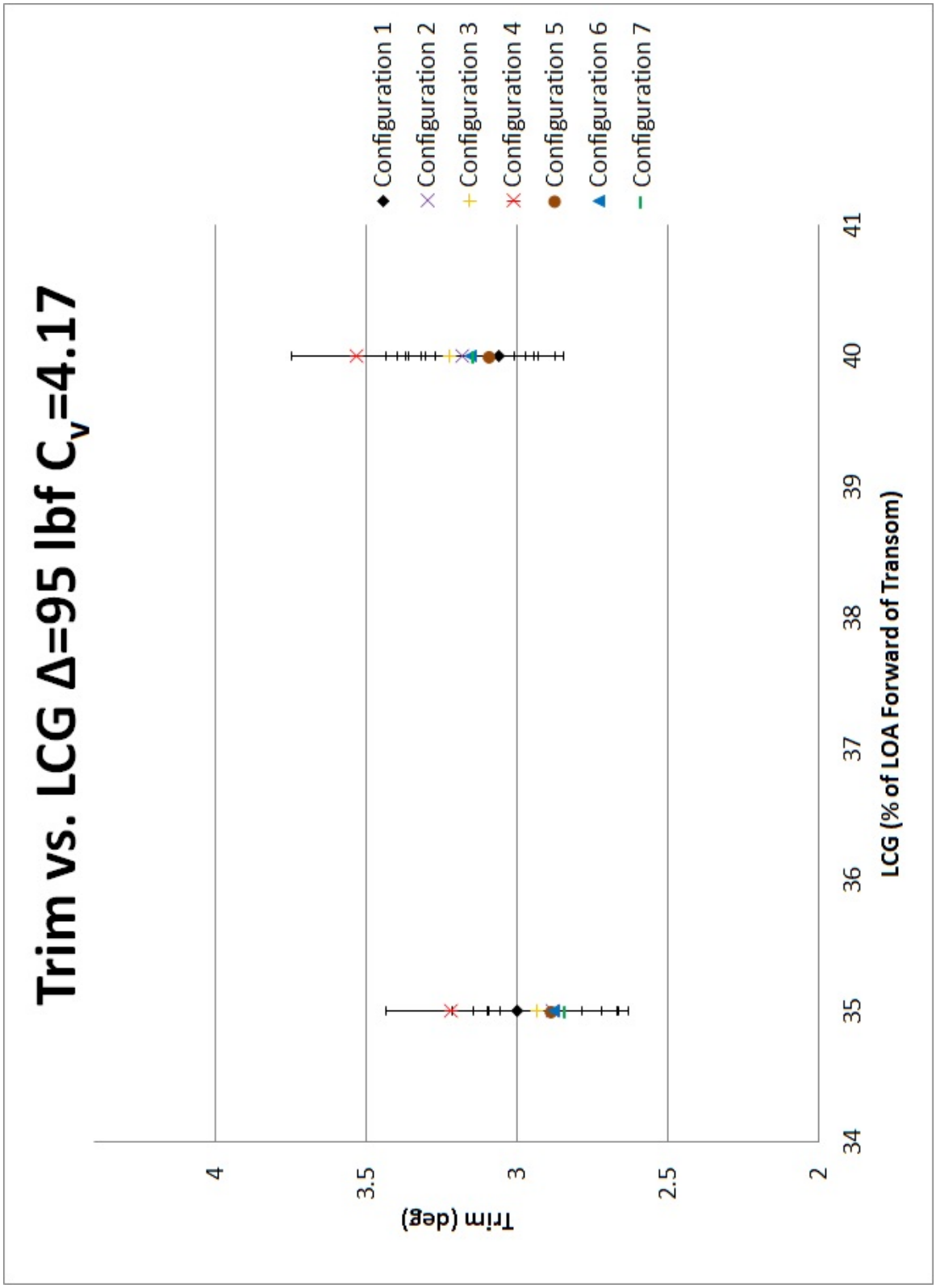

Figure B.83: Trim vs. Longitudinal Center of Gravity at Δ=95 C_v=4.17

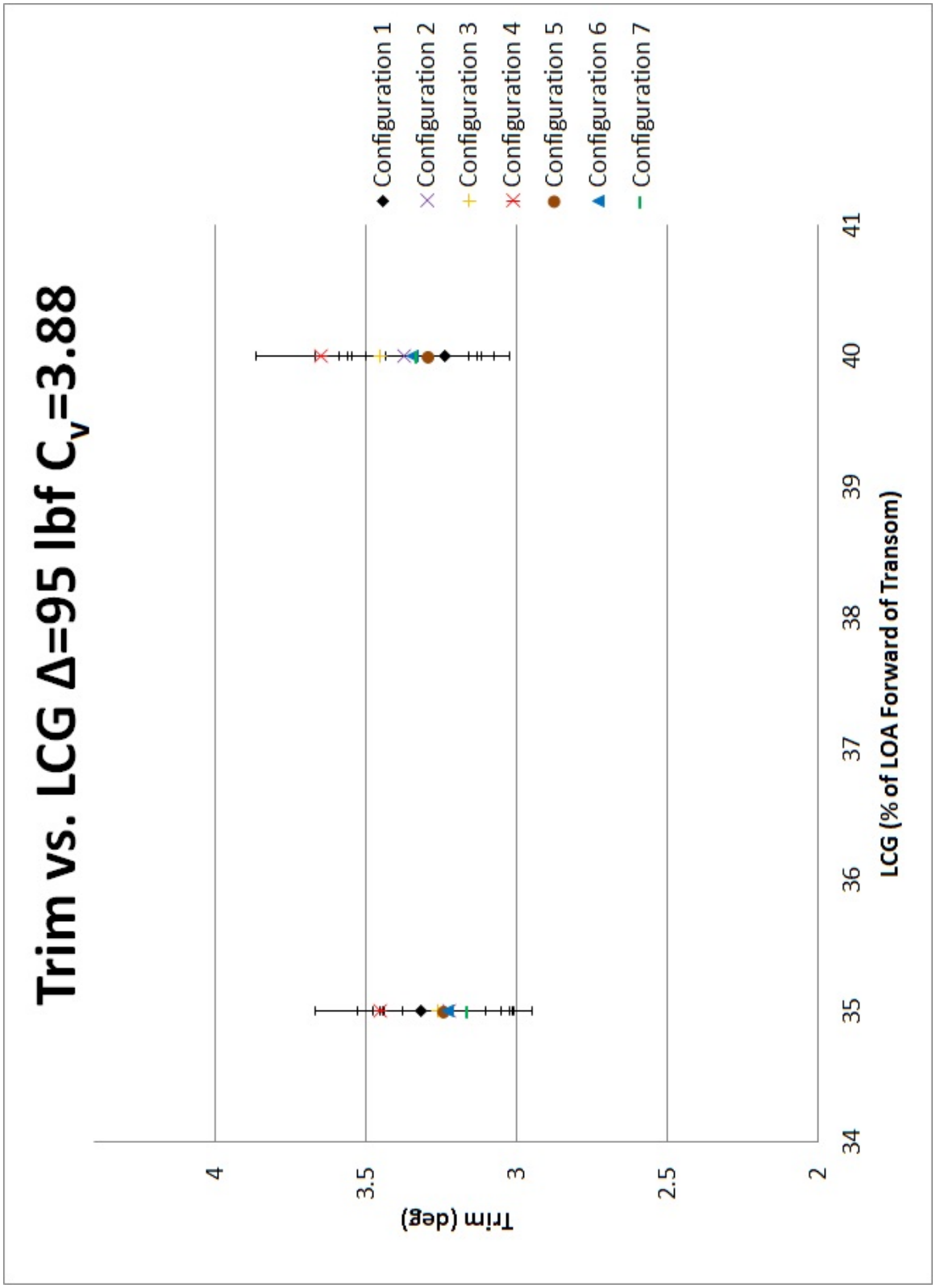

Figure B.84: Trim vs. Longitudinal Center of Gravity at Δ=95 C_v=3.88

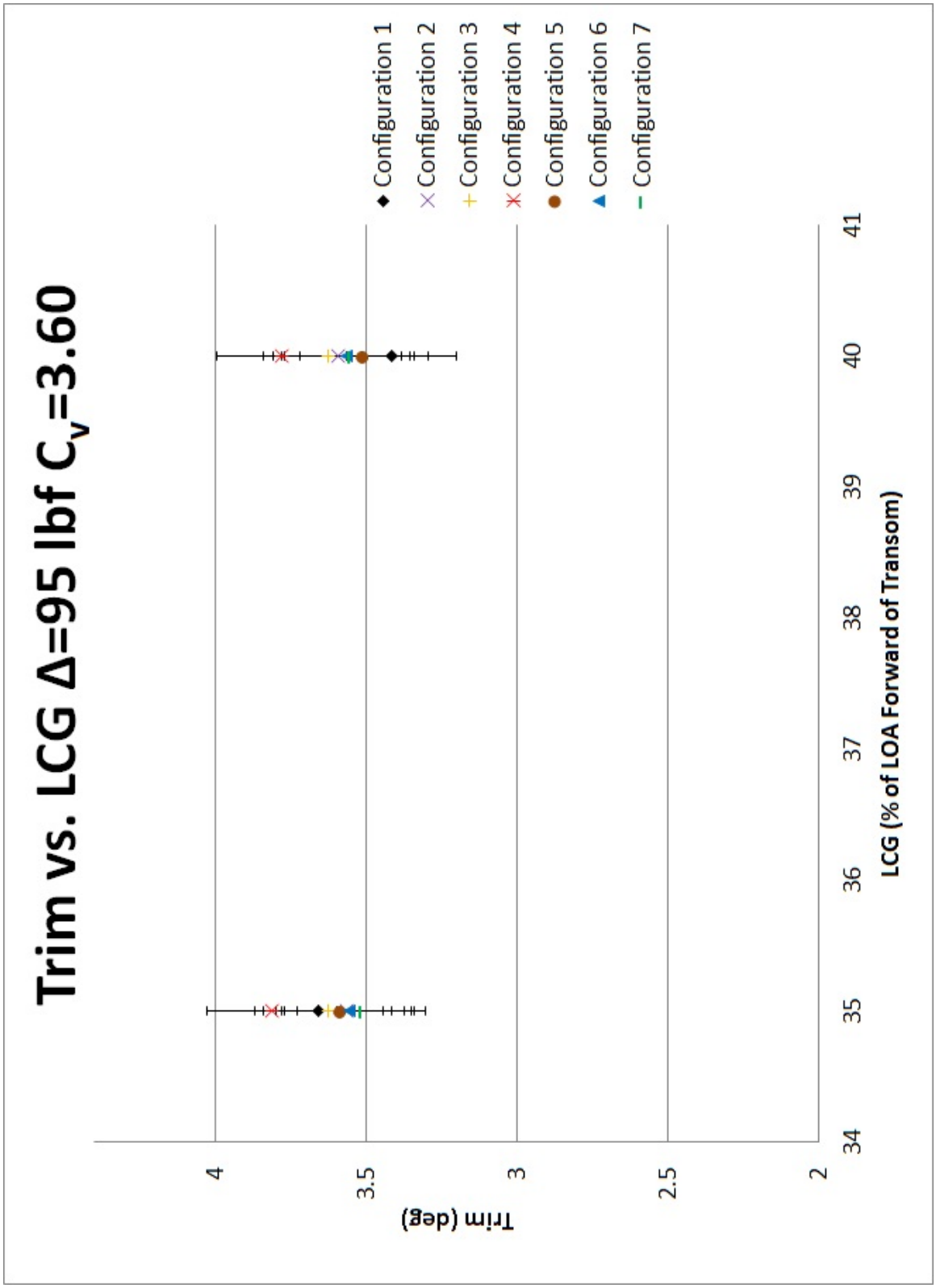

Figure B.85: Trim vs. Longitudinal Center of Gravity at Δ=95 C_v=3.60

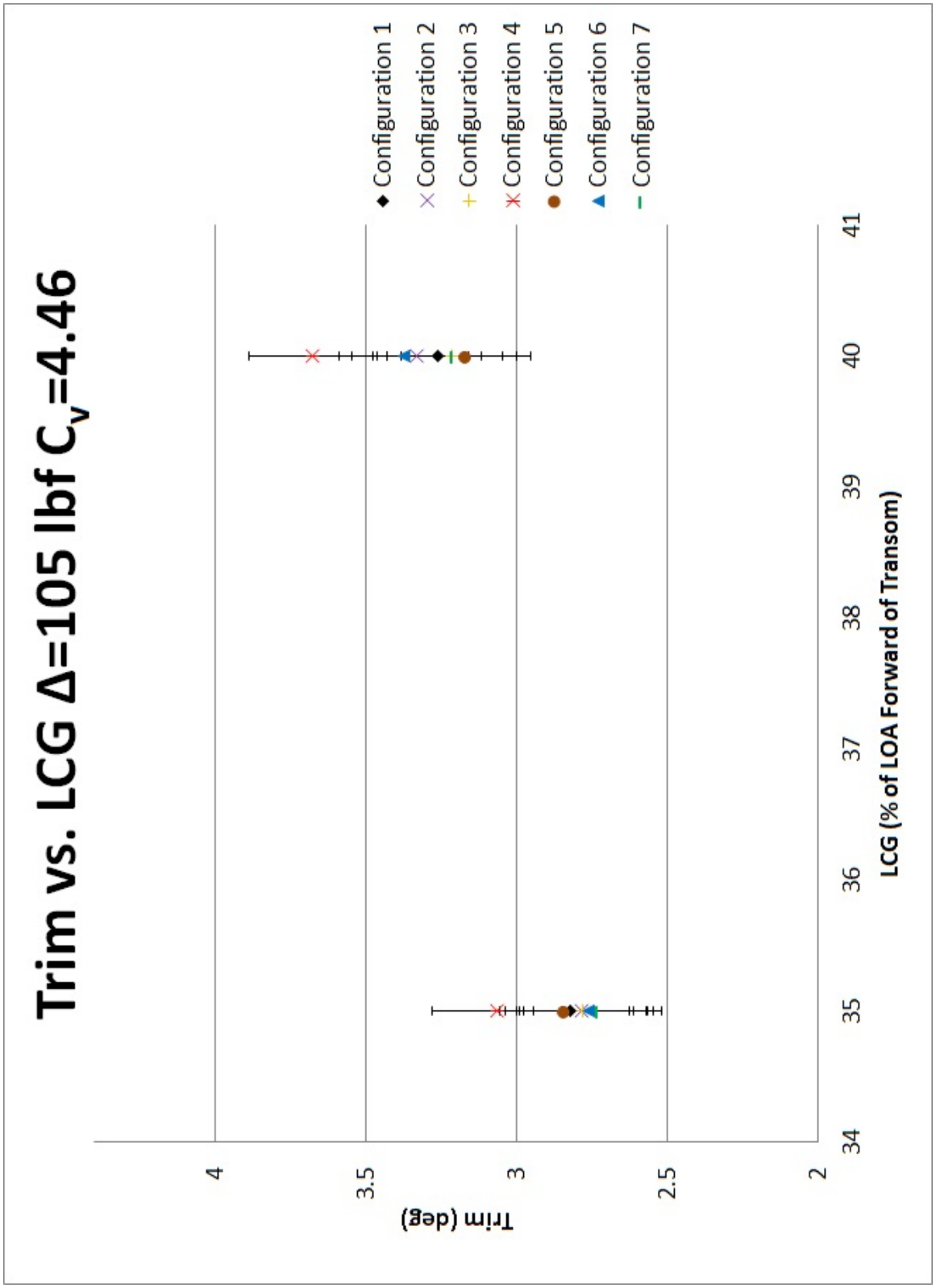

Figure B.86: Trim vs. Longitudinal Center of Gravity at Δ=105 C_v=4.46

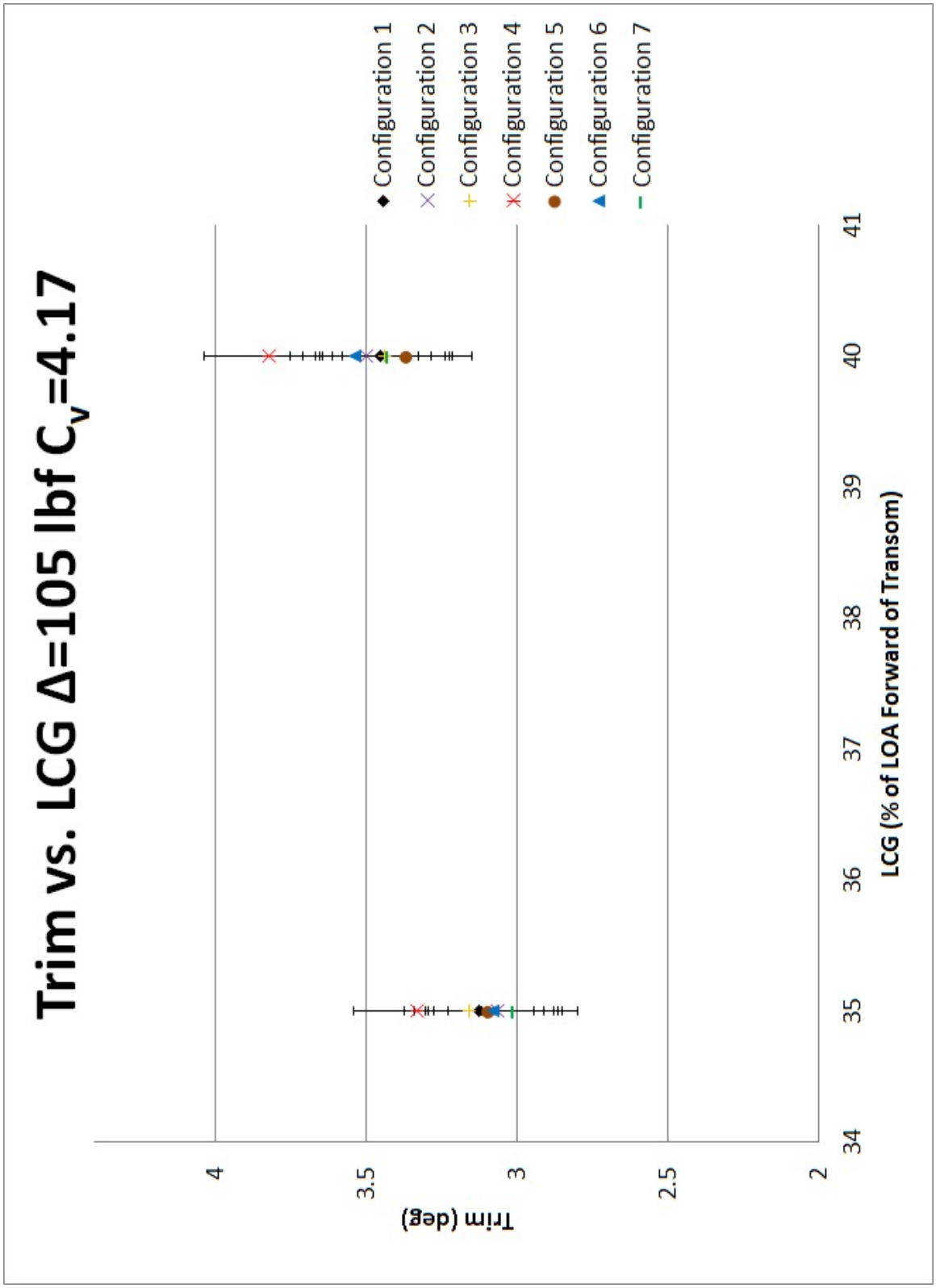

Figure B.87: Trim vs. Longitudinal Center of Gravity at Δ=105 C_v=4.17

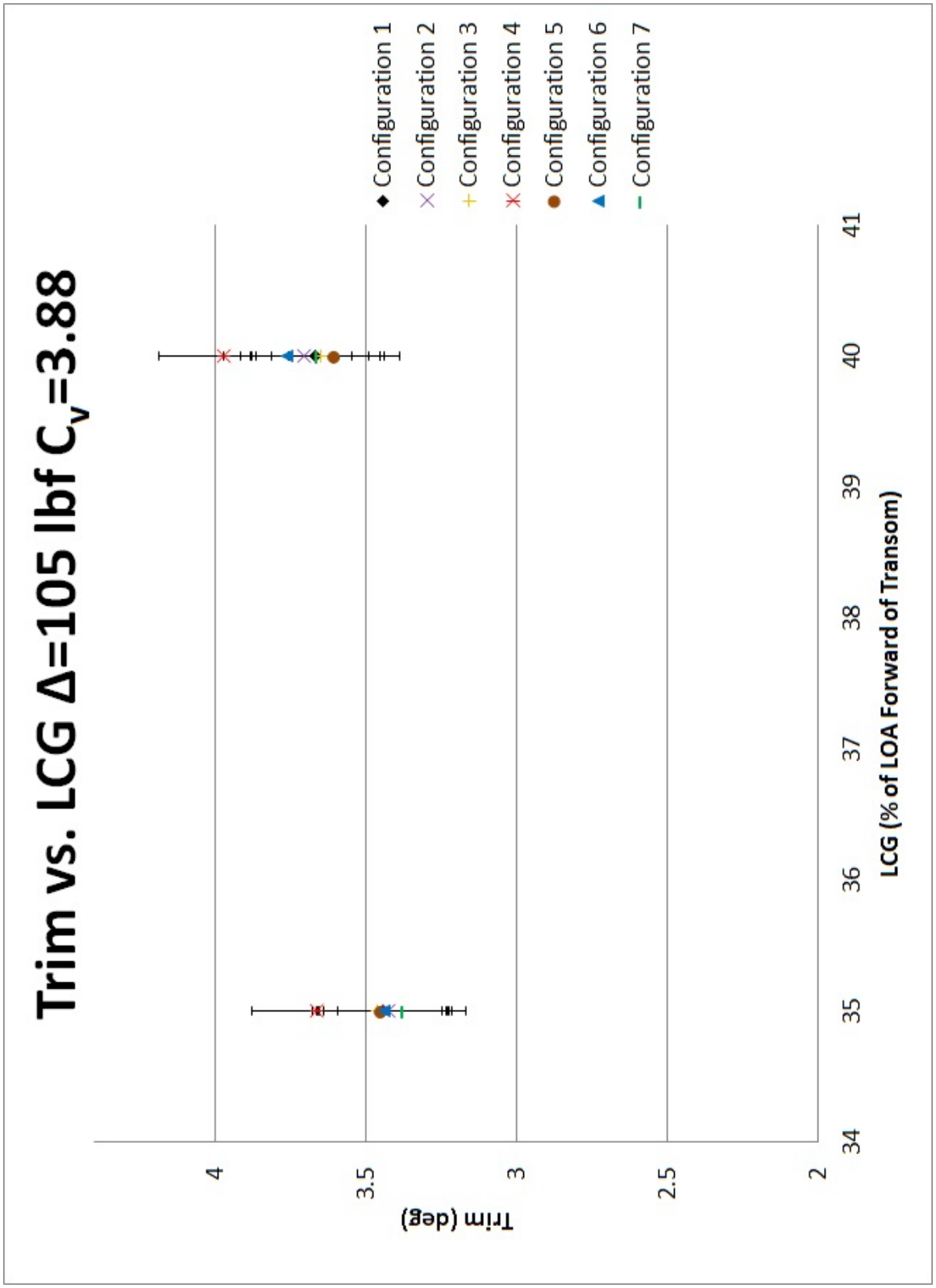

Figure B.88: Trim vs. Longitudinal Center of Gravity at Δ=105 C_v=3.88

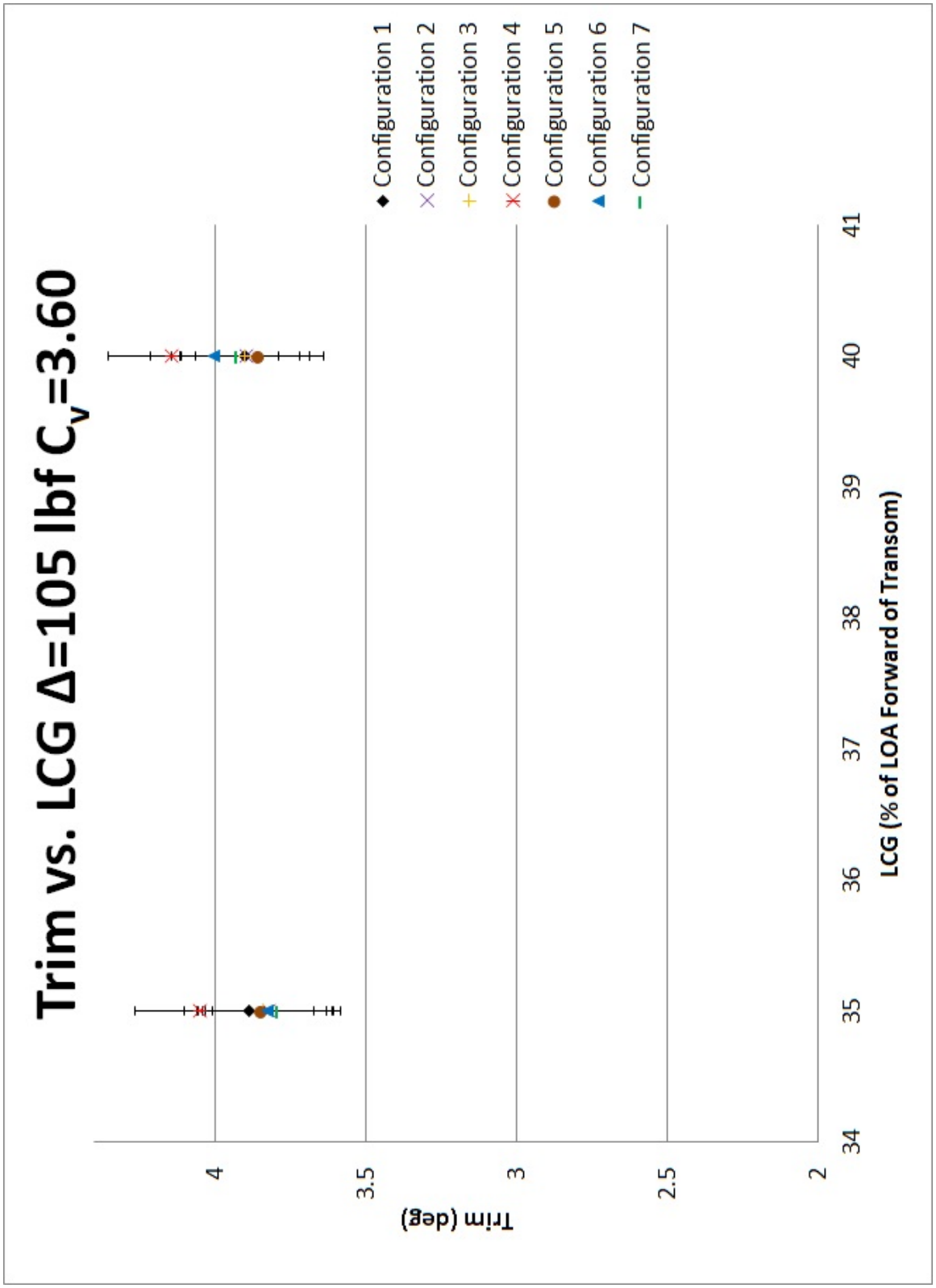

Figure B.89: Trim vs. Longitudinal Center of Gravity at Δ=105 C_v=3.60

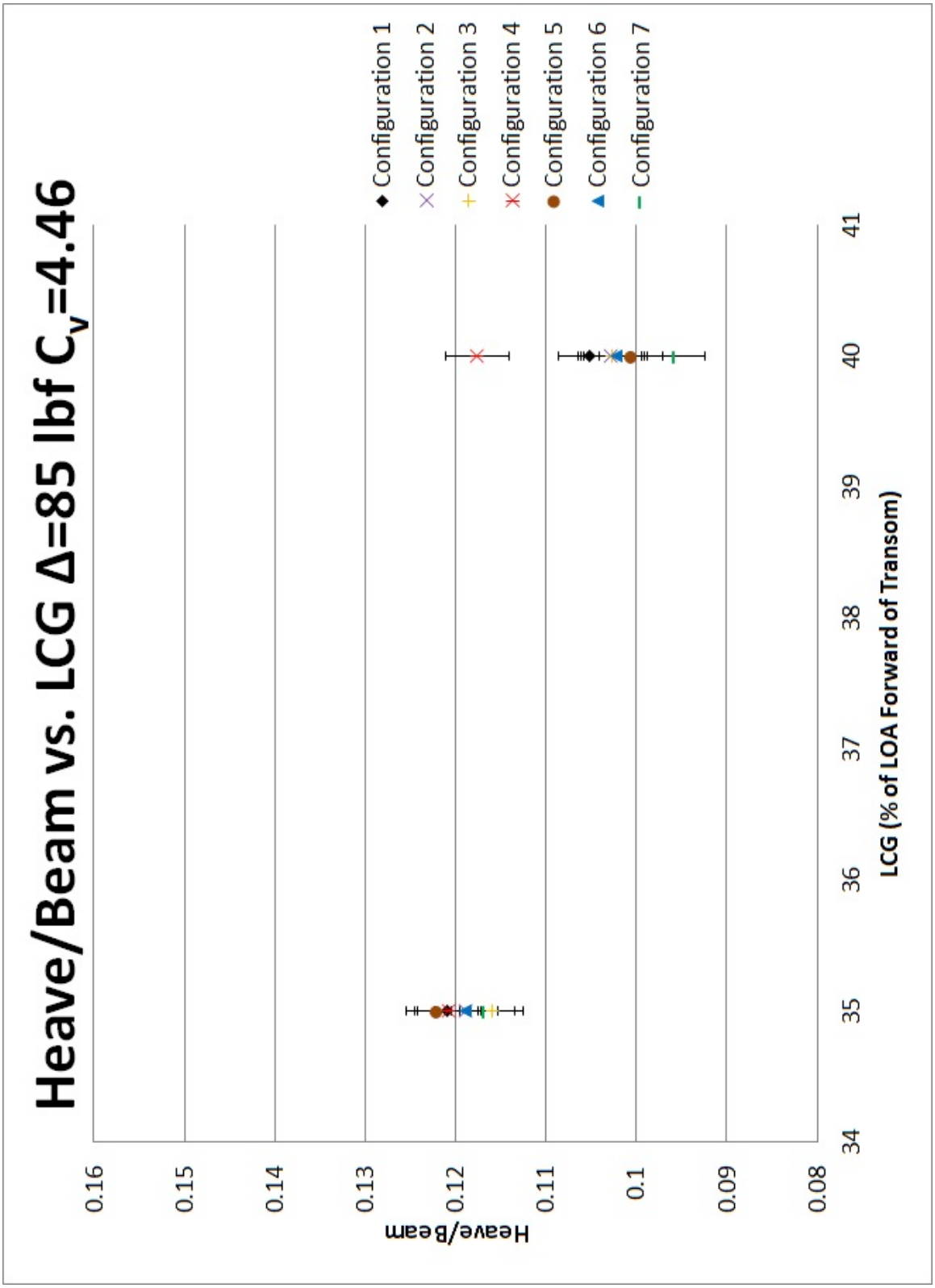

Figure B.90: Heave/Beam vs. Longitudinal Center of Gravity at Δ=85 C_v=4.46

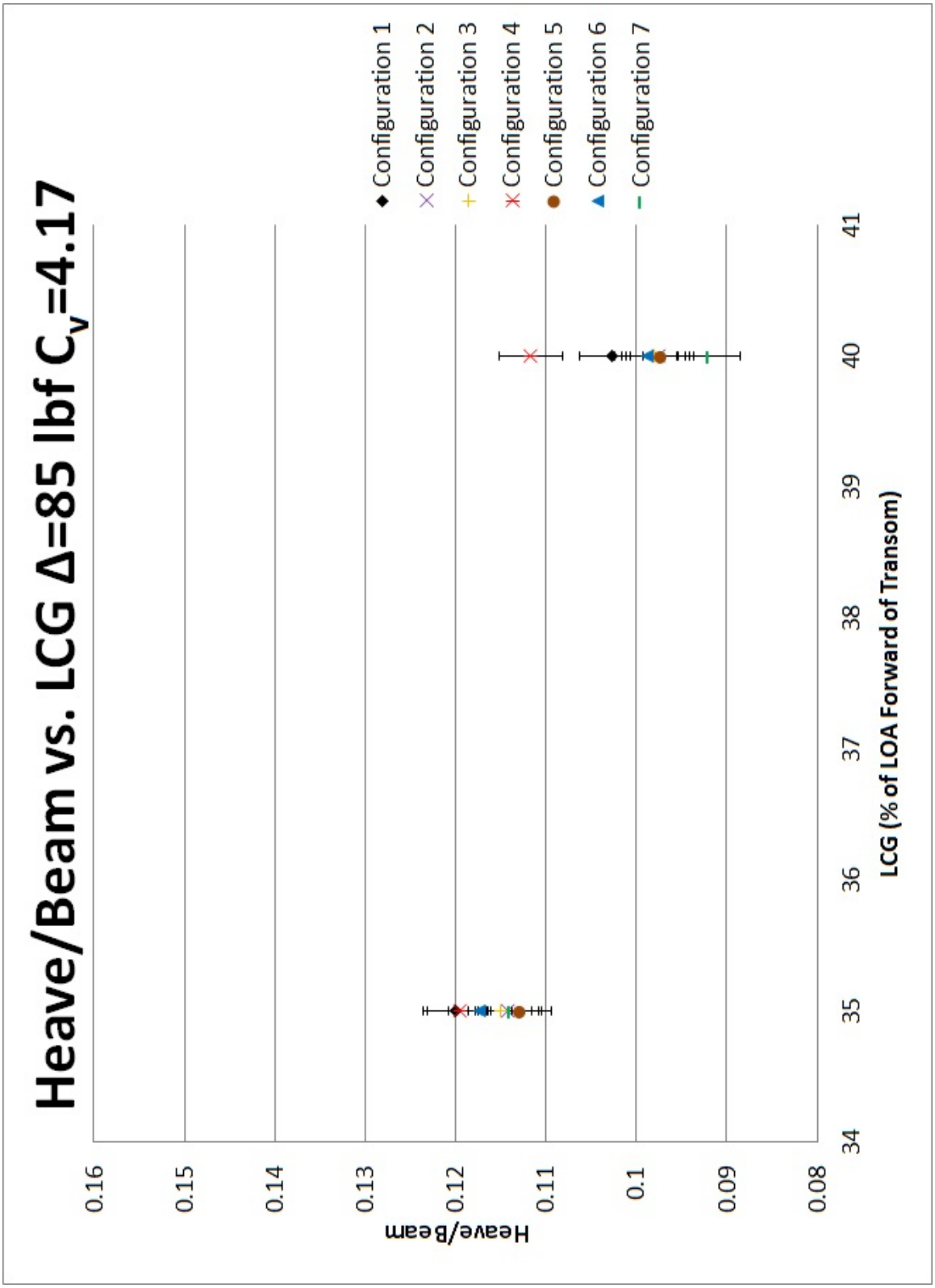

Figure B.91: Heave/Beam vs. Longitudinal Center of Gravity at Δ=85 C_v=4.17

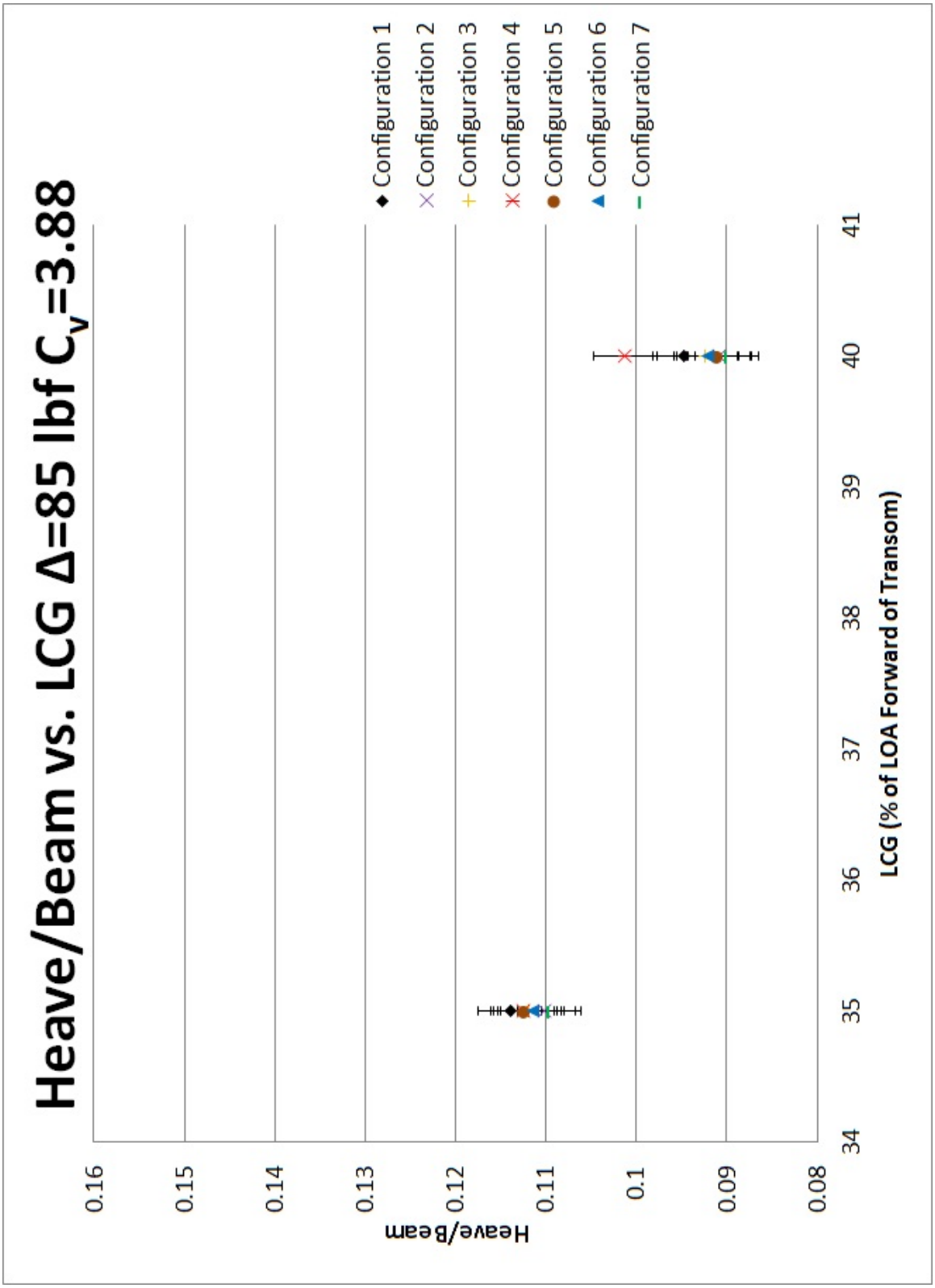

Figure B.92: Heave/Beam vs. Longitudinal Center of Gravity at Δ=85 C_v=3.88

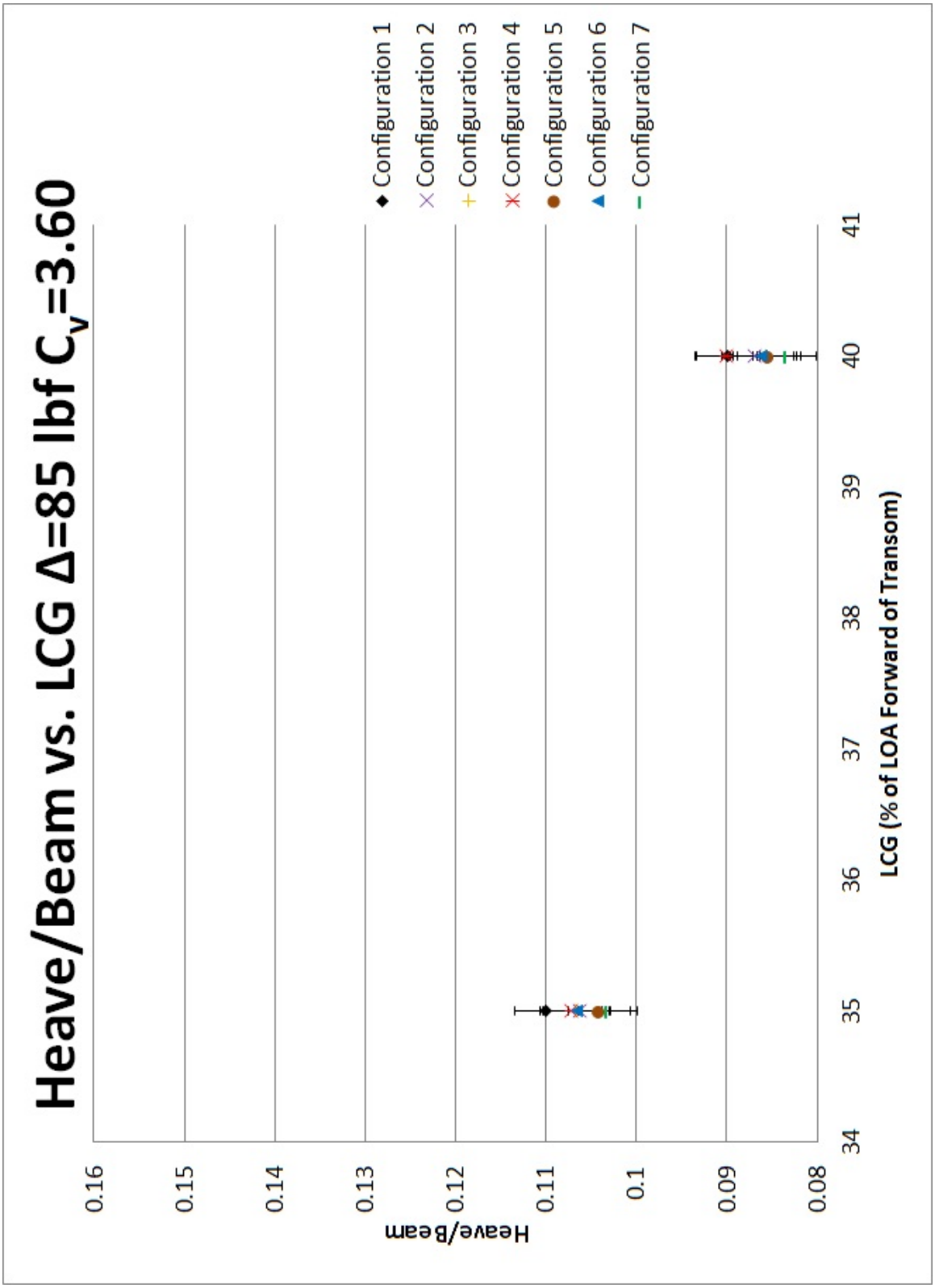

Figure B.93: Heave/Beam vs. Longitudinal Center of Gravity at Δ=85 C_v=3.60

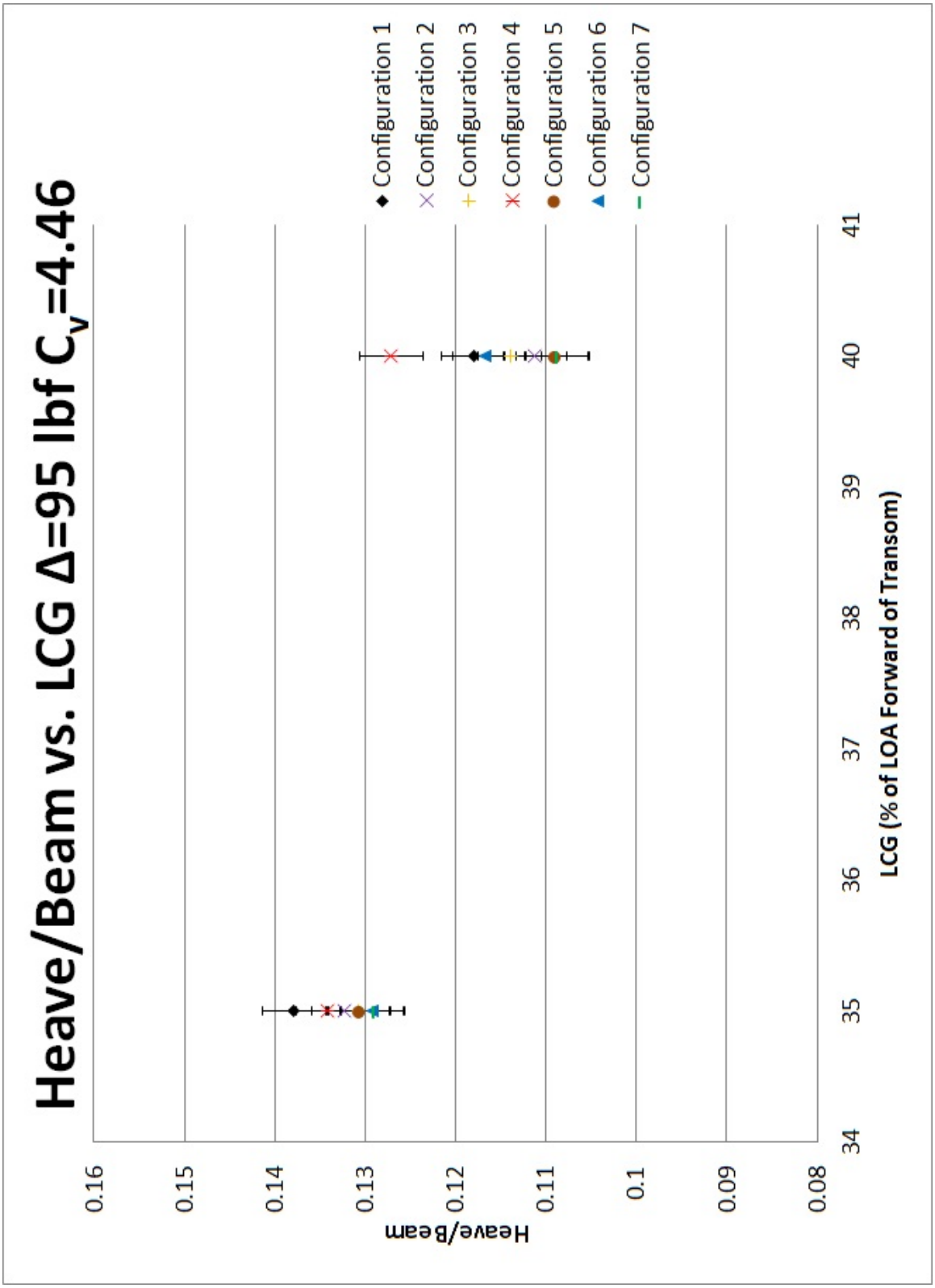

Figure B.94: Heave/Beam vs. Longitudinal Center of Gravity at Δ=95 C_v=4.46

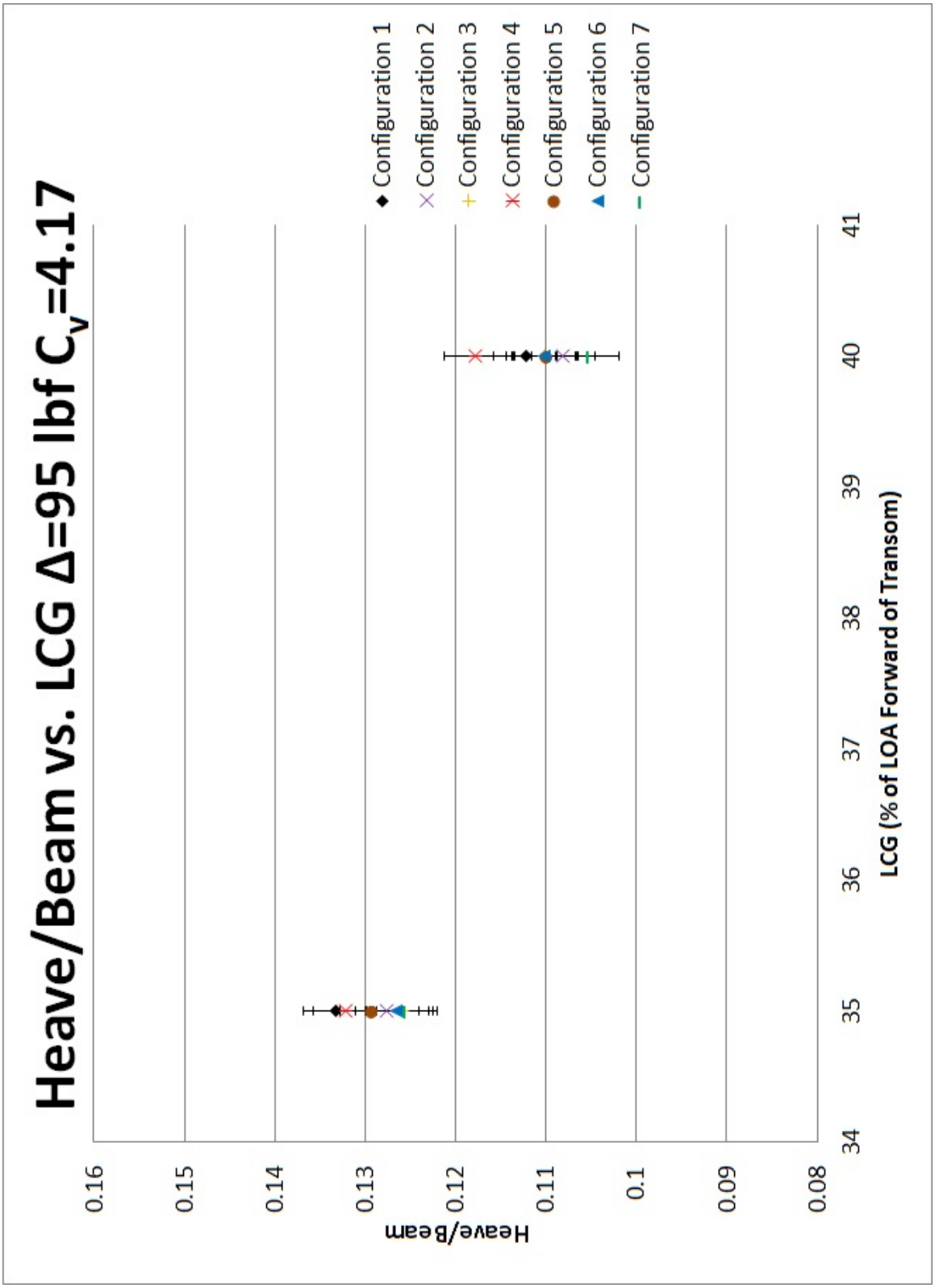

Figure B.95: Heave/Beam vs. Longitudinal Center of Gravity at Δ=95 C_v=4.17

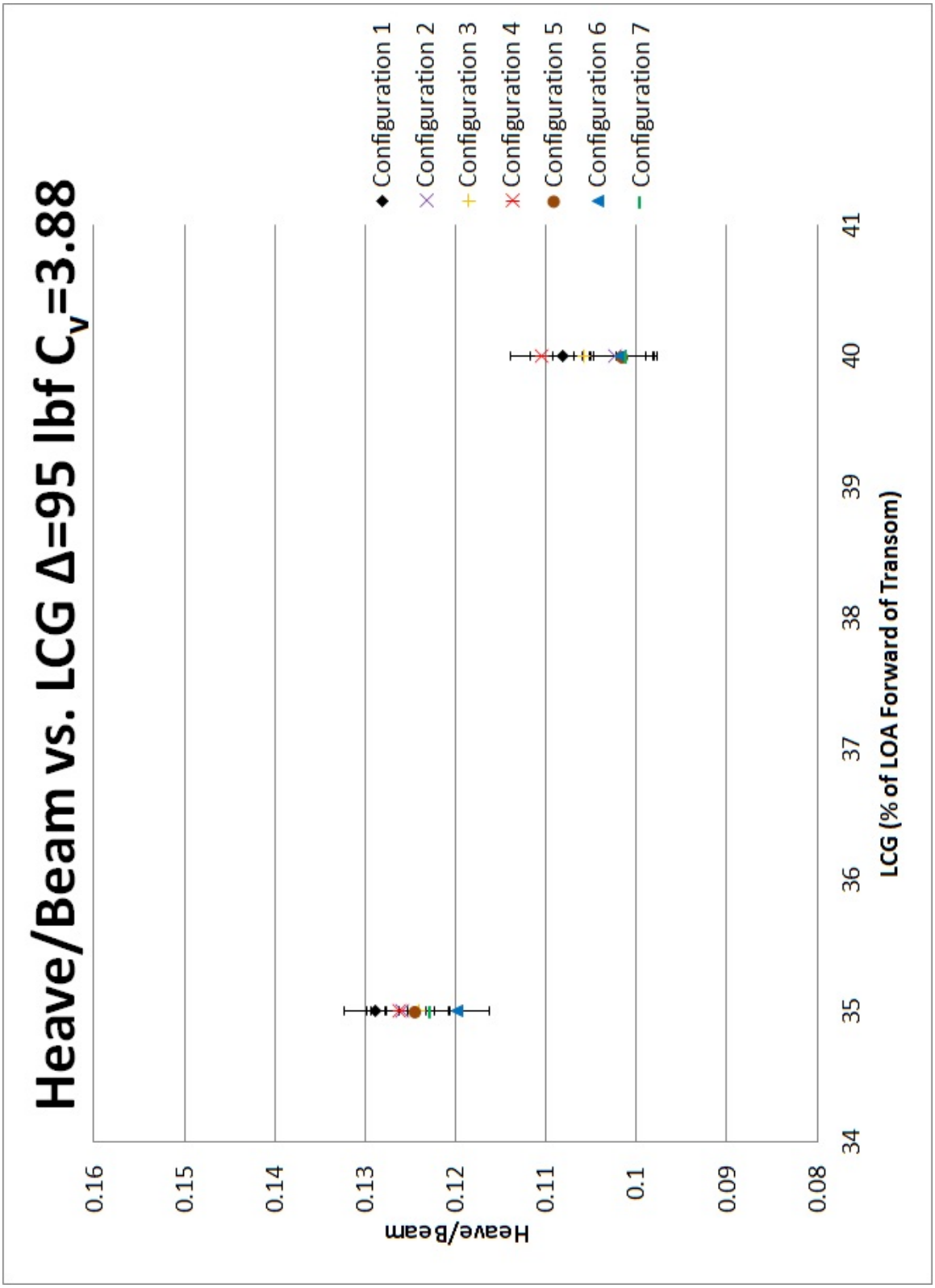

Figure B.96: Heave/Beam vs. Longitudinal Center of Gravity at Δ=95 C_v=3.88

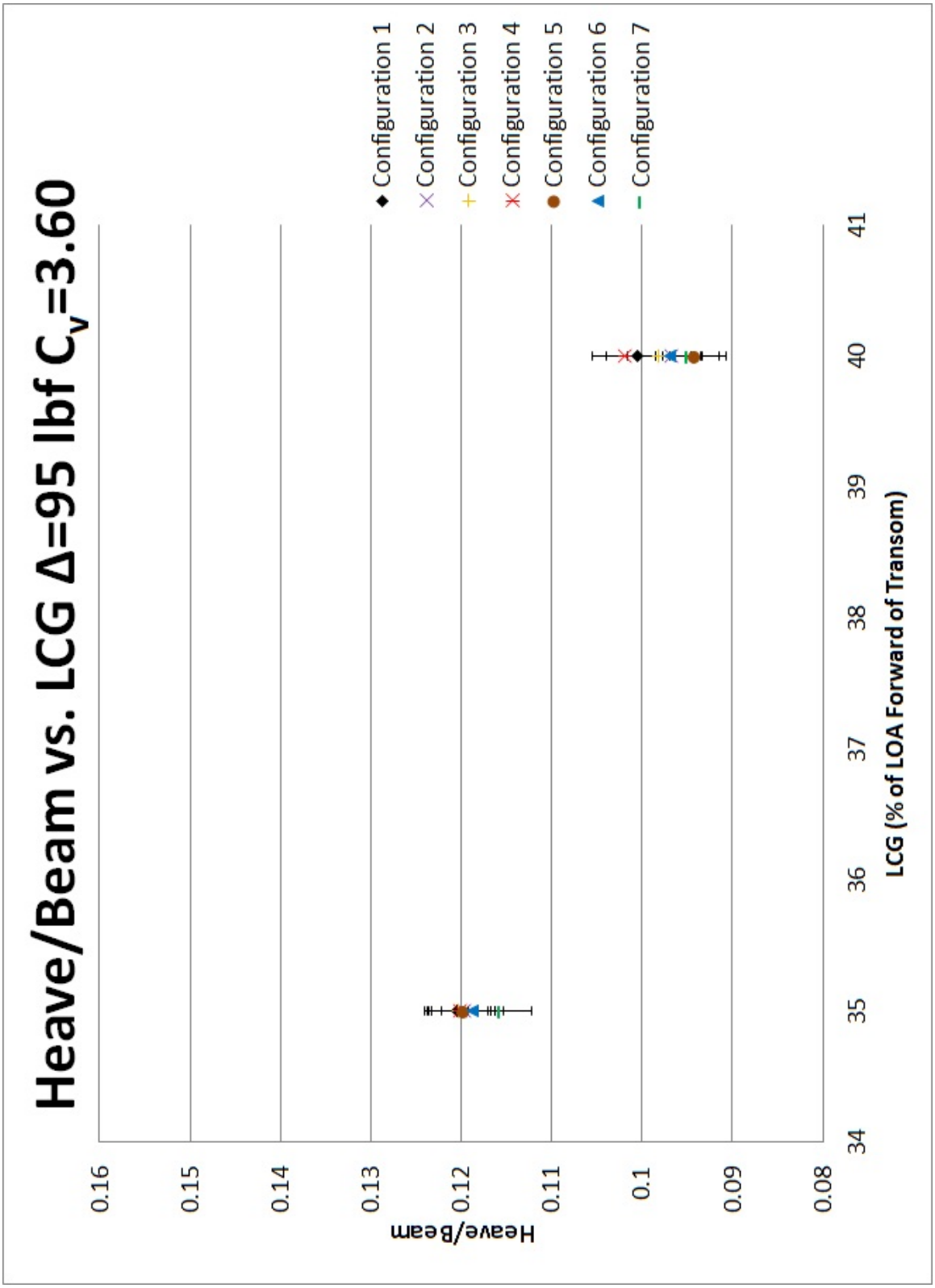

Figure B.97: Heave/Beam vs. Longitudinal Center of Gravity at Δ=95 C_v=3.60

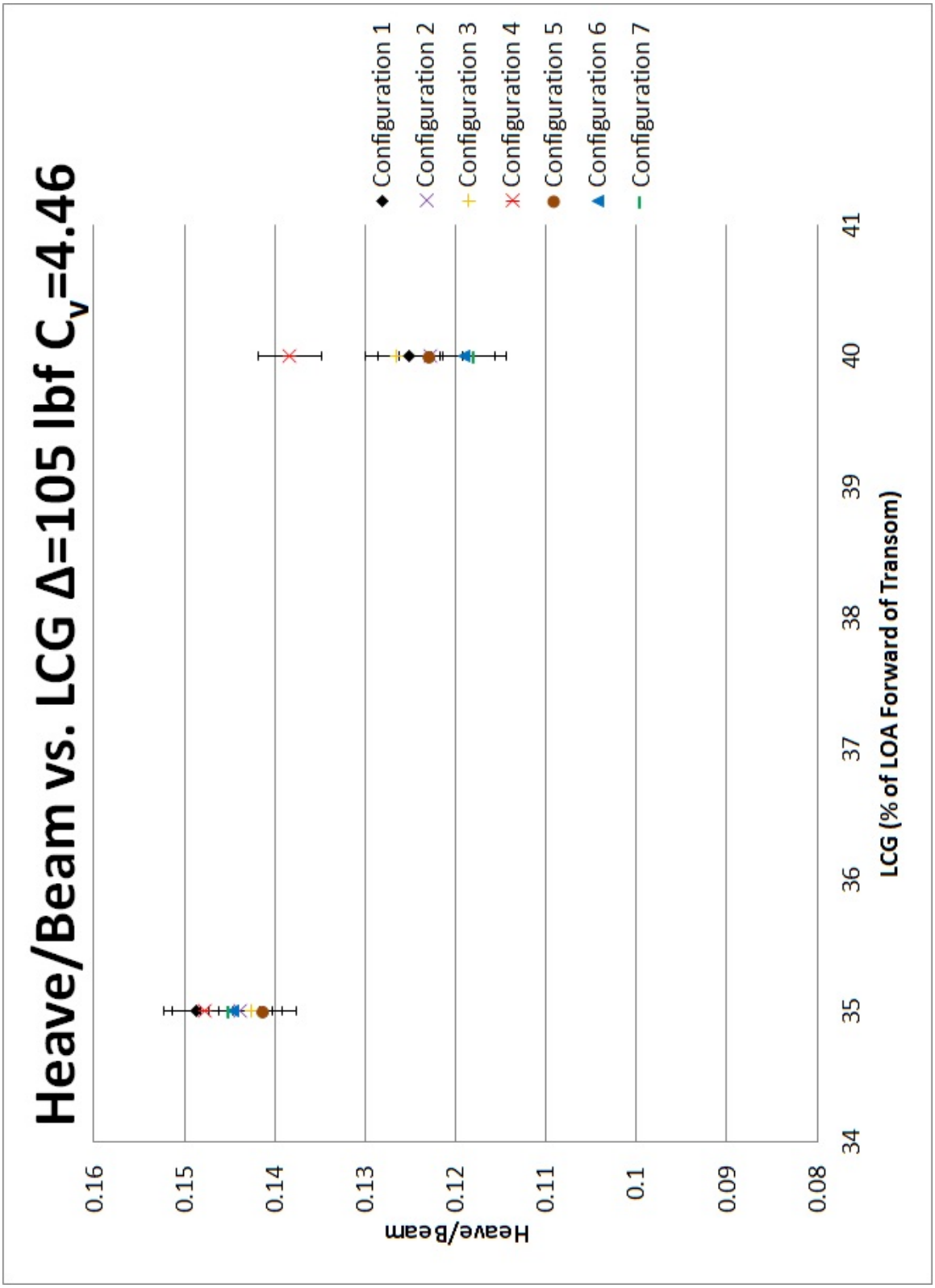

Figure B.98: Heave/Beam vs. Longitudinal Center of Gravity at Δ=105 C_v=4.46

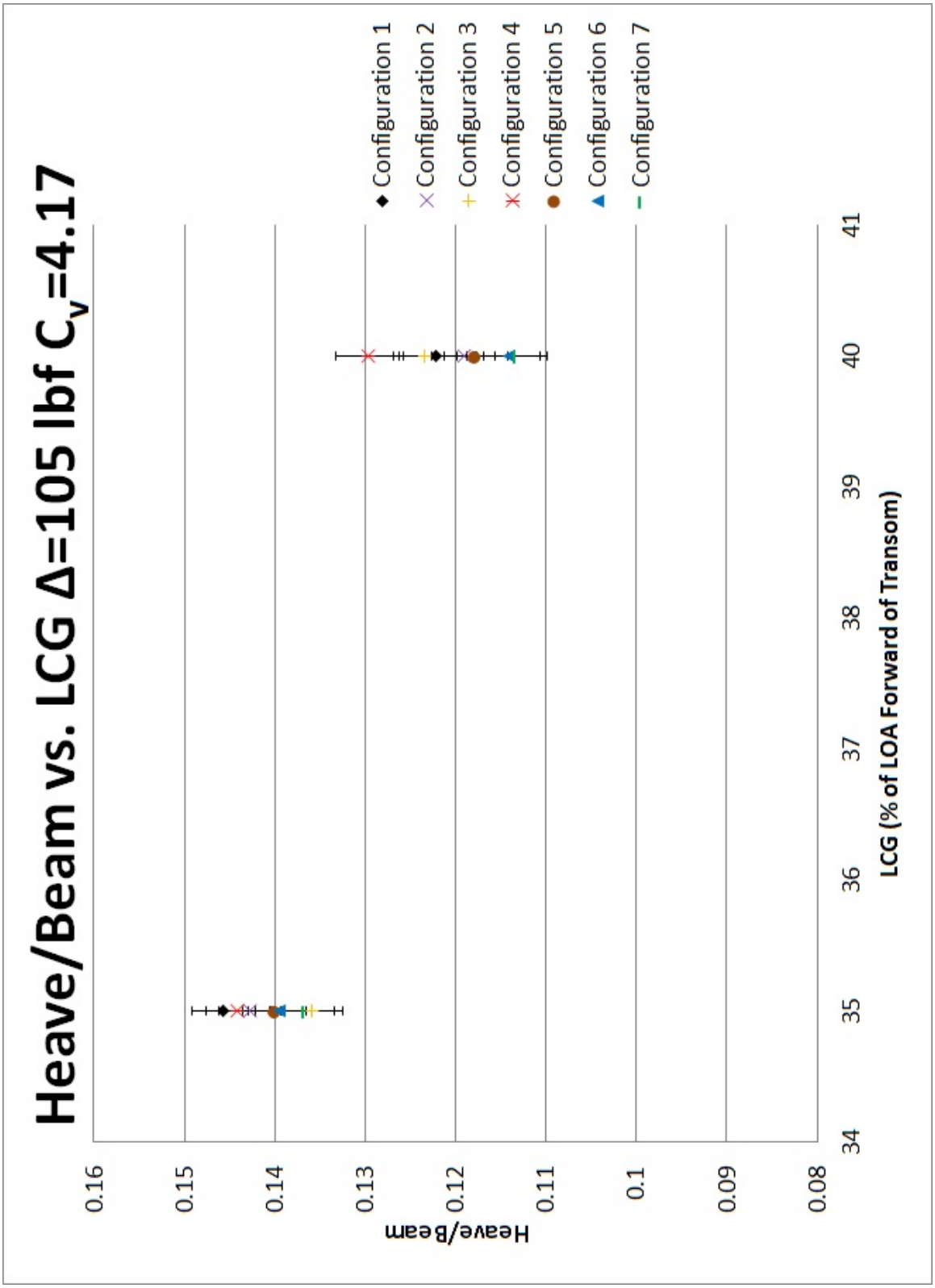

Figure B.99: Heave/Beam vs. Longitudinal Center of Gravity at Δ=105 C_v=4.17

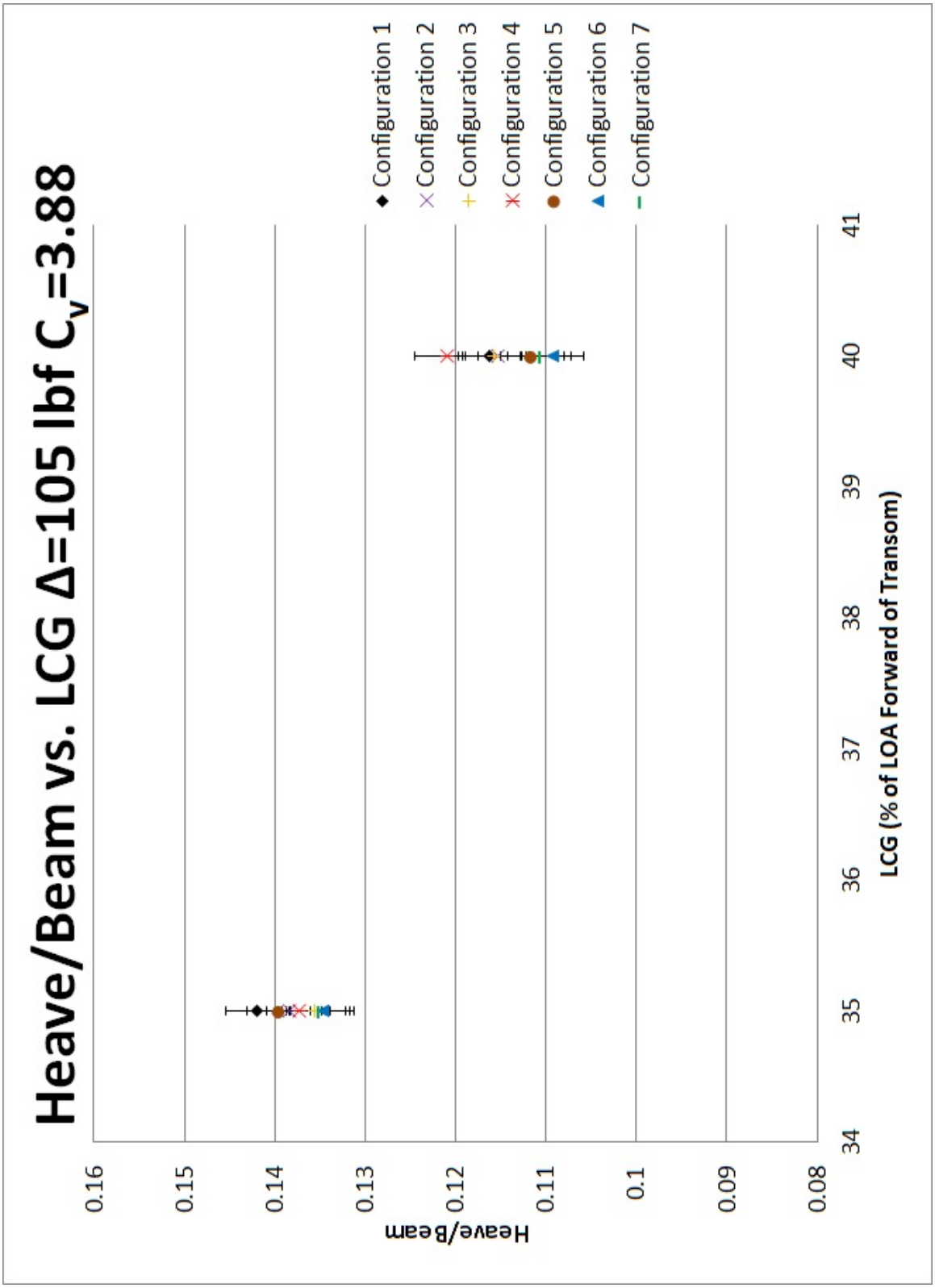

Figure B.100: Heave/Beam vs. Longitudinal Center of Gravity at Δ=105 C_v=3.88

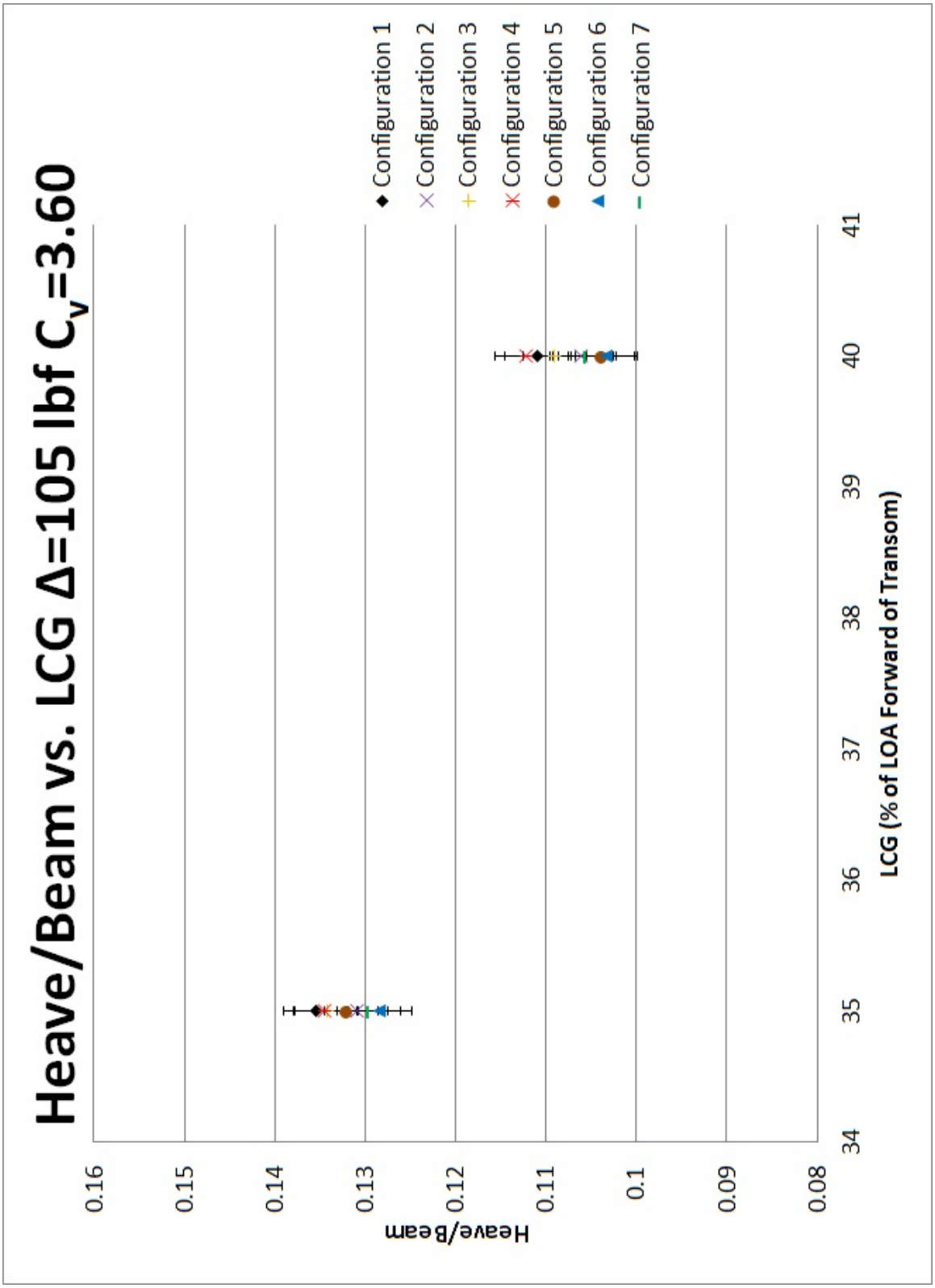

Figure B.101: Heave/Beam vs. Longitudinal Center of Gravity at Δ=105 C_v=3.60

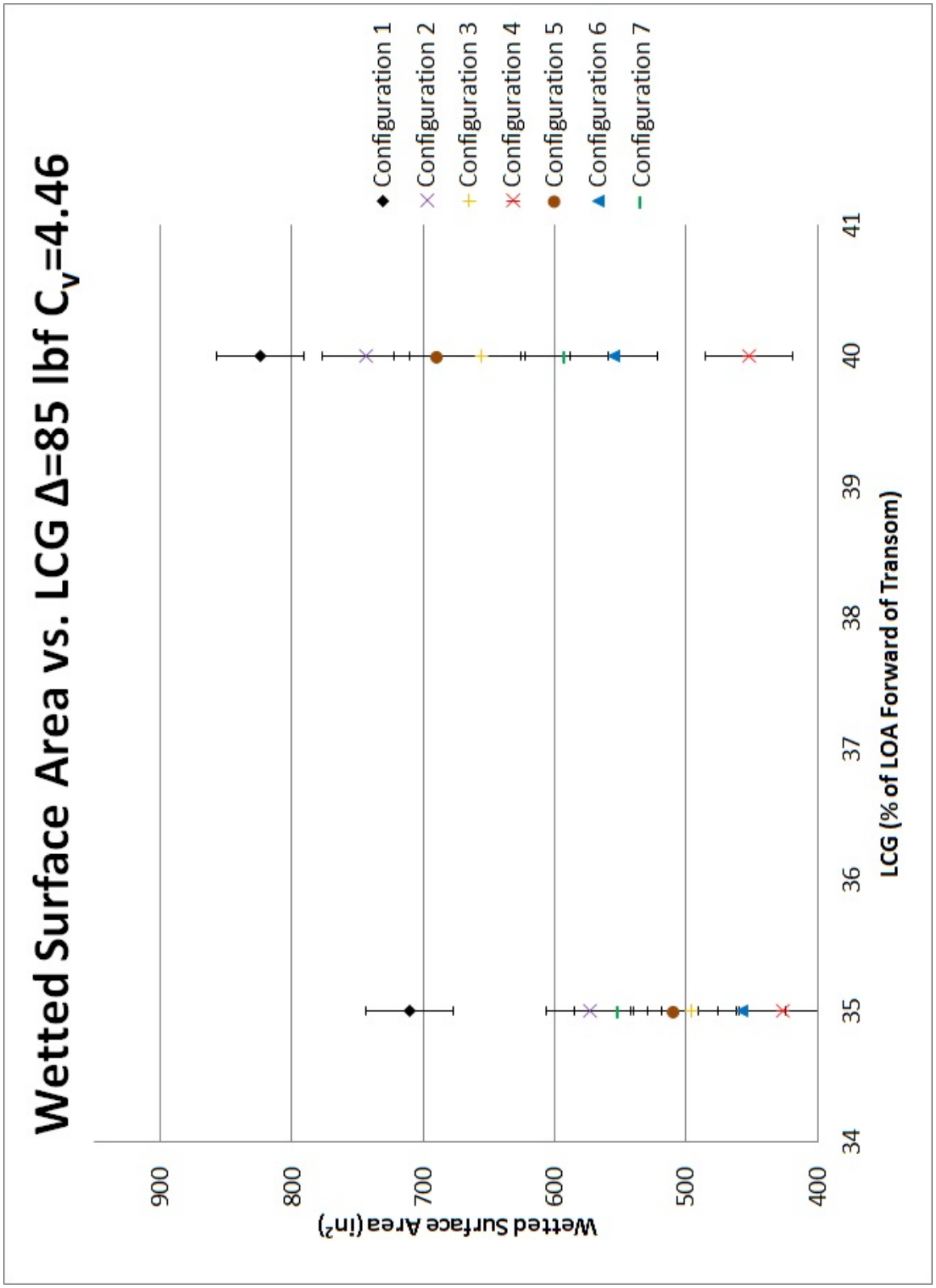

Figure B.102: Wetted Surface Area vs. Longitudinal Center of Gravity at Δ=85 C_v=4.46

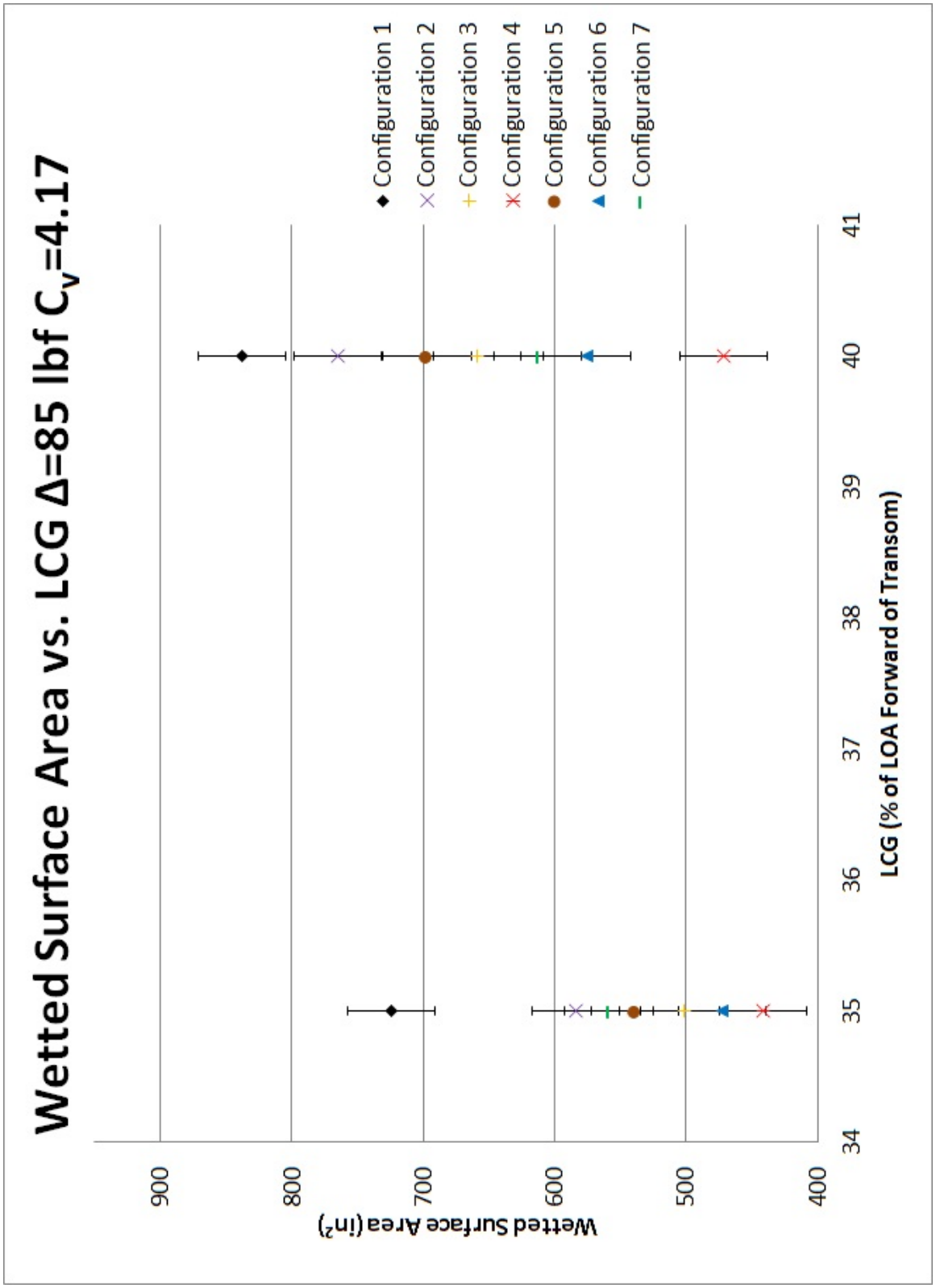

Figure B.103: Wetted Surface Area vs. Longitudinal Center of Gravity at Δ=85 C_v=4.17

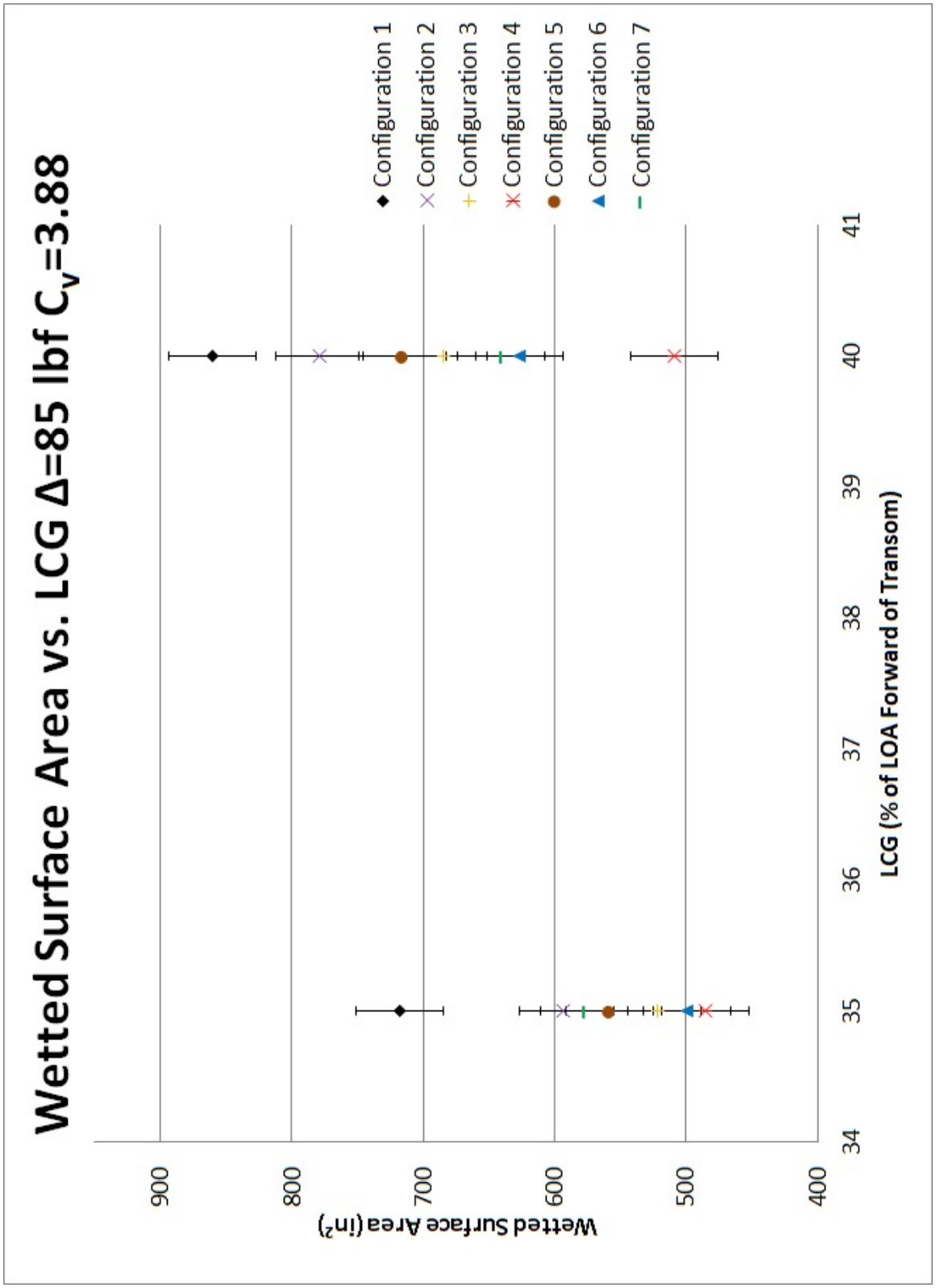

Figure B.104: Wetted Surface Area vs. Longitudinal Center of Gravity at Δ=85 C_v=3.88

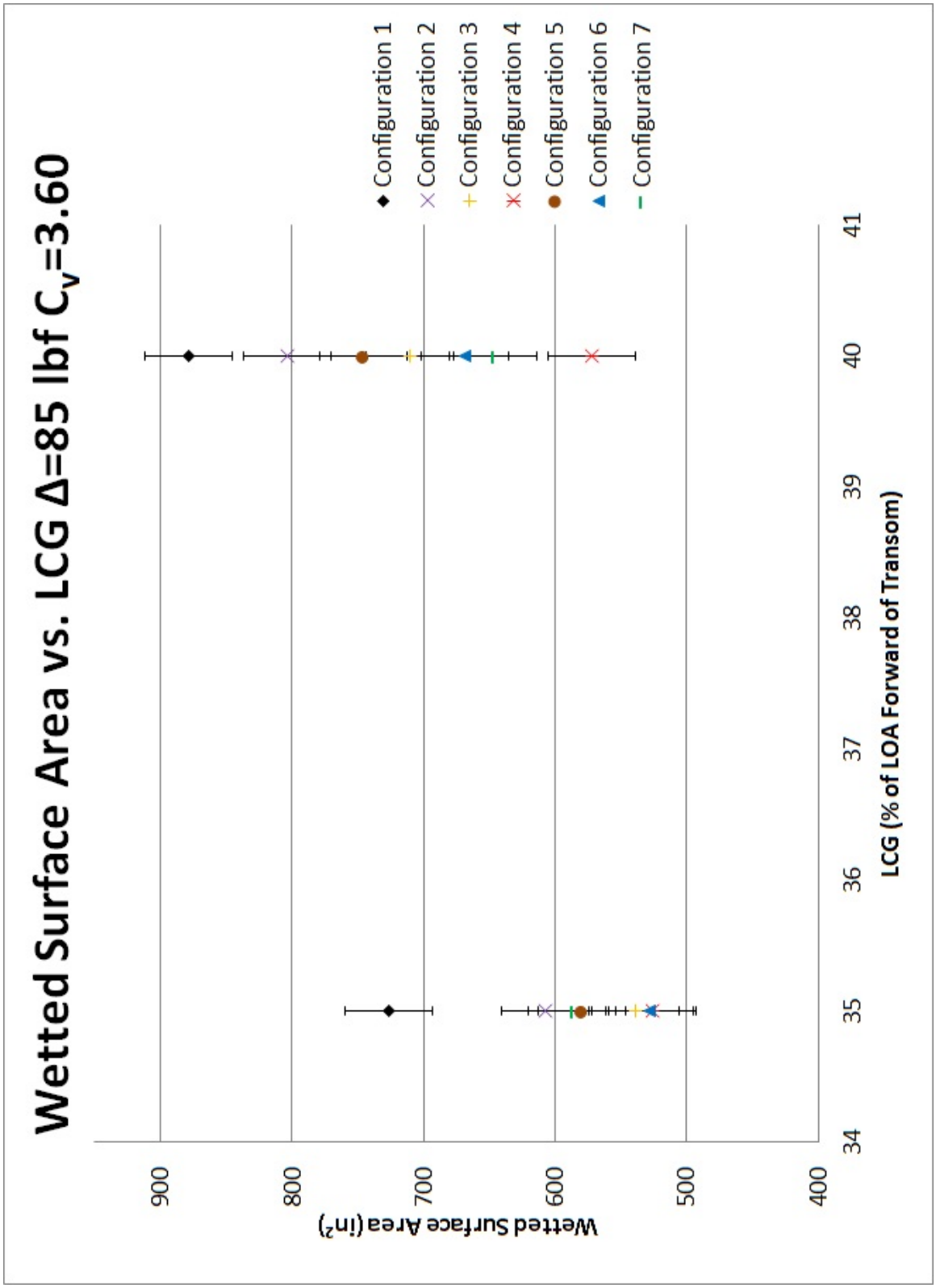

Figure B.105: Wetted Surface Area vs. Longitudinal Center of Gravity at Δ=85 C_v=3.60

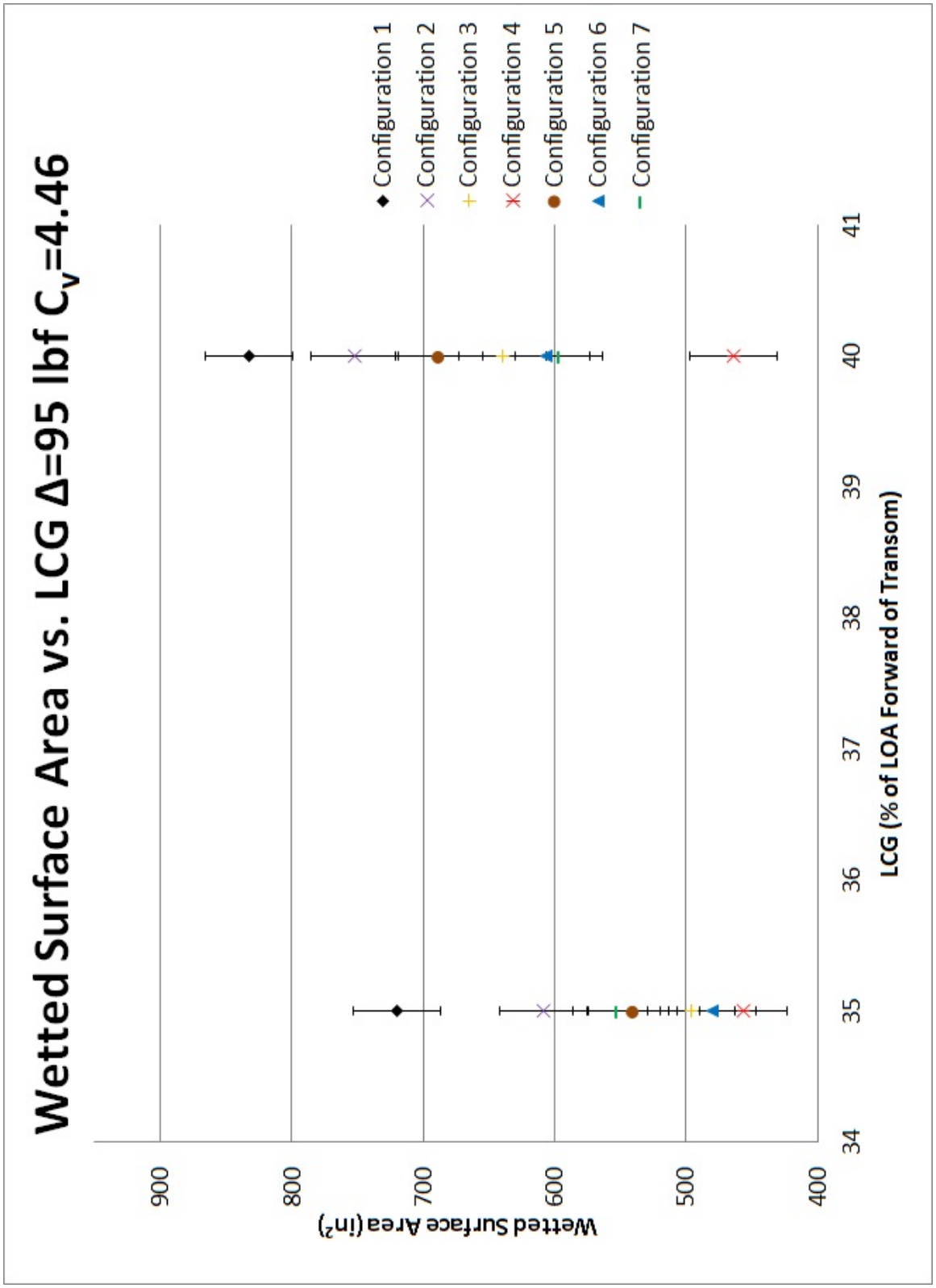

Figure B.106: Wetted Surface Area vs. Longitudinal Center of Gravity at Δ=95 C_v=4.46

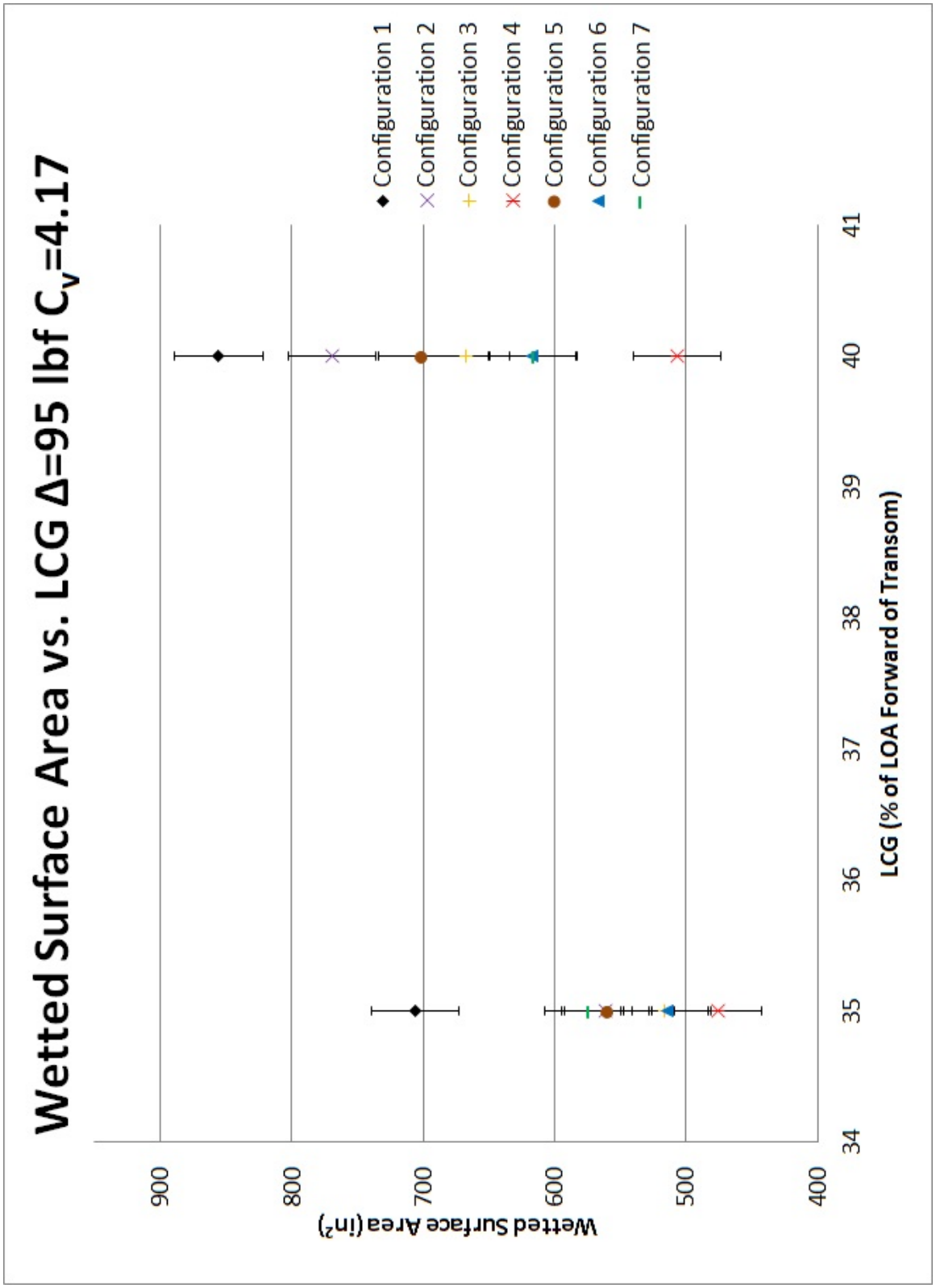

Figure B.107: Wetted Surface Area vs. Longitudinal Center of Gravity at Δ=95 C_v=4.17

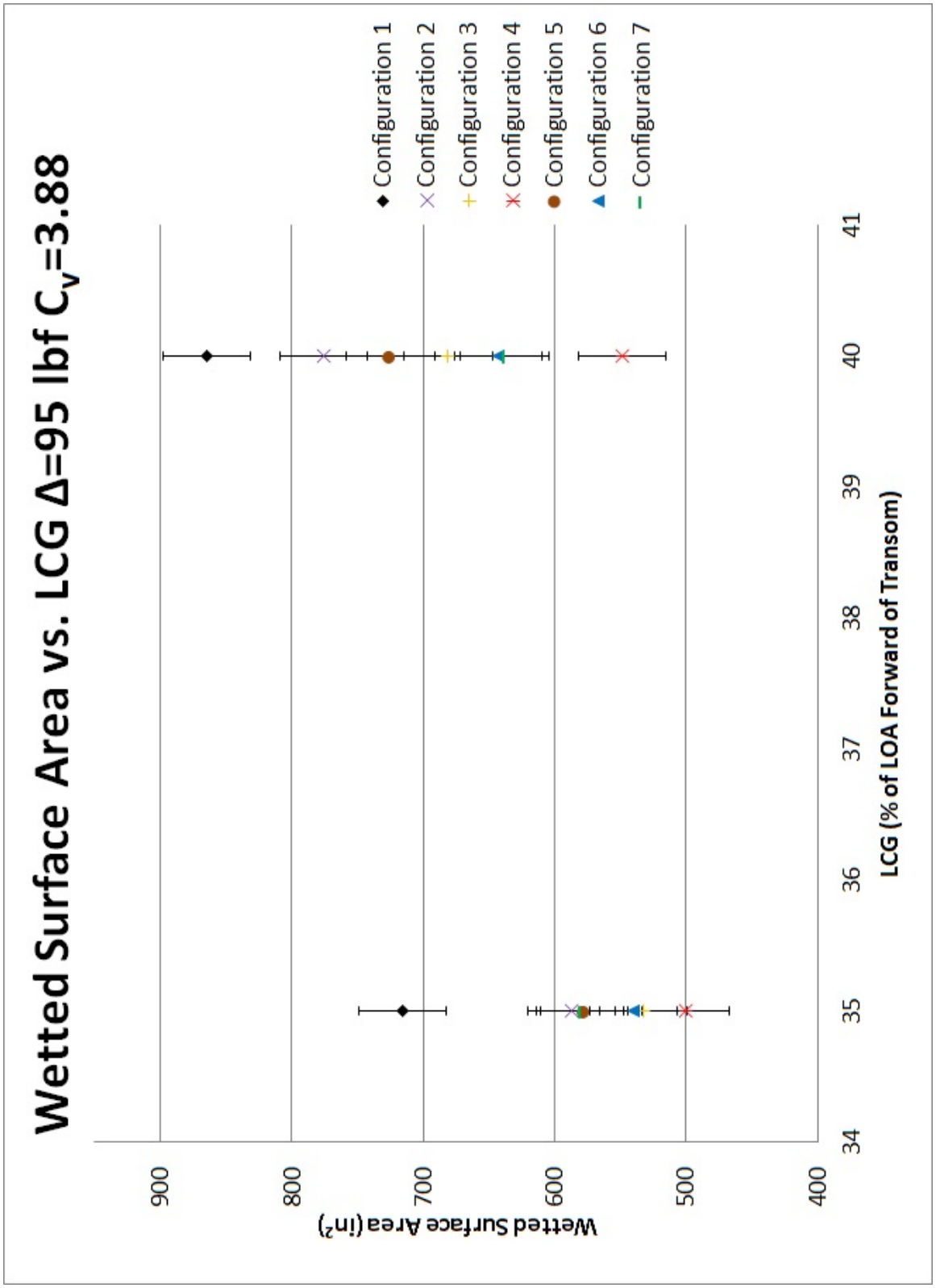

Figure B.108: Wetted Surface Area vs. Longitudinal Center of Gravity at Δ=95 C_v=3.88

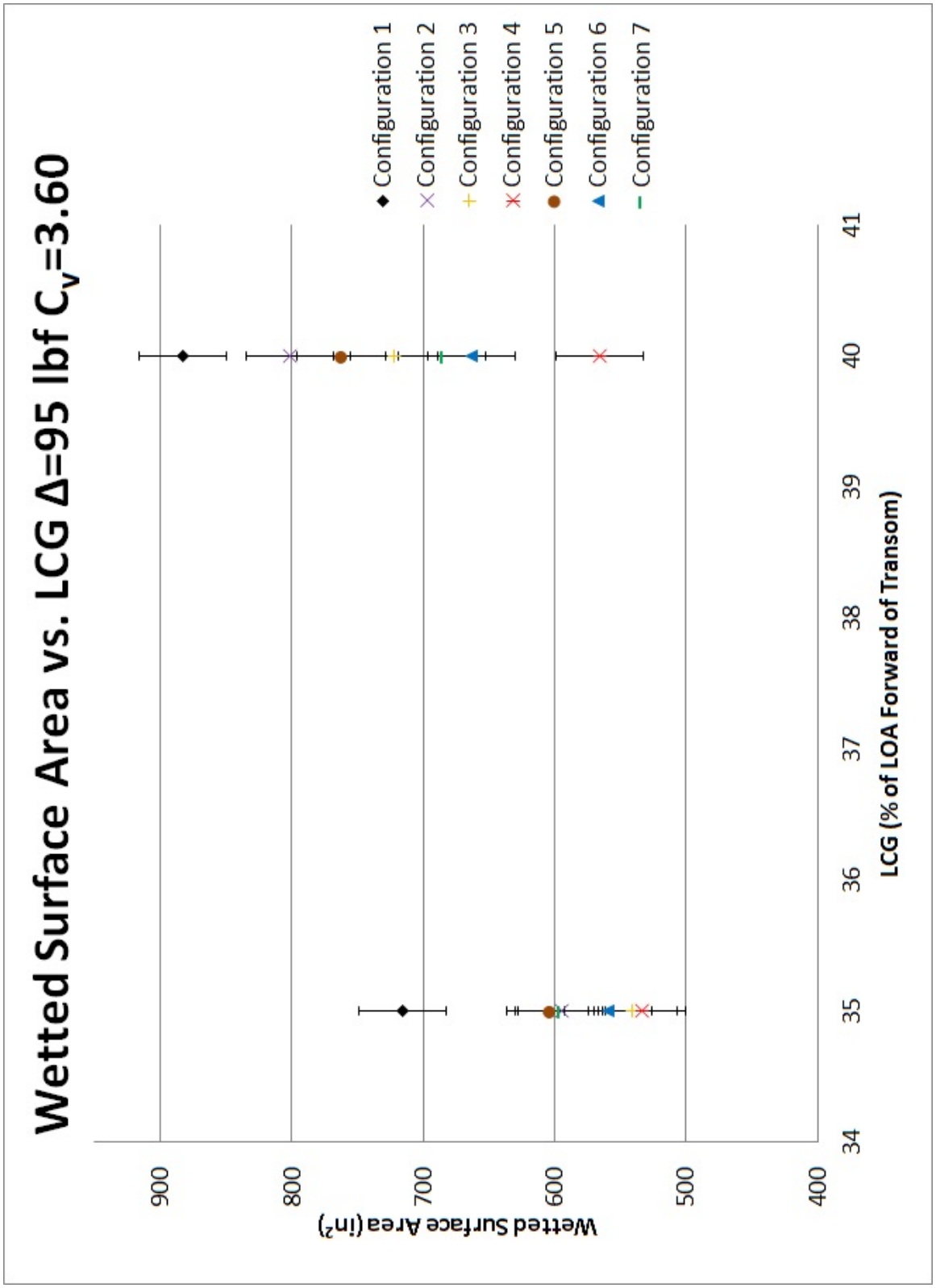

Figure B.109: Wetted Surface Area vs. Longitudinal Center of Gravity at Δ=95 C_v=3.60

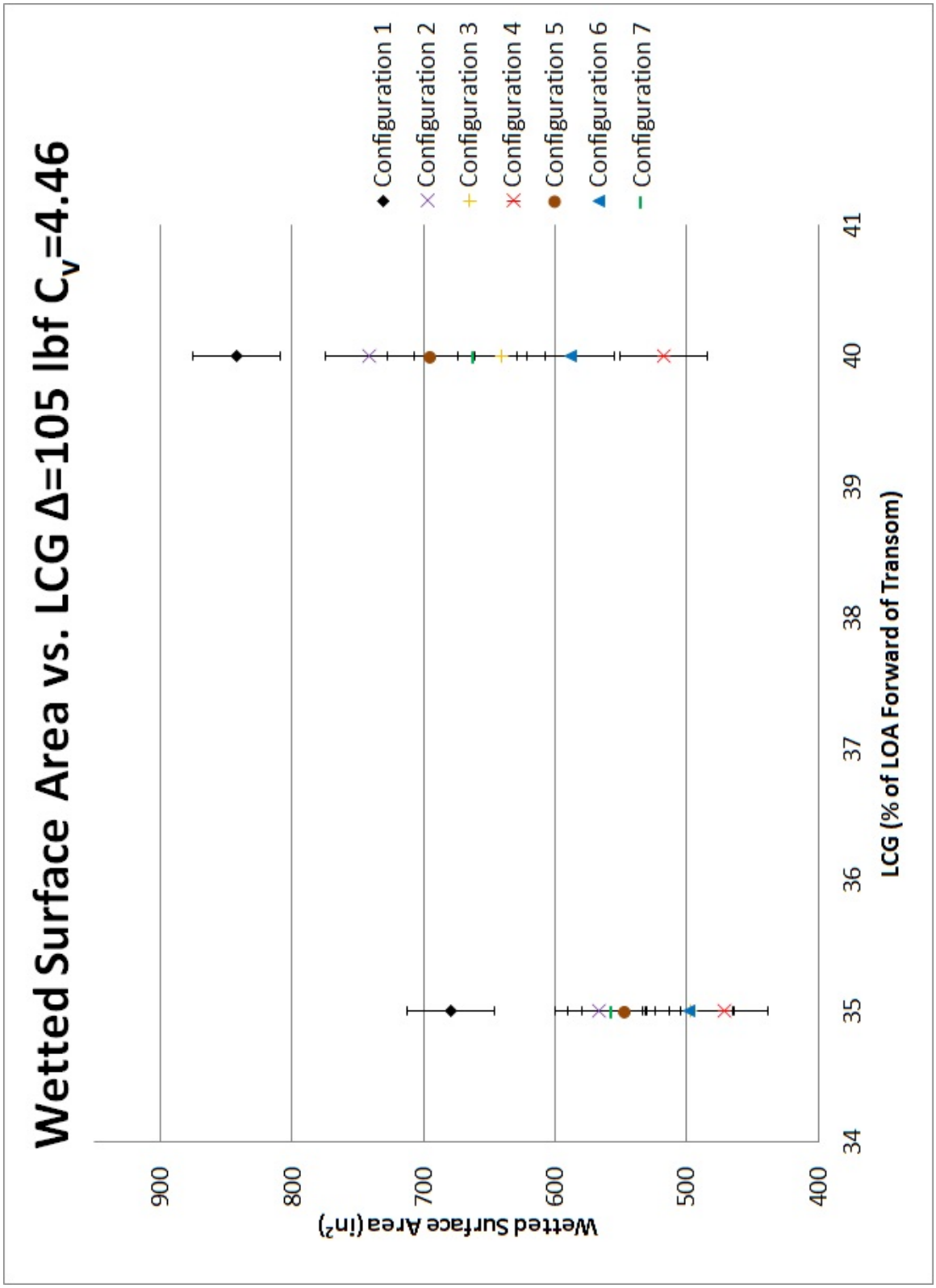

Figure B.110: Wetted Surface Area vs. Longitudinal Center of Gravity at Δ=105 C_v=4.46

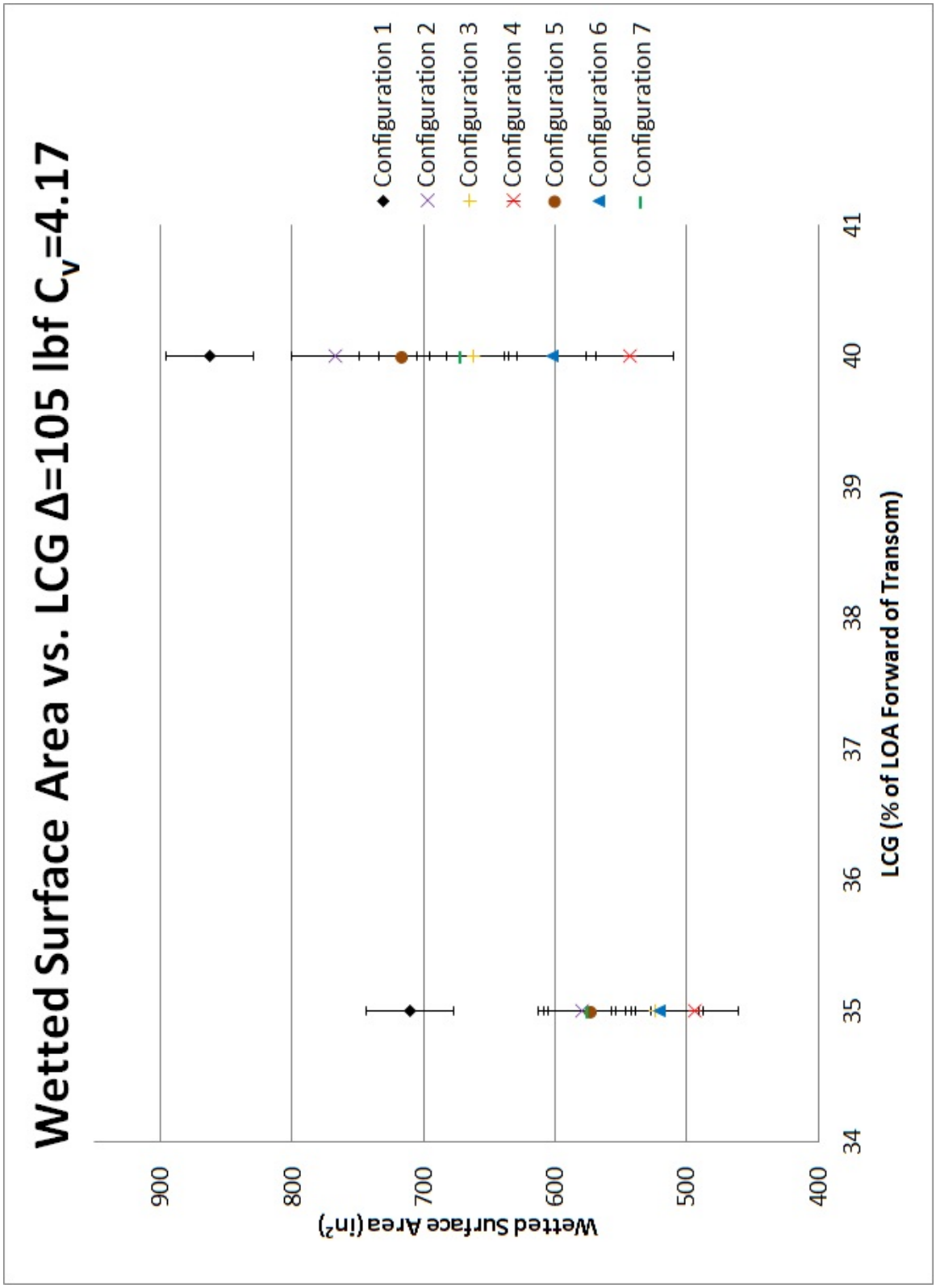

Figure B.111: Wetted Surface Area vs. Longitudinal Center of Gravity at Δ=105 C_v=4.17

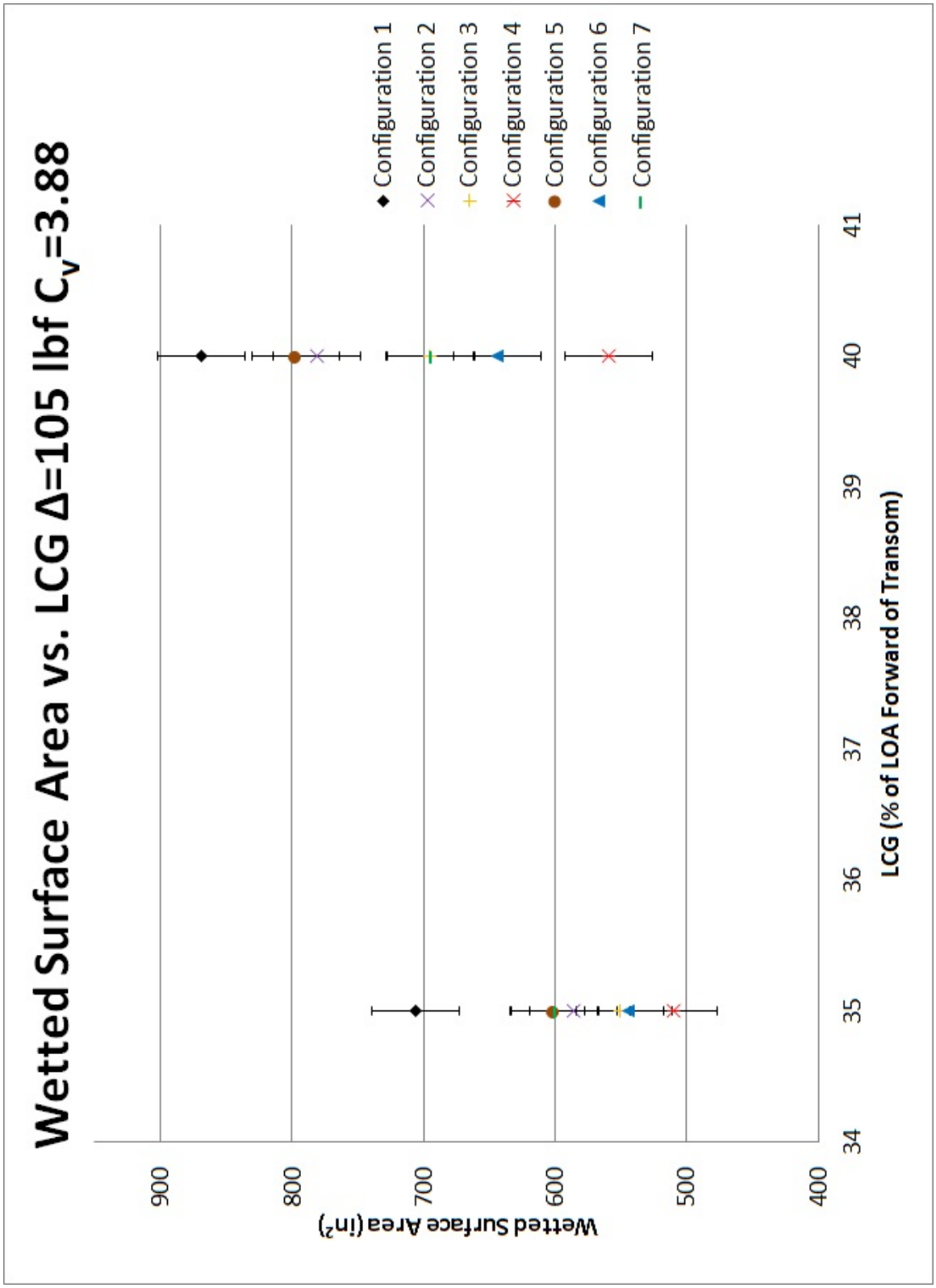

Figure B.112: Wetted Surface Area vs. Longitudinal Center of Gravity at Δ=105 C_v=3.88

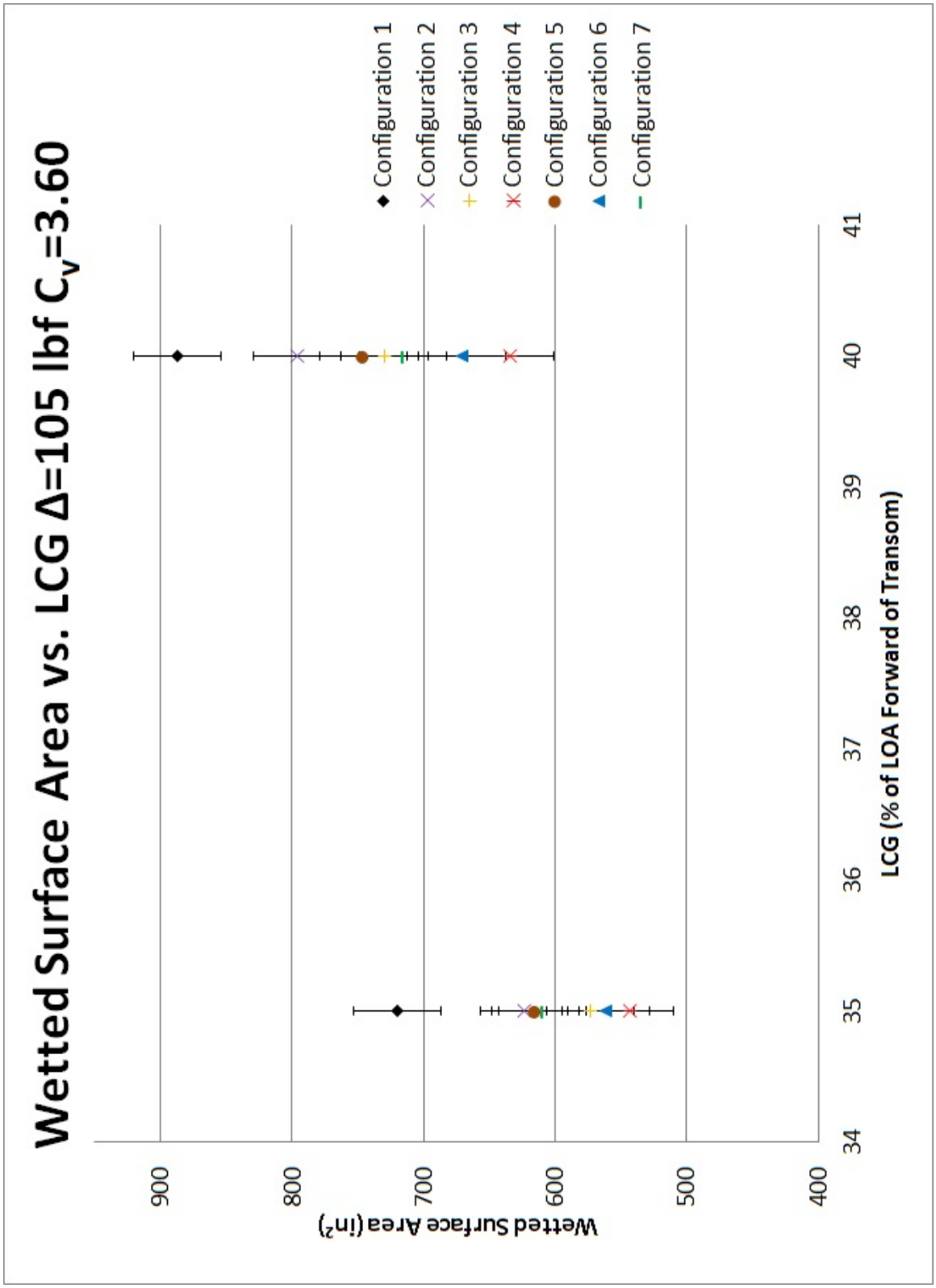

Figure B.113: Wetted Surface Area vs. Longitudinal Center of Gravity at Δ=105 C_v=3.60

Appendix C

Wave Profile Curve Fitting

β	10	deg
τ	4	deg
C_v	3.69	
λ	0.84	
V	8.00802	knots
Lk	0.517218	ft
B	0.416667	ft

	Measured			New			Error Squared		
X	0	0.2B	0.4B	0	.2B	0.4B	0B	0.2B	.4B
0	-0.087	-0.05215	-0.02305	-0.08659	-0.05132	-0.01606	0.00041	0.000827	0.006986
0.33	-0.09222	-0.07338	-0.0386	-0.10102	-0.06867	-0.03457	0.008805	0.004706	0.00403
0.66	-0.09879	-0.08969	-0.05035	-0.10834	-0.08132	-0.04935	0.009549	0.008371	0.000997
1	-0.10443	-0.09941	-0.07035	-0.11103	-0.09091	-0.0617	0.006602	0.0085	0.008649
1.33	-0.11007	-0.10354	-0.07786	-0.10998	-0.09803	-0.07209	8.92E-05	0.005503	0.005771
1.66	-0.10687	-0.10154	-0.08596	-0.10569	-0.10301	-0.08077	0.001177	0.001476	0.00519
2	-0.1017	-0.10048	-0.09326	-0.09852	-0.10609	-0.08795	0.003181	0.005608	0.005315
2.33	-0.09722	-0.09688	-0.09763	-0.08871	-0.10743	-0.09374	0.008516	0.010547	0.003896
2.66	-0.08974	-0.09309	-0.09553	-0.07646	-0.10715	-0.09825	0.013282	0.014063	0.00272
3	-0.07907	-0.08371	-0.09085	-0.06194	-0.10537	-0.10156	0.017131	0.021667	0.010712

β	10	deg
τ	4	deg
Cv	5.47	
λ	0.86	
V	11.87097	knots
Lk	0.525552	ft
B	0.416667	ft

	Measured			New			Error Squared		
X(B)	0	0.2B	0.4B	0	.2B	0.4B	0B	0.2B	.4B
0	-0.088	-0.07236	-0.02686	-0.08799	-0.05272	-0.01745	1.45E-05	0.019644	0.00941
0.33	-0.10714	-0.08758	-0.04618	-0.1052	-0.0719	-0.03742	0.00194	0.01568	0.008764
0.66	-0.12507	-0.10536	-0.06741	-0.11759	-0.08789	-0.05485	0.007481	0.017469	0.012565
1	-0.14286	-0.11658	-0.08451	-0.12686	-0.10181	-0.07063	0.015997	0.01477	0.013884
1.33	-0.15485	-0.13219	-0.10324	-0.13359	-0.11406	-0.08508	0.02126	0.018138	0.018165
1.66	-0.16422	-0.14637	-0.11649	-0.13813	-0.12485	-0.09837	0.026087	0.021517	0.018112
2	-0.171	-0.15432	-0.1277	-0.14072	-0.13436	-0.11064	0.03028	0.019959	0.017061
2.33	-0.17552	-0.15935	-0.13578	-0.14153	-0.14269	-0.12197	0.03399	0.016665	0.013803
2.66	-0.17899	-0.16248	-0.14638	-0.14069	-0.14992	-0.13244	0.038298	0.012561	0.013937
3	-0.18199	-0.16711	-0.15021	-0.13831	-0.15614	-0.14209	0.043681	0.010972	0.008116

β	10	deg
τ	4	deg
Cv	3.69	
λ	1.23	
V	8.00802	knots
Lk	0.679718	ft
B	0.416667	ft

	Measured			New			Error Squared		
X(B)	0	0.2B	0.4B	0	.2B	0.4B	0B	0.2B	.4B
0	-0.114	-0.07814	-0.04635	-0.1138	-0.07853	-0.04326	0.000205	0.000388	0.003087
0.33	-0.11632	-0.09382	-0.07107	-0.12773	-0.09538	-0.06128	0.011411	0.00156	0.009789
0.66	-0.12683	-0.10902	-0.09322	-0.13415	-0.10713	-0.07516	0.007326	0.001888	0.018058
1	-0.13099	-0.11713	-0.10637	-0.13567	-0.11555	-0.08634	0.004684	0.001583	0.020029
1.33	-0.13531	-0.1241	-0.10786	-0.13323	-0.12128	-0.09534	0.002078	0.002813	0.012521
1.66	-0.13232	-0.12895	-0.10968	-0.12737	-0.1247	-0.10246	0.004944	0.004257	0.007222
2	-0.12338	-0.13363	-0.10848	-0.11846	-0.12603	-0.10789	0.004924	0.007591	0.000594
2.33	-0.11883	-0.1266	-0.10287	-0.10676	-0.12548	-0.11179	0.012065	0.001118	0.008925
2.66	-0.10894	-0.12031	-0.09659	-0.09249	-0.12318	-0.11427	0.016458	0.002871	0.017686
3	-0.09115	-0.11222	-0.08608	-0.0758	-0.11924	-0.11543	0.015352	0.007014	0.029347

Figure C.1: Wave Profile Curve Fitting

β	10	deg
τ	4	deg
Cv	3.02	
λ	1.36	
V	6.553989	knots
Lk	0.733885	ft
B	0.416667	ft

	Measured			New			Error Squared		
X(B)	0	0.2B	0.4B	0	.2B	0.4B	0B	0.2B	.4B
0	-0.115	-0.07352	-0.04713	-0.12286	-0.0876	-0.05233	0.007864	0.014081	0.005203
0.33	-0.11851	-0.09116	-0.07007	-0.13459	-0.10288	-0.06904	0.01608	0.011726	0.001027
0.66	-0.12577	-0.10651	-0.08417	-0.13695	-0.11176	-0.08052	0.011184	0.005254	0.00365
1	-0.12934	-0.11406	-0.09438	-0.13323	-0.11647	-0.0886	0.003886	0.002409	0.005785
1.33	-0.12197	-0.11406	-0.09938	-0.12457	-0.1178	-0.09392	0.002604	0.003742	0.005453
1.66	-0.11439	-0.11608	-0.10212	-0.11167	-0.11622	-0.09687	0.00272	0.000139	0.005254
2	-0.09702	-0.11282	-0.1009	-0.09496	-0.11204	-0.0977	0.002055	0.000779	0.003206
2.33	-0.07465	-0.10806	-0.098	-0.07479	-0.10549	-0.09659	0.000145	0.002571	0.001416
2.66	-0.03287	-0.09644	-0.09612	-0.05142	-0.09674	-0.09369	0.018546	0.000298	0.002433
3	0.002707	-0.08639	-0.09193	-0.02504	-0.08594	-0.08911	0.027751	0.000451	0.002816

β	10	deg
τ	4	deg
Cv	4.39	
λ	2.29	
V	9.527157	knots
Lk	1.121385	ft
B	0.416667	ft

	Measured			New			Error Squared		
X(B)	0	0.2B	0.4B	0	.2B	0.4B	0B	0.2B	.4B
0	-0.186	-0.15647	-0.11451	-0.18774	-0.15247	-0.11721	0.001737	0.004002	0.002692
0.33	-0.20161	-0.1749	-0.12825	-0.202	-0.16918	-0.13489	0.000387	0.00572	0.00664
0.66	-0.21452	-0.18989	-0.14605	-0.209	-0.18066	-0.14816	0.005526	0.009231	0.002112
1	-0.22265	-0.20597	-0.1597	-0.21127	-0.18874	-0.15856	0.011382	0.017229	0.001138
1.33	-0.22451	-0.21435	-0.16724	-0.20973	-0.19406	-0.16663	0.014786	0.02029	0.000614
1.66	-0.22881	-0.21664	-0.16968	-0.20488	-0.19701	-0.17269	0.023933	0.019631	0.003013
2	-0.23106	-0.21087	-0.16323	-0.19709	-0.19784	-0.17696	0.033969	0.013031	0.013729
2.33	-0.23318	-0.20909	-0.15255	-0.18661	-0.19673	-0.1796	0.046564	0.012364	0.027047
2.66	-0.22183	-0.20274	-0.13738	-0.17365	-0.19382	-0.18072	0.048176	0.008913	0.04334
3	-0.20827	-0.1939	-0.12675	-0.15836	-0.18925	-0.18042	0.049912	0.004648	0.053668

β	10	deg
τ	4	deg
Cv	3.69	
λ	2.41	
V	8.00802	knots
Lk	1.171385	ft
B	0.416667	ft

	Measured			New			Error Squared		
X(B)	0	0.2B	0.4B	0	.2B	0.4B	0B	0.2B	.4B
0	-0.195	-0.16224	-0.12789	-0.19611	-0.16084	-0.12558	0.001108	0.001395	0.002313
0.33	-0.19558	-0.17765	-0.13784	-0.20855	-0.1762	-0.1421	0.012977	0.00145	0.004259
0.66	-0.20102	-0.18578	-0.14461	-0.21224	-0.18522	-0.15324	0.011214	0.000567	0.008635
1	-0.20317	-0.19702	-0.15079	-0.21022	-0.1901	-0.16088	0.007048	0.00692	0.010095
1.33	-0.20205	-0.20129	-0.15341	-0.20358	-0.19164	-0.16569	0.001534	0.009647	0.012282
1.66	-0.19737	-0.19826	-0.14721	-0.19297	-0.19029	-0.16805	0.004397	0.007969	0.020841
2	-0.18775	-0.18795	-0.14205	-0.1788	-0.18638	-0.16823	0.008944	0.001569	0.026186
2.33	-0.17639	-0.1768	-0.13591	-0.16139	-0.18011	-0.16642	0.015006	0.003311	0.030508
2.66	-0.16027	-0.16371	-0.13032	-0.14097	-0.17166	-0.16276	0.019301	0.007955	0.032445
3	-0.13127	-0.14588	-0.11925	-0.11775	-0.16119	-0.15738	0.013515	0.015312	0.038126

Figure C.2: Wave Profile Curve Fitting

β	10	deg
τ	4	deg
Cv	3.69	
λ	3.36	
V	8.00802	knots
Lk	1.567218	ft
B	0.416667	ft

	Measured			New			Error Squared		
X(B)	0	0.2B	0.4B	0	.2B	0.4B	0B	0.2B	.4B
0	-0.26	-0.23078	-0.18031	-0.26238	-0.22711	-0.19185	0.002377	0.003665	0.011535
0.33	-0.27092	-0.23697	-0.18635	-0.27362	-0.24127	-0.20717	0.002695	0.004302	0.020818
0.66	-0.2677	-0.23991	-0.18932	-0.2751	-0.24808	-0.21611	0.007402	0.008168	0.026784
1	-0.26349	-0.23514	-0.18178	-0.27023	-0.25011	-0.2209	0.006737	0.014975	0.039119
1.33	-0.25303	-0.22459	-0.17476	-0.26022	-0.24828	-0.22233	0.007194	0.023689	0.047572
1.66	-0.23073	-0.21855	-0.16728	-0.24578	-0.24311	-0.22087	0.015054	0.024559	0.053587
2	-0.20797	-0.20302	-0.15245	-0.22738	-0.23496	-0.21681	0.019416	0.03194	0.064364
2.33	-0.18446	-0.18795	-0.13757	-0.20537	-0.22409	-0.2104	0.020906	0.036141	0.072832
2.66	-0.15312	-0.16845	-0.11405	-0.18001	-0.2107	-0.2018	0.026888	0.04225	0.087745
3	-0.11782	-0.14889	-0.09901	-0.15152	-0.19496	-0.19115	0.033706	0.046076	0.092138

β	20	deg
τ	4	deg
Cv	3.69	
λ	1.68	
V	8.00802	knots
Lk	1.045168	ft
B	0.416667	ft

	Measured			New			Error Squared		
X(B)	0	0.2B	0.4B	0	.2B	0.4B	0B	0.2B	.4B
0	-0.182	-0.11438	-0.04221	-0.17498	-0.10218	-0.02939	0.007023	0.012192	0.012823
0.33	-0.18903	-0.12351	-0.05073	-0.18781	-0.11793	-0.0463	0.001226	0.005579	0.004432
0.66	-0.1905	-0.13229	-0.06088	-0.19219	-0.12764	-0.05814	0.001687	0.004645	0.002737
1	-0.19261	-0.13346	-0.06506	-0.19108	-0.13343	-0.06669	0.001528	2.9E-05	0.001632
1.33	-0.1839	-0.13444	-0.06971	-0.18552	-0.13605	-0.07257	0.001623	0.001609	0.002865
1.66	-0.17404	-0.13051	-0.07076	-0.17613	-0.13593	-0.07616	0.002091	0.005413	0.005399
2	-0.16205	-0.1261	-0.06726	-0.16331	-0.13336	-0.07768	0.001257	0.007257	0.01042
2.33	-0.14876	-0.12076	-0.0594	-0.14736	-0.12856	-0.07734	0.001393	0.007792	0.017934
2.66	-0.12804	-0.11325	-0.05288	-0.12853	-0.12169	-0.07526	0.000485	0.00844	0.022378
3	-0.1046	-0.1054	-0.04525	-0.10698	-0.11289	-0.07155	0.002382	0.007495	0.026299

β	20	deg
τ	4	deg
Cv	3.02	
λ	1.87	
V	6.553989	knots
Lk	1.124335	ft
B	0.416667	ft

	Measured			New			Error Squared		
X(B)	0	0.2B	0.4B	0	.2B	0.4B	0B	0.2B	.4B
0	-0.188	-0.11868	-0.04324	-0.18823	-0.11544	-0.04264	0.000231	0.003243	0.000597
0.33	-0.19007	-0.13068	-0.05106	-0.1985	-0.12927	-0.0579	0.00843	0.00141	0.006837
0.66	-0.18698	-0.13569	-0.06315	-0.19822	-0.1355	-0.06673	0.011238	0.000192	0.003577
1	-0.17845	-0.13351	-0.07034	-0.19106	-0.13677	-0.07137	0.012606	0.003258	0.00103
1.33	-0.15359	-0.12887	-0.07456	-0.17834	-0.13403	-0.07263	0.024743	0.00516	0.001931
1.66	-0.12959	-0.1172	-0.07387	-0.16082	-0.12784	-0.07096	0.031229	0.010645	0.002907
2	-0.09658	-0.09987	-0.07249	-0.13901	-0.11856	-0.06669	0.042431	0.018691	0.005806
2.33	-0.05722	-0.08526	-0.06527	-0.1133	-0.10646	-0.06003	0.056076	0.021207	0.005236
2.66	-0.01139	-0.06139	-0.06179	-0.08396	-0.09176	-0.05117	0.072578	0.030372	0.010617
3	-0.01063	-0.03717	-0.05717	-0.05125	-0.07462	-0.04025	0.040615	0.037443	0.016914

Figure C.3: Wave Profile Curve Fitting

β	20	deg
τ	4	deg
Cv	3.68	
λ	1.9	
V	7.986318	knots
Lk	1.136835	ft
B	0.416667	ft

	Measured			New			Error Squared		
X(B)	0	0.2B	0.4B	0	.2B	0.4B	0B	0.2B	.4B
0	-0.188	-0.10687	-0.03869	-0.19032	-0.11753	-0.04474	0.002324	0.010657	0.006045
0.33	-0.19363	-0.11955	-0.04739	-0.20284	-0.13297	-0.06135	0.009219	0.01342	0.013954
0.66	-0.19634	-0.13262	-0.05574	-0.20667	-0.14214	-0.07265	0.010325	0.009519	0.016915
1	-0.19883	-0.1441	-0.0641	-0.20483	-0.14722	-0.0805	0.006001	0.003127	0.016399
1.33	-0.19459	-0.14724	-0.06857	-0.19841	-0.149	-0.08555	0.003822	0.001758	0.016985
1.66	-0.1893	-0.15488	-0.07415	-0.18804	-0.14793	-0.08819	0.001259	0.006953	0.014044
2	-0.18095	-0.14954	-0.07641	-0.17414	-0.14431	-0.08868	0.006804	0.005236	0.012274
2.33	-0.16677	-0.1402	-0.07863	-0.15702	-0.13836	-0.0872	0.00975	0.001839	0.008574
2.66	-0.15131	-0.13473	-0.08059	-0.13692	-0.13026	-0.0839	0.014384	0.004466	0.003311
3	-0.12394	-0.125	-0.08194	-0.11404	-0.12016	-0.0789	0.009906	0.004844	0.003037

β	20	deg
τ	4	deg
Cv	4.25	
λ	2.02	
V	9.22333	knots
Lk	1.186835	ft
B	0.416667	ft

	Measured			New			Error Squared		
X(B)	0	0.2B	0.4B	0	.2B	0.4B	0B	0.2B	.4B
0	-0.195	-0.12104	-0.04454	-0.19869	-0.1259	-0.05311	0.003695	0.00486	0.00857
0.33	-0.20273	-0.13735	-0.06066	-0.21249	-0.14223	-0.07045	0.009764	0.004877	0.009789
0.66	-0.20124	-0.15367	-0.06843	-0.21865	-0.15301	-0.08308	0.017405	0.000654	0.014652
1	-0.20028	-0.16529	-0.08463	-0.21983	-0.16019	-0.09265	0.019556	0.0051	0.008018
1.33	-0.19744	-0.16969	-0.08901	-0.21699	-0.16444	-0.09974	0.019557	0.005248	0.010737
1.66	-0.19392	-0.1735	-0.10056	-0.21068	-0.16618	-0.1047	0.016757	0.007319	0.004132
2	-0.18195	-0.1668	-0.10246	-0.20127	-0.16567	-0.10774	0.019322	0.001129	0.005279
2.33	-0.178	-0.16385	-0.10926	-0.18903	-0.1631	-0.10904	0.011022	0.000743	0.000219
2.66	-0.16192	-0.15866	-0.11065	-0.17417	-0.15864	-0.10873	0.012246	2.03E-05	0.001913
3	-0.14249	-0.14742	-0.10744	-0.15686	-0.1524	-0.10691	0.014374	0.004976	0.000528

β	20	deg
τ	4	deg
Cv	5.47	
λ	2.02	
V	11.87097	knots
Lk	1.186835	ft
B	0.416667	ft

	Measured			New			Error Squared		
X(B)	0	0.2B	0.4B	0	.2B	0.4B	0B	0.2B	.4B
0	-0.199	-0.11971	-0.03951	-0.19869	-0.1259	-0.05311	0.000305	0.006194	0.013596
0.33	-0.20228	-0.12868	-0.05692	-0.21455	-0.14372	-0.07171	0.012271	0.015039	0.014792
0.66	-0.21146	-0.1375	-0.07504	-0.22447	-0.15723	-0.08666	0.013011	0.01973	0.011619
1	-0.21702	-0.15082	-0.09449	-0.23052	-0.16794	-0.09923	0.013497	0.017126	0.004747
1.33	-0.22136	-0.15871	-0.11117	-0.23345	-0.17638	-0.10988	0.012092	0.017679	0.001296
1.66	-0.22639	-0.16838	-0.1242	-0.23368	-0.18287	-0.11886	0.007283	0.01449	0.00534
2	-0.23133	-0.17707	-0.13679	-0.2315	-0.1876	-0.12636	0.000164	0.010535	0.010426
2.33	-0.23233	-0.1821	-0.15033	-0.22712	-0.19075	-0.13251	0.00521	0.008641	0.01782
2.66	-0.23757	-0.19134	-0.15882	-0.22071	-0.19241	-0.1374	0.016864	0.001071	0.021419
3	-0.23453	-0.20058	-0.16057	-0.2124	-0.1927	-0.14112	0.02213	0.007888	0.019449

Figure C.4: Wave Profile Curve Fitting

β	20	deg
τ	4	deg
Cv	3.69	
λ	2.64	
V	8.00802	knots
Lk	1.445168	ft
B	0.416667	ft

	Measured			New			Error Squared		
X(B)	0	0.2B	0.4B	0	.2B	0.4B	0B	0.2B	.4B
0	-0.242	-0.14059	-0.0339	-0.24194	-0.16915	-0.09636	5.64E-05	0.028561	0.062454
0.33	-0.23995	-0.15947	-0.05431	-0.25356	-0.18368	-0.11205	0.013605	0.024205	0.057737
0.66	-0.23567	-0.17566	-0.07393	-0.25572	-0.19117	-0.12167	0.020046	0.015503	0.047743
1	-0.22838	-0.18628	-0.08711	-0.25173	-0.19408	-0.12734	0.023349	0.0078	0.040227
1.33	-0.22075	-0.19046	-0.09746	-0.24276	-0.19329	-0.12981	0.02201	0.00283	0.03235
1.66	-0.21301	-0.19432	-0.10138	-0.2295	-0.18929	-0.12953	0.016486	0.005021	0.028143
2	-0.20222	-0.18852	-0.10377	-0.2124	-0.18245	-0.12678	0.010183	0.006068	0.023006
2.33	-0.18533	-0.1795	-0.10604	-0.19181	-0.173	-0.12178	0.00648	0.0065	0.01574
2.66	-0.16277	-0.16154	-0.10546	-0.16797	-0.16114	-0.1147	0.005202	0.000407	0.009243
3	-0.13936	-0.13795	-0.10492	-0.14111	-0.14702	-0.10568	0.001748	0.009066	0.000765

β	30	deg
τ	4	deg
Cv	3.69	
λ	2.24	
V	8.00802	knots
Lk	1.480859	ft
B	0.416667	ft

	Measured			New			Error Squared		
X(B)	0	0.2B	0.4B	0	.2B	0.4B	0B	0.2B	.4B
0	-0.257	-0.14059	-0.0339	-0.24792	-0.13245	-0.01698	0.009081	0.00814	0.016923
0.33	-0.24922	-0.15947	-0.05431	-0.25942	-0.14687	-0.03256	0.010198	0.012604	0.021749
0.66	-0.24494	-0.17566	-0.07393	-0.26139	-0.15416	-0.04198	0.016441	0.021505	0.03194
1	-0.23765	-0.18628	-0.08711	-0.25714	-0.15681	-0.0474	0.019487	0.029464	0.039714
1.33	-0.23002	-0.19046	-0.09746	-0.24787	-0.15572	-0.04957	0.017844	0.034739	0.047895
1.66	-0.22229	-0.19432	-0.10138	-0.23426	-0.15138	-0.04894	0.011974	0.042935	0.052447
2	-0.21149	-0.18852	-0.10377	-0.21678	-0.14415	-0.0458	0.00529	0.044363	0.057966
2.33	-0.1946	-0.1795	-0.10604	-0.19577	-0.13429	-0.04039	0.001172	0.04521	0.065647
2.66	-0.17204	-0.16154	-0.10546	-0.17149	-0.12198	-0.03287	0.000552	0.039563	0.072589
3	-0.14864	-0.13795	-0.10492	-0.14416	-0.10739	-0.02337	0.00448	0.030565	0.081542

β	30	deg
τ	4	deg
Cv	3.69	
λ	2.33	
V	8.00802	knots
Lk	1.518359	ft
B	0.416667	ft

	Measured			New			Error Squared		
X(B)	0	0.2B	0.4B	0	.2B	0.4B	0B	0.2B	.4B
0	-0.255	-0.13675	-0.02566	-0.2542	-0.13873	-0.02326	0.000803	0.001973	0.002399
0.33	-0.25621	-0.1556	-0.04855	-0.26559	-0.15303	-0.03873	0.009377	0.002568	0.009825
0.66	-0.26025	-0.16483	-0.06557	-0.26734	-0.16012	-0.04794	0.007095	0.004719	0.017627
1	-0.26285	-0.17407	-0.07849	-0.26282	-0.1625	-0.05308	2.31E-05	0.011571	0.025411
1.33	-0.26467	-0.18342	-0.08782	-0.25323	-0.16108	-0.05493	0.011438	0.022341	0.032885
1.66	-0.26197	-0.18521	-0.09683	-0.23926	-0.15638	-0.05394	0.022709	0.028826	0.042887
2	-0.25974	-0.1843	-0.10078	-0.22139	-0.14876	-0.05041	0.038351	0.035545	0.050369
2.33	-0.2502	-0.17588	-0.10376	-0.19994	-0.13845	-0.04456	0.050264	0.037427	0.059197
2.66	-0.24464	-0.16535	-0.10506	-0.17519	-0.12568	-0.03657	0.06945	0.039677	0.06849
3	-0.2359	-0.15118	-0.10171	-0.14736	-0.11059	-0.02657	0.088546	0.040591	0.075137

Figure C.5: Wave Profile Curve Fitting

β	30	deg
τ	4	deg
Cv	5.47	
λ	2.62	
V	11.87097	knots
Lk	1.639192	ft
B	0.416667	ft

	Measured			New			Error Squared		
X(B)	0	0.2B	0.4B	0	.2B	0.4B	0B	0.2B	.4B
0	-0.276	-0.16155	-0.03762	-0.27443	-0.15896	-0.04349	0.001574	0.002598	0.005868
0.33	-0.27834	-0.17999	-0.05807	-0.28935	-0.17585	-0.06116	0.011008	0.00414	0.003099
0.66	-0.28229	-0.19272	-0.08448	-0.29757	-0.18767	-0.07442	0.015281	0.005055	0.010058
1	-0.28484	-0.20721	-0.07035	-0.30143	-0.19618	-0.08479	0.016594	0.01103	0.01444
1.33	-0.28662	-0.21703	-0.12064	-0.30176	-0.20202	-0.09283	0.015135	0.015011	0.027809
1.66	-0.28398	-0.22556	-0.13117	-0.29904	-0.20555	-0.09887	0.015054	0.020007	0.032303
2	-0.28179	-0.23562	-0.13902	-0.29359	-0.20702	-0.1031	0.0118	0.028598	0.035917
2.33	-0.27247	-0.22952	-0.14306	-0.28567	-0.20662	-0.1057	0.013202	0.022901	0.037362
2.66	-0.26703	-0.2263	-0.14639	-0.27545	-0.20447	-0.10678	0.00842	0.021831	0.039604
3	-0.25848	-0.21859	-0.14971	-0.26308	-0.2007	-0.10645	0.004599	0.017891	0.043263

Figure C.6: Wave Profile Curve Fitting

Appendix D

Files for Reproduction of Prediction Method

D.1 Stepped Main

```
clear all
close all
clc
gridnumx=200;  %Number of grid points in x
gridnumy=200;  %Number of grid points in y

%% Batch Code
[FileName,PathName,FilterIndex] = uigetfile('*.txt','MultiSelect','on');

Data = strcat(PathName,FileName);

% Load files into cell arrays
fileID = fopen(Data);
% Loads contents of input file into cell array, ignoring header
% info
Data = textscan(fileID,'%f %f %f %f %f %f %f %f %f %f %f %f %f %f %f %f
%f','HeaderLines',1);
fclose(fileID);

%Number of Steps
Snum=2;
%Snum=0;
Tauavg=zeros(1,Snum+1);
Lambdaavg=zeros(1,Snum+1);
Betaavg=zeros(1,Snum+1);
B=zeros(1,Snum+1);
BL=zeros(1,Snum+1);
Beta=zeros(1,Snum+1);
Lf=zeros(1,Snum+1);
Df=zeros(1,Snum+1);
Cp=zeros(1,Snum+1);
Lp=zeros(1,Snum+1);
LkL=zeros(1,Snum+1);
L=zeros(Snum+2,1);
LL=zeros(Snum+2,1);
hL=0;
M=0;
D=0;

%LOA (feet)
LOA=80/12;

%Beam (feet)
B=ones(1,Snum+1)*1.47;

%Deadrise (degrees)
Beta=ones(1,Snum+1)*15;
Betaavg=Beta;

%Water Temp (Deg F)
T=59.5;
```

Figure D.1: Stepped Main Page 1

```
%VCG (feet above Baseline)
VCG=.4166666666666;

%Distance Thrust Line Below VCG (feet)
f=0;

%Angle of Thrust Line (degrees)
Epsilon=0;

%Friction Factor
dCf=0;

%Step Location (feet forward of Transom)
Ls(2)=40/12;
Ls(3)=20/12;
Ls(4)=0;
Ls(5)=0;

%Planing Surface Angle After Step (degrees)
Theta=zeros(Snum+1,1);
Taur=ones(length(Data{1}),1);
Dr=ones(length(Data{1}),1);
Lkr=ones(length(Data{1}),1);
for run=4:4%length(Data{1})
    %% Setup Calculations
    %Speed (ft/s)
    V=Data{6}(run);

    %Displacement (lbf)
    Disp=Data{4}(run);

    %Unit Conversions
    TC=(T-32)*5/9;

    %Step Height (feet)
    h(1)=0;
    h(2)=Data{2}(run)/12;
    h(3)=Data{3}(run)/12;

    %LCG (feet from Transom)
    LCG=Data{5}(run);

    %Calculate Dynamic Viscosity
    %     mum=(0.000000032451574*TC^4 - 0.000009061289916*TC^3 +
0.000984509345712*TC^2 - 0.055211010387108*TC + 1.778370453327440)*10^-3;
%Dynamic Viscosity (Ns/m^2)
    %     mu=mum*0.0208854342; %Dynamic Viscosity (lbfs/ft^2)
```

Figure D.2: Stepped Main Page 2

```
    %Calculate Density
    %     rho0=1000;  %Initial Denisty (kg/m^3) at 4 deg. C
    %     T0=4;       %Initial Temperature (deg. C)
    %     VTC=.0002;  %Volumetric Temperature Coefficient (m^3/m^3 deg.
C)
    %     rhom=rho0/(1+VTC*(TC-T0)); %Denisity (kg/m^3)
    %     rho=rhom*.0624279606; %Denisity (lbf/ft^3)
    rho=62.2;

    %Calculate Kinematic Viscosity
    %     num=mum/rhom; %Kinematic Viscosity (m^2/s)
    %     nu=32.2*mu/rho; %Kinematic Viscosity (ft^2/s)
    nu=1*10^-5; %Kinematic Viscosity (ft^2/s)

    Taul=2;%1;
    Tauu=5.5;
    dTau=0.1;
    Lkll=0.2;
    Lklu=LOA;
    Lkul=0.2;
    Lkuu=LOA;

    [ FVll,Lift,Cp,Df,BL,Betaavg,Lambdaavg,Tauavg ] = SteppedVertical8(
B,gridnumy,rho,V,Taul,Beta,Lkll,nu,dCf,Disp,Snum,Ls,h,Theta);
    [ FVlu,Lift,Cp,Df,BL,Betaavg,Lambdaavg,Tauavg ] = SteppedVertical8(
B,gridnumy,rho,V,Taul,Beta,Lklu,nu,dCf,Disp,Snum,Ls,h,Theta);
    while abs(imag(FVll))>0||abs(imag(FVlu))>0||sign(FVll)==sign(FVlu)
        Taul=Taul+dTau;
        [ FVll,Lift,Cp,Df,BL,Betaavg,Lambdaavg,Tauavg ] =
SteppedVertical8(
B,gridnumy,rho,V,Taul,Beta,Lkll,nu,dCf,Disp,Snum,Ls,h,Theta);
        [ FVlu,Lift,Cp,Df,BL,Betaavg,Lambdaavg,Tauavg ] =
SteppedVertical8(
B,gridnumy,rho,V,Taul,Beta,Lklu,nu,dCf,Disp,Snum,Ls,h,Theta);
        Taul;
    end
    [ FVul,Lift,Cp,Df,BL,Betaavg,Lambdaavg,Tauavg ] = SteppedVertical8(
B,gridnumy,rho,V,Tauu,Beta,Lkul,nu,dCf,Disp,Snum,Ls,h,Theta);
    [ FVuu,Lift,Cp,Df,BL,Betaavg,Lambdaavg,Tauavg ] = SteppedVertical8(
B,gridnumy,rho,V,Tauu,Beta,Lkuu,nu,dCf,Disp,Snum,Ls,h,Theta);
```

Figure D.3: Stepped Main Page 3

```
    while abs(imag(FVul))>0||abs(imag(FVuu))>0||sign(FVul)==sign(FVuu)
        Tauu=Tauu-dTau;
        [ FVul,Lift,Cp,Df,BL,Betaavg,Lambdaavg,Tauavg ] =
SteppedVertical8(
B,gridnumy,rho,V,Tauu,Beta,Lkul,nu,dCf,Disp,Snum,Ls,h,Theta);
        [ FVuu,Lift,Cp,Df,BL,Betaavg,Lambdaavg,Tauavg ] =
SteppedVertical8(
B,gridnumy,rho,V,Tauu,Beta,Lkuu,nu,dCf,Disp,Snum,Ls,h,Theta);
        Tauu;
    end

    M=1000;
    [ D,Ml ] = Stepped8(
B,gridnumy,rho,V,Taul,Beta,nu,dCf,LCG,VCG,f,Disp,LOA,Snum,Ls,h,Theta );
    [ D,Mu ] = Stepped8(
B,gridnumy,rho,V,Tauu,Beta,nu,dCf,LCG,VCG,f,Disp,LOA,Snum,Ls,h,Theta );
    if Ml>0&&Mu>0
        Tauu=Taul;
        Mu=Ml;
        Taul=Taul-dTau;
        [ FVll,Lift,Cp,Df,BL,Betaavg,Lambdaavg,Tauavg ] =
SteppedVertical8(
B,gridnumy,rho,V,Taul,Beta,Lkll,nu,dCf,Disp,Snum,Ls,h,Theta);
        [ FVlu,Lift,Cp,Df,BL,Betaavg,Lambdaavg,Tauavg ] =
SteppedVertical8(
B,gridnumy,rho,V,Taul,Beta,Lklu,nu,dCf,Disp,Snum,Ls,h,Theta);
        while sign(FVll)==sign(FVlu)
            Taul=Taul+.001;
            [ FVll,Lift,Cp,Df,BL,Betaavg,Lambdaavg,Tauavg ] =
SteppedVertical8(
B,gridnumy,rho,V,Taul,Beta,Lkll,nu,dCf,Disp,Snum,Ls,h,Theta);
            [ FVlu,Lift,Cp,Df,BL,Betaavg,Lambdaavg,Tauavg ] =
SteppedVertical8(
B,gridnumy,rho,V,Taul,Beta,Lklu,nu,dCf,Disp,Snum,Ls,h,Theta);
            Taul
        end

        [ D,Ml ] = Stepped8(
B,gridnumy,rho,V,Taul,Beta,gridnumx,nu,dCf,LCG,VCG,f,Disp,LOA,Snum,Ls,h,T
heta );

    End
```

Figure D.4: Stepped Main Page 4

```
    if Ml<0&&Mu<0
        Taul=Tauu;
        Ml=Mu;
        Tauu=Tauu+dTau;
        [ FVul,Lift,Cp,Df,BL,Betaavg,Lambdaavg,Tauavg ] =
SteppedVertical8(
B,gridnumy,rho,V,Tauu,Beta,Lkul,nu,dCf,Disp,Snum,Ls,h,Theta);
        [ FVuu,Lift,Cp,Df,BL,Betaavg,Lambdaavg,Tauavg ] =
SteppedVertical8(
B,gridnumy,rho,V,Tauu,Beta,Lkuu,nu,dCf,Disp,Snum,Ls,h,Theta);
        while sign(FVul)==sign(FVuu)
            Tauu=Tauu-.001;
            [ FVul,Lift,Cp,Df,BL,Betaavg,Lambdaavg,Tauavg ] =
SteppedVertical8(
B,gridnumy,rho,V,Tauu,Beta,Lkul,nu,dCf,Disp,Snum,Ls,h,Theta);
            [ FVuu,Lift,Cp,Df,BL,Betaavg,Lambdaavg,Tauavg ] =
SteppedVertical8(
B,gridnumy,rho,V,Tauu,Beta,Lkuu,nu,dCf,Disp,Snum,Ls,h,Theta);
            Tauu;
        end
        [ D,Mu ] = Stepped8(
B,gridnumy,rho,V,Tauu,Beta,gridnumx,nu,dCf,LCG,VCG,f,Disp,LOA,Snum,Ls,h,T
heta );
    end

    Mll=Ml;
    Taull=Taul;

    while abs(M)>0.001
        Tau=(Tauu+Taul)/2;
        [ D,M ] = Stepped8(
B,gridnumy,rho,V,Tau,Beta,nu,dCf,LCG,VCG,f,Disp,LOA,Snum,Ls,h,Theta );

        if abs(Taul-Tauu)<1e-05
            M=0;
        end
        if sign(Ml)==sign(M)
            Taul=Tau;
            Ml=M;
        else
            Tauu=Tau;
            Mu=M;
        end
    end
    [ Dr(run),Mr(run), Lkr(run) ] = Stepped8(
B,gridnumy,rho,V,Tau,Beta,gridnumx,nu,dCf,LCG,VCG,f,Disp,LOA,Snum,Ls,h,Th
eta );
    Taur(run)=Tau;
    run
end
```

Figure D.5: Stepped Main Page 5

D.2 Stepped

```
function [ D,M,LkG ] = Stepped8(
B,gridnumy,rho,V,Tau,Beta,nu,dCf,LCG,VCG,f,Disp,LOA,Snum,Ls,h,Theta )
%% Initialize Variables
FV=1000;
i=0;
M=0;
hL=0;
D=0;

%% Initialize Wetted Keel Length
Lkl=0.2;
Lku=LOA;

%% Calculate Sum of Vertical Forces at Upper and Lower Bound
[ FVl,Lift,Cp,Df,BL,Betaavg,Lambdaavg,Tauavg ] = SteppedVertical8(
B,gridnumy,rho,V,Tau,Beta,Lkl,nu,dCf,Disp,Snum,Ls,h,Theta);
[ FVu,Lift,Cp,Df,BL,Betaavg,Lambdaavg,Tauavg ] = SteppedVertical8(
B,gridnumy,rho,V,Tau,Beta,Lku,nu,dCf,Disp,Snum,Ls,h,Theta);
FV=1000;

%Iterate until Sum of Vertical Forces Equals Zero
while abs(FV)>1*10^-3
Lkc=(Lkl+Lku)/2;
[ FV,Lift,Cp,Df,BL,Betaavg,Lambdaavg,Tauavg ] = SteppedVertical8(
B,gridnumy,rho,V,Tau,Beta,Lkc,nu,dCf,Disp,Snum,Ls,h,Theta);
        if abs(Lkl-Lku)<1e-05
            FV=0;
        end
if sign(FVl)==sign(FV)
        Lkl=Lkc;
        FVl=FV;
    else
        Lku=Lkc;
        FVu=FV;
    end
Lk=Lkc;
    Lk;
    FV;
end
[ FV,Lift,Cp,Df,BL,Betaavg,Lambdaavg,Tauavg,L ] = SteppedVertical8(
B,gridnumy,rho,V,Tau,Beta,Lk,nu,dCf,Disp,Snum,Ls,h,Theta);
%% Calculate Sum of the Moments
M=0;
D=0;
```

Figure D.6: Stepped Page 1

```
for i=1:Snum+1;
    hL=hL+h(i);
    %Calculate distance from friction drag to center of gravity (ft)
    a(i)=VCG-hL-BL(i)/4*tan(Betaavg(i)*pi/180);
    %Calculate distance from normal force to center of gravity (ft)
    c(i)=LCG-(Cp(i)*Lambdaavg(i)*BL(i)+Ls(i+1));
    %Calculate moment (ft-lbf)
    M=M+Lift(i)/cos(Tau*pi/180)*c(i)+Df(i)*a(i);
    %Calculate Total Drag (lbf)
    D=D+Lift(i)*tan(Tau*pi/180)+Df(i)/cos(Tau*pi/180);
end
LkG=L(1,1);
end
```

Figure D.7: Stepped Page 2

D.3 Stepped Vertical

```
function [ FV,Lift,Cp,Df,BL,Betaavg,Lambdaavg,Tauavg,L] =
SteppedVertical8(
B,gridnumy,rho,V,Tau,Beta,Lk,nu,dCf,Disp,Snum,Ls,h,Theta)
%% Initialize Variables
FV=0;
Tauavg=zeros(1,Snum+1);
Tauavg(1)=Tau;
Lambdaavg=zeros(1,Snum+1);
Betaavg=zeros(1,Snum+1);
Betaavg(1)=Beta(1);
Lift=zeros(1,Snum+1);
Df=zeros(1,Snum+1);
Cp=zeros(1,Snum+1);
LkL=zeros(1,Snum+1);
BL=zeros(1,Snum+1);
Cv=zeros(1,Snum+1);
y=B(1)/(2*gridnumy)*(0:gridnumy);
L=inf*ones(Snum+2,length(y));
LL=inf*ones(Snum+2,length(y));
LStag=inf*ones(Snum+2,length(y));
LLStag=inf*ones(Snum+2,length(y));
LExtra=inf*ones(Snum+2,length(y));
LLExtra=inf*ones(Snum+2,length(y));
LWake=inf*ones(Snum+2,length(y));
LLWake=inf*ones(Snum+2,length(y));

%% Calculate parameters on forward planing surface
%Determine if forward planing surface is chines wet or chines dry
if Lk < B(1)/pi*tan(Beta(1)*pi/180)/tan(Tau(1)*pi/180)

    %Calculate Wetted Beam (ft)
    BL(1)=Lk*pi*tan(Tau(1)*pi/180)/(tan(Beta(1)*pi/180));
    %yL=BL(1)/(2*(gridnumy-1))*(0:gridnumy-1);

    %Calculate Mean Wetted Length to Beam Ratio
    Lambda=Lk/(2*BL(1));
    Lc=0;

    for j = 1:length(y)
        %Local Wetted Length (Feet from Next Aft Step)
                LLStag(1,j)=-2*Lk/BL(1)*abs(y(j))+Lk;
        %Wetted Length (Feet from Transom)
        LStag(1,j)=LLStag(1,j)+Ls(2);

    end

else

    %Calculate Mean Wetted Length to Beam Ratio
    Lambda=Lk/B(1)-tan(Beta(1)*pi/180)/(2*pi*tan(Tau(1)*pi/180));
```

Figure D.8: Stepped Vertical Page 1

```
    %Calculate Wetted Chine Length (ft)
    Lc=Lambda*B(1)-B(1)*tan(Beta(1)*pi/180)/(2*pi*tan(Tau(1)*pi/180));

    BL(1)=B(1);
    for j = 1:length(y)

        %Local Wetted Length (Feet from Next Aft Step)
        LLStag(1,j)=2*(Lc-Lk)/BL(1)*abs(y(j))+Lk;
        %Wetted Length (Feet from Transom)
        LStag(1,j)=LLStag(1,j)+Ls(2);
        %LB(1,j)=0;
    end
end
for j = 1:length(y)
    for k=2:Snum+2
        if LStag(k-1,j)-Ls(k)<0 %&& L(k-1,j)>0
            LStag(k,j)=LStag(k-1,j);%-Ls(k+1)
            LLStag(k,j)=LStag(k-1,j)-Ls(k+1);
            LLStag(k-1,j)=0;%0
            LStag(k-1,j)=0;%0
        end
    end
end
LL(1,:)=LLStag(1,:);
L(1,:)=LStag(1,:);
%Calculate Averages
Betaavg(1)=Beta(1);
Lambdaavg(1)=Lambda(1);
Cv(1)=V/(32.2*BL(1))^(1/2);
LkL(1)=LL(1,1);
%Calculate lift and drag on the forward planing surface
[Lift,Df,V1,Re,Cf, Cp] =
LandD8(Lift,Df,1,V,Tauavg,Lambdaavg,Betaavg,BL,nu,rho,dCf,Cv,B,Cp,LkL);
%% Calculate for the after planing surfaces
ThetaL=0;
for i=2:Snum+1
    %Calculate wave profile and reattachment line

[Tauavg,Betaavg,BL,Lambdaavg,Lavg,LkL,L,LL,TauL,BetaL,chines,LStag,LLStag
,LExtra,LLExtra,LWake,LLWake]=Wake8(L,i,Cv,B,BL,LkL,Theta,Beta,h,Ls,Tauav
g,Betaavg,Lambdaavg,LL,y,LStag,LLStag,LExtra,LLExtra,LWake,LLWake);

%[Tauavg,Betaavg,BL,Lambdaavg,Lavg,LkL,L,x,y,LL,chines,LStag,LLStag,LExtr
a,LLExtra,LWake,LLWake]=Wake2D8(L,i,Cv,B,BL,LkL,Tau,Theta,Beta,h,Ls,Tauav
g,Betaavg,Lambdaavg,gridnumy,LL,y,Snum,LStag,LLStag,LExtra,LLExtra,LWake,
LLWake);
    Cv(i)=V/(32.2*BL(i))^(1/2);
    Tauavg(i)=Tau;
    %Calculate lift and drag on aft planing surfaces
    [Lift,Df,V1,Re,Cf, Cp] =
LandD8(Lift,Df,i,V,Tauavg,Lambdaavg,Betaavg,BL,nu,rho,dCf,Cv,B,Cp,LkL);
end
```

Figure D.9: Stepped Vertical Page 2

```
%% Calculate sum of the vertical forces
for i=1:Snum+1
FV=FV+Lift(i);%*cos(Tauavg(i)*pi/180)-Df(i)*sin(Tauavg(i)*pi/180);
end
FV=FV-Disp;
end

%figure
%plot(L(1,:)*12,y*12,L(2,:)*12,y*12,L(3,:)*12,y*12)
%xlim([0,80])
%axis equal
% figure
%title('Predicted Wetted Surface','FontSize',16);
%xlabel('Distance from Transom (in)','FontSize',14);
%ylabel('Distance from Centerline (in)','FontSize',14);
% legend('Forward Planing Surface','Middle Planing Surface','Aft Planing
Surface');
% set(legend,'FontSize',6,'Location','NorthWest');
% xlim([3.5,4.5]);
```

Figure D.10: Stepped Vertical Page 3

D.4 Wake

```
function
[Tauavg,Betaavg,BL,Lambdaavg,Lavg,LkL,L,LL,TauL,BetaL,chines,LStag,LLStag
,LExtra,LLExtra,LWake,LLWake]=Wake8(L,i,Cv,B,BL,LkL,Theta,Beta,h,Ls,Tauav
g,Betaavg,Lambdaavg,LL,y,LStag,LLStag,LExtra,LLExtra,LWake,LLWake)
%% 3D Wave Profile Constants
C1=4.14389041296706*1;
C2=-3.58981846107602*1;
C3=1.32869538817665*1;
x=zeros(3,length(y));
TauL=zeros(1,length(y));
BetaL=zeros(1,length(y));
%% Discretization in the y (transverse) directiom
chines=0;
count=0;
BL(i-1)=BL(i-1);

%% Calculate at each y location
for j = 1:length(y)
    %Reattachment Point (feet aft of step)
    x(i,j)=fzero(@(a) .103*1/Cv(i-1)*(a/BL(i-1))^(3/2)*(C1*(y(j)/BL(i-
1))^2+C2*(y(j)/BL(i-1))+C3+0.03*LkL(i-1)/BL(i-1)*Tauavg(i-1)^(3/2))-
h(i)/BL(i-1)-(a/BL(i-1))*tan(Theta(i)*pi/180)-(y(j)/BL(i-
1))*(tan(Beta(i)*pi/180)-tan(Beta(i-1)*pi/180)),[0,1000]);
    LWake(i,j)=Ls(i)-x(i,j)/cos(Theta(i)*pi/180);
    if LExtra(i,j)==0
        LExtra(i,j)=Inf;
    end
    L(i,j)=min(min(LWake(i,j),LStag(i,j)),LExtra(i,j));
    if LExtra(i,j)==inf
        LExtra(i,j)=0;
    end
    %Local Wetted Length (Feet from Next Aft Step)
    LL(i,j)=L(i,j)-Ls(i+1);
    LLWake(i,j)=LWake(i,j)-Ls(i+1);

end
BL(i)=B(i);
Lavg(i)=sum(LL(i,:))/length(y);
%% Check if Chines are Dry
if min(LL(i,:))<0
    bcount=1;
    Bj(1)=0;
    %Calculated new Beam at step based on deadrise angle
    for j = 1:length(y)-1
        if sign(LL(i,j))==-sign(LL(i,j+1))
            bcount=bcount+1;
        Bj(bcount)=(y(j)+y(j+1))/2;
        end
    end
```

Figure D.11: Wake Page 1

```
    Bj(bcount+1)=B(i)/2;
    Bj(bcount+2)=B(i)/2;
    BL(i)=0;
    for j=1:(bcount+1)/2
        BL(i)=BL(i)+(Bj(2*(j-1)+2)-Bj(2*(j-1)+1));
    end
    BL(i)=2*BL(i);
    for j = 1:length(y)
         if LL(i,j)<0
            LLExtra(i+1,j)=L(i,j)-Ls(i+2);
            LExtra(i+1,j)=L(i,j);
            L(i,j)=0;
            LL(i,j)=0;
        else
            count=count+1;
        end
    end
    Lavg(i)=sum(LL(i,:))/count;
end

LkL(i)=LL(i,1);
%% Calculate Local Trim Angle, Deadrise Angle
for j = 1:length(y)
    if L(i,j)==Ls(i)-x(i,j)/cos(Theta(i)*pi/180);
    TauL(j)=(.1545*1/(Cv(i-1)*BL(i-1))*(x(i,j)/BL(i-
1))^(1/2)*(C1*(y(j)/BL(i-1))^2+C2*(y(j)/BL(i-1))+C3+0.03*LkL(i-1)/BL(i-
1)*Tauavg(i-1)^(3/2)))*BL(i-1)*180/pi-Theta(i);
    BetaL(j)=Beta(i)-atan((.103*1/Cv(i-1)*(Lavg(i)/BL(i-
1))^(3/2)*(2*C1*y(j)*(1/BL(i-1))^2+C2/BL(i-1)))*BL(i-1))*180/pi;
    else
        TauL(j)=Tauavg(i-1);
        BetaL(j)=Betaavg(i-1);
    end
end
%% Calculate Averages
if count>0
    Tauavg(i)=sum(TauL(1:count))/count;
    Betaavg(i)=sum(BetaL(1:count))/count;
else
    Tauavg(i)=sum(TauL)/length(y);
    Betaavg(i)=sum(BetaL)/length(y);
end
Lambdaavg(i)=Lavg(i)/BL(i);
end
```

Figure D.12: Wake Page 2

D.5 Lift and Drag

```
function [Lift,Df,V1,Re,Cf, Cp] =
LandD8(Lift,Df,i,V,Tauavg,Lambdaavg,Betaavg,BL,nu,rho,dCf,Cv,B,Cp,LkL)
%Calculate Average Bottom Velocity
V1=V*sqrt(1-
.0120*Tauavg(i)^1.1/(Lambdaavg(i)^(1/2)*cos(Tauavg(i)*pi/180)));
V1=V1-.0065*Betaavg(i)*V1^0.6;

%Calculate Reynolds number
Re=V1*Lambdaavg(i)*BL(i)/nu;

%Calculate Friction Coefficient
Cf=0.075/(log(Re)/log(10)-2)^2;

%Cff=@(x)0.242/sqrt(x)-log(Re*x)/log(10);
%Cf=fzero(Cff,CLb/4);
Cf=Cf+dCf;

%Calculate Friction Drag (lbf)
Df(i)=1/2*rho/32.2*V1^2*Lambdaavg(i)*BL(i)^2*Cf/cos(Betaavg(i)*pi/180);


%Calculate Lift Force (lbf)
if BL(i)<B(i)
%Calculate Lift Coefficient
    CL=pi*(pi/(2*Betaavg(i)*pi/180)-1)^2*sin(Tauavg(i)*pi/180)^3*(1-
tan(Tauavg(i)*pi/180)/(2*tan(Betaavg(i)*pi/180)));
Lift(i)=1/2*CL*rho/32.2*V^2*LkL(i)^2;
else
 if Cv<12
CLo=Tauavg(i)^1.1*(0.012*Lambdaavg(i)^(1/2)+0.0055*Lambdaavg(i)^(5/2)/Cv(
i)^2);
CLb=(CLo-0.0065*Betaavg(i)*CLo^0.6);
Lift(i)=CLb*(1/2*rho/32.2*V^2*BL(i)^2);
 else

CLb=((0.5*pi*sin(Tauavg(i)*pi/180)*cos(Tauavg(i)*pi/180)^2)/(1+1/Lambdaav
g(i))*(1-
sin(Betaavg(i)*pi/180))+4/3*Lambdaavg(i)*sin(Tauavg(i)*pi/180)^2*cos(Taua
vg(i)*pi/180)^3*cos(Betaavg(i)*pi/180)+Tauavg(i)*0.0109*Lambdaavg(i)^2/Cv
(i)^2);
     Lift(i)=CLb*(1/2*rho/32.2*V^2*BL(i)^2);
 end
end
if BL(i)<B(i)
%Calculate Center of Pressure Coefficient
    Cp(i)=0.4;

else
Cp(i)=0.75-1/(5.21*Cv(i)^2/Lambdaavg(i)^2+2.39);
end

end
```

Figure D.13: Lift and Drag